Characterisation of the conserved mycobacterial penicillin binding protein LpqF

by

Clare Joan Thomas

A thesis submitted to the University of Birmingham for the degree of

DOCTOR OF PHILOSOPHY

School of Biosciences
College of Life and Environmental Sciences
University of Birmingham
September 2024

UNIVERSITY OF
BIRMINGHAM

University of Birmingham Research Archive

e-theses repository

This unpublished thesis/dissertation is copyright of the author and/or third parties. The intellectual property rights of the author or third parties in respect of this work are as defined by The Copyright Designs and Patents Act 1988 or as modified by any successor legislation.

Any use made of information contained in this thesis/dissertation must be in accordance with that legislation and must be properly acknowledged. Further distribution or reproduction in any format is prohibited without the permission of the copyright holder.

Abstract

Tuberculosis is a global disease affecting humans, animals, and marine life. In humans, it is primarily caused by the bacterium *Mycobacterium tuberculosis* and a few closely related species. *M. tuberculosis* was responsible for 1.6 million deaths in 2022, equating to one death every 20 seconds. Antibiotic resistance in *M. tuberculosis* is a major concern and a significant driver of mortality. The *Mycobacterium* genus has a unique, impermeable cell wall built on a foundation of peptidoglycan, which provides tensile strength and resists osmotic pressure. Peptidoglycan, an extensive cell wall polymer of alternating *N*-acetylglucosamine and *N*-acetylmuramic acid residues, is cross-linked by short peptides. Peptidoglycan-targeting enzymes, such as D,D-carboxypeptidases, are tightly regulated to enable growth and division.

Building on the observation that the loss of LpqF leads to altered colony morphology in *M. marinum*, this thesis characterises the function of this protein. LpqF is a low molecular weight penicillin-binding protein (PBP) conserved in mycobacteria. Our data support classifying LpqF as a D,D-carboxypeptidase that is inhibited by meropenem. These data show that LpqF has a unique N-terminal NTF2-like domain that binds to peptidoglycan, suggesting a positioning mechanism for the catalytic domain to access its substrate. Additionally, two of eight mutants (D85A and R98A) designed in the N-terminal NTF2-like domain further support this hypothesis by showing that these residues likely have roles in anchoring LpqF to peptidoglycan. Furthermore, this thesis presents evidence that Δ*lpqf* causes an accumulation of the fluorescent D-amino acid (FDAA) 3-[7-nitrobenzofurazan]-carboxamide-D-alanine (NADA) along the lateral cell wall in *M. marinum*, indicating the involvement of LpqF in peptidoglycan incorporation.

This work provides a strong foundation for further analysis and elucidation of D,D-carboxypeptidases. Understanding the function and regulation of LpqF could offer valuable insights into developing inhibitors targeting proteins involved in peptidoglycan biosynthesis, potentially aiding in the creation of new therapeutics against drug-resistant strains of *M. tuberculosis*.

Declaration

The work presented in this thesis has been carried out under the supervision of Dr Patrick J. Moynihan and Prof Gurdyal S. Besra in the School of Biosciences at the University of Birmingham, UK, B15 2TT during the period of June 2020-December 2023. I hereby declare the work in this thesis is original except where acknowledged by reference. No part of this work is being, or has been submitted for a degree, diploma or any other qualification at any other university.

Covid-19 statement

My PhD project was affected by the 2019-ongoing pandemic. During 2020-2022 there were three lockdowns halting the time in the lab for months at time. In between these times, due to social distancing there was limited, allocated time slots in the lab based on a rota system. This limited preliminary data acquisition and long term experimental planning. The pandemic also affected reagents acquisition, normal conferencing, presenting and collaborative opportunities between labs.

This thesis is dedicated to my two sons, Zayan and Toby. To you I give the future.

Acknowledgements

It is with enormous gratitude I thank my supervisor Dr Patrick Moynihan for his support and advice over the course of my PhD. I would like to thank Aaron Franklin, Sam Benedict, Abi Layton, Rudi Sullivan and Greg Gouge and everyone else in the Moynihan lab for their support and camaraderie. Thank you to Greg for all the coffees and laughs.

I would like to thank Sarah Bhat, Alex Kingdon, Kat Abrahams and everyone else in the Besra lab and Bhatt lab for their advice and chats.

I especially would like to thank and am so proud of my children, Zayan and Tobias for understanding, for the hugs, for your belief in me and for making me laugh out loud when I needed to. Without your presence none of this would have been worth it.

To everyone whom I may have forgotten, you all have had a positive influence on my life over the past three years and I thank you.

Contents

Abstract……. ii

Declaration……. iii

Covid-19 statement…… iv

Acknowledgements…… vi

Table of Contents……. viii

Figure List……. xiii

Table List……..... xvi

Abbreviation List…… xvii

Table of Contents

1 Chapter 1. General introduction…… 1

1.0 The *Mycobacterium* genus……... 1
1.2 History of tuberculosis……. 2
1.3 Environmental and social implications of mycobacterial infection……. 4
1.4 Epidemiology of Tuberculosis……. 5
1.4.1 Global prevalence of *M. tuberculosis* infection…….. 5
1.4.2 Drug resistant strains of *M. tuberculosis*…… 6
1.4.3 HIV-associated *M. tuberculosis* infection…….. 8
1.4.4 United Nations (UN) Sustainable Development Goals (SDGs)……..... 8
1.5 Infection and pathogenesis…….. 9
1.6 Treatment of *M. tuberculosis*…….. 11
1.7 The cell wall of Mycobacteria……..... 15
1.7.1 Mycobacterial outer membrane…… 16
1.7.2 Mycobacterial inner membrane (MIM)…… 17
1.7.3 Mycolic acids…… 22
1.7.4 Arabinogalactan…… 26
1.7.5 Peptidoglycan……..... 29
1.7.6 Mycobacterial classification…….. 30
1.7.7 Modifications of peptidoglycan……. 30
1.7.7.1 Admidation……. 30
1.7.7.2 *N*-deacteylation……... 31
1.7.7.3 *N*-glycolylation……... 31
1.7.8 Mycobacterial cross linking…….. 32
1.7.9 Peptidoglycan cytoplasmic biosynthesis……... 33
1.7.10 Formation of lipid linked muropeptides…… 34
1.7.11 Translocation of lipid linked muropeptide across the plasma membrane……. 36
1.7.12 Peptidoglycan periplasmic biosynthesis…… 37
1.7.13 D,D-transpeptidases…… 40
1.7.14 L,D-transpeptidation……... 41
1.7.15 Penicillin binding protein catalytic mechanism……. 43
1.7.16 Peptidoglycan cleaving enzymes……... 44

1.7.16.1 Muramidases…….. 45
1.7.16.2 *N*-acetylglucosaminidases…….. 47
1.7.16.3 *N*-acetylmuramoyl-L-alanine amidases…….. 48
1.7.16.4 Endopeptidases……... 48
1.7.16.5 Carboxypeptidases……. 49
1.7.17 Cleaved peptidoglycan……...51
1.8 Inhibitors of peptidoglycan synthesis……. 52
1.8.1 D-cycloserine…….. 52
1.8.2 β-lactams and adjuvants for targeting L,D-TPases and PBPs…… 54
1.8.3 Penams……... 56
1.8.4 Penems……... 56
1.8.5 Carbapenems……. 57
1.8.6 Cephams…… 57
1.8.7 Monobactams…… 59
1.8.8 Clavams……. 59
1.8.9 Mode of action of β-lactams…….. 60
1.9 Resistance to β-lactams; β-lactamases…….. 61
1.10 The use of model organisms and systems to study genes in pathogenic mycobacteria…….. 64
1.11 The use of genetic tools to identify new enzymes in TB research……... 65
1.11.1 Transposons……... 66
Aims and Objectives…… 69

2 Chapter 2. Materials and Methods…….. 70
2.1 Culture media…….. 71
2.1.1 Lysogeny broth……. 71
2.1.2 Lysogeny broth agar……..... 71
2.1.3 Middlebrook 7H9 Media……... 72
2.1.4 Middlebrook 7H10 Agar…… 72
2.2 *in silico* analysis……. 72
2.2.1 Multiple sequence alignments……... 72
2.2.2 Synteny for *lpqf*……. 73
2.2.3 Conservation of motifs and domain analysis…… 73

2.3 Cloning…… 73
2.3.1 Oligonucleotides…… 73
2.3.2 Polymerase Chain Reaction (PCR)…….. 74
2.3.3 Restriction free PCR (RF cloning)…… 74
2.3.4 Preparation of plasmid DNA…… 74
2.3.5 DNA concentration determination…… 75
2.4 Site directed mutagenesis and PCR…… 75
2.4.1 Generic method for Agarose Gel Electrophoresis…… 77
2.4.2 Generic method DNA extraction from Agarose Gel…… 78
2.4.3 Purification of DNA product…… 78
2.4.4 Digestion, Ligation and recirculation mixture…….. 78
2.5 Electroporation and transformation into competent cells…… 79
2.5.1 Electroporation into *M. marinum* competent cells…… 79
2.5.2 Transformation of *E. coli* strains…….. 79
2.6 Preparation of glycerol stocks…… 80
2.6.1 Protein expression and harvesting…… 80
2.7 Protein purification…… 81
2.7.1 Buffer exchange and salt removal using dialysis…….. 82
2.7.2 Concentration of purified protein…….. 82
2.7.3 Anion Exchange…… 83
2.7.4 Size Exclusion Chromatography…….. 83
2.7.5 Sodium Dodecyl Sulphate-Polyacrylamide Gel Electrophoresis…….. 83
2.8 Transposon mutagenesis library…… 84
2.8.1 Microbial growth curves…… 86
2.9 Microscopy (confocal and phase contrast)…… 86
2.10 Biochemistry…… 87
2.10.1 Bocillin fluorescence assay…… 87
2.10.2 Cephalosporinase assay using nitrocefin as a substrate…….. 88
2.10.3 Purification of peptidoglycan …… 89
2.10.4 Degradation assay using FITC …… 89
2.10.5 Sample preparation and RP-HPLC…… 90
2.10.6 Thin Layer Chromatography…….. 91
2.10.7 Peptidoglycan binding assay…….. 92

2.10.7.1 Classical SDS-PAGE peptidoglycan binding assay…… 92
2.10.7.2 NHS-Rhodamine adapted peptidoglycan binding assay……. 92

3 Chapter 3. Identification and bioinformatic analysis of LpqF……. 95
3.0 Introduction……... 95
3.1 An archived *Tn* library contains putative cell wall enzymes identified as having altered colony morphology in *M. marinum*…… 98
3.1.1 phAE181 as a delivery system……... 98
3.1.2 Experimental aim……... 99
3.1.3 MMAR_5092……... 101
3.1.4 Morphological screen for genes involved in cell wall assembly……... 104
3.1.5 LpqF (Rv3593)…… 107
3.1.6 The N-terminal domain of LpqF has an NTF2-like fold……. 114
3.1.7 LpqF is a low molecular weight PBP with a unique motif III within the catalytic triad…….. 118
3.2 Discussion…….. 126
3.3 Conclusion……. 130

4 Chapter 4. Rv3593 (LpqF) is a low molecular weight penicillin binding protein and is selectively inhibited by carbapenems……. 131
4.0 Expression and purification of LpqF…… 131
4.1 Functional analysis of LpqF……. 132
4.1.1 LpqF is unlikely to be a β-lactamase……... 133
4.1.2 LpqF selectively binds to β-lactams and is inhibited by meropenem…….. 134
4.2 Discussion…….. 136
4.3 Conclusion……. 139

5 Chapter 5. Biochemical analysis of LpqF…… 141
5.0 Introduction……..... 141
5.1 LpqF does not perform a D-amino acid exchange reaction *in vitro*……... 142
5.2 LpqF has weak or no hydrolytic activity on polymerised peptidoglycan…….. 143
5.3 LpqF cleaves L-alanine-γ-D-glutamate-L-lysine-D-alanine-D-alanine pentapeptide…. 151
5.4 Discussion…….. 153

5.5 Conclusion……. 159

6 Chapter 6. LpqF binds to peptidoglycan via its NTF2-like domain……... 161

6.0 Introduction……... 161

6.1 The NTF2 domain of LpqF binds peptidoglycan…….. 162

6.2 The NTF2 domain of LpqF mediates peptidoglycan binding……... 163

6.3 Discussion……. 173

6.4 Conclusion……. 176

7 Chapter 7. LpqF plays a role in peptidoglycan incorporation…… 178

7.0 Introduction…….. 178

7.1 Fitness analysis of Δ*lpqf* mutant strains…… 179

7.2 An *lpqf* transposon mutant has altered peptidoglycan incorporation relative to wildtype *M. marinum*……. 187

7.3 Discussion……... 189

7.4 Conclusion…….. 192

8 Chapter 8. General discussion……. 193

8.1 Future work…… 196

8.2 General conclusion…… 199

References…….. 200

List of Figures

Figure 1. UKHSA statistics of total number of people reporting TB cases in England from 2020-22……. 5
Figure 2. Global map of estimated tuberculosis incidence rates for 2022……. 6
Figure 3. The WHO global map of the incidence of multidrug/rifampicin resistant TB... 7
Figure 4. The WHO global map of estimated distribution of cases……... 8
Figure 5. Diagram outlining potential routes for pathogenic outcome for *M. tuberculosis* infection……... 11
Figure 6. Schematic representation of a cross-section of the cell wall structure in mycobacteria……. 16
Figure 7. A presentation of the biosynthetic pathway for PIMs and inositol acylation… 19
Figure 8. The structure of LAM from *M. smegmatis* and *M. tuberculosis*…… 22
Figure 9. A basic representation of the biosynthetic pathway for the generation of mycolic acids……. 25
Figure 10. Representation of arabinogalactan structure in *M. tuberculosis*……... 27
Figure 11. A schematic of the arabinogalactan biosynthesis in *Mycobacteria*…….. 29
Figure 12. Schematic of the basic chemical composition of mycobacterium peptidoglycan…… 33
Figure 13. Diagrammatic representation of the cytosolic phase of peptidoglycan synthesis in the cell wall of mycobacteria……. 36
Figure 14. Representative motifs in PBPs for Gram positive and Gram negative bacteria as well as mycobacteria responsible for lipid II integration into the existing peptidoglycan structure…….. 39
Figure 15. A schematic outlining the transpeptidation reaction resulting in the 3,4 cross-link, bridging two stem peptides and carboxypeptidation……. 41
Figure 16. Schematic of the steps depicting the 3,3 cross-linking created by the L,D-transpeptidases……... 43
Figure 17. A description of the bacilli cell responses during PG repair and maintenance……... 45
Figure 18. A schematic of the formation of the di-peptide, converting L-alanine to D-alanine……... 52
Figure 19. A basic depiction of the modes of action for the lipid II inhibitors

preventing incorporation into mature peptidoglycan…… 53
Figure 20. The similarity of the β-lactam ring……. 61
Figure 21. Confirmation of *M. marinum* colony morphology defects from an *Tn* library.. 106
Figure 22. A spot assay using wildtype and Δ*lpqf*^{Mm} (12C3)…… 107
Figure 23. Phylogenetic analysis of *lpqf* and its relationship to evolutionary distance in mycobacteria…… 109
Figure 24. Synteny analysis reveals the approximate loci for Rv3591, Rv3592, Rv3593, and Rv3594…….. 112
Figure 25. LpqF is predicted to belong to the PBP/B-lactamase family of enzymes……. 113
Figure 26. LpqF has two domains, an N-terminal NTF2-like domain and a C-terminal PBP domain……. 116
Figure 27. LpqF bears the signature motifs of a LMW PBP…….. 122
Figure 28. SDS-PAGE analysis of LpqF purification…… 132
Figure 29. LpqF β-lactamase activity assay……... 134
Figure 30. LpqF is inhibited by a variety of β-lactams…….. 136
Figure 31. Assessment of the capability of LpqF to exchange D-alanine in an *in vitro* Assay……... 143
Figure 32. LpqF does not hydrolyse polymerised *M. smegmatis* peptidoglycan in an *in vitro* degradation assay…… 145
Figure 33. Determination of LpqF hydrolytic activity on FITC-PG by thin layer chromatography…….. 148
Figure 34. HPLC separation of reaction products derived from LpqF digestion of *E. coli* and *M. smegmatis* peptidoglycan…… 150
Figure 35. LpqF-catalysed reaction products against pentapeptide……... 153
Figure 36. Structural comparison of the NTF2^{LpqF} and Bd1075 NTF2 domain suggests that NTF2^{LpqF} is unlikely to function in the same way……... 163
Figure 37. LpqF binds to peptidoglycan via the NTF2^{LpqF} domain……... 165
Figure 38. Structure of the NTF2^{LpqF} and residue selections for site-directed mutagenesis……. 166
Figure 39. Purification of NTF2^{LpqF} variants with putative binding residue substitutions.. 167
Figure 40. Development of a medium-throughput peptidoglycan-binding assay…….. 169
Figure 41. NHS-rhodamine NTF2 conjugated peptidoglycan binding assay…… 172
Figure 42. Morphological evaluation of an *M. marinum lpqf* transposon mutant……. 180

Figure 43. Morphological evaluation of Δ*lpqf* in *Mycobacterium smegmatis*……... 182
Figure 44. Growth kinetics for wildtype and Δ*lpqf in M. marinum*……... 183
Figure 45. Analysis of Δ*lpqf* ^{Sm} and wildtype in *M. smegmatis* liquid cultures……. 184
Figure 46. Cell wall labelling of wildtype and Δ*lpqf M. marinum* strains with FDAA dyes HADA and NADA…….. 188
Figure 47. A description of the function for LpqF a new mycobacteria D,D-CPase…….. 195

List of Tables

Table 1. A summary of mycobacterial species causing disease in animals and humans… 2
Table 2. 1st line antibiotics in the DOTS programme……. 12
Table 3. Reduced antibiotic regime in the DOTS programme…….. 13
Table 4. Drugs used for TB regimens associated with multi-drug resistant strains……... 14
Table 5. The nomenclature of the most common β-lactams and a representative structure from each class is outlined…….. 55
Table 6. Outlines the strains and plasmids that were used in this study…… 70
Table 7. Plasmids used in this study……..… 71
Table 8. Primers and melting temperatures (Tm) for site directed mutagenesis of NTF2 domain…….. 76
Table 9. Reaction mixture for RFP1 PCR……..…… 76
Table 10. Reaction mixture for RFP2 PCR…….. 77
Table 11. PCR thermocycler parameter settings…….. 77
Table 12. List of transposon mutagenesis library as labelled in original *Tn* library (Chen., 2010)…… 85
Table 13. A list of β-lactam antibiotic used in the fluorescence assay……. 88
Table 14. Twenty two isolated mutants in *M. marinum* from the Chen et al. (2010) study with morphological changes…… 104
Table 15. A representation of the structural alignments of NTF2 domains……. 117
Table 16. Alignment of 3h3h and NTF2 of LpqF structures for assessment of conservation of ligand binding residues…….. 118
Table 17. A summary of statistics for representing the diversity of the 18 enzymes from S11 and S13 groups utilised in Figure 27…..……..…….. 123
Table 18. Muropeptides from *E. coli* analysed by HPLC…….……... 150

List of abbreviations

ADC	Albumin, Dextrose, Catalase
Å	angstrom
BCG	Bacillus Calmette-Guérin
$CalC_2$	Calcium Chloride
D	Amino acid: aspartic acid
dH_2O	Distilled water
DAT	Diacyltrehalose
D-*iso*-Glu	D-*iso*-glutamine
DNA	Deoxyribonucleic Acid
EDTA	Ethylenediaminetetraacetic acid
EMB	Ethambutol
Glc*N*Ac	*N*-acetylglucosamine
HIV	Human Immunodeficiency Virus
HMW	High molecular weight
I	Amino acid: isoleucine
INH	Isoniazid
IPTG	Isopropyl-β-D-thiogalactopyranoside
kDa	Kilodalton
KOH	Potassium Hydroxide
LAM	Lipoarabinomannan
LB	Lysogeny Broth
LM	Lipomannan
LMW	Low molecular weight
M	Molar
Mur*N*Ac	*N*-acetylmuramic acid
MWCO	Molecular weight cut-off
mAGP	Mycolyl-arabinogalactan-peptidoglycan
mg	Milli Gram
mM	Milli Molar
*m*eso-DAP	*meso*-diaminopimelic acid
NaOH	Sodium hydroxide

Na_2CO_3	Sodium Carbonate
Ni^{2+}-NTA	Nickel Nitrilotriacetic Acid
NTF2	Nuclear transport factor like domain/fold
ng	Nano Gram
OADC	Oleic Acid, Albumin, Dextrose, Catalase
OD_{600nm}	Optical Density at 600 nm
PBP	Penicillin Binding Protein
PBS	Phosphate Buffered Saline
PCR	Polymerase Chain Reaction
PDIM	Phthiocerol dimycocerosate
PG	Peptidoglycan
PI	Phosphatidyl-myo-inositol
PIM	Phosphoinositol mannoside
PPM	Polyprenyl-phosphate-mannopyranose
pH	Power of Hydrogen
PZA	Pyrazinamide
Q	Amino acid: glutamine
R	Amino acid: arginine
RIF	Rifampin
RNA	Ribonucleic Acid
RP-HPLC	Reverse phase high performance liquid chromatography
SDS	Sodium Dodecyl Sulfate
SDMs	Site Directed Mutagenesis
SDS-PAGE	Sodium Dodecyl Sulfate-Polyacrylamide Gel Electrophoresis
TB	Tuberculosis
TLC	Thin layer chromatography
TDM	Trehalose dimycolate
TMM	Trehalose monomycolate
v/v	Volume per Volume
v/w	Weight per Volume
W	Amino acid: tryptophan
WHO	World Health Organisation
µg	Micro Gram

µL	Micro Litre
µm	Micro Meter
µM	Micro Molar

Chapter 1. General introduction

1.0 The *Mycobacterium* genus

The etiological agent of tuberculosis (TB) is *Mycobacterium tuberculosis*, along with other closely related strains grouped into the *M. tuberculosis* complex (MTBC), within the genus *Mycobacterium*. This genus belongs to the phylum *Actinomycetota* and the family *Mycobacteriaceae* (Velayati et al., 2017). Members of the MTBC share high genetic similarity but exhibit variability in host specificity, geographic distribution, and pathogenicity (Reva et al., 2015; Taiana Tainá Silva-Pereira, Naila Cristina Soler-Camargo and Marcia, 2024). The genus *Mycobacterium* was originally classified based on the characteristics of *M. tuberculosis*, including differences in cell wall composition (e.g., mycolic acids), cellular morphology (e.g., pigmentation), and the ability to grow under aerobic conditions (Lehmann & Neumann, 1896; Ramakrishnan et al., 1997; Chen et al., 2010; Hashish et al., 2018; Liang et al., 2020; Liu et al., 2023). However, these classifications have been updated with the integration of comparative genomics, which has helped identify conserved gene sequences specific to *Mycobacterium*, improving phylogenetic accuracy (Advani et al., 2019; Kumaragurubaran Karthik et al., 2023). Differences in 16S rRNA genomic data have also become a cornerstone of modern data analysis (Tortoli et al., 2017). There are approximately 190 species within this genus, which have adapted over millennia to diverse environments such as water, soil, air, and dust (Reva et al., 2015). Many of these species can cause infections in immunocompromised individuals, highlighting the genus's adaptability. Notable examples include the clinically significant human pathogens *M. tuberculosis* and *Mycobacterium leprae*, as well as non-tuberculous species such as *Mycobacterium abscessus* and *Mycobacterium avium* (Tortoli et al., 2017; Tortoli et al., 2019). The genus *Mycobacterium* is divided into slow- and fast-growing species (Fedrizzi et al., 2017). The slow growers are further subdivided into two complexes: the *M. tuberculosis* complex (MTBC) and the *Mycobacterium avium* complex (MAC), as summarised in Table 1. Fast growers include both pathogenic and non-pathogenic strains, also detailed in Table 1.

Table 1: A summary of mycobacterial species causing disease in animals and humans. Highlighting the groupings of fast and slow growers in the mycobacterial genus and a summary of the host and epidemiology for MTBC, MAC and MCAC. Table adapted from Reva et al., 2015; Forbes, 2017; Kanabalan et al., 202; Besiatykh et al., 2021; Zhou et al., 2021.

		***Mycobacterium tuberculosis complex* (MTBC)**	**Primary Reservoir Host**	**Geography**
Slow growing	MTBC	*Mycobacterium tuberculosis*	Humans	Global
		Mycobacterium aficanum	Humans	West and Central Africa
		Mycobacterium bovis	Cattle, deer, elk, bison, badger, oppossum	Global
		Mycobacterium cannetii	Human	East Africa
		Mycobacterium microti	Vole, field rodents	
		Mycobacterium orygis	Ruminants (oryx, rhinos dairy cattle)	South Africa
		Mycobacterium leprae	Human	Africa, South East Asia
	Non-tuberculosis mycobacteria	*Mycobacterium marinum*	Fish, Humans	Europe, Asia and United States
		Mycobacterium ulcerans	Fish, Humans	Africa, South America and Western Pacific regions
		***Mycobacterium avium complex* (MAC)**	**Primary Reservoir Host**	**Geography**
		Mycobacterium avium	Environment, Humans	Americas, Asia, and Europe
		Mycobacterium intracellulare	Environment, Humans	Americas, Asia, and Europe
		Mycobacterium chimaera	Environment, Humans	Global
		Mycobacterium haemophilum	Environment, Humans	Europe, Israel, Africa, Australia, Canada, Americas.
		Mycobacterium xenopi	Environment, Humans	Europe, Africa, Australia, Canada, South America.
		Mycobacterium kansasii	Environment, Humans	UK and North America
		Mycobacterium simiae	Environment, Humans	Europe, North America, Africa, Mediterranean, Middle East, Asian-Pacific
Fast growing		***Myobacterium chelonae-abscessus complex***	**Primary Reservoir Host**	**Geography**
		Mycobacterium abscessus subsp. abscessus	Environment, Humans	UK, North America, Europe, Asia
		Mycobacterium abscessus subsp. bolletii	Environment, Humans	UK, North America, Europe, Asia
		Mycobacterium chelonae	Environment, Humans	UK, North America, Canada, Eurasia, Austraila

1.2 History of tuberculosis

Studies conflict on how long tuberculosis has afflicted humans, with early research suggesting its presence as far back as 9000 years ago (Hershkovitz et al., 2008; WHO, 2023; CDC, 2019). Evidence includes studies on ancient mummies from Egypt dating back to 2050 BC, where PCR and spoligotyping techniques identified *M. tuberculosis* DNA (Zink et al., 2003). However, low genetic variation and analysis of mosaic gene sequences suggest that the

progenitor of *M. tuberculosis* infected hominids approximately 3 million years ago (Gutierrez et al., 2005). Later studies propose that the co-divergence of *M. tuberculosis* into humans occurred around 70,000 years ago during the Neolithic era (Comas et al., 2013). MTBC is divided into human- and animal-adapted strains, facilitating studies of *M. tuberculosis* and *M. bovis*, which have provided insights into the co-evolution of MTBC with human migration patterns out of Africa (Gordon and Behr, 2015). Recent research suggests that both human- and animal-adapted MTBC strains underwent dual evolution to adapt to their respective hosts (Brites et al., 2018; Gagneux, 2012; Gordon and Behr, 2015).

Over the centuries, before the advent of infection science and the identification of the etiological agents responsible for tuberculosis, the disease was described in various ways across many cultures. In ancient Greece, Hippocrates referred to it as phthisis (from "phthiein" meaning to waste away), characterising it by emaciation of the individual and ulceration of lung tissue (Daniel & Iversen, 2015). He noted that the disease was more common during the temperate months, and primarily affected individuals between the ages of 18 and 35 years (Daniel & Iversen, 2015). By 1720, the disease was known as consumption, and a new theory of its origin was proposed by Benjamin Marten in his publication "A New Theory of Consumption" where he suggested that microscopic "animacul" could survive in the host and cause TB (Hardy, 1999; Daniel, 2001).

A century later, during the 1800s, studies into the causative agent of infected lung and liver tissues from animals were conducted. The French physician René Laënnec and later Dr. Philipp Friedrich Hermann Klencke studied the pathology caused by small masses of fibrotic and necrotic caseous lesions (referred to as tubercles by pathologist Mathew Baillie in 1793) in both humans and animals (Roguin, 2006; Smith., 2023; Crainz et al., 1982). These studies led to Theodor Albrecht Edwin Kleb's, attempts to isolate the TB bacillus in 1867 by using TB-containing material on egg white, stored in sterile flasks. The culture medium turned turbid and was then used to infect guinea pigs, leading to the conclusion that the inoculation material contained the causative agent of TB (Susser and Stein, 2009; CURIOSity Digital Collections, 2022). Twenty years later, in 1882, Robert Koch published his findings on the isolation of *M. tuberculosis*, declaring that he had discovered the cause of TB (Blackswan et al., 2013). Koch demonstrated that *Mycobacterium* along with other bacterium could be grown outside of the host and could reproduce disease in a new host (Tabrah., 2011). In 1884, he published "Koch's Postulates," which outlined four principles: 1) the microorganism must be found in all diseased

hosts but not in healthy ones, 2) the microorganism can be isolated from the infected host and grown in culture, 3) when the cultured microorganism is inoculated into a new healthy host, it must cause disease, and 4) the microorganism must be re-isolated from the inoculated host and identified as the same microorganism (Tabrah., 2011). These postulates became the foundational principles for studying all infectious diseases. Koch continued his research on tuberculosis in search of a cure, and in 1890, he announced the discovery of tuberculin, derived from TB bacilli. Although tuberculin was initially thought to attenuate mycobacterial growth *in vitro* and in animal studies, it was later found to be ineffective as a therapeutic but proved valuable in 1931 for diagnosing TB using purified tuberculin protein derivative (Daniel., 2006; Yang, Kruh-Garcia, and Dobos, 2012; Akkermans, 2014).

1.3 Environmental and social implications of mycobacterial infection

During the time of Robert Koch's discoveries, the death rate from TB infection was approximately 900 deaths per 100,000 people. This high mortality rate coincided with the urbanization of Europe and the Americas between the 18th and 19th centuries, as people migrated to major city hubs in search of employment (Daniel, 2006). TB infection was closely linked to poverty, malnutrition, poor hygiene, and overcrowded living conditions (Hargreaves et al., 2011; Duarte et al., 2018). Additionally, cattle were often kept near living quarters, increasing the prevalence of *M. bovis* in milk and meat products (Waddington, 2004). These conditions facilitated zoonosis, the transmission of diseases from animals to humans, prompting efforts to limit the spread of infection through contaminated meat and dairy (Waddington, 2004). Despite the introduction of milk pasteurisation in the 1930s, zoonotic transmission remains a major health concern, not only for *M. bovis* but also for *M. tuberculosis* infections (Rowe & Donaghy, 2008).

The UK has a relatively low human-to-human transmission rate of TB at 7.8%, giving it one of the lowest incidence rates in Europe (GOV.UK, 2023, see Figure 1). In contrast, Ukraine reports the highest incidence rate at 27%, with 7.3 deaths per 100,000, a figure exacerbated by the ongoing Russian-Ukrainian conflict (Mencarini et al., 2023). Despite its overall low incidence, TB remains a concern in the UK; between 1999 and 2010, there was a 50% increase in TB cases in London, leading The Telegraph to label the city as "The TB Capital of Europe" (The Telegraph, 2010; UCL, 2010).

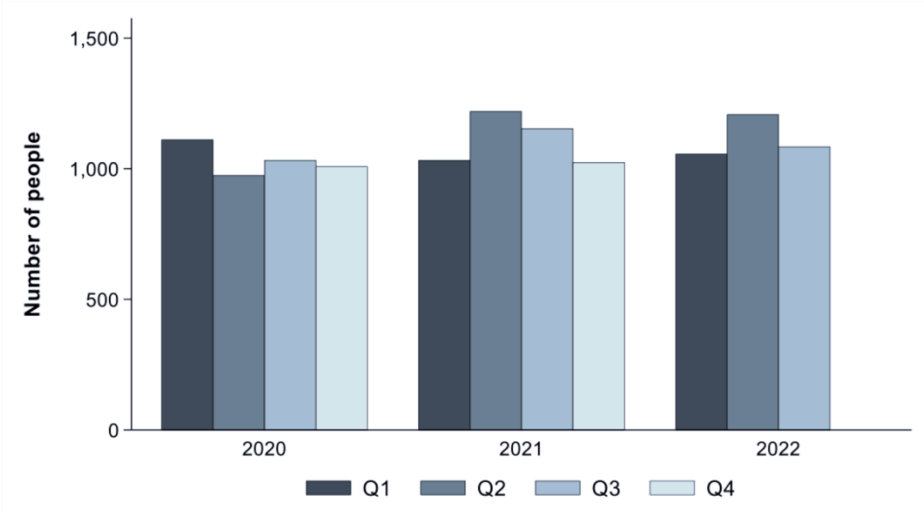


Figure 1: UKHSA statistics of total number of people reporting TB cases in England from 2020-22. These statistics reflect the number of reported cases of TB per region 1,084 of the population overall. In 2022, London had the highest number of cases (1220) but has decreased from 1,572 in 2021. From 2021-22; increase of 20% of population in the Southwest, East, Northeast, Northwest, Southwest and Yorkshire and the Humber remained comparable and decreased in East and West Midland (-10.1%, -31.1% respectively) (Figure adapted from; GOV.UK, 2022).

In the UK, the prevalence of *M. bovis* in cattle has steadily increased since the early 2000s, leading to the annual slaughter of over 40,000 cattle. This situation imposes a substantial financial burden on taxpayers, amounting to approximately £150 million per year, with additional costs impacting the farming industry (Hogarth & Sawyer, 2023). These circumstances highlight the critical importance of updating and implementing One Health policies that address the interconnections between human, animal, and environmental health. Additionally, the use of high-throughput, rapid diagnostics during outbreaks is essential for promptly identifying and managing cases, thereby limiting transmission and reducing the overall economic burden.

1.4 Epidemiology of Tuberculosis

1.4.1 Global prevalence of *M. tuberculosis* infection

TB is present in every country worldwide and is responsible for causing long-term disease in humans. Globally, TB is classified as the second most common cause of death from a single infectious pathogen, following SARS-CoV-2 (Global Tuberculosis, 2023). In 2019, 7.1 million new TB cases were reported (World Health Organisation, 2022; Gavi.org, 2022). According to the 2023 Global Tuberculosis Report, the number of newly diagnosed TB cases in 2022 increased to 7.5 million, up from 5.8 million in 2020, with a reduction in death rates to 1.3

million (Global Tuberculosis Report, 2023, Figure 1). However, the total number of people with an active infection was estimated at 10.6 million (5.8 million men, 3.5 million women, and 1.3 million children), similar to the levels in 2021 (WHO, 2023). This disparity in case reporting is attributed to limited access to medical care and diagnostics during the COVID-19 pandemic (World Health Organisation, 2022, 2023). Notably, 11% of these cases were among individuals under 15 years of age, with 250,000 children dying from tuberculosis each year (World Health Organisation, 2022). The incidence rate per 100,000 population varied between countries, with the highest numbers reported in Africa, Southeast Asia, the Western Pacific, the Eastern Mediterranean, the Americas, and Europe (Global Tuberculosis Report, 2023, Figure 2). TB is endemic in low- and middle-income countries and those experiencing conflict, with Africa currently having the highest incidence rates of pulmonary TB (WHO, 2023).

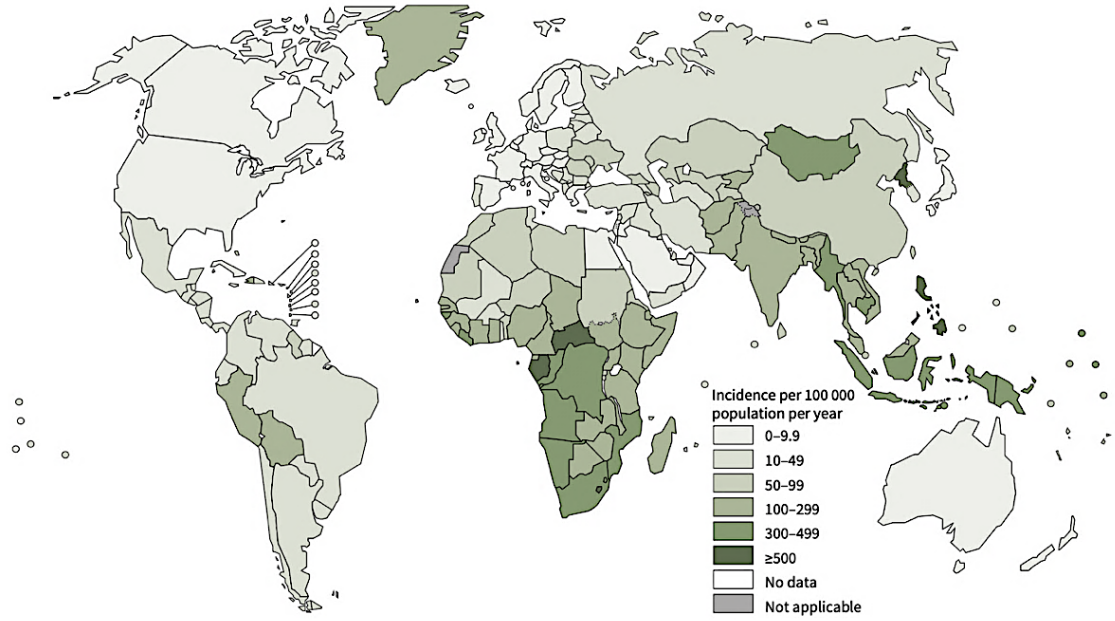


Figure 2: Global map of estimated tuberculosis incidence rates for 2022 (Figure adapted from; WHO Global TB Report., 2023).

1.4.2 Drug resistant strains of *M. tuberculosis*

In 2022, approximately 450,000 individuals were diagnosed globally with multidrug-resistant and rifampicin-resistant TB, with a cure success rate of 63% (World Health Organisation, 2022; Rich et al., 2023). However, only 40% of those diagnosed with multidrug resistant TB

sought treatment, leading to an increased mortality rate estimated between 191,000 and 264,000 (World Health Organisation, 2022).

Rifampicin-resistant, multidrug-resistant, totally drug-resistant, and extensively drug-resistant tuberculosis strains are resistant to isoniazid, rifampin (RIF), and fluoroquinolones, posing a significant global health security threat (Zhao et al., 2012; Zhang et al., 2014; Migliori et al., 2012). The World Health Organisation's 2022 guidelines for treating multidrug-resistant and rifampicin-resistant TB outline a hierarchical treatment regime based on patient outcomes (WHO Consolidated Guidelines on Tuberculosis, 2022; Rich et al., 2023). WHO statistics indicate that the incidence of multidrug-resistant and rifampicin-resistant TB cases varies significantly between countries and regions. New cases range from less than 4% in Africa, the Americas, the Western Pacific, and South-East Asia to over 26% in Europe (World Health Organisation, 2022). Recurring cases are predominantly found in the Eastern Mediterranean and Europe, with rates ranging from 7.9% to 57%, respectively. The highest incidence rates are observed in the Russian Federation, Eastern Europe, and Central Asia (Figure 3).

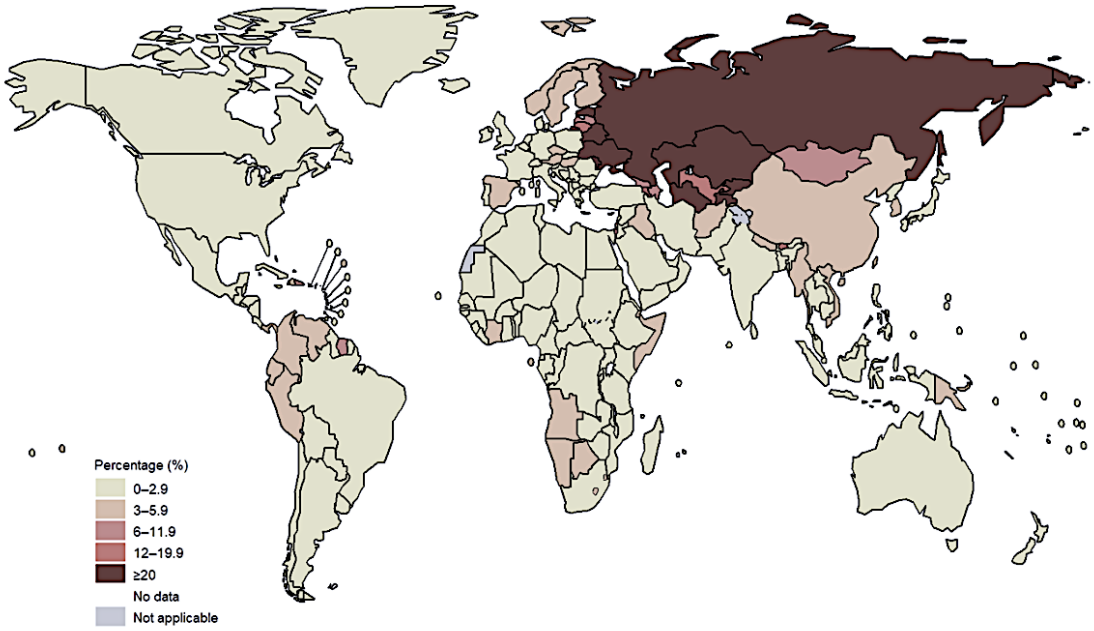


Figure 3: The WHO global map of the incidence of multidrug/rifampicin resistant TB for newly infected cases in 2022. Figure adapted from; WHO Global TB Report., 2023.

1.4.3 HIV-associated *M. tuberculosis* infection

People with HIV are approximately 30% more susceptible to developing a co-infection with *M. tuberculosis*, which significantly contributes to AIDS-related mortality rates (Salomon et al., 2022). WHO statistics estimated that in 2022, there were 710,000 individuals co-infected with HIV and TB, accounting for around 7% of all TB cases and resulting in 187,000 deaths (World Health Organisation, 2023). The epidemiological patterns of TB+HIV cases closely mirror those of TB-only cases (Figure 4; Suthar et al., 2012; Gupta et al., 2012; Odone et al., 2014). The highest number of co-infected individuals was recorded in low- to middle-income countries, with over 50% in the southern African region (Figure 4). Combined antiretroviral and anti-tubercular therapy can improve survival rates for co-infected individuals (Mukonzo et al., 2019). However, long-term treatment can complicate the therapeutic process due to drug interactions and synergistic complications, as well as hyperimmune responses (Dooley et al., 2019).

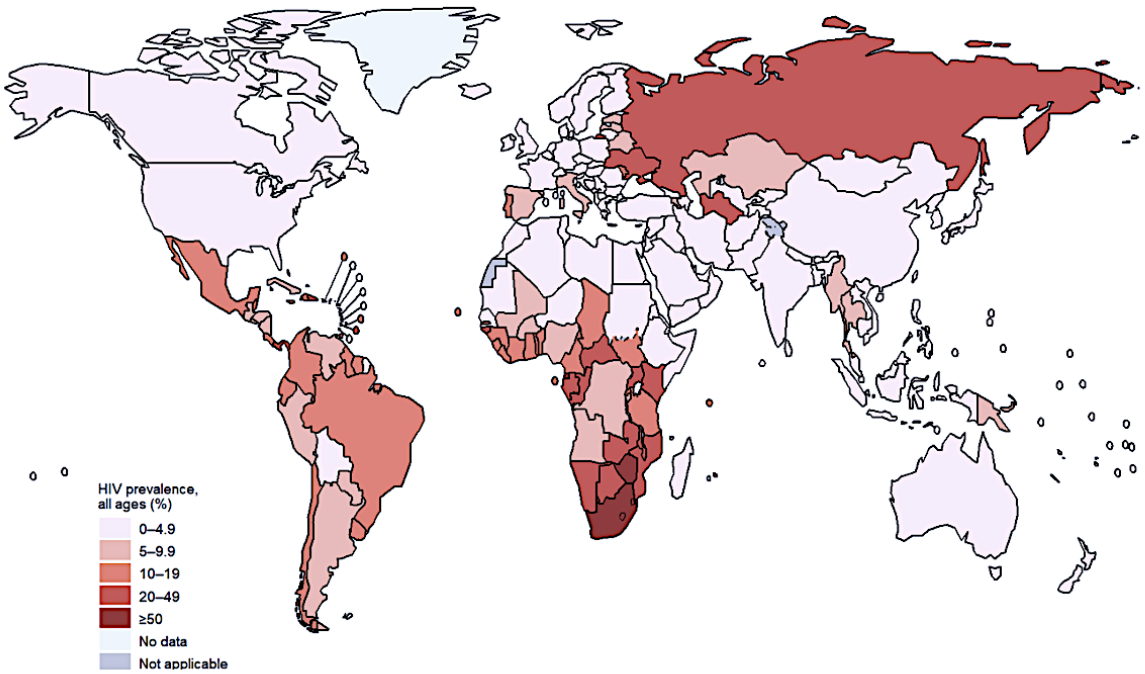


Figure 4: The WHO global map of estimated distribution of cases for co-infection (TB+HIV) from newly infected cases in 2022. Figure adapted from; WHO Global TB Report., 2023.

1.4.4 United Nations (UN) Sustainable Development Goals (SDGs)

In 2014, WHO member nations initiated a global strategy to address preventable but dangerous neglected diseases such as TB, HIV/AIDS, and malaria, with goals set for the period between

2015 and 2030 (United Nations, 2023). This strategy outlined seventeen goals aimed at addressing the root causes of persistent health threats, such as hunger, poverty, inequality to accessible medicine, education, and clean water (United Nations, 2023). In 2018, the United Nations (UN) agreed on a prevention policy specifically targeting unmet needs in TB care, which included implementing TB intervention strategies, investing in diagnostics and treatment centres, and conducting research into therapeutics and vaccines. To achieve these targets, it is estimated that $13 billion (US) is needed annually. The initial goal was to reduce TB mortality rates by 2030, improve access to treatment centres for up to 80% of individuals, and achieve a 90% improvement in the implementation of appropriate TB therapy regimens (World Health Organisation, 2023; United Nations, 2023).

However, the UN Sustainable Development Goals (SDG) report in 2023 indicates that these objectives have been significantly impacted by the COVID-19 pandemic, the climate crisis, the war in Ukraine, and the Israel-HAMAS conflict. These events have shifted the timeline for ending the TB epidemic to 2030. The report highlights that global conditions have become more challenging for the world's poorest populations and emphasises the need to adapt the EndTB goals outlined in the SDG manifesto to meet a revised agenda that aims to improve socio-economic and global health outcomes by 2030 (United Nations, 2023).

1.5 Infection and pathogenesis

The direct transmission of *M. tuberculosis* occurs through the air, with as few as ~5 bacilli, each 1-5 microns in size, needed to successfully enter the host (Loudon & Roberts, 1967; Fennelly & Jones-López, 2015; Tellier et al., 2019). The outcome of infection varies depending on the individual's circumstances. Approximately 25% of the global population is infected with *M. tuberculosis*, meaning they carry the bacterium in a latent, non-contagious state. Among these individuals, an estimated 5-15% are at risk of developing active tuberculosis, the symptomatic and contagious form, within two years of the initial infection. This two-year period represents the highest risk for progression, though active tuberculosis can still develop at a later stage (Behr, Edelstein, & Ramakrishnan, 2018; Gill et al., 2022; Dartois & Rubin, 2022). Individuals at higher risk of developing an active infection include those with immunocompromised conditions such as HIV, diabetes, or long-term complications from long COVID (Udoakang et al., 2023; Nowiński, Wesołowski, & Korzeniewska-Koseła, 2023). It is common for immunocompromised individuals and young children (~10%) to develop a

primary active TB infection (Young, Gideon, & Wilkinson, 2009). Active infection typically results in lung damage due to primary active pulmonary TB, where granulomas form tubercle cysts that consist of macrophages containing bacilli, cell debris, foam cells, and innate effector cells as a measure of infection control (Johansen et al., 2018). Individuals with active TB will experience acute symptoms, including coughing up blood or cloudy sputum, malaise, weight loss, and COPD-like shortness of breath. These individuals may recover from active infection but the bacilli become metabolically inactive. Post-primary or secondary infection may occur if the individual becomes for example immune comprised (World Health Organisation, 2023).

In contrast, 90% of individuals exposed to TB bacilli will not develop an active infection, as the bacilli are contained within granulomas or tubercles (Allen et al., 2015). These individuals will not experience symptoms because the bacilli become metabolically inactive, leading to latent tuberculosis infection, where the bacilli can reside in the lungs for long periods (World Health Organisation, 2023; Klink et al., 2013; Zhang et al., 2018). However, in approximately 10% of individuals with an inactive *M. tuberculosis* infection, reactivation can occur if the individual becomes immunosuppressed due to comorbidities such as HIV, diabetes, or cancer (Shaler et al., 2012; Ai et al., 2016; World Health Organisation, 2023). The precise factors that trigger reactivation and disease progression are currently under investigation (Carranza et al., 2020). Figure 5 outlines potential progression routes that individuals with *M. tuberculosis* infection may experience within their lifetime.

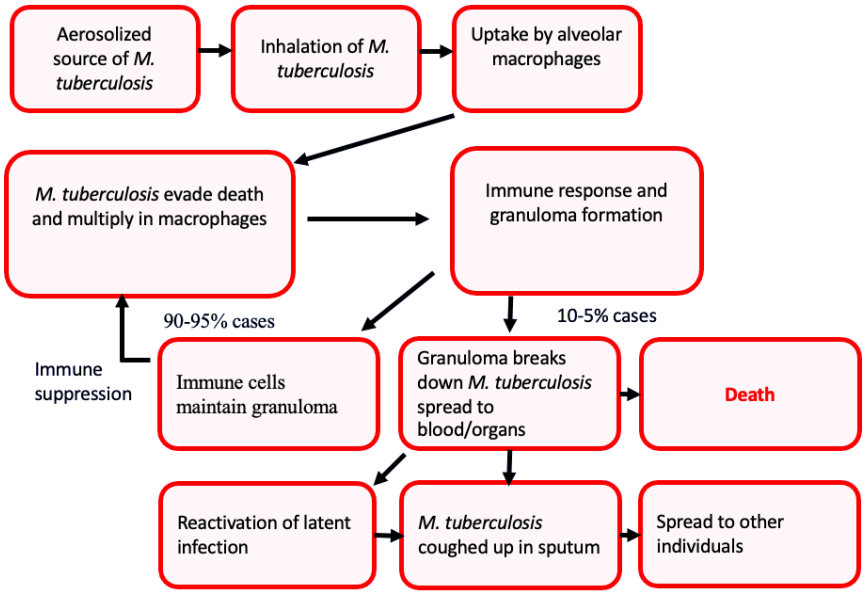


Figure 5: Diagram outlining potential routes for pathogenic outcome for *M. tuberculosis* infection. Flow chart data based on Shaler et al., 2012.

Opinions on the classical disease progression paradigm for tuberculosis (TB) have changed significantly over the last decade, prompting increased research into areas such as the incubation periods of *M. tuberculosis*. Current studies and opinions suggest much shorter incubation periods than previously believed, and that the underlying causes of infection reactivation may be linked to antimicrobial resistance rather than aging or declining immunity (Behr, Edelstein and Ramakrishnan, 2018). These developments underscore the need to reassess symptom-based diagnostic methods to account for a spectrum of disease states between active (infectious) and non-infectious TB. Such an approach could reduce the risk of misdiagnosing individuals with infectious TB (Richards et al., 2023).

1.6 Treatment of *M. tuberculosis*

Most cases of tuberculosis (TB) are curable; however, without treatment, individuals infected with *M. tuberculosis* are 60% more likely to succumb to the disease (World Health Organisation, 2023). For drug-susceptible *M. tuberculosis*, treatment involves combinations of first- and second-line drugs, collectively referred to as Directly Observed Treatment (DOT) (Larkins-Ford et al., 2022). The DOT approach was introduced to help reduce the risk of resistance, enhance adherence to the regimen, and shorten the duration of therapy (Larkins-Ford et al., 2022). By 2005, over 187 countries had implemented DOTs programmes

(Pasipanodya and Gumbo, 2013). However, challenges such as the emergence of multi-drug resistance strains, limited access to a continuous supply of medicines, and the affordability of treatment in some high burden countries have led to adherence failures. These challenges highlight the need for additional treatment strategies, including on-site microbiology testing labs and individualised treatment plans (Bastian et al., 2000).

The global standard for first-line antibiotics includes rifampin, isoniazid, pyrazinamide, and ethambutol, with ethionamide recently added for adolescents (Larkins-Ford et al., 2022; World Health Organisation, 2023). For example, a combination of isoniazid (INH), rifampin (RIF), pyrazinamide (PZA), and ethambutol (EMB) is used for 4-6 months, followed by an additional 4 months of isoniazid and rifampin to treat active TB (Dartois & Rubin, 2022; World Health Organisation, 2023). Table 2 outlines examples of drug-susceptible TB treatment at three different stages of the DOTS program.

Table 2: 1st line antibiotics in the DOTS programme for susceptible strains. EMB; ethambutol, STP; streptomycin.

Case type	Phase 1 (1-2 months)	Phase 2 (1-4 months)	Phase 3 (1 month)
New	INH, RIF, PZA, EMB	INH, RIF	N/A
Relapse	INH, RIF, PZA, EMB, STP	INH, RIF, PZA, EMB	INH, RIF, EMB (1 month)

In 2019, a treatment plan for multidrug-resistant tuberculosis was approved and implemented, incorporating the drugs bedaquiline, pretomanid, and linezolid in combination with drugs outlined in Table 2 (Conradie et al., 2020; World Health Organisation, 2023). This regimen significantly increased the cure rate from less than 50% to over 90% and reduced the treatment duration from 24 months to just 6-9 months (Conradie et al., 2020; Larkins-Ford et al., 2022; Table 3).

Table 3: Reduced antibiotic regime in the DOTS programme for drug resistant strains used in WHO member countries. BDQ; bedaquiline, PA; pretomanid, LZD; linezolid, MDR; multi-drug resistant, RR-TB; rifampicin resistant, XDR-TB; extremely drug resistant.

Case type	Regimen (6 months)	Regimen (9 months)	Regimen (4-9 months)
MDR/RR-TB + fluoroquinolones	BDQ, PA, LZD moxifloxacin[2]	-	-
MDR/RR-TB	-	BDQ, EMB[1], INH[1] levofloxacin/moxifloxacin[2], ethionamide[2] (after 2 months of LZD)	BDQ, EMB[1], INH[1], PZA[1], levofloxacin/moxifloxacin[2]
XDR-TB	N/A	N/A	N/A

[1] In combination with drugs see Table 2, [2] In combination with drugs see Table 4

Second-line antibiotics include kanamycin, streptomycin, capreomycin, amikacin, levofloxacin, and moxifloxacin (CDC MPEP MTBC DST Report, 2018). The specific treatment regimen depends on factors such as the type of infection (active, latent, or mixed sub-populations of culturable and non-culturable bacilli) and whether the isolates are rifampin-susceptible and isoniazid-resistant (Mukamolova et al., 2010; Loraine et al., 2016). Drug-tolerant strains, non-adherence to treatment, misdiagnosis, and malnutrition have impacted eradication efforts and contributed to drug resistance in *M. tuberculosis* (Liebenberg, Gordhan, & Kana, 2022). Table 4 outlines the drug regimen for patients infected with a strain of *M. tuberculosis* that is resistant to at least one drug (NICE, 2024; Mirzayev et al., 2020).

Table 4: Drugs used for TB regimens associated with multi-drug resistant strains. Regimens for multidrug strains are grouped into classes. Group A drug can comprise one or two drugs and with at least one from B group. Drugs from group C are only used if groups A and B cannot be completed (Mirzayev et al., 2020).

Groups	Drugs	Drug target	Mechanism of action
A Drugs used in combination for multi/rifampicin resistant strains with 2 or more in this group	levofloxacin or moxifloxacin	DNA gyrase and topoisomerase II & IV	DNA damage, preventing replication, transcription, and repair
	bedaquiline	ATP synthase	Inhibits ATP synthase
	linezolid	23S ribosomal RNA of the 50S subunit	Inhibits protein synthesis
B Drugs used in combination with Group A	clofazimine	Membrane associated physiological processes including cell respirations and ion transport (ATPase)	Cellular growth
	D-cycloserine/terizidone	L-alanine racemase and D-alanine-D-alanine ligase	Inhibits cytoplasmic PG synthesis
C 1st and 2nd line drugs used for sensitive /multi and rifampicin resistant in combination with others in groups A and C	Ethambutol	Glutamate racemase	Inhibits arabinosyl transferase
	delamanid or pretomanid	Dpr2 subunit of Decaprenylphosphoribose-2'-epimerase	Inhibits methoxy/keto mycolic acids /arabinogalactan
	Pyrazinamide	RpsA, GpsI, PanD	At acidic pH: Inhibits protein translation, nucleic acid metabolism, coenzyme A synthesis
	Amikacin	30S ribosomal subunit	Inhibits protein synthesis
	ethionamide	ethA	Disruption of mycolic acids
	para-aminosalicyclic acid	Dihydrofolate reductase	Inhibits folic acid synthesis
	Imipenem-cilastatin or meropenem	L,D-transpeptidase	Inhibits periplasmic PG synthesis

DOTS regimens are applicable for individuals co-infected with HIV and TB; however, the potential for comorbidities and drug-drug interactions must be carefully considered (De Cock & Re, 1999; Wood et al., 2007). Similar to TB-only DOTS programs, DOTs regimens for co-infected individuals in high-burden countries, such as Ethiopia, have shown limited success, with an unsuccessful TB cure rate 2.6 times higher than that of TB-only DOTs programs (Mekonen et al., 2024). Incorporating DOTs programs into local health policies is

particularly challenging in countries where consistent follow-up on adherence is difficult. The World Health Organisation's (2023) report uses lessons from the SARS-CoV-2 pandemic to refine its strategies for achieving SDG targets. Given the global rise of extensively drug-resistant TB isolates, exploring alternative approaches for improving therapeutic delivery and ensuring equitable access is critical.

1.7 The cell wall of Mycobacteria

The *Mycobacterium* cell wall is a complex structure composed of multiple layers, including long-chain fatty acids, polypeptides, and polysaccharides (Singh et al., 2018; Ghazaei, 2018). While the mycobacterial cell wall shares similarities with that of Gram-positive bacteria, such as a thick peptidoglycan layer, it differs significantly in lipid content; mycobacteria have a lipid content of 60%, compared to 30% in *Bacillus subtilis* (dry mass) (Alderwick et al., 2015; Nickels et al., 2017).

Gram-positive organisms like *Staphylococcus aureus* and *Streptococcus pneumoniae* have a broad peptidoglycan layer, comprising 30-70% of the total cell wall structure, with a thickness of 20-80 nm (Schleifer & Kandler, 1972). In contrast, Gram-negative bacteria have a thinner peptidoglycan layer, only 2-8 nm thick (Leduc et al., 1989; Labischinski et al., 1991; Matias et al., 2003; Gan, Chen & Jensen, 2008).

Despite some similarities to Gram-negative bacteria, such as the presence of an outer membrane, *Mycobacterium* has an atypical outer membrane that contributes to the cell wall's high hydrophobicity and impermeability to antibiotics (Brennan, 2003; Mahapatra et al., 2008; Alderwick et al., 2015; Al-Jourani et al., 2023). The mycobacterial cell wall consists of an outer mycobacterial membrane (MOM) and an inner membrane (MIM), with three intercalating covalently linked layers known as the mycolyl-arabinogalactan-peptidoglycan (mAGP) complex (Maitra et al., 2019; Al-Jourani et al., 2023).

The mAGP complex consists of peptidoglycan, which is common to most bacteria but with some adaptations, covalently attached to arabinogalactan, a polysaccharide layer made up of a D-galactofuranose backbone with branched structures of polymerised D-arabinofuranose chains. The outermost layer, mycolic acids, contributes to the hydrophobicity and impermeability of the cell wall (Abrahams & Besra, 2018; Maitra et al., 2019). Figure 6

provides a basic diagram of the cell wall in *M. tuberculosis*. The next section will discuss the structure and biosynthesis of each layer, with a focus on peptidoglycan.

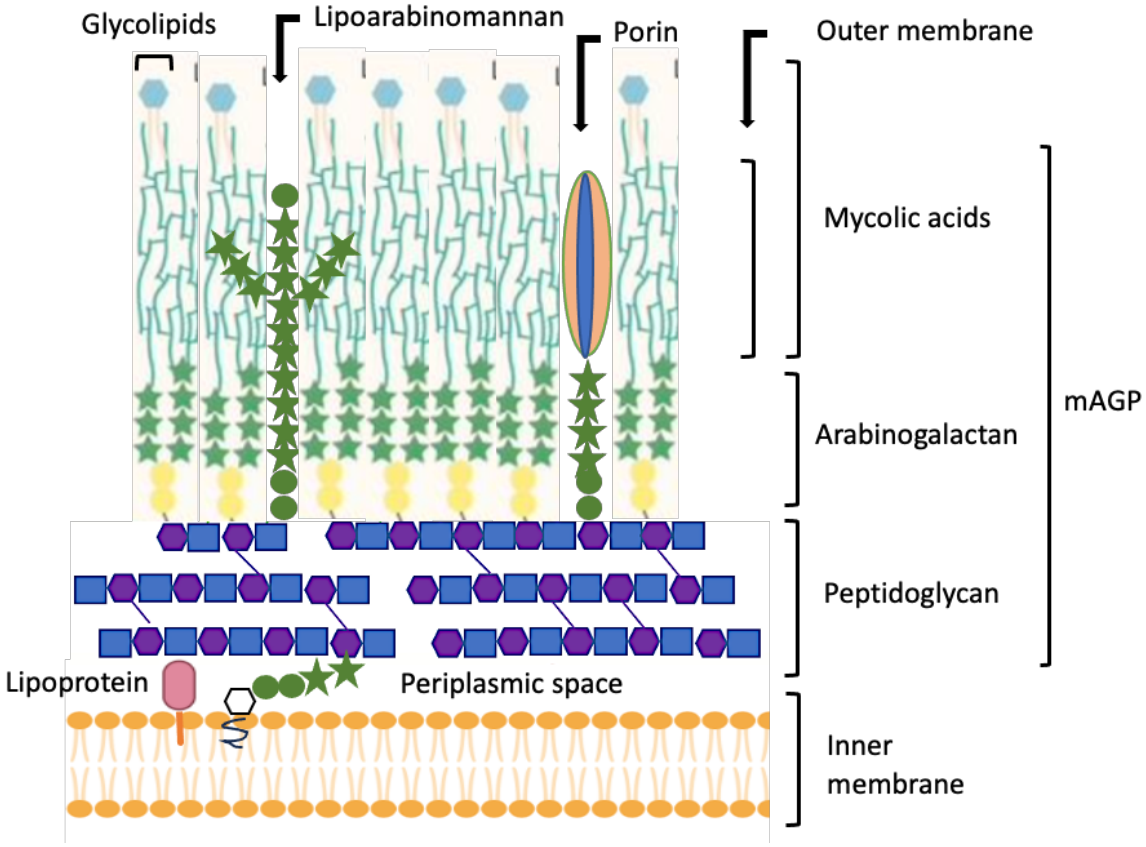


Figure 6: Schematic representation of a cross-section of the cell wall structure in mycobacteria. The inner cell membrane (MIM) is depicted alongside the mycolyl-arabinogalactan-peptidoglycan complex, which consists of the hydrophilic portion of peptidoglycan, arabinogalactan, and the hydrophobic layer of mycolic acids. The figure also shows the intercalating lipoarabinomannan and a single linker unit from Mur*N*ac to L-rhamnose (represented as black sticks) at the base of galactan, as well as the attachment sites to the mycolic acids via the non-reducing end of arabinogalactan (Minnikin et al., 2015; Dmitriev et al., 2000). The outer membrane region (MOM) is where mycolic acids are located within the hydrophobic region, with glycolipids situated above. For simplicity, other lipids such as phospholipids, higher phosphoinositol mannosides (PIMs), and lipomannan have been omitted. Adapted from (Hett and Rubin, 2008; Kieser and Rubin, 2014; Porfírio et al., 2019). Green circles represent mannan; yellow circles, D-galactofuranose; green stars, D-arabinose; and white hexagons, inositol with diacylglycerol.

1.7.1 Mycobacterial outer membrane

The outer membrane of *M. tuberculosis* contains components such as sulfoglycolipids, phthiocerol dimycocerosate (PDIM), trehalose dimycolate (TDM), diacyltrehalose (DAT), polyacyltrehalose (PAT), trehalose monomycolate (TMM), and trehalose dimycolate (TDM), which are intercalated into the mycolic acid layer (Chiaradia et al., 2017; Abrahams & Besra, 2018; Maitra et al., 2019). These components confer pathogenesis and virulence properties to

the mycobacterial cell (Mishra et al., 2011; Chiaradia et al., 2017; Maitra et al., 2019). Additionally, the composition of the outer membrane renders it highly hydrophobic, restricting the permeability of hydrophilic molecules. Nutrients such as glycerol, vitamin B12, and iron as well as drugs are believed to cross this barrier predominantly via porins or transporters (Niederweis et al., 2010b; Chiaradia et al., 2017). *M. tuberculosis* encodes approximately 140 outer membrane proteins which perform a variety of functions, including the transport of extracellular materials to build biofilm and capsule, processes essential for survival within the host (Niederweis et al., 2010b). However, *M. tuberculosis* encodes two non-classical porins: a small, cation selective, heat sensitive porin with a short lived open state, and a 60 KDa porin with a long lived open state (Kartmann, Stengler and Niederweis, 1999). These porins resemble those found in fast growing mycobacteria, despite the functional differences in the proteins across each strain. Research suggests that slow growing mycobacteria, such as *M. tuberculosis*, have adapted to utilise a family of proteins called PE/PPE for nutrient uptake (Kartmann, Stengler and Niederweis, 1999; Melek Özkan et al., 2024).

1.7.2 Mycobacterial inner membrane (MIM)

The cytoplasmic membrane is primarily composed of phospholipids, including phosphatidyl-myo-inositol (PI), phosphatidyl-myo-inositol mannosides (PIMs), phosphatidylethanolamine (PE), and diphosphatidylglycerol (DPG). PI serves as a stabilising anchor for PIMs by acting as a lipid acceptor (Figures 6 & 7). PE and DPG interact through hydrogen bonding, which is critical for inner membrane permeability and packing density (Murzyn, Róg, & Pasenkiewicz-Gierula, 2005). These lipids also act as building blocks for lipoglycans, such as lipomannan (LM), lipoarabinomannan (LAM), and mannose-capped lipoarabinomannan (ManLAM) (Chatterjee et al., 1998; Nigou et al., 2002; Kovacevic et al., 2006; Siegrist & Bertozzi, 2014; Harrison et al., 2016; Carranza & Chavez-Galan, 2019). LM and LAM are non-covalently attached to the cell wall via a PIM anchor (Minnikin et al., 2015; Turner & Torelless, 2018; Franklin et al., 2024). LM, LAM, and ManLAM play integral structural roles in *M. tuberculosis* cell growth. They are processed by LamH, a glycoside hydrolase that cleaves the α1-6 bonds within LM and LAM, producing arabinomannan facilitating its transport to the capsule. This mechanism enables the pathogenicity associated with mycobacteria (Franklin et al., 2024).

Phosphatidyl-myo-inositol (PI) is a critical component of both the inner and outer membranes of *Mycobacterium* species, serving as an anchor for PIMs and as a mannose acceptor during

PIMs synthesis (Boldrin et al., 2014). There is some disagreement in the literature regarding the abundance of diacyl-phosphatidyl-di-mannoside (Ac_2PIM_2) in the mycobacterial plasma membrane. While many studies agree that PI and four types of PIMs constitute 56% of the phospholipid content of the cell wall, with Ac_2PIM_2 being the most abundant at 40%, followed by mono-phosphatidyl-inositol-di-mannosides ($AcPIM_2$), and mono- and diacyl-phosphatidyl-inositol-hexa-mannosides ($AcPIM_6$ and Ac_2PIM_6) (Bansal-Mutalik & Nikaido, 2014; Minnikin et al., 2015). Studies indicate that PIMs such as Ac_2PIM_2 and Ac_2PIM_6 are quantitatively minor with PI with DPG, PE, being the most dominant structural phospholipids within the inner membrane (Haites et al., 2005; Nguyen et al., 2022; Kitsmiller et al., 2024). However, Kitsmiller et al. (2024) highlight a rapid response mechanism in the mycoplasma membrane under membrane-fluidising stress wherein $AcPIM_2$ and $AcPIM_6$ undergo rapid inositol acylation and are converted to their diacyl forms, Ac_2PIM_2 and Ac_2PIM_6 suggesting that PIMs are dynamic and increase in abundance upon stressors. This finding provides a clearer understanding of the mycobacterial plasma membrane composition and its response to environmental stresses, facilitating better modelling of this crucial bacterial structure. Figure 7 presents a basic representation of the PIM biosynthesis pathway.

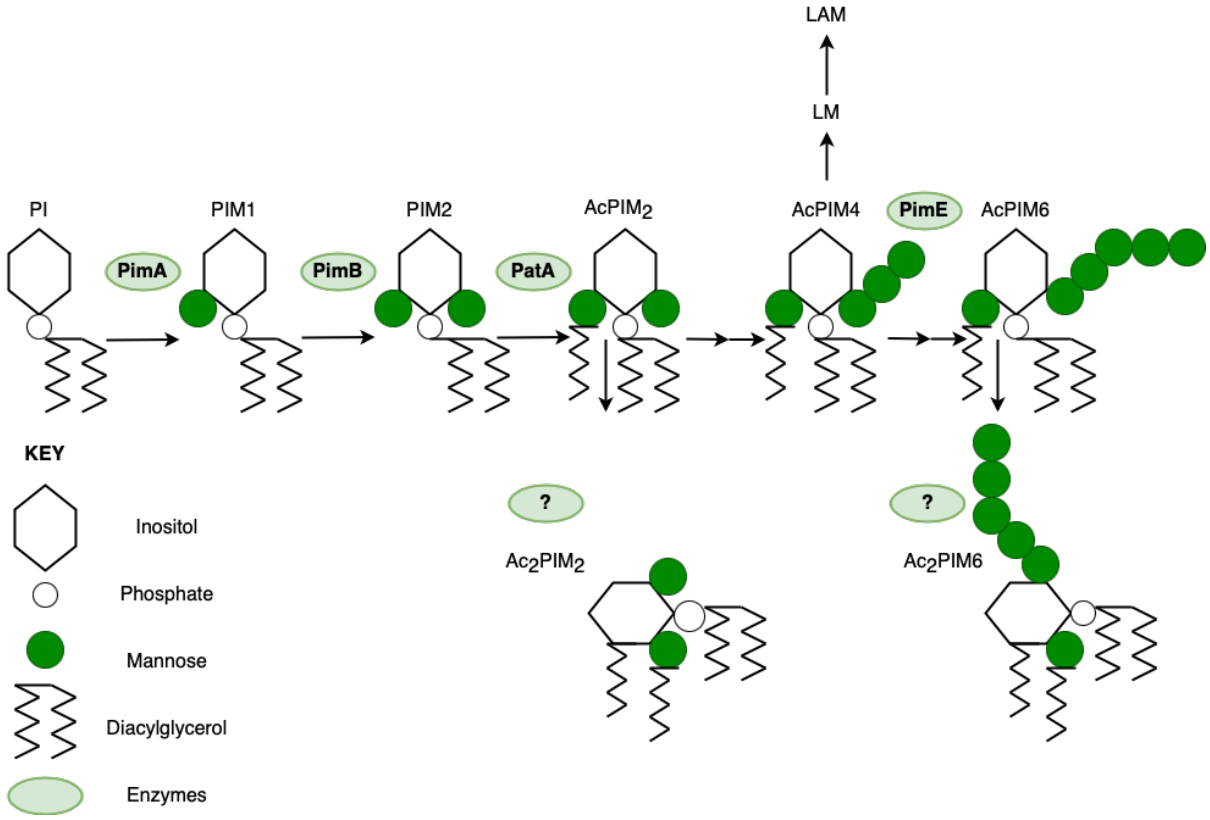


Figure 7: A presentation of the biosynthetic pathway for PIMs and inositol acylation. PIM biosynthesis takes place in the plasma membrane. Each step is mediated via a mannosyltransferase or an acyltransferase. This diagram shows that $AcPIM_2$ and $AcPIM_6$ are the abundant forms of PIMS whereas Ac_2PIM_2 and Ac_2PIM_6 are minor secondary constituents with the potential for other PIM intermediates that may be present at lower levels. The transfer of the fifth mannose by PimE the enzymes that transfer the 3, fourth and fifth are currently unknown. The enzymes with the question marks are unknown acyltransferases responsible for converting monoacyl to diacyl PIMs is also unknown. For clarity LM and LAM biosynthetic enzymes have been omitted. $AcPIM_2$, monoacyl phosphatidylinositol dimannoside; Ac_2PIM_2, diacyl phosphatidylinositol dimannoside; PIM, phosphatidylinositol mannoside; LAM, lipoarabinomannan; LM, lipomannan. Diagram adapted from Nguyen et al., 2022.

PI is composed of a diacylglycerol backbone attached to a myo-inositol sugar ring, which is inserted into the membrane (Bhattacharjee, Ghosh, & Das, 2022). The synthesis of phosphatidylinositol mannosides (PIMs) occurs via the addition of one to six mannose residues to the inositol's carbon positions 2 and 6 by the mannosyltransferases PimA and PimB (Daffé, Crick, & Jackson, 2014). The acyltransferase Acy1T (Rv2611c in *M. tuberculosis*) can acylate PIMs (PIM_1 and PIM_2) at positions C3 or C6 of the mannose ring, creating the basic PIM units Ac_1PIM_4, Ac_2PIM_4, Ac_1PIM_2, Ac_2PIM_2, and $AcPIM_6$ (Tran et al., 2019). From these basic units, more elaborate PIMs can be synthesised, forming LM and LAM (Kaur et al., 2009; Mishra et al., 2011).

Phosphatidyl-myo-inositol phosphate synthase, PgsA1, initiates PI biosynthesis by cleaving CDP from CDP-diacylglycerol and adding diacylglycerol to the main carbon of D-*myo*-inositol-3-phosphate (Grāve, Bennett, & Högbom, 2019). This reaction produces phosphatidyl-myo-inositol-3-phosphate, which is then dephosphorylated by an uncharacterised phosphatase to produce PI. On the cytoplasmic side of the membrane, PimA adds a mannopyranose from GDP-Mannose to the two-position of an inositol moiety of PI to produce PIM_1 (Korduláková et al., 2002; Guerin et al., 2007; Daffé, Crick, & Jackson, 2014). PimB then adds another mannopyranose to the six-position of inositol to form PIM_2, which is acylated by Rv2611c (Guerin et al., 2009; Daffé, Crick, & Jackson, 2014). Further acylation at the three-position on the inositol moiety, carried out by an unknown acyltransferase, converts Ac_1PIM_2 to Ac_2PIM_2 (Enea Sancho-Vaello et al., 2017). PimC and PimD sequentially add mannopyranose residues, producing Ac_1PIM_4/Ac_2PIM_4 (Bhattacharje, Ghosh, & Das, 2022). Ac_1PIM_2 can also be further modified to produce $AcPIM_6$, which may be acylated to produce Ac_2PIM_6 [(Morita et al., 2006). For further mannosylation, Ac_1PIM_4/Ac_2PIM_4 must be flipped across the lipid bilayer by an enzyme or flippase that is yet to be identified. Polyprenyl-phosphate-mannopyranose (PPM) is synthesized by Ppm1, which transfers a mannopyranose from GDP-Mannose to a C50/C35 polyprenyl-phosphate (Gibson et al., 2003). Under different conditions, $AcPIM_2$, Ac_2PIM_2, $AcPIM_6$, and Ac_2PIM_6 accumulate in the cell envelope (Nguyen et al., 2022; Kitsmiller et al., 2024).

Once the PIM units are in the outer membrane, synthesis of higher PIMs, LM, and LAM can commence. The PPM-dependent glycosyltransferase PimE adds two α(1,2) terminal mannopyranoses to Ac_1PIM_4/Ac_2PIM_4, producing mature Ac_1PIM_6/Ac_2PIM_6 [(Morita et al., 2006; Boldrin et al., 2014; Bhattacharje, Ghosh, & Das, 2022). The mannosyltransferases MptA and MptB then add an α(1,6) mannopyranose residue from PPM to Ac_1PIM_4/Ac_2PIM_4 for the synthesis of LM and LAM (Arun Kumar Mishra et al., 2007; Arun Kumar Mishra et al., 2008). Branching occurs via the addition of α(1,2) side chains by MptC [(Mishra et al., 2011; Jankute et al., 2015). LM serves as a precursor for LAM; if no further additions are made, LM is produced. LAM is created by attaching arabinose to the mannose backbone (Jankute et al., 2015). Approximately 55-70 arabinofuranose residues are added to LM by an unknown arabinofuranosyltransferase, producing an arabinan structure similar to arabinogalactan (AG) (Jankute et al., 2015). Approximately 12-16 α(1,5) arabinofuranose residues are polymerised by the arabinosyltransferase EmbC to the priming arabinofuranose (Shi et al., 2006; Alderwick et al., 2011). The AftC and AftD enzymes, responsible for branching arabinogalactan, also

undertake branching in LAM and incorporate branches at α(1,3) followed by α(1,5) polymerisation (Alderwick et al., 2006; Birch et al., 2008). As in arabinogalactan, the arabinose chains in LAM are capped by AftB with a β(1,2) linkage (Seidel et al., 2007). resulting in LAM production. In slow-growing mycobacteria, LAM can be further modified by MptC and CapA with additional α(1,2) mannopyranose residues, producing ManLAM (Dinadayala et al., 2006; Kaur et al., 2008). As a final step, an unknown enzyme terminates the mannose cap by adding an α(1,4) 5-deoxy-5-methyl-thio-xylofuranose (Maeda et al., 2002; Ludwiczak et al., 2002; Turnbull et al., 2004). In *M. smegmatis*, the LAM cap is phosphatidyl-*myo*-inositol instead of mannose (Sparkes et al., 2024). Sparkes et al. (2024) also found that in *M. smegmatis*, LAM and MptA-deficient strains affect cell division and cell shape in a RipA-independent manner. Taken together, PIMs, LM, and LAM contribute to structural integrity and are potential targets for anti-tubercular drugs (Mishra et al., 2011; Källenius et al., 2016; Sparkes et al., 2024; see Figure 6). Figure 8 is a representation of the LAM structure in *M. tuberculosis* and *M. smegmatis*.

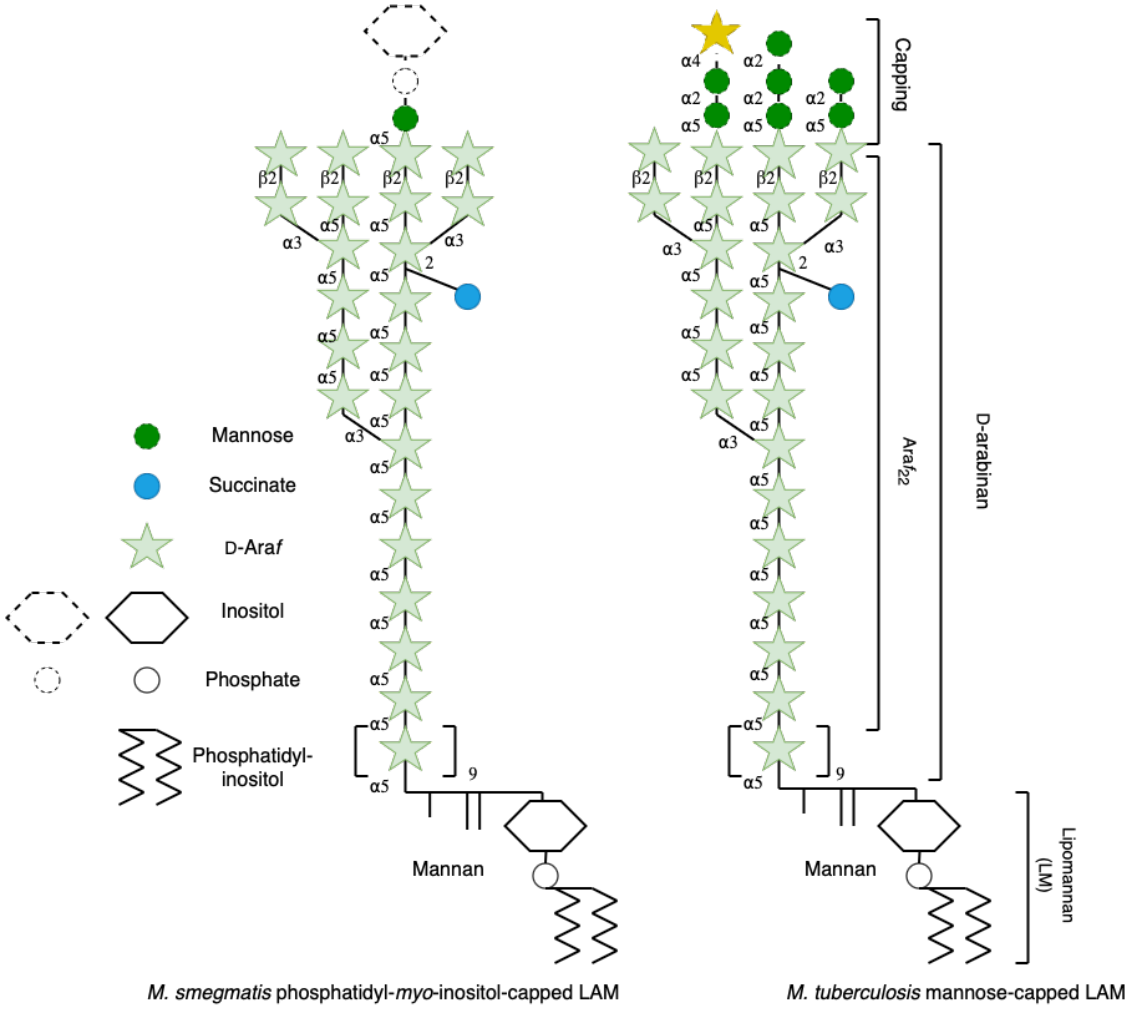


Figure 8: The structure of LAM from *M. smegmatis* and *M. tuberculosis*. The structure predominantly consists of α-links collectively known as D-arabinan, while the terminal of the D-arabinan ends in β-links. In pathogenic mycobacteria such as *M. tuberculosis*, mannose caps the β-linked D-Ara*f* residues. In contrast, some non-pathogenic species, such as *M. smegmatis*, are capped by phosphatidyl-*myo*-inositol. LM, lipomannan domain. Diagram adapted from Shimokawa et al., 2023.

1.7.3 Mycolic acids

Mycolic acids form an outer waxy layer composed of two branched fatty acid chains, providing an additional layer of defence by acting as a barrier to hydrophilic drugs and small molecules (Nataraj et al., 2015; Hett & Rubin, 2008). The meromycolate chains consist of 24-26 α-alkyl carbon atoms and 42-62 β-hydroxy carbon atoms (Sridharan et al., 2007; Hett et al., 2008; Schiebel et al., 2013). Mycolic acids undergo bifurcation, with some covalently linked via ester bonds to arabinogalactan, others are attached to trehalose monomycolate (TMM) or trehalose dimycolate (TDM), and some existing as free lipids (Draper et al., 1997; Bhamidi et al., 2008; Alderwick et al., 2015). TMM and TDM intercalate into mycolic acids, forming the interlinked

mAGP network (Crick et al., 2001; Crick et al., 2008; Hett et al., 2008; Alderwick et al., 2015). The structure of mycolic acids can vary, featuring modifications such as α, α′ epoxy, methoxy, keto, and carboxy groups, depending on the species of mycobacteria (Liu et al., 2023). For example, *M. smegmatis* mc^2155 possesses epoxy but not keto or methoxy modifications, which are present in *M. tuberculosis* and *M. marinum*, both of which contain α, α′, and keto mycolates (Liu et al., 2023). These modifications may play a species-specific role in contributing to antimicrobial resistance, intracellular modulation of the host immune response, cholesterol accumulation, and biofilm formation (Morris et al., 2005; Marrakchi, Lanéelle, & Daffé, 2014; Pawełczyk & Kremer, 2014).

The biosynthesis of mycolic acid precursors is facilitated by the fatty acid biosynthetic cycle, involving two fatty acid synthases: FAS I and the acyl carrier protein-dependent FAS II (Lefebvre et al., 2020). FAS I elongates the C14-CoA fatty acid chain to 26 carbon lengths, generating C24-C26 acyl-CoA, which is essential for the α-branch of mycolic acids (Jamet et al., 2015). FAS II utilises malonyl-AcpM, a unit that extends C16-C18 fatty acids to produce mycolic acids (Kremer et al., 2001). Before entering the FAS II pathways, malonyl-AcpM is produced by the ACP transacylase FabD, which acylates AcpM, an acyl carrier protein (Kremer et al., 2001). Subsequently, a condensation reaction facilitated by β-ketoacyl-ACP FabH produces C16-AcpM from C14-CoA via malonyl-AcpM (Choi et al., 2000). The resulting C16-AcpM is then channelled into the FAS II cycle, where MabA catalyses a keto reduction reaction, creating a hydroxyl group (Marrakchi et al., 2002; Bhatt et al., 2007). The 3-hydroxy-ACP dehydratase enzymes HadAB and HadBC perform a dehydration reaction on the hydroxyl group, resulting in a double bond formation (Sacco et al., 2007; Singh et al., 2022). Finally, the cycle is completed by a reduction reaction catalysed by acyl carrier reductase InhA on the double bond (Xu et al., 2022; Melanny Ika Sulistyowaty et al., 2023). Each iteration of the cycle adds two carbon atoms, with β-ketoacyl-AcpM synthases KasA and KasB catalysing the condensation reaction of the elongated lipid with additional malonyl-AcpM, until 42-62 carbon atoms are produced, completing the FAS II cycle (Schaeffer et al., 2001; Kremer et al., 2002).

Modifications to the meromycolate involve the addition of a cyclopropane ring, resulting in α, α′ keto, methoxy, and epoxy variations that define the types of mycolic acids [(Glickman, Cox, & Jacobs, 2000; Glickman, 2003; Dubnau et al., 2002; Barkman et al., 2010; Liu et al., 2023). C26-α-alkyl-CoA synthesised by polyketide synthase PKS13, produced by FAS I, is added to

AMP-ligated meromycolates by acyl-AMP ligase FabD32 (Trivedi et al., 2004; Gande et al., 2004; Portevin et al., 2004; Khun et al., 2016; Kim et al., 2023). In the final steps of the mycolic biosynthesis pathway, maturation of the meromycolate is achieved via a reduction reaction catalysed by the reductase Rv2509 (Bhatt et al., 2008; Javid et al., 2019). The mature mycolic acid chain is then attached to trehalose to form TMM, which is transferred by the efflux transporter MmpL3 to the periplasmic side of the membrane in collaboration with the chaperone lipoprotein LpqN, which also interacts with the mycoltransferase Ag85 (Xu et al., 2017; Melly et al., 2019). Once TMM reaches the periplasmic space, Ag85 isoforms can either transfer the mycolyl moiety of TMM to arabinogalactan or convert it to TDM (Backus et al., 2014). Figure 9 is a basic representation of the biosynthetic pathway of mycolic acids.

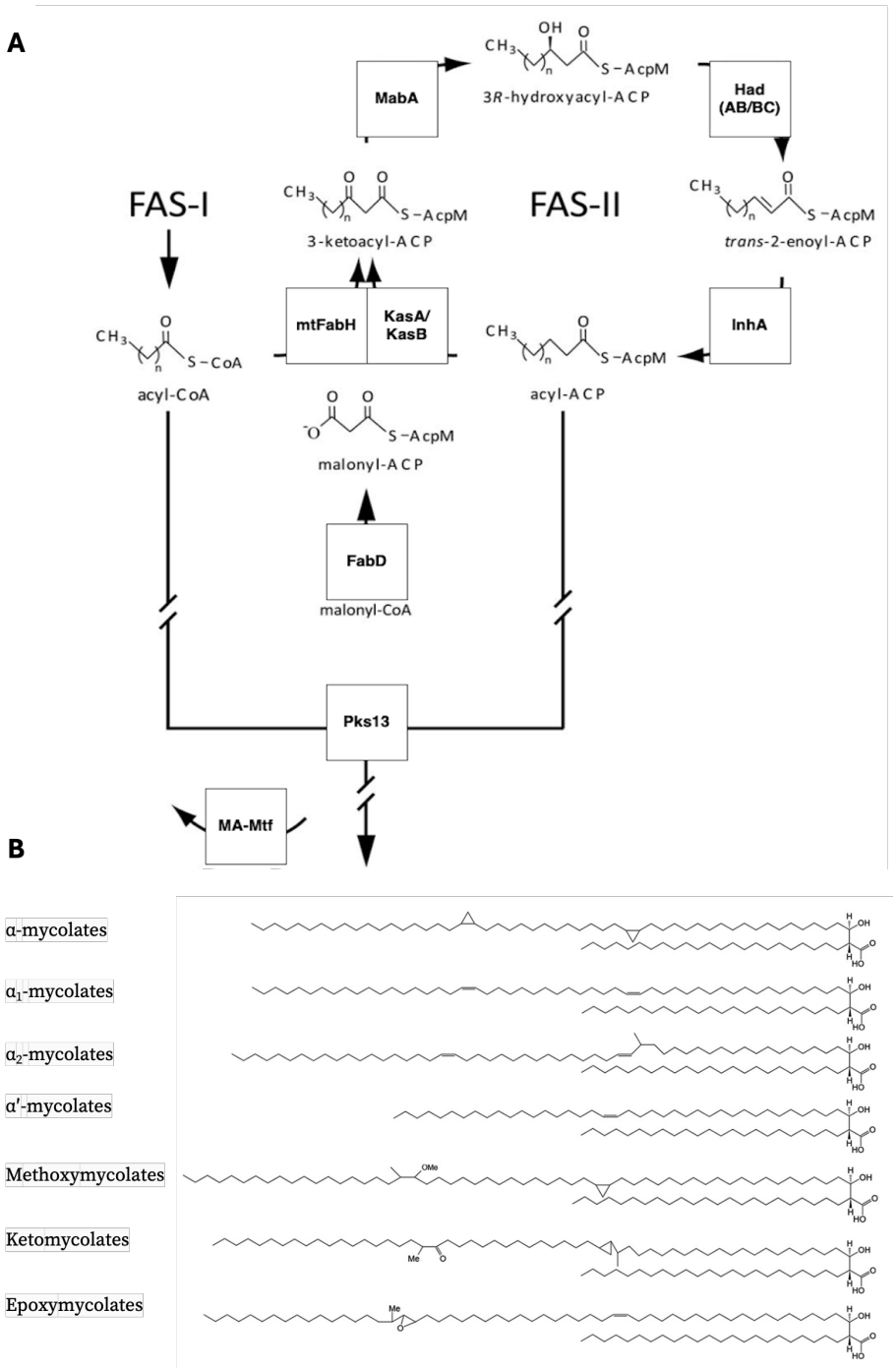


Figure 9: A basic representation of the biosynthetic pathway for the generation of mycolic acids. (**A**) The biochemical reactions necessary to achieve the biosynthesis of mature mycolic acids are symbolized with black arrows. The enzymes responsible for each reaction are named in black square boxes. For clarity the cofactors that are needed for reactions to occur such as NADPH and NADH and some biochemical intermediates reactions have been omitted and are symbolised by interrupted arrows. The different proximal and distal modifications meromycolate chain are via the condensing interacting mycolic acid-Mtfs (MA-Mtfs). Acyl-CoA, acetyl-coenzyme A; FAS-I and II, fatty acid synthase type I and II; HadAB/BC, beta-hydroxyacyl-ACP dehydratase complex; InhA, 2-*trans*-enoyl-acyl carrier protein reductase; KasA/KasB, beta-ketoacyl-acyl carrier protein synthases A/B; MabA, beta-ketoacyl-acyl carrier protein reductase. (**B**) The chemical structure of the mycolic acids that exist in the mycobacterial cell envelope. The nonoxygenated mycolates, α-mycolates; α- (78 to 80 carbons), α1- and α2- (78 and 79 carbons, respectively), and α′- (64 carbons); The oxygenated mycolic acids are the keto, methoxy, and epoxy mycolates. Diagram adapted from Cantaloube et al., 2011; Beatriz et al., 2022.

1.7.4 Arabinogalactan

Arabinogalactan is a polysaccharide composed of branched protrusions from the cell membrane, made up of the two monosaccharides D-arabinofuranose and D-galactofuranose (Lechevalier & Lechevalier, 1970; McNeil et al., 1987; Lowry, 2016; Dulberger, Rubin, & Boutte, 2019). These are the most abundant monosaccharides in the mycobacterial cell wall (Belete, 2022). The primary chain is linear, consisting of 30 alternating β-1,5 and β-1,6 linked D-galactofuranose residues (Besra et al., 1995; Hett & Rubin, 2008; Abrahams & Besra, 2018). There are three points on the galactan chain, located at positions 8, 10, and 12 (see Figure 10), where D-arabinofuranose residues are attached via α-1,3 linkages (Besra et al., 1995; Alderwick et al., 2015). These D-arabinofuranose chains are extended by 13 D-arabinofuranose residues, which are bifurcated at the α-1,3 position on each branch point (Daffe, Brennan, & McNeil, 1990; Alderwick et al., 2015). The D-arabinofuranose can be further branched to produce a tree-like structure, with the termini consisting of a D-arabinofuranose chain linked at branch point positions α-1,3 and α-1,5, which are extended by β-1,2 linked D-arabinofuranose (Daffe, Brennan, & McNeil, 1990). The hexa-arabinofuranose unit structures provide anchor sites for mycolic acids. In *M. tuberculosis*, approximately 66% of the D-arabinofuranose residues are mycolated (McNeil, Daffe, & Brennan, 1991). Modifications to the arabinose residues from the tree-branching structure on the chain can occur with the addition of α(1→2)-D-galactosamine or succinyl residues, depending on the mycolate composition, to provide structural stability (Draper et al., 1997; Lee et al., 2006; Bhamidi et al., 2008; Škovierová et al., 2010; Peng et al., 2012). Figure 10 shows a basic representation of the biochemical structure of arabinogalactan in *M. tuberculosis*.

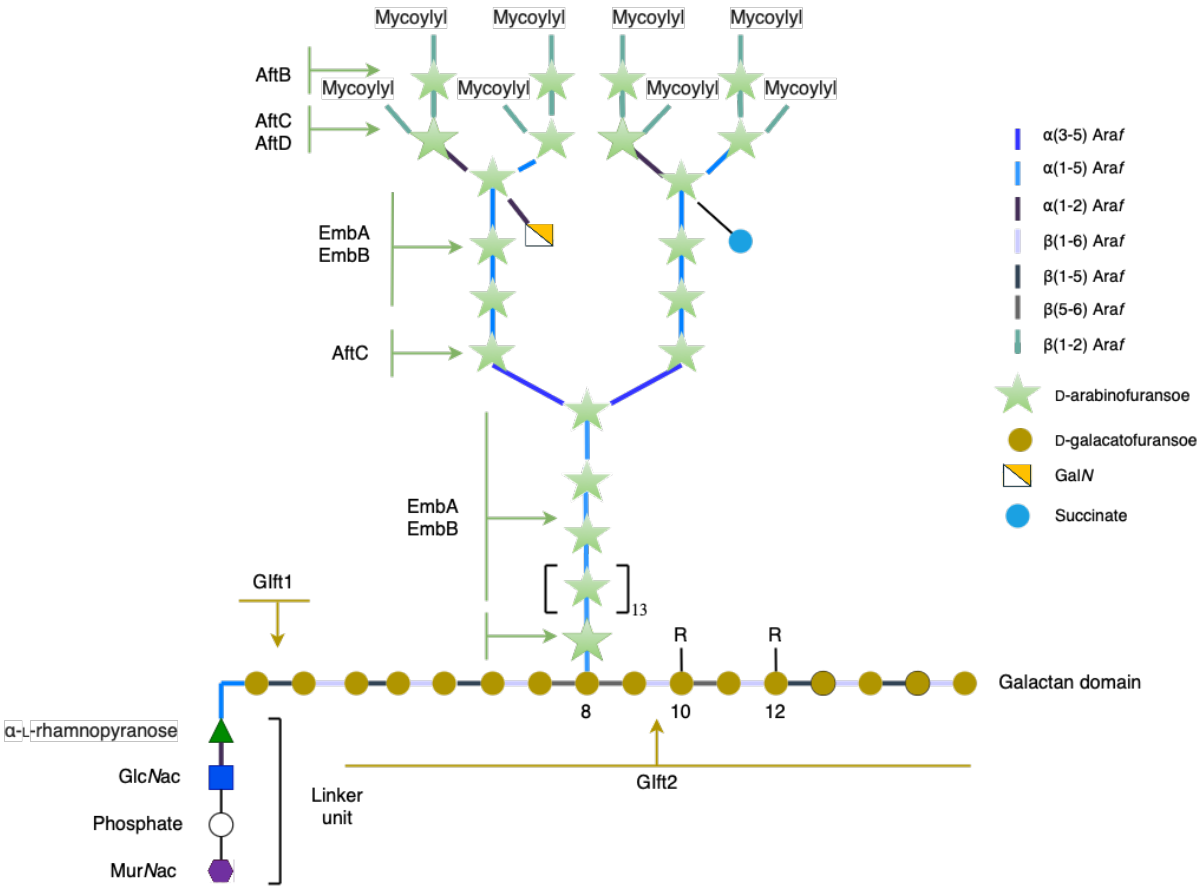


Figure 10: Representation of arabinogalactan structure in *M. tuberculosis*. Schematic shows an arabinogalactan structure with mycolate attachment sites at the non-reducing terminal ends of the arabinofuranose chain. Each branched tree like structure is called a *hexa*-arabinoside unit. Galactosamine and succinyl residues shown allow for structural stability (Bhamidi et al., 2008). For clarity the hydrolases that have recently been discovered have been omitted. Gal*f*; D-galactofuranosyl, Ara*f*; D-arabinofuranosyl. Gal*N*; D-galactosamine. Diagram is adapted from Jankute & Cox., 2015.

Arabinogalactan is synthesised starting from decaprenyl precursors (D-P) in the cytoplasm and polymerised in the periplasm, following the pathway depicted in Figure 11. Briefly, the *N*-acetyl glucosaminyl-1-P transferase WecA (Rv1302 in *M. tuberculosis*) combines N-acetylglucosamine-1-phosphate and C_{50}-phosphate (C_{50}-P) to produce C_{50}-P-P-*N*-acetyl-glucosamine, a precursor to the linker unit between arabinogalactan and peptidoglycan (Alderwick et al., 2015; Jin et al., 2010; Huszár et al., 2017; Batt et al., 2020). The linker unit is completed by the dTDP-4-dehydro-rhamnose reductase RmlD (Rv3266c in *M. tuberculosis*), which utilises the sugar donor UDP-L-rhamnose to add an L-rhamnose sugar moiety to the rhamnosyl-transferase WbbL (Rv3265c) (Ma, Pan, & McNeil, 2002; Mills et al., 2004). WbbL transfers an α-L-rhamnopyranose moiety from dTDP-L-rhamnose to decaprenyl-di-

phosphoryl-α-D-*N*-acetylglucosamine, producing α-L-rhamnopyranose-α-D-Glc*N*Ac-P-P-DP at positions 1,3 (Grzegorzewicz et al., 2008).

Two galactofuranose units are then added at positions β-1,4 and β-1,5, respectively, by the galactosyltransferases GIfT1 (Rv3782c) and GifT2 (Kremer et al., 2001; Mikušová et al., 2006; Rose et al., 2006; Alderwick et al., 2008; Beláňová et al., 2008; Larrouy-Maumus et al., 2012). This forms a lipid-linked linker with a galactofuranose chain attached that must be transferred to the outer membrane. This step is completed by an unknown translocase; however, research studies have implicated Rv3781, Rv3783 in the GIfT-wzm operon, or Rv3789 as potential candidates for this action (Dianišková et al., 2011; Larrouy-Maumus et al., 2012; Savková et al., 2021). Furthermore, Rv3789 is located upstream of the phosphoryl-D-arabinose biosynthetic gene cluster *dprE1* and *dprE2* (Larrouy-Maumus et al., 2012), which donates arabinofuranose to elongate the arabinose chain. The subunit Dpr2 of decaprenyl-phosphoribose-2'-epimerase, a target for delamanid and pretomanid, is involved in the final steps of synthesising phosphoryl-D-arabinose (Mikusová et al., 2005; Abrahams et al., 2023).

Arabinogalactan synthesis continues with the arabinosyl-transferase AftA, which uses decaprenyl-monophosphoryl-arabinose to catalyse the transfer of the arabinofuranosyl moiety to a galactan chain, a process known as priming (Alderwick et al., 2008; Gong et al., 2023). An unknown glycosyltransferase then elongates the arabinofuranose linked at position α-1,5, with bifurcation occurring via AftC and further polymerisation by AftD (Alderwick et al., 2005; Birch et al., 2008; Škovierová et al., 2009). At a branch point on the galactan chain at position α-1,3, AftB caps arabinofuranose at the β-1,2 position to terminate arabinogalactan synthesis (Seidel et al., 2007).

Finally, glycosyltransferases make further modifications: either Rv3779 adds D-galactosamine, or an unknown glycosyltransferase adds a succinyl group (for non-mycolated arabinogalactan) to the arabinogalactan structure (Scherman et al., 2009; Škovierová et al., 2010; Peng et al., 2012; Rana et al., 2012). The mature arabinogalactan is then translocated and ligated to peptidoglycan at the 6-position of approximately 10% Mur*N*Ac residues by the phosphotransferase Lcp1 (McNeil et al., 1987; Barry et al., 2007; Harrison). Figure 11 illustrates the biosynthetic pathway of arabinogalactan in *M. tuberculosis*.

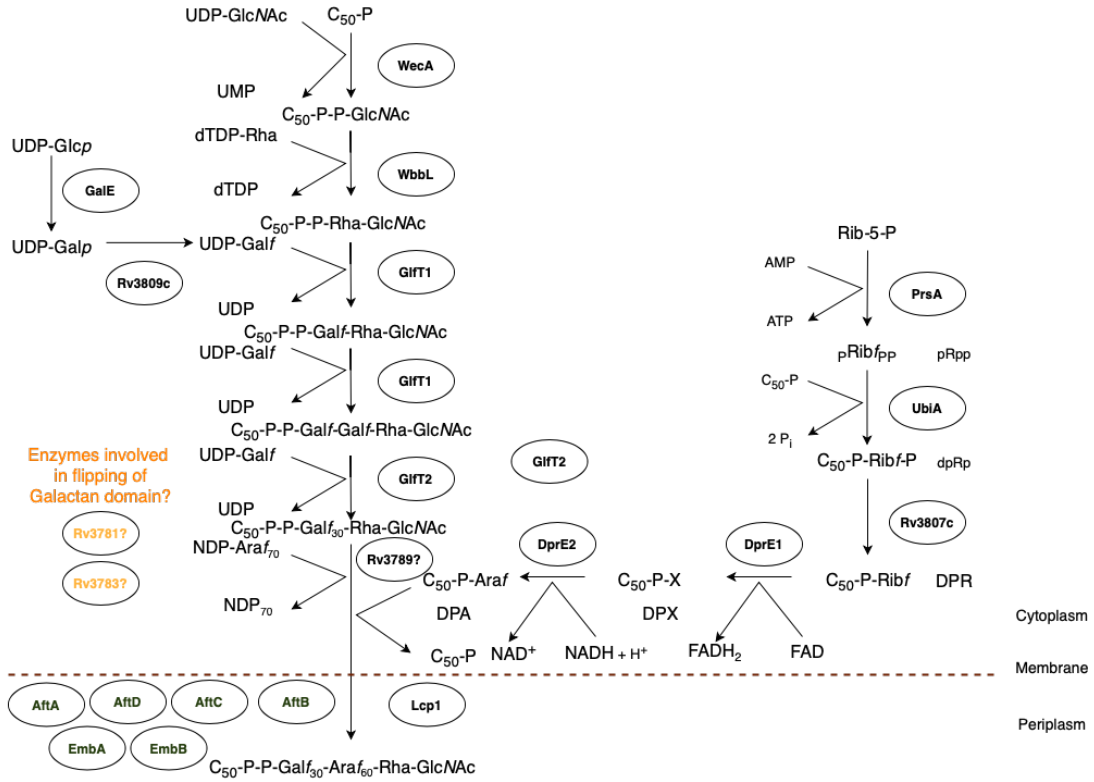


Figure 11: A schematic of the arabinogalactan biosynthesis in *Mycobacteria*. Synthesis occurs in a stepwise action of *N*-acetyl glucosaminyl-1-P transferase, WecA, rhamnosyl-transferase WbbL, and galactosyltransferase GlfT1 followed by polymerisation of 30 galactan residues catalysed by galactosyltransferase GlfT2. Translocation of galactan chain to the periplasm through Wzm-Wzt that make up a transporter complex (Rv3781, Rv3783 & Rv3789) (Dianišková et al., 2011; Gérald Larrouy-Maumus et al., 2012; Savková et al., 2021). Abbreviations: phospho-α-d-ribosyl-1-pyrophosphate (pRpp), decaprenylphosphoryl-D-arabinose (DPA), DPX-decaprenylphosphoryl 2′-keto-β-d-*erythro*-pentofuranose, decaprenol-1-phosphoribose (DPR), D-arabinose in furanose ring form (D-Ara*f*), D-galactose in furanose ring form (D-Gal*f*), l-rhamnose in pyranose ring form (l-Rha*p*). Diagram adapted from Birch et al., 2008; Savková et al., 2021; Rose et al., 2006.

1.7.5 Peptidoglycan

The overall structure of peptidoglycan is conserved in the bacterial kingdom, with some modifications discussed below (Schleifer and Kandler, 1973; Brennan et al., 1995). Peptidoglycan plays a critical role in maintaining cell shape and size, withstanding osmotic pressure, providing a protective barrier against drug/compound penetration, and serving as a scaffold for proteins (Nguyen et al., 2006; Turner et al., 2014; Meeske *et al*., 2016). In mycobacteria, peptidoglycan supports the entire mAGP complex, playing roles in cell signalling, antimicrobial resistance, and coordination of cell elongation and division (Hett and Rubin 2008; Abraham and Besra, 2018; Squeglia et al. 2018).

The conserved core structure of peptidoglycan consists of long glycan strands composed of a repeating dissacharide of *N*-acetylmuramic acid (Mur*N*Ac) and *N*-acetylglucosamine (Glc*N*Ac), linked at β-1,4 positions. These strands are linked to amino acids via a lactoyl moiety on Mur*N*Ac, forming stem-peptides that vary by species and will be discussed further below (Vollmer and Höltje, 2004; Vermassen et al., 2019). In mycobacteria, these peptide chains contain L-alanine, D-*iso*-glutamine, *meso*-diaminopimelic acid, D-alanine, and the terminal D-alanine, producing the final pentapeptide, L-alanine-D-*iso*-glutamine-*meso*-diaminopimelic-acid-D-alanine-D-alanine (Brennan *et al*., 1995, Kumar *et al*., 2012).

Peptidoglycan biosynthesis occurs in three stages: (1) cytoplasmic, (2) transport across the membrane, and (3) and polymerisation and incorporation of new peptidoglycan (Figures 14 &17). The next section will describe the generic composition of peptidoglycan at each stage in detail, followed by a discussion of mycobacterial-specific adaptions.

1.7.6 Mycobacterial classification

The classification system devised by Schleifer and Kandler (1973) assigned the peptidoglycan in mycobacteria to the A1γ=A31 chemotype, which is the same as found in *E. coli* and *Bacillus* species. This classification is based on the presence of *meso*-diaminopimelic acid (*meso*-DAP) as ε-amino group of 3rd amino acid in the stem peptide, which is linked to the carboxyl group of 4th D-alanine on an adjacent peptide stem (Schleifer and Kandler.,1973).

1.7.7 Modifications of peptidoglycan

1.7.7.1 Amidation

Modifications to D-*iso*-glutamate and *meso*-DAP residues in the stem peptides of peptidoglycan may contribute to resistance against lysozyme digestion. Amidation of these residues via the ε-carboxylic group could reduce the net charge of the peptidoglycan, potentially hindering enzymatic digestion (Konati et al., 1970; Mahapatra et al., 2008). While D-*iso*-glutamate modifications have been implicated in TPase activity, *meso*-DAP modifications are crucial for modulating peptidoglycan hydrolysis in both Gram-positive bacteria, such as *B. subtilis*, and mycobacteria (Ghuysen et al., 1971; Figueiredo et al., 2012; Zapun et al., 2013; Dajkovic et al., 2017).

In mycobacteria, a deviation from the canonical peptidoglycan structure occurs when the stem peptides undergo amidation at position 3 of the ε-carboxy group of *meso*-A2pm, yielding *meso*-DAP, and/or at position 2 of D-glutamate, yielding D-*iso*-glutamine (D-*iso*-Glu) residues (Kumar et al., 2012; Shaku et al., 2023). In *M. smegmatis*, amidation occurs at the pentapeptide lipid II stage of peptidoglycan synthesis in the periplasm, resulting in non-, mono, and di-amidated molecules (Mahapatra et al., 2005).

Amidation of D-glutamate is carried out by the MurT-GatD complex and is essential for both D,D- and D,L-TPase reactions, which are vital for 3,4 and 3,3 cross-links, respectively (Zapun et al., 2013; Shaku et al., 2023). Amidation of *meso*-DAP is facilitated by the glutamate amidotransferase AsnB and is crucial for peptidoglycan cross-linking in *M. tuberculosis* (Ngadjeua et al., 2018). However, the amidotransferase LstA, responsible for *meso*-DAP amidation, is not essential for cross-linking in Corynebacteria. Depletion of LstA led to reduced *meso*-DAP amidation and increased susceptibility to lysozyme (Levefaudes et al., 2015). These modifications regulate stem peptide cross-linking, contribute to resistance against lysozyme, and may play a role in resistance to endopeptidases in mycobacteria (Levefaudes et al., 2015; Ngadjeua et al., 2018; Shaku et al., 2023).

1.7.7.2 *N*-deacteylation

In mycobacteria, *N*-deacetylation occurs, which involves the removal of the C2-acetyl group from Mur*N*Ac or Glc*N*Ac moieties in polymerised peptidoglycan by the deacetylase PgdA (Vollmer & Tomasz, 2000). Until recently, Rv1096, a homologue of PgdA, was identified in *M. tuberculosis* as having deacetylase activity (Lu et al., 2020). This modification ablates lysozyme activity because the interaction between the acetyl group and the lysozyme active site is disrupted, leading to a predominance of un-deacetylated glycan strands and decreased recognition of peptidoglycan via nucleotide-binding oligomerisation domain-containing protein (NOD) receptors (Boneca et al., 2007; Callewaert & Michiels, 2010).

1.7.7.3 *N*-glycolylation

Peptidoglycan in some mycobacteria undergoes several modifications. For example, in most mycobacteria, with *Mycobacterium leprae* being a notable exception, some Mur*N*Ac residues can be modified by *N*-acetylmuramic hydroxylase (NamH) to become *N*-glycoylmuramic acid

(Mur*N*Glyc) (Mahapatra *et al*., 2007; Lavollay *et al*., 2008; Catalão *et al*., 2019; Birhanu *et al*., 2019). This modification involves the oxidation of Mur*N*Ac from an *N*-acetyl group to a *N*-glycolyl group, resulting in the formation of *N*-glycoylmuramic acid (Mur*N*Glyc) (Raymond et al., 2004; Gateau, Bordet and Michel, 1976). The degree of Mur*N*Glyc modification varies among mycobacterial species and can be influenced by growth conditions and treatment with D-cycloserine (Mahapatra *et al*., 2005; Hett and Rubin 2008; Birhanu *et al*., 2019).

For instance, the Mahapatra et al (2005) study observed a 100% conversion to Mur*N*Gly in isolated nucleotide-linked peptidoglycan precursors when *M. tuberculosis* cultures were treated with D-cycloserine, whereas *M. smegmatis* showed a mixture of both Mur*N*Ac and Mur*N*Glyc. These results highlight differential enzymatic responses to cell wall stressors in mycobacteria. NamH is not essential in *M. tuberculosis in vitro*, and depletion of NamH did not affect the growth or pathogenicity of bacilli in a mouse model (Raymond et al., 2005).

Hydroxylation by NamH of the *N*-acetyl group and to an *N*-glycolyl group by NamH contributes to the immunogenicity of *M. tuberculosis* by inducing NOD2 host immune cell responses (Hansen *et al.* 2013). It is hypothesised that this modification increases the abundance of hydrogen bonds in the linkages, thereby stablishing the cross-linking (Brennan *et al*., 1995; Raymond *et al*., 2005). It may also enhance resistance to exogenous lytic enzymes such as muramidases and β-lactam antibiotics (Raymond *et al*., 2005). Thus, *N*-glycolylation of peptidoglycan in mycobacteria may play a crucial role in the structural stability of the cell wall and in successful host invasion.

1.7.8 Mycobacterial cross linking

There are approximately 70-80% of the peptides in mycobacterial peptidoglycan that are cross-linked, in contrast to *E. coli* and other Gram-negative bacteria, which typically exhibit ~50% cross-linking. This makes mycobacterial peptidoglycan among the most highly cross-linked in bacteria (Matsuhashi et al., 1966; Kumar et al., 2012; Vollmer et al., 2004). In mycobacteria, peptidoglycan is initially cross-linked at positions 3 and 4 (D,D cross-links) between the acceptor peptide at position 3 and the donor peptide at position 4, forming *meso*-DAP-D-Ala residues at the cell poles. As the cell matures, these cross-links transition to 3,3 (D,L cross-links), forming *meso*-DAP-*meso*-DAP connections in the lateral wall (Kumar et al., 2012; Lavollay et al., 2008; Ghuysen et al., 1968; Wietzerbin-Falszpan et al., 1970).

The 3,3 cross-links are also common in spore-forming bacteria and during entry into the stationary phase (Kumar et al., 2012; Lavollay et al., 2008). The study by Lavollay et al. (2008) demonstrated that peptidoglycan purified from stationary phase mycobacterial cells contained ~80% 3,3 cross-linked residues, suggesting that the increase in these cross-links is an adaptation to growth conditions and nutrient scarcity during the stationary phase (Lavollay et al., 2008; Mahapatra et al., 2007).

Overall, adaptation of peptidoglycan structure is essential for survival in nutrient-limited environments. Ongoing research into how peptidoglycan-active enzymes in mycobacteria are affected by these modifications could lead to the identification of potential targets for inhibitors. Figure 12 outlines the chemical composition of peptidoglycan in mycobacteria.

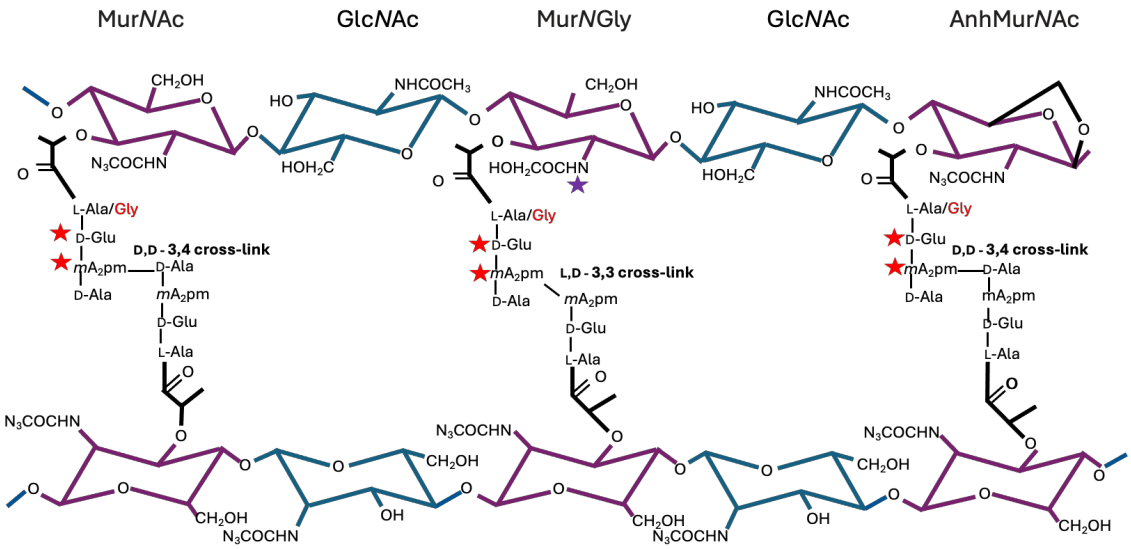


Figure 12: Schematic of the basic chemical composition of mycobacterium peptidoglycan. The glycan backbone (Glc*N*Ac and Mur*N*Ac) is depicted with the modifications Mur*N*Gly (blue, purple). Outlined are the 3→3 and 3→4 cross-links of the stem-peptides carried out by the D,D- and L,D-TPases. Stars highlight the representation of peptidoglycan modifications. Purple star; *N*-glycolylation and red star; amidation points in the stem peptide. Also shown is 1,6-AnhMur*N*Ac a termination of the glycan chain polymerisation in the upper right. Also highlighted is the Gly substitution in place of L-alanine on the stem peptide. Adapted from (Maitra et al., 2019).

1.7.9 Peptidoglycan cytoplasmic biosynthesis

Peptidoglycan biosynthesis begins in the cytoplasm, utilising the glucosamine biosynthesis pathway and carbohydrate metabolism (Craggs et al., 2018). This section will describe the enzymes involved in this initial stage of peptidoglycan biosynthesis (Figure 13). The first

enzyme in the cytoplasmic pathway for synthesising disaccharide-pentapeptides, which are later used as peptidoglycan building blocks, is *N*-acetyl-glucosamine-1-phosphate acetyltransferase uridylyl-transferase (GlmU). In *M. tuberculosis*, GlmU is encoded by the gene Rv1018c. GlmU functions through its two domains to produce the first precursor in the peptidoglycan synthesis pathway, uridine-diphosphate-*N*-acetyl-glucosamine (UDP-Glc*N*Ac) (Craggs et al., 2018). The acetyltransferase domain of GlmU is responsible for producing *N*-acetylglucosamine-1-phosphate by transferring an acetyl group from acetyl-coenzyme A (Zhang et al., 2009). The uridyl-transferase domain then catalyses the uridylation of *N*-acetylglucosamine-1-phosphate into UDP-Glc*N*Ac (Zhang et al., 2009).

Following this, the Mur enzymes convert UDP-Glc*N*Ac into UDP-Mur*N*Ac, also known as Park's nucleotide. The MurA-F enzymes sequentially incorporate the amino acids L-Ala, D-*iso*-Glu, *meso*-DAP, and D-alanyl-D-alanine, with the latter being added by the ligase Ddl, as described below (Babajan et al., 2011; Munshi et al., 2013). The conversion of UDP-Glc*N*Ac into UDP-Mur*N*Ac occurs via a two-step process involving the enzymes UDP-Glc*N*Ac enol-pyruvyl transferase (MurA; Rv1315) and UDP-*N*-acetyl-enol-pyruvyl-glucosamine reductase (MurB; Rv0482) (Babajan et al., 2011). MurA transfers an enol-pyruvate group from phosphoenolpyruvate (PEP) to Glc*N*Ac at the carbon 3 position, producing UDP-Glc*N*Ac-enol-pyruvate (Babajan et al., 2011; De Smet et al., 1999). MurB then reduces enol-pyruvate to the D-lactoyl group with the help of the co-factors NADPH and FAD, ultimately producing UDP-Mur*N*Ac (Eniyan et al., 2018). Additionally, some UDP-Mur*N*Ac is modified to UDP-Mur*N*Glyc at this stage of peptidoglycan synthesis by the hydroxylase NamH (Birhanu et al., 2019; Raymond et al., 2005).

1.7.10 Formation of lipid linked muropeptides

The latter part of the cytoplasmic peptidoglycan biosynthesis pathway is dedicated to the selection of amino acids that will be appended to UDP-Mur*N*Glyc and UDP-Mur*N*Ac, creating the disaccharide-pentapeptides that form Park's nucleotide (discussed below). The amino acids L-alanine, D-iso-glutamine, and *meso*-Dap are sequentially added to UDP-Mur*N*Glyc and UDP-Mur*N*Ac by the ligases MurC, MurD, and MurE (encoded by *Rv2152c*, *Rv2155c*, and *Rv2158c*, respectively) via ATP. This process ensures the correct amino acid is attached to the peptide chain, extending the stem up to the third amino acid (Kurosu et al., 2007; Munshi et al., 2013) (Figure 13). Finally, the D-alanine-D-alanine dipeptide is synthesised by an alanine

racemase, Alr, and the Ddl ligase, which is specific for D-alanine. This dipeptide is then added to the peptide subunit by MurF (*Rv2157c*), forming the complete muramyl-pentapeptide, Park's nucleotide (Munshi et al., 2013). The nucleotide is then anchored to the inner membrane by phospho-*N*-acetyl-muramoyl-pentapeptide transferase (MurX, *Rv2156c*), producing decaprenyl diphospho-Mur*N*Ac-pentapeptide (lipid I) via coupling to decaprenyl-phosphate (C_{50}-phosphate) (Bruning et al., 2011; Chen et al., 2016). Lipid I is subsequently converted to lipid II by the glycosyltransferase MurG (*Rv2153c*), which transfers UDP-Glc*N*Ac onto the Mur*N*Ac or Mur*N*Glyc residue, forming a glycosidic bond at the β(C1→C4) position. This ultimately produces decaprenyl pyrophosphoryl-Mur*N*Ac-Glc*N*Ac-pentapeptide (lipid II) (Mengin-Lecreulx et al., 1991; Mahapatra et al., 2005; Bouhss et al., 2008).

The MurA-F enzymes are crucial in peptidoglycan biosynthesis and are the products of essential genes in most bacteria. *M. tuberculosis* is no exception, making these enzymes attractive targets for inhibitor design (Sassetti et al., 2003; Griffin et al., 2011; DeJesus et al., 2017). Several studies have shown that the regulation of Mur enzymes is key to bacterial survival against environmental stressors such as antibiotics, competition, or host immunity. For example, a study by Sapkota et al. (2020) using antisense genetic studies found that MurA and MurC enzymes are crucial for endospore formation in *Clostridioides difficile*. In *M. smegmatis*, MurA is upregulated 30-fold by the inactive peptidoglycan amidase CwlM, which is phosphorylated by the serine/threonine protein kinase PknB (Boutte et al., 2016). The study by Boutte et al. (2016) also found that under nutrient-deficient conditions, CwlM is dephosphorylated, resulting in antibiotic tolerance. Additionally, CwlM is vital for polar growth in *M. smegmatis*. Furthermore, the PknA and PknB serine/threonine protein kinases regulate the attachment of the pentapeptide to UDP-Mur*N*Ac by phosphorylating the Mur ligases in response to host-induced stimulatory factors, a process that is essential for cell growth (Munshi et al., 2013; Turapov et al., 2018; Zeng et al., 2020). A diagrammatic outline of the mycobacterial peptidoglycan biosynthesis pathway within the cytoplasm and the inhibitors used against the Mur, GlmU, and Ddl enzymes is depicted in Figure 13.

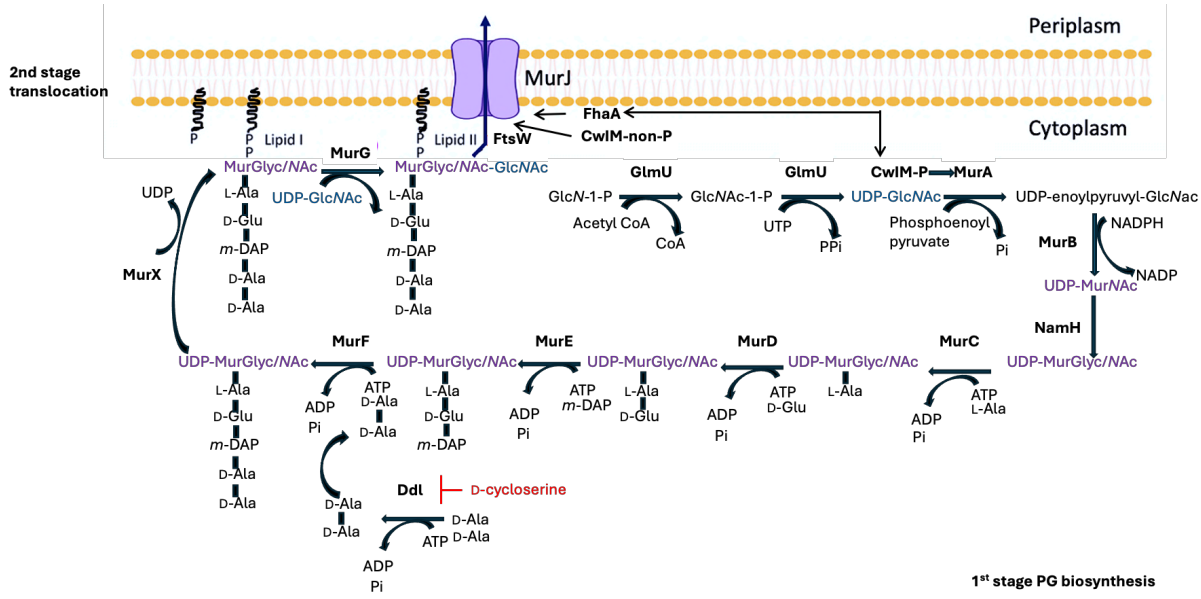


Figure 13: Diagrammatic representation of the cytosolic phase of peptidoglycan synthesis in the cell wall of mycobacteria. The 1st stage of PG biosynthesis begins with the Mur enzymes, Mur A & B convert UDP-Glc*N*Ac to UDP-Mur*N*Ac and UDP-Mur*N*Glyc. Then the synthetases Mur C-F specific for an amino-acid residue is attached to the growing pentapeptide L-Ala (orange), D-*iso*-Glu (yellow), *meso*-Dap (green) and the dipeptide subunit, D-Ala- D-Ala (light blue). Once the L-Ala-UDP-Mur*N*Ac-D-*iso*-Glu-*meso*-Dap-D-Ala-D-Ala (lipid I) is complete it is then anchored to the inner membrane and UDP-Glc*N*Ac is then added via MurG forming lipid II. This disaccharide-pentapeptide subunit is now ready to be transported out into the periplasm via the MurJ/FtsW complex (2nd stage translocation). Also shown is CwIM role in regulation of MurA and the inhibitor for Ddl enzyme and the D-Ala-D-Ala ligation. Abbreviations: L-Ala; L-Alanine, D-*iso*-Glu; D-*iso*-glutamine, D-*meso*-2,6, diaminopimelic acid, D-Ala; D-Alanine UDP: Uridine diphosphate, ATP; Adenosine triphosphate, ADP; Adenosine diphosphate. Figure created using (BioRender., 2022). Adapted from (Batt., 2020).

1.7.11 Translocation of lipid linked muropeptide across the plasma membrane

Before the disaccharide-pentapeptide subunit (lipid II) can be incorporated into the existing peptidoglycan structure, it must be translocated across the plasma membrane into the periplasm (Figure 14). Recent studies have identified two proteins, MurJ (*Rv3910*) and FtsW (*Rv2154c*), that play a role in the "flipping" of lipid II across the membrane. However, the mechanism of lipid II translocation in mycobacteria was only uncovered recently (Butler et al., 2013; Ruiz et al., 2015). FtsW is a Shape, Elongation, Division, and Sporulation (SEDS) protein that was first identified by Mohammadi et al. (2011) as capable of translocating a fluorescently tagged lipid II-homologue across the membrane of liposomes and lipid vesicles (Mohammadi et al., 2011). In contrast, studies by Sham et al. (2004, 2014) suggested that FtsW was deficient in transferring lipid II, indicating instead that MurJ is responsible for the translocation mechanism (Sham et al., 2014). The role of MurJ as a "flippase" has been further supported by recent studies using *E. coli* as a model organism. Bolla et al. (2018) and Zheng et al. (2018) demonstrated through native mass spectrometry and high-throughput mutagenesis,

respectively, that MurJ interacts with lipid II (Bolla et al., 2018; Zheng et al., 2018). Additionally, Kuk et al. (2016) used MurJ from *Thermosipho africanus* to identify structural features consistent with a transporter, including a cytoplasmic opening and a gated central cavity leading to the periplasm, further suggesting its role in lipid II translocation (Kuk et al., 2016; Meeske et al., 2016).

Taguchi et al. (2009) proposed that FtsW functions as a peptidoglycan glycosyltransferase, with lipid II as its substrate, delivering it to MurJ. However, they could not rule out the possibility that FtsW also acts as a lipid II transporter (Emami et al., 2017; Meeske et al., 2016; Taguchi et al., 2019). Overall, the currently accepted view, based on the majority of studies, is that MurJ is the primary transporter responsible for lipid II translocation across the membrane. Additionally, it has been shown that in *B. subtilis*, MurJ, along with Amj, plays a crucial role in coordinating peptidoglycan synthesis (Meeske et al., 2016). Together, these findings suggest a working hypothesis of a MurJ/FtsW complex, possibly in conjunction with other SEDS proteins, to facilitate the transfer of lipid II into the periplasm. A diagrammatic representation of this mechanism is shown in Figure 14.

1.7.12 Peptidoglycan periplasmic biosynthesis

There are two known classes of enzymes that use lipid II as a substrate to generate peptidoglycan strands: the division (FtsW-FtsI) and elongation (RodA-PBP2) SEDS complex proteins, as discussed above, and the high molecular weight penicillin-binding proteins (HMW-PBPs) (Sauvage et al., 2008; Keiser et al., 2015; Sassine et al., 2017). Unlike the SEDS proteins, which are monofunctional glycosyltransferases, the HMW-PBPs perform both glycosyltransferase and peptidyltransferase reactions. Once lipid II has been translocated to the periplasm, the final stage of peptidoglycan synthesis involves the incorporation and polymerization of the disaccharide-pentapeptide dimer into the existing multi-layered peptidoglycan structure (Figure 14). This process is carried out by monofunctional and bifunctional synthases that possess transpeptidase and transglycosylase domains, respectively, and are collectively referred to as penicillin-binding proteins (PBPs) (Sauvage et al., 2008; Keiser et al., 2015).

Most PBPs are extracellular, membrane-bound enzymes classified into A, B, or C groups based on their function, domain organisation, and molecular weight (Waxman & Strominger, 1983; Goffin & Ghuysen, 2002). For example, the monofunctional and bifunctional PBPs are

classified as class A and B, respectively, and are considered high molecular weight (HMW) enzymes. In contrast, class C PBPs, such as carboxypeptidases, are low molecular weight (LMW) enzymes (Sauvage et al., 2008; Figure 14, A). The most prominent polymerising PBPs carry out specific multifunctional roles, such as the class A synthases PonA1 (PBP1; *Rv0050*) and PonA2 (PBP2; *Rv3682*) in *M. tuberculosis*, and PonA3 in *M. smegmatis*. PBP1 and PBP2 are products of the *ponA1* and *ponA2* genes, and unlike the class B and C PBPs, they are responsible for attaching a lipid II molecule with a Glc*N*Ac at the OH group at position 4 to another lipid II molecule at position 1 of a Mur*N*Ac, forming a β-1,4 glycosidic bond. Lipid II then loses its decaprenyl phosphate group (Mahapatra et al., 2005). This step is regulated by PknB, which, as discussed above, plays a species-specific role in modulating the Mur enzymes, as well as PBP1 and PBP2 activity, by phosphorylating the lipid-linked anchor, subsequently affecting the rate of cell elongation (Kieser et al., 2015; Kaur et al., 2019). The bifunctional PBPs can be indispensable, whereas the monofunctional class B synthases and class C hydrolases often exhibit redundancy (Suzuki et al., 1978; Denome et al 1999; Meberg et al., 2001; Sauvage et al., 2008). Despite their differences in function and essentiality, these enzymes are important drug targets (Sauvage et al., 2008; Crick et al., 2001; Waxman & Strominger, 1983; Sassine et al., 2017). An overview of the lipid II insertion, polymerisation, and cross-linking pathways carried out by these enzymes is outlined in Figure 14 B.

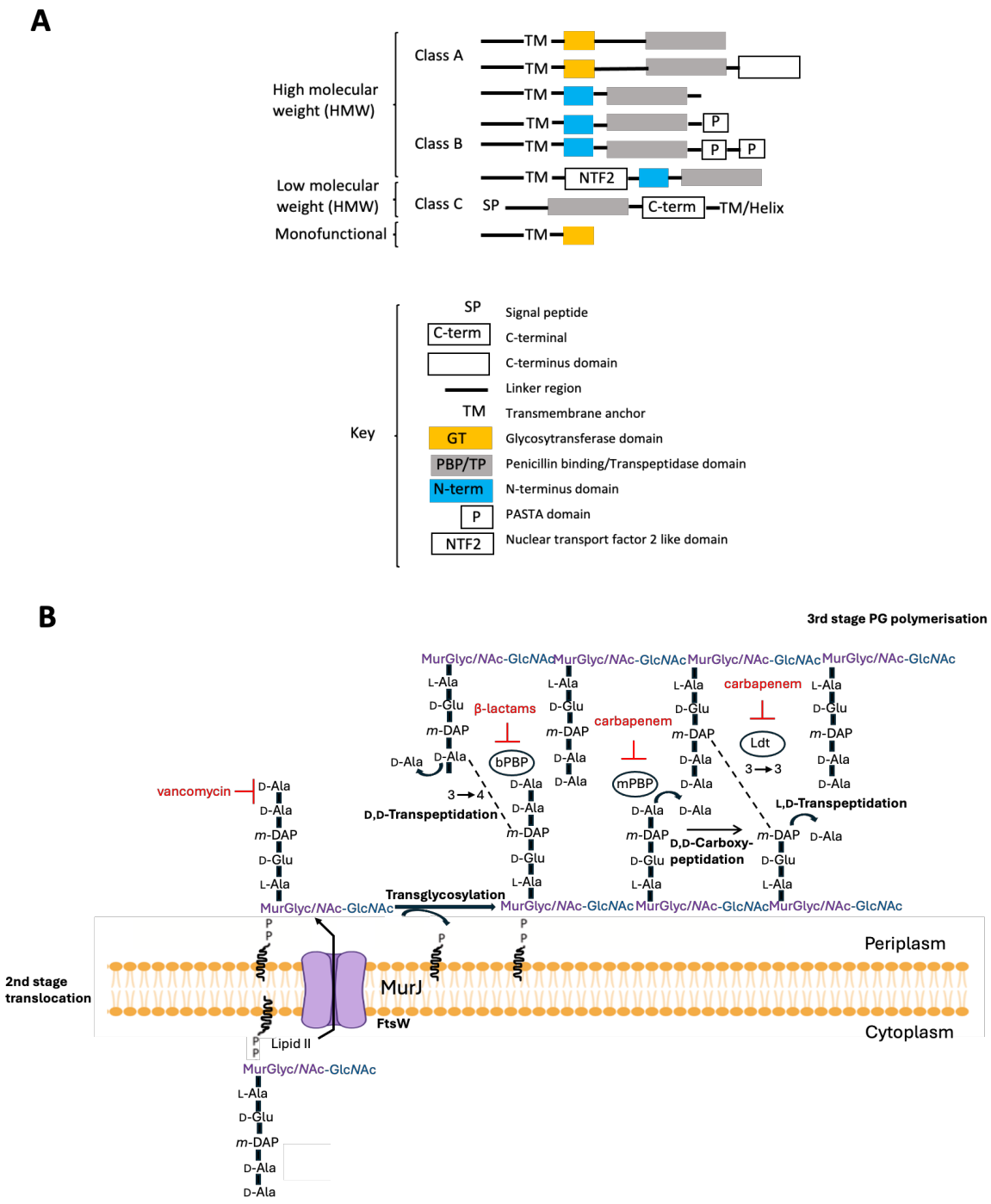


Figure 14: Representative motifs in PBPs for Gram positive and Gram negative bacteria as well as mycobacteria responsible for lipid II integration into the existing peptidoglycan structure. (**A**) Modular domains for each class of PBPs and description of each functional domain, schematic is representative of 10 different domains in 213 eubacteria. Figure adapted from Macheboeuf et al., 2006. (**B**) The third stage begins once Lipid II has been transported into the cytoplasm it is incorporated into the nascent PG by the transglycosylation domain of PBP1 and PBP2 (bPBP), forming and adding to the glycan chains of repeating MurGlyc/MurGlyc-Gly*N*Ac units. The pentapeptide chains are added to the peptidoglycan via transpeptidation by the D,D-peptidases with adjacent peptide stems in a 'zippering' effect. Subsequent L,D reactions occur to reinforce peptidoglycan adding to stability. The recycling of lipid II carrier occurs by its removal and its return to the cytoplasmic space ready to be reused. Also outlined are the inhibitors for lipid II, D,D and L,D peptidases in red colour. mPBP; monofunctional penicillin binding proteins, bPBP; bifunctional penicillin binding proteins. Adapted from (Batt et al., 2020).

1.7.13 D,D-transpeptidases

The 3,4 cross-links made by D,D-transpeptidases (D,D-TPases) are the most abundant in many bacteria. However, in mycobacteria, only about 20% of the peptides form 3,4 cross-links, where the ε-amine (NH_2) group on the D-centre of *meso*-DAP (acyl acceptor stem) binds to the α-carbonyl (COOH) group on D-alanine (acyl donor stem), forming a D,D bond (Wietzerbin et al., 1974). This forms the 3,4 interpeptide stem cross-link, fully incorporating the disaccharide-pentapeptide subunit into the existing peptidoglycan (see Figures 12, 15) (Kumar et al., 2012; Kieser et al., 2015; Sauvage & Terrak, 2016; Sauvage et al., 2008).

For successful transpeptidation, three steps must occur in succession: 1) a rapid, non-covalent complex forms between a penicillin-binding protein (PBP) and the peptidoglycan pentapeptide; 2) an acyl-PBP intermediate is produced between the α-carboxyl group at the C-terminus of the 4th and 5th D-alanine on the donor pentapeptide stem and the active site serine residue in the D,D-TPase domain of the PBP. To form this acyl-PBP intermediate, the PBP active site utilises a deprotonated lysine to abstract a proton, activating the nucleophilic activity of the catalytic serine (Kumarasiri et al., 2014); and 3) deacylation occurs as carboxypeptidation or transpeptidation releases the PBP, and in the case of transpeptidation, a covalent bond is formed with an adjacent acceptor tetra-peptide (Sauvage et al., 2008; Pandey et al., 2018; Kumarasiri et al., 2014; Macheboeuf et al., 2008).

In contrast, D,D-endopeptidases function opposite to D,D-TPases by hydrolysing the cross-links within the peptide stems. Thus, effective communication between different PBPs must be established before new peptidoglycan fragments can be integrated into the nascent peptidoglycan. An outline of the 3,4 cross-link process is presented in Figure 15.

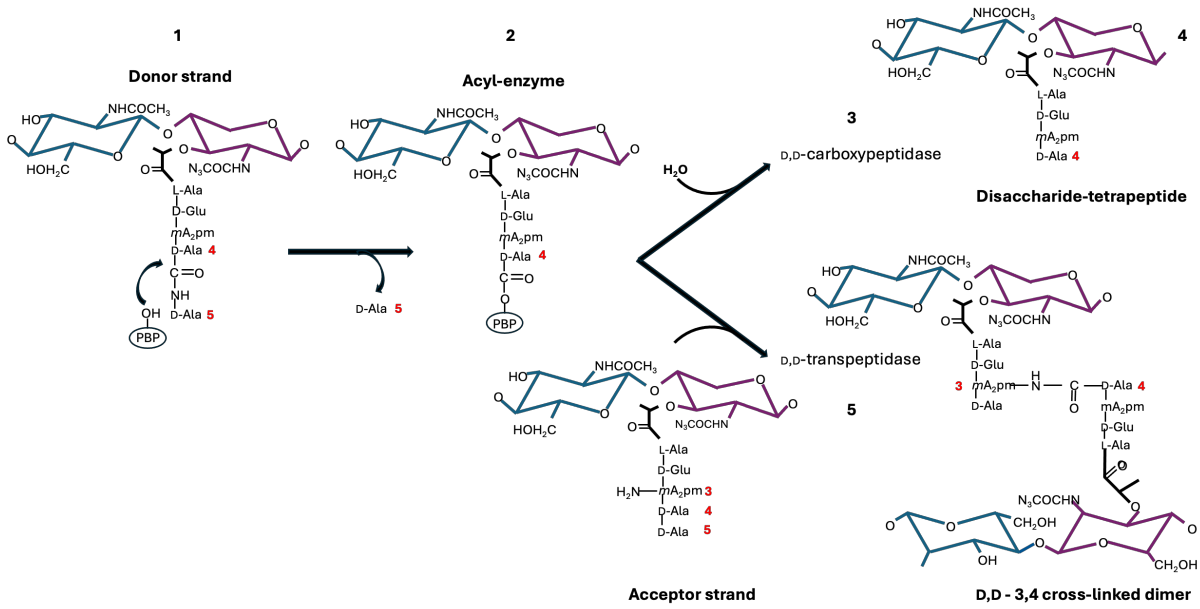


Figure 15: A schematic outlining the transpeptidation reaction resulting in the 3,4 cross-link, bridging two stem peptides and carboxypeptidation. The serine of the PBP attacks the amide bond between D-alanine[4]-D-alanine[5] activates and forms a complex with a donor peptide stem (1). This creates an acyl-PBP intermediate forming an ester bond where the lysine in the active site of TPase or C-TPase removes a proton from the serine (lysine-serine system) initiating an attack on the amine group on the acyl-PBP enabling deacylation to occur (2). These reactions result in the terminal D-alanine[5] on a donor stem-peptide being released in the deacylation step, whereby the PBP is also displaced. Depending on the reaction i.e., carboxypeptidation or transpeptidation, hydrolysis of a water molecule occurs on the donor peptide and forms a disaccharide-tetrapeptide (4), or a covalent bond (cross-link) to an amide group of *m*A2pm on an acceptor stem peptide is made producing the 3,4 cross-linked dimer respectively. Adapted from (Lupoli et al., 2011).

1.7.14 L,D-transpeptidation

In mycobacteria, the predominant cross-linkages occur at positions 3,3 between *meso*-DAP residues on adjacent tetrapeptides carried out by L, D-TPases (Kumar et al., 2012; Lavollay et al., 2008). This L,D cross-linkage has been identified in various species, such as *E. coli* during the stationary phase, where it constitutes 6-15% of cross-links (Goffin & Ghuysen, 2002; Templin et al., 1999; Pisabarro et al., 1985; Glauner et al., 1988), and in *Clostridium perfringens* and *Streptomyces* spp. (Leyh-Bouille et al., 1970). Similar to the 3,4 cross-links, the terminal D-alanine is removed from the stem peptide by a D,D-CPase, creating a substrate for the L,D-TPases LdtA (*Rv0116c*) and LdtB (*Rv2518c*), which are products of the *ldtMt1* and *ldtMt2* genes in *M. tuberculosis* (Correale et al., 2013; Bianchet et al., 2017).

Unlike D,D-TPases, L,D-TPases have a cysteine residue in their active site instead of a serine (Biarrotte-Sorin et al., 2006; Mainardi et al., 2005). Additionally, the substrate for L,D-peptidases is a tetrapeptide rather than a pentapeptide (Figure 16). Acylation begins when the

L,D-TPases interact with the tetrapeptide (donor strand) via the cysteine residue, forming an acyl-enzyme intermediate at the 3rd position, which subsequently removes the other D-alanine (Pandey et al., 2018). Deacylation then occurs when the L,D-TPase is removed by the amine group on the *meso*-DAP at the 3rd position of the acceptor stem peptide (Figure 16). This creates a covalently L,D cross-linked bridge between the COOH group of the L-centre of *meso*-DAP on the donor peptide and the NH_2 group of the adjacent D-centre of *meso*-DAP on the acceptor peptide, allowing the formation of the 3,3 linkage (Wietzerbin et al., 1974; Silva et al., 2014).

The 3,3 linkages help reinforce the cell wall, providing protection against β-lactam antibiotics or during the transition into the stationary phase (Peddireddy et al., 2017; Pidgeon et al., 2019). However, ongoing studies are uncovering differences between 3,3 and 3,4 cross-link compositions in mycobacteria (Rimal et al., 2022; Baranowski et al., 2018). The L,D-TPases are targets for carbapenems such as meropenem. Studies by Kieser et al. (2013) and Pidgeon et al. (2019) demonstrated that the deletion of *ponA1*, *ponA2*, and *ldtB* rendered *M. tuberculosis* susceptible to β-lactams, highlighting their vital role in the periplasmic phase of the peptidoglycan biosynthetic pathway (Kieser et al., 2013; Pidgeon et al., 2019). A diagrammatic representation of the steps for cross-linking carried out by L,D-TPases is outlined in Figure 16.

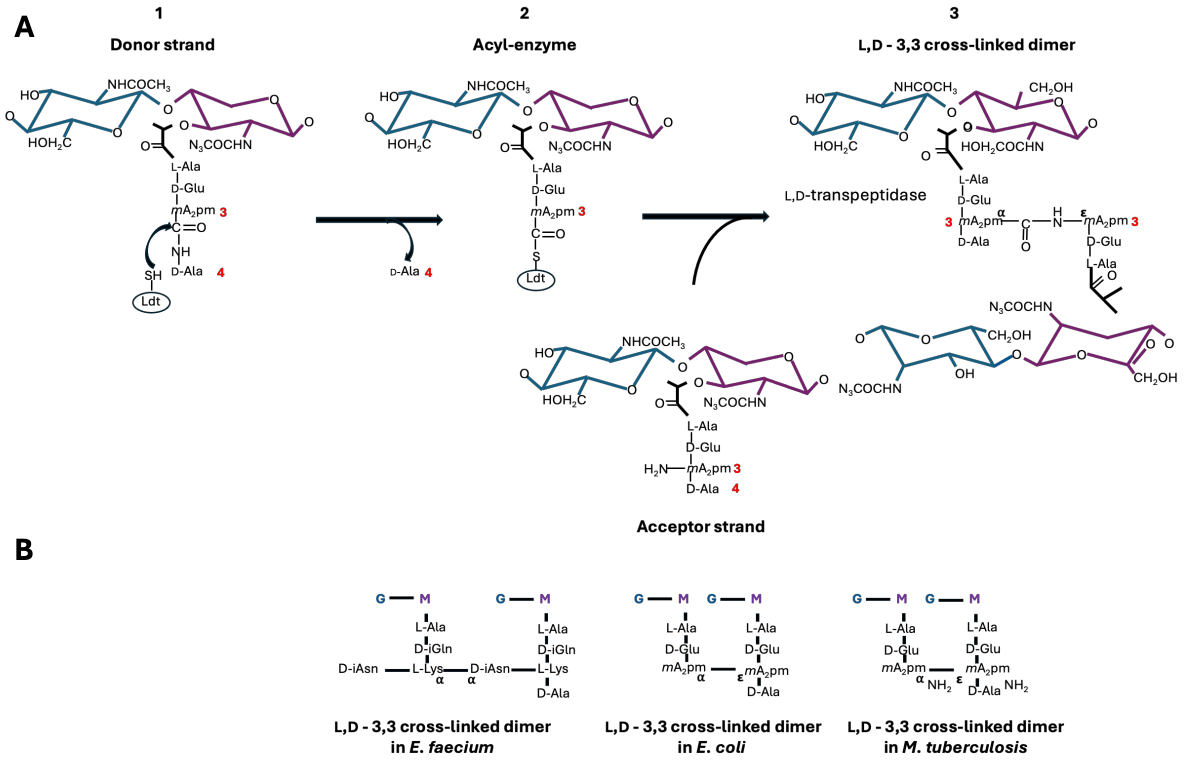


Figure 16: Schematic of the steps depicting the 3,3 cross-linking created by the L,D-transpeptidases. (**A**) Acylation takes place by a L,D peptidase attaching to amide bond between fourth position, D-alanine[4] and the third position, *m*A2pm[3] on the disaccharide-tetrapeptide via the cysteine in the active site L,D-peptidase, and the carboxyl group on the donor disaccharide-tetrapetide (1). This releases D-alanine[4] and forms an enzyme-intermediate complex that contains a thioester bond between cysteine in the active site of L,D peptidase and the now tripeptide (2). Subsequently, deacylation takes place when the L,D-peptidase is released from its substrate (donor peptide) and nucleophilic attack of amine group on the *m*A2pm[3] on the acceptor strand forming a thioester interbridge link and the 3,3 cross-linked dimer (3). (**B**) A representation of variations on the species level of the 3,3 cross-linked dimer formation for three taxa (Lecoq et al., 2013). In *E. faecium* (left), a 3,3 cross-linked dimer is created between the third amino-acids on the stem peptide via α-carboxyl of L-lysine and α-amine of D-*iso*-asparagine in the D–Ala[4]-D–iAsn-l–Lys[3] link to an acceptor strand (Mainardi et al., 2025). In *E. coli* (middle), the 3,3 cross-link occurs between the α-mine of A2pm[3] on a donor tripeptide and ε-amine of A2pm[3] on an acceptor tetra-peptide strand (Höltje, 1998; Magnet et al., 2007; Magnet et al., 2008; Sanders & Pavelka, 2013). In *M. tuberculosis* (right), the 3,3 cross-link dimer occurs via amidated *meso*-DAP (A2pm[3]) on a donor tripeptide and ε-amine of amidated A2pm[3] on an acceptor tetra-peptide strand (Lavollay et al., 2008). G, Glc*N*Ac; M, Mur*N*Ac. (A) is adapted from Alaman-Zarate et al., 2024.

1.7.15 Penicillin binding protein catalytic mechanism

PBPs have a conserved catalytic triad. The first motif, SxxK, contains an activating serine and a lysine, which acts as a general base. The second and third motifs are (S/Y)X(N/C) and (K/H)(S/T)G, respectively (Lovering et al., 2012). The reaction initiates when the peptidase domain binds to the muropeptide substrate. During acylation, the lysine in the SxxK motif interacts with the SxN motif, accepting a proton to facilitate the nucleophilic attack by the serine in the SxxK tetrad. This process forms an acyl-intermediate with the muropeptide and removes the terminal D-alanine (Lovering et al., 2012). To free the enzyme, deacylation occurs,

where the SxN motif, activated by the KTG motif, plays a crucial role. The KTG motif serves as an electrostatic anchor for substrate binding (Zhang et al., 2007; Nicola et al., 2005), forming a hydrogen bond with a water molecule at the carbonyl group of the acyl-enzyme intermediate. This releases the D-alanine in a D,D-CPase, or in the case of a TPase, cross-linking occurs via an attack from an amino group on a neighbouring peptide branch, which hydrolyses the acyl-enzyme intermediate (Nicola et al., 2010). Notably, residues such as asparagine, histidine, and threonine near the KTG motif may regulate enzyme activity and are essential for interacting with β-lactams (Sauvage et al., 2008; Lovering et al., 2012).

1.7.16 Peptidoglycan cleaving enzymes

Enzymes that cleave peptidoglycan are essential in cell wall biosynthesis, peptidoglycan remodelling, septation of daughter cells during cell division, bacterial signalling, and autolysis (Shockman & Höltje, 1994; Lee & Huang, 2013). The hydrolytic activity of these enzymes must be tightly regulated to prevent uncontrolled peptidoglycan degradation, which could lead to cell lysis. This regulation is achieved through multi-enzyme complexes that include peptidoglycan synthases, other hydrolases, or non-catalytic proteins acting as their cognate regulators (Uehara et al., 2009; Banzhaf et al., 2020; Morlot et al., 2010). In *E. coli*, approximately twenty hydrolases exist, with multiple enzymes responsible for each hydrolytic activity. None of these are essential for cell viability; mutants lacking several hydrolases show mild to no morphological changes, indicating compensatory mechanisms within the cell (Morlot et al., 2010). In contrast, the consensus on how the exact number of hydrolyses there are in mycobacteria is not yet currently defined (Kumar et al. 2022). With the emphasis on specific hydrolase function such as the endopeptidase, RipA or the *N*-acetylglucosaminidase LpqI (Hett & Rubin, 2010; Moynihan et al., 2019; Kumar et al., 2022) These enzymes facilitate the insertion of newly synthesised peptidoglycan by cleaving the mesh-like structure to create space for new glycan strands, without increasing susceptibility to antibiotics or inducing cell lysis (Typas et al., 2011; Egan et al., 2015). Peptidoglycan-cleaving enzymes are categorized into five groups based on their cleavage sites: muramidases, *N*-acetylglucosaminidases, *N*-acetylmuramoyl-L-alanine amidases, endopeptidases, and carboxypeptidases (Vollmer et al., 2008). Their activity must be precisely controlled to avoid uncontrolled peptidoglycan cleavage, which can result in cell lysis. This section will describe the activities of each of these peptidoglycan hydrolase enzymes and their associated signalling cascades during cell wall

remodelling. A diagrammatic overview illustrating the roles these enzymes play in maintaining cell wall homeostasis is presented in Figure 17.

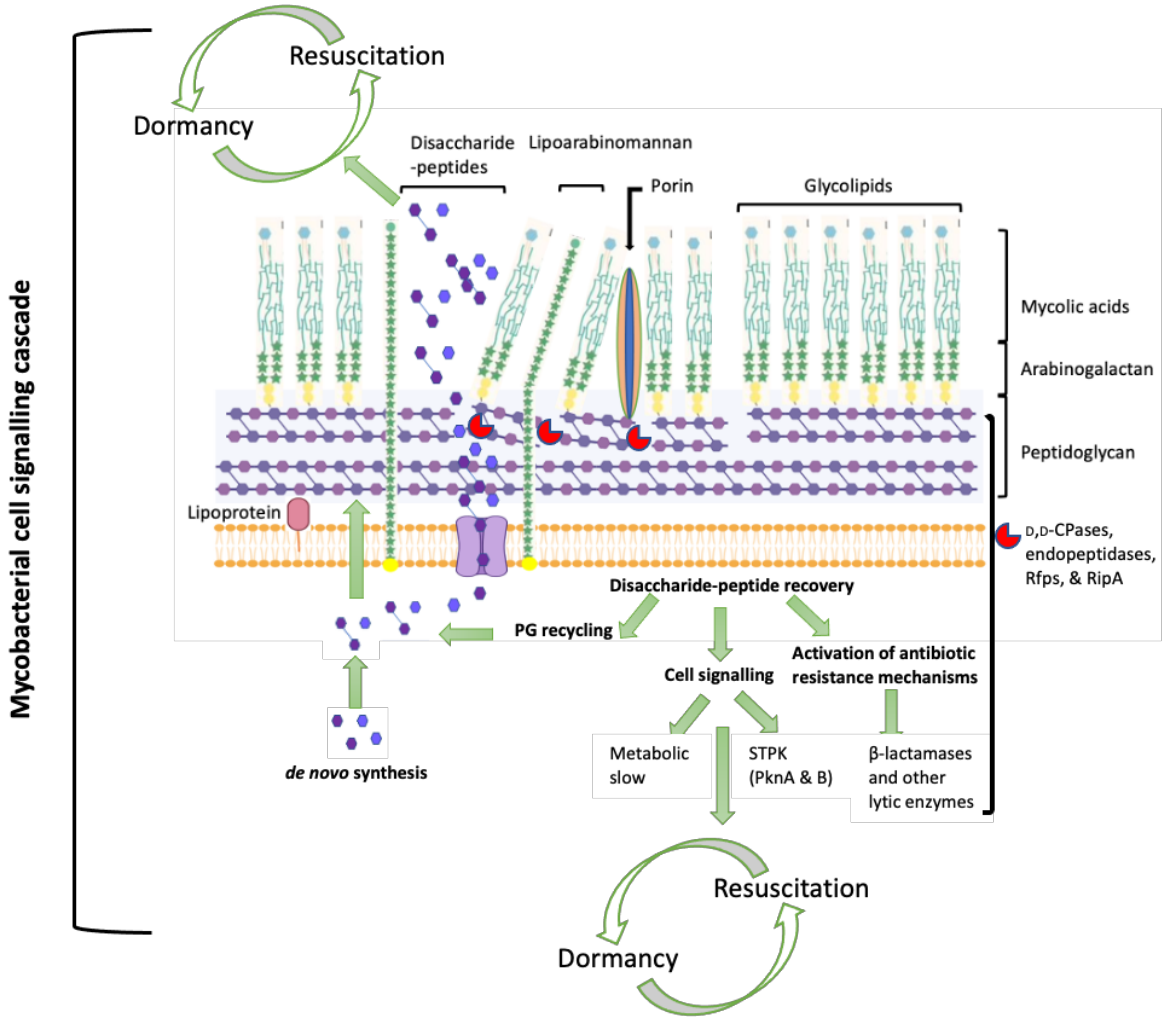


Figure 17: A description of the bacilli cell responses during PG repair and maintenance. Digested fragments of PG by various hydrolases generates muropeptides (disaccharide-di-, tripeptides) sub-units. The digestion of PG releases muropeptides into the environment and/or recycled back into the cytoplasm. These induce a variety of pathways leading to the cycling between dormancy and reactivation. The release of muropeptides may also lead to the induction of β-lactamases in the presence of antibiotics. Adapted from (Porfírio *et al*., 2019, Maitra *et al*., 2019).

1.7.16.1 Muramidases

Peptidoglycan turnover products can signal the expression of chromosomally encoded β-lactamases, which degrade β-lactam antibiotics (Jacobs et al., 1997). Inhibition of glycan strand transpeptidation by β-lactams can induce the turnover of nascent peptidoglycan by lytic transglycosylases, such as the Slt in *E.coli* (Cho et al., 2014). This cycle of peptidoglycan synthesis and degradation depletes the pool of peptidoglycan precursors, contributing to the

bactericidal activity of β-lactams (Figure 17). Lytic transglycosylases are non-hydrolytic proteins that regulate peptidoglycan in a coordinated manner, enabling cell division without rupture due to osmotic pressure imbalances (Vollmer et al., 2008; Den Blaauwen, 2008; Uehara et al., 2009). These enzymes cleave the glycosidic bond between Glc*N*Ac and Mur*N*Ac, forming a disaccharide-muropeptide with a 1,6-anhydroMur*N*Ac on the Mur*N*Ac in Gram-positive bacteria (Johnson et al., 2012; Höltje et al., 1975; Vermassen et al., 2019). This released fragment can contribute to the pathology caused by the cytotoxin of *Bordetella pertussis* (Cookson et al., 1989).

Muramidases such as lysozyme although catalyse reactions at the same site as lytic transglycosylases, they differ by catalysing a hydrolysis reaction, cleaving the β(1,4) glycosidic bond between Glc*N*Ac and Mur*N*Ac in bacterial cell walls, compromising the integrity of the cell wall and leading to bacterial lysis (Geiger et al., 2018; Jana et al., 2017). While lysozyme can inhibit the growth of *M. tuberculosis* and *M. smegmatis*, the peptidoglycan structure in these bacteria is often refractory to lysozyme because of modifications such as *N*-glycolylation they require addition and alternative hydrolytic enzymes to fully degrade the cell wall (Raymond et al., 2005; Mahapatra et al., 2013).

M. tuberculosis, *M. bovis*, *M. smegmatis*, and *M. marinum* present unique challenges for cell elongation and division due to their complex cell wall structure. The functions of lytic transglycosylases in *M. tuberculosis*, *M. bovis*, *M. smegmatis*, and *M. marinum* are currently under investigation. The cleavage of peptidoglycan plays a crucial role in recycling, which is further complicated by the need for specialised enzymes and regulatory mechanisms distinct from those in other bacteria. Key enzymes involved in mycobacterial cell elongation and division include resuscitation-promoting factors (Rpfs), which cleave peptidoglycan and play an essential role in resuscitating dormant cells and facilitating cell division (Ruggiero et al., 2016).

There are five resuscitation-promoting factors (Rpfs), RpfA, RpfB, RpfC, RpfD, and RpfE each functioning as lytic transglycosylases with lysozyme-like domains that cleave the glycan chains in peptidoglycan (Wivagg et al., 2012; Ruggiero et al., 2016). While all Rpfs are mutually dispensable, RpfB and RpfE have been shown to be essential for the resuscitation of metabolically inactive bacilli in *M. tuberculosis* and *M. Bovis* (Ruggiero et al., 2016; Tufariello et al., 2004; Tufariello et al., 2008). Peptidoglycan fragments released by Rpfs act as signals to

stimulate growth. For instance, recombinant Rpfs have been shown to resuscitate *M. bovis in vitro* and enhance the recovery of *M. tuberculosis* from sputum samples of patients with active tuberculosis (Wu et al., 2008; Mukamolova et al., 2010; Ealand et al., 2019). Additionally, Kana et al. (2008) reported that the deletion of three *rpf* genes results in a loss of pathogenicity *in vivo*, indicating a hierarchy or potency of expression among Rpfs (Kana et al., 2008; Downing et al., 2005). Similarly, Russell-Goldman et al. (2008) observed that double deletion of *rpfA* and *rpfE* led to altered phenotypes and failed resuscitation of dormant cells (Romano et al., 2012). Expression of Rpfs also varies across growth phases and environmental conditions. RpfA and RpfD are predominantly expressed during early resuscitation, whereas RpfC and RpfE are crucial under hypoxic and acidic conditions (Gupta et al., 2011). These findings suggest that Rpfs act synergistically and play a crucial role in mycobacterial virulence (Gupta et al., 2011).

1.7.16.2 *N*-acetylglucosaminidases

N-acetylglucosaminidases, also called NagZ, are glycoside hydrolases that specifically target the glycosidic bonds within peptidoglycan, a critical component of bacterial cell walls. These enzymes catalyse the hydrolysis of the β-1,4 linkages between Glc*N*Ac and Mur*N*Ac within the peptidoglycan, removing the terminal Glc*N*Ac and facilitating cell wall remodelling during bacterial growth, division, and autolysis. The activity of *N*-acetylglucosaminidases, such as Atla and Acp, has been shown to be essential for processes like cell separation in *Enterococcus faecalis* and *Clostridium perfringens,* respectively, by enabling the cleavage of septal peptidoglycan after cell division (Eckert et al., 2006; Camiade et al., 2010). In *Bacillus subtilis*, the BsNagZ enzyme plays a crucial role in peptidoglycan turnover and recycling, especially under conditions of nutrient limitation (Su et al., 2016). Additionally, *N*-acetylglucosaminidases are important in maintaining bacterial cell wall integrity and can influence bacterial virulence by modulating the susceptibility of the cell wall to host lysozymes (Vollmer & Tomasz, 2000).

Similar to *B. subtilis*, *M. tuberculosis* has an exo-acting β-*N*-acetylglucosaminidase encoded by the *lpqI* gene, which was identified by Moynihan et al. (2019). This enzyme is responsible for recycling peptidoglycan fragments released by hydrolase activity back into the cytoplasm. It cleaves the link between the glycan backbone and the peptidoglycan fragments, allowing them to enter metabolic or recycling pathways. Some of the cleaved disaccharide units are

further hydrolysed by various enzymes and reused as a carbon source, stimulate host immune factors, or reintegrate into the peptidoglycan biosynthesis pathway (Moynihan et al., 2019).

1.7.16.3 *N*-acetylmuramoyl-L-alanine amidases

Some hydrolases have defined functions. For instance, amidases cleave the lactyl-amide bond between Mur*N*Ac and L-alanine on the peptide stem (Vermassen et al., 2019; Healy et al., 2020). The AmiA, AmiB, and AmiC amidases in *E. coli* and their EnvC, NlpD, and ActS regulators play redundant roles in septation, essential for separating daughter cells. Depletion of all three amidases results in long, undivided cells (Boelter et al., 2022). EnvC interacts with and activates AmiA and AmiB, while NlpD binds and activates AmiC (Gurnani et al., 2021). This aberrant morphology is exacerbated in the absence of lytic transglycosylases and endopeptidases (Heidrich et al., 2001). Additionally, ActS, an inactive member of LytM-type peptidoglycan endopeptidases, activates AmiA, AmiB, and AmiC in *E. coli* (Gurnani et al., 2021). Furthermore, in *Bacillus subtilis*, for example, the SpoIIP amidase interacts with the lytic transglycosylase SpoIID to form the IIP-IID complex at cell wall hydrolysis sites, stimulating the amidase activity of SpoIIP during pore morphogenesis (Morlot et al., 2010). Overall, underscoring that no one enzyme works alone.

In *M. tuberculosis*, there are at least four amidases: Ami1 (Rv3717), Ami2 (Rv3915), Ami3 (Rv3811), and Ami4 (Rv3594) (Machowski et al., 2014). Despite the genes *ami1* and *ami2* whose product is Ami1 and Ami2 (also called Cw1M) being highly conserved, only *ami2* is well-categorised in *M. tuberculosis*. It consists of two peptidoglycan-binding domains and is essential for growth and cell survival (Boutte et al., 2016; Turapov et al., 2018). *ami4*, on the other hand, is less studied and is unique to *M. tuberculosis* (Kieswetter et al., 2021). Additionally, Ami1 has been shown to have a synergistic role with the endopeptidase RipA in mediating cell division (Healy et al., 2020).

1.7.16.4 Endopeptidases

Endopeptidases have a broad range of functions and can cleave within any part of the stem peptide (Figure 17). They catalyse the hydrolysis of amide bonds within peptide stems, including cross-links catalysed by PBPs or L,D-CPase. For instance, the D,D-endopeptidases

like MepS, MepM, and MepH are responsible for cleaving 4,3 cross-links between D-alanine and *meso*-DAP, which inhibits cell elongation and peptidoglycan synthesis, ultimately leading to cell lysis (Singh et al., 2015; Singh et al., 2012; Chodisetti & Reddy, 2019). Other endopeptidases, such as MepK, specifically hydrolyse L,D-TPase-catalysed 3,3 cross-links (Chodisetti & Reddy, 2019).

In *M. tuberculosis*, the NlpC/P60-type D,L-endopeptidase RipA is the most well-characterised protein out of the four Rip-family members: RipA (Rv1477), RipB (Rv1478), RipC (Rv2190c), and RipD (Rv1566) Mavrici et al., 2014; Martinelli & Pavelka, 2016). RipA cleaves between the 2nd and 3rd positions within the stem peptide (Hett & Rubin, 2010). RipA interacts with PonA1 and RpfB, forming a complex that cleaves the amide bond between D-*iso*-Glu at position 2 and *meso*-DAP at position 3 on the peptide (Hett et al., 2008; Hett & Rubin, 2010; Nikitushkin et al., 2015). RipA is recruited to the septum of dividing cells, and its absence results in growth defects and abnormal cell morphology (Ruggiero et al., 2010). PonA1 polymerises peptidoglycan, and its activity is regulated through its interaction with RipA, which is crucial for cell elongation (Hett & Rubin, 2010; Kieser et al., 2015) The RipA-PonA1 complex produces *N*-acetyl-glucosaminyl-β(1,4)-*N*-glycolyl-1,6-anhydromuramyl-L-alanyl-D-*iso*Glu (Machowski et al., 2014). The RipA-RpfB-PonA1 complex is essential for peptidoglycan cleavage at the septum site, and thus for growth at the poles, elongation, and septum formation (Kang et al., 2008; Hett & Rubin, 2010). Critically the activity of RipA is regulated by an acid-resistant serine protease, MarP (Rv3671c) (Botella et al., 2017). Additionally, this complex initiates stress-response enzymes encoded by the DoSR regulon, facilitating the recovery of dormant mycobacterial cells (Nikitushkin et al., 2015).

1.7.16.5 Carboxypeptidases

D,D-carboxypeptidases (D,D-CPases) are crucial for regulating cross-linking and homeostasis in peptidoglycan. These multi-domain enzymes cleave the terminal D-alanine residues from the 3,4 cross-links of peptidoglycan precursors or pentapeptides, generating tetrapeptide stems that serve as substrates for L,D-transpeptidases (L,D-TPases) (Popham, Gilmore, & Setlow, 1999; Vollmer et al., 2008; Pandey et al., 2018; Vermassen et al., 2019; Espaillat et al., 2024). This process is essential for the maturation and restructuring of the bacterial cell wall.

For example, D,D-CPases like PBP5 cleave the terminal D-alanine on lipid II after it has been added to a glycan strand, allowing transpeptidases to crosslink the newly free *meso*-DAP peptide to the D-alanine from the new glycan strand (Egan et al., 2020; Garde et al., 2021). Incidentally, the L,D-CPases also cleave in the same place but between the L- and D-amino acids (Dousa et al., 2020). The balance of hydrolysis and peptidoglycan biosynthesis coordinates cell wall elongation before division takes place.

The D,D-CPases in mycobacteria, such as those identified in *M. smegmatis* and *M. tuberculosis*, have been shown to be integral to cell wall remodelling processes. For instance, studies have demonstrated that these enzymes help maintain cell shape and contribute to resistance to β-lactam antibiotics by remodelling the peptidoglycan layer (Eun, Yapo, & Petit, 1978). Similarly, the gene MSMEG_2433 in *M. smegmatis* exhibits both D,D-CPases and β-lactamase activities, highlighting its role in antibiotic resistance (Bansal et al., 2015). Other D,D-CPases such as PBP6b in *E. coli* have also been shown to be important in maintaining cell shape, becoming increasingly active as pH rises to 5.0 and contributing to cell shape and elongation under acidic conditions (Peters et al., 2016). PBP5, PBP6 and PBP6b constitute up to 50% of the PBPs in *E.coli* (Meiresonne et al., 2017). Peters et al. (2016) showed that deletion of PBP6 caused the cells to lyse in acidic conditions. Site-directed mutagenesis has also been used to target and characterise the D,D-CPase genes *pbp5*, *pbp6*, *pbp6B*, and *dacD* in *E. coli* (Waxman, Arima and Strominger, 1982; Baquero et al., 1996; Nicola et al., 2005; Zhang et al., 2007; Shi et al., 2008; Peters et al., 2016). In addition, the catalytic motifs for the function of D,D-CPases have proven to be crucial. For example, PBP4 in *S. aureus* contains the motifs SMTK, SSN, KTG, with serine of SMTK proposed to be activated by losing a proton to the lysine located in KTG. Mutating amino acids such as these abolishes enzymatic activity, inhibiting the terminal D-alanine on the pentapeptide from interacting with the serine of the SxxK tetrad and lysine of KTG (van der Linden et al., 1994; Malhotra & Nicholas, 1992).

However, the mechanisms and timing of how D,D-CPases carry out their functions are not that well understood. Studies such as Ealand (2019) have found shared homology for the SMEG_1661, SMEG_2432, SMEG_2433, and MEG_6113 (DacB) D,D-CPases in the S11 (InterPro IPR012338) and S13 (InterPro IPR000667) peptidase families between *E. coli* and *M. smegmatis*. Kang and Kim (2024) describe structural insights into PBP4, a D,D-CPase present in *M. tuberculosis*, *E. coli*, *Haemophilus influenzae*, and Actinomycetes R39, showing

a two-domain enzyme with a PBP domain (domain I) sandwiched between a peptidoglycan-binding domain (domain II).

Other studies are uncovering their multi-functional roles. For instance, the Pandey et al. (2020) study showed MSMEG_2432 from *M. smegmatis* exhibited both D,D-CPase and β-lactamase activities, playing a role in peptidoglycan remodelling and antibiotic resistance. Similarly, MSMEG_2433 has both D,D-CPase and β-lactamase activities, contributing to cell shape restoration and antibiotic resistance (Bansal et al., 2015). Moreover, the gene Rv3627c in *M. tuberculosis*, encoding a novel D,D-CPase, was shown to affect mycobacterial cell morphology and cell division, promoting elongation and Z-ring formation in *M. smegmatis* (Zhang et al., 2019).

D,D-CPases and their peptidoglycan-binding domains are crucial for bacterial cell wall remodelling, enzyme specificity, and adaptation to environmental stresses. The physiological roles of D,D-CPases in peptidoglycan turnover underscore their contribution to the structural integrity and antibiotic resistance mechanisms of the bacterial cell wall (Squeglia et al., 2018). Despite the importance of these enzymes, their actions in mycobacteria are not fully understood. Understanding their structure and function provides insights into their roles in bacterial physiology and potential targets for antibiotics and novel therapeutic approaches for combating mycobacterial infections, especially in the face of increasing antibiotic resistance.

1.7.17 Cleaved peptidoglycan

Mycobacteria shed a wide range of pathogen-associated molecular patterns (Kleinnijenhuis et al., 2011). Of particular relevance to this thesis is peptidoglycan fragments, which are detected by the pattern recognition receptor NOD2, expressed on innate immune cells. NOD2 specifically recognises the muramyl dipeptide component of peptidoglycan (Boneca, et al. 2007; Callewaert and Michiels, 2010; Moynihan and Clarke, 2011; Kleinnijenhuis et al., 2011; Li, Wang, & Liu, 2012; Giovanna Valle Germano et al., 2022; Dubé, McIntosh, and Behr, 2022). Upon recognition of *M. tuberculosis* by host immune factors, NOD2 modulates host effector cells (Li & Wu, 2021; Cagliero et al., 2022; Giovanna Valle Germano et al., 2022; Dubé, McIntosh, and Behr, 2022). This receptor can distinguish between self and non-self-components, including microbial peptides from peptidoglycan and lipoproteins secreted by *M. tuberculosis* (Duan et al., 2022; Killick et al., 2013). Consequently, this process elicits an initial effector response by macrophages, leading to the phagocytosis and control of the intracellular

proliferation of *M. tuberculosis*, thus contributing to the characteristic granulomatous pathology of TB infection (Gold et al., 2010; Harriff et al., 2014; Arango Duque & Descoteaux, 2014; Sharma et al., 2020).

1.8 Inhibitors of peptidoglycan synthesis

Peptidoglycan is essential and unique to most bacteria, as it maintains cell shape and resists turgor pressure. Glycopeptide antibiotics target lipid II, which is delivered by enzymes responsible for the insertion and maintenance of peptidoglycan, such as the transglycosylases (Figures 19). Consequently, this part of the cytoplasmic peptidoglycan biosynthetic pathway is a significant focus for the research and development of new therapeutics. Peptidoglycan synthesis is inhibited by several classes of antibiotics, including glycopeptides, D-cycloserine, and various classes of β-lactams. The specifics of these classes will be described below.

1.8.1 D-cycloserine

D-cycloserine is a second-line, toxic compound used only as a last resort for multi- and extremely drug resistant infections (Bhat et al., 2018, Table 4). It is a structural analogue of D-alanine, competing with the natural substrates of D-alanine racemase (Alr, Rv3423c) (de Chiara et al., 2020). Alr converts L-alanine to D-alanine, thus facilitating dipeptide formation for the final step of pentapeptide formation (Prosser et al., 2013; Figure 18). A recent study highlighted that mutations in the promoter of *alr* are responsible for resistance, and in addition, they identified 16 other gene mutations associated with D-cycloserine resistance (Chen et al., 2017).

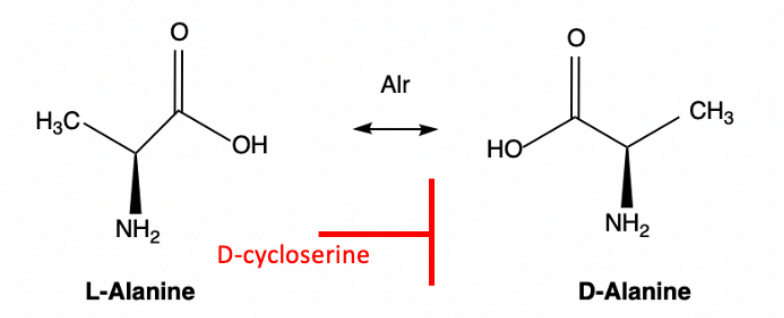


Figure 18: A schematic of the formation of the di-peptide, converting L-alanine to D-alanine. Also outlined is the mechanism of D-cycloserine preventing Alr from its substrate by binding to its active site instead. Figure adapted from Trivedi et al., 2018.

Lipid II inhibitors include vancomycin and teicoplanin among others, all of which are structurally similar (Svetitsky et al., 2009). These molecules are tricyclic glycosylated non-ribosomal peptides used for multi- and extremely drug resistant infections with Gram-positive bacteria like *Staphylococcus aureus* and *Enterococcus faecalis* (Barna et al., 1984; Stogios & Savchenko, 2020). Vancomycin and teicoplanin bind via hydrogen bonding to the C-terminal D-alanine-D-alanine on lipid II (Figure 19) (Sarkar et al., 2017), inhibiting polymerisation of muropeptides via steric hindrance and halting the transpeptidase responsible for 3,4 cross-linking between D-alanine and the *meso*-DAP on the 3rd position on the adjacent peptide stem (Sarkar et al., 2017). Although not traditionally used against mycobacteria, Soetaert et al. (2015) showed that a synergistic effect was observed with vancomycin in combination with a lipid biogenesis inhibitor, cerulenin, in *M. bovis* and *M. tuberculosis* XDR strains (Soetaert et al., 2015).

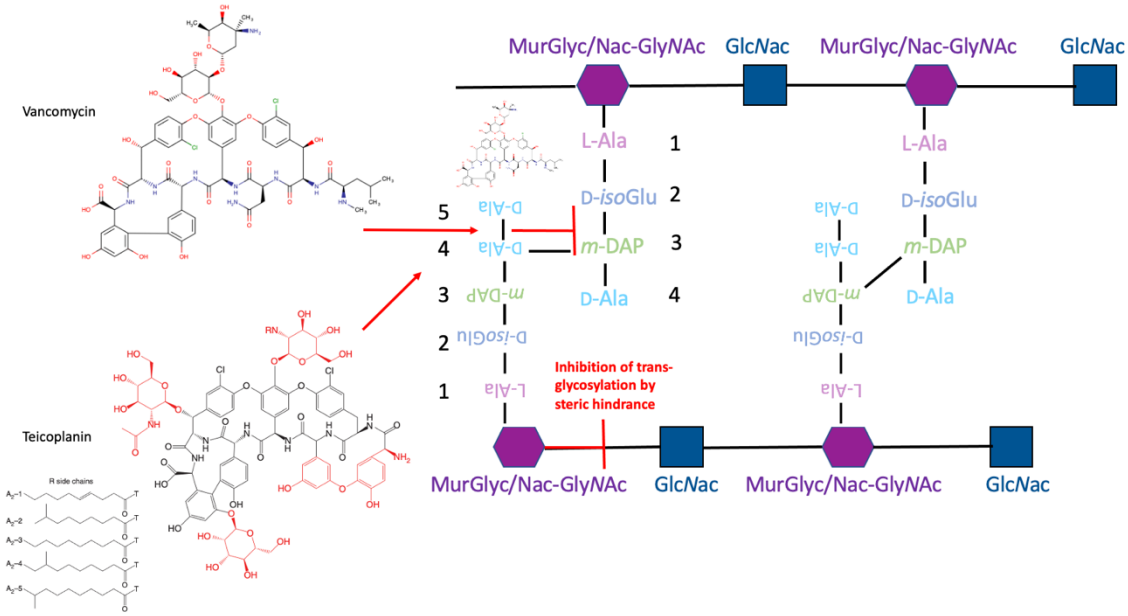


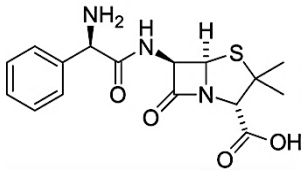
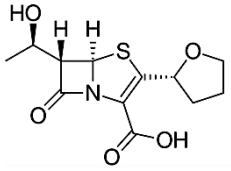
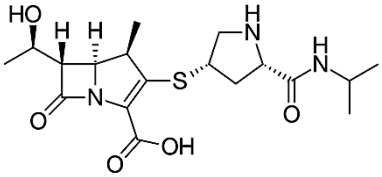
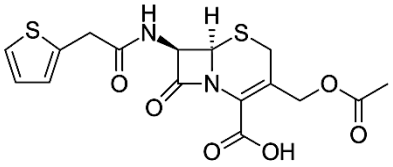
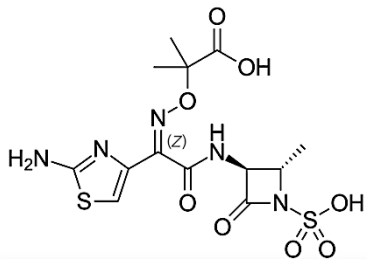
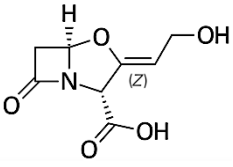
Figure 19: A basic depiction of the modes of action for the lipid II inhibitors preventing incorporation into mature peptidoglycan. On the left are the chemical structures of the teicoplanin (plus 5 R side groups) and vancomycin (Zeng et al., 2016). Vancomycin sequesters the substrate by binding to the to the terminal D-alanine on lipid II interrupting transpeptidation activities of the D,D transpeptidase and halting the cross-linkage between 3rd *m*-DAP and 4th D-alanine on the adjacent peptide stem. Teicoplanin also has the same mode of action as vancomycin but both peptides sterically hinder the formation of the lipid II and interfering with the peptidoglycan layer maturation process and ultimately leading to cell lysis.

1.8.2 β-lactams and adjuvants for targeting L,D-TPases and PBPs

The first β-lactam, penicillin, was discovered in 1928 by Sir Alexander Fleming (Bellamy et al., 1948; Fleming et al., 1945). The structure of penicillin was solved by Dorothy Hodgkin in 1945 using X-ray crystallography (Hodgkin et al., 1965; Crowfoot et al., 1949). This structural elucidation aided Sir Howard Florey and Dr. Ernst Boris Chain in purifying penicillin, eventually making it fit for clinical use (Bellamy et al., 1948).

In the interim years, new classes of β-lactams have been developed. β-lactams are broad-spectrum, bactericidal compounds that covalently modify the active site of penicillin-binding proteins (PBPs) (Lai et al., 2017; Dalhoff et al., 2020). The β-lactam antibiotics currently used clinically are natural, semi-synthetic, or completely synthetic compounds (Turner et al., 2022). They share a common structure of the four-member β-lactam (azetidine-2-one) ring. β-lactams are grouped into classes including penams, penems, carbapenems, cephams, monobactams, and clavulans (Table 5). Each class has unique chemical modifications, giving them an affinity for different subsets of PBPs and transpeptidases (D,D- L,D-transpeptidases) (Zandi et al., 2021).

Table 5: The nomenclature of the most common β-lactams and a representative structure from each class is outlined. Chemical structures adapted from (Papp-Wallace et al., 2011; Lee et al., 2016; Batchelder et al., 2020; Turner et al., 2022;).

Class	Example of structure
Penam	 ampicillin
Penem	 faropenem
Carbapenem	 meropenem
Cepham	 cephalothin
Monobactam	 aztreonam
Clavum	 clavulanic acid

1.8.3 Penams

Penams, also called penicillins, possess a thiazolidine ring and a sulfur atom at position one (Turner et al., 2022). The most well-known natural β-lactams in the penam class are benzylpenicillin (penicillin G), derived from *Penicillium chrysogenum* (Fleming et al., 2001), and phenoxymethylpenicillin (penicillin V). Penicillins have excellent activity against Gram-positives in the absence of β-lactamases but are not potent against Gram-negatives (Libby and Holmberg, 1945; Eagle, 1946; Eagle, 1947; E. Ellen. Nell and Hill, 1947; Thomsen Vf and So, 1962; Davies, 2018; Barrie et al., 2024). Modifications of the structure at carbon position 6, where the R side chain resides, have been undertaken to broaden the therapeutic range of the penems (Table 5). Amoxicillin is the most clinically prescribed β-lactam globally (Tao et al., 2019).

1.8.4 Penems

Penems are derivatives of the penam class of β-lactams and have structural similarities to carbapenems, except for a sulfur atom at position 1 (Batchelder et al., 2022). They contain a bicyclic core and an unsaturated five-membered ring which imposes stress on the β-lactam ring, enhancing its reactivity (Batchelder et al., 2020). Penems are currently being investigated as potential candidates for new β-lactam development. For example, the compound T405 has shown high antimicrobial potency against *M. tuberculosis* (H37Rv) and *M. abscessus* (ATCC 19977) (Batchelder et al., 2022). Others in this class being researched for improved clinical potential against infections include faropenem and sulopenem (Batchelder et al., 2020; Zhanel et al., 2022).

Unlike carbapenems, faropenem is orally administered with approximately 70-80% oral bioavailability and has shown *in vitro* anti-tubercular properties (Gandra et al., 2022; Shangguan et al., 2023). However, research is also being undertaken to improve the bioavailability of carbapenems (Gandra et al., 2022).

1.8.5 Carbapenems

Carbapenems are a subclass of penems that contain a pyrroline ring unsaturated at C2-C3 (Papp-Wallace et al., 2011; Armstrong, Fenn, and Hardie, 2021; Metha et al., 2021). The structural arrangements of carbapenems are responsible for their antibacterial properties against Gram-positive and Gram-negative bacteria within this class of β-lactams (Armstrong, Fenn, and Hardie, 2021). Unlike penams and cephams, which have aminoacyl substituents at C6, carbapenems contain an *R*-hydroxymethyl side chain at C6 on the β-lactam ring (Metha et al., 2021). Thioether modification is the main feature of carbapenems, characterised by the presence of a sulfur atom in the R1 side chain at position 3. Except for imipenem, all carbapenems are substituted with a methyl group (R2) at position 4 on the pyrroline ring. This increases stability *in vivo* towards renal dehydropeptidase (DHP-1). Without the methyl group, drugs like imipenem need to be co-administered with cilastatin (Table 4; Armstrong, Fenn, and Hardie, 2021). Another departure from the *cis* configuration at C5-C6 of penams and cephams is the *trans* hydrogen bond at C5-C6 in carbapenems, which attributes β-lactamase resistance (Armstrong, Fenn, and Hardie, 2021). Examples of highly potent carbapenems include meropenem, doripenem, and ertapenem. They have been clinically considered useful for treating multidrug-resistant infections such as carbapenem-resistant Enterobacteriaceae (Bush et al., 2017; Doi et al., 2019; Li et al., 2020). Carbapenems such as meropenem, having shown activity against pulmonary TB *in vitro* mouse models and in clinical trials, are being reconsidered for anti-tubercular treatment in combination with clavam adjuvants (Hugonnet et al., 2009; England et al., 2012; Payen et al., 2012; Diacon et al., 2016; Veronique De Jager et al., 2022). For example, Hugonnet et al.'s (2009) study showed that meropenem-clavulanate killed 13 different strains of extremely drug-resistant *M. tuberculosis* (XDR) with MICs between 1-1.25 μg/mL.

1.8.6 Cephams

Cephams, originally isolated from the mold *Acremonium*, are also called cephalosporins. They possess a 6-membered dihydrothiazine ring fused to the β-lactam ring, which is unsaturated at C2-C3 with a sulfur at position 5. Antibacterial activity is attributed to positions C3, C4, and C7 (Hughes et al., 2017, parts 1 & 2; Shchelik and Gademann, 2021; Lekshmi Narendrakumar et al., 2023). They are the most prescribed antibiotics due to their general tolerability, low

toxicity, and low allergic reporting (Bush and Bradford, 2016). There have been five generations of cephams with variations in the structures developed to combat resistance in Gram-negatives while maintaining a broad range of antibacterial activity (Bui and Preuss, 2023).

The majority of cephams in this class are semi-synthetically derived from amino-cephalosporins acid with broad spectrum activity (Lin and Kück, 2022). For example, the first-generation cephalothin is active against Gram-positive bacteria such as *Staphylococcus* spp. and *Streptococcus* spp., as well as the Gram-negative *Proteus mirabilis*. Additionally, *Escherichia coli* and *Klebsiella pneumoniae* are more susceptible to first-generation cephalosporins (Bui and Preuss, 2023).

The second-generation cefoxitin was developed to prevent hydrolysis by β-lactamases due to a change from hydrogen to a methoxy group at position 7. It has moderate activity against Gram-positives and Gram-negatives. However, it can induce cephalosporinase expression (a β-lactamase that can hydrolyse cephalosporins) (Neu., 1974). The methoxy group also reduces the antibacterial activity of cephamycins against Gram-negatives (Page., 2007).

Third generation cephalosporins, including cefotaxime, ceftriaxone, ceftazidime, ceftazidime-avibactam, cefdinir, cefpodoxime, and cefixime, were developed to improve robustness against β-lactamases and have a broader antibacterial spectrum (Donowitz, 1989; NICE., 2024). They are more susceptible to being hydrolysed by broad-spectrum β-lactamases and AmpC-producing organisms (Jacoby, 2009; Bui and Preuss, 2023).

Fourth generation cephams, such as cefepime, have a nitrogen at C3 to help passive transport through the outer membrane of Gram-negatives (Okamoto et al., 1994). They are effective against methicillin-susceptible *Staphylococcus aureus* (MSSA), *Streptococcus* spp., *Pseudomonas aeruginosa*, and enteric Gram-negative bacteria (Bui and Preuss, 2023).

Fifth generation cephams, such as ceftaroline and ceftobiprole, were developed to have a broader antibacterial spectrum, including extended-spectrum β-lactamase producers like *Acinetobacter baumanii* and *Stenotrophomonas maltophilia*. Other organisms susceptible to fifth generation cephams include methicillin-resistant *S. aureus* (MRSA), *Streptococcus* spp., Gram-negative enteric bacteria, and Gram-positive cocci (Bui and Preuss, 2023).

1.8.7 Monobactams

Monobactams represent a single cyclic structure, namely the β-lactam ring, that was first isolated in Chromobacterium violaceum (Asai et al., 1981; Imada et al., 1981; Sykes et al., 1981; Decuyper et al., 2018; Goldberg et al., 2021). Monobactams have a narrow spectrum of antimicrobial activity compared to other classes of β-lactams. The only licensed monobactam, Aztreonam, targets aerobic Gram-negative class B PBPs and PBP3, which targets the divisome of *E. coli* and *M. tuberculosis* (Lu et al., 2020; Liu, Miller, and Miller, 2021; Park and Cho et al., 2022). Ongoing studies for Aztreonam include its use against multidrug Gram-negative and Gram-positive infections in combination with other β-lactam classes and diazbicyclooctane monobactams (Bhatnagar et al., 2020; Bassetti et al., 2021). Research into the development of a second generation (LYS228) of monobactam is currently underway (Osborn et al., 2019).

1.8.8 Clavams

Clavulans are β-lactamase inhibitors that include subclasses of penams resistant to being hydrolysed by β-lactamases (Lang et al., 2022). β-lactamase inhibitors containing a β-lactam ring currently include clavulanic acid, sulbactam, and tazobactam. Other synthesized variations include boronate and diazabicyclooctane scaffolds such as vaborbactam, avibactam, and relebactam, respectively (Nordmann, Bouvier, and Laurent Poirel, 2023; Alsenani et al., 2023). These newer inhibitor combinations are currently being researched for infections with Carbapenemase-producing Enterobacterales (Nordmann, Bouvier, and Laurent Poirel, 2023; Alsenani et al., 2023). Meropenem-vaborbactam is in preclinical trials for multi-drug-resistant pulmonary TB and non-tuberculosis TB (Kaushik et al., 2019; Sing et al., 2023). Sing et al. (2023) study showed using a fibre model system meropenem-vaborbactam restored rifampin in a dose-dependent response. They do not possess antibacterial activity but enhance the performance of the β-lactam partner such as amoxicillin by binding to β-lactamases and leaving an unobstructed β-lactam free to deactivate its target (Lang et al., 2022; Shapiro et al., 2021). Hugonnet's study (2009) showed that the meropenem-clavulanate combination was potent against XDR strains of *M. tuberculosis*, proving clavulanate to be an effective adjuvant for anti-tubercular drug therapy by inhibiting the BlaC (Hugonnet and Blanchard, 2007; Hugonnet et al., 2009).

1.8.9 Mode of action of β-lactams

The mechanism of penicillin was not elucidated until 1974 by Blumberg and Strominger (Blumberg and Strominger, 1974). β-lactams mimic the natural substrate of D,D-TPase, which is the dipeptide D-alanine-D-alanine during peptidoglycan synthesis (Tipper and Strominger, 1965; Tipper et al., 1965; Maya-Martinez et al., 2019). Under normal conditions, peptidoglycan construction involves cross-linking the stem peptide by the activity of D,D-TPases of penicillin-binding proteins (PBPs) and/or L,D-TPase (Pandey et al., 2018). L,D-TPase recognise the mirror image of the α-carbon on the 4th D-alanine and are also targets for carbapenems (Wivagg, Bhattacharyya, and Hung, 2014). Transpeptidases recognise the dipeptide D-alanine-D-alanine, and β-lactams covalently bind to transpeptidases, blocking D-alanine-D-alanine from entering the active site. This mechanism is attributed to the reactive β-lactam ring, which mimics the electrostatic negative wells on D-alanine- D-alanine (Tipper et al., 1965; Maya-Martinez et al., 2019).

An acyl-transpeptidase intermediate is formed between the carboxy group on a β-lactam ring that opens and forms a covalent bond with the active site serine in the transpeptidase domain of the PBP (Sauvage et al., 2008; Mora-Ochomogo and Lohans, 2021). Through a slow de-acylation rate, β-lactams render the transpeptidase inactive, leading to a build-up of uncross-linked tetra-penta-peptides and initiation of cell signalling mechanisms, activating the upregulation of the L,D- and D,L-TPases (Sauvage et al., 2008). Figure 20 shows the similarity of structures of β-lactam and the di-peptide D-alanine- D-alanine.

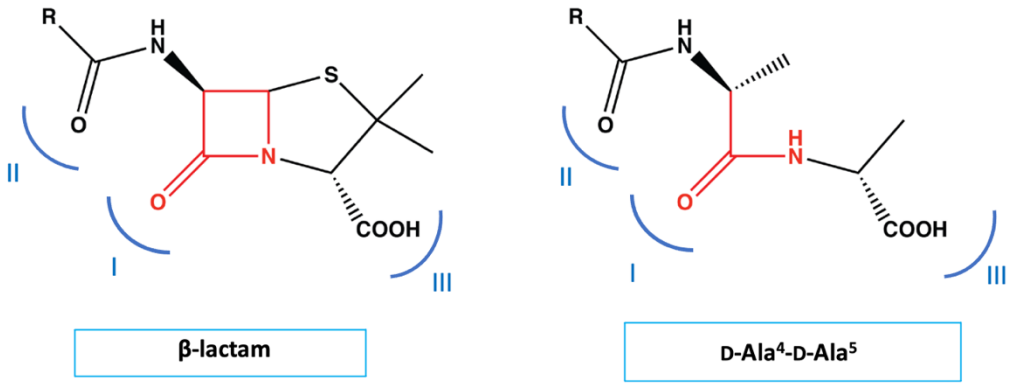


Figure 20: The similarity of the β-lactam ring (shown in red) between the pentapeptide containing D-alanine--D-alanine (D-Ala^4- D-Ala^5) and the β-lactam, in this case penicillin. A comparison can be made between the electron distribution for both structures facilitating the mimetic of the PBPs natural substrate (Blue, I, II & III). The R group can also be modified which gives rise to a plethora of antibiotic derivates with different binding efficacies. The R group on the D-Ala^4- D-Ala^5 is what remains of the peptide. Diagram adapted from (Zeng and Lin, 2013; André Zapun, Macheboeuf and Vernet, 2017; Kim et al., 2023).

The use of β-lactams for treatment of TB infection is limited due to the production of ambler class of β-lactamase BlaC that can inactivate the β-lactam ring. However, since the discovery of clavulanic acid the WHO has recommended amoxicillin-clavulanic acid in combination with meropenem as a potential treatment of multi-drug or rifampicin-resistant TB. Clinical studies for evidence based outcomes are still a work in progress.

1.9 Resistance to β-lactams; β-lactamases

A primary resistance mechanism that bacteria employ is the utilisation of enzymes that inactivate most β-lactams by hydrolysing the four-membered ring of β-lactams. This allows transpeptidases to continue building the cell wall. Although Gram-positive bacteria do produce β-lactamases, this resistance mechanism is mainly observed in Gram-negative bacteria (Fisher & Mobashery, 2016). The main mechanism for Gram-positive bacteria is the production of low-affinity PBPs (Fisher & Mobashery, 2016).

There are four classes of β-lactamases: A, B, C, and D, based on their conserved and distinct amino acid motifs (Ambler, 1980; Jaurin & Grundstrom, 1981; Huovinen et al., 1988; Ouellette, Bissonnette, and Roy, 1987; Ambler et al., 1991). β-lactamases are further subdivided into 17 classes depending on substrate specificity (Bush & Jacoby, 2010; Antunes et al., 2014; Naas et al., 2017). The substrate preferences include carbapenemases, penicillinases, cephalosporinases, and extended-spectrum β-lactamases (ESBLs), which

hydrolyse penams, broad-spectrum cephems, and carbapenems (Pisabarro, de Pedro, and Vázquez, 1985).

Serine β-lactamases possess structural motifs and have a conserved serine in their active site, which they share with PBPs, the ancestral enzymes of β-lactamases (SxxK, KTG, SDN) (Knott-Hunziker et al., 1974; Massova & Mobashery, 1998). The interaction of serine β-lactamases with β-lactams leads to the formation of a non-covalent Michaelis-Menten complex, similar to the reaction of PBPs with β-lactams (Mora-Ochomogo and Lohans, 2021). Serine β-lactamases use their active-site serine to form an intermediate covalent acyl enzyme by nucleophilic attack on the carbonyl group of the lactam ring, which is then hydrolysed. The hydrolytic reaction step deviates from the PBP process, exhibiting a much higher rate of hydrolysis in β-lactamases compared to PBPs.

The mechanisms of action for hydrolysis in Class A β-lactamases are currently debated and are proposed to be different from Class C, utilising a lysine or glutamine in place of an active serine (Chen et al., 2007; Tomanicek et al., 2010). The active site amino acid residues are conserved for the recognition of certain substrates. Examples of Class A β-lactamases include the clinically relevant extended-spectrum β-lactamases such as TEM, SHV, cephalosporinase CTX-M, and the carbapenemase KPC (Rapp & Urban, 2012; Bush, 2018; Chong et al., 2018).

In mycobacteria, there are four known β-lactamases (Rv0406c, Rv3677c, BlaC, and CrfA), with the class A serine β-lactamase BlaC being the most potent (Kumar et al., 2022; Nantongo et al., 2024). BlaC, encoded by the *blaC* gene on the chromosome, can hydrolyse penams, cephams, and, at low affinity, carbapenems (Wivagg et al., 2014; Hugonnet et al., 2009). Although the blaC gene is not essential, its deletion renders *M. tuberculosis* susceptible to β-lactams, making BlaC an essential enzyme in the presence of these drugs (van Alen et al., 2021). Hugonnet & Blanchard (2007) demonstrated that BlaC is inhibited by clavulanic acid (Hugonnet et al., 2007).

Directed evolution studies on *M. tuberculosis* identified mutations that increase resistance to –β-lactams. For example, the mutation at position 105 (I105F) enhances resistance and catalytic efficiency of BlaC (Feiler et al., 2013). Other studies have shown that combinatorial active-site variants, with mutations at positions 69, 130, 220, and 234, synergistically enhance resistance

to clavulanate in BlaC (Egesborg et al., 2014). Additionally, mutations G132N and N132G have shown higher resistance to both clavulanate and avibactam (Soroka et al., 2016). While the antibacterial activity of meropenem has been shown to be enhanced by clavulanic acid (Hugonnet et al., 2009). Other inhibitors of BlaC enzymes in clinical use include sulbactam, tazobactam, avibactam and durlobactam (van Alen et al., 2021; Nantongo et al., 2024). Class A enzymes such as BlaC significantly contribute to the resistance of mycobacteria to β-lactam antibiotics (Flores et al., 2005). Mutational adaptations and structural features of BlaC enzymes enhance resistance, complicating treatment with β-lactam antibiotics and their inhibitors.

Class C β-lactamases (cephalosporinases), also called AmpC enzymes, are encoded by chromosomal *ampC* genes and inducible genes, with some class C enzymes found on mobile genetic elements (Jacoby, 2009; Philippon et al., 2022). In some bacteria, the *ampC* gene expression is controlled by the transcriptional regulator AmpR, which represses *ampC* expression under normal conditions (Juan et al., 2017). The degradation of nascent peptidoglycan by lytic transglycosylases, such as Slt, has been shown to be caused by the presence of β-lactams (Cho et al., 2014). Consequently, this leads to the accumulation of anhydro Mur*N*Ac-peptide turnover products in the cytoplasm, which serves as a signal for the induction of *ampC* and upregulation of β-lactamase activity (Fisher & Mobashery, 2014; Fisher & Mobashery, 2016). Class C enzymes are extended-spectrum β-lactamases with higher resistance to carbapenems (Philippon et al., 2022).

Class B and D β-lactamases do not have a catalytic serine; instead, they are metallo-β-lactamases that use a water molecule to hydrolyse the lactam ring (Zang et al., 2011). Metallo-β-lactamases consist of an HXHXD motif forming a metal core activated by a water molecule, which is central to the function of the enzyme. These enzymes are resistant to most β-lactams, including the carbapenem class of inhibitors, except for monobactams (Lohans et al., 2017).

Class D β-lactamases (oxacillinases) are encoded chromosomally and found on mobile genetic elements (Poirel, Potron, & Nordmann, 2012; Toth et al., 2016). They can hydrolyse a broad spectrum of β-lactams, including penams, extended-spectrum cephems, and carbapenems (Leonard, Bonomo, & Powers, 2013; Boyd et al., 2022). The emergence of β-lactam-resistant OXA-producing bacteria, such as enterobacterial species, *Pseudomonas aeruginosa*, and *Acinetobacter baumannii*, has become increasingly worrisome (Potron, Poirel, & Nordmann, 2015; Mairi et al., 2017). Thus, these classes of enzymes pose a significant clinical problem that urgently needs to be addressed.

1.10 The use of model organisms and systems to study genes in pathogenic mycobacteria

The study of genes in highly pathogenic species of mycobacteria, such as *M. tuberculosis* is restricted to high containment laboratories. To overcome this limitation and accelerate the pace of discovery, model species with high genome similarity and comparable cell wall profiles to *M. tuberculosis* can be used. Examples include *M. marinum* (1218R), *M. bovis* (BCG Danish 1331) and *M. smegmatis* (mc^2155). One advantage of using these model species is their faster growth rates compared to *M. tuberculosis*. For example, *M. marinum* has a doubling time of approximately 6 days whereas *M. tuberculosis* takes ~28 days and *M. smegmatis* is even faster with a doubling time of 3-5 h (Stinear et al., 2008; Eun Seon Chung et al., 2023 PREPRINT). The *M. tuberculosis* genome consists of 4.4 $x10^6$ base-pairs and encodes for approximately 4173 genes. It shares genome similarity to *M. bovis* (99.6%) , *M. marinum* (77%) and *M. smegmatis* (62 %) (Cole *et al*., 1998)). For example, there are approximately 3000 orthologues between *M. tuberculosis* and *M. marinum*, and 2,800 between *M. tuberculosis* and *M. smegmatis* (Stinear et al., 2008; Sparks et al., 2023). Phylogenetic comparisons indicate that *M. tuberculosis* is more closely related to and *M. marinum* are than to *M. smegmatis*, with some differences attributable to horizontal gene transfer (Stinear et al., 2008; Sparks et al., 2023; Figure 23). While *M. marinum, M. smegmatis,* and *M. tuberculosis* share similarities, there are notable differences in cell wall composition, lipid content, virulence factors, and environmental adaptations, which highlight limitations in their use as model organisms for tuberculosis research. The choice of an appropriate model depends on the specific aspect of mycobacterial biology or pathogenesis under investigation. For example, *M. marinum* lacks the lipid PDIM which plays a role in *M. tuberculosis* virulence (Stinear et al., 2008). Similarly, *M. smegmatis* has functional differences in chain lengths of its mycolic acids and in lipid biosynthetic pathways compared to *M. tuberculosis*, which can affect drug susceptibility studies (Zuber et al., 2008).

Phylogenetic analyses by Stinear et al. (2008) place *M. marinum*, *M. ulcerans*, *M. tuberculosis* and *M. leprae* with *M. smegmatis* in close evolutionary proximity, with *M. smegmatis* being more distantly related (Stinear et al., 2008). Their study suggests that *M. tuberculosis* evolved into a specialist adapted to mammalian hosts via lateral gene transfer, whereas *M. marinum* retained its ability to thrive in a broader ecological niche such as aquatic environments (Stinear

et al., 2008). The close evolutionary relationship among these organisms make them valuable suitable tools for the tuberculosis research, enabling studies that would otherwise be impractical with highly pathogenic *M. tuberculosis*.

1.11 The use of genetic tools to identify new enzymes in TB research

There are many genetic tools that have been applied to study gene function in common model organisms such as *E. coli, Bacillis subtilis* and *Pseudomonas aeruginosa* (Kulasekara, 2014; Freed, 2017; Dempwolff, Sanchez and Kearns, 2020; Vitale et al., 2020; Holden et al., 2021). In contrast, the mycobacterial genetic toolkit has historically lagged behind due to limitations such as inefficiencies in DNA recombination, gene editing, and gene silencing (Rahman et al., 2021; Calvet-Seral et al., 2023; Feng et al., 2023). However, methods such as and one- or two-step allelic exchange using the L5 mycobacteriophage and high-density mutagenesis techniques specific to mycobacterial species have been developed (Hatfull and Sarkis, 1993; Sassetti, Boyd and Rubin, 2003; Griffin et al., 2011; DeJesus et al., 2017). These studies, particularly by Sassetti et al., 2003, Griffin et al., 2011 and DeJesus et al., 2017 laid the groundwork for assigning gene functions in *M. tuberculosis* provided valuable datasets and databases (Sassetti, Boyd and Rubin, 2003; Griffin et al., 2011; DeJesus et al., 2017). Building upon these foundational studies, ever-evolving technologies for researching the pathophysiology of slow-growing, fast-growing, and non-tuberculosis mycobacteria now include advanced, adapted methods. One such method is oligonucleotide-mediated recombineering followed by Bxb1 integrase targeting (ORBIT), which employs two recombination systems: the integration of an oligonucleotide into the chromosome and the use of a payload plasmid containing a selectable marker to facilitate the selection of drug resistant recombinants (Borgers et al., 2019). Other approaches include RNA interference (CRISPRi/Cas9) strategies, where Cas9 protein binds to guide RNA to specifically interrupt to gene of interest, and enhancements to high-density transposon mutagenesis, which enable gene disruption and analysis (Rahman et al., 2021; Feng et al., 2023; Akusobi et al., 2022). More recently, counter-selectable transposons have been designed to unmark mutants and reduce biases introduced by resistance gene markers (Borgers et al., 2020). These tools are particularly effective for generating single and multi-targeted mutants (Borgers et al., 2019). For applications requiring the creation of libraries of random mutants, high-density transposon mutagenesis remains widely utilised (Rahman et al., 2021; Akusobi et al., 2022).

Transposon mutagenesis (*Tn*-mutagenesis) is now broadly applicable to multiple species, accessible, and a low-cost technique for probing gene discovery and function in various conditions for prokaryotes (DeJesus et al., 2017). *Tn*-mutagenesis is based on the principle of random insertion and excision events into integration sites across the bacterial genome by DNA sequences or mobile genetic elements called transposons (DeJesus et al., 2017; Hutchison et al., 2019). A marker attached to the transposon such as a hygromycin or kanamycin resistance gene allows for positive selection and screening of mutants (Saavedra, Schwartzman, and Gilmore, 2017; Dempwolff, Sanchez and Kearns, 2020).

1.11.1 Transposons

The study of mycobacterial peptidoglycan-active enzymes has benefited from many different genetic tools. Transposons were first discovered in corn by Barbara McClintock in the 1950s (McClintock, 1950 & 1953; Pray, 2013). Since that time, transposons have been discovered in all domains of life. In bacteria, they are classified into two groups. The Class I group are non-replicative retrotransposons and carry an insertion sequence at each end. They can cut the double helix at an original site before moving, but in some cases, the cut does not need to occur for the transposon to move (Domingues, da Silva, and Nielsen, 2012). Retrotransposons carry reverse transcriptase and an endonuclease. They begin as DNA, which is then transcribed into RNA. The reverse transcriptase and endonuclease are used to reverse transcribe the RNA back into DNA. This DNA is then inserted back into the chromosome at a new location (Beauregard, Curcio, and Belfort, 2008).

In bacteria, the Class II replication transposons carry elements essential for transposition, including an inverted repeat sequence, transposase, resolvase, and non-essential elements such as genes associated with antibiotic resistance (Blackwell, Iqbal, and Thomson, 2019). Transposons insert themselves semi-randomly into new locations across the genome with insertion biases and recognition for dinucleotide sequences (Behr, Stevenson, and Kapur, 2020). These biases vary depending on the GC content of the genome and therefore species (Choudhery et al., 2021).

Some transposons are active in different species. For example, *Tn10* used for *E. coli* can also integrate into the *M. smegmatis* genome (Bardarov et al., 1997; Rubin et al., 1999). Transposable elements that contain the insertion sequences IS16110 and IS1096 are found in

mycobacterial species such as *M. tuberculosis*, *M. bovis*, and *Mycobacterium africanum*, with IS1096 unique to *M. smegmatis* (Comín, Otal, and Samper, 2022). The insertion sequences are limited to mycobacteria, but they do not have equal activation in all Mycobacterium species (Rubin et al., 1999; Comín, Otal, and Samper, 2022). IS1096 has been shown to insert itself into the *lrs2* gene under the pressure of phage activity at a rate of 7.2 x 10-5 per cell to incur mycobacterial phage resistance (Cirillo et al., 1991; Li et al., 2024). While the IS1610 occurs at a frequency of 7.9 x 10-5 per cell, it is activated during infection of macrophages and acts as a promoter of transcription, contributing to virulence (Gonzalo-Asensio et al., 2018). A caveat to using transposons derived from these insertion sequences is the requirement for a low-abundance integration recognition site comprising 5'-NNPy(A/T)A(A/T)NN-3', making them rather unsuitable for large-scale mutagenesis studies (Behr, Stevenson, and Kapur, 2020). Advancements in the genetic engineering field for creating random insertional mutants have expanded to the use of *Himar1 mariner*-based transposons from organisms such as Drosophila melanogaster and the horn fly *Haematobia irritans* (Gao et al., 2003; Chen et al., 2010). The advantage of these mariner-based transposons is their higher transposition frequency, usability in many species, fewer insertion biases, and a smaller target sequence (5'-TA-3') compared to the elements derived from IS1610 (Gao et al., 2003). This makes them very useful bacterial molecular 'copy and paste' tools, especially in the context of screening for gene essentiality (Gao et al., 2003). The *Tn*-mutagenesis study described below utilised the *Haematobia irritans*-derived mariner-based element *Tn5371* with a hygromycin resistance gene (Chen et al., 2010).

Studies using transposon mutagenesis to study mycobacterial biology include the Riggs-Shute, Falkinham, and Yang (2020) study, who used *tetr*-expressing plasmid to produce a specific strain *M. smegmatis* (VTY123) via hygromycin selection which than accepted a *mycotetOP*^{2} delivery plasmid to be transformed into this strain which identified 13 conditional mutants in Atc-dependent growth conditions, leading to the identification of essential genes in *M. smegmatis* and *M. tuberculosis*. Additionally, and even more relevant to this thesis, is the Akusobi et al. (2022) study that identified a new essential PBP involved in septum formation in *Mycobacterium abscessus* using CRISPRi/Cas9 methods to interrupt target genes of interest in peptidoglycan biosynthesis. They found that deletion of DacB, PBP1, and D,D-CPase (MAB_0519) inhibited growth in *M. abscessus* identifying the importance of these genes in *M. abscessus*. The authors reported that this morphological outcome for homologs was absent and therefore not essential in *M. smegmatis*, indicating distinct genetic networks in each organism.

A previous Birmingham PhD student used transposon mutagenesis to generate mutants in genes involved in cell wall metabolism and synthesis by applying *mariner*-based transposon *Tn5371* delivered by the mycobacteriophage phAE181. This library generated a mutant that was found in the gene *lpqf*, whose predicted product is akin to a D,D-CPase. LpqF is an uncharacterised enzyme, and therefore, taking inspiration from related studies this thesis will focus on and describe the characterisation of LpqF.

Aims and objectives.

Peptidoglycan-targeting enzymes play a crucial role in cell division, elongation, and overall cell survival. In mycobacteria, some of these enzymes, such as D,D-CPases, are not as well characterised. It is essential to study the enzymes that maintain the cell envelope in mycobacteria. Therefore, the aim of this project was to characterise a highly conserved PBP in mycobacteria, known as LpqF (Rv3593) identified through re-screening of the mutagenesis library. The objectives were divided into five smaller aims, as follows:

- **Identify and validate putative cell wall-active enzymes derived from a transposon mutagenesis library:** This aim focused on validating cell wall-active enzymes identified from a mutagenesis library using automated high-throughput pinning and dilution assays.
- **Purify full-length and generate truncated derivatives of LpqF for biochemical study:** This aim involved purifying full-length, generating and cloning N-terminal LpqF constructs to near homogeneity in *E. coli* using techniques such as metal affinity chromatography, sodium dodecyl sulfate-polyacrylamide gel electrophoresis (SDS-PAGE), and size exclusion chromatography.
- **Use a bocillin FL protection assay to assess the binding and inhibition of LpqF by β-lactams:** This aim was to test the affinity of LpqF for against a range of β-lactams by using purified LpqF in the presence of a fluorescent penicillin derivative (bocillin FL).
- **Perform phenotypic screens in *M. marinum* and *M. smegmatis* backgrounds:** This aim involved conducting growth curve and solid media assays with wild-type and Δ*lpqf* constructs to evaluate susceptibility. Additionally, microscopy was performed on *lpqf* and Δ*lpqf* cultures stained with cell wall dyes to study growth dynamics in *M. marinum*.
- **Conduct biochemical assays to determine whether LpqF interacts with peptidoglycan:** This aim involved conducting various biochemical assays to investigate the interaction of LpqF with peptidoglycan derived from *M. smegmatis* and peptidoglycan fragments. Techniques included fluorescent based degradation assays, thin-layer and reverse-phase high-pressure liquid chromatography. Additionally, a new fluorescent peptidoglycan assay was designed, optimised, and applied to test the ability of LpqF to bind to peptidoglycan.

Chapter 2. Methods and materials

For experiments involving *M. smegmatis* or derivatives thereof we used the mc^{2}155 strain (Snapper et al., 1990). For experiments involving *M. marinum* or derivatives thereof we used (1218R, ATCC927). Hereafter any reference to *M. smegmatis* (Δ*lpqf*^{Sm}) and *M. marinum* (Δ*lpqf*^{Mm}) will refer to these strains. See Tables 5 and 5.1 for a complete description of strains and plasmids used in this thesis.

Table 6: Outlines the strains and plasmids that were used in this study.

Organism	Strain	Genotype	Source/Reference
M. smegmatis	mc^{2}155	Parental (wild type strain) strain pTIC-Δ*lpqf*	Snapper et al., (1990)
M. marinum	1218R 12C3	Parental (wild type strain) strain pTIC6a-*lpqf*	ATCC927
E.coli	Top10	*Δ(ara-leu) 7697 araD139 fhuA ΔlacX74 galK16 galE15 e14- ϕ80dlacZΔM15 recA1 relA1 endA1 nupG rpsL (Str^R) rph spoT1 Δ(mrr-hsdRMS-mcrBC)*	NEB (C3019H)
E.coli	SHuffle T7 K12	F′ *lac, pro, lacI^q / Δ(ara-leu)7697 araD139 fhuA2 lacZ::T7 gene1 Δ(phoA)PvuII phoR ahpC* galE (or U) galK λatt::pNEB3-r1-cDsbC* (Spec^R, *lacI^q*) *ΔtrxB rpsL150*(Str^R) *Δgor Δ(malF)3*	NEB (C3026J)

Table 7: Plasmids used in this study

Organism	Strain	Plasmid	Source/Reference
E.coli	Top10 SHuffle T7 K12	pET26SUMORv3593N-terminal	This study
E.coli	Top10 SHuffle T7 K12	pET26SUMORv3593	This study
E.coli	Top10 SHuffle T7 K12	pET26SUMORv3593N-terminal-SDMs (Q104A, D85A, R98A, R87A, R98A;R87A, W56A, W28A, I33A and wildtype	This study

All chemicals and reagents were obtained at analytical or HPLC grade with 99.8-9% purity from Sigma Aldrich unless otherwise stated. MilliQ purified water was used to make all buffers. The pH of solutions was measured using a WPA pH meter CD720 from Hanna Instruments with pH 4, pH 7 and pH 10 buffer standards. For chromatography (gravity flow and fast protein liquid chromatography (FPLC), buffers were filtered prior to use with a 0.2 μm filter and degassed (FPLC).

2.1 Culture media

2.1.1 Lysogeny broth

7.5 g of Lysogeny (LB) granules were dissolved in 300 mL of dH_2O and sterilised by autoclaving at 121 °C for 25 min.

2.1.2 Lysogeny broth agar

11.1 g of LB agar granules were dissolved in 300 mL of dH_2O and sterilised by autoclaving at 121 °C for 25 min.

2.1.3 Middlebrook 7H9 Media

2.35 g of Middlebrook 7H9 broth base powder was dissolved in 450 mL of distilled water (dH_2O). 2 mL of 50% glycerol (0.2% final) and 1.25 mL of 20% Tween 80 (0.05% final) were added. 50 mL (10% final) of either OADC (Oleic Acid, Albumin, Dextrose, Catalase) or ADC (Albumin, Dextrose, Catalase) was added depending on the cultured organism. The final mixture was filter sterilised. 2x 7H9 was prepared as above but with 225 mL of dH_2O instead of 450 mL.

2.1.4 Middlebrook 7H10 Agar

7 g of Middlebrook 7H10 Agar Base was dissolved in 270 mL of dH_2O. 3 mL of 50% glycerol (0.5% final) was added. The mixture was autoclaved at 121 °C for 25 min. Then 30 mL of OADC was added.

2.2 *in silico* analysis

2.2.1 Multiple sequence alignments

A basic alignment was conducted using the Uniprot sequence O06155_MYCTU as the query sequence. O06155_MYCTU was input into the NCBI platform using the ProteinP parameters, selecting the Uniprot/Swissprot sequences database, auto BLOSUM62, and the algorithm BlastP-protein-protein BLAST, with no filters applied.

For the domain and classification analysis, the default parameter was used for specific domain architecture analysis. This produced 250 NTF2 domains, 174 D-alanyl-D-alanine (peptidase S11 IPR001967) domains, and 29 PBP domains. The Uniprot LpqF sequence was submitted to the InterProScan platform to predict homologous domains and motifs from known proteins with sequences similar to the domains found in LpqF (www.ebi.ac.uk, 2023).

For the phylogenetic relationship of *lpqf* among species of *Mycobacterium*, the Rv3593 (O06155_MYCTU) FASTA sequence was input into the Protein BLAST alignment tool (NCBI, 2023), which produced 250 diverse alignments. For simplicity, sequences were filtered to include only Mycobacteriaceae taxonomy (id:1762), trimming down to 87 FASTA sequences that were uploaded to NGPhylogeny.fr using the OneClick setting (Lemoine et al.,

2018). The resulting tree was refined and annotated in the Interactive Tree of Life platform (itol.embl.de) (Letunic and Bork, 2021).

2.2.2 Synteny for *lpqf*

LpqF uniprot sequence (O06155) was submitted to Uniprot and aligned to 250 sequences. This alignment was then submitted to EMBL platform using Clustal Omega to generate sequences with gaps. The sequences were then submitted to the Webflags with the default parameter settings, 4 flanking genes, for the maximum number of sequences (200). This produced a synteny plot for LpqF in mycobacteria. As a comparison LpqF O06155 was submitted to fast.genomics producing 250 alignments for homologues using the setting for diverse and within mycobacteria taxa.

2.2.3 Conservation of motifs and domain analysis

The LpqF sequence was inputted into the Conservfold platform: Protein Conservation to 3D Structure Generator platform using MMSEQ generating alignments with known published PDB files in diverse bacteria (Mirdita et al., 2022; Graham et al., 2023). The output generated a Weblogo plot of 18 highest scoring structurally conserved amino acids and motifs in homologous proteins (Crooks et al., 2004). The PDB files used to construct the conservation plot for analysis are listed in legend of Figure 27. Additionally, the RMSD scores for protein structure files recorded in Table 12 were obtained using ChimeraX 1.6.1 (Meng et al., 2006; Meng et al., 2023) and RSCB database using the analysis and pairwise structural alignment.

2.3 Cloning

2.3.1 Oligonucleotides

DNA oligonucleotides for PCR amplification were designed against the target gene and ordered from Sigma (Merck) and Integrated DNA Technologies (UK), see Table 8.

2.3.2 Polymerase Chain Reaction (PCR)

Q5® 2 x High-Fidelity DNA master mix (NEB) was used according to the manufacturer's instructions to carry out DNA amplification. Unless otherwise stated, a 100 µL mix of reagents was made and divided into four 25 µL aliquots. All PCR reactions were undertaken using an Eppendorf Gradient thermocycler with an annealing temperature optimised according to the primers used (between 55-68 °C).

2.3.3 Restriction free PCR (RF cloning)

RF cloning allows for the insertion of any sequence into any position within any plasmid without the need for restriction enzymes, recognition sites, or homologous recombination sites within these sequences (van den Ent and Löwe, 2006). Using this principle, forward and reverse primers were designed that were 50 base pairs in length. This allowed for 25 base pair overhangs with the start and end of the gene (NTF2 substitutions), flanking the target plasmid (pETSUMORv3593N-terminal), as outlined in Table 8. These primers are used to amplify the insert using high-fidelity PCR conditions (Tables 9 and 10). The PCR product is then purified (see sections 2.4.1-2.4.3) and used as a primer in a secondary PCR reaction (RFP2, see Table 10), with the target plasmid acting as a template. Amplification of the plasmid proceeds in both directions, and the primers in RFP2 act as long single-stranded overhangs. This allows the complementary strands of the plasmid to anneal, forming a nicked hybrid molecule. The controls consisted of template only without any target DNA or target DNA and template but no primers were added in RF1 PCR. DpnI was used to digest any parental/methylated plasmid that may still be present (see section 2.4.4), and the final product was used to identify the presence of an insert via colony PCR and then transformed into competent *E.coli* SHuffle K12 T7 cells (NEB, C3026J) (see section 2.5.2) and selected for using 50 mg/mL of kanamycin.

2.3.4 Preparation of plasmid DNA

The vectors used for LpqF full-length and N-terminal in this study contain a kanamycin-resistant gene for selection. The gene variants of LpqF (Rv3593) - N-terminal ([pET26SUMORv3593N-terminal]) and full-length ([pET26SUMORv3593]) - were cloned into the vectors pET28a and pET26, respectively, prior to the start of this project (see Tables 7

& 7). Vectors were designed with a 6x His-tag followed by a SUMO solubility tag, upstream of the SUMO sequence at the 5' end of *Rv3593*.

Plasmid DNA was extracted from *E. coli* TOP10 beta (NEB, C3019H) cells following transformation and overnight culture using a Qiagen miniprep extraction kit see (sections 2.4.2 and 2.5.2) according to the manufacturer's instructions. After verifying the sequences for the presence of gene products, DNA was transformed into *E. coli* Top10 beta competent cells (NEB, C3019H) for storage or into *E. coli* K12 T7 (NEB, C3026J) competent cells for protein expression and purification (see section 2.5.2, Table 6).

2.3.5 DNA concentration determination

A NanoDrop ND-1000 spectrophotometer (Thermo Scientific) was used to obtain DNA concentrations. The protein settings were selected and set to A280/A555. The extinction coefficient (ε/1000) of the polypeptide sequence along with the molecular weight of the protein was added before testing the sample test. Two μL of protein sample was added to sampling arm after washing with water and blanking with sample storage buffer.

2.4 Site directed mutagenesis and PCR

The selected residues were mutated to alanine the NEB Q5 mutagenesis kit, PCR reaction products were transformed into *E. coli* Top10 beta cells (as described in sections 2.4.2), Plasmids were isolated and extracted using a Qiagen Miniprep kit (see section 2.4.2) and verified by sequencing (MicrobesNG) to confirm the presence of mutants. The resulting proteins were expressed and purified using established procedures as described below.

Primers listed in Table 8 were designed using the NEB base changer http://nebasechanger.neb.com/. Briefly, the N-terminus sequence from LpqF containing the NTF2 was pasted into the NEB basechanger website, using the setting for substitution and the sequence that need to be changed was highlighted and the desired 3 base change in this case alanine (GCG) was inserted into the programme. Output was a set of forward and reverse primers for desired sequence.

Table 8: Primers and melting temperatures (Tm) for site directed mutagenesis of NTF2 domain.

Mutant	Forward primer **5' > 3'**	Tm	Reverse primer **5' > 3'**	Tm	Ta
W28A (732-734 bps)	CAACTCGGACgcgCCGATCGGCG	65°C	AGCATGTCCATGGTCTGTTG	65°C	66°C
W56A (163-165 bps)	GCGCTCTGGgccGATCGCCCGT	65°C	TCCATGGTGGTCTTGACC	64°C	65°C
Q104A (960-963 bps)	CGTCGAAACGgcgGCGCCGTCGA	68°C	TCGAATCGGTCAACCCAG	64°C	65°C
I33A (747-750 bps)	GATCGGCGAGgcgGGCGTTGGCAC	65°C	GGCCAGTCCGAGTTGAGC	68°C	66°C
R98A (942-945 bps)	CTGGGTTGACgcgTTCGACGTCGAAACGC	64°C	CCGTCGTCGTCGGTATGA	67°C	65°C
R87A (909 – 912 bps)	ACAAGACATCgcgATTCATACCGACGACGACGGC	66°C	TGCGCGCCGTAAGAGGAG	71°C	67°C
D85A (903-905 bps)	CGCGCAACAAgcgATCCGCATTC	64°C	CCGTAAGAGGAGATGAGG	61°C	62°C
R98A+R87A (double mutant) (909-912, 942-945 bps)	See above for primers				

All reagents for RF PCR were prepared on ice. These included DNA template and autoclaved milliQ water along with Q5 High-Fidelity 2x master mix, primers, was thawed, placed on ice. For primers a working solution of 100 µM was made, using 1 µL of each primer and 8 µl of water achieving a 200 nM concentration. Reactions were gently mixed before PCR. Reactions mixtures for RF1 (Table 9) and RF2 (Table 10) were made up to a master mix of 150 µL and 100 µL and aliquoted into PCR tubes immediately prior to placing into the PCR machine.
The following reaction was prepared:

Table 9: Reaction mixture for RFP1 PCR

component	**25 µL reaction**	**Final concentration**
Q5 High Fidelity 2x master mix	12.5 µL	1 X
Primers	1.25 µL	200 nM
DNA template	1 µL	10 ng
Water	10 µL	

Table 10: Reaction mixture for RFP2 PCR

component	*33 µL reaction	Final concentration
Q5 High Fidelity 2x master mix	16.6 µL	1 X
RF1 product	1 µL	5 ng
Destination template	0.25 µL	10 ng
Water	14.6 µL	-

*Note: reaction mixtures represent volumes per tube

PCR parameters were as follows:

Table 11: PCR thermocycler parameter settings

Step	Temp	Time
Initial denaturation	98 °C	1 minute
25 cycles: Denaturation Annealing Extension	 98 °C 55-68 °C 72 °C	 30s 30s 5 min
Final extension	72 °C	3 min
Hold	4 °C	

2.4.1 Generic method for Agarose Gel Electrophoresis

PCR products were confirmed by adding 4 µL of product to a 1% w/v agarose gel. The agarose gel was prepared by adding 1 g of agarose powder to 100 mL of 1x TAE Buffer (40 mM Tris-acetate, 2 mM Na_2EDTA). The agarose was dissolved by heating in a microwave. The heated agarose was poured into a mold, and 2.5 µL/100 mL of Midori Green Advance (Nippon Genetics) was mixed in as a DNA dye to visualise the DNA. A gel comb was inserted into the mold, and the gel was allowed to set. Once set, the gel was removed from the mold and placed into a gel tank filled with 1x TAE Buffer. The comb was removed from the gel. DNA samples were mixed with 6x Gel Loading Dye Purple (NEB, B7024S) and loaded into the gel wells along with a well of Quick-Load Purple 1 kb DNA Ladder (NEB, N0552S). The gel was run at 140 V, 400 mA for 40 min. The gel was visualised using a Bio-Rad Gel Dock XR+ UV imager or a blue light box. Bands were excised from the gel using a scalpel for DNA extraction.

2.4.2 Generic method DNA extraction from Agarose Gel

A Qiagen QIAquick Gel Extraction Kit was used to extract DNA from agarose gel. DNA bands excised from the gel were weighed in a tube. Three volumes of QG Buffer (5.5 M guanidine thiocyanate, 20 mM Tris-HCl pH 6.6) were added to one volume of gel (100 mg gel = 100 µL QG Buffer). The tube was agitated until the gel dissolved, and 10 µL of 3 M sodium acetate pH 5 was then added. One volume of isopropanol was subsequently added, and the mixture was applied to a QIAquick column or a Monarch DNA Clean-Up column (NEB, T1034L). The column was centrifuged in a microcentrifuge at 13,000 rpm for 1 minute. The flow-through was discarded, and 500 µL of QG Buffer was applied to the column and centrifuged again. The flow-through was discarded again, and 750 µL of PE Buffer (10 mM Tris-HCl pH 7.5, 80% ethanol) was applied to the column and centrifuged once more. The flow-through was discarded again, and the residual buffer was removed by centrifugation. The column was placed into a 1.5 mL microcentrifuge tube, and 30 µL of EB Buffer (10 mM Tris-HCl pH 8.5) was added. The column was allowed to stand for 1 minute and then centrifuged again to elute the DNA.

2.4.3 Purification of DNA product

DNA produced by PCR was cleaned using a Qiagen QIAquick PCR Purification Kit. Five volumes of PB Buffer (5 M guanidinium chloride, 30% isopropanol) were added to one volume of PCR mix. Sodium acetate pH 5.0 (10 µL) was added, and the mixture was applied to a QIAquick column or a Monarch DNA Clean-Up column (NEB, T1034L). The column was centrifuged in a microcentrifuge at 13,000 rpm for 1 minute. PE Buffer (10 mM Tris-HCl pH 7.5, containing 80% ethanol, 750 µL) was applied to the column and centrifuged again. The flow-through was discarded, and the residual buffer was removed by centrifugation. The column was placed into a 1.5 mL microcentrifuge tube, and 30 µL of EB Buffer (10 mM Tris-HCl pH 8.5) was added. The column was allowed to stand for 1 minute and then centrifuged again to elute the DNA.

2.4.4 Digestion, Ligation and recirculation mixture

Once product was confirmed as present the rest of the sample was used in the next step. From 1 µL of product was added to Kinase Ligase Digestion reaction (KLD) reagent mix (NEB,

M0554S) in the were added in the following volumes listed below and incubated at room temperature for 1-2 h. Mixture was then purified with PCR purification protocol and transformed into *E. coli* SHuffle K12 T7 competent cells (NEB, C3026J).

Component	Volume (µL)
Product	1
T4 ligase buffer	1
T4 ligase	0.75
DpnI	0.5
Polynucleotide kinase	0.75
Water	6

2.5 Electroporation and transformation into competent cells

2.5.1 Electroporation into *M. marinum* competent cells

Competent cells were prepared from *M. marinum* wildtype (1218R) , and 5 µL of Δ*lpqf*^{Mm} were electroporated into 100 µL of wildtype electrocompetent cells containing the construct *lpqf* on a pTIC6a plasmid using settings of 2.5 V, 25 µF, and 1000 Ω. The cells were immediately placed into 7H9 recovery media and then plated onto plates containing 75 µg/mL of hygromycin. Briefly, 5 mL of M. marinum culture was grown at 30 °C in 7H9 containing 0.05% Tween 80 and 10% OADC until the culture reached saturation (6 days). The OD was read, and subcultures were made and grown until an OD_{600nm} of 0.8 was reached. Cultures were then transferred to ice and incubated for 1.5 h. The culture was then transferred to a 50 mL conical tube and centrifuged for 10 min at 4 °C. The supernatant was poured off, and the pellet was resuspended in 2 mL of 10% chilled glycerol. The volume was increased to 20 mL, inverted three times, and centrifuged at 17,000 x g for 10 min at 4 °C. These steps were repeated three times, and the pellet was resuspended in 2 mL of 10% glycerol prior to electroporation. Cells not used were aliquoted and stored at -80 °C for 3-6 months.

2.5.2 Transformation of *E. coli* strains

Commercially purchased competent cells (NEB) (50 µL) were thawed on ice for 10 min prior to use. Then, 2.5 ng of DNA was added to the cells and incubated on ice for 30 min. The cells

were then heat-shocked at 42 °C for 30 seconds using a heat block and subsequently incubated on ice for 5 min. Immediately after, 500 µL of SOC (super optimal broth plus glucose) or LB media was added, and the cells were incubated at 37 °C for 60-90 min with shaking at 180 rpm. In a pre-sterilised environment, 50-100 µL of the transformed cells were plated onto LB-agar plates containing the appropriate antibiotic and incubated at 37 °C overnight in a static incubator.

2.6 Preparation of glycerol stocks

10-20 mL of sterile LB containing the appropriate antibiotic was inoculated with an *E. coli* colony from a fresh transformation and cultured overnight at 37 °C with shaking at 180 rpm. In a pre-sterilised environment, 0.5 mL of culture was mixed with 0.5 mL of sterile 100% (v/v) glycerol in a Corning cryo-vial, frozen in liquid nitrogen, and stored at -80 °C.

2.6.1 Protein expression and harvesting

The use of pET26 plasmid encoding *lpqf*, *ntf2*^{lpqf} and *ntf2* variants was used to aid in protein folding, increases soluble protein concentrations by inducible protein chaperones and enabling the ability to titrate the expression of the gene product LpqF and its variants. Transformed cells were then grown on antibiotic-selective agar. Individual colonies were inoculated and incubated overnight at 37 °C with 180 rpm agitation in a 5 mL volume of LB media with the required antibiotics. Overnight cultures were then used to inoculate 1-litre baffled culture flasks containing LB media supplemented with 25 µg/mL kanamycin and grown at 37 °C with agitation at 180 rpm until an OD_{600nm}: of 0.5-0.6 was achieved. Recombinant protein expression was induced by adding 1 mM Isopropyl-β-D-thiogalactopyranoside (IPTG), followed by incubation at 16 °C for 18 h. Small volume expression trials were conducted to identify optimal induction temperatures and obtain the optimum quantity of recombinant protein. IPTG-induction conditions investigated included 37 °C, 25 °C, 18 °C, and 16 °C for 4 h, and then 16 °C overnight. Cells were pelleted by centrifugation in a Beckman JLA-8.1000 rotor at 20,000 x g, and the resulting cell pellets were transferred to containers and stored at -20 °C.

2.7 Protein purification

$NTF2^{LpqF}$ and full-length LpqF, were purified on an ÄKTA Pure 25 FPLC system using a 1 mL/min HisTrap Fast Flow column (GE Healthcare). Cell pellets were resuspended in a lysis buffer consisting of 25 mM Bis-Tris (pH 8.0, Merck), 50 mM NaCl (pH 8.0, Thermo Scientific), 10 mg/mL lysozyme (Sigma), DNase, 50 µg/mL RNase, and a protease inhibitor tablet (Roche). The pellet and lysis suspension were left to thaw and mix completely at 4 °C for 30 min.

Pellets were then lysed by sonication (Ultrasonic Processor XL) on ice for 6 min (pulsing for 30 seconds on, 40 seconds off). The lysed suspension was centrifuged at 20,000 rpm for 30 min at 4 °C. The lysate was collected from the pellet, filtered through a 0.45 µM filter syringe, and 100 mL of lysate was loaded onto a HisTrap Fast Flow purification column (Cytiva) by FPLC. Fractions were collected at 1 mL/min using a gradient of 0-500 mM imidazole (25 mM Bis-Tris and 50 mM NaCl, pH 8.0). Imidazole washes were obtained using an optimised protocol of 10% increments yielded eluent fractions set to 7%, 17%, 47%, and 100%.

Four microliters of lysate, wash, and 10 µL of the 7%, 17%, 47%, and 100% fractions were taken and loaded into 1x SDS loading dye, then boiled at 95 °C for 10 min. Samples were loaded onto a 15% SDS-PAGE gel and run for 1 h at 180 volts, 60 mA. The ladder used for all gels (Sigma Broad Range) ranged from 10 kDa to 250 kDa.

Protein fractions at 17%, 47%, and 100% were pooled and placed in dialysis tubing with a 3 kDa molecular weight cutoff (MWCO) in buffer (50 mM Bis-Tris, 250 mM NaCl, pH 8.0) and left overnight to remove imidazole salt from the solution (section 2.7.1). Additionally, 50 µL of Ulp protease and 1 mM β-mercaptoethanol (BME) were added to cleave the SUMO tag (since the His-tag is upstream of SUMO, it is also removed in the cleaving process). A 50 µL sample was taken from each protein solution before adding protease to assess cleavage efficiency via gel electrophoresis.

Proteins were then incubated with nickel charged affinity (Ni^{2+}-NTA) resin (Jena Bioscience) beads overnight and run through a gravity column (PD10) to remove cleaved SUMO. Fractions were collected as flow-through (FT), 25 mM, and 500 mM imidazole (25 mM Bis-Tris, 250

mM NaCl, pH 8.0). To assess SUMO cleavage and protein purity, samples from each protein solution were collected and analysed by running on a 15% SDS-PAGE gel at 180 volts, 60 mA. Samples eluted in the FT and 25 mM fractions. If the FT fraction was pure (containing only one band and no presence of the SUMO band), it was concentrated down to 1 mL and stored at -80 °C until further use. If the sample was not pure in the FT fraction, the FT and 25 mM fractions were taken for size exclusion.

For the site directed mutants (SDMs) that were size excluded (see section 2.7.4), fractions were separated into 'peak' and 'shoulder' in 20 mL, 17 mL, 30 mL, and 9.5 mL volumes, respectively. Ten microliters of each sample were taken and assessed for protein via a 15% SDS-PAGE gel. The 'shoulder' fractions not containing protein were discarded, and the 'peak' fractions containing protein were concentrated down to 500 µL and stored at -80 °C.

2.7.1 Buffer exchange and salt removal using dialysis

Four litres of dialysis buffer were prepared and stored at 4 °C. The protein of interest was loaded into washed dialysis tubing (Spectra/Por®3 & Medicell Membranes Ltd, molecular weight cut-off (MWCO) 3.5 and 12-14 kilodaltons), which was then tied off and clamped at both ends. The tubing was placed into 4 litres of chilled buffer and left in the refrigerator for 4 h with gentle mixing. The buffer was then replaced with 4 litres of fresh chilled buffer and left overnight at 4 °C with a magnetic stirring bar on a magnetic stirrer to facilitate buffer exchange. The protein was then removed from the dialysis tubing and transferred into a 50 mL tube (Falcon) .

2.7.2 Concentration of purified protein

Dilute proteins were concentrated using a Millipore centrifugal concentrator. The choice of concentrator depended on the molecular weight of the protein being concentrated, with concentrators having molecular weight cutoffs of 10 or 30 kDa used as appropriate. Large volumes were concentrated in stages using a 4 °C centrifuge (Eppendorf Centrifuge 5810R) at 1,800 x g until the desired protein volumes and concentrations were achieved.

2.7.3 Anion Exchange

A Hi-Trap Q HP anion exchange chromatography column (GE Healthcare) was equilibrated with Buffer A (25 mM Bis-Tris and 10 mM NaCl) connected to an ÄKTA Pure 25 purification system (Cytiva). The desalted protein was then applied to the column, and a gradient from Buffer A to Buffer B (25 mM Bis-Tris and 500 mM NaCl) was started, progressively increasing the concentration of NaCl. The eluate was monitored for ultraviolet absorbance at 280 nm and collected in 1 mL fractions. Fractions with high absorbance were analysed by SDS-PAGE.

2.7.4 Size Exclusion Chromatography

Samples were separated at 4 °C by size using a Superdex 200 column (GE Healthcare) for protein purification. The Superdex 200 column was connected to the ÄKTA 10/100 system (GE Healthcare) and equilibrated overnight in 2 column volumes (CV) of gel filtration buffer (25 mM Bis-Tris, pH 8.0, 250 mM NaCl) at a flow rate of 1 mL/min. Samples were concentrated to 2 mL prior to loading onto the column using a 5 mL injection loop. The column was then eluted at a flow rate of 1 mL/min, and 0.5 mL fractions were collected. Elution of proteins was monitored by a change in absorbance at 280 nm. The column was washed in 5 column volumes of sterile dH_2O and stored in 20% (v/v) ethanol. Protein fractions containing the highest level of purity (as determined by SDS-PAGE, section 2.7.5) were pooled, concentrated and stored at -20 °C.

2.7.5 Sodium Dodecyl Sulphate-Polyacrylamide Gel Electrophoresis

For SDS-PAGE, Mini-Protean TGX Any kD precast gel gels were either purchased from Bio-Rad or made as follows: A polyacrylamide resolving gel was cast in an acrylamide Mini-Protean casting gel kit (Bio-Rad), comprising 12% or 15% acrylamide:bis-acrylamide (37.5:1), 375 mM Tris pH 8.8, and 0.4% (w/v) SDS. Once the resolving gel had set, a stacking gel (6% acrylamide:bis-acrylamide (37.5:1), 125 mM Tris pH 6.8, 0.4% (w/v) SDS) was cast above the resolving gel. Both the stacking and resolving gels were polymerised using 10% (w/v) ammonium persulfate (APS) and *N,N,N',N'*-tetramethylethylenediamine (TEMED). To enable a straight interface between both gels, 97% (v/v) ethanol was pipetted onto the resolving gel while it set. The ethanol was then removed, and the stacking gel was poured. A well-shaped comb was inserted into the unpolymerised stacking gel to create wells of the selected size and number, and the gel was left to set for 20 min. The gels were loaded into a Bio-Rad protein

gel tank. The tank was filled with 1x Tris/Glycine/SDS Buffer (25 mM Tris-HCl, 192 mM glycine, 0.1% SDS), and the sample was loaded into the gel wells.

Protein samples (15 µL) were mixed with 5 µL of protein loading dye (10% SDS, 500 mM dithiothreitol, 50% glycerol, 250 mM Tris-HCl pH 6.8, 0.5% bromophenol blue). The protein samples were heat-denatured by a 10-minute incubation at 95 °C using an Eppendorf Mastercycler Gradient thermocycler. A maximum sample volume of 20 µL was used for the samples and protein molecular weight standards (Blue Pre-stained Protein Standard Broad Range; NEB 5 µL, P7718S, or Page Ruler Plus Pre-stained, Thermo Scientific) and pipetted into SDS-PAGE wells. The casting gels were run at 180 volts (V) once submerged in SDS-PAGE running buffer (25 mM Tris pH 8.3, 190 mM glycine, 0.1% (w/v) SDS). The pre-cast gels were run at 200 V and 50 mA for 35 min. The procedure was concluded once the dye front migrated to the bottom of the gel. After running, the gels were then removed from the plastic outer case, stained overnight in Instant Blue (Expedeon), and then excess stain was removed by soaking in water.

2.8 Transposon mutagenesis library

Contribution statement: In the following experiments Rudi Sullivan supported me in using the S & P Robotics BM3-BC robot to pin mycobacteria onto solid media.

Streak plates containing 23 strains derived from a parent strain *M. marinum* 1218R which was a kind gift from Dr Apoorva Bhatt. Plates were re-streaked on 7H10 agar containing 75 ug/mL of hygromycin except for wildtype. Strains are listed in Table 12 below. Highlighted in red is 12C3 the strain that was found to contain the interrupted gene Rv3593.

Table 12: List of transposon mutagenesis library as labelled in original *Tn* library (Chen., 2010).

Number	**Strain name**
1	3ES
2	14D3
3	5G3
4	13E7
5	16D10
6	3D7
7	13E3
8	9D9
9	16F6
10	12B4
11	10G2
12	11F5
13	6B11
14	8D9
15	9B4
16	6G3
17	7D3
18	10C3
19	1G2
20	10E9
21	8G10
22	12C3
23	WT

Glycerol stocks were made of all 23 strains, and cultures were grown in 7H9 medium supplemented with 0.05% Tween 80, 10% OADC, and 75 µg/mL hygromycin in 10 mL for 4 days until an OD_{600nm} of 0.6 was reached. Cultures were readjusted to an OD_{600nm} of 0.1, and 100 µL was added to 96-well microplates (Greiner, PS, F-bottom, black, sterile. Ref: 655086), used for inoculating source plates for pinning.

Briefly, source plates were prepared by adding 42 mL of 7H9 with 2% agar, with or without 75 µg/mL hygromycin, and left to dry for 30 min at room temperature in a sterile HEPA hood. For strain preparation, 40 mL of culture containing each strain intended for pinning was grown to an OD_{600nm} of 0.8 in 7H9 supplemented with 0.05% Tween 80 and 10% OADC. Each culture

was resuspended to an OD_{600nm} of 0.1, and 200 µL of each starting culture was added to a 96-well plate and placed into the robot. A protocol program was created with the parameters for a 96-well Greiner VWR source plate. The source plates were then placed on the stacker, ready for pinning. Cultures were shaken to resuspend cells before 5 µL of each strain was pinned onto a plate. Plates were pinned in triplicate, and strains were left to grow for 7 days before imaging. Cells were imaged using the colony imaging system with spImager software and an *in situ* camera in the robot.

2.8.1 Microbial growth curves

Ten µL of *M. smegmatis* or *M. marinum* were used to inoculate 20 mL of 7H9 medium supplemented with 0.05% Tween 80 and 10% OADC until an OD_{600nm} of 0.6 was reached. Cell suspensions were then diluted to an OD_{600nm} of 0.01 and used to inoculate 5 mL of fresh media in 20 mL sterile Hungate test tubes containing glass beads to prevent clumping. Along with a blank control (7H9 media only), the tubes were placed into a MicrobeMeter v 1.0 (Sasidharan et al., 2018) where cells were automatically read at a sampling rate of 31372.55 Hz. Cells were allowed to grow for 6 days for *M. marinum* and 3 days for *M. smegmatis*. The conversion factor provided by the manufacturer was used to calculate OD readings. Briefly, turbidity calculation was based on the ratios of each measurement from each test tube versus the blank value. The -log of the ratios was calculated, and path-length was corrected by multiplying by 1/1.6 (1.6 cm being the inner diameter of the Hungate tube).

Antibiotics used in the *M. smegmatis* growth curve were in the volumes and concentrations described in Chapter 7. Rifampicin and chloramphenicol were a gift from Dr. Rudi Sullivan.

2.9 Microscopy (confocal and phase contrast)

3-[7-Hydroxycoumarin]-carboxamide-D-alanine (HADA) and 3-[7-nitrobenzofurazan]-carboxamide-D-alanine (NADA) were purchased from TOCRIS (UK). Ten mL of *M. marinum* cultures were grown to an OD_{600nm} of 0.6, adjusted to an OD of 0.01, then aliquoted into 0.5 mL volumes and grown for 6 h at 30 °C with shaking at 180 rpm. The ODs were measured and adjusted to 0.01. At this point, 500 µM HADA was added, and the cultures were grown for an additional 6 h (one generation time).

Cells were then washed at 17,709 x g with 7H9 with 0.05% Tween80 and 25 μM NADA was added. The cells were incubated for 16 h under the same conditions. After incubation, the cells were washed twice with 7H9 supplemented with 0.05% Tween80. They were then centrifuged at 1,200 rpm for 2 min, and the pellets were resuspended in 1x PBS supplemented with 0.05% Tween80.

Ten μL of supernatant from each strain containing separated cells was added to a 1% w/v agarose pad, left to dry for 5 min, and then covered with a cover slip. Slides were examined using an epifluorescence microscope with Zeiss Black software settings for FDAA. The fluorescence parameters were the excitation/emission filters λ for HADA, 405 nm/450 nm: for NADA, 450 nm/555 nm, along with phase contrast. Each slide contained 600-800 cells, with 10-20 cells per area. Images were acquired based on these parameters.

Images were processed using the FIJI plugin MicrobeJ (Ducret, Quardokus and Brun, 2016) to collect length, width, and maxima values for each cell. The files were colourised and auto scaled. Length values were set from 1 μm to maximum, width from 0.3 to 1 μm for rod-shaped cells. Maxima were assessed as follows: HADA foci (length 1 μm to maximum, width 0.3 to 7 μm), NADA filament (length 1 μm to maximum, width 0.3 to 7 μm, smooth). The collected data were collated and quantified using Prism 9.

2.10 Biochemistry

2.10.1 Bocillin fluorescence assay

Purified protein (5 μM) was incubated with or without β-lactam antibiotic (Table 13) for 60 min and 18 h at 25 °C. The protein reaction was then labelled by addition of 25 μM of Bocillin_FL (Invitrogen, 1809310), to each sample and incubated for 30 min before quenching the reaction with 1x SDS loading dye and boiling the sample for 10 min at 65 °C (samples were boiled at 65 °C to prevent degradation of the protein-β-lactam binding complex in the reaction mixture). Samples were then loaded onto 15% polyacrylamide gel SDS-PAGE gels and run for 1.5 h at 180 V, 200 ma. Quantitation of band density was obtained using Image Lab platform and normalising the bands to control sample (untreated). Coomassie gels were used as a

reference for loading control. Assays were run in triplicate, n = 3. Protein to Bocillin_FL, 1:5 ratio. Bocillin fluorescence was analysed using the BioRad ChemiDoc imaging system, SYBR® Green DNA setting.

Table 13: A list of β-lactam antibiotic used in the fluorescence assay

B-lactam	Class	Reference
meropenem	Carbapenems	TCI M2279
doripenem		Sigma 32138
imipenem		Acros Organics (USA) A0410734
nitrocefin	cephalosporins	Acros Organics (USA) B6052
cefsulodin		Cayman 14227
cephalothin		Sigma C4520
penicillin G	penicillins	Alfa Aesar J63032
amoxicillin		A054
oxacillin		Sigma 28221
mecillinam		Alfa Aesar J66774
piperacillin		Alfa Aesar J66143
cloxacillin		Alfa Aesar J64314
aztreonam	monobactam	Acros Organic A03532118

2.10.2 Cephalosporinase assay using nitrocefin as a substrate

To evaluate the serine β-lactamase activity of LpqF, 5, 10, 18, and 36 µM concentrations of the protein (LpqF) and a control (penicillinase) were added to 1 mg/mL nitrocefin (Acros Organics). A dilution series of the enzyme was prepared in buffers with the following conditions: citrate (pH 5.4), phosphate (pH 6.5), and Bis-Tris (pH 8.0), with concentrations ranging from 0.3, 0.5, 1, 2, 4, 9, 18, and 36 µM, at a final volume of 100 µL. All reaction series were kept on ice until ready to be added to wells containing the substrate. Reactions were then carried out at 25 °C in a 96-well plate.

The nitrocefin substrate and the enzyme dilution series were set up in the plate prior to adding the enzyme to the substrate. The enzyme was added to nitrocefin, mixed, and the plate was immediately read in a plate reader at an absorbance (OD) of 486 nm, with readings taken every 30 seconds for 60 min. Measurements were taken using a Mars microplate reader (BMG Labtech), with excitation/emission filter λ; 488 nm and 530 nm. Kinetic analysis was performed using Prism 9. Reactions were performed in triplicate for each condition.

2.10.3 Purification of peptidoglycan

Purification of peptidoglycan from *M. smegmatis* was achieved following established protocols (Shenderov et al., 2013; Moynihan group). Eight litres of *M. smegmatis* were grown with aeration at 37 ℃ to mid-exponential phase (OD_{600nm}: ~0.6), at which point they were harvested by centrifugation, resuspended in a minimal volume of PBS, and lysed by sonication. The resulting lysate was treated with 4% SDS and boiled under reflux for 3 h. The insoluble material was collected by centrifugation and washed with water until the SDS was completely removed (at least seven washes), yielding mAGP. The mAGP was incubated for 4 days in 0.5% (w/v) KOH in methanol at 37 °C before being washed three times with methanol. The mycolic acids were extracted with three washes of diethyl ether. The phosphodiester linkage in the arabinogalactan-peptidoglycan complex was cleaved using 0.2 M H_2SO_4, and the peptidoglycan was separated from the solubilised arabinogalactan by centrifugation. Then Na_2CO_3 was added to peptidoglycan as a neutralisation step and washed with water three times. The insoluble peptidoglycan pellet (250 mgs) was sequentially digested with α-amylase (100 µg/mL), DNase (10 µg/mL), and RNase (5 µg/mL) for 8 h, followed by proteinase K (100 µg/mL) digestion overnight at 37 °C. The peptidoglycan pellet was resuspended in a minimal volume of 1% SDS and boiled under reflux for 3 h. Afterward, the SDS was removed by centrifugation and washing with water (at least seven times). The resulting material was lyophilised and stored at -20 °C until needed. Digestion and quantitation of this material were carried out as described above.

2.10.4 Degradation assay using FITC

For peptidoglycan conjugated to fluorescein-5-Isothiocyanate (PG-FITC) dye the assay was conducted as previously reported with some modifications (Moynihan et al., 2019). Briefly,

lyophilized peptidoglycan is mixed with FITC powder (Sigma) at a 2:1 ratio. Then, 4 mL of 0.5 M sodium carbonate was added, and the PG-FITC mixture was stirred at 37 °C overnight. Unreacted FITC is washed out with sodium bicarbonate buffer (0.5 M), followed by centrifugation and resuspension in filter-sterile dH_2O. Washing continued until the water was no longer yellow. The sample was tested for reduced fluorescence background using a microplate reader with absorbance/emission λ of 490 nm and 520 nm.

The mixture was washed with ethanol to remove any remaining unbound FITC, followed by washing with acetone (with centrifugation at 4,000 rpm for 10 min). After discarding the acetone, the PG-FITC conjugate was left overnight in the fume cupboard to evaporate remaining acetone. PG-FITC was used immediately or stored at 4 °C for up to one week.

For the assay, purified protein (5 µM) in phosphate buffer (pH 6.0) and Bis-Tris buffer (pH 8.0) was incubated with 5 mg/mL of sonicated peptidoglycan-FITC conjugate for 1 to 18 h with shaking at 1,200 rpm at 4 °C, in a final volume of 100 µL. The samples were then filtered with a 0.22 µm filter to separate the undigested peptidoglycan from the supernatant. Fifty µL of supernatant was added to each well of a black flat-bottomed 96-well plate (Greiner, 96-well, PS, F-bottom, black, sterile; Ref: 655086). To ensure consistent fluorescence, 50 µL of NaOH (0.5 M) was added to 50 µL of supernatant and mixed thoroughly. Plates were read at excitation/emission filter λ; 490 nm and 520 nm using a ClarioStar microplate reader (BMG Labtech) and Mars software, with the gain adjusted to the highest fluorescence well (set at 90% threshold) to minimise background noise. Quantitation of readout values is performed using Prism 9. Reactions were performed in triplicate for each condition (n = 3).

2.10.5 Sample preparation and RP-HPLC

Optimisation of peptidoglycan degradation was carried out before analysing with LpqF (5 µM) enzymatic hydrolysis of *M. smegmatis*-derived peptidoglycan.

Five mg/mL of peptidoglycan was incubated with 43 µM mutanolysin (Sigma, M9901) for 18 h at 37 °C in 25 mM phosphate buffer, pH 6.5. The samples were then pelleted and subjected to a double digest by resuspending in phosphate buffer at pH 6.0 with the addition of lysozyme (Sigma, L3790) or mutanolysin (25 mM phosphate buffer, pH 6.5). The pellets were washed,

and the supernatants were reduced with 0.5 M sodium borohydride (pH 9.0) and quenched with 20% phosphoric acid, which lowered the pH of the samples to 3.5. The supernatants were then washed to remove any debris and analysed via reverse phase high performance liquid chromatography (RP-HPLC). HPLC separation was achieved using a Dionex UltiMate 3000 uHPLC (Thermo Scientific,) with a constant flow rate of 0.200 mL/min using a Phenomenex 150 x 2.1 mm C18 column with a 1.7 μm particle size containing 100 Å pores. Solvents were degassed and comprised: Solvent A, formic acid (0.1%) in acetonitrile, and Solvent B, formic acid (0.1%) in HPLC-grade dH_2O.

The column was equilibrated with Buffer A at 99% for 20 min, then Buffer A was reduced to 1% while Buffer B was increased to 99% for 20 min. Analytes were monitored for ultraviolet absorbance at 210 nm. Chromatograms were obtained using Chromeleon™ (Thermo Scientific) software.

2.10.6 Thin Layer Chromatography

LpqF was incubated with or without pentapeptide (Sigma), D-alanine (Sigma) and D-alanine-D-alanine (Sigma), in 100 μL of phosphate buffer (pH 7.0) for 18 h at 25 °C with agitation. Controls included D-alanine-D-alanine, D-alanine, and pentapeptide. After incubation, the samples were centrifuged, and the supernatants were collected, lyophilised, and resuspended in 25 mM phosphate buffer, pH 7.0.

TLC silica gel plates (Merck, 60 F254) were marked with a pencil at the origin, 2.5 cm from the bottom of the plate and 1.5 cm from the side, to ensure evenly separated samples. The TLC plates were heated to 60 °C for 30 min before use. A total of 10 μL of each sample was spotted (using aliquots of 1 μL, allowing each spot to dry before applying the next) onto the silica gel plate. The plate was then placed into a pre-equilibrated closed tank at room temperature containing 1 cm depth of mobile phase solvent (1-n-butanol-methanol-ammonium hydroxide-dH_2O, 5:4:2:1 v/v).

The plate was left for approximately 45-60 min until the solvent front reached about 1.5 cm from the top of the plate. To visualise the separated species, the plates were stained with 1.5%

ninhydrin and scanned immediately using ImageDoc (Bio-Rad). For preparation of samples for PG-FITC TLC except for filtration see section 2.10.4.

2.10.7 Peptidoglycan binding assay

2.10.7.1 Classical SDS-PAGE peptidoglycan binding assay

Purified protein (5 µM) was mixed with phosphate buffer (25 mM, with added salt) and incubated with 1 mg/mL of polymerised *M. smegmatis* peptidoglycan for 1 h on ice. For a negative control, protein without peptidoglycan was treated in the same manner as the samples with peptidoglycan throughout the assay process. The equivalent amount of protein, minus peptidoglycan, was used as a loading control and labelled as "load."

The samples were then centrifuged for 10 min (5 min at high speed, followed by 5 min at low speed) at 103,100 x g and 4 °C. The supernatant was carefully removed without disturbing the pellet and transferred to fresh Eppendorf tubes, then stored on ice until analysis; this fraction was labelled "unbound" (UB). The pellet was resuspended in 150 µL of cold buffer, and the centrifugation step was repeated. The supernatant from this step was collected and labelled "wash 1" (W1). This process was repeated until the supernatant from wash 2 (W2) was collected. The pellet was then resuspended in 150 µL of 1x SDS.

Ten µL of the "load" sample and each of the supernatants (UB, W1, and W2) were mixed with 5 µL of 5x SDS. The samples were then loaded onto a 15% SDS-PAGE gels (section 2.7.5). All samples were analysed in triplicate, and the bands were quantified using Image Lab software by normalising the samples to the loading control. Reactions were performed in triplicate for each condition (n = 3).

2.10.7.2 NHS-Rhodamine adapted peptidoglycan binding assay

NHS-rhodamine was first conjugated to wheat germ agglutinin (WGA) using the protocol provided by Sigma and previous studies involving NHS-rhodamine-WGA. The amount of NHS-rhodamine needed was calculated using the conversion factor for the probe (Sigma)

before adding it to 1 mg/mL of WGA or $NTF2^{LpqF}$ and SDMs. Briefly, NHS-rhodamine (Sigma) was resuspended in DMSO to a concentration of 25 mg/mL to make a stock solution. Forty µL of this stock solution were then diluted with 60 µL of DMSO to make a 10 mg/mL working solution.

Purified $NTF2^{LpqF}$ and SDM variants were dialysed in 1x PBS (25 mM, pH 7.3) and adjusted to a concentration of 1 mg/mL. Forty-six microliters of the 10 mg/mL NHS-rhodamine solution were added to the proteins. For the positive control, 6 µL of NHS-rhodamine was added to 1 mg/mL of WGA (in 1x PBS, 25 mM + 0.5 mM $CalC_2$, pH 7.3). The negative control with WGA was treated under the same conditions, but with $CalC_2$ replaced by 10 mM EDTA.

All protein conjugates were incubated for 2 h at 4 °C with periodic agitation. Excess NHS-rhodamine was quenched with the addition of 1M Tris pH 8.0. NHS-rhodamine-conjugated proteins were either dialysed overnight in 1x PBS or passed through a Sephadex desalting column to remove excess rhodamine. In the case of dialysis, the NHS-rhodamine and protein conjugate were dialysed in 4,000 mL of 1x PBS overnight for 4 days, with the buffer changed daily. On the fourth day, conjugates were transferred to 3 kDa MWCO Amicon filters, 10 mL of 1x PBS was added, and the remaining free NHS-rhodamine was removed.

One hundred µL of the eluate were placed in a 96-well flat-bottomed plate (Greiner, 96-well, PS, F-bottom, black, sterile; Ref: 655086), and fluorescence was read using a plate reader with the gain adjusted to minimise background noise. If the readout was in the low 100s, the A280 and concentration of conjugates were measured on a nanodrop, and the A555 was read using 100 µL of each conjugate. This information was used to calculate the degree of labelling (DOL) using the correction factor for rhodamine (0.3400) and the extinction coefficient (ε = 80,000 M^{-1} cm^{-1}).

$$\frac{\text{Amax} = \text{A555 x molecular weight (WGA)}}{\text{WGA x } \varepsilon\text{dye}}$$

The next stage involved using the conjugates in a similar manner to the SDS-PAGE version of the peptidoglycan assay. However, after the washes, the samples were read in a 500 µL volume in a 96-well flat-bottom plate (Greiner, 96-well, PS, F-bottom, black, sterile; Ref: 655086) using a plate reader (Mars microplate, BMG Labtech) with fluorescence parameters set to

absorbance/emission filter λ; 550 nm and 605 nm, and gain adjusted to 80% threshold. To corroborate the assay, 50 µL of the remaining volume from each conjugate was mixed with 1x SDS dye, loaded onto 15% SDS-PAGE gels, and visualised using a Cytiva Typhoon scanner. Quantitation and analysis of the raw data were performed using Prism 10.

To calculate the binding of the bound sample, the values for unbound (from the first wash after loading) and all wash samples were subtracted from the total load value. This process was repeated for protein-only samples. The resulting value was then subtracted from the protein plus peptidoglycan samples to obtain the final bound value. Data analysis for both methods involved normalizing the samples to the load control. The percent bound was calculated by taking the load (L) minus the unbound (UB) plus the washes 1 (W1) and 2 (W2), using the formula: percent bound (b) = (L - UB + W1 + W2) / L × 100%.

Chapter 3. Identification and bioinformatic analysis of LpqF

3.0 Introduction

This thesis focused on the characterisation of *lpqf* (Rv3593 in *M. tuberculosis* and MAR_5092 in *M. marinum*, see sections 3.1.3 and 3.1.5), a gene identified from an old mutagenesis library containing genes involved in cell wall metabolism (Chen et al., 2010). *lpqf* is an unclassified gene, automatically categorised as potentially belonging to the S11 family of peptidoglycan-active enzymes. It contains a C-terminal PBP/transpeptidase/D,D-CPase/β-lactamase domain and an N-terminal domain of also of unknown function, which is homologous to an NTF2-like/ORF12 (Cpe) domain from the clavulanic acid biosynthetic cluster from *Streptomyces clavuligerus* (UniProt ID O06155_MYCTU; Valegård et al., 2013). The rationale for focusing on *lpqf* stemmed from the re-screening of the mutants from this library to identify genes potentially involved in peptidoglycan biogenesis and degradation.

The unique mechanisms by which peptidoglycan is synthesised, ligated, and hydrolysed result in a highly complex structure in Actinomycetes. This complexity depends on species-specific enzymes, many of which remain unknown or uncharacterised in pathogenic mycobacteria (Baranowski et al., 2018). These enzymes broadly include the low molecular weight PBPs, which are involved in peptidoglycan remodelling. While this structural class may serve several functions, most are likely responsible for cleaving the peptide stems in peptidoglycan (Sauvage et al., 2008). Mycobacteria have 60% more 3,3 cross-links than *E. coli* during the exponential phase, highlighting the vital role of D,D-CPases in regulating cell elongation and division (Pandey et al., 2017; Baranowski et al., 2018; Aliashkevich & Cava, 2021).

Previous studies have shown abnormalities in double or multiple carboxypeptidase mutants in various species, including model organisms like *B. subtilis*, *E. coli*, and *M. smegmatis* (Popham, Gilmore, & Setlow, 1999; Peters et al., 2016; Pandey et al., 2018). For instance, Pandey et al. (2018) generated single and double mutants of MSMEG_2433 and MSMEG_2432 in an *M. smegmatis* mc^2155 background, both enzymes belonging to the S11 class of peptidases. The double mutant exhibited significant growth anomalies, including a 16% growth defect in liquid culture compared to the wildtype, an increase in 3,4 cross-links, and an elongated cell phenotype (Pandey et al., 2018). Furthermore, a study by Bansal et al. (2015) found that MSMEG_2433 exhibits dual D,D-CPase and β-lactamase activity. Recent investigations have elucidated the mechanism by which D,D-CPases reach the stem peptide,

revealing that it is facilitated by a second domain containing a nuclear transport factor-like 2 domain (NTF2) (Lin et al., 2021; Banks et al., 2022). NTF2 domains in peptidoglycan-targeting enzymes will be discussed in the following section.

Overall, D,D-CPases are functionally redundant in most bacteria, with multiple enzymes compensating for the loss of others in maintaining peptidoglycan integrity and resistance to cell wall-targeting antibiotics. This redundancy may lead to phenotypic abnormalities without causing lysis. This underscores the role D,D-CPases play in β-lactam resistance, normal growth, peptidoglycan synthesis and elongation under different conditions.

NTF2-fold proteins are ubiquitous in bacteria, fungi, plants, and mammals (Eberhardt et al., 2013). These folds exhibit high conservation and are characterised by a cone-like shape with a hydrophobic cavity inside, which accommodates various molecular cargoes to facilitate diverse processes (Nagata et al., 2001). In mammalian cells, NTF2 originally named for its role in nuclear transport, was first identified in *Rattus norvegicus* (Bullock et al., 1996). NTF2 interacts with Ran, a molecular switch that cycles between inactive GDP-bound and active GTP-bound states, shuttling between the cytoplasm and nucleus (Lu et al., 2022). Ran binds to the importin α/ß transport complex, crucial for transporting cargo into and out of the nucleus (Lu et al., 2022). NTF2 acts as an entry and stability receptor, facilitating the entry of Ran into the nucleus (Smith, Brownawell, & Macara, 1998; Ribbeck, 1997), and serves as a dissociation inhibitor from Ran by maintaining the inactive GDP-bound state (Yamada et al., 1998). Additionally, in mammals, NTF2 proteins play distinct roles, such as regulating calmodulin-dependent protein kinase (CaMKIIa), crucial for synaptic strength in *Rattus norvegicus* (Myers et al., 2017).

NTF2-like proteins exhibit a wide range of activities, including facilitating protein transport to the nuclear envelope, signal transduction, transcription, translation, stress response, and cell cycle control mechanisms (Steggerda, Black, & Paschal, 2000). Ran, highly conserved in plants and mammals, results in similar binding affinities with homologous NTF2 proteins (Zhao et al., 2006). Studies by Zhao et al. (2006) have demonstrated that orthologs of NTF2 in *Arabidopsis thaliana* can rescue mutants in *Saccharomyces cerevisiae*. Furthermore, Reuper, Amari, and Krenz (2021) investigated the acquisition of NTF2 domain of GB31, a Ras GTPase-activating protein by the Turnip Mosaic virus to facilitate viral RNA transcription machinery. This mechanism mirrors pathways observed in orthologs for NTF2 in humans and Semi-Lekki virus infection (Panas et al., 2012; Panas, Ahola and McInerney, 2014; Panas et al., 2015).

Notably, a study by Mahamaya Biswal, Lu, & Song (2023) indicates that Sars-Cov2 targets the NTF2 domain of GB31. These studies, among others, underscore the high conservation of the NTF2-like family and its vital role in cell viability.

Narrowing the focus to bacterial cell wall-active proteins, NTF2-like domains are widely distributed among peptidoglycan (PG)-targeting enzymes, including PBP2a (MecA) from *Staphylococcus aureus*, PBP5 from *Streptococcus faecium*, and the L,D-CPase Pgp2 from *Campylobacter jejuni*, *Helicobacter pylori* (Csd6), and *Bdellovibrio bacteriovorus* (Hyoun Woo Kim et al., 2015; Lin et al., 2021; Banks et al., 2022). In bacterial systems, similar to their mammalian and eukaryotic counterparts, these NTF2-like domains are critical for protein-ligand interactions, enzyme regulation, and spatial positioning necessary for cell wall maintenance and cell division (Eberhardt et al., 2013).

Studies have demonstrated that NTF2-like folds in these proteins play a critical role in maintaining cell shape by positioning the PBP domains of cell wall proteins to effectively reach their substrates (See Chapter 6, Sections 6.0 and 6.1) (Hyoun Woo Kim et al., 2015; Lin et al., 2021; Banks et al., 2022). For example, Banks et al. (2022) showed that the NTF2-fold located in the C-terminus of Bd1075 facilitates the enzymes translocation to the outer convex surface of *B. bacteriovorus*. This positioning enables access to the substrate, a peptidoglycan tetrapeptide, and the subsequent removal of D-alanine to form a tripeptide. This process is essential for maintaining cell curvature, which is crucial for the successful invasion of prey cells. Using single-cell time-lapse microscopy, Banks et al. (2022) demonstrated that mutants lacking L,D-CTPase activty exhibited significantly slower invasion of predator cells, highlighting the importance of cell shape maintenance for the virulence of *B. bacteriovorus* (Banks et al., 2022).

Structurally similar proteins with an NTF2-like fold, such as Pgp2 and Csd6, are also involved in binding to peptidoglycan and localising the L,D-CPase domains. Lin et al. (2021) found that the binding pocket in the NTF2 fold is crucial for Pgp2's interaction with peptidoglycan, as demonstrated by a *Campylobacter jejuni* Δ*pgp2* pulldown assay. Specifically, the mutation of lysine 307 (K307A) within in the NTF2-like fold of Pgp2, abolished its presence in the pulldown assay, indicating that both the NTF2-fold and K307 are essential for peptidoglycan binding and localisation function of the L,D-CPase and K307 is important for binding (See Chapter 6, Section 6.0; Lin et al., 2021). These findings align with the Banks et al. (2022), who reported that deletion of residues in the NTF2 binding pocket led to a partial helical shape in

B. bacteriovorus. Similarly, Houn-Sook Kim et al. (2015) demonstrated that Csd6 contains a deep pocket for peptidoglycan binding, enabling the localisation of L,D-CPase to access tetrapeptides. Collectively, these studies suggest that the NTF2-like domain is critical for the function of peptidoglycan binding enzymes irrespective of their specific roles. The following section will detail the characterisation of LpqF, a novel peptidoglycan-targeting enzyme in mycobacteria.

3.1 An archived *Tn* library contains putative cell wall enzymes identified as having altered colony morphology in *M. marinum*

3.1.1 phAE181 as a delivery system

A previous study investigating cell wall metabolism in mycobacteria utilised *Tn*-mutagenesis in *M. marinum* 1218R and *M. smegmatis* mc^2155. In this study, Chen and colleagues developed *Tn5371* mutant libraries to identify genes when disrupted the bacteria have altered colony morphology (Chen et al., 2010). The *Tn*-mutagenesis method employed the recombinant phage phAE181, a derivative of the temperature-sensitive TM4 lytic bacteriophage, which carries the mariner-based transposon, *Tn5371* (Chen et al., 2010; Kriakov, Lee, & Jacobs, 2003). This phage can infect both fast and slow growing Mycobacteria, including *M. smegmatis*, *M. marinum* and *M. tuberculosis* (Rubin et al., 1999; Chen et al., 2010).

The temperature sensitivity of phAE181 is due to mutations in genes essential for replication, which render its replication machinery sensitive to higher temperatures. At the permissive at the permissive temperature of 30 °C, phAE181 can replicate within mycobacterial cells and grow, but at the non-permissive temperature of 37 °C, it cannot fully complete its replication cycle, leading to lysis. This property enables the *Tn5371* transposon, which contains a hygromycin resistance gene, to insert into the mycobacterial genome during infection at 37 °C, facilitating the selection of mutants on hygromycin-containing plates at this temperature (Bardarov et al., 1997; Rubin et al., 1999; Sassetti, Boyd, & Rubin, 2001).

Isolated genomic DNA from a *Tn*-mutant containing the *Tn5371* transposon can be digested with a restriction enzyme that does not cut site within the *Tn5371* sequence. This ensures that the *Tn5371* element remains intact in the resulting fragments. After digestion, the DNA fragments are ligated under conditions that promote re-circularisation of fragments containing the intact *Tn5371* element. The ligated DNA can then be transformed into *E. coli* cells, allowing

for replication and selection of the circularised DNA fragments containing *Tn5371* on hygromycin-containing plates to isolate colonies (Kriakov, Lee, & Jacobs, 2003). The following section will describe a library of mutants (*Tn*-library) derived from *Tn5371*-based transposon mutagenesis in *M. marinum* and *M. smegmatis* backgrounds, with a particular focus on uncharacterised *M. marinum* mutants exhibiting altered colony morphology.

3.1.2 Experimental aim

One of the primary aims of this thesis was to validate the colony morphology defects identified in the original study led by Dr. Apoorva Bhatt at the University of Birmingham, conducted in 2010. Unfortunately, the original image files depicting the mutant morphologies could not be located. However, the archived *Tn*-library containing 22 *M. marinum* 1218R strains, identified in the study as involved in cell wall metabolism, was obtained from Dr. Apoorva Bhatt. This facilitated a reinvestigation into altered morphologies for genes implicated in peptidoglycan (PG) homeostasis (Chen et al., 2010, Table 14).

Chen et al. (2010) isolated a total of 1,675 hygromycin-resistant colonies: 715 from the *M. smegmatis* (mc^2155) background and 960 from the *M. marinum* (1218R) background. For library coverage and sequencing details, refer to Chen et al. (2010). Briefly, cultures of *M. marinum* or *M. smegmatis* were grown to the late exponential phase and inoculated with high-titre lysate at 10^{10} and 10^{11} pfu/mL, at a multiplicity of 10. The cells were incubated overnight at 37 °C, as previously discussed, and then plated onto TSB agar (for *M. smegmatis*) and 7H9 agar (for *M. marinum*) containing hygromycin. Plasmids isolated from the colonies were sequenced using primers designed for *Tn5371* flanking regions. Sequencing results were analysed by aligning fragments with the BLAST and Xbase databases (Chen et al., 2010). In total, 8 mutants with altered morphology were identified in the *M. smegmatis* library, and 22 in the *M. marinum* library. In *M. smegmatis*, two transposon insertions were located in genes related to cell-wall genes: MSMEG_0031, a penicillin-binding protein (*pbpa*), and MSMEG_0035 (FhaA), a substrate for the serine/threonine kinase PknB (Roumestand et al., 2011; Arora et al., 2018). These two genes are part of the same operon and are linked to peptidoglycan synthesis and cell wall division (Arora et al., 2018). Additionally, the *M. smegmatis Tn*-library revealed four genes indirectly involved in cell wall synthesis and metabolism, along with two uncharacterised genes (Chen et al., 2010; Table 14). Given that

only 8 mutants were identified in the *M. smegmatis Tn*-library, of which 6 have been characterised, the subsequent efforts focused on the *M. marinum Tn*-library.

The *M. marinum Tn*-library identified 22 genes, 17 of which had indirect links to cell wall and lipid synthesis (Chen et al., 2010; Table 14). Among these, genes encoding ESX-1 secreted proteins EspF and EspB were notable (7D3, 9B4 & 10C3). ESX secretion proteins have been demonstrated to be crucial for successful entry into macrophages, dissemination, and host cell lysis, as well as phagosome damage during infection (Chen et al., 2010; Cronin et al., 2022).

Five genes in the *M. marinum Tn*-library were found to have insertions in cell wall-related genes: MMAR_2327, MMAR_2352, MMAR_2913, MMAR_3250, and MMAR_5092. MMAR_2327, homologous to Rv1508c in *M. tuberculosis*, encodes a predicted glycosyltransferase with 99.7% sequence conservation across *M. tuberculosis* strains. It is located in the region of difference (RD) 4, part of a genomic region characterised by unique gene insertions and deletions (RD1-4). Notably, RD1 is associated with virulence genes, while RD4 includes genes involved in the synthesis of acyl trehalose-containing glycolipids (Brodin et al., 2010; Qin et al., 2013). MMAR_2352 encodes an unclassified transmembrane protein implicated in lipo-oligosaccharide biosynthesis. Its homologue, Rv1517 in *M. tuberculosis*, has been linked to biosynthetic pathways (Seeliger et al., 2012). MMAR_2913 encodes BetP, an integral glycine betaine transport protein. Its homologue in *M. tuberculosis*, Rv0917, is known to be upregulated during nutrient depletion, suggesting a role in stress response (Betts et al., 2002; Chen et al., 2017). MMAR_3250 is orthologous to Rv2206 in *M. tuberculosis* and is a component of the Type VII protein secretion system. This system contributes to bacterial survival within in macrophages during infection, highlighting its importance in pathogenicity (MacGurn and Cox, 2007; Weerdenburg et al., 2015; Ates, Houben & Bitter, 2015).

Since the study by Chen et al. (2010), subsequent research by Perkowski et al. (2017) identified Rv1517 and Rv1508c as part of a repertoire of exported proteins essential for both *in vitro* and *in vivo* infection models. Furthermore, the *Tn*-mutant for Rv1508c severely impaired intracellular growth compared to the parent strain, underscoring its critical role in pathogenicity (Perkowski et al., 2017).

The focus of this thesis is on the gene MAR_5092 (Rv3593) from the *M. marinum Tn*-library, which is predicted to encode a β-lactamase/penicillin binding protein. In the study by Chen et al. (2010), the MAR_5092 mutant (12C3) exhibited a moderate change in colony morphology,

specifically forming smaller colonies, as described below. Overall, the *M. marinum Tn*-library revealed insertions in genes whose homologues in *M. tuberculosis* are directly involved in cell wall homeostasis, host-bacterial interaction dynamics, and virulence.

3.1.3 MMAR_5092

In addition to the genes described above, MMAR_5092 (*lpqf*) was identified in the colony morphology screen. This gene encodes a putative conserved lipoprotein called LpqF. MMAR_5092, along with its homologue in *M. tuberculosis*, Rv3593, are uncharacterised proteins, exhibiting high conservation in mycobacteria (Figure 24).

While the study by Chen et al. (2010) suggested that LpqF is non-essential in *M. marinum*, *Tn*-sequencing (*Tn*-seq) studies in *M. tuberculosis* have yielded conflicting results (DeJesus et al., 2017; Sassetti, Boyd, & Rubin, 2003). These discrepancies may be attributed to differences in methodology and experimental approaches. For example, the seminal study by Sassetti, Boyd, and Rubin (2003), employed a genome-wide transposon mutagenesis study in *M. tuberculosis* H37Rv using the Himar1 transposon, identifying 614 essential genes, including Rv3593, for *in vitro* growth. Their study provided a comprehensive map of essential and non-essential genes critical for bacterial survival under laboratory conditions through high-density mutagenesis and microarray analysis (TrasH). In contrast, Chen et al. (2010) investigated *M. smegmatis* and *M. marinum* using the *Tn5371* transposon, focusing on genes involved in cell wall biosynthesis and virulence. This approach emphasised phenotypic screening, identifying mutants with altered colony morphology and impaired intracellular growth, highlighting specific functional roles in targeted pathways and a small subset of genes rather than a broad essentiality profile.

Further supporting the findings of Sassetti et al. (2003), Griffin et al. (2011) used high-density transposon mutagenesis combined with deep sequencing to map transposon insertion sites across the in *M. tuberculosis* genome at single base pair resolution. This study incorporated phenotypic profiling of mutant libraries under different conditions, including media containing cholesterol as a sole carbon source, to identify genes essential for growth under specific environmental stresses. Griffin et al. (2011) found the C-terminal domain of Rv3593 to be essential, while the N-terminal domain. Given that the export signal is encoded at the N-terminus and is likely required for any C-terminus activity, this finding underscores the importance of combining genetic approaches to delineate essential functional domains.

In contrast, DeJesus et al. (2017) employed a high-saturation *Tn*-seq approach using Himar1 transposon with over 35 million independent insertions, coupled with a hidden Markov model to classify essential and non-essential genes. They reported Rv3593 as non-essential for *in vitro* growth under rich media conditions (DeJesus et al., 2017). Unlike Griffin et al. (2011), this study addressed insertion biases in multiple prokaryotic libraries by identifying sequence motifs less permissive to transposon insertion and acknowledged how methodological differences impact the interpretation of essentiality. For example, Griffin et al. (2011) excluded small genes with fewer than 6 TA insertions sites, eliminating 583 genes (approximately 13%) with 1-5 TA sites in *M. tuberculosis*. Despite these methodological differences, Dejesus et al. (2017) aligned with Chen et al. (2010) in concluding that Rv3593 is a non-essential gene. Together, these studies provide complementary insights. Sassetti et al. (2003) and Griffin et al. (2011) offer foundational frameworks and detailed genetic mapping, while Chen et al. (2010) and DeJesus et al. (2017) highlight targeted functional roles and methodological variability in essentiality assessment.

M. leprae is often considered to contain the minimal mycobacterial genome, and thus, genes conserved in this organism are likely to be important for survival at some point in the pathogen's life cycle. More recently, Das et al. (2023) reported the *M. leprae lpqf* homologue ML1923 to be downregulated in a hybridisation array derived from RNA from skin lesions, suggesting a potential role as a marker for diagnostics (Das et al., 2023). In the *Tn*-library, the MMAR_5092::Tn5371 strain was labelled as 12C3. From this point onwards, 12C3 will be referred to as Δ*lpqf*^{Mm} for *M. marinum* unless otherwise stated (Figure 21, Table 14).

Table 14: Twenty two isolated mutants in *M. marinum* from the Chen et al. (2010) study with morphological changes.

Gene reference	Gene number	*M. tuberculosis* homologue	Gene name	Function	Studies
9D9	MMAR_2327	Rv1508c	Probable membrane protein (glycosyltransferase)	Cell wall Probable glycosyltransferase	Chen et al., 2010. This study
14D3	MMAR_2352	Rv1517	Conserved hypothetical transmembrane protein. Probable triacylglycerol synthase.	Cell wall Probable (LysE like) peptidoglycolipid transporter (Seeliger et al., 2012)	Chen et al., 2010. This study
10E9	MMAR_2913	Rv0917	Possible glycine betaine transport integral membrane protein BetP	Cell wall. High-affinity uptake of glycine betaine Potential regulation protein during nutrient depletion (Betts et at., 2002)	Chen et al., 2010 This study
16D10	MMAR_3250	Rv2206	Transmembrane protein (ESX transport protein) involved in survival in macrophages	Cell wall Function unknown	Chen et al., 2010 This study
12C3	MMAR_5092	Rv3593 (LpqF)	Lipoprotein LpqF	Cell wall Probable class C – LMW penicillin binding protein	Chen et al., 2010 This study
9B4	MMAR_5457	Rv3881c	Secreted ESX-1 substrate protein B, EspB. Conserved alanine and glycine rich protein	Cell wall and cell wall process Function unknown	Chen et al., 2010 This study
12B4	MMAR_0992	Rv0653c	Possible transcriptional regulatory protein (probably TetR-family)	Regulatory proteins - Involved in transcription mechanism	Chen et al., 2010 This study
6B11	MMAR_5449	Rv3874 (esxB)	EsaT-6 like protein, EsxB	10 kDa culture filtrate antigen EsxB (LHP) (CFP10)	Chen et al., 2010 This study
10C3	MMAR_5457	Rv3881c	ESX-1 secreted protein, EspB	Cell wall and cell processes Probable secreted ESX-1 substrate protein B, EspB. Conserved alanine and glycine rich protein)	Chen et al., 2010 This study
7D3	MMAR_5440	Rv3865	ESX-1 secretion-associated protein EspF	Cell wall and cell processes Type VIII secretion system – interacts with EsxA, EccA1, and EspC	Chen et al., 2010 This study
3D7	/	/	Not described in Chen et al., 2010	/	Chen et al., 2010 This study
8D9-1 8D9-2	1 MMAR_4214 2 MMAR_1180	(1) Rv1223 (2) Rv1662	(1) Probable serine protease HtrA (DEGP protein)	Cell wall and cell processes (1) Possibly hydrolyses peptides and/or proteins (2) Potentially involved in some	Chen et al., 2010 This study Chen et al., 2010

			(2) Probable polyketide synthase Pks8	intermediate steps for the synthesis of a polyketide molecule	
3E5	MMAR_4806	Rv3829c	Phytoene dehydrogenase CrtI (lipid metabolism)	Cell wall and cell processes Probable dehydrogenase	Chen et al., 2010 This study
13E3	MMAR_3223	Rv2179c	Conserved hypothetical protein	Function unknown Conserved hypotheticals	Chen et al., 2010 This study
13E7	/	/	Not described in Chen et al., 2010	/	Chen et al., 2010 This study
11F5	promotor region of MMAR_3235	Rv2191	Conserved hypothetical protein	Function unknown Information pathways	Chen et al., 2010 This study
16F6	/	/	PGL and PDIM biosynthesis Described in text Chen et al., 2010 different colony fringes similar to 5G3, bigger in colony size compared to wildtype	/	Chen et al., 2010
1G2	MMAR_1767	Rv2940c	Multifunctional mycocerosic acid synthase membrane-associated Mas	Catalyses the elongation of N-fatty acyl-CoA with methylamalonyl-CoA to form mycocerosyl lipids	Chen et al., 2010 This study
10G2	MMAR_2341	Rv1521 (fadD2)	Probable fatty-acid-CoA ligase FadD25	Involved in lipid degradation	Chen et al., 2010 This study
5G3			Described in text Chen et al., 2010 different colony fringes similar to 16F6		Chen et al., 2010 This study
6G3	MMAR_1775	Rv2932	Phenolpthiocerol synthesis type-I polyketide synthase (PpsB)	Involved in phenolphthiocerol and phthiocerol dimycocerosate (DIM) biosynthesis	Chen et al., 2010 This study
8G10	Promoter of MMAR0978	Rv0643c	probable fatty-acid-CoA ligase FadD25	Involved in mycolic acid modification	Chen et al., 2010 This study

3.1.4 Morphological screen for genes involved in cell wall assembly

The 22 *Tn*-mutants, along with the parental strain, were cultured in 7H9 media supplemented with 10% OADC at 30 °C until an optical density (OD) 0.6 at 600 nm ($OD_{600\ nm}$). The $OD_{600\ nm}$ was then adjusted to 0.1, and the cultures were pinned onto 7H9 agar plates containing 0.05% Tween80 using a pinning robot to replicate from a source plate. The plates were then incubated for 7 days at 30 °C (Figure 21, A). To confirm that the colonies were indeed *M.*

marinum strains free from contamination, the plates were exposed to ultraviolet (UV) light and left overnight (Figure 21, B). This method leveraged the natural ability of *M. marinum* to genetically regulate the carotenoid biosynthesis and *de novo* pigmentation production under UV illumination. Specifically, UV exposure induces the expression of the gene MMAR_3806 (*ctr1*), the *crtB* homologue in *Streptomyces griseus* and *Myxococcus xanthus*. This gene encodes phytoene dehydrogenase, a key enzyme in the photochromogenic carotenoid biosynthetic pathway (Ramakrishnan et al., 1997; Gao et al., 2003; Hashish et al., 2018).

All colonies, except for mutant 3E5, developed the characteristic yellow stress pigmentation commonly observed in photochromogenic organisms such as *M. marinum* upon UV exposure. The pigmentation was attributed to carotenoid activity of Ctr1. Strain 3E5, however, harbours a *Tn* insertion in MMAR_3806, disrupting the *ctr1* gene that encodes phytoene dehydrogenase. The disruption of *ctr1* impairs carotenoid biosynthesis, thereby preventing pigmentation production (Ramakrishnan et al., 1997; Chen et al., 2010; Liang et al., 2020).

The pinning assay revealed colony morphological alterations in the mutants consistent with those reported and described previously in the Chen study, in agreement with the original reference *Tn*-library (Chen et al., 2010). Although the wild-type (WT) and 12C3 strains both exhibited a rough dry texture characteristic of *M. marinum*, strain 12C3 displayed a smaller colony with a thin crust compared to WT in both non-UV and UV-exposed plates (Figure 21, B). Conversely, WT colonies appeared larger with a wider crust surrounding the circumference of the colony (Figure 21, B).

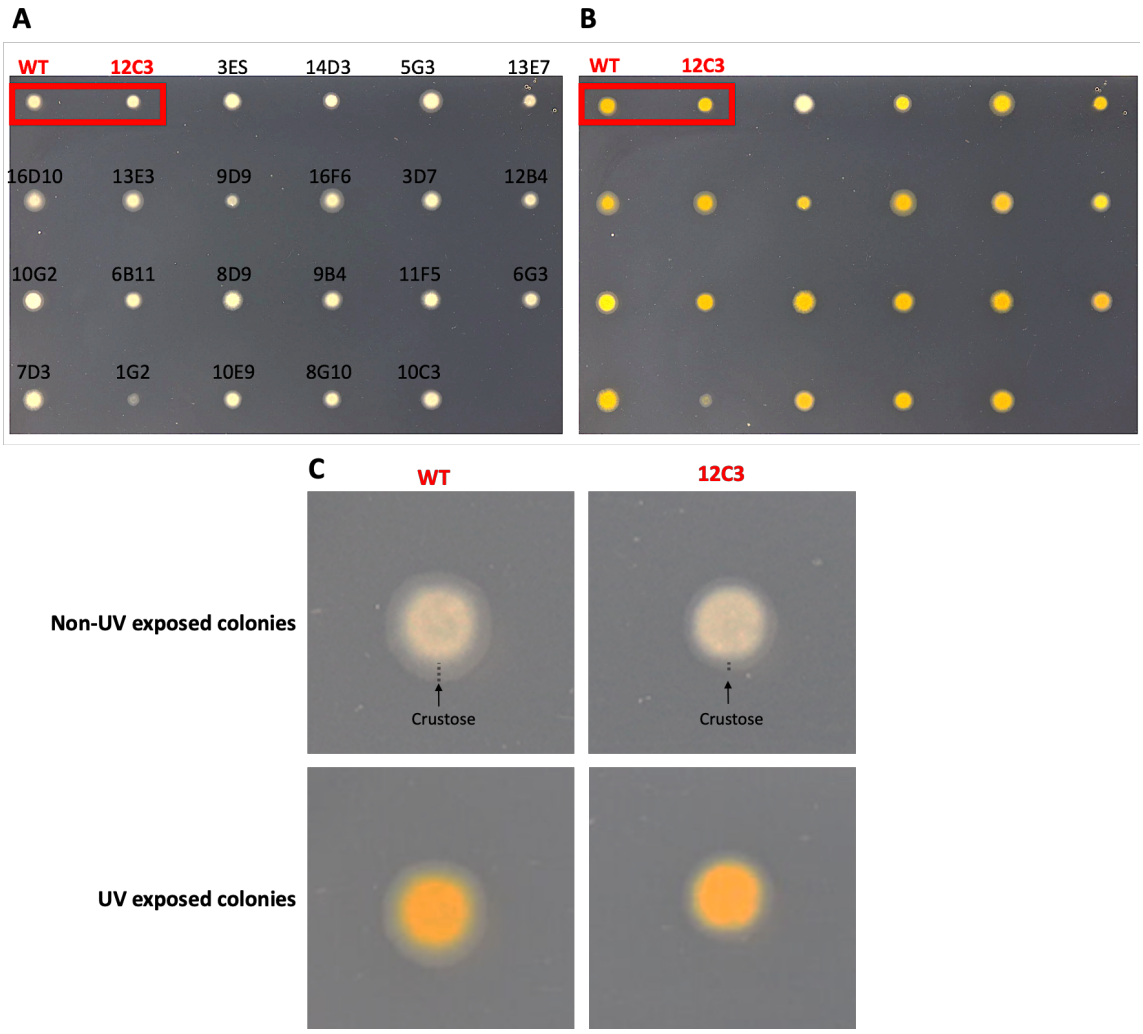


Figure 21: Confirmation of *M. marinum* colony morphology defects from an *Tn* library. (**A**) The 22 strains harbouring an insertion into genes predicted to be involved in cell wall synthesis in *M. marinum* were pinned onto 7H10 + 2 % agarose plates using the S & P Robotics BM3-BC platform. Arrayed mutants and wild-type from the *Tn*-library ID produced by Chen et al. (**B**) Colonies exposed to UV light for 24 h left indicating the induction of beta-carotene and production of yellow pigmentation colonies. Highlighted in red boxes are the wildtype and 12C3 (Δ*lpqf*) strains. (**C**) Higher resolution images of non-UV and UV exposed colonies of WT and 12C3 highlighting the morphological difference. Crustose; the diameter of the outer edge or frill of the colony. The plates represent 1 of 3 replicates.

MMAR_5092 was annotated as a low molecular weight penicillin binding protein, suggesting a potential role in peptidoglycan metabolism. Based on this annotation, the mutant strain was selected for further investigation. A dilution assay was performed to determine whether the Δ*lpqf* (12C3) mutant from the *Tn*-library exhibited any morphological or fitness defects, such as an altered growth rate on solid agar (Figure 22). The results demonstrated that the Δ*lpqf* mutant displayed a moderate growth defect under these conditions, as shown in Figure 22. Specifically, the Δ*lpqf* strain produced fewer and smaller colonies despite being inoculated at the same density of starting inoculum (OD_{600nm} = 0.001).

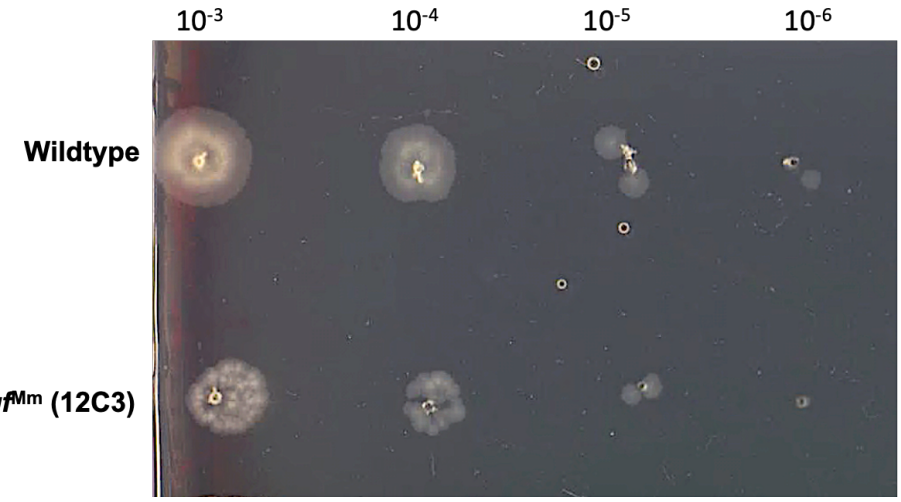


Figure 22: A spot assay using wildtype and Δ*lpqf*^{Mm} (12C3). A tenfold serial dilution of the parental wildtype strain and Δ*lpqf*^{Mm} (12C3) (from transposon *Tn*-library) in the *M. marinum* (1218R) background was spotted onto 7H10 plates. A culture at an OD_{600} of 0.6 was serially diluted in 7H9 media. Shown is a representative plate, with 2 uL of the 10^{-3} to 10^{-6} dilutions pipetted onto 7H10 agar, incubated at 30 °C for 6 days. Plates were monitored for growth every two days, and images were taken on day 6. The image is representative of triplicate experiments (n = 3).

Colony morphology defects can result from changes in bacterial shape, which are often linked to deficiencies in cell wall biosynthesis. These deficiencies may arise from the absence of biosynthetic or cell wall maintenance enzymes, exposure to chemical agents, or variations in nutrient availability in the environment (van Teeseling, de Pedro, & Cava, 2017; Baranowski et al., 2018; Akusobi et al., 2022). Considering its predicted role in peptidoglycan metabolism, it is plausible that the colony morphology of Δ*lpqf* strain and fitness defects results from disruptions in these pathways.

3.1.5 LpqF (Rv3593)

After identifying *lpqf* as a gene contributing to colony morphology alterations in *M. marinum*, our next objective was to assess its conservation across mycobacteria and other bacterial species. To examine the genetic distance and conservation of LpqF in mycobacteria, a basic alignment was conducted using the *M. tuberculosis* H37Rv LpqF homolog (Rv3593) as the query sequence. The UniProt ID O06155_MYCTU was retrieved from UniProt and inputted into the NCBI platform, employing blastP with parameters set to a cut-off of 250 sequences. The initial iteration yielded 250 aligned sequences, comprising 29 homologous protein sequences to the catalytic domain of LpqF and 241 predicted domains from diverse taxa. These

alignments were then used to generate 239 groups based on sequence identity, utilising a cut-off of 50% identity.

Compositional biases within sequences can result from changes in nucleotide or amino acid frequencies due to adaptations to the bacterial species' ecological niche, function, or localisation of the gene product (Antonets and Nizhnikov, 2013). In this study, sequences obtained from the alignments were trimmed by setting the taxonomy to Mycobacteriaceae, focusing on *M. tuberculosis*, *M. bovis*, *M. marinum*, *M. leprae*, and *M. smegmatis*. Eighty-seven sequences exhibiting the highest homology to the catalytic domain were inputted into the ngphylogeny.fr platform using the OneClick setting (Lemoine et al., 2018). This produced a phylogenetic tree, further refined and annotated using the iTOL platform (Letunic and Bork, 2021). Figure 23 illustrates the conservation of LpqF among the top-scoring hits in mycobacteria. Each colour represents a different species, providing a visual representation of how *lpqf* orthologues are conserved across these species. Notably, *M. tuberculosis* (red), and *M. bovis* (blue) are the most closely related species, clustering together within the same clade on the phylogenetic tree. In contrast, *M. leprae* (purple) is positioned outside of this clade, indicating a greater evolutionary distance. *M. marinum* (yellow) appears farther from *M. tuberculosis* (red), *M. bovis* (blue), and *M. leprae* (purple) on the tree, forming a distinct clade. Finally, *M. smegmatis* (green) is positioned at the greatest distance, located on a separate node, highlighting its evolutionary divergence from the other species. This phylogenetic arrangement reflects both genomic and functional adaptations. Environmental mycobacteria like *M. smegmatis* and *M. marinum* exhibit broader ecological niches, while host-specific pathogens such as *M. tuberculosis* and *M. leprae* have evolved traits that specialise them for survival and virulence within their respective hosts.

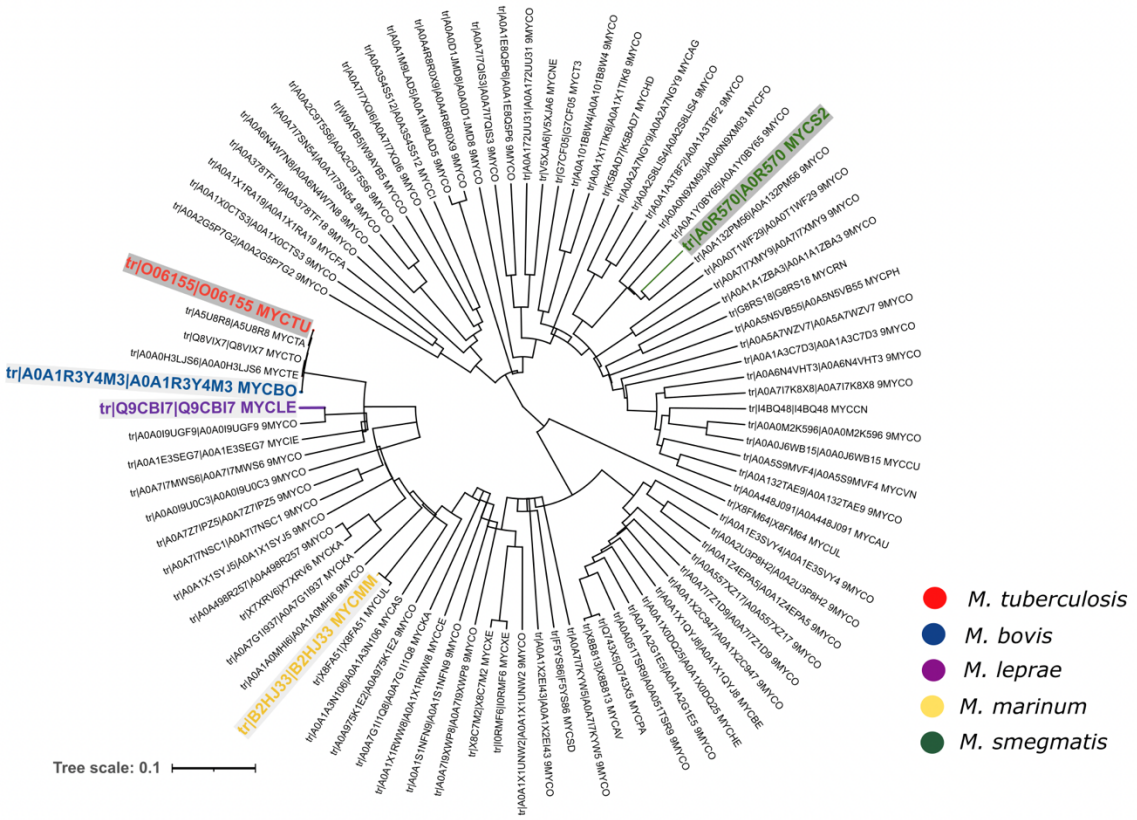
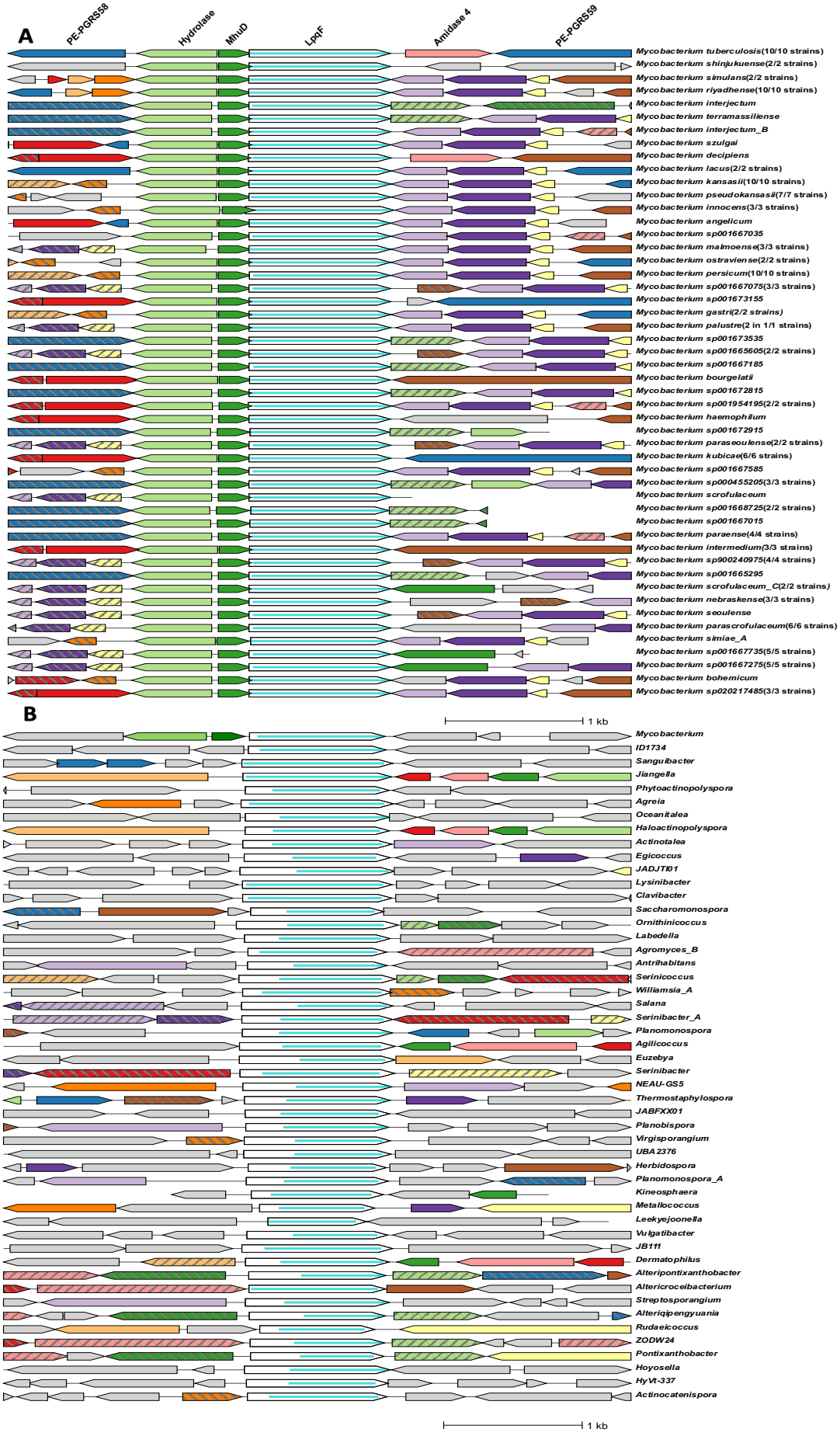


Figure 23: Phylogenetic analysis of *lpqf* and its relationship to evolutionary distance in mycobacteria. Phylogenetic relationship of *lpqf* amongst species of *Mycobacterium*. Rv3593 (O06155_MYCTU) fasta sequence was inputted into the Protein BLAST alignment tool (NCBI, 2023) which produced 250 diverse alignments. For simplicity sequences were filtered to include Mycobacteriaceae taxonomy (id:1762) only trimming down to 87 Fasta sequences that were uploaded to NGPhylogeny.fr (Lemoine et al., 2018) resulting tree was refined and annotated in the interactive tree of life platform (itol.embl.de) (Letunic and Bork, 2021). Highlighted labels indicate the closely related genes for *M. tuberculosis* (red), *M. bovis* (blue), *M. leprae* (purple), *M. marinum* (yellow) and the more distant related *M. smegmatis* (green). The boot strap distances are represented by a tree scale between 0.1-1.

Synteny analysis of MMAR_5092 (Rv3593) revealed its proximity to six genes, including two uncharacterised PE_PGRS genes, Rv3590 and Rv3595, which flank MMAR_5092. PPE and PE_PGRS gene families are known for their diverse functions in host-pathogen interactions (De Maio et al., 2020). Downstream of Rv3595c is Rv3596c, which encodes the protease ClpC1, a key regulator of proteins involved in bacterial growth that is highly conserved in mycobacteria (Lunge et al., 2020). The homologous genes in *M. marinum* are MMAR_2596, MMAR_5555, and MMAR_5100, respectively. Upstream and adjacent to MMAR_5092 are a predicted hydrolase, MMAR_5090 (Rv3591), and the gene *mhud* (Rv3592), which encodes a heme oxygenase involved in iron acquisition during macrophage infection (Chim et al., 2009). The C- and N-termini of Rv3593, along Rv3591 and Rv3592 and its with its homologs in *M. marinum* MMAR_5092, MMAR_5090 and MMAR_5091 respectively exhibit high

conservation across Actinomycetes (Figure 24, A, C). In contrast, a gene that encodes a putative amidase, Rv3594, is unique to *M. tuberculosis* and closely related species. Located downstream of Rv3593, Rv3594 is predicted to participate in peptidoglycan homeostasis (light pink, Figure 24, A, C). Overall, these analyses demonstrate that MhuD and LpqF are highly conserved across Actinomycetes.

Synteny analysis also revealed the presence of orthologs of the LpqF PBP domain in a diverse range of bacteria (Figure 24, B), likely due to the conservation of classical catalytic residues present in most PBP/transpeptidase domains. However, the high conservation of the N-terminal domain in LpqF gene among mycobacteria is largely absent in orthologs from more diverse bacterial species, highlighting the uniqueness of the N-terminal domain of LpqF in Actinomycetes. The predicted operon depicting the gene arrangement in mycobacteria is outlined in Figure 24, panel C.


A
PE-PGRS58
Hydrolase
MhuD
LpqF
Amidase 4
PE-PGRS59
Mycobacterium tuberculosis(10/10 strains)
Mycobacterium shinjukuense(2/2 strains)
Mycobacterium simulans(2/2 strains)
Mycobacterium riyadhense(10/10 strains)
Mycobacterium interjectum
Mycobacterium terramassiliense
Mycobacterium interjectum_B
Mycobacterium szulgai
Mycobacterium decipiens
Mycobacterium lacus(2/2 strains)
Mycobacterium kansasii(10/10 strains)
Mycobacterium pseudokansasii(7/7 strains)
Mycobacterium innocens(3/3 strains)
Mycobacterium angelicum
Mycobacterium sp001667035
Mycobacterium malmoense(3/3 strains)
Mycobacterium ostraviense(2/2 strains)
Mycobacterium persicum(10/10 strains)
Mycobacterium sp001667075(3/3 strains)
Mycobacterium sp001673155
Mycobacterium gastri(2/2 strains)
Mycobacterium palustre(2 in 1/1 strains)
Mycobacterium sp001673535
Mycobacterium sp001665605(2/2 strains)
Mycobacterium sp001667185
Mycobacterium bourgelatii
Mycobacterium sp001672815
Mycobacterium sp001954195(2/2 strains)
Mycobacterium haemophilum
Mycobacterium sp001672915
Mycobacterium paraseoulense(2/2 strains)
Mycobacterium kubicae(6/6 strains)
Mycobacterium sp001667585
Mycobacterium sp000455205(3/3 strains)
Mycobacterium scrofulaceum
Mycobacterium sp001668725(2/2 strains)
Mycobacterium sp001667015
Mycobacterium paraense(4/4 strains)
Mycobacterium intermedium(3/3 strains)
Mycobacterium sp900240975(4/4 strains)
Mycobacterium sp001665295
Mycobacterium scrofulaceum_C(2/2 strains)
Mycobacterium nebraskense(3/3 strains)
Mycobacterium seoulense
Mycobacterium parascrofulaceum(6/6 strains)
Mycobacterium simiae_A
Mycobacterium sp001667735(5/5 strains)
Mycobacterium sp001667275(5/5 strains)
Mycobacterium bohemicum
Mycobacterium sp020217485(3/3 strains)
B
1 kb
Mycobacterium
ID1734
Sanguibacter
Jiangella
Phytoactinopolyspora
Agreia
Oceanitalea
Haloactinopolyspora
Actinotalea
Egicoccus
JADJTI01
Lysinibacter
Clavibacter
Saccharomonospora
Ornithinicoccus
Labedella
Agromyces_B
Antrihabitans
Serinicoccus
Williamsia_A
Salana
Serinibacter_A
Planomonospora
Agilicoccus
Euzebya
Serinibacter
NEAU-GS5
Thermostaphylospora
JABFXX01
Planobispora
Virgisporangium
UBA2376
Herbidospora
Planomonospora_A
Kineosphaera
Metallococcus
Leekyejoonella
Vulgatibacter
JB111
Dermatophilus
Alteripontixanthobacter
Altericroceibacterium
Streptosporangium
Alteriqipengyuania
Rudaeicoccus
ZODW24
Pontixanthobacter
Hoyosella
HyVt-337
Actinocatenispora
1 kb

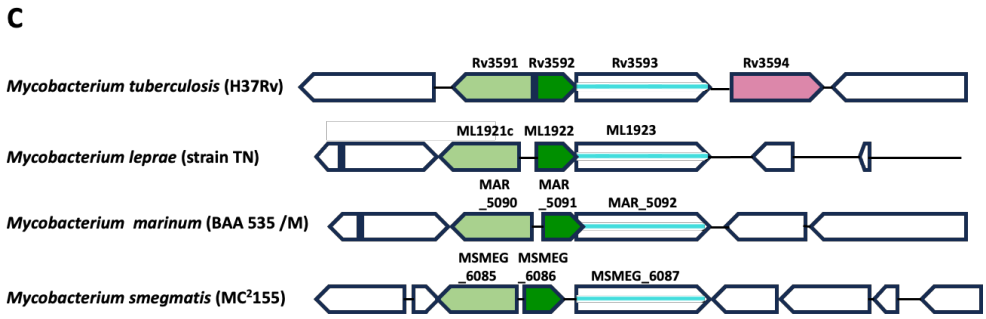


Figure 24: Synteny analysis reveals the approximate loci for *Rv3591*, *Rv3592*, *Rv3593*, and *Rv3594*. (**A**) The sequence alignments produced 1,101 homologous hits from 997 genomes within Mycobacteriales, with bars below the diagram representing genome distance in kilobases. (**B**) Rv3593 was further analysed in diverse bacteria to identify orthologous operons, yielding 100 hits out of 258 genomes from 6,377 diverse bacterial genomes. Operons are grouped into species clusters, with the length of the blue bar indicating the length of domain conservation for LpqF orthologs, while dark and light green bars represent MhuD and the predicted hydrolase, respectively. (**C**) A focused synteny analysis showcases the orthologs of the predicted hydrolase (light green), MhuD (dark green), and LpqF (light blue stripe within bar) in *M. tuberculosis* (Rv3593), *M. marinum*, *M. leprae*, and *M. smegmatis*. Gene colours correspond to specific functional categories, with Rv3594 depicted in salmon, PE_PGRS59 in blue bars, histidine phosphatase family protein in pink bars, CbtA family protein in aubergine bars, CbtB domain containing protein in yellow bars, and A/G specific adenine glycosylase in red bars. Non-conserved genes are represented by grey bars. Images rendered via fast genomics (www.genome.jp, 2021, fast.genomics.lbl.gov, 2023, Webflags, Saha et al., 2020).

Motif analysis of LpqF revealed distinct conservation patterns between the N- and C-terminal domains, as depicted in Figure 25. The conservation associated with LpqF outside of mycobacteria is predominantly associated with the C-terminal domain, consistent with the predicted penicillin-binding protein domain (Figure 25, A). InterProScan analysis of LpqF from H37Rv (O06155-MYCTU) highlighted key motifs within the domains. Residues 173-283 corresponded to the catalytic motif, labelled as a transpeptidase/β-lactamase in the peptidase S11 family (Figure 25, A, C). Conversely, the N-terminal domain exhibits much lower conservation across species. To identify orthologs of the N-terminal domain, a search was conducted, yielding several results including the N-terminal domain of ORF12 (Cpe) from the clavulanic acid synthesis pathway in *S. clavuligerus* (PDB:2xep chain A03, Valegård et al., 2013). The N-terminal domain showed 28.8% identity to the ORF12-NTF2-like motif from amino acids 51-138 (Figure 25, B, D). This analysis provides insights into the putative functional domains of LpqF and identifies potential orthologs.

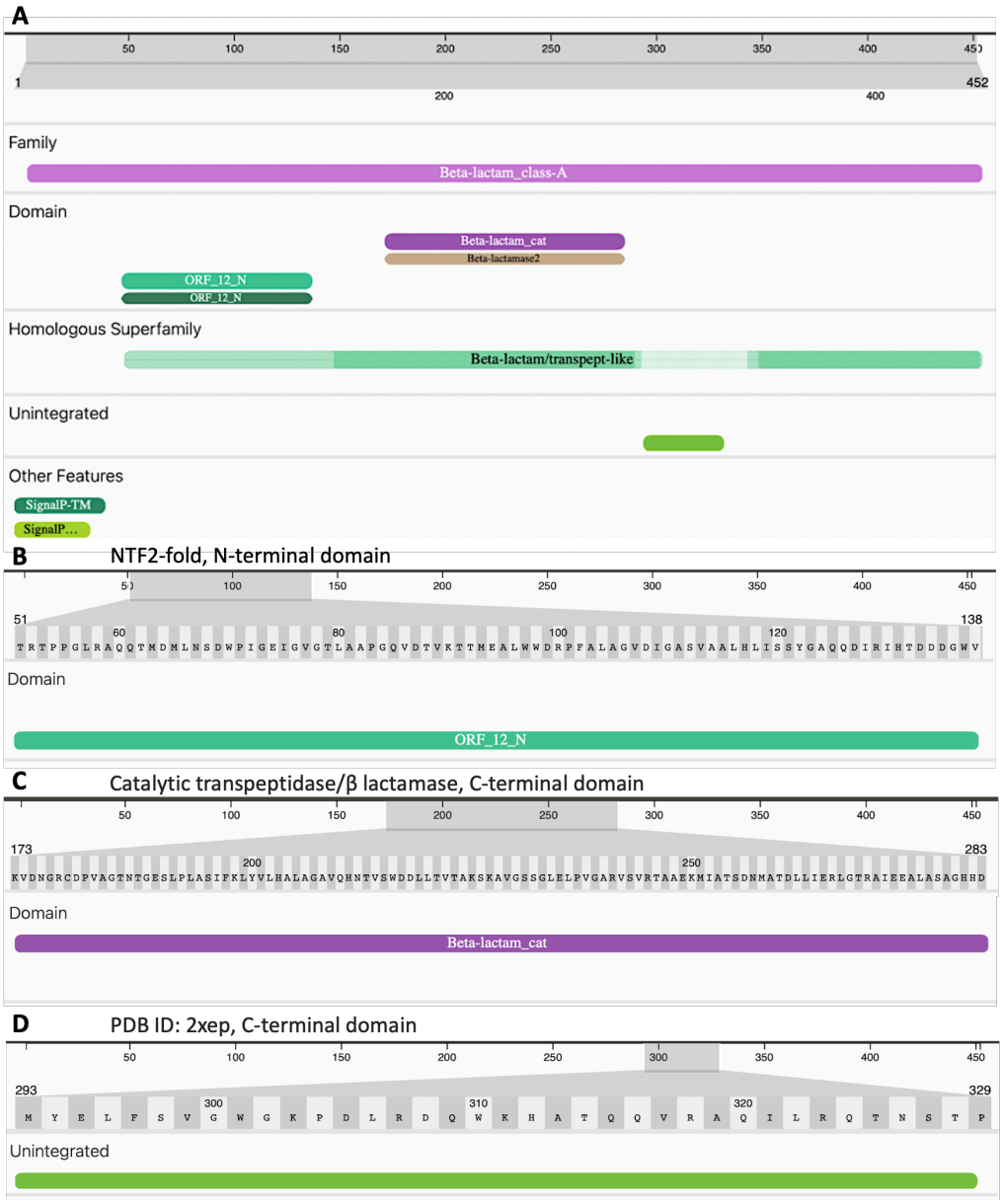


Figure 25: LpqF is predicted to belong to the PBP/B-lactamase family of enzymes. The Rv3593 (LpqF) sequence obtained from Uniprot (O06155_MYCTU) was analysed using InterProScan to predict homologous domains from known proteins with sequences similar to the domains found in LpqF (www.ebi.ac.uk., 2023). (**A**) The full-length sequence is depicted, showing all predicted domains with the homologous superfamily highlighted. (**B-D**) Individual sequences aligned to homologous domains are presented. (**B**) In the alignment, the ORF12-like domain is highlighted in cyan (ORF 12 N–IPR040846), indicating regions of similarity between LpqF and the ORF12 protein from *S. clavuligerus*. (**C**) The catalytic domain is outlined in purple (β-lactam cat, IPR045155), which encompasses groups such as penicillin-binding proteins (PBP), β-lactamases, and peptidase S11 D-alanyl D-alanine carboxypeptidase. These annotations provide insights into the potential functional domains present in the LpqF protein. (**D**) The sequence in LpqF exhibits similarity to the published PDB 2xep, specifically to helical bundle domains 9, 10, and 11, flanking the catalytic motif within ORF12 (Cpe) from *Streptomyces clavuligerus* (Valegård et al., 2013.

3.1.6 The N-terminal domain of LpqF has an NTF2-like fold

The investigation into the role of the NTF2-like fold for LpqF began with an examination of the structure of its catalytic domain. The 2.1 Å X-ray crystal structure of LpqF (Rv3593) from *M. tuberculosis* was resolved in 2019 by Dr. Patrick Moynihan and Professor Andrew Lovering. Surprisingly, the experimental structure revealed the presence of a second NTF2 domain bound to the gap between the catalytic domain and the NTF2-domain, completely occluding the active site of the protein (Figure 26, A). This unexpected discovery suggested the possibility that LpqF might be regulated by this additional NTF2 domain. This regulatory mechanism could be analogous to the inhibitory properties observed in IseA, an NTF2-like protein which inhibits the D,L-EPase LytF in *Bacillus subtilis* (Arai et al., 2012). However, due to time constraints, the focus of this thesis will be on the intact protein, setting aside further exploration of the regulatory implications of the second NTF2 domain for future investigation.

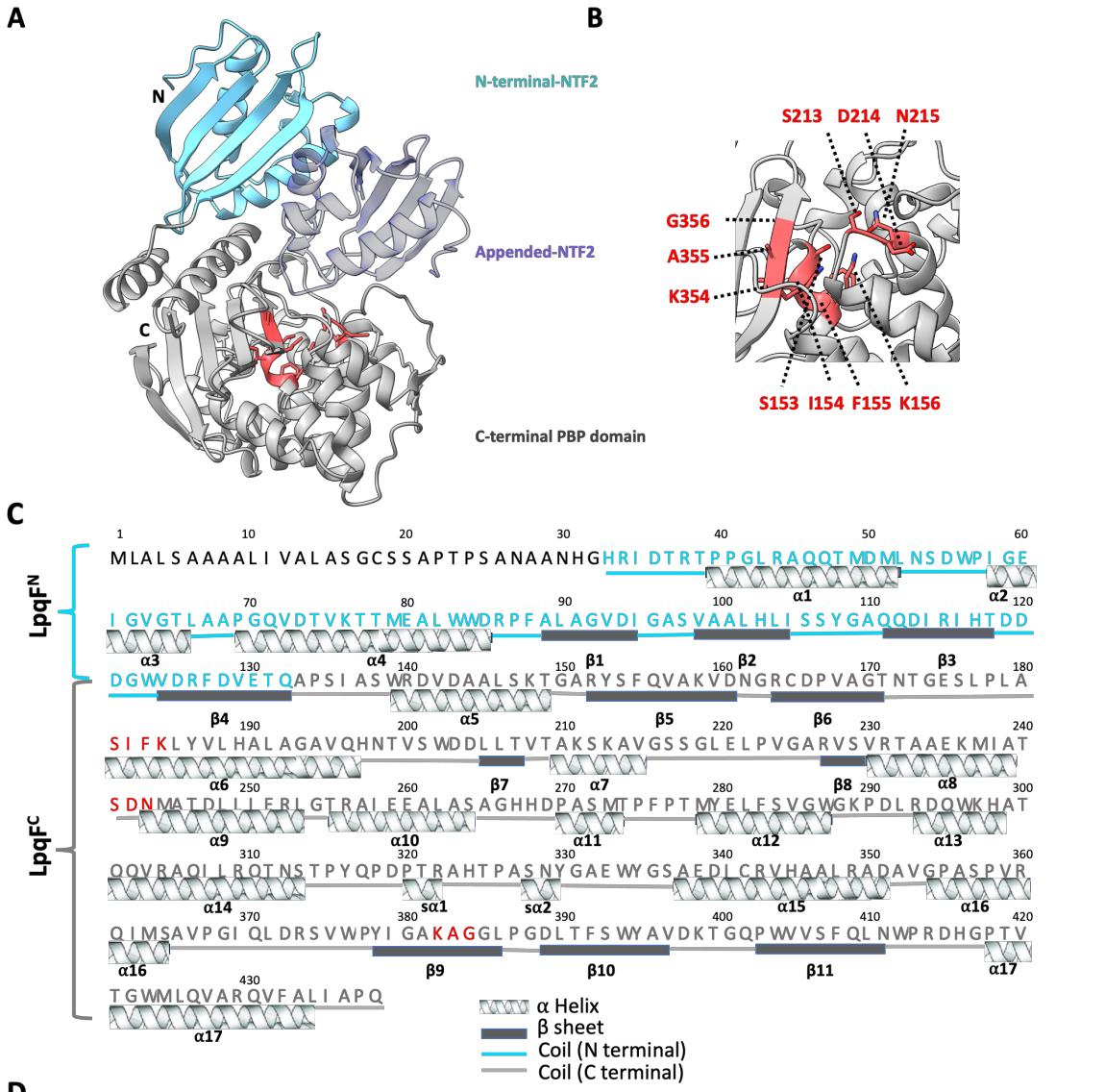

A
N
C
N-terminal-NTF2
Appended-NTF2
C-terminal PBP domain
B
S213 D214 N215
G356
A355
K354
S153 I154 F155 K156
C
LpqF^N
LpqF^C
α Helix
β sheet
Coil (N terminal)
Coil (C terminal)
D
NTF2-fold of LpqF in Mycobacterium tuberculosis
NTF2-fold of Cpe in S. clavuligerus
PDB 2xh9
RMSD: 3.56 Å
NTF2-fold of protein with unknown function in B. thailandensis
PDB 3h3h
RMSD: 4.86 Å
NTF2-fold of protein with unknown function in P. aeruginosa
PDB 1tp6
RMSD 6.61 Å

Figure 26: LpqF has two domains, an N-terminal NTF2-like domain and a C-terminal PBP domain. (**A**) The experimental structure of LpqF highlights the C-terminal PBP (grey) domain, the N-terminal NTF2 domain (cyan), and an appended second NTF2 domain (light purple). (**B**) Zoom in of the catalytic site in the PBP domain with functional residues highlighted in light red. The amino acid sequence of LpqF showing the experimentally derived secondary structure, with α-helices shown in light grey and β-strands in dark grey. (**C**) Highlighted in red are the catalytic triad motifs identified in panel B (SIFK, SDN, KAG). A structural alignment using ChimeraX of the NTF2 domain in LpqF with known NTF2 domains: Cpe (PDB ID: 2xh9) in *S. clavuligerus* (light green), protein of unknown function (PDB ID: 3h3h) (Uniprot, Q2T8S1) from *B. thailandensis* (purple, with ligand bound shown inset), and protein of unknown function (PDB ID: 1tp6) from *P. aeruginosa* (dark blue). (**D**) The NTF2-fold of LpqF (light blue) overlaid with NTF2-like folds of Cpe, the unknown protein in *B. thailandensis*, and from *P. aeruginosa* is shown as the far right of panel D. The RMSDs are 3.56 Å, 4.86 Å, 6.21 Å, and 6.61 Å, respectively. Search.foldseek was used to find suitable structural comparisons structure for NTF2 domain of LpqF. The search produced 747 alignments to PDBs published in the protein data bank (RSCB) that were obtained and further parsed with RMSDs. (Joint Centre for Structural Genomics., unpublished; Valegård et al., 2013; Michel van Kempen et al., 2023; EBI Web Team 2023).

The *in silico* analyses conducted in this study indicated that the N-terminal (a small α/β domain) of LpqF is less conserved outside of the Mycobacteriales. However, given the potential differences between sequence and structural conservation, it was important to identify NTF2 homologues for LpqF among structurally characterised proteins in a diverse set of organisms. To accomplish this, the N-terminal motif-only domain-specific criterion was employed using the Search.foldseek.com platform, inputting the PDB file and generating a list of PDBs of two published structural homologues with a root mean square deviation (RMSD) below the threshold of 5.0 for robust fitting of structural alignments (Figure 26, D). The Foldseek platform (Michel van Kempen et al., 2023; Barrio-Hernandez et al., 2023) produced several high-scoring alignments to similar NTF2 domains in *S. clavuligerus* and *Burkholderia thailandensis* derived from Alphafold and published structures. The top-scoring Foldseek hit was ORF12 (Cpe) from *S. cavuligerus* (PDB: 2xh9). This protein shares 28.8% sequence identity with the NTF2 domain of LpqF, and the Foldseek structural alignment gives an RMSD of 3.56 Å, confirming previous *in silico* results (Figure 26, C). Analyses of the structural overlay revealed the absence of conserved residues between the Cpe and NTF2 of LpqF.

The next highest matching structures with sequence coverage to the NTF2 domain of LpqF, identified via Foldseek (Michel van Kempen et al., 2023; Barrio-Hernandez et al., 2023), were structurally aligned. The quality of these alignments ranged from 3.56 Å RMSD to 6.61 Å RMSD, indicating a generally low RMSD that reflects the high conservation of the NTF2 domain. The lower RMSD values support the hypothesis of structural similarity and potential functional conservation across these proteins. Table 15 describes the other structural alignments shown in Figure 26, D, focusing on those with RMSD values lower than the cut-off score of 5 Å.

Table 15: A representation of the structural alignments of NTF2 domains.

Gene name/PDB file	Organism	Sequence identity (%)	Coverage	RMSD (Å)	TM-score	Function
Cpe esterase	*S. clavuligerus*	28.8	91	3.56	0.82419	The clavulanic biosynthetic pathway
Unknown protein (3h3h)	*B. thailandensis*	13.1	<30	4.86	0.57248	Unknown function
Unknown protein (5ne2)	*Stenotrophomonas maltophilia*	25.5	15	5.44	0.71937	Unknown function
pa1314 (1tp6)	*P. aeruginosa*	15	<30	6.61	-	Unknown function
Unknown protein (4RZM)	*Streptomyces lasalocidi*	21	14	6.66	0.59274	Unknown function
Unknown protein (AF-A0A1B7LWH1-F1))	*Enteractinococcus helveticum*	18.6	20	17.48	0.64708	Unknown function

An uncharacterised protein in *B. thailandensis* (EMBL-EBI, 3h3h) aligned to the N-terminal domain of LpqF with an RMSD of 4.86 Å (Figure 26, D, light green structure). The structure of *B. thailandensis* (Joint Centre for Structural Genomics, unpublished), which aligned second highest with the NTF2 domain, is associated with a ligand of unknown function that resembles a peptide. The contact residues were verified using MotiveValidator (EBI Web Team, 2023; Sehnal, 2023). This ligand binds to residues W16, W20, M38, Y63, W64, A67, L74, Y92, and E102, located within a cleft that resembles the NTF2 domain of LpqF (Vacekova et al., 2014; EBI Web Team, 2023, Figure 26, coloured purple and inset).

However, the structural alignment using PDB ID 3h3h from PDBsum with the NTF2 domain of LpqF, revealed overlapping residues within a similarly shaped cleft. The aperture size of the cleft for 3h3h is larger compared to that of the cleft containing the putative binding pocket of the NTF2 domain of LpqF, where α-helices 1 and 3 occlude the aperture space (12.1 Å vs. 4.2 Å, respectively). Additionally, there was no conservation of the residues lining the binding pocket, with some residues exhibiting polarity differences, for example, T20>W16 and I86>E102. The overall shape of the domain structure differs as well: 3h3h forms an oval, closed shape, whereas the NTF2 domain of LpqF forms a semi-circular, non-closed clamp-like shape.

These differences in features suggest unique ligand preferences for each domain (Figure 26, D; see Table 16).

Table 16: Alignment of 3h3h and NTF2 of LpqF structures for assessment of conservation of ligand binding residues.

Structure	NTF2-LpqF	NTF2-3h3h
residues	T20	W16
	L24	W20
	L54	R58
	L76	Y92
	V47	Y63
	K48	W64
	M51	A67
	I86	E102

In summary, NTF2 domains have been reported for peptidoglycan targeting enzymes. While the structure of the NTF2 domain is conserved, variation in the fine structure of the domain suggests that the NTF2 of LpqF likely has a function which is unique to this enzyme. In the discussion the published functional NTF2-like structures for peptidoglycan targeting enzymes, their functions, and their structural differences will be described.

3.1.7 LpqF is a low molecular weight PBP with a unique motif III within the catalytic triad

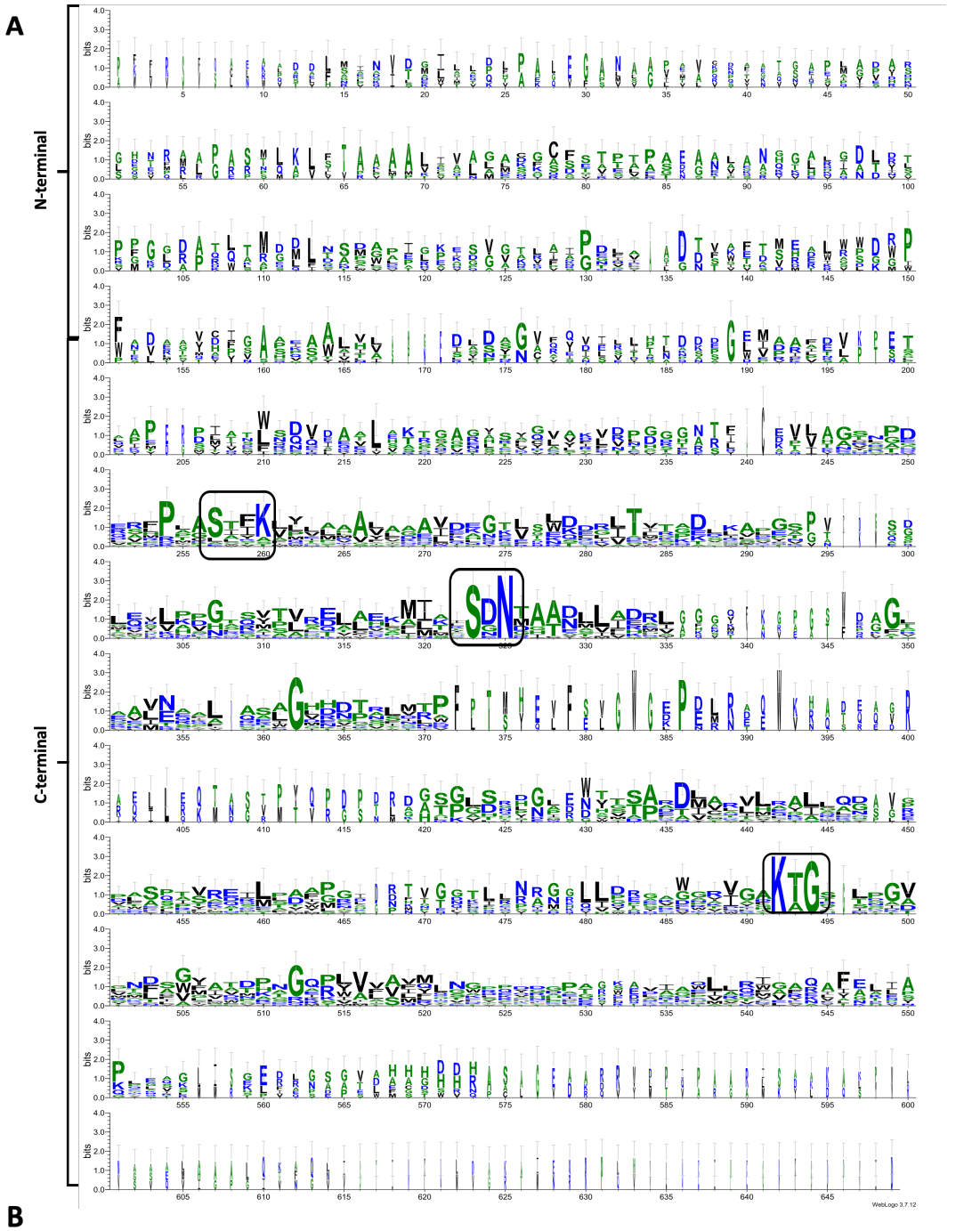
Given that the experimental structure and basic *in silico* analyses revealed that LpqF consists of two domains: a large α/β domain similar to other PBPs and serine β-lactamases, this domain annotated as PBP/transpeptidase/D,D-CPase/β-lactamase, was further investigated to identify homologues and predict its function. The PBP-domain includes 17 α-helices and 7 β-sheets, with the catalytic pocket situated between specific helices and sheets (Figures 26, A). Notably, the PBP-domain of LpqF lacks the canonical omega loop present in β-lactamases (Egorov et al., 2019; Pandey et al., 2020); however, it contains an alternative loop that sits above the active. Structural analyses revealed that LpqF possesses a catalytic triad (SxxK, SxN, KxG) within its active site, with residue positioning and distances strikingly similar to those observed in the PBP-domain of PBP5, where these residues also face into the active site cleft. PBP5 was

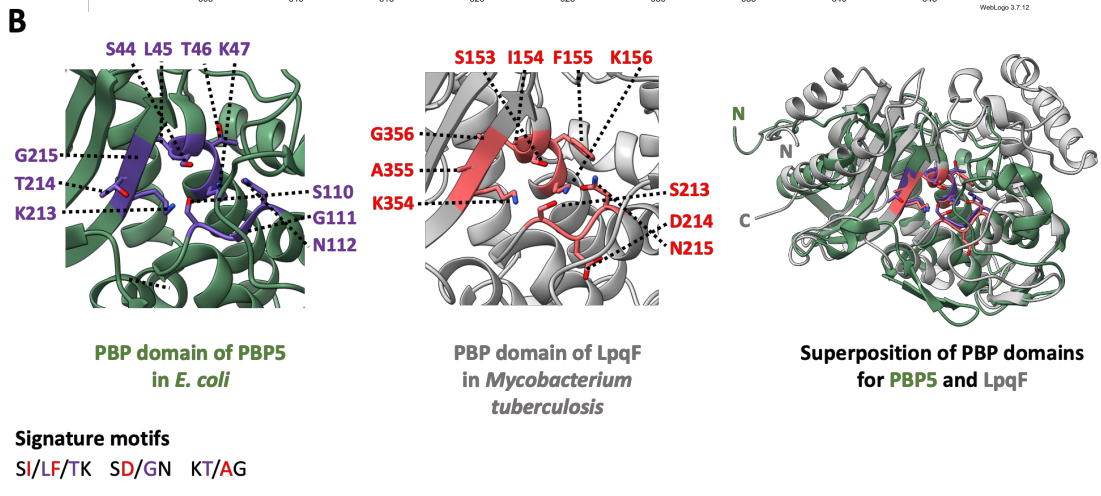
chosen from the list of templates to compare to LpqF because it has a structurally similar PBP-domain from *E.coli*, also belonging to the S11 family (Figure 26, B). In PBPs, the peptidase domain containing the catalytic triad motifs is typically located at the N-terminus, followed by a C-terminal region rich in β-strands (Sauvage et al., 2008; Welsh et al., 2017; Alexander et al., 2018). Many low molecular weight PBPs, including LpqF, harbour a catalytic domain belonging to the S11 family of peptidases (Welsh et al., 2017). Structural analyses confirmed that LpqF (Rv3593) contains a canonical catalytic triad in its PBP-domain, supporting its classification within the S11 family of peptidases (Figure 26, B, C and Figure 27).

Characterisation of the conservation of catalytic residues in orthologues of LpqF was undertaken by aligning of PBP sequences. The LpqF sequence was uploaded to ConservFold (Mirdita et al., 2022) using the MMSEQ2 setting with 20 iterations (AlphaFoldmultimer3) (Mirdita et al., 2022), and aligned against a taxonomy subset. This analysis identified the 10 highest scoring PDB templates for structural similarity to the PBP domain of LpqF (Methods & Materials, section 2.0). Among these templates were Cpe in *S. clavuligerus* (Valegård et al., 2013), PBPA from *Synechoccus elongatus* (Urbach et al., 2009), and a β-lactamase from *Sphaerobacter thermophilus* (Wu, Clancy, and A. Joachimiak, 2012). The list of hits was filtered for redundant sequences, resulting in a Weblogo conservation plot that displayed a degree of conservation for the catalytic residues and the PBP-domain in a small subset of structures.

To evaluate the conservation of residues among the three catalytic motifs across a broader spectrum of bacterial orthologues, including those from the mycobacterial class of D,D-endopeptidases (D,D-EPases) and D,D-CPases, two groups (the S11 and S13 families of peptidases) from diverse species were selected based on their structural similarities to LpqF and the presence of an activating nucleophilic serine in motif I. The S11 and S13 families generally encompass low molecular weight PBPs, with the S13 family including both CPases and EPases. The first group consisted of D,D-CPases from *Actinomadura sp*. R39 (Sauvage et al., 2005), PBP4, PBP7, and β-lactamases from *E. coli* (Kishida et al., 2006; Risso et al., 2014), PBP4a from *B. subtilis* (Sauvage et al., 2007), and PBP4 from *Haemophilus influenzae* (Kawai et al., 2010). The mycobacterial homologs were represented by enzymes from *M. tuberculosis* (Prigozhin et al., 2014; Cuff et al., 2015), and predicted AlphaFold models for LpqF from *M. tuberculosis*, *M. marinum, M. smegmatis, S. clavuligerus* and *E. coli*. The sequences were pooled and the fasta files were submitted to Clustal Omega to generate a sequence alignment

with gaps and then resubmitted to Weblogo 3 (Crooks et al., 2004). This produced a Weblogo plot showing high conservation of catalytic residues in the PBP-domain for mycobacterial D,D-CPases (Figure 27).





PBP domain of PBP5 in *E. coli*

PBP domain of LpqF in *Mycobacterium tuberculosis*

Superposition of PBP domains for PBP5 and LpqF

Signature motifs

SI/LF/TK SD/GN KT/AG

Figure 27: LpqF bears the signature motifs of a LMW PBP. (**A**) A Weblogo for conservation of the amino acid sequences of LpqF homologs from a diverse range of bacteria. The x-axis represents the amino-acid position, and the y-axis is set to 4 bits. Highlighted in black boxes are the catalytic motifs . The LpqF sequence was inputted into the Conservfold: Protein Conservation to 3D Structure Generator platform using MMSEQ generating alignments with known published PDB files in diverse bacteria (Mirdita et al., 2022; Graham et al., 2023). The output generated a Weblogo plot of 18 highest scoring structurally conserved amino acids and motifs in homologous proteins (Crooks et al., 2004). Weblogo plot residue colour scheme represents a hydrophobicity scale: hydrophilic, blue; neutral, green; hydrophobic, black. The structures used to build the Weblogo conservation alignment are as follows: the LpqF (unpublished structure Rv3593, $LpqF^{Mtb}$), Alphafold predicted structures for LpqF from *M. smegmatis* (AFA0R570-F1, $LpqF^{Sm}$) and *M. marinum* (AFB2HJ33-F, $LpqF^{Mm}$), the D,D-CPases, Rv2911 (PDB ID: 4RYE, Cuff et al., 2015) & Rv3330 (PDB ID: 4PPR, Prigozhin et al., 2014). Cpe from *S. clavuligerus* (PDBs ID: 2xgn, 2xep, Valegård et al., 2013), PBP5 from *E. coli* (PDB ID: 3mzf), PBP4 from *E. coli* (PDB ID: 2ex2), PBP4 from *H. influenzae* (PDB ID: 3a3d, Kawai et al., 2010), PBP4a from *B. subtilis* (PDB ID: 1w5d, Sauvage et al., 2007), Actinomycetes, R39 (PDB ID: 1w79, Sauvage et al., 2005), The D,D-endopeptidase PBP7 from *E.coli*, (Alphafold predicted structure: P0AFI5), PBPA from *Synechoccus elongatus* (PDBs ID: 2j7v, 2jbf, Urbach et al., 2009), β-lactamase A from *E. coli* (PDB ID: 4c75, 5fqq, Risso et al., 2014), a β-lactamase from *Sphaerobacter thermophilus* (PDB ID: 4ewf, Wu, Clancy and A. Joachimiak, 2012). Colour coded superposition of PBP domains of LpqF and PBP5 showing the catalytic triad motifs of PBP5 from *E. coli* (aubergine) and LpqF from *M. tuberculosis* (red). (**B**) Superposition of the catalytic domains in the PBP-domains of LpqF from *M. tuberculosis* and PBP5 (3mzf, DacB) from *E. coli* indicating the conservation for D,D-CPases in different species and the slight deviation for the K/TAG motif.

The results revealed the presence of three conserved PBP sequence motifs (SxxK, SxN, and K/AT/G) that constitute the catalytic centre of the active site within the PBP-domains of 13 orthologous proteins in the S11 and S13 classes of peptidases. These highly conserved residues, typical of low molecular weight PBPs, are anticipated to play a crucial role in D,D-CPase activity within the mycobacterial cell wall. However, notable sequence was observed divergence within the binding pocket of LpqF orthologues. Based on sequence alignments, three catalytic motifs in LpqF were identified as S153-IFK (motif I), S213-DN (motif II), and K354-AG (motif III) (Figures 26, A, B; 27, A, B). These residues are likely to be crucial for enzymatic function. Specifically, mutating S153 in motif I to disrupt potential activation and G356 in motif III to impair deacylation could validate their functional importance (see section 3.1.7). These residues are located within the putative binding pocket spanning residues 174-280, a region consistently conserved across PBP orthologues (Figures 32, 33 B) (Ghosh et al., 2008). Table 17 summarises the diversity statistics for the proteins used in the alignments shown in Figure 27.

Table 17: A summary of statistics for representing the diversity of the 18 enzymes from S11 and S13 groups utilised in Figure 27.

Enzyme (PDB/ID)	Class	RMSD	TM-score	Sequence identity (%)	Aligned residues	Sequence length	Modelled residues
$LpqF^{Mtb}$	S11	-	-	-	-	452	429
$LpqF^{Mm}$	S11	1.76	0.93	78	401	456	456
$LpqF^{Sm}$	S11	2.13	0.90	62	386	439	439
Cpe (2xgn)	S11	2.85	0.66	30	283	458	420
Cpe (2xep)	S11	2.67	0.66	30	284	458	419
β-lactamase (5fqq)	S11	2.63	0.49	21	212	269	262
β-lactamase (4ewf)	S11	2.62	0.49	21	211	275	268
β-lactamase (4c75)	S11	2.83	0.48	19	209	262	262
PBP-A (2j7v)	S11	2.72	0.47	18	210	298	265
(2jbf)	S11	2.75	0.47	18	210	298	264
Rv3330 (4PPR)	S11	2.86	0.45	18	205	334	300
Rv2911 (4RYE)	S11	2.86	0.45	17	210	269	264
PBP7 (POAF15)	S13	2.89	0.43	16	184	310	310
PBP5 (3mzf)	S11	2.78	0.44	16	196	363	355
PBP4 (2ex2)	S13	3.87	0.43	15	178	458	456
PBP4a (1w5d)	S13	3.51	0.45	15	190	462	458
R39 D,D-peptidase (1w79)	S13	3.61	0.44	14	186	489	466
D,D-CPase (3a3d)	S13	3.85	0.43	13	179	453	453

In the analyses of the S11 and S13 enzyme classes, serine and lysine within the SxxK motif at the first and fourth positions are conserved 100 % of the time. In contrast, the second and third positions of the SxxK motif are less conserved, with isoleucine and phenylalanine occurring at frequencies of 16.6% and 30%, respectively. However, these positions are 100% conserved in

LpqF homologs. The SDN motifs across the S11 and S13 PBP sequences exhibit a higher degree of conservation, with asparagine conservation at 100% and aspartic acid conserved at 66.6% of the time with 100% conservation in the mycobacterial homologues. Moderate conservation is observed in the third motif (K/AT/G). The second residue in this motif is threonine in 77.8% of cases, whereas mycobacterial LpqF homologues encode alanine in this position, except for *M. smegmatis*, which encodes glycine at a prevalence of 5.5% (Figure 27, B). Notably, the substitution of alanine for threonine (KA>TG) is less frequent in the S11 class but highly conserved in LpqF homologues of *M. marinum* and *M. tuberculosis*, where it occurs at a prevalence of 22.2%, in these alignments. These percentages might increase with the inclusion of additional LpqF sequences from a more diverse set of mycobacterial homologues. The lower conservation of the third motif has been noted previously in the literature (Ryu et al., 2016).

Tryptophan residues lining the hydrophobic wall within the binding cavity have been reported for PBP3 in *E. coli* and *Pseudomonas aeruginosa*, indicating their importance for binding to peptides (Han et al., 2012; Rowland et al., 2024). Additionally, moderate conservation was observed in the S11 class for tryptophan residues (27.7%) lining the outside edge of the catalytic binding pocket, suggesting a role in catalysis via a hydrophobic binding groove, as observed for some PBP active site clefts (Ryu et al., 2016; Han et al., 2012; Rowland et al., 2024). Moreover, glycine was highly conserved across the S11 and S13 classes at positions 116, 128, and 192 (94.5%, 100%, and 100%, respectively), with the last residue forming part of the KxG motif. Interestingly, positions 280-283 showed a GHHD motif conserved between Cpe (positions 259-262) and LpqF orthologues with a prevalence of 22.2%, potentially indicating a motif of unknown function within the PBP domain of LpqF. As expected, the N-terminal region exhibited a lower degree of conservation (Figure 27, A).

These analyses also revealed homology of motifs I, II, and III between LpqF and the β-lactamases from *E. coli* and *Sphaerobacter thermophilus* (PDB ID: 4c75, 5fqq, Risso et al., 2014; PDB ID: 4ewf, Wu, Clancy, and A. Joachimiak, 2012) with STFK (11%) for 4c75 and 5fqq and STVK (5.5%) for 4wef, and SDN for all three with 25% predominance from the 18 sequences. Though showing a lower degree of conservation, these results highlight the presence of the SxxK, SxN, and KxG motifs across PBPs and β-lactamases (Kumer et al., 2022). Since β-lactamases have evolved from PBPs and use a similar catalytic mechanism, this result is not surprising.

Given that PBP5 is a well-studied D,D-CPase within the S11 class and is structurally similar to the PBP domain of LpqF, it was chosen for comparison to analyse the conservation of the catalytic triad in LpqF across diverse taxa. The superposition of the PBP-domain of LpqF with PBP5 from *E. coli* revealed a structurally conserved catalytic cleft, although PBP5 exhibits a divergent catalytic triad motif comprising 44-SLTK-47, 110-KTG-112, and 213-SGN-215 (Figure 27, B). These alignments showed that the near identical catalytic triad in LpqF with PBP5 is characteristic of the S11 class of low molecular weight peptidoglycan-active enzymes (Figures 26 and 27). While the serine and lysine residues are fully conserved, variations in the intervening residues suggest they are less critical for catalysis. These differences may indicate a specific binding mechanism; however, since the motifs in both LpqF and PBP5 share similar orientation and spatial clustering, it can be inferred that both enzymes may prefer similar peptide substrates, with species-specific peptide modifications playing a lesser role (Nelson & Young, 2001; Nicola et al., 2010; Welsh et al., 2017).

PBP5 functions by cleaving the terminal D-alanine from the stem peptide, providing a substrate for YcbB, an L,D-TPase (Caveney et al., 2019). The crystal structure of PBP5 reveals a binding pocket that accommodates the D-alanine-D-alanine dipeptide, optimally positioning it for catalysis (Nicola et al., 2010; Skoog et al., 2011; Caveney et al., 2019). PBP5 has been shown to bind via its SLTK motif and is inhibited by meropenem, a carbapenem-class antibiotic targeting L,D-TPases (Caveney et al., 2019).

The soluble PBP-domain of PBP5, lacking its membrane anchor, exists in a monomeric form. However, experimental data from the study by Skoog et al. (2011) have been used to model homo-oligomeric complexes in the *E. coli* inner membrane, suggesting that the catalytic domains have sufficient flexibility to access pentapeptides at varying distances from the membrane. This oligomerisation likely enhances the stability and D,D-CPase activity of PBP5 within the bacterial membrane (Skoog et al., 2011). The structural and residue similarities between LpqF and PBP5 have important implications for guiding on future functional studies on LpqF.

In conclusion, these data suggest that the active site of LpqF closely resembles that of the S11 class of proteins and shows high conservation with PBP5, a D,D-CPase, supporting the hypothesis that LpqF functions as a D,D-CPase. However, because the serine catalytic triad motif is widely conserved among peptidoglycan-modifying and β-lactamase enzymes, further biochemical studies are necessary to definitively characterise the function of LpqF.

3.2 Discussion

The active site of LpqF is positioned in its PBP-domain at the C-terminal. The structural arrangement suggests that the flexibility between the PBP and NTF2 domains may influence the enzyme's binding capacity and substrate specificity. Flexibility in protein structure is often associated with functional versatility, allowing enzymes to accommodate a range of substrates and perform diverse biochemical reactions (Lim & Strynadka, 2002). The interplay between the PBP-domain and the NTF2-like domain in LpqF could facilitate conformational changes that are essential for substrate recognition and catalysis. Such dynamic interactions may enable LpqF to adapt to different substrates and perform its enzymatic function effectively. Understanding the structural dynamics of LpqF is crucial for deciphering its biochemical activity and substrate specificity. Further structural studies coupled with functional assays will provide valuable insights into the molecular mechanisms underlying the function of LpqF.

The aim of this chapter was to identify orthologues of LpqF, a gene identified in an archived *Tn*-library from a study conducted 14 years prior to this project. Using high-throughput pinning and serial dilution assays, this study confirmed the morphological differences observed by Chen et al. (2010) (Figures 27, 28). The *Tn*-inserted gene producing Δ*lpqf* exhibited a smaller colony with a thinner crust compared to wild-type. Similar gene deletion mutant strains of PBPs from transposon-mutagenesis studies have been recorded previously. For instance, mutants of HMW PBP1b, PBP2a, and PBP2b in *Streptococcus agalactiae*, although they did not alter colony morphology, grew in a pellet formation in spent media compared to wildtype. This phenotype was later shown to alter the expression of genes involved in peptidoglycan cell wall synthesis (Zhu et al., 2021).The lack of colony morphology change in this context is not surprising as these genes are essential for peptidoglycan elongation.

Keiser et al. (2015) used PonA1, PonA2, and the L,D-TPase (LdtB) in *M. tuberculosis* and showed that deleting *ponA1* and *ponA2* via *Tn*-mutagenesis did not alter growth; however, LdtB reduced the population density in the stationary phase culture. They demonstrated that PonA2 can compensate for PonA1 depletion and that the Ldt interacts with PonA1 and PonA2, they further demonstrate that the Ldt is crucial for growth in the absence of both *ponA1* and *ponA2* genes. Another relevant example of *Tn*-inserted genes is the Baranowski et al. (2018) study focusing on Ldts in *M. smegmatis*. Using *Tn*-sequencing, the authors showed that 6 Ldts

(Δ*ldtAEBCGF)* interact with PBP2 and PonA1 and that in the absence of Ldts, the PBPs are inactive, leading to morphological defects when 3 of the 6 Ldts are depleted. Given the literature for both HMW and LMW PBPs, the delayed growth pattern and difference in colony edge thickness on solid agar, and morphological defects observed using similar methods in LpqF, an uncharacterised PBP in *M. marinum*, it was decided to investigate LpqF further.

An analysis of the genetic distance of *lpqf* in mycobacteria was conducted. The phylogenetic tree depicted in Figure 23 showcases the evolutionary relationships among various mycobacteria specifically highlighting orthologues of LpqF in *M. tuberculosis, M. bovis*, *M. leprae*, *M. marinum*, and *M. smegmatis*. The tree illustrates the clustering of these orthologues, indicating the degree of genetic similarity of *lpqf* and the divergence of genomes among the different species. The divergence between the strains has been reported in previous studies (Gey van Pittius et al., 2006; Mickael Orgeur et al., 2024). The tree scale in these analyses also includes the evolutionary distance, quantifying the genetic divergence between the orthologues. This phylogenetic analysis underscores the evolutionary conservation and potential functional similarities of *lpqf* across different *Mycobacterium* species.

The next investigation undertaken was synteny analyses of *lpqf* using 200 Mycobacteriaceae species and 200 species that encode a *lpqf* orthologue. In the comparative analyses within Mycobacteriales, a pattern of conservation emerged, with 100% sequence coverage for a putative hydrolase, the heme-degrading monooxygenase (*mhud*), and *lpqf* (Rv3591, Rv3592, Rv3593 in *M. tuberculosis*) (Figure 24, A, D). In contrast, the alignments across taxa with 260 hits from 243 genomes, showed potential orthologs. The analysis of the conservation of LpqF across Mycobacteriales species and diverse genera indicate that while the PBP domain is highly conserved, the inclusion of an NTF2 domain appears to be restricted to mycobacteria (Figure 24, B).

In conclusion, these data demonstrate for the first time that *lpqf* is a highly conserved gene in Mycobacteriales, along with two other putative flanking genes: one encoding an uncharacterised hydrolase and *mhud*, which encodes a heme-degrading enzyme. The high degree of conservation of these neighbouring genes among orthologues suggests that *lpqf* may be part of a predicted operon that is co-transcribed, as described for *mhud* and *lpqf* (Blanco and Bigi, 2023). Further analysis of *mhud* could determine whether the absence of *lpqf* impairs

mhud expression. However, since this assumption has not been validated, it should be confirmed through additional studies such as chemical genomics or RNA sequencing.

Structural and bioinformatic analyses of the domains and motifs in the LpqF sequence revealed that LpqF possesses a PBP/transpeptidase/β-lactamase domain in the C-terminal region and an NTF2-like domain in the N-terminal region, with sequence similarity to ORF12 (Cpe), an esterase in *S. clavuligerus* (Figures 25 and 26, A, B). The N-terminal NTF2-like domain consists of 7 α-helices and one large β-sheet. Structural similarity to the NTF2 domain was assessed using Foldseek, which identified 100 PDB templates containing uncharacterised proteins with Cpe as the top hit. Other notable hits included a Snoal-like protein from *B. thailandensis* and an NTF2-like protein from *Pseudomonas aeruginosa*, both uncharacterised but available in the PDB database. All three structures were superimposed onto the NTF2-like domain of LpqF (Figure 25; Figure 26, C). The RMSD for Cpe was the closest match with a score of 3.56 Å, followed by the snoal-like protein with 4.86 Å, and the third uncharacterised protein at 6.61 Å. This structural similarity suggests a conserved motif between LpqF, Cpe, and the snoal-NTF2-like proteins, supporting the possibility of functional homology across different bacterial species.

Motifs I, II, and III have been reported to be present in most PBPs or their homologues, including D,D-peptidases, making them highly conserved (Sauvage et al., 2008; Peitsaro et al., 2008). These motifs adopt similar structural spacing in the polypeptide sequence, indicative of an evolutionary origin (Goffin and Ghuysen, 1998; Pratt and McLeish, 2010).To investigate the residue composition for motifs of LpqF in the context of low molecular weight PBPs, the S11 and S13 class of low molecular weight EPases and CPases were selected. These classes were chosen based on the prediction of the motifs, domain organisation, and automated annotated databases. A residue conservation plot was generated by uploading 18 of the highest scoring hits.

The results show that motif I consists of the catalytic serine residue in the tetra-peptide. Generally, the serine in this motif acts as a nucleophile while the lysine residue is involved in the acylation step (153-SIFK-156 in LpqF and 44SLTK-47 in PBP5). In motif II, for most PBPs, the important residue is either tyrosine or serine, which initiates the deacylation of the active serine (Sauvage et al., 2008). In LpqF, motif II, the conserved residues serine and asparagine were present, and therefore are conserved among these orthologs. In contrast, motif

III consists of lysine (K), aspartic acid (A), and asparagine (G) (354-KAG-356), whereas in PBP5 motif III consists of lysine (K), threonine (T), and glycine (G) (213-KTG-215) (Figure 27). This conservation with changes to the non-conserved amino acids in motif III have been reported across the PBP family and its homologs (Sauvage et al., 2008; Ryu et al., 2016). It could be postulated that the substitution of alanine instead of threonine in motif III of LpqF could indicate a species specific mechanism for substrate peptidoglycan binding as reported for motif III in other PBPs (Ryu et al., 2016; Moon et al., 2018).

Despite the motif analyses not producing high homology scores with any of the β-lactamases in mycobacteria, such as BlaC, Rv0406c, Rv3677c, and CrfA (Voladri et al., 1998; Wang, Cassidy, and Sacchettini, 2006; K.M. Nampoothiri et al., 2008; Kumar et al., 2017), hits for shared homology between LpqF and β-lactamases from *E. coli* (PDB ID: 4c75, 5fqq, Risso et al., 2014) and *S. thermophilus* (PDB ID: 4ewf, Wu, Clancy, and A. Joachimiak, 2012) were present. These are class A serine β-lactamases, which also encompass the BlaC gene family of β-lactamases (Kaderabkova et al., 2022).

Although LpqF lacks the canonical omega loop typical of β-lactamases, some dual-function enzymes have a loop-like structure at the bottom of the active site, such as the D,D-CPase MSMEG_2432, with D179 in the active site important for dual activity and substrate specificity (Egorov et al., 2019; Pandey et al., 2020). BlaC has this conserved residue, which is representative in 98.8% of class A β-lactamases; however, this is absent in LpqF (Ilona van Alen et al., 2023). An example of dual activity comes from studies such as Bansal et al. (2015) and Pandey et al. (2020) of MSMEG_2432 and MSMEG_2433, which exhibit both β-lactamase and D,D-CPase activity. Therefore, although structural differences exist between β-lactamases and LpqF, these analyses suggest a conserved catalytic mechanism. Considering the structure of PBP-domain of LpqF coupled with research on dual functionality (D,D-CPase and β-lactamase) in peptidoglycan-targeting enzymes, it is unlikely that LpqF functions solely as a β-lactamase. However, these results do not rule out the possibility that LpqF may possess dual activity, and thus, this hypothesis will need to be validated through further testing.

PBP5 was selected from these analyses for its structural and functional similarity to LpqF, and its PBP-domain was superimposed over the PBP-domain of LpqF. In LpqF, the observed differences in motifs I and II affect the non-conserved residues that have been reported as common in PBP-domains of peptidoglycan targeting enzymes (Sauvage et al, 2008; Ryu et al.,

2016; Moon et al., 2018). In contrast, motif III consists of lysine (K), alanine (A), and glycine (G), whereas in PBP5, motif III consists of lysine (K), threonine (T), and glycine (G) (Figure 27). However, the lysine and glycine are conserved, and these residues are reported in the literature to be vital for correct positioning of substrate, with glycine of motif III utilised to avoid steric hindrance (Sauvage et al., 2007). The glycine is also important for specificity of PBP-domain towards the last D-alanine on the stem peptide of peptidoglycan (Adediran, et al., 2005). Indeed, the presence of the KAG motif in motif III of Cpe in *S. clavuligerus* further emphasises the importance of these motifs in substrate binding and catalysis across enzymes with diverse functions. This observation underscores the significance of conserved motifs in determining the functional properties of enzymes and highlights their crucial role in substrate recognition and enzymatic activity.

In summary, conservation of the PBP triad motifs I, II, and III, along with structural similarities with PBP5, a D,D-CPase, suggests that LpqF is a D,D-CPase, most likely acting on peptidoglycan stem peptides and could potentially have a β-lactamase dual function, as described in the literature for other D,D-CPases (Pandey et al., 2020). The next chapter describes the biochemical characterisation assays undertaken to understand LpqF function.

3.3 Conclusion

Based on these data, it is likely that LpqF is a low molecular weight penicillin binding protein, potentially belonging to the peptidase S11 class, and is likely a D,D-CPase. It may participate in cleaving D-amino acids from stem peptides or in regulating other penicillin binding proteins and/or L,D-TPases. In the next section, the first step in the biochemical characterisation of LpqF will be described.

Chapter 4: Rv3593 (LpqF) is a low molecular weight penicillin binding protein and is selectively inhibited by carbapenems

4.0 Expression and purification of LpqF

Prior to the start of this project, the portion of the *M. tuberculosis lpqf* gene that encodes amino acids 36-452, which removes the predicted secretion signal, was cloned into the pET-SUMO expression vector. This construct includes an N-terminal His_6-tag followed by a small ubiquitin-like modifier (SUMO) tag to aid in solubility (Malakhov et al., 2004; Marblestone, 2006; Wilson and Heaton, 2008). Expression of SUMO-LpqF was induced with the addition of IPTG (See Materials and Methods). The inclusion of the SUMO tag was previously found to be necessary to produce soluble protein (Moynihan, P. private communication).

LpqF was successfully purified using standard methods (Figure 28) and it was found that unless it was immediately buffer-exchanged into 25 mM Bis-Tris, pH 8.0, the protein was prone to degradation. The predicted molecular weight of His_6-SUMO-LpqF is 57 kDa. The apparent molecular weight of the protein, based on comparison to the molecular weight standard, is 58 kDa, suggesting that the protein was not truncated or degraded during expression (Figure 28, A).

The SUMO tag and thus the 6x His-tag were successfully removed via cleavage by incubating LpqF with Ulp1, a SUMO-specific protease (Figure 28, B, lanes 2 and 3). A second IMAC was conducted to remove the remaining cleaved His_6-SUMO tag, the protease and any uncleaved protein. Cleavage of LpqF was verified by SDS-PAGE analysis, yielding the expected size of 44 kDa (Figure 28, B). The cleaved SUMO-tag is predicted to be 13 kDa, which is observed in Figure 28, B, lane 3. A control sample of uncleaved LpqF was also included on the gel (Figure 28, B, lane 1).

Densitometry analysis of the gel using ImageLab indicated that the protein was approximately 70% pure. The presence of contaminating proteins in the sample was likely due to the purification process. To improve sample purity, LpqF was subjected to size exclusion chromatography. SDS-PAGE analysis of the size exclusion chromatography fractions

confirmed the purity of the protein, showing a single band at the expected molecular weight size of 44 kDa (Figures 28, C and D).

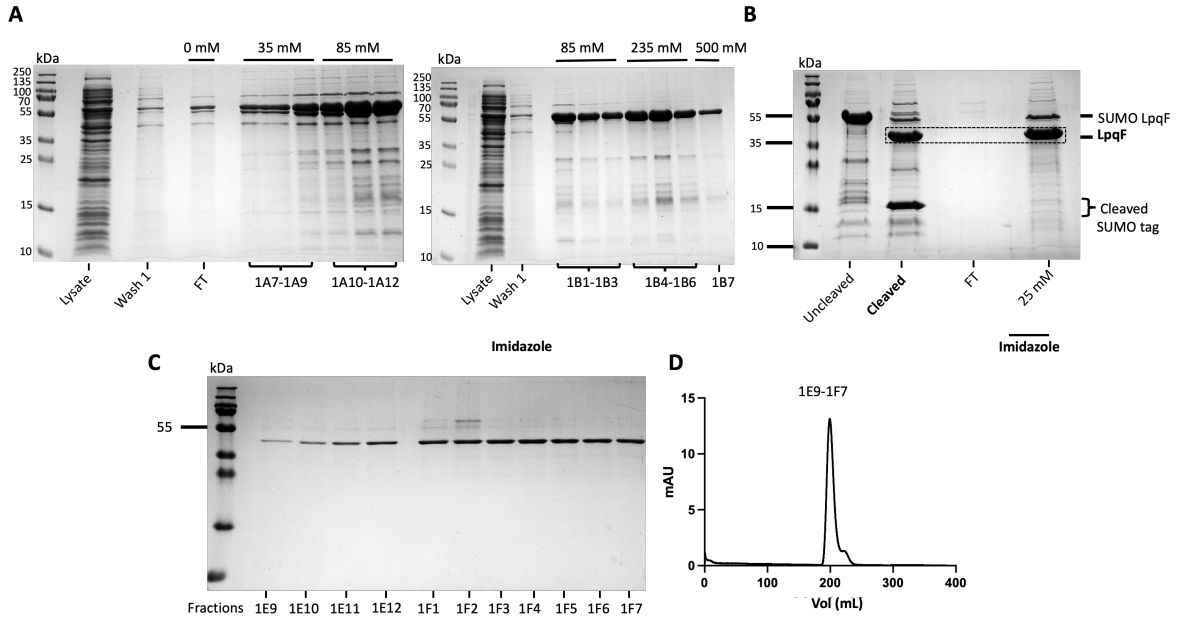


Figure 28: SDS-PAGE analysis of LpqF purification. (**A, B**) An SDS-page showing metal affinity chromatography on an ÄKTA Pure 25 system with a 1 mL GE HisTrap fast-flow column of clarified lysate containing the expressed protein LpqF in *E. coli* with gradients of imidazole (0, 35, 85, 235, and 500 mM) for eluent fractions of LpqF. (**B**) An SDS-page showing purified protein and confirmation of removal of 6 x histidine tag and SUMO tag in the N-terminal using SUMO protease. (**C**) An SDS-PAGE with the size excluded fractions of purified protein. (**D**) A chromatogram of size excluded monomeric form of LpqF according to lab standardised molecular weights.

4.1 Functional analysis of LpqF

The *in silico* analysis of LpqF led to the prediction that the LpqF will have D,D-CPase activity. However, low molecular weight PBPs such as D,D-CPases and β-lactamases are relatively unexplored in *M. tuberculosis* (Kumer et al., 2022). To test this hypotheses, the purified protein was used in an *in vitro* context to assess the ability of LpqF to form an acylation intermediate with β-lactams, as has been reported in the literature for low molecular weight PBPs. For example, Shapiro et al. (2013) utilised bocillin, a derivative of penicillin V attached to a fluorescent dye, to test acylation or binding rate for PBP3 in *P. aeruginosa*. Studies such as Pandey et al. (2018) and Bansal et al. (2015) also used bocillin as well as nitrocefin, a chromogen, to test the activity of the D,D-CPases MSMEG_2432 and MSMEG_2433 in *M. smegmatis*. Both bocillin and nitrocefin have a core structure of a β-lactam ring that shares similarity with the D-alanine-D-alanine backbone structure, a natural substrate of PBPs (Bansal

et al., 2015; Kim et al., 2023; Pandey et al., 2018). Nitrocefin is a chromogen that changes colour upon hydrolysis of the β-lactam ring from yellow to red, indicating β-lactamase activity and the colour change intensity is an indication of hydrolytic potency (Calbiochem). This similarity allows these compounds to be utilised for visualizing the hydrolysis of substrates in the active site of the PBP domain in an assay-specific context (Shapiro et al., 2013; Bansal et al., 2015; Ryu et al., 2016; Pandey et al., 2018).

4.1.1 LpqF is unlikely to be a β-lactamase

A nitrocefin chromogenic enzyme assay was performed to determine whether LpqF can hydrolyse the amide bond of the β-lactam ring of the cephalosporin substrate nitrocefin (Figure 29). The enzyme was tested across a range of pH values (5.4-8.0) to assess potential β-lactamase activity under these conditions (Figure 29). Cephalosporinase (SigmaAldrich) from *Bacillus* was used as a positive control and exhibited activity under all tested conditions (Figure 29). In all conditions, the control was able to hydrolyse the substrate therefore the conditions for concentrations 18 µM and 36 µM are shown in Figure 29 as a representation of the data obtained in this assay. Since the control consistently hydrolysed the substrate, the results for 18 µM and 36 µM concentrations are presented in Figure 29 as representative data from this assay. At 18 µM enzyme concentration (Figure 29, A, B, and C), a slower increase in absorbance (2×10^{-3} vs 9×10^{-4} nmols/sec) was observed compared to the 36 µM concentration. For cephalosporinase, saturation where the maximum number of substrate molecules is converted into the product per unit of time (k_{cat}), was reached at 60 minutes for the 18 µM condition vs 20 minutes for the 36 µM condition respectively across all experimental setups (Figure 29, D, E & F). In contrast, under the conditions tested, LpqF did not hydrolyse nitrocefin even at the higher enzyme concentration of 36 uM. Notably, absorbance measurements for LpqF at 36 µM were below zero, indicating that increasing the concentration had no impact in this assay. These findings suggest that LpqF is unable to hydrolyse the β-lactam ring of nitrocefin, indicating that LpqF does not function as a β-lactamase.

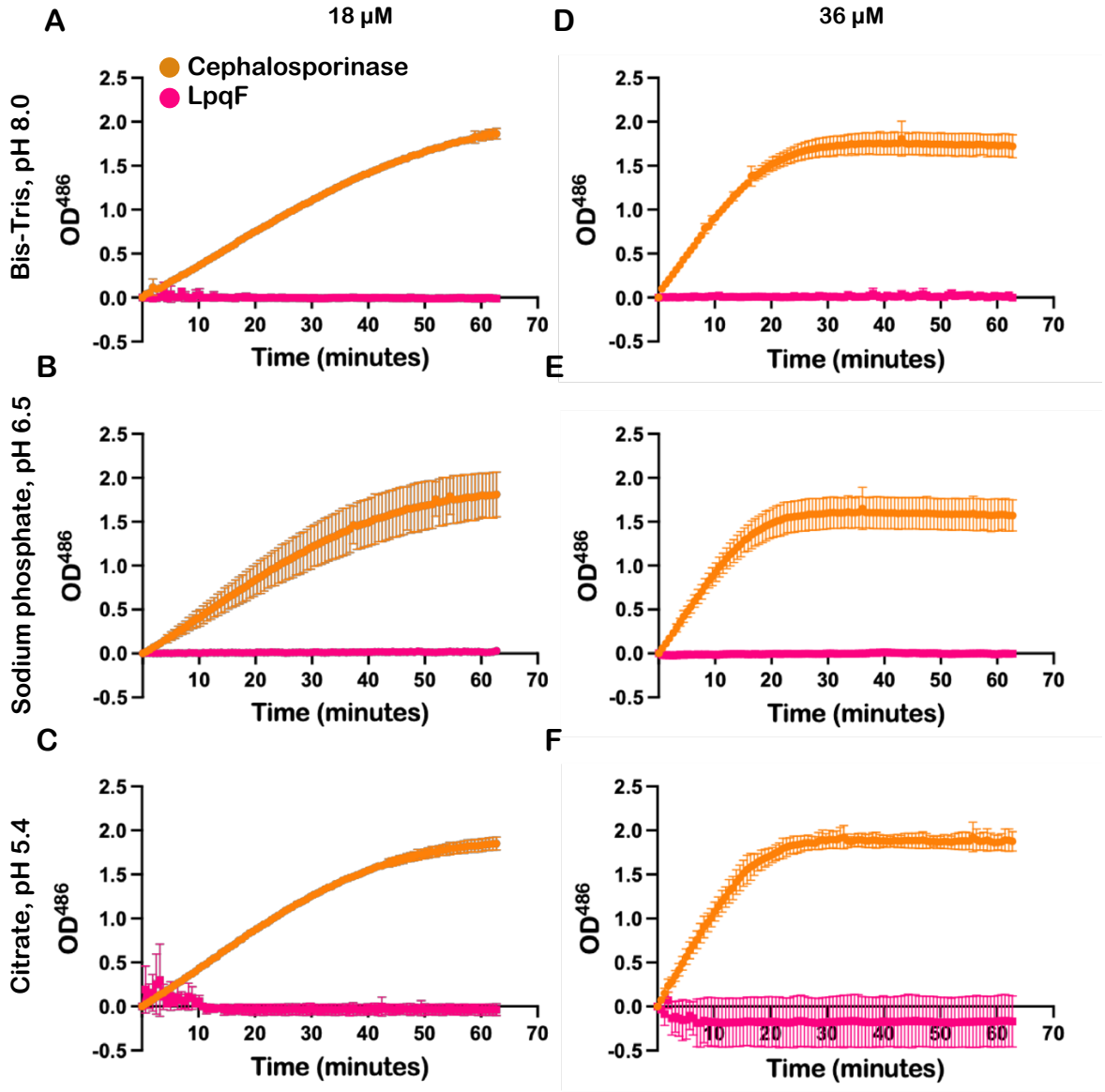


Figure 29: LpqF β-lactamase activity assay. Reactions were initiated by addition of LpqF or cephalosporinase at concentrations of enzymes 18 and 36 µM respectively to a reaction containing 1 mg/mL nitrocefin at a range of pH conditions: (**A, D**) Bis-Tris, pH 8.0, (**B, E**) sodium phosphate, pH 6.5 (**C, F**), and citrate, pH 5.4. The reaction was followed for 30 min. Data represent triplicate assays and error bars are the standard deviation.

4.1.2 LpqF selectively binds to β-lactams and is inhibited by meropenem

To determine if LpqF behaves as a classical PBP, the degree to which it could be inhibited by β-lactams was assessed using a bocillin-FL protection assay. In this assay, the enzyme is first incubated with a given β-lactam and then with bocillin-FL. If the β-lactam reacts covalently with the enzyme, bocillin-FL will be unable to bind to the protein. These reactions can then be monitored by SDS-PAGE by comparing Coomassie-staining and fluorescence imaging of the

proteins. Under these conditions, the absence of fluorescence indicates inhibition by the β-lactam.

A broad range of β-lactam antibiotics were chosen for this experiment, including carbapenems (imipenem, meropenem, doripenem), cephalosporins (cefsulodin, cephalothin, nitrocefin), penicillins (penicillin G, amoxicillin, oxacillin, mecillinam, piperacillin, cloxacillin), and the monobactam aztreonam. As a control, LpqF incubated with no β-lactam prior to bocillin-FL and was set at 0% inhibition.

The results of this assay demonstrate that LpqF binds to carbapenems, as evidenced by the complete absence of bocillin-FL signal (100%) in the LpqF-treated samples with meropenem and doripenem treated samples. The related compound, imipenem, reduced fluorescence by only 60% suggesting some degree of carbapenem selectivity for LpqF. In contrast to the carbapenems, cefsulodin and cephalothin did not reduce the fluorescence intensity, suggesting that LpqF is not sensitive to cephalosporins. In addition, nitrocefin was included in this assay to assess if the lack of nitrocefin cleavage was due to LpqF inhibition or the enzyme's inability to cleave the molecule. These data coupled with the nitrocefin data indicate that LpqF can weakly bind to nitrocefin but does not hydrolyse it. There was a similar level of fluorescence observed for the penicillin class of inhibitors, with a decrease of approximately 10% for penicillin G, amoxicillin, and oxacillin. This result is surprising given that bocillin-FL, a penicillin derivative, showed fluorescence in the absence of treatment indicating the ability of Bocillin-FL to enter the unobstructed active site of LpqF. Finally, mecillinam, piperacillin, cloxacillin, and aztreonam also showed no reduction in fluorescence. This assay demonstrated that bocillin_FL can enter the active site, where its attached fluorophore becomes excited after forming the acyl-enzyme intermediate complex. These results suggest that the compounds tested can also access the active site of LpqF; however, no cleavage occurs (Figure 29). Overall, this assay indicates that LpqF is strongly inhibited by the carbapenem class of β-lactams, while the penicillins and cephalosporins tested had no effect on LpqF, aside from bocillin-FL itself.

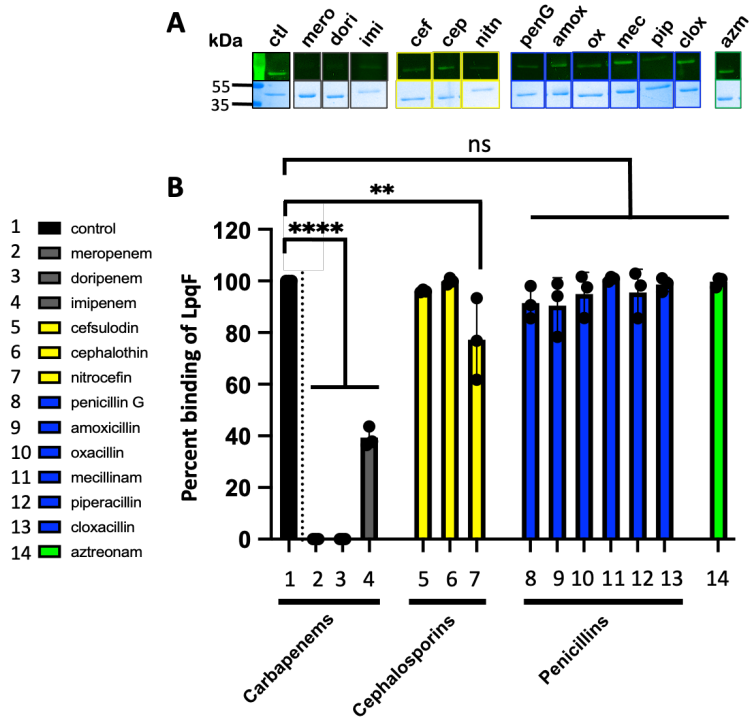


Figure 30: LpqF is inhibited by a variety of β-lactams. LpqF (5 µM) was incubated with the indicated β-lactam for 60 min at 25 ºC in 25mM phosphate buffer, pH 7.0. Bocillin_FL was then added to these reactions at a final concentration of 50 µM. (**A**) The reactions were subsequently analysed via SDS-PAGE and imaged on a ChemiDoc (BioRad) using the UV setting followed by Coomassie staining. (**B**) The fluorescence intensity of LpqF in triplicate reactions was determined using ImageLab and plotted in GraphPad Prism 10. Significance was determined using a One-way ANOVA and Dunnett's multiple comparisons test, Error bars represent mean with ± standard deviation. Ns non-significant ($p > 0.05$), **** $p < 0.0001$. Data represent n = 3 biological replicates and these are indicated. Ctl; untreated LpqF, mero; meropenem, dori; doripenem, imi; imipenem, cef; cefsulodin, cep; cephalothin, nitfn; nitrocefin, pen; penicillin G, amox; amoxicillin, ox, oxacillin, mec; mecillinam, pip; piperacillin, clox; cloxacillin, azm; aztreonam.

4.2 Discussion

In chapter 3 the *in silico* analysis of LpqF suggested that it most likely belongs to the β-lactamase or D,D-CPase families of enzymes. However, results indicate that the enzyme does not possess β-lactamase activity but is inhibited by the penam class of β-lactams. Although LpqF shares a common PBP-domain fold with conserved motifs I and II, its motif III is less conserved. Most PBPs, including D,D-CPases, share structural homology, particularly in catalytic motifs similar to those of class A serine β-lactamases, supporting the evolutionary link between penicillin binding proteins and β-lactamases as demonstrated in the literature (Sauvage et al., 2008; Bush et al., 2018).

As a preliminary step in assessing the function of LpqF, the purified enzyme was tested for its ability to hydrolyse the chromogenic β-lactam substrate nitrocefin. When tested in the buffer used for optimal purification of the enzyme, LpqF exhibited no activity. To account for the possibility of a narrow pH optimum, LpqF was also tested at (pH) 6.5 and 5.4, but similar results were obtained. This contrasts with the rapid turnover of nitrocefin by a known class A β-lactamase, the cephalosporinase from *B. cereus*, under identical assay conditions (Figure 29). This confirmed that the assay conditions were suitable for detecting β-lactamase activity.

Although LpqF has not been previously assayed, both DacB1 and DacB2 have been shown to degrade nitrocefin, albeit slowly (Kumar et al., 2022). The absence of detectable β-lactamase activity for LpqF may suggest a narrow substrate specificity. LpqF may bind nitrocefin similar to DacB1 and DacB2 but could have a higher affinity for peptidoglycan peptides, with a slower deacylation rate. In contrast, β-lactamases like BlaC rapidly hydrolyse β-lactams, such as penicillins, due to significantly higher deacylation and hydrolysis rates (Kumar et al., 2022). These data indicate that LpqF lacks β-lactamase activity under the conditions tested and is therefore unlikely to function as a β-lactamase.

The subsequent investigation focused on testing the affinity of LpqF for β-lactam antibiotics using the bocillin-FL assay, which utilises a penicillin V derivative. The results for penicillins and cephalosporins were non-significant, clearly indicating that LpqF is not susceptible to these classes of β-lactams (Figure 30). These results demonstrate that the carbapenems meropenem, and doripenem, have a higher binding affinity for LpqF compared to penicillins and cephalosporins. However, since this assay relies on the percentage of fluorescent dye bound, this finding requires further validation through quantitative analysis of binding kinetics, hydrolysis rates, and potential active site modifications (Shapiro et al., 2013).

Additionally, these results illustrate that imipenem exhibits a weaker substrate binding mechanism in this context, whereas the penicillins and cephalosporins show no measurable affinity for LpqF. This could potentially arise to the structural differences between imipenem and meropenem, despite both belonging the carbapenem class. Specifically, the addition of a methyl group at C1 position of the carbapenem moiety of meropenem facilitates the stability of the meropenem-acyl-intermediate complex. In contrast, the hydrogen atom at C1 in imipenem is more prone to degradation (Pryka and Haig, 1994) (See Table 5).

Imipenem has been shown to have more activity against Gram-positive bacteria, whereas meropenem is more active against Gram-negative bacteria (Kitzis, Acar, and Gutmann, 1989; Davies et el., 2008). For example, meropenem has been shown to have high binding affinity for PBP3 and PBP6 in Gram-negative bacteria such as *E. coli* and *P. aeruginosa*, compared with imipenem (Kitzis, Acar, and Gutmann, 1989). While, in *E. coli* imipenem has four-fold binding activity for PBP1a and PBP1b (Davies et el., 2008). However, both imipenem and meropenem have equal potency in *E. coli* for PBP2 and in *Staphylococcus aureus* for PBP1, PBP2, and PBP4 (Kitzis, Acar, and Gutmann, 1989). While the literature reports meropenem to be a broad-spectrum carbapenem for the synthase PBPs, it has also been shown to have high affinity for Ldt2 in *M. tuberculosis* (Li et al., 2013). However, unlike in Gram-negative bacteria, meropenem is highly susceptible to hydrolysis by BlaC, the most potent β-lactamase known in the Mycobacteriales (Li et al., 2013).

The results of LpqF and imipenem contrast with findings on D,D-CPases such as PBP5 in *E. coli*, which has been shown to be inhibited by meropenem and imipenem in substrate-bound crystal structures (Caveney et al., 2019). The Caveney et al. (2019) study noted that PBP5 exhibits a similar acylation rate for meropenem and imipenem. In their study, they showed that PBP5 bound more quickly and deacylated more slowly than the L,D-TPase YukD, despite both enzymes being capable of binding to a similar stem peptide in peptidoglycan. Interestingly, PBP5-β-lactam complexes have been shown to have differing acylation rates with other compounds, such as cloxacillin and cefoxitin via an unknown mechanism (Nicola et al., 2010). Furthermore, in a study by Kumar et al. (2012), purified DacB2 (Rv2911) was shown to form an acyl-adduct with meropenem using a fluorescent coupled assay and a synthetic pentapeptide substrate. Given that LpqF is a low molecular weight enzyme with structural homology to PBP5, it is hypothesised that the binding of meropenem to form an meropenem-acyl-adduct with LpqF is similar to PBP5. These discrepancies in native substrate specificity of each of these enzymes could drive the specificity for different β-lactams. It could be that LpqF might have a specific affinity for carbapenems due to structural differences, such as the capping loop that covers the active site of YkuD (residues 426-491), which is absent in LpqF and PBP5. This absence could allow for structural modifications depending on the class of bound β-lactams, explaining the difference between imipenem and meropenem acylation. In addition, PBP5 has an open active site cleft, whereas the active site cleft of LpqF is occluded by a coil and short α-helix consisting of the residues T286-A299. Interestingly, these residues in PBP5 consist of T145-T149. Although capping loops have not been reported in the literature for PBP5, both

potential capping loops of LpqF and PBP5 are proximal to the active site. The ‘loop’ in LpqF sits above the active site, while the ‘loop’ in PBP5 is positioned adjacent to its active site. Both loops could play a role in stabilising the carbapenem-intermediate (Figure 27).

In this study both meropenem and doripenem treated LpqF inhibited bocillin-FL in an *in vitro* assay, indicating potential functional differences similar to those reported for PBP5. As meropenem primarily targets L,D-transpeptidases (Ldts) responsible for 3,3 cross-linking in peptidoglycan stem peptides (Caveney et al., 2019), the apparent high specificity of meropenem for LpqF could suggest a mechanism that involves limiting D,D-CPase activity after a certain point in peptidoglycan insertion. This would prevent tetrapeptide production and subsequently inhibit Ldts, impeding 3,3 cross-link production, as reported by Kumar et al. (2012). This suggests enzyme complex or crosstalk activity, as detailed in the Caveney et al. (2019) study.

Other examples include the lipoprotein Rv2864c, which functions as a D,D-transpeptidase and exhibits susceptibility to carbapenems in *in vivo* assays, albeit to a lesser extent (Olivença et al., 2022; Kumar et al., 2022). This indicates that meropenem-acylation is common among enzymes with the SxxK motif, as suggested by Caveney et al. (2019). According to these authors, it is proposed that PBP5 interacts with the carbonyl oxygen on C7 of meropenem, enabling it to occupy the oxyanion hole, which helps in stabilisation and formation of the acylation intermediate. The side chain of the serine in the SDN motif, adjacent to the leaving group nitrogen on meropenem, promotes acylation intermediate formation. The asparagine residue from this motif then forms a hydrogen bond with the hydroxyethyl group on C6 of meropenem, while the threonine residue from the KA/TG motif forms hydrogen bonds with C3 of meropenem and is further stabilised by the lysine residue of the KA/TG motif. Although, a mechanism for LpqF is highly likely, this has not been proven for LpqF, and it will need to be validated as described above.

4.3 Conclusion

Although nitrocefin has been reported to undergo recycling in L,D-TPases from *Enterococcus faecium*, forming a reversible acyl-intermediate that diffuses out of the active site, similar processes in D,D-CPases or low molecular weight PBPs have not been reported (Edoo, Arthur

and Hugonnet, 2017). The data obtained from the first set of biochemical tests suggest that LpqF is unlikely to possess β-lactamase activity. The results from the nitrocefin assay indicated that LpqF does not appear to hydrolyse nitrocefin under any of the tested conditions (Figure 29).

These data point to a narrow range of substrate specificity for the binding site cleft of LpqF. This specificity is suggested by the enzyme's selective affinity for certain β-lactam antibiotics, such as meropenem and doripenem, which inhibited bocillin-FL treated LpqF *in vitro*. The structural features of LpqF, including its active site motifs (SIFK, SDN, and KAG), appear to play a critical role in substrate recognition and binding; however, mutagenesis studies are required to confirm this. The interaction of these motifs with the functional groups of β-lactam antibiotics, as hypothesised from studies on similar enzymes like PBP5, indicates a precise mechanism that limits the activity of LpqF to specific substrates. This specificity might involve interactions with the carbonyl oxygen and hydroxyethyl groups of the antibiotics, stabilising the acylation intermediate and facilitating the inhibition of D,D-CPase activity similar to the mechanism reported for Ldts and PBP5, thereby impacting peptidoglycan synthesis and cross-linking. However, these assumptions need further validation through detailed kinetic studies and structural analyses.

In summary, the results of these biochemical assays suggest that LpqF is not a β-lactamase and is unlikely to exhibit the same dual mechanisms as reported for MSMEG_2432 and MSMEG_2433 in previous studies (Pandey et al., 2018; Bansal, 2015). Moreover, LpqF appears to be susceptible to the carbapenem class of β-lactams, similar to other D,D-CPases. However, these data do not conclusively distinguish specific substrate binding for a D,D-TPase. The next section will describe macromolecular peptidoglycan and peptidoglycan fragment-specific assays aimed at further examining this hypothesis.

Chapter 5. Biochemical analysis of LpqF

5.0 Introduction

In the previous chapters, it was demonstrated that LpqF has structural similarities with PBP5 from *E.coli,* which is a low molecular weight, S11 D,D-CPase (Caveney et al., 2019). Following these results, basic binding studies showed that the LpqF can be acylated by β-lactams, with a strong preference for carbapenems. This indicates that the protein is catalytically competent. In this chapter, the evaluation of LpqF and its capacity to degrade peptidoglycan will be discussed.

Carbapenems such as meropenem, imipenem, doripenem, and ertapenem are broad spectrum, last-line defence antibiotics and potent inhibitors have been shown to inhibit several peptidase enzymes by targeting the domain of PBPs involved in peptidoglycan biogenesis, including synthases (L,D-TPases), and hydrolases (D,D-CPase) (For mechanism see Chapter 1, Sections 1.8.5 and 1.8.9). This inhibition affects peptide crosslinking and other peptidase reactions (Silva et al., 2015; Papp-Wallace et al., 2011; Armstrong et al., 2021). Moreover, carbapenems are effective inhibitors of various β-lactamase enzymes, including class A β-lactamases such as TEM-1, SHV-1, and *M. tuberculosis* BlaC, by forming stable, long-lived acyl-enzyme complexes (Mehta et al., 2021; Chudyk et al., 2022). The main mechanism of resistance against carbapenems arises from metallo-β-lactamases (Lisa et al., 2017). These enzymes, such as OXA variants, particularly in *A. baumannii*, have been associated with conferring resistance to carbapenems, significantly impacting their clinical efficacy (See Chapter 1, Section 1.9) (Evans & Amyes, 2014). This underscores the broad-spectrum efficacy of carbapenems against a wide range of peptidoglycan targeting enzymes. Consequently, reverse mutagenesis studies aimed at determining the function of uncharacterised enzymes are more challenging.

One avenue of investigation considered the relationship between synthases and hydrolases, specifically the L,D-TPases and D,D-CPases. The L,D-TPases are responsible for performing 3-3 cross-linking in peptidoglycan and have been shown to carry out a side reaction where they perform D-amino acid exchange by substituting D-alanine for other amino acids, including fluorescent D-amino acids both *in vitro* and *in vivo* (Hammes, 1978; Kuru et al., 2014; Kuru et al., 2019). PBPs such as D,D-CPases play a critical role in this process by cleaving the terminal D-alanine prior to L,D-TPases executing their function. As stated above, some PBPs responsible

for 3-4 cross-linking have also been shown to be inhibited by carbapenems. Additionally, certain PBPs possess secondary functions. For example, Qiao et al. (2014) demonstrated that PBP4 preferentially acts as a TPase *in vitro* and is primarily responsible for incorporating exogenous D-amino acids into cellular peptidoglycan polymers, monomers, Lipid I, and Lipid II, suggesting that it also has TPase activity *in vivo*. Given that LpqF is specifically inhibited by carbapenems and is a PBP in S11 class of enzymes, it was hypothesised that it may recognise a substrate with a chemical structure similar to that of the TPases and also mediate the exchange of D-amino acids into peptidoglycan.

5.1 LpqF does not perform a D-amino acid exchange reaction *in vitro*

Fluorescent D-amino acids (FDAAs) have been utilised as tools in microscopy studies to demonstrate the incorporation, utilisation, and accumulation of peptides into peptidoglycan by PBPs and L,D-TPases during cell elongation in both Gram-positive and Gram-negative bacteria (Kuru et al., 2014; Kuru et al., 2019). The fluorescent D-amino acid 3-[[(7-Hydroxy-2-oxo-2H-1-benzopyran-3-yl)carbonyl]amino]-D-alanine hydrochloride (HADA; Bio-techne, TOCRIS) is a derivative of D-alanine attached to a dye and can be used *in vitro* to quantify D-alanine exchange. Espaillat et al. (2024) demonstrated a method for this with an L,D-TPase in *Gluconobacter oxydans*. Based on this approach, the ability of LpqF was tested, in the presence of macromolecular peptidoglycan, to catalyse an exchange reaction using HADA as a substrate.

An exchange assay was conducted using either LpqF or RipA. The proteins were incubated with 5 mg/mL of peptidoglycan derived from *Mycobacterium smegmatis* and 500 μM of HADA in 25 mM phosphate buffer (pH 7.0) for 18 hours. Given that the optimal pH range for mycobacterial peptidoglycan enzyme kinetics spans from 5 to 7.5, and considering the similarity of this assay to the exchange reaction assay reported by Espaillat et al. (2024) in the context of HADA and purified LpqF, the experiment was performed under physiological conditions (pH 7.0) (Yao et al., 2012; Botella et al., 2017; Peters et al., 2019; Melzer et al., 2022). This setup aimed to determine whether LpqF acts as a synthase or facilitates synthetic reactions. RipA, a known peptidoglycan endopeptidase, was included as a negative control. Following the incubation, samples were washed to remove excess HADA, and the pellets were resuspended in phosphate buffer. Fluorescence was measured at an excitation wavelength of 405 nm and an emission wavelength of 450 nm.

In this assay, an exchange reaction would result in a fluorescence increase above the peptidoglycan control, indicating the enzyme's ability to append free D-alanine. However, LpqF showed no significant fluorescence (pink bar) compared to the enzyme-free reaction (peptidoglycan only, red bar), suggesting that no D-alanine exchange was catalysed (Figure 31). RipA exhibited a much lower fluorescence level than LpqF (66%, black bar) and the peptidoglycan-only control (85%), further indicating that RipA could not catalyse D-alanine transfer as expected. This result confirmed that the assay was functioning correctly. In summary, these data do not support the hypothesis that an exchange reaction occurs in the presence of LpqF. However, the absence of a positive control limits the ability to completely rule out this possibility.

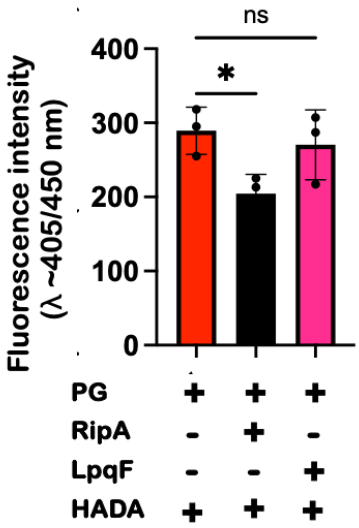


Figure 31: Assessment of the capability of LpqF to exchange D-alanine in an *in vitro* assay. To evaluate the ability of LpqF to perform an exchange reaction**,** the enzymes were incubated with HADA and *M. smegmatis* mc^2155 PG for 18 h in phosphate buffer, pH 7.0. Samples were washed with buffer then fluorescence was monitored at Ex: 405 nm, Em: 450 nm. The reported fluorescence associated with the PG-pellet is after 3 washes (**C**). Bars represent the mean with individual data points shown and error bars represent standard deviation. Quantitation of HADA uptake was analysed via GraphPad Prism 10. Significance was determined using a one-way ANOVA with Tukey's multiple comparison test. ns - non-significant (* = $p < 0.05$).

5.2 LpqF has weak or no hydrolytic activity on polymerised peptidoglycan

Given the previous data that LpqF is low molecular weight PBP capable of binding to β-lactams and appears not to have synthase activity. The next logical step was test if LpqF possesses hydrolytic activity using a peptidoglycan-degradation assay. For this assay, peptidoglycan was

conjugated to fluorescein isothiocyanate (FITC) and used as a substrate. Upon hydrolysis of the insoluble peptidoglycan, the reaction products, which are conjugated to the fluorophore are solubilised, providing a clear readout for peptidoglycan-cleaving enzymes. As a positive control, RipA was used, a known mycobacterial peptidoglycan endopeptidase (Ruggiero et al., 2010; Böth, Schneider, and Schnell, 2011).

One consideration in this assay was to set up reactions at multiple pHs, allowing for a range of possible pH optima, as observed for other peptidoglycan-degrading enzymes (Pizarro, Fernández, and Orce, 1988; Ohnishi, Ishikawa, and Sekiguchi, 1999; Botella et al., 2017; Peters et al., 2019; Schaefer et al., 2020; Xie et al., 2021; Wysocka et al., 2022; Melzer et al., 2022). In this assay, to preclude a lack of activity caused by a similar phenomenon, LpqF was tested at pH 6.0, 7.0, and 8.0 (Figure 32, A). In this experimental setup, the fluorescence intensity generated by RipA served as the standard, with the highest single RipA replicate set to 100% activity and all other readings normalised accordingly. Under these conditions, LpqF did not release a significant amount of fluorescent product from the substrate compared to the enzyme-free control. In contrast, RipA consistently catalysed product formation, with its activity peaking at pH 7.0.

Having established that LpqF had little or no activity, with the highest value being at pH 7.0, a second assay was conducted at pH 7.0 to investigate the potential for pre-digestion by RipA to potentiate LpqF activity like that observed for RipA and amidase 1 in the study by Healy, Gouzy, and Ehrt (2020) (Figure 32, B). The combination of RipA and LpqF yielded the same fluorescence release as samples with RipA alone, and LpqF did not demonstrate activity independently. This suggests that RipA had no effect on LpqF under these assay conditions. The fluorescence release by LpqF was measured at 21 ± 1%, which was only 5% above the no-enzyme control and was not found to be statistically significant. These data demonstrate that LpqF does not appear to be influenced by RipA under the conditions tested. Taken together, these results suggest that it is unlikely that LpqF has endopeptidase activity.

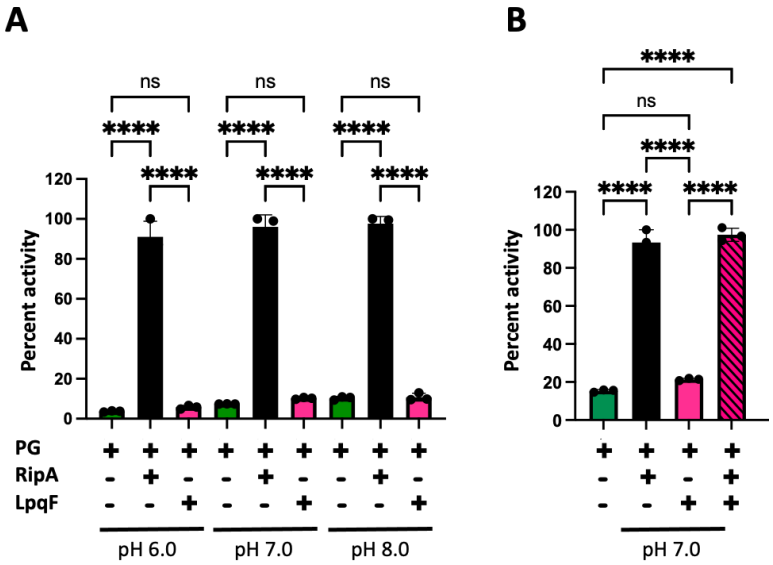


Figure 32: LpqF does not hydrolyse polymerised *M. smegmatis* peptidoglycan in an *in vitro* degradation assay. (**A** & **B**) The indicated enzymes were incubated with FITC-labelled peptidoglycan for 18 h at 25 °C in phosphate buffer, pH 6.0, 7.0 and 8.0. Supernatants were collected, centrifuged, and filtered through a 0.2 microfilter to remove debris. Supernatant and 500 mM sodium hydroxide were mixed in a 50:50 ratio and fluorescence quantified (Em = 490 nm, Ex = 520 nm). (**A**) Data for each buffer condition is shown as percent activity normalised to RipA at pH 8.0. (**B**) Using conditions identical to the pH 7.0 assay, we also tested if RipA activity would potentiate LpqF. Activity here is normalised to RipA. Data are representative of three independent experiments. Statistical significance was determined using a one-way ANOVA and Kruskal-Wallis test. Error bars represent mean with ± standard deviation. ns non-significant ($p > 0.05$), ****$p < 0.0001$.

Despite the fluorescence release not being statistically significant in the preceding assay, a small amount of product formation above the no-enzyme control was consistently observed. It was reasoned that this product might be too minor relative to the background in the assay, prompting an evaluation of the reaction composition using thin-layer chromatography (TLC). Cross-linked peptidoglycan derived from *M. smegmatis* (mc^2155) was used as a standard. Using this experimental setup, the enzymes LpqF, RipA, and a combination of the two were tested alongside an additional control, mutanolysin, as shown in Figure 33. Mutanolysin was included as a positive control to confirm peptidoglycan degradation and validate the functionality of the assay. For the TLC, a solvent system consisting of 1-n-butanol, methanol, ammonium hydroxide, and deionised water in a ratio of 5:4:2:1 (v/v) was used to detect the FITC-conjugated products, following the method of Moynihan et al. (2019). Numerous products were observed on the TLC for both RipA and mutanolysin, consistent with their known ability to solubilise the complex peptidoglycan structure (Figure 33).

Given that detection by fluorescence can be quantitative, it was possible to measure liberated fluorescence from the origin for each lane and as a percent of the total fluorescence using ImageJ. Only a small amount of released fluorescence in the supernatant migrated away from the origin in the peptidoglycan-only control. This is expected because macromolecular peptidoglycan is insoluble and would not leave the origin, resulting in only small, soluble products visualised as fluorescent bands migrating away from the origin. Two products were observed at the top of each lane, irrespective of sample type. These are speculated to be either artefacts resulting from background noise or, more likely, the presence of other labelled products in the reaction and/or undigested peptidoglycan. This may include small soluble amine side groups, either present in the buffer or co-purified within peptidoglycan (Figure 33, A, lane 1). The values for relative fluorescence intensity for each lane were normalised to RipA from the origin to the solvent front, which released the most product and was therefore set to 100% activity (Figure 33, A, lane 3). As expected, mutanolysin had the next highest amount of liberated fluorescence at ~76% (Figure 33, A, lanes 1 & 2).

In the LpqF lane, a band was detected that is absent in the no-enzyme lane that represented 11.7% liberated fluorescence as a total percentage of that lane (Figure 39, A, lanes 1 and 4, outlined in red boxes). The LpqF and RipA combination showed 74% activity relative to RipA, which unexpectedly indicated a decrease in the cleaved product compared to RipA alone, as outlined in Figure 33, A, lanes 3 and 5. Additionally, to compare the levels of quenched background, LpqF, RipA, and the combination of RipA and LpqF were normalised to the no-enzyme control (10%), resulting in values of 1%, 9%, and 7%, respectively.

Overall, these results agree with the plate reader assay, suggesting that LpqF is not releasing a product associated with endopeptidase or amidase activity. The presence of a small product in the LpqF lane could indicate a low-abundance reaction product. However, this could also reflect background fluorescence. Additionally, the unexpected results for the RipA and LpqF combination are not consistent with the previous degradation assay, suggesting that LpqF may affect RipA activity under the conditions tested. However, this discrepancy may be explained by the differences in sample processing and visualisation.

To determine whether the potential product from LpqF aligns with the data shown in panel A of Figure 33, a second assay was performed at pH 6.0. This condition was chosen based on the pH range tested in the data presented in Figure 32. Reaction products were analysed via TLC

to evaluate the impact of the lower pH on the product profile of LpqF, providing additional insights (Figure 33, panel B). The results of this TLC indicated that the product migration was impeded under these conditions, as shown in Figure 33, B (red box, lane 5). Despite n = 3, the poor separation may suggest insufficient drying of the TLC plate or the polarity of the solvent used in this TLC was suboptimal, rather than being attributable to pH differences. All fluorescence measurements were normalised to RipA, consistent with the normalisation approach used in the previous TLC experiment. For LpqF, the fluorescent value was 9.2 ± 4%, with a non-significant increase of 2.5% compared to the peptidoglycan-only (6.5 ± 0%) and the peptidoglycan and meropenem (6.0 ± 2%) controls.

Under these conditions, the susceptibility of RipA and LpqF to meropenem was also evaluated. Unexpectedly, meropenem appeared to decrease RipA activity by 70% (16 ± 7%) (Figure 33, B, C, lanes 3 & 4). Similar to RipA, LpqF samples treated with meropenem showed a decrease in fluorescence to 8.3 ± 4%, a reduction of 1% compared to LpqF only, and a reduction of 2.3% compared to the peptidoglycan with meropenem control, which had fluorescence values of 6.0 ± 2% (Figure 33, B, C, lanes 4 & 5). Taken together, these results show a single species released by LpqF. This species may indicate cleavage of the stem peptide by LpqF, but it is more likely to be artefactual based on results discussed further on.

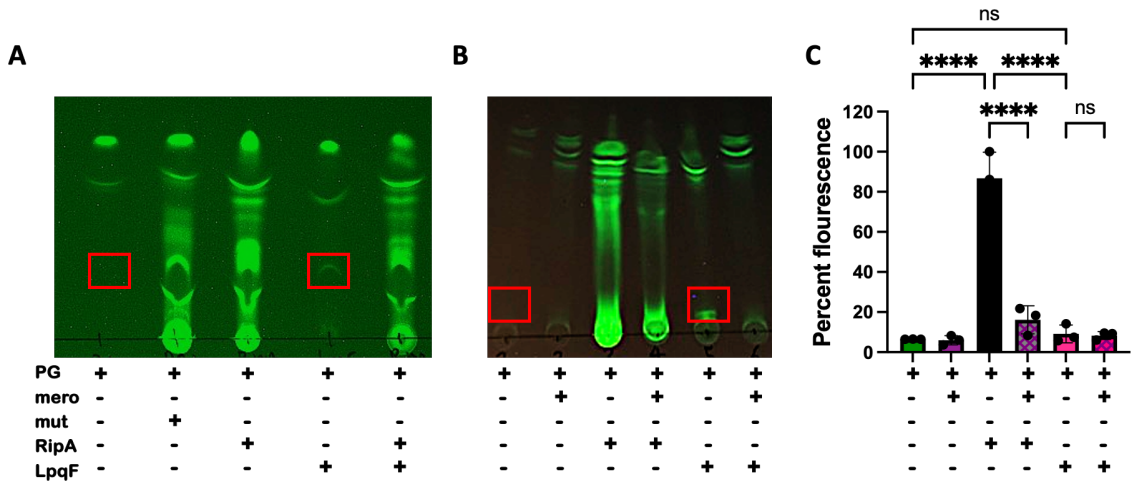


Figure 33: Determination of LpqF hydrolytic activity on FITC-PG by thin layer chromatography. The indicated enzymes were incubated with FITC-labelled peptidoglycan for 18 h at 25 °C in phosphate buffer, (**A**) pH 7.3 and (**B**) pH 6.0. 10 µL of the total reaction was subsequently spotted onto the origin of a TLC plate which was then dried and developed in a solvent system of 1-n-butanol-methanol-ammonium hydroxide-dH_2O 5:4:2:1 (v/v). TLC fluorescence was analysed using a BioRad ChemiDoc XRS+ using the UV setting 365 nm. The red box indicates potential cleavage product of LpqF. Red boxes represent the presence of a product in the LpqF lane and absence in the PG only lane. The values obtained from each TLC are given by the total fluorescence liberated from the origin for each lane and is a percent of the total fluorescence. (**C**) The values from Panel B are presented in panel C with colours for each bar from left to right areas follows; PG only (green), PG+mero (dark purple), RipA (black), RipA+mero (grey+drak purple), LpqF (pink), LpqF+mero (pink+dark purple). Mero; meropenem, mut, mutanolysin. Data values were obtained using FIJI, ImageJ and lanes quantitated using Excel v 16.8 and Graphpad, Prism 10. Statistical analysis, One way ANOVA, Tukey's multiple comparisons test. Error bars represent mean and standard error of the mean. ns non-significant ($p > 0.05$), ****$p < 0.0001$.

The role of D,D-CPases in facilitating the formation of 3-3 cross-links via L,D-TPases is critical in peptidoglycan remodelling, as they provide tetrapeptide substrates necessary for this process (Pandey et al., 2018). Given that LpqF did not produce significant detectable products in the FITC release assay, it was reasoned that the FITC may sterically hinder the enzyme or LpqF might release a product not labelled by this molecule. The compositional analysis of peptidoglycan by reverse-phase HPLC is a robust and quantitative method for analysing the reaction products of lytic enzymes (Glauner, 1988). Accordingly, the reaction products of LpqF were analysed with peptidoglycan from mid-exponential *M. smegmatis* or *E. coli* by RP-HPLC. The chromatograms are presented in Figure 34.

LpqF was incubated with peptidoglycan from *E. coli* or *M. smegmatis* for 18 h in phosphate buffer (pH 6.0) and processed according to the methods outlined in Methods and Materials (sections 2.10.4 & 2.10.5). The chromatographic separation of the mutanolysin products derived from *E. coli* peptidoglycan yielded the expected pattern of peaks consistent with prior studies (Glauner, 1988; Höltje & Young, 2004; Kühner et al., 2014; Figure 34, A, B). Kühner et al. (2014) utilised *E. coli* to analyse muropeptide composition via ultra-performance liquid

chromatography, confirmed by mass spectrometry. They reported the monomeric forms of tri- and tetrapeptides (with abundances of 11.6% and 6.4%) as well as dimers of tetrapeptide-glycine, tetra-tetrapeptide, and tetra-tetrapeptide (with abundances of 12%, 19%, and 19.9%, respectively). Despite methodological deviations, similar retention times and relative abundance values were observed in the *E. coli* chromatograms shown in Figure 39, panels A and B (Table 18). These results confirm that muramidase digestion and subsequent muropeptide separation by RP-HPLC were successful for *E. coli*-derived peptidoglycan. However, no difference was observed between samples incubated without LpqF (Figure 34, A) and those treated with the enzyme (Figure 34, B, C). Therefore, under these conditions, the data suggest an absence of activity for LpqF on *E. coli* peptidoglycan.

In contrast to the *E. coli* chromatograms, the *M. smegmatis* chromatograms exhibited only one peak (Peak 6) under identical separation conditions (Figure 34, D). This peak with a retention time of 14.06 minutes, with peak areas of 13.06% and 5.02%, respectively (Figure 34, D, E). This peak appeared to be reduced by 2.6 fold in the presence of LpqF (Figure 34, E, F). This observation contrasts with prior analyses of peptidoglycan degradation techniques for *M. smegmatis* (see section 5.4) (Pandey et al., 2018). Moreover, since only Peak 6 was present in *M. smegmatis* chromatograms, this suggests incomplete or no digestion of *M. smegmatis* peptidoglycan with mutanolysin, or a failure in the chromatographic conditions.

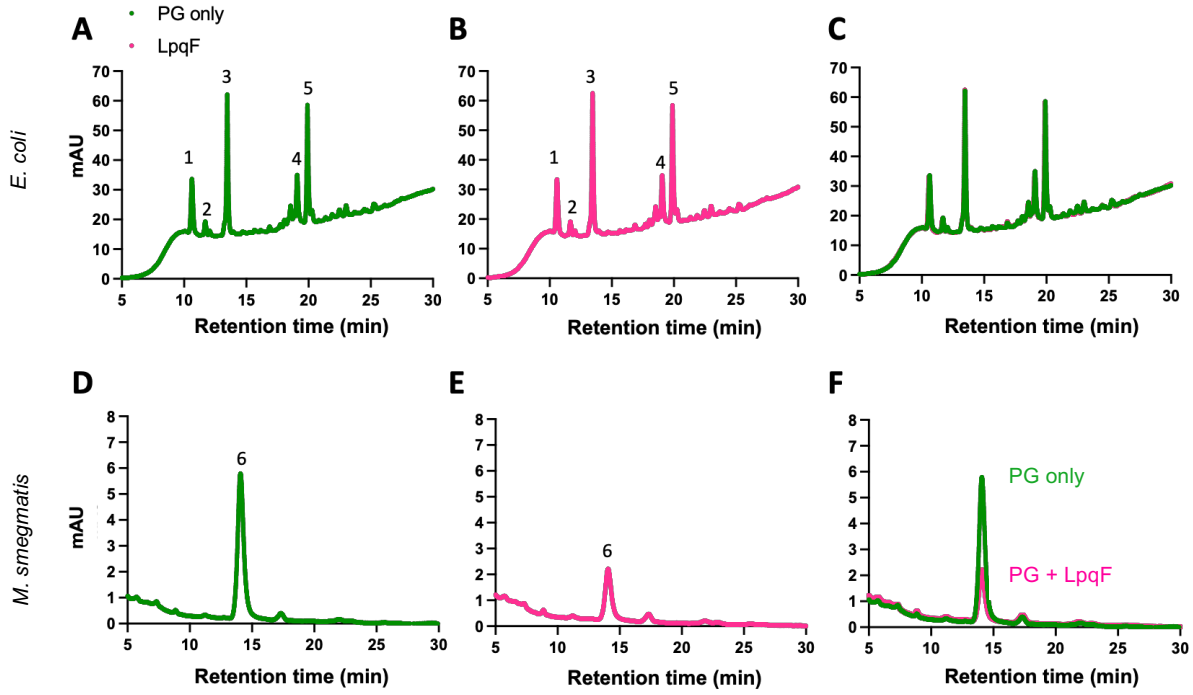


Figure 34: HPLC separation of reaction products derived from LpqF digestion of *E. coli* and *M. smegmatis* peptidoglycan. Muropeptide elution profiles of mutanolysin-digested peptidoglycan isolated from *E. coli* (K12) and *M. smegmatis* mc^{2}155 with and without LpqF. Respective sacculi were incubated with LpqF (for enzyme treated) and then mutanolysin, the resulting muropeptides were reduced with sodium borohydride and analysed by RP-HPLC. (**A**, **D**) Chromatographs for PG only, (**B**, **E**) PG incubated with LpqF, (C, **F**) and an overlay of PG only and LpqF. Chromatograms are representative of three biological repeats. Retention time and purported composition of muropeptides can be found in Table 18. Peak identifications correspond to Table 18 for retention times (Kumar et al., 2012; Kühner et al.,2014; Rimal et al., 2022).

Leveraging the stability of the elution profile for *E. coli* K12 peptidoglycan, certain peaks in the traces can be tentatively identified, as outlined in Table 18. However, the situation differs for the *M. smegmatis* data, where assigning peak identifications is not possible.

Table 18: Muropeptides from *E. coli* analysed by HPLC. Peak identities for this study are highlighted in column three. Peak identities derived with similar elution times from the Kühner et al.,(2014) study for *E. coli* are outlined in column four and referenced in column five. Information relating to retention times, peak areas and relative abundance are in reference to this study.

Peak ID	Retention time (mins)	Peak area (mAU*min)	Relative abundance (%)	Presumed stem peptide composition	Study
1	11.6	3.9	2.81	Tri	Kühner et al.,2014
2	12.0	0.23	0.16	Tetra-Gly	Kühner et al.,2014
3	13.4	8.9	6.4	Tetra	Kühner et al.,2014
4	19.0	2.5	1.8	Tetra-Tri	Kühner et al.,2014
5	19.9	6.4	4.5	Tetra-Tetra	Kühner et al.,2014

5.3 LpqF cleaves L-alanine-γ-D-glutamate-L-lysine-D-alanine-D-alanine pentapeptide

The FITC release assay requires that LpqF releases a product that is connected to FITC. However, for D,D-CPase activity, this would not be the case, as the terminal D-alanine residues do not have a free amine to conjugate with FITC. To address this limitation, an alternative approach using TLC was explored.

This aimed to test whether LpqF could degrade soluble peptides. The rationale for probing the substrate preference of LpqF stems from observations that peptidoglycan regulatory enzymes, like the D,D-CPases Rv2911 and Rv3330 in *M. tuberculosis,* have demonstrated a weak preference for sacculi *in vitro*, with varying affinities for different pentapeptide compositions (Kumar et al., 2012; Prigozhin et al., 2014). Additionally, low molecular weight D,D-peptidases, such as those found in *Streptomyces*, like R39 and R61, have specificity for stem peptide fragments (Adediran et al., 2010; Nemmara et al., 2011).

One major hurdle encountered during this work was the limited availability of muropeptides and peptide substrates tailored for mycobacterial-specific enzymes. This is in contrast to model organisms like *Staphylococcus aureus,* for which such substrates are readily available commercially. To address this limitation, it would be necessary to purify mycobacterial-derived peptide fragments within the laboratory. However, due to time constraints, a pentapeptide, L-alanine-γ-D-glutamate-L-lysine-D-alanine-D-alanine abbreviated to penta-L (Sigma), was used as a substitute. The major differences between this stem-peptide and the mycobacterial substrate is the presence of L-lysine where *meso*-diaminopimelic acid would be found at the 3rd positions in mycobacterial peptidoglycan. Minor changes can be further modified such as the amidation of *meso*-diaminopimelic acid and D-glutamate in mycobacterial species (Kumar et al., 2005; Ngadjeua et al., 2018; Shaku et al., 2023), which could potentially impact enzyme affinity for stem peptide substrates (Kumar et al., 2005).

Following the precedent set by previous tests for LpqF in the FITC-PG degradation assays, conditions were maintained at pH 7.0 for this assay. Considering that the commercial pentapeptide used substituted *meso*-diaminopimelic acid with L-lysine, it is likely that the enzyme would not be highly active on this substrate. Therefore, an optimisation process was undertaken to explore enzyme concentrations prior to the assay and mitigate streaking or merging. In preliminary experiments, lower enzyme concentrations were tested, but the data

were inconclusive. However, at 100 µM for both LpqF and RipA, the assay showed robust clear product formation. To drive product formation to a level that would be detectable by TLC, relatively high concentrations of 100 µM were needed and were therefore chosen to represent the data. This approach also aligns with established literature on peptidoglycan analysis via TLC methods (Hoyland et al., 2014). This clearly showed the presence of the reaction products. The solvent system used was the same as described in the Moynihan et al. (2019) study for LpqI, a β-*N*-acetylglucosaminidase. This was paired with ninhydrin staining as described previously (Hoyland et al., 2014).

The TLC analysis conducted with 100 µM LpqF incubated with penta-L as a substrate revealed a product inconsistent with cleaved D-alanine (R*f* of 0.3) and unfortunately could not be identified (black box, Figure 35). Consistent with previous degradation assays using polymerised *M. smegmatis* peptidoglycan, LpqF and RipA were tested together to determine whether one could activate the other in the context of penta-L and D-alanine-D-alanine substrates. The results suggest that LpqF was unable to cleave penta-L in the presence of RipA, as no product was detected in the RipA only lane, indicating that RipA alone it is not active against penta-L (black box, Figure 35). In comparison, the lane containing the D-alanine-D-alanine substrate in the presence of LpqF, a product with the same R*f* value as the D-alanine standard was detected, indicating cleavage of the di-peptide substrate (red box, Figure 35). This observation was also evident in the lane containing both LpqF and RipA but was notably absent in lanes containing RipA reaction products only as expected. These findings suggest that LpqF can cleave the substrate independently, even in the presence of RipA. Although this assay demonstrates that LpqF can release a product from the di-peptide substrate or potentially from penta-L, it does not definitively confirm if this is activity occurs under physiologically conditions. Future studies should reevaluate these results using an appropriate positive control, such as DacB, alongside additional controls like *meso*-DAP and pentapeptides derived from *E. coli* and mycobacteria (Ealand et al., 2019; Kumar et al., 2022), to complement the standards and RipA controls. Unfortunately, these controls were omitted due to time constraints. Furthermore, the data indicate that LpqF retains catalytic activity at pH 7.0. In conclusion, the identification of D-alanine as a product of the LpqF-catalysed reaction strongly suggests that LpqF functions as a D,D-CPase. However, further validation is warranted, particularly to quantify the unidentified band observed with penta-L in the presence of LpqF and assess LpqF activity with tetrapeptides and pentapeptides.

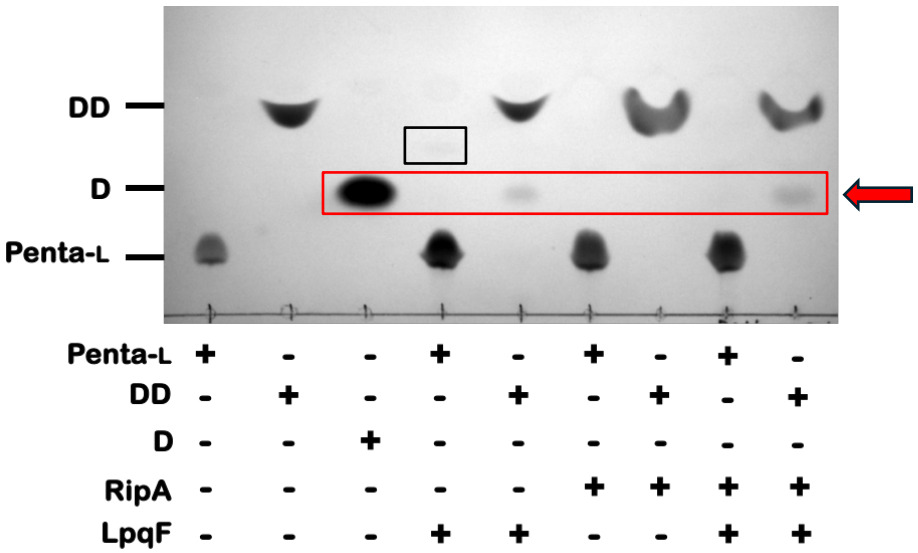


Figure 35: LpqF-catalysed reaction products against pentapeptide by TLC. The indicated enzymes were incubated with pentapeptide or D-alanine-D-alanine for 18 h at 25 °C in 25 mM phosphate buffer (pH 7.0). Red arrow indicates the reaction products assumed to be D-alanine. Supernatants were collected, lyophilised, and then resuspended in phosphate buffer pH 7.0 and spotted onto silica plates. The TLCs represent 100 µM (**A**) To visualise the reaction products, 10 µL of the total reaction was subsequently spotted onto the origin of a TLC plate which was then dried and developed in a solvent system of 1-n-butanol-methanol-ammonium-hydroxide-dH_2O 5:4:2:1 (v/v) followed by detection with ninhydrin. Controls samples contained no enzymes and are as follows; D; D-alanine, penta-L; pentapeptide; DD; D-alanine-D-alanine. TLCs are representative of n = 3.

5.4 Discussion

In this chapter, it was demonstrated that LpqF may have D,D-CPase activity. Various assays ranging from transpeptidase to hydrolase on an array of substrates were used to come to this conclusion. The first of these was the investigation into the potential of D-alanine exchange facilitated by LpqF using the presence of HADA and peptidoglycan derived from *M. smegmatis*. The results revealed LpqF was not non-significant in fluorescence compared to peptidoglycan alone, suggesting that LpqF is not capable of driving a synthetic reaction (Figure 31). To further validate these results, a positive control such as an L,D-TPase should be used in this assay.

Though the method in this study deviates from published data, similar methodology has been described. For example, Montón Silva et al., (2018) used *in vitro* analysis for orthogonal FDAA probes and apply HPLC to determine the ability of LdtD in *E. coli* to exchange D-alanine, using HADA as a marker for labelling muropeptides. The authors observed that while LdtD could carry out an exchange reaction, the overall fluorescence of the reaction decreased. They

attributed this phenomenon to the enzyme simultaneously catalysing a hydrolysis reaction, which was favoured under their experimental conditions. While it has been shown that Ldts (L,D-TPases) can append and transfer D-amino acids, this is the first time to my knowledge that this methodology using a novel *in vitro* assay has been applied in the context of testing a mycobacterial D,D-CPase.

In the degradation assay using FITC-conjugated *M. smegmatis* polymerised peptidoglycan (FITC-PG), peptidoglycan was incubated with purified LpqF to investigate its activity by measuring the liberated soluble peptidoglycan fragments in the supernatant. Unlike RipA, LpqF did not significantly release digested products (Figure 32). This difference could be due to the distinct cleavage sites of each enzyme: D-glutamate-*meso*-diaminopimelic acid for RipA and potentially D-alanine-D-alanine for LpqF. Given that FITC forms a covalent bond with primary amines , it does not bind to the D-alanine-D-alanine portion of the stem peptide, which lacks primary amine groups (López-Zabalza et al., 1990; Hernandez et al., 2009).

Despite the semi-quantitative assessment of FITC-labelled digested peptidoglycan and TLC-resolved products for LpqF not demonstrating clear hydrolytic activity for LpqF, the appearance of a minor product suggests two possibilities. These bands may be artefacts of the analysis, or LpqF cleaves at an alternative site on the pentapeptide other than the terminal D-alanine (Figure 33, A, lane 5). The former explanation is more likely, especially considering that this band is also present in the RipA lane of the TLC. Additionally, TLC-resolved products formed by RipA were evident in lane 3 of Figure 33, A, indicating that RipA effectively cleaved the peptidoglycan at the third position, supporting the proof of principle and application of FITC-TLC analyses for peptidoglycan-targeting enzymes. Furthermore, the multiple products present in the lane combining RipA and LpqF (Figure 33, A, lane 6) could suggest that LpqF may cleave the tripeptide formed by RipA, indicating a potential synergistic or regulatory effect. As expected, these constituents were absent in the mutanolysin control, due to its exolytic β-1,4 glycosidic bond cleavage between Glc*N*Ac and Mur*N*Ac, rather than on the stem peptides (Figure 33, A, lane 2). Based on the results, these data suggest, but do not prove, that LpqF may act downstream of RipA cleavage and could potentially have a second or alternative cleavage site. Interpretation of these results would be enhanced by including a D,D-CPase control, such as DacB, or multifunctional D,D-EPases like Rv2911 or AmpH.

Critically, to further validate the use of TLC-resolved products, LpqF digesting RipA reaction products would not increase the total fluorescence release, so this activity would not be captured in the plate-based FITC-PG assay. The higher-resolution approach of FITC-TLC enhances the visualisation of products from enzymes that cleave between amino acids, providing a clearer understanding of their enzymatic activities. To our knowledge, this represents the first application of TLC to visualise hydrolase reaction products of FITC-conjugated peptidoglycan.

Using a reactive dye like FITC comes with several caveats, including sensitivity to pH changes, photobleaching, and the necessity to remove any unbound dye to prevent a reduced signal-to-noise ratio. While these challenges were addressed during the optimisation process, there was also the potential for steric occlusion to alter binding efficiency if LpqF had endopeptidase activity. Supporting the argument that FITC might sterically hinder the binding of LpqF, a study by Fei et al. (2011) demonstrated an altered affinity profile for wheat-germ agglutinin (WGA) conjugated to FITC with GlcNAc, compared to non-FITC-conjugated WGA.

Other studies have used fluorescein isothiocyanate (FITC)-conjugated peptidoglycan, initially described by Maeda et al. (1980). In recent years, FITC has emerged as a valuable tool for assessing the hydrolytic activity of peptidoglycan-active enzymes. This method has since been applied by Moynihan et al. (2019) and Boelter et al. (2022) for the characterization of LpqI, a β-*N*-acetyl-glucosaminidase in mycobacteria, and for amidase activation regulators in *E. coli*. Additionally, the study by Gurnani et al. (2021) investigated *E. coli* amidases (AmiA, AmiB, and AmiC) and their activator ActS via a degradation assay using FITC-conjugated peptidoglycan. Furthermore, synergistic effects have been documented between RipA and enzymes such as the synthase PonA1 in previous findings in mycobacteria (Hett, Chao, and Rubin, 2010; Healy, Gouzy, and Ehrt, 2020). This method allows for sensitive detection of enzymatic activity due to the covalent attachment of FITC to peptidoglycan, which emits fluorescence when hydrolysed, making it ideal for high-throughput assays.

Despite the challenges in achieving robust separation for digested products in the RP-HPLC analysis. A reduced peak in the chromatogram of *M. smegmatis* incubated with LpqF was detected compared to the non-LpqF control. The 2.6-fold reduction of peak 6 in the LpqF-incubated sample may indicate a product released by LpqF under these conditions. However, the reliability of these data is low given the unusual nature of the chromatogram. Due to the

lack of separation via RP-HPLC, I was unable to perform mass spectrometry and assign a mass to peak 6 in the *M. smegmatis* chromatogram, preventing an in-depth analysis or comparison with known literature or databases. Although liquid chromatography-based methods for mycobacterial peptidoglycan analysis were being optimised in the Moynihan laboratory, they became available too late during my PhD for application to LpqF.

In contrast, the *E. coli* traces demonstrated good separation via RP-HPLC and confirmed that LpqF had no activity on *E. coli* polymerised peptidoglycan. Therefore, the chromatographic separation was deemed to be nominal. The peptidoglycan used in this experiment may not have been pure or adequate for HPLC. The failure points in starting material could be related to digestion or peptidoglycan purification. The discrepancy between the chromatographic separation of *M. smegmatis* and *E. coli* may stem differences in peptidoglycan digestion. For instance, *M. smegmatis* peptidoglycan contains approximately 50% more cross-linked peptides (around 80%) compared to *E. coli*, which typically has 40%-50% cross-linked stem peptides (Wietzerbin et al., 1974; Glauner, Holtje, and Schwarz, 1988; Bahadur, Chodisetti, & Reddy, 2021; Rimal et al., 2022). Addtionally, *E. coli* produce more tetra- rather than pentapeptides and contains Braun's lipoprotein, which is attached to stem peptides and cleaved by LtdF, an L,D-TPase (Rimal et al., 2022; Bahadur, Chodisetti, & Reddy, 2021). Recent studies have also highlighted modifications in mycobacterial peptidoglycan such as O-acetylation of Mur*N*Ac, *N*-deacetylation of Glc*N*Ac, and D-glutamate amidation, which are absent in *E. coli* (Moynihan and Clarke, 2010; Garde, Chodisetti, and Reddy, 2021; Rimal et al., 2022; Shaku et al., 2023). These modifications could make mycobacterial glycans less susceptible to muramidase lysis, contributing to differences in digestion efficiency between the two species, which may have led to poor chromatographic separation (Mahapatra et al., 2005; Rimal et al., 2005).

Other factors may also contribute to the purification challenges for *M. smegmatis* peptidoglycan. Incomplete hydrolysis and washing during the extraction process could result in the presence of lipids, proteins, or cytoplasmic contents that co-purify with the peptidoglycan. Additionally, inefficient or incomplete digestion with muramidase and lysozyme could leave behind peptidoglycan fragments that are not fully representative of the native structure. The retention of small, soluble components like amine side groups or short peptide chains, if not adequately separated during purification, can be difficult to distinguish from genuine peptidoglycan components. Lastly, harsh chemical treatments used during purification, such as strong acids or bases, can modify the peptidoglycan structure, including

deacetylation or depolymerisation leading to impure samples (Moynihan group unpublished). These caveats are now being addressed and optimised for mycobacterial peptidoglycan in the Moynihan group along with appropriate controls and validation methods to ensure the purity and integrity of the final peptidoglycan product.

Due to challenges posed by peptidoglycan degradation resulting from its heterogeneity in solution, different groups have employed fluorescent or colorimetric conjugates in combination with HPLC. These methods enable visualisation and quantitation of insoluble products. Gao et al. (2023) investigated probiotic bi-functional hydrolases in the gut microbiome of mice, employing a Remazol Brilliant Blue release assay to demonstrate the hydrolytic activity of LPH in *Lactobacillus*. Subsequently, they used ANTS-labelled gel electrophoresis and high-performance liquid chromatography-electrospray tandem mass spectrometry (HPLC-MS/MS) to elucidate the precise reaction products.

HPLC with UV or MS detection is the most common method to assay peptidoglycan hydrolases to visualise and quantitate the reaction product profiles. This well-established approach identifies reaction products of peptidoglycan-targeting enzymes. Researchers often focus on peptidoglycan derived from exponentially growing bacteria, reflecting its complex composition. Hoyland et al. (2014) employed HPLC for muropeptide product analysis, incubating the purified L,D-CPase, LdcB, in *Streptococcus pneumoniae* and *B. subtilis* with purified peptidoglycan, demonstrating LdcB substrate specificity using synthetic tetrapeptides L-alanine-D-glutamic acid-L-lysine-D-alanine and its L-isomer. Rimal et al. (2022) used stationary phase peptidoglycan derived from *M. smegmatis* mc^2155, distinguishing a wide range of muropeptide species. Pandey et al. (2018) used *M. smegmatis* peptidoglycan from all growth phases to ascertain the muropeptide profile via RP-HPLC, focusing on strains lacking MSMEG_2432 and MSMEG_2433, two D,D-CPases. They analysed three peaks with retention times of 4, 5.7, and 7 minutes in both wildtype and mutant strains, reporting relative abundances of 16.4%, 1.1%, and 3.8% in the wildtype, and 6.2%, 21.0%, and 0.4% in the mutant strains, respectively. These peaks were identified as muropeptides, specifically tetrapeptide (tetra), tetra-tripeptide (tetra-tri), and tri-tripeptide (tri-tri), based on their masses. Kumar et al. (2012) used similar methods, employing *M. tuberculosis*-derived peptidoglycan to characterise DacB2 via RP-HPLC. They reported monomeric muropeptides with relative abundances akin to those documented by Pandey et al. (2018). Although there are slight adaptations that make direct comparisons challenging, these studies collectively suggest a

robust separation method for characterising peptides released from muropeptides in the presence of D,D-CPases in mycobacteria.

Many peptidoglycan-active enzymes preferentially cleave soluble fragments of peptidoglycan (Jensen & Campbell, 1976; Sinha & Rosenthal, 1980; Anderson et al., 2003; Vollmer et al., 2008; Kwan & Qiao, 2023). The TLC method used to assess the activity of LpqF with a commercial pentapeptide containing L-lysine at the 3rd position revealed a product that did not correspond to the R*f* value of the D-alanine control, as observed with LpqF and D-alanine-D-alanine reaction (black box, Figure 35). This indicates that LpqF was active against both penta-L albeit it weaker, and D-alanine-D-alanine (red box, Figure 35). These findings align with previous studies on D,D-CPases, such as Kumar et al. (2012) and Prigozhin et al. (2014), which demonstrated that Rv2911, a D,D-CPase, can cleave pentapeptides containing L-lysine. This suggests that the substitution of L-lysine in place of *meso*-DAP is important, indicating the amino acid at the 3rd position may be crucial for LpqF activity. Additionally, the results imply that amidated D-*iso*-glutamate and *meso*-DAP at the 2nd and 3rd positions may be essential for LpqF to recognise and bind to the pentapeptide. This contrasts with some D,D-TPases in *M. smegmatis*, that have been shown to lack substrate preference (Shaku et al., 2023). However, the higher enzyme concentration required to observe the product suggests that LpqF exhibits higher activity in the presence of L-alanine-D-glutamine-*meso*-diaminopelmic-acid-D-alanine-D-alanine, characteristic of mycobacterial pentapeptides. In the presence of LpqF and RipA, the penta-L substrate showed a faint product, indicating LpqF activity on this substrate when RipA was present (red box, Figure 35). However, these results suggest RipA does not modulate LpqF activity. These results will need to be reevaluated using appropriate controls, including L-alanine-D-glutamine-*meso*-diaminopelmic-acid-D-alanine-D-alanine from *E. coli* and mycobacteria, along with *meso*-DAP to enable a definitive evaluation of D,D-CPase activity.

The TLC method employed in this study has limitations compared to techniques like RP-HPLC. One limitation is buffer artifacts at the solvent front, which can distort the D-alanine-D-alanine dipeptide control. Although efforts were made to minimise these effects, completely eliminating buffer components was challenging. Additionally, high amounts of enzyme were required for product visualisation, potentially generating misleading results. For example, Hoyland et al. (2014) used 700 µM of L,D-CPase in *Streptococcus pneumoniae*, whereas Moynihan et al. (2019) used only 1 µM of LpqI to release Glc*N*Ac from soluble muropeptides derived from *M. smegmatis* peptidoglycan. Such variability underscores the artificial nature of

these assays and the difficulties in working with peptidoglycan as a substrate. To address these challenges and validate TLC findings, future studies should consider employing RP-HPLC with the substrates mentioned, followed by mass spectrometric analysis. This method would allow for the determination of peptide masses derived from incubation with LpqF, providing a more comprehensive understanding of LpqF activity and substrate specificity under physiological conditions.

A caveat to these data is that only *M. smegmatis* peptidoglycan substrate was tested in the assays for Figures 32-35. If LpqF is indeed a D,D-CPase, using fragments of peptidoglycan such as muropeptides (Glc*N*Ac-Mur*N*Ac-di-, tri-, tetra- and pentapeptides) and pentapeptides with *meso*-DAP at the 3rd position instead of polymerised peptidoglycan, could initiate LpqF binding activity, especially when used alongside an appropriate positive control, such as DacB (Ealand et al., 2019; Kumar et al., 2022). LpqF might bind to peptidoglycan only after a certain growth point, such as the early stationary phase when more cross-linking is produced by L,D-TPases, necessitating cleaving of the terminal D-alanine to produce substrates for L,D-TPases. LpqF might also be involved in the peptidoglycan recycling pathway. Accumulation of recycled tetrapeptides, influenced by D,D-CPase activity, has regulatory consequences for peptidoglycan synthesis in mycobacteria, reducing D,D-cross-linkage and modulating cell wall integrity (Hernández et al., 2020; González-Leiza et al., 2011).

While some peptidoglycan-targeting enzymes have multiple functions, others are monofunctional or have functions not detected by these assays. This validates further research into potential mechanisms for LpqF and other similar mycobacterial enzymes yet to be characterised. The function of the proposed peptidoglycan-binding/stabilisation domain located in the N-terminus of LpqF will be addressed in the next chapter.

5.5 Conclusion

There was no activity observed for LpqF in the FITC-PG digestion assays, indicating that if LpqF is indeed a D,D-CPase, it would not function in this assay. To further investigate this, an adapted semi-quantitative FITC-PG TLC method corroborated these findings, showing that the digestion assay was working as a point of principle. The negative results in these assays could be interpreted as a need to change to a carboxypeptidase assay, which could verify the activity of LpqF. The RP-HPLC data indicate incomplete digestion of peptidoglycan, and thus, the

activity of LpqF could not be conclusively verified under these conditions (Figure 34, D, E). These data need to be repeated to ensure robust repeatability of the peaks seen in chromatograms corresponding to the specific activity of LpqF. Confirmation by mass spectrometry is also necessary to definitively verify these findings. Improvements to the methodology for peptidoglycan have since been optimised, and these discrepancies can now be addressed in future studies with LpqF.

The data on LpqF activity with pentapeptide substrate indicate that the *meso*-DAP amino acid is essential, and potentially amidated peptides are required for tight contact and binding to occur (Figure 35). The results under these conditions strongly suggest that LpqF cleaves within the D-alanine-D-alanine dipeptide, supporting the hypothesis that LpqF functions as a D,D-CPase.

Chapter 6. LpqF binds to peptidoglycan via its NTF2-like domain

6.0 Introduction

In bacteria, proteins featuring the NTF2-like fold exhibit a range of activities, categorised into catalytic and non-catalytic functions (Eberhardt et al., 2013). For instance, certain NTF2-containing proteins act as anti-toxins within operons alongside toxin genes in systems like the Tox-JAB-2 family polymorphic toxin system (Zhang et al., 2012). Additionally, NTF2-like proteins have been identified in inner membrane complexes such as VirB8 in *Brucella suis* and the VirB10 homologue in *Helicobacter pylori* Type IV secretion systems, playing crucial roles in antibiotic resistance and virulence by facilitating plasmid DNA transfer (Terradot et al., 2005; Porter et al., 2011; Goessweiner-Mohr et al., 2013; Fercher et al., 2016).

Of more relevance to this study, NTF2s have also been associated with several peptidoglycan-active enzymes. Recent studies on L,D-CPases, including Csd6 in *H. pylori*, Pgp2 in *C. jejuni*, and Bd1075 in *Bdellovibrio bacteriovorus*, have shed light on the importance of the NTF2-like domains in guiding the catalytic domain to the substrate (Houn-Sook-Kim et al., 2015; Lin et al., 2021; Banks et al., 2022). In the case of multi-domain peptidoglycan hydrolases, the presence of a peptidoglycan-binding domain has been shown to enhance the activity of the catalytic domain. These domains are crucial for the proper functioning of several peptidoglycan-active enzymes (Mesnage et al., 2014; Rocaboy et al., 2013; Woo Cheol Lee., 2021). While the mechanistic studies of NTF2-fold domains in D,D-CPases are a work in progress, insights from these studies underscore the structural, conservation, and functional significance of NTF2-like domains in peptidoglycan-active enzymes.

NTF2-like domains have been identified in high- and low-molecular-weight peptidoglycan-active enzymes. For example, the NTF2 domain in the hydrolase PBP2a in *Staphylococcus aureus* is important for ligand binding and catalysis. Some low molecular weight enzymes that possess NTF2 domains have a non-catalytic binding pocket for interacting with small molecules (Lim and Strynadka, 2002; Eberhardt et al., 2013). NTF2-folds identified in L,D-CPases such as Pgp2, Csd6, and Bd1075 exhibit moderate structural similarity (Houn-Sook-Kim et al., 2015; Lin et al., 2021; Banks et al., 2022). However, despite variations in the length of the β-strands within the NTF2 domain, these enzymes maintain cell shape by facilitating the activity of the L,D-CPase domain. Notably, Bd1075 binds to peptidoglycan, with residue W303

within the extended loop of its NTF2-like domain playing a key role in targeting the L,D-CPase to peptidoglycan and maintaining cell curvature (Banks et al., 2022). Additionally, mutations in residues E302 and Y274 within the binding pocket of Bd1075 have been linked to incomplete formation of the NTF2-like domain and partial localisation to peptidoglycan, respectively.

Lin et al. (2021) demonstrated via a pull-down assay that the NTF2-fold of Pgp2 is required for catalytic activity and cell curvature, showing this through amino acid substitutions. Their work revealed that residues K307, Y233, and K257 contribute to binding, while C174, H157, and G158 contribute to catalysis. Moreover, studies by Kim et al. (2015) revealed that Csd6 features a deep pocket potentially involved in binding hydrophobic substrates. Given these insights, it is reasonable to hypothesise that the NTF2-like domain of LpqF may also play a role in positioning the catalytic domain and binding to peptidoglycan. Consequently, this chapter aims to characterise the NTF2-like domain of LpqF and investigate potential residues implicated in peptidoglycan binding.

6.1 The NTF2 domain of LpqF binds peptidoglycan

In silico analyses revealed that Cpe (PDB: 2xh9) in *S. clavuligerus* and the unknown proteins, bth_ii0226 (PDB: 3h3h) in *B. thalandensis* and PA1314 (PDB: 1tp6) in *P. aeruginosa* possess an NTF2 domain that is structurally similar to $NTF2^{LpqF}$ (Figure 32, C, D, E). These structures provided limited information regarding the function and binding mechanisms of the NTF2 domains due to the lack of published biochemical characterisation. Therefore, to gain insights into the function of $NTF2^{LpqF}$ and based on conserved residues in the published structure of the L,D-CPase Bd1075, similar analyses were undertaken for LpqF (Banks et al., 2022).

In Bd1075, a pocket is formed by eight residues (F231, H239, L243, Y247, Y274, H279, D281, W303), creating an aperture that is 9.062 Å by 1.38 Å in size, necessary for binding to peptidoglycan. It was also found that residues E302, W303, and Y274 are required for this binding interaction (Figure 36, B). There are not equivalent residues in the $NTF2^{LpqF}$. Instead, when Bd1075 NTF2-domain was compared to that of $NTF2^{LpqF}$, a similarity was revealed in the two N-terminal helices (helix 1: Y233-Y247, helix 2: S188-N212 for Bd1075; helix 1: P41-D57, helix 2: P12-P24 for $NTF2^{LpqF}$). However, the binding cavity of $NTF2^{LpqF}$ is partially occluded by its β-sheet compared to the cavity space of Bd1075 (measuring 4.2 Å in width vs.

9.062 Å) (Figure 36, A, B, C). Bd1075 exhibits a more extended and open NTF2-fold structure where residue W303 is located, whereas LpqF does not possess this extended loop and therefore lacks W303 or an equivalent residue (Figure 36, C). The distance measurements of apertures for Bd1075 between residues K240 and W303 is 9.062 Å, while for LpqF between T50 and V101 it is 4.226 Å. This structural variation suggests potential differences in the binding interactions and substrate recognition between the two NTF2 domains. It remains possible that $NTF2^{LpqF}$ enlarges its aperture when in contact with peptidoglycan. This, however, contrasts with Bd1075, which is 'open' even in the absence of substrate. Further analysis is needed to parse these differences for $NTF2^{LpqF}$, which could provide valuable insights into which residues play a role in binding to peptidoglycan.

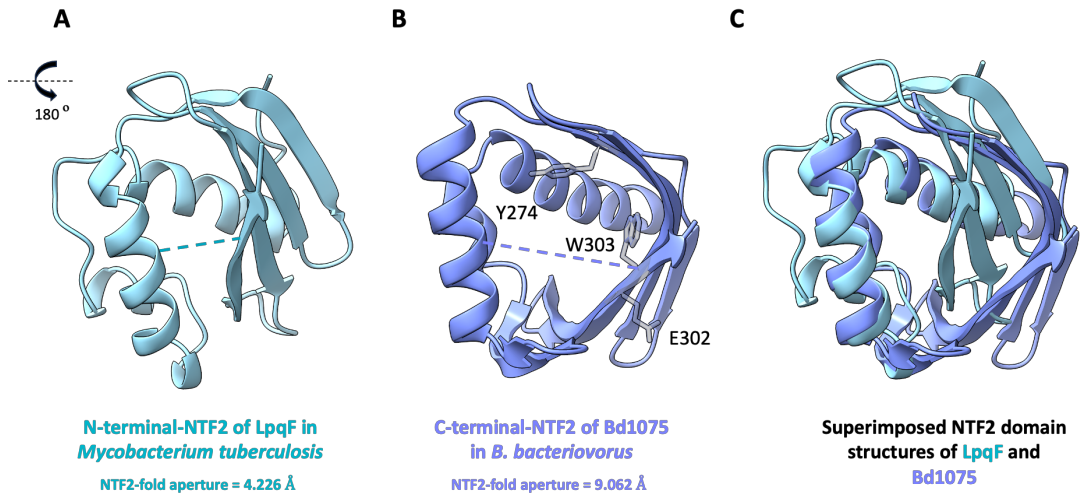


Figure 36. Structural comparison of the $NTF2^{LpqF}$ and Bd1075 NTF2 domain suggests that $NTF2^{LpqF}$ is unlikely to function in the same way. (**A**) The N-terminal-NTF2 domain of LpqF. (**B**) The C-terminal NTF2 domain of Bd1075 (PDB ID: BD7021) is shown with the residues highlighted from the Banks et al. (2022) study that were shown to be pivotal for localisation of the L,D-CPase either fully (E302, W303) or partially (Y274). (**C**) The superimposition of NTF2 domains for Bd1075 and LpqF shows the occlusion NTF2-fold of LpqF in comparison to Bd1075 for. Images rendered via ChimeraX-.6.1.1. Dashed lines represent distance of aperture between residues located on each of the α-helices to opposite β-sheet of the NTF2-fold for each structure.

6.2 The NTF2 domain of LpqF mediates peptidoglycan binding

The structural analysis of $NTF2^{LpqF}$ revealed a distinct shape, lacking an apparent open binding pocket compared to characterised NTF2 domains such as those of Bd1075, Csd6, and Pgp2. Despite these structural variations, $NTF2^{LpqF}$ may still bind to peptidoglycan. To investigate this, a classical substrate binding assay was employed where the amount of bound protein

eluted from the peptidoglycan is visualised by SDS-PAGE with Coomassie staining (Vasstrand, Miron and Jensen, 1987; Bernadsky, Beveridge and Clarke, 1994; Watt and Clarke, 1994).

The NTF2^{LpqF} was purified using the same method as the full-length protein, and macromolecular *M. smegmatis* mc^{2}155 peptidoglycan was incubated with both the full-length and NTF2^{LpqF} for 1 h on ice. The samples were then washed twice, with the supernatant collected each time, and the supernatants were analysed by SDS-PAGE. Percent bound values were obtained via densitometric analysis of bound protein using ImageJ (Figure 37, A, B). The full-length protein showed binding to peptidoglycan, calculated at 6.7 ± 3% of the total protein in the assay (load), while 7.1 ± 5% of the NTF2^{LpqF} was bound, indicating that both NTF2^{LpqF} and full-length proteins have an affinity for *M. smegmatis* peptidoglycan under these conditions (Figure 37, A, B). Given there is no substrate in the protein-only samples, the presence of a band in the 'bound' fraction for the full-length protein (Figure 37, A, lane 9) indicates that the full length protein is moderately unstable whereas the isolated NTF2 domain is not (Figure 37, B). Overall, these results demonstrate that both the NTF2^{LpqF} and full-length LpqF can bind to and has a similar binding affinity for cross-linked peptidoglycan, suggesting that NTF2^{LpqF} has capacity for binding to peptidoglycan. Despite repeated efforts, the PBP domain proved insoluble, and so the peptidoglycan-binding capacity of this domain in isolation could not be measured.

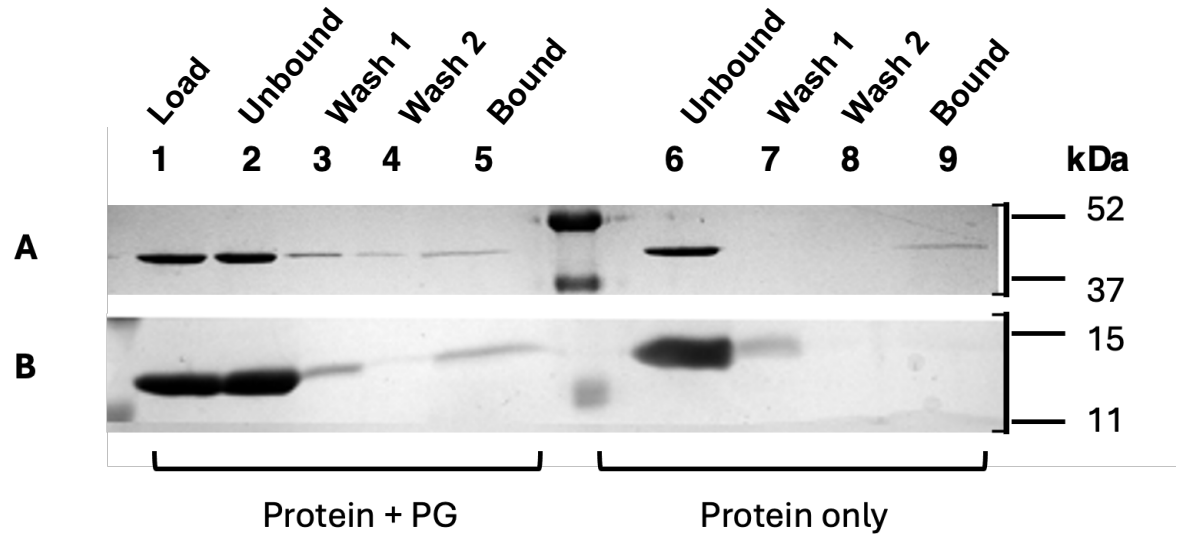


Figure 37: LpqF binds to peptidoglycan via the NTF2^{LpqF} domain. (**A**) A representation of quantitation from the SDS-PAGE of unbound, washes and bound fractions for full length LpqF. (**B**) A representation of quantitation from the SDS-PAGE showing the same as full length for the NTF2 domain of LpqF. SDS-PAGE analysis of PG binding for NTF2 was incubated with peptidoglycan derived from *M. smegmatis* for 60 min after which time samples were washed in sodium phosphate buffer, pH 6.0 except for the sample labelled load which was collected as a control. The pellet, along with supernatants from each wash step, was resuspended with SDS loading dye and was analysed by SDS-PAGE and detected by staining with Coomassie Brilliant Blue. To control for non-specific precipitation, a control assay without PG was also analysed. These data are representative of triplicates. Raw data was obtained using BioRad Gel Doc XR + and analysed via Imagelab. PG; peptidoglycan.

The next objective was to identify the residues that contributed to peptidoglycan binding. Given that NTF2^{LpqF} is proposed to bind a peptide-containing substrate but lacks conservation of key residues found in well-studied NTF2-like domains of enzymes such as Bd1075, Pgp2 or Csd6, it was hypothesised that the crystal contacts observed in the experimentally derived structure could provide insights into the residues responsible for interacting with peptides in peptidoglycan (Figure 38). Analysis of the crystal contacts identified eight candidate residues potentially involved in binding to peptidoglycan fragments or peptides. The shortest distance between interacting sites was observed for R98A and W28A at 3.15 Å, W28 and R87 at 3.9 Å, D85 and I33 at 3.78 Å, D85A and R87A at 5.35 Å, and I33A and Q104A at 3.9 Å. Expression constructs were made with alanine substituted for the residues listed above (Figure 38). In addition, a double substitution, NTF2$^{R98A;R87A}$, was also generated to further understand any cooperative roles of these residues might have.

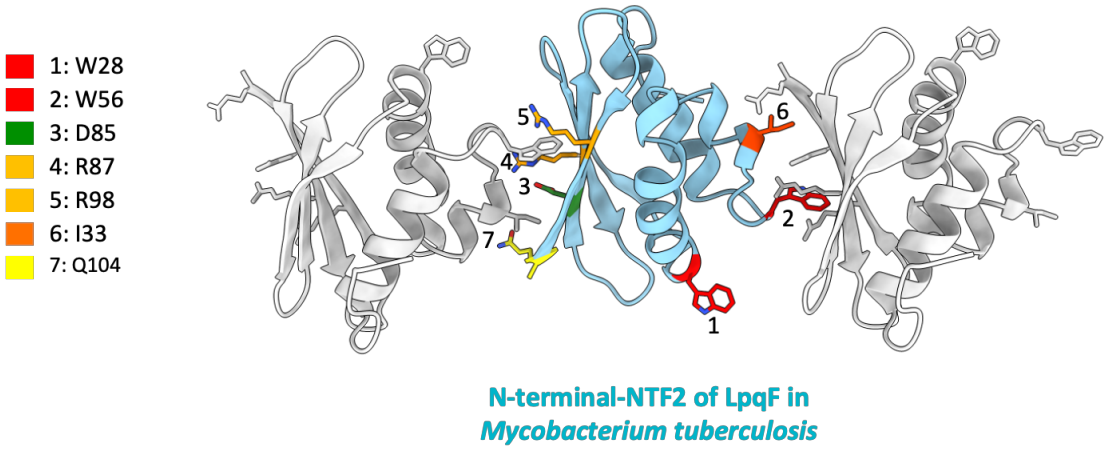


Figure 38: Structure of the NTF2^{LpqF} and residue selections for site-directed mutagenesis. Highlighted are the NTF2^{LpqF} contact points, implicating the eight potential candidate residues for peptidoglycan (PG) binding. Colour coded for the residues chosen for site directed mutagenesis is indicated by the legend at the left. W28 and W56 (NTF2^{W28A} and NTF2^{W56A}), D85 (NTF2^{D85}), R87 and R98 (NTF2^{R87A} and NTF2^{R98A}), I33 (NTF2^{I33A}), Q104 (NTF2^{Q104A}). Only 3 NTF2^{LpqF} structures are shown with all crystal contact highlighted except for W28 that is out of plane of the image. Images rendered via ChimeraX-.6.1.1.

The resulting NTF2^{LpqF} variants were expressed and purified following the established procedures described above. All variants were analysed for protein purity and stability via SDS-PAGE (Figure 39, A, B). NTF2^{I33A}, NTF2^{W56A}, NTF2^{R98A}, and NTF2$^{R98A;R87A}$ showed varying degrees of instability as evidenced by degraded protein fragments (Figure 39, C, D, E). Consequently, the NTF2^{I33A}, NTF2^{W56A}, NTF2^{R98A} variants required size exclusion chromatography to further purify them (Figure 39, C-F). Among these, NTF2^{W56A} was prone to proteolysis, as evidenced by two peaks in the chromatogram: a smaller shoulder (to the right) to the main peak indicating an apparent shift in protein conformation or contamination with smaller proteins (Figure 39, D, F).

Conversely, NTF2^{Q104A}, NTF2^{W28A}, NTF2^{R87A}, NTF2^{R98A}, and NTF2^{D85A} exhibited high purity after the SUMO-tag removal and did not require size exclusion chromatography (Figure 39, F). Additionally, analysis by SDS-PAGE revealed a second contaminating protein with an apparent molecular weight of 6.5 kDa in the preparation of NTF2^{W56A}. Despite repeated purification efforts, this contaminant could not be separated from the protein, which migrated to its expected size (11.47 kDa) (Figure 39, D, F). The additional steps, such as size exclusion chromatography for the unstable variants, ensured that the proteins were of sufficient quality for further analysis. Overall, all NTF2 variants were successfully purified to near homogeneity (≥80%), with W56A at ~70% purity for downstream investigation.

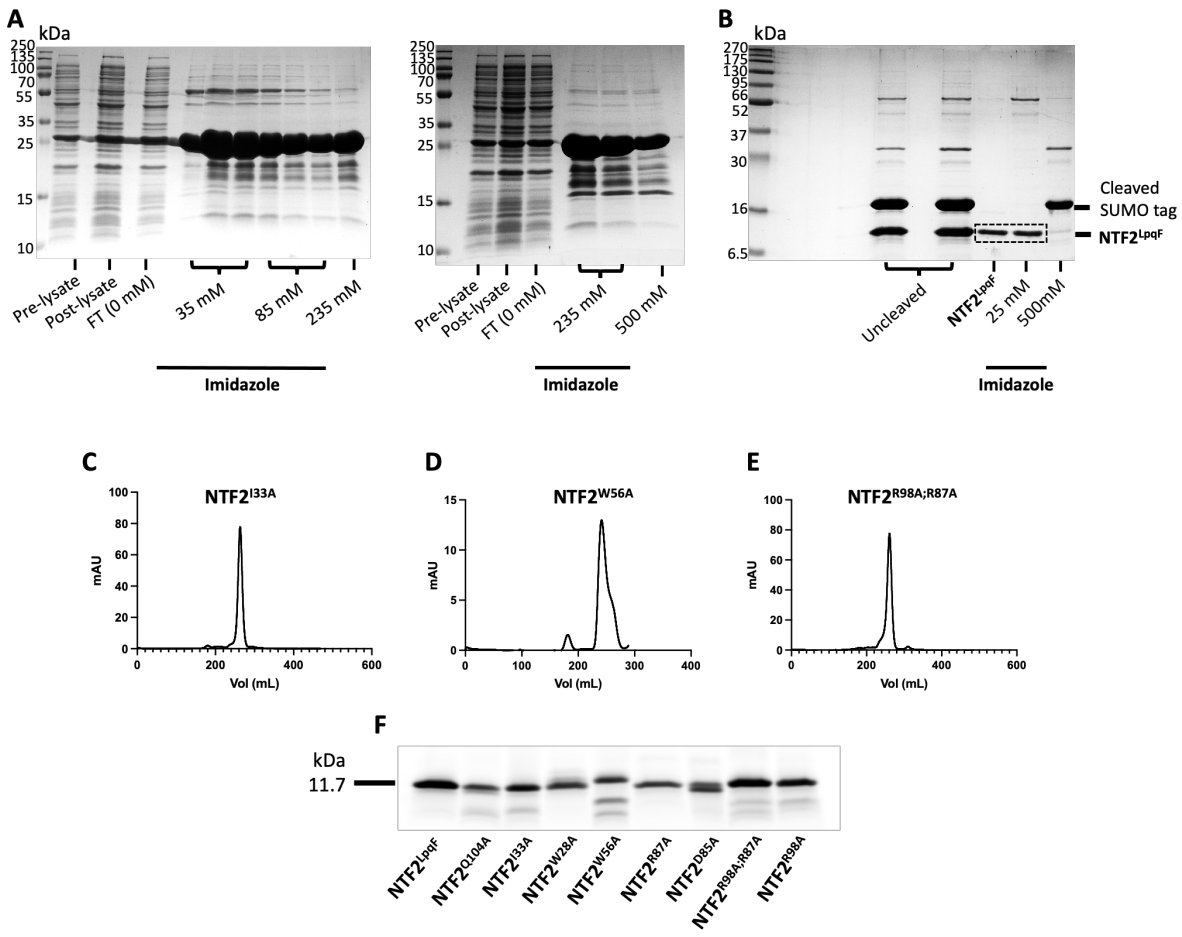


Figure 39: Purification of NTF2^{LpqF} variants with putative binding residue substitutions. An SDS-PAGE of metal affinity chromatography shows the expression and purification of NTF2 variants using an ÄKTA Pure 25 system with a 5 mL GE HisTrap fast-flow column. NTF2^{LpqF} is presented as a representative example, with stepwise elution fractions collected at increasing imidazole concentration (0, 35, 85, 235 and 500 mM) (**A**). (**B**) Ulp1-protease digestion products of SUMO-NTF2 as visualised by SDS-PAGE with Coomassie brilliant blue staining on an 15% acrylamide gel. The dash box and bold text indicates the purified NTF2^{LpqF}. Chromatograms for size excluded protein samples showing the monomeric NTF2 mutants for (**C**) NTF2^{I33A}, (**D**) NTF2^{W56A} and (**E**) NTF2$^{R98A:R98A}$. (**F**) SDS-PAGE show purified mutants (NTF2^{W28A}, NTF2^{W56A}, NTF2^{R87A}, NTF2$^{R98A-R87A}$, NTF2^{R98A}, NTF2^{Q104A}, NTF2^{I33A} and NTF2^{D85A} respectively) from the ÄKTA Fast Flow column after SUMO-HIS tag removal. IMI, imidazole.

While functional for detecting protein-peptidoglycan interactions, the in-gel detection method suffers from low throughput and sensitivity. Coomassie Brilliant Blue typically has a detection range of 0.1 to 1 µg of protein per band, depending on the staining protocol and the type of Coomassie dye used (e.g., G-250 or R-250) (Diezel, Kopperschläger, and Hofmann, 1972; Neuhoff, Stamm, and Eibl, 1985). In contrast, fluorescent labelling of proteins is more sensitive with a higher detection limit of 33-66 pg per band and, depending on the detection mechanism to measure the fluorescence intensity, can detect protein as low as 3 pg (Fuchs, 2023). A higher throughput method also has the advantage over SDS-PAGE analyses in minimising errors

when designing and applying multiple mutations, especially when running replicates, as the in-gel method becomes impractical. A refined peptidoglycan-binding assay was developed to leverage the superior sensitivity of fluorescence detection. This work was conducted in collaboration with Greg Goudge, a colleague in the Moynihan group.

NHS-rhodamine (Sigma 46406) contains an *N*-hydroxy-succinimide (NHS) ester group. In the presence of proteins, the NHS ester reacts specifically with primary amines (-NH2) at a slightly basic pH (pH 7.0-9.0), forming a covalent bond. This reaction is preferential at the N-terminus of a protein, forming a stable amide bond between the N-terminal amine and the NHS-rhodamine molecule, releasing the NHS group. Each mutant protein was treated with NHS-rhodamine at a 1:1 molar ratio, allowing the dye to selectively react with and label the amine group on the N-terminus, followed by post-reaction quenching to remove excess unreacted NHS-Rhodamine.

The fluorescently labelled protein was incubated with peptidoglycan before collecting the insoluble material by centrifugation. The fluorescence of the supernatant was then measured to indicate the total unbound protein. The pellet was then washed twice with buffer, retaining the supernatant each time to remove and quantify any weakly bound protein. The total percentage of bound protein was calculated by subtracting the sum of the fluorescence of all wash steps and unbound protein from the starting sample (load) fluorescence. A schematic representation of the protocol is outlined in Figure 40, A.

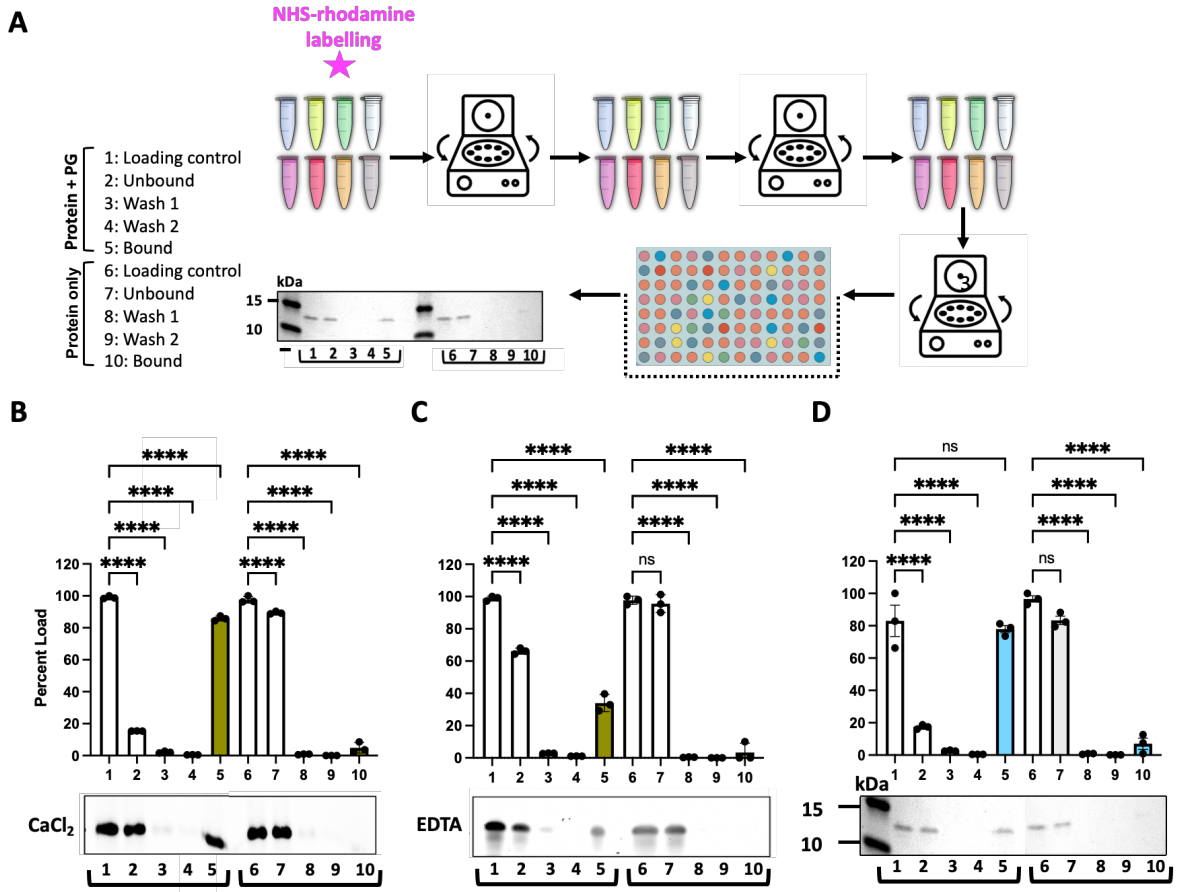


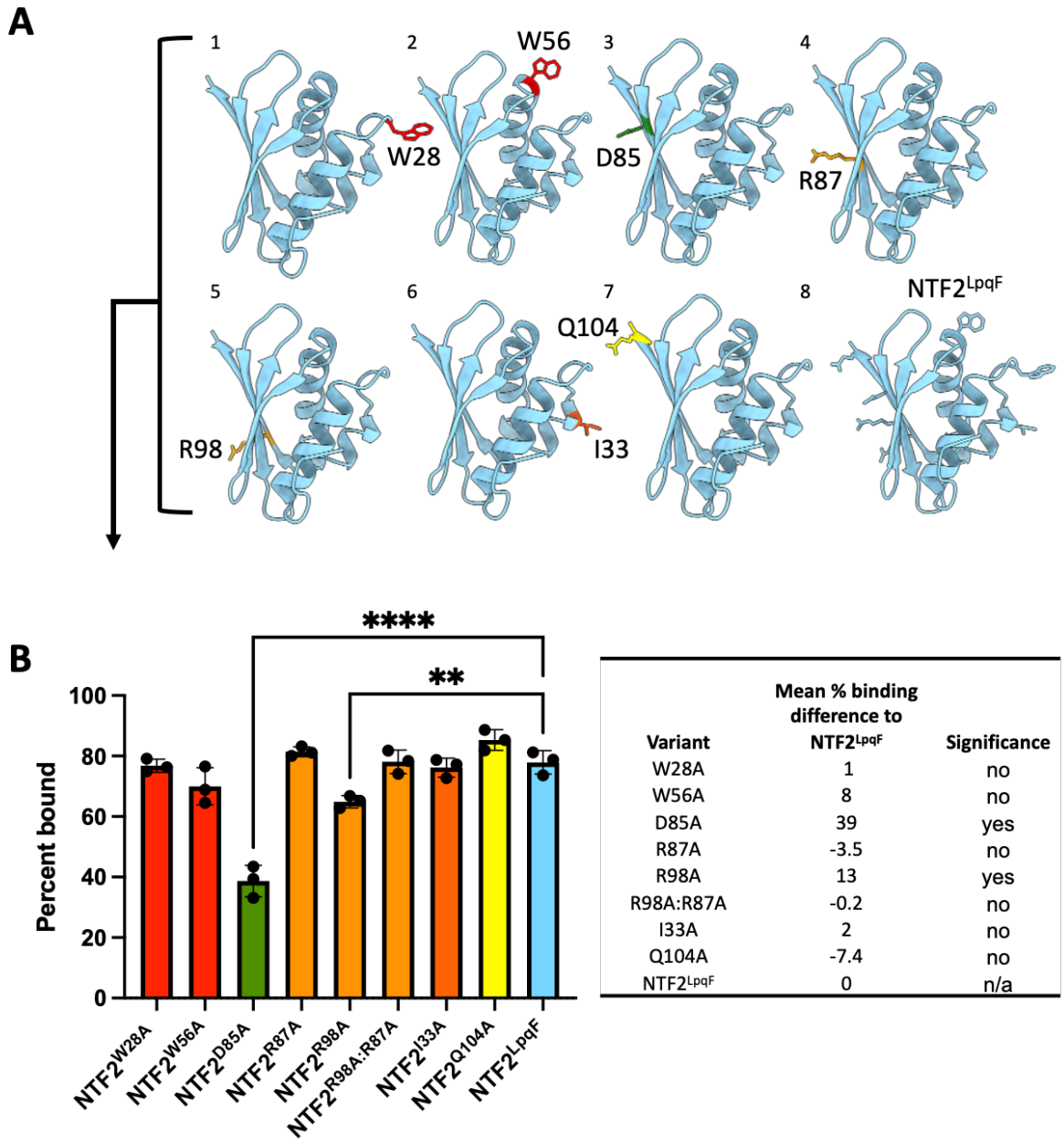
Figure 40: Development of a medium-throughput peptidoglycan-binding assay. (**A**) A schematic representation of a high throughput, fluorescence assay for labelling protein with NHS-rhodamine. NHS-rhodamine conjugated proteins were incubated with PG derived from *Mycobacterium smegmatis* PG (5 mg/mL) for 1 h and then samples representing total load, and 2 washes were collected and labelled as unbound, washes 1-3. (**B-C**) The fluorescence data was reported as a percentage of the total starting material (load), and the bound fraction of protein was calculated by subtracting the unbound, wash 1, and wash 2 fractions from the initial load. (**B**) WGA with $CaCl_2$, (**C**) WGA treated with EDTA and (**D**) wildtype NTF2 domain. Below each figure are the corresponding SDS-page gels for the NHS-rhodamine conjugated samples matching the figures and includes the bound (pellets) sample (lanes 5 and 10). Key for each number is inset to the left of panel **B**. Samples were read at Ex 550-20 nm: Em 605-40 nm. The pellet (bound protein) along with protein remaining in the unbound and supernatants from each wash step was resuspend with SDS loading dye and were analysed for binding by associated protein by SDS-PAGE after staining with Coomassie. WGA, wheat germ agglutinins. Raw data was quantitated using Excel version 16.8 and GraphPad, Prism 10. Key colour code corresponds to a residue number. Error bars represent mean and standard deviation. Significant values; P > 0.05 ns non-significant; p >0.9999, **** p <0.0001. One-way ANOVA with Šídák's multiple comparison test.

A known peptidoglycan-binding protein, WGA, was first tested to validate the assay. WGA was selected as a positive control in the peptidoglycan binding assay due to its high affinity for Glc*N*Ac, a component present in peptidoglycan (Gallagher, Morris, and Dexter, 1985). WGA-rhodamine was evaluated for its ability to bind to peptidoglycan by comparing it to a negative control lacking peptidoglycan. The NHS-rhodamine-WGA conjugate was added to 0.75 mg/mL of *M. smegmatis* peptidoglycan. NHS-rhodamine-WGA was adjusted to a concentration of 0.25 µM.

In the pull-down assay, the percentage of the fluorescent protein associated with the peptidoglycan pellet after incubation with the protein was calculated. There are two main sources of false-positive data for this experiment. First, unbound protein in the supernatant must be removed from the final pellet to ensure only bound protein is being quantified. To address this, we washed the pellet three times. The fluorescence associated with these washes is added to our total 'unbound' protein signal. Secondly, if the protein binds non-specifically to the plastics or is prone to precipitation, it will contribute to the fluorescence measurement at the end of the assay despite not being associated with peptidoglycan. As discussed above; to circumvent this, we always conduct a no-peptidoglycan control. The value of the final 'non-specific bound' sample from this assay is subtracted from our 'bound' readings. This gives the following formula for calculating percentage bound: Percent Bound = (Load – (Wash 1 + Wash 2 + Wash 3) – Non-specific bound) / Load * 100 (Figure 40, B-D, lanes 1-9). To compare to existing methods, we also analysed these samples via SDS-PAGE (Figure 40, B-D, lanes 5 and 10).

WGA showed robust binding in the presence of $CaCl_2$, as evidenced by a low percentage of the starting material in the unbound and wash wells and strong signal in the SDS-PAGE (Figure 40, B). To test the discriminatory capacity of the assay and to demonstrate that the WGA-peptidoglycan interaction we are measuring is specific, we took advantage of the fact that WGA binding is $CaCl_2$-dependent by adding 10 mM EDTA to the sample. In the EDTA-free condition, 86 ± 2% of the protein was bound to the peptidoglycan. As expected, the EDTA-treated condition reduced this binding to 34 ± 5% (Figure 40, C). Under similar conditions, 78 ± 4% of $NTF2^{LpqF}$ was bound to peptidoglycan (Figure 40, D). These data showed a 60% increase in $NTF2^{LpqF}$ bound protein compared to the classical SDS-PAGE analysis method results. The 50% lower percentage of bound protein observed in the SDS-PAGE method in Figure 37 could be explained by several factors. First, different batches of peptidoglycan were used for each method, potentially affecting purity. Second, the lower peptidoglycan-to-enzyme ratio was lower (2mg/ mL) compared to the plate reader (5mg/ mL), resulting in fewer binding sites. Additionally, the presence of starting material in the unbound and wash fractions due to cross contamination of the wells could have lowered the percentage of total bound protein. Lastly, protein degradation was observed in the SDS-PAGE method, which could account for protein detected in the bound lane in peptidoglycan-only controls. Overall, these findings indicate that an efficient and more practical moderate-throughput alternative to the classical SDS-PAGE method for assessing peptidoglycan-binding proteins was successfully optimised.

The NTF2 variants were evaluated using the above assay to test for any impact on peptidoglycan binding. The $NTF2^{D85A}$ variant had 39% less binding than wildtype binding compared to $NTF2^{LpqF}$. The second single amino acid mutation that exhibited a significant difference was $NTF2^{R98A}$, which overall 13% less bound protein with a significant difference of $p < 0.0021$. All other mutants did not exhibit statistically significant changes in binding relative to the wildtype protein (Figure 41, B). Overall, these data suggest that the residues D85 and R98 play a potential role in positioning LpqF and binding to peptidoglycan.



Variant	Mean % binding difference to NTF2^{LpqF}	Significance
W28A	1	no
W56A	8	no
D85A	39	yes
R87A	-3.5	no
R98A	13	yes
R98A:R87A	-0.2	no
I33A	2	no
Q104A	-7.4	no
NTF2^{LpqF}	0	n/a

Figure 41: NHS-rhodamine NTF2 conjugated peptidoglycan binding assay. Variants of the NTF2 domain with amino acid substitutions were incubated with NHS-rhodamine to assess their binding affinity to peptidoglycan. (**A**) The residues changed to alanine are shown as an example of the conjugation procedure and wildtype NTF2 is shown with all residues in blue. Analysis of site-directed mutants of the NTF2^{LpqF} using our newly developed peptidoglycan-binding assay. Individual NTF2^{LpqF} variants were conjugated to rhodamine and then assayed as described above. (**B**) The final percentage bound represents the total percent binding. The data are reported as absolute percent bonding of each NTF2 variant protein. Raw data was inputted into Excel v16.8 and calculation of percent bound obtained before quantifying via GraphPad Prism 10. Statistical analysis, Bars represent the mean with individual data points shown and error bars represent standard deviation. ns non-significant; $p > 0.9999$, Significant values; ** $p < 0.0021$, **** $p < 0.0001$. Significance was determined using a one-way ANOVA with Šídák's multiple comparison.

6.3 Discussion

Prior to recent studies by Lin et al. (2021) on the NTF2 domain of Pgp2 and Banks et al. (2022) on the NTF2 domain of Bd1075, very little was known about the mechanisms underpinning peptidoglycan recognition in these domains. These studies identified specific features within NTF2 domains, such as a conserved binding pocket crucial for peptidoglycan binding and residues like W303 and Y274 in Bd1075, which are important for binding to peptides (Banks et al., 2022). However, W303 is absent in other L,D-CPases due shorter sequences, such as those terminating at E302 in Pgp2, whereas Y274 is conserved. In the case of LpqF, the absence of these residues and the structurally closed pocket suggest that LpqF binds to peptidoglycan through a different mechanism. The NTF2 domain of LpqF shows low conservation with the well-characterised NTF2 domains of Bd1075, Pgp2, and Csd6, making it difficult to identify binding residues through comparison with these proteins.

To circumvent this, the X-ray crystal structure of LpqF to analyse the intermolecular contacts was utilised. Based on this analysis, residues that appeared to be make crystal contacts were substituted with alanine, identifying eight potential candidate residues involved in peptidoglycan interactions (Figure 41). These are surface-exposed residues that surround the $NTF2^{LpqF}$ binding pocket and could be involved in making contact with peptidoglycan. These residues appeared to interact with residues on the juxtaposed NTF2 structures. For example, W28 was observed to be sandwiched between R98 and R87, I33 sits between D85 and Q104, and W56 points outward in the crystal contact analysis, sitting in a groove adjacent to the appended NTF2 (Figure 32A).

The rationale substituting each residue with alanine was to eliminate the ability to interact with peptidoglycan, though this may affect protein stability. A double mutant ($NTF2^{R98A;R87A}$) was also designed to determine whether two substitutions would have a greater impact on the attachment of the NTF2 domain to the peptide substrate than one substitution alone. The forward primer of R87 and the reverse primer for R98 were used to make $NTF2^{R98A;R87A}$ mutant. All substitutions were successfully purified and subsequently used for downstream analyses (Figure 36).

To understand the molecular determinants of peptidoglycan binding by the $NTF2^{LpqF}$, site-directed mutants for residues proposed to be involved in making crystal contacts in the previously solved structure of LpqF. A new fluorescence assay was applied to evaluate their role in substrate recognition. NHS-rhodamine-conjugated $NTF2^{LpqF}$ variants were incubated at a final concentration of 5 μM with 5 mg/mL of peptidoglycan, except for WGA controls. At higher concentrations, WGA showed saturation of binding sites, limiting its binding by 50%. Therefore, WGA was optimised to a concentration of 0.25 μM and 0.75 μg/ml of peptidoglycan (Figure 40). While most mutations had no effect on binding, two significantly reduced the interaction with peptidoglycan. These residues, D85 and R98, are located proximally on the outer edge of the β-sheet, are surface-exposed and are separated by 5.35 Å in the crystal contacts analysis. Intriguingly, $NTF2^{R98A;R87A}$ mutation appears to rescue the partial binding defect of the $NTF2^{R98A}$ mutation. However, if these residues exerted a cumulative effect on binding to peptidoglycan, it would be expected that the multiple mutations would result in weaker binding to peptidoglycan than what was observed. Although difficult to explain, one possibility is that the loss of the first residue causes a conformational change that is somehow compensated upon the loss of the second. The proximity of D85 and R98 suggests that these residues may perform cooperative or distinct roles in the binding process, with D85 potentially playing a more dominant role than R98 (Figure 41). This will need further investigation to decipher and explain these results.

Structurally, the NTF2 domain of $NTF2^{LpqF}$ is unique compared to other published NTF2-containing proteins. The residues D85 and R98 are not present in Bd1075, suggesting that LpqF binds to peptidoglycan through a different mechanism. The putative binding residues R98 in $NTF2^{LpqF}$ and the known binding residue E302 in Bd1075 are both located on the first β-strand of an anti-parallel β-sheet, with both facing outward (Figures 42 & 47). The putative binding residue D85 and the established Y274 are located on the second β-strand in each respective protein, with D85 facing 180 degrees in the opposite direction to Y274, which faces inward into its binding pocket (Figure 41). These structural differences could be due to a specific loop containing W303 that sits above the binding pocket at the C-terminus, found only in Bd1075, which is responsible for pocket-formation (Banks et al., 2022). The closed cleft space in $NTF2^{LpqF}$ is indicative of a flexible substrate acquisition mechanism, similar to that reported for the NTF2-like domains DUF4887 (Eberhardt et al., 2013) and Pgp2 (Lin et al., 2021). Despite both belonging to the NTF2 superfamily, the available data would suggest that LpqF

and Bd1075 bind to peptidoglycan through different mechanisms. The mechanism in $NTF2^{LpqF}$ likely involves D85 and R98, as supported by our data.

Although very few studies directly implicate aspartic acid in peptidoglycan-binding domain functionality, research on negatively charged residues such as glutamic acid in peptidoglycan-binding domains of peptidoglycan-active enzymes indicates that these residues play roles in cell shape and binding. For example, Lin et al. (2021) showed that E324 in the pocket of NTF2 of Pgp2 made a specific interaction with monomeric tetrapeptides. Removal of the negative charge and its ability to interact with a positively charged side chain of D-glutamine in a stem peptide, reduced the abundance of tripeptides, indicating a loss of binding to the substrate. Similarly, Eberhardt et al. (2013) describe a conserved aspartic acid in the middle of the NTF2-like fold domains DUF3828, DUF3887, and DUF4878, positioned close to a conserved glutamine. These domains have predicted structurally different binding pockets in the N-terminal and a peptidase in the C-terminal. Additionally, like $NTF2^{LpqF}$, DUF4887 was shown to have a shallower binding pocket but is predicted to bind larger substrates than DUF3828 and DUF3887. Yao et al. (2012) showed that Rv0899 (ArfA), a peptidoglycan-binding protein, binds to both peptidoglycan and peptide fragments containing diaminopimelic acid. This mechanism is driven by two arginine residues (R277, R213) and one aspartic acid residue (D262) at acidic pH, specifically for *meso*-DAP interaction. This interaction allows ArfA to adopt a more stable structure, indicating that these amino acids are vital for the enzyme's protection in acidic environments.

D85 is a negatively charged amino acid positioned 3.78 Å away from I33 on the adjacent NTF2 domain, as shown in Figure 38. Although an electrostatic interaction between D85 and a positively charged component on the peptide, such as *meso*-DAP, is highly likely, the attraction between hydrophobic residues like I33 and uncharged residues could also contribute to stabilisation. This interaction may be part of a larger set of interfacing residues involved in peptidoglycan binding, as described for I215, I280, and I323 in ArfA (Yao et al., 2012). Similarly, an interaction between either of the positively charged arginines (R87 and R98) and a peptide substrate via electrostatic potential is likely, with these residues potentially playing a cooperative role in binding to the stem peptide (Nath, Jha, Vishveshwara, and Banavar, 2010).

In this study, the substitutions of W28 or W56 with alanine did not impact binding. It is possible that substituting both W28 and W56 for hydrophilic and/or neutral residues would have an

additive effect, and removing only one tryptophan is not enough to reduce or abrogate binding to the substrate. An example of the hydrophobic cooperativity comes from a study on gene 32 in phage T4 (Casas-Finet et al., 1988), where the authors showed that two tryptophan residues undergo stacking interactions with polynucleotides, and deletion of five tryptophan residues abrogates protein binding. While this study shows complete loss of activity, other studies, such as Mikoulinskaia et al. (2023), show that in a bacteriophage endolysin (MC15 family, zinc-containing enzyme), substitution of W114A abrogated its catalytic activity, while W109A retained 5% activity. The authors also showed that replacing tryptophan with phenylalanine reduced the activity of the endolysin by ~60%.

Taken together, it is important to note that these data for $NTF2^{LpqF}$ are based on structural analysis of the crystal contacts as a proxy for residue binding. These data need to be further tested to delineate and validate the real interaction partner between D85 and the amino acid on a peptide and investigate the residues in the binding pocket (see Future Work). Overall, this study shows that the NTF2-like domain of LpqF binds peptidoglycan through a unique, non-catalytic mechanism, similar to other peptidoglycan-targeting enzymes with NTF2-like domains.

6.4 Conclusion

NTF2-like domains in peptidoglycan-targeting enzymes play a major role in localising proteins to peptidoglycan fragments and maintaining cell shape (Banks et al., 2022). Structural analysis and comparison with the NTF2 domain of Bd1075 revealed that the NTF2 fold in LpqF is not fully open, possessing 44% less internal space than Bd1075 (Figure 36). Intermolecular contact analysis identified key residues with potential for peptidoglycan binding. Despite the difference in pocket confirmation, the NTF2-like domain of LpqF was shown to bind peptidoglycan. This structural insight into $NTF2^{LpqF}$ may guid future research on the functional mechanisms of similar domains in other proteins.

In collaboration with my colleague Greg Goudge, a new medium-throughput assay was designed and optimised. The results showed that $NTF2^{LpqF}$ exhibited repeatable and robust binding to peptidoglycan. In our assay, 80% of the $NTF2^{LpqF}$ was bound, comparable to the binding observed with WGA (Figure 41). This suggests that the binding is both tight and

specific. The data also identified D85 and R98 as key residues likely responsible for peptidoglycan binding. To the best of our knowledge, this is the first assay to use fluorescently labelled proteins in a peptidoglycan-binding context. However, these findings should be further validated by designing double and multiple mutants, incorporating neutral and charge reversals, to test for cumulative effects alongside single residue substitution evaluation.

Chapter 7. LpqF plays a role in peptidoglycan incorporation

7.0 Introduction

Meropenem has been shown to target L,D-TPases as well as PBPs in mycobacteria, despite their resistance to many β-lactams (Flores et al., 2005; Dubée et al., 2012; Zandi and Townsend, 2021). Following the morphological defect observed in the Δ*lpqf*^{Mm} mutant from the *Tn*-library on solid media, and the previous biochemical evidence demonstrating that both meropenem and doripenem can inhibit LpqF (Chapter 3), this section will address the impact of the *lpqf* gene and its deletion Δ*lpqf* in *M. marinum* cells (Δ*lpqf*^{Mm}) by evaluating bacterial fitness in liquid media under antibiotic exposure, alongside visualisation of cell wall changes associated with the absence of *lpqf*.

Given that the formation of peptidoglycan crosslinks is a validated therapeutic target for carbapenems, characterising the enzymes involved in this pathway could lead to new targets for mycobacterial drug discovery. In this context, the use of FDAAs was applied to visualise the impact of *lpqf* on peptidoglycan incorporation. FDAAs are powerful tools for visualising peptidoglycan synthesis and incorporation. They work by integrating into the bacterial cell wall during peptidoglycan synthesis, allowing real-time observation of the process using fluorescence microscopy. If *lpqf* is crucial for proper peptidoglycan synthesis, its disruption should result in visible alterations in the pattern or amount of peptidoglycan incorporation. These alterations can be observed as changes in fluorescence intensity or distribution, indicating that *lpqf* is a potential target for new drug discovery efforts.

Early studies by Kuru et al. (2012) investigated FDAA incorporation in *E. coli*, *B. subtilis*, and *Agrobacterium tumefaciens*. They found that using FDAAs did not adversely affect peptidoglycan metabolism and could reliably report D-amino acid incorporation. Additionally, they observed that FDAAs were incorporated at the 4th position in *E. coli* and *A. tumefaciens*, while in *B. subtilis*, FDAAs were incorporated into the 5th position of the peptide, with labelling at the poles and lateral cell wall. This method was later optimised and adapted to analyse peptidoglycan synthesis at earlier steps, such as the cytoplasmic pathway (Kuru et al., 2014). Since then, *in vivo* peptide incorporation has been documented in a wider variety of bacteria using various FDAAs (Hsu et al., 2017; Peters et al., 2019; Kuru et al., 2019; Shaku et al.,

2023; Castanheira & García-del Portillo, 2023). In these model organisms, the FDAA HADA is typically taken up through the periplasmic synthetic peptidoglycan pathway and is appended onto the di-peptide via D,D-TPases and, if present, L,D-TPases (Kuru et al., 2019).

In mycobacteria, high-resolution confocal and epifluorescence microscopy have shown that FDAA accumulation varies depending on the species, with debate ongoing regarding whether FDAAs are taken up via the extracellular or intracellular peptidoglycan synthesis pathways (García-Heredia et al., 2018; Baronowski et al., 2018). For example, Botella et al. (2017) demonstrated that peptidoglycan elongation in *M. smegmatis* occurs from the old pole. They also showed that in *M. tuberculosis*, cell elongation depends on cell length and eventually occurs from both poles. FDAA is incorporated at both poles prior to cell division and then at one pole after cell division occurs. This reflects the differential peptidoglycan synthetic pathways utilised by these species. In this chapter, data will be described on the impact of peptidoglycan insertion and cell shape in the absence of *lpqf*.

7.1 Fitness analysis of Δ*lpqf* mutant strains

In Chapter 3, a transposon mutant (Δ*lpqf*^{Mm}) in *lpqf* was identified, which exhibited an altered colony morphology. In this chapter, I will further examine this strain concerning cell size compared to the wildtype, 1218R. To assess this, cells were analysed by phase contrast microscopy to study length and width at lag, mid-exponential, and stationary phases of growth (OD_{600nm}: 0.2, 0.6, and 1.0, respectively, Figure, A & B). Under these conditions, the Δ*lpqf*^{Mm} cells (600-800 cells analysed with 10-20 cells counted per area) were significantly longer at the mid-exponential phase (wildtype: 2.7 ± 1 μm vs. Δ*lpqf*^{Mm}: 3.4 ± 2 μm) and had a wider diameter during the lag phase (wildtype: 0.64 ± 0.1 μm vs. Δ*lpqf*^{Mm}: 0.70 ± 0.1 μm) and mid-exponential phase (wildtype: 0.65 ± 0.1 μm, vs. Δ*lpqf*^{Mm}: 0.72 ± 0.1 μm), as shown in Figure 42, A & B.

In addition to measuring width and length, HADA staining was used to label the peptidoglycan, and the total number of septa per cell was counted (Figure 42, C). Significant differences in septation distribution were observed during the lag and mid-exponential growth phases for the Δ*lpqf*^{Mm} strain, with an average of 1.2 ± 1 septa per cell compared to 1.5 ± 1 septa per cell in a total of 637 cells during the lag phase, and 0.8 ± 1 septa per cell compared to 1.10 ± 0.4 septa

per cell in 426 cells during the mid-exponential phase (including an average of 5 cells with 3 or more septa). However, there was no difference in the average number of septa per cell between the wild type and Δ*lpqf*^{Mm} strains during the late growth phase, with 1.30 ± 0.5 septa per cell in the wild type versus 1.40 ± 0.6 septa per cell in 1079 cells. Each strain exhibited a minimum of one and a maximum of five septa events per cell, as shown in Figure 42, C. Although the cell length and width are significantly different, the change from the wildtype strain appears modest.

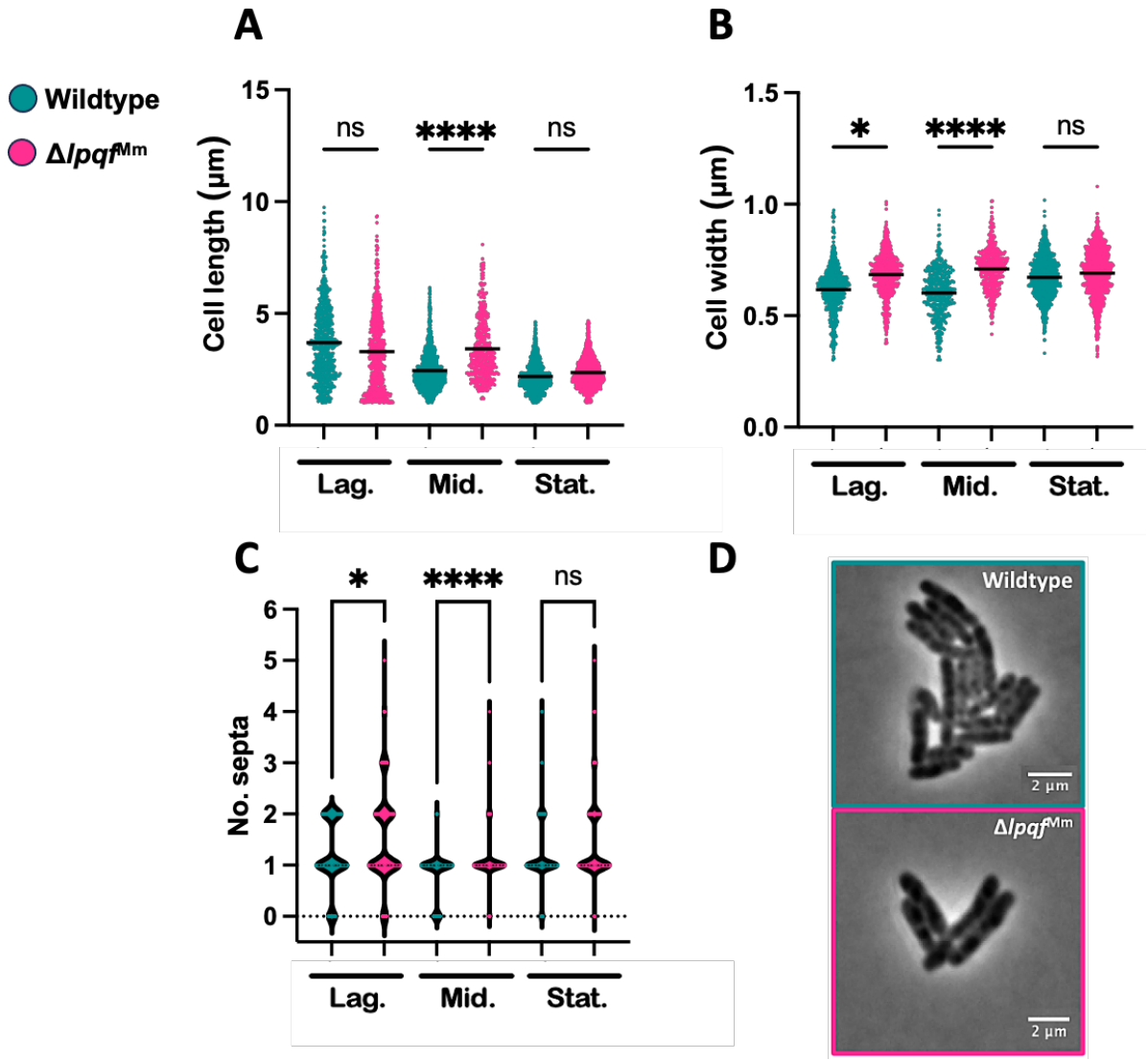


Figure 42: Morphological evaluation of an *M. marinum lpqf* transposon mutant. At the indicated optical densities, 5 uL of culture was analysed by brightfield microscopy on an Ziess, Axio, microscope. *M. marinum* wildtype and Δ*lpqf*^{Mm} was measured at early, mid and late phase for (**A**) length and (**B**) width. (**C**) Septation events were also measured for lag, mid exponential and early stationary phase. **(D)** Phase images are representative of Δ*lpqf* and wildtype at mid-exponential phase ($OD_{600\,nm}$, 0.6, scale bar 2 µm. Measurements filters of wildtype and Δ*lpqf*^{Mm} in *M. marinum* background were undertaken using10-20 cells per frame. Error bars represent standard error of the mean. ns non-significant ($p > 0.05$), ****$p < 0.0001$, * $p < 0.01$. Welches (Dunnett's T3 multiple comparison test) ANOVA.

In previous work by Dr. Patrick Moynihan, a Δ*lpqf* deletion mutant was generated in *M. smegmatis* mc^2155 using ORBIT-mediated mutagenesis (Murphy et al., 2018). To explore whether *lpqf* contributed to cell morphology in this organism, similar measurements were repeated. This investigation was conducted in collaboration with Dr Rudi Sullivan, at the time of this study, a fellow PhD student in the Moynihan laboratory. The data presented in Figure 43 were primarily collected by Rudi, with my involvement in the experimental design and execution.

The previous data indicated that the Δ*lpqf*^{Mm} mutant exhibited significantly longer and wider cell morphology. To build on these findings, an examination was undertaken on whether Δ*lpqf*^{Sm} also affected cell morphology in *M. smegmatis.* Similar to the *M. marinum* study, the Δ*lpqf*^{Sm} strain in *M. smegmatis* was analysed to determine its impact on cell size in liquid media. For this assessment, wild-type *M. smegmatis* and Δ*lpqf*^{Sm} cells (500 cells analysed with 10-20 cells counted per area) were examined by phase contrast microscopy to measure length and width at the mid-exponential growth phase (OD_{600nm}: 0.6). There was no significant difference in cell length between the Δ*lpqf*^{Sm} strain and the wild type (Figure 43, A). However, the Δ*lpqf*^{Sm} strain showed a significant decrease in mid-cell diameter (0.79 ± 0.1 μm) compared to the wild type (0.82 ± 0.1 μm) during exponential growth (Figure 43, B).

Additionally, septation was measured. Similar to the *M. marinum* data, a slight but significant difference was observed in the distribution of pre-cell division events for the Δ*lpqf*^{Sm} strain compared to the wild type. The average number of septa per cell was slightly higher in the Δ*lpqf*^{Sm} strain (1.40 ± 0.5 septa per cell in 339 cells) compared to wildtype (1.30 ± 0.5 septa per cell in 407 cells, respectively), as shown in Figure 43, C. In contrast to the previous results in *M. marinum*, these data indicate a decrease in cell diameter only. However, both datasets suggest that *lpqf* play may a role in affecting cell division.

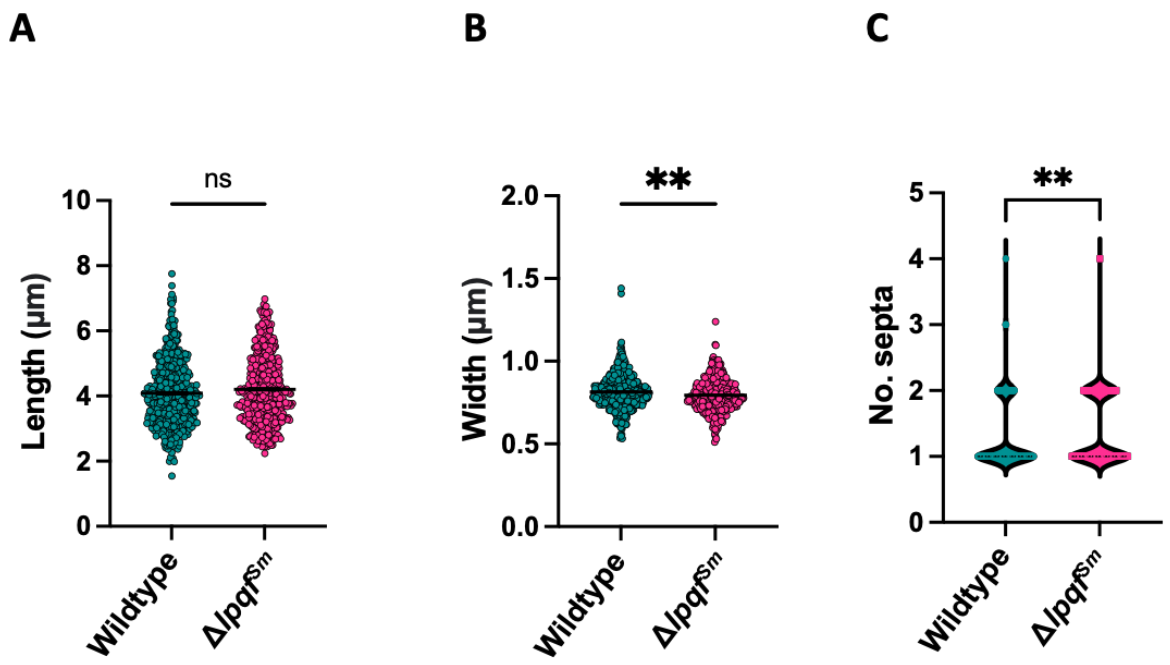


Figure 43: Morphological evaluation of Δ*lpqf* in *Mycobacterium smegmatis*. Wildtype and Δ*lpqf*^{Sm} were measured at the indicated growth phases for (**A**) length, (**B**) width and (**C**) septation. Cell cultures of the respective strains were grown to mid-exponential phase. Aliquots of cultures at growth time points of $OD_{600nm:}$ 0.6 were taken and 5 µL of culture was spotted on to a preprepared slide with agar pads and visualised phase contrast microscopy. Measurements of wildtype and Δ*lpqf*^{Sm} in *M. smegmatis* were undertaken using10-20 cells per frame. Error bars represent standard error of the mean. ns non-significant ($p > 0.05$), ** $p < 0.0022$, $p < 0.0034$), unpaired Welches T test.

Having identified moderate shape defects in *lpqf* deletion strains in both *M. marinum* and *M. smegmatis*, this study aimed to understand whether *lpqf* also contributed to bacterial growth kinetics. For this study, we used the wildtype and Δ*lpqf*^{Mm} strains in 7H9 medium supplemented with 0.05% Tween80 and 10% OADC over a period of 60 h.

Analysis of the growth kinetics revealed that the lag phase lasted approximately 20 h for all wildtype strains under these conditions. The wildtype strain then entered the exponential phase at around 20 h, reaching the late exponential phase-plateau stage at around 36 h ($OD_{600\ nm}$:1.2). In contrast, the Δ*lpqf*^{Mm} strain had a more prolonged lag phase, beginning to enter the exponential phase at approximately 27 h and reaching the late exponential phase-plateau at around 40 h ($OD_{600\ nm}$:1.2). The exponential phase lasted 10 h for the wildtype strain compared to 20 h for the Δ*lpqf*^{Mm} strain (Figure 44).

A complemented strain was also created by electroporating a pTIC6a construct containing the *lpqf* gene into the Δ*lpqf*^{Mm} mutant cells. This plasmid allows for conditional expression and is inducible with anhydrotetracycline for conditional expression. Overall, these preliminary data

(Figure 44) show a non-significant difference in the growth kinetics for Δ*lpqf*^{Mm} compared to the wildtype under these conditions.

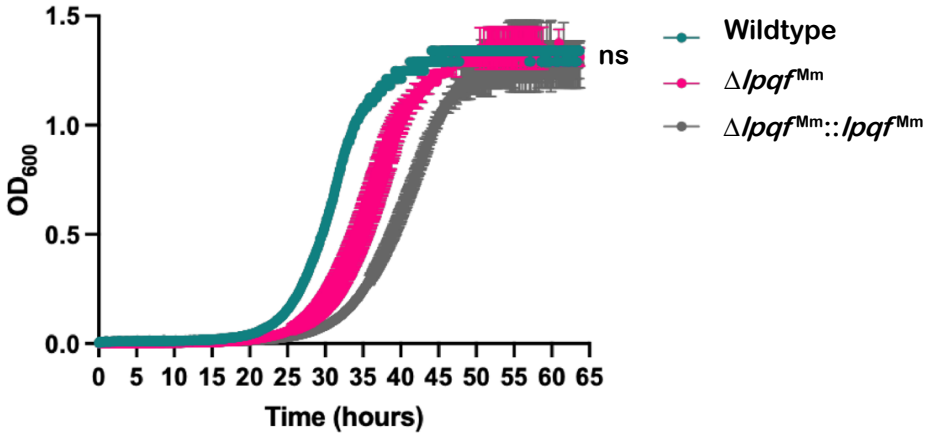


Figure 44: Growth kinetics for wildtype and Δ*lpqf* in *M. marinum*. The indicated strains were grown in 7h9 media for 60 h in a MicrobeMeter (Sasidharan et al., 2018) at 300 rpm in a total volume of 5 mL. To aid in mixing, two 3 mm glass beads were included in the sample tube. The sampling rate of the MicroMeter was 31372.55 Hz, with measurements taken every 30 seconds. The growth curve with error bars represents standard deviation of duplicate data from two independent experiments. Wildtype (turquoise), Δ*lpqf*^{Mm} (pink) and compliment strain (silver) in an *M. marinum* background. Statistics: non-linear regression with Gompertz growth, with sum of squares values = $p > 0.05$. ns non-significant ($p > 0.05$).

Having identified that the penam class of antibiotics could inhibit LpqF and considering the preliminary data obtained in an *M. marinum* background for Δ*lpqf* (Figures 30 & 44), A collaboration with Dr Rudi Sullivan was established to conduct growth kinetic studies as detailed in Figure 45. The aim was to investigate the potential impact of a knockout strain Δ*lpqf*^{Sm} on cell growth in *M. smegmatis* and determine if the Δ*lpqf*^{Sm} strain had an altered response to these antibiotics. To this end, the growth kinetics of the wildtype and mutant Δ*lpqf*^{Sm} strains in the presence and absence of the carbapenems meropenem and amoxicillin-clavulanic acid were evaluated. Additionally, to assess potential indirect effects of carbapenems, rifamycin and chloramphenicol were tested at sub-MIC concentrations (1 µg/mL, 2 µg/mL, 2.5 µg/mL, and 5 µg/mL, respectively). Chloramphenicol inhibits protein synthesis by binding to the 50S subunit of the 70S ribosome, thereby inhibiting peptidyl transferase activity, which subsequently prevents the aminoacyl transfer of aminoacyl-tRNA to its active site and peptide bond formation. While rifamycin binds to DNA dependant RNA polymerase, RpoB, thereby preventing RNA synthesis. To assess mutant sensitivity, two conditions were used: 7H9 supplemented with 0.5% OADC at pH 7.0 and lysogeny broth (LB), pH 7.0. All cultures were grown for 2 days until they reached the stationary phase (Figure 45).

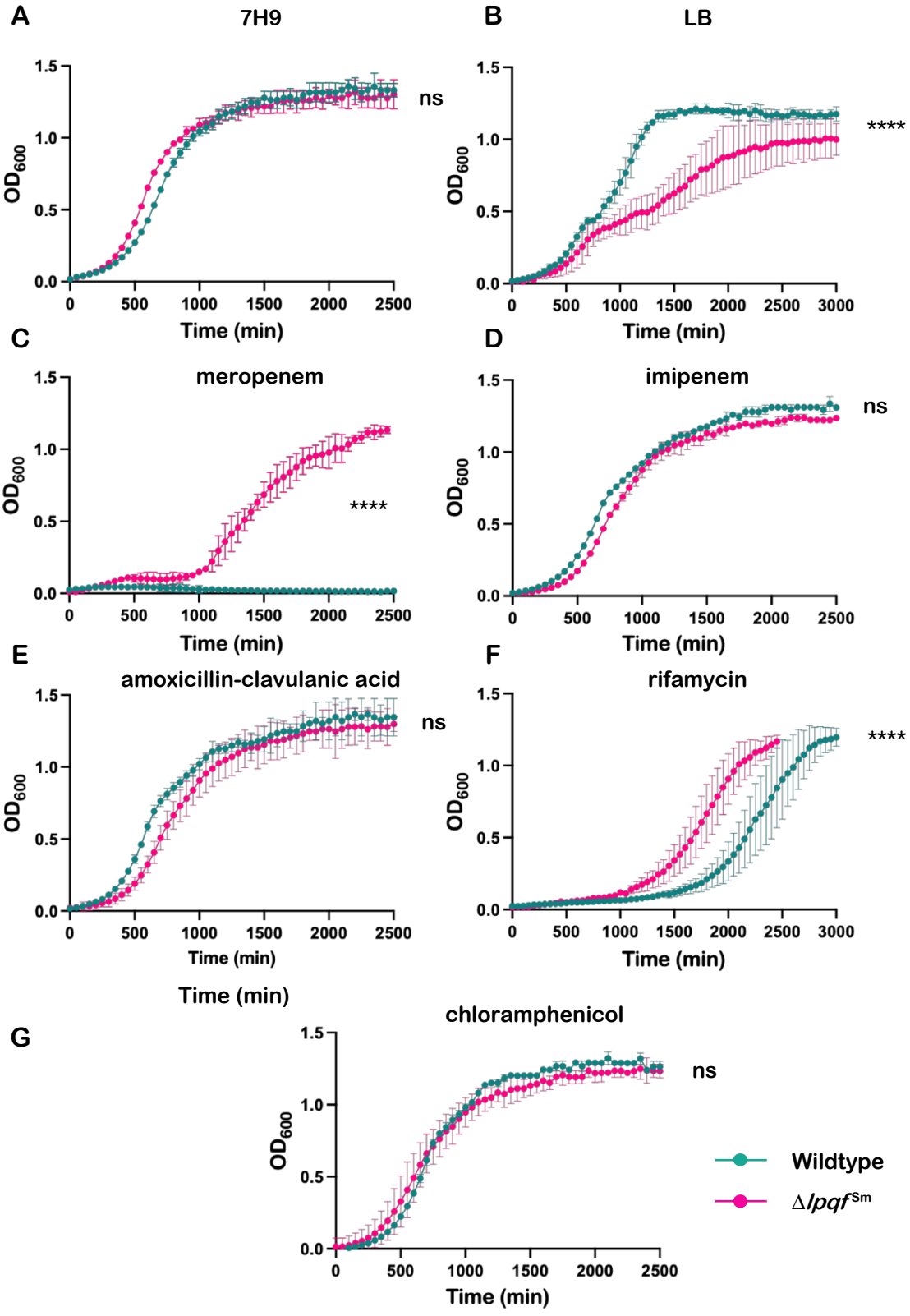


Figure 45. Analysis of knockout strain (Δ*lpqf* ^{Sm}) and wildtype in *M. smegmatis* liquid cultures. (**A** & **B**) Growth curves of wildtype and Δ*lpqf M. smegmatis* mc^{2}155 in 7H9 and LB. (**C-G**) The respective strains were measured every 5 minutes and tested with and without treatment of antibiotics in 7H9 media. (**C**) Treated cultures consisted of 1 µg/ml of meropenem, (**D**) 4 µg/mL imipenem, (**E**) 2 µg/ml of amoxicillin-clavulanic acid, (**F**) 2.5 µg/mL of rifamycin and (**G**) 5 µg/mL of chloramphenicol. The growth curves with error bars are representative of standard deviation of triplicate data from three independent experiments. Statistics: non-linear regression with Gompertz growth, with sum of squares values = $p > 0.05$. ns non-significant ($p > 0.05$, $p > 0.0001$).

The cultures grown in 7H9 media showed no difference in growth rate between the wildtype and Δ*lpqf*^{Sm} strains (Figure 45, A). Both strains exited the lag phase and entered the exponential phase at around 300 minutes. In LB medium, although both strains grew similarly during the lag phase, the Δ*lpqf*^{Sm} strain entered the exponential phase at 600 min and displayed slower growth compared to the wild type (mean difference between the two curves: -0.03 ± 0.0). The wildtype entered the exponential phase at 550 min and continued to grow normally. The fitted growth curve model, as indicated by R^2 values of 0.9755 (sum of squares = 9.553) for wildtype and 0.9082 (sum of squares = 28.17) for Δ*lpqf*^{Sm} strain , suggests a relatively strong fit to the observed growth trajectories. A discrepancy was observed in one set of replicates, with OD600 values ranging from 0.8 to 1.0 at the stationary phase for Δ*lpqf*^{Sm}, resulting in a larger margin of error (Figure 45, B). These data indicate that the loss of *lpqf* in *M. smegmatis* caused no growth defect when grown in 7H9 media. However, the loss of *lpqf* led to slower growth in LB media by the 1000-minute mark, although the strain was still able to grow under these conditions. The larger margin of error makes it challenging to draw a definitive conclusion. Based on these results, there may be a fitness defect in the Δ*lpqf*^{Sm} strain when grown in media not specifically formulated to meet its unique metabolic requirements, particularly the absence of oleic acids and glycerol essential for energy and cell wall biosynthesis (Figure 45, B).

For the treated cells, the wild-type strain did not grow in the presence of meropenem (wildtype: R^2 = 0.9248, sum of squares: 0.9667); while the Δ*lpqf*^{Sm} strain was unaffected (R^2 = 0.9724, sum of squares = 6.496) with a mean difference of 0.37 ± 0.0 (Figure 45, C). The Δ*lpqf*^{Sm} strain displayed a longer lag phase, eventually reaching an OD_{600nm} of 1.2, while the wildtype did not grow at all (Figure 45, A & C). Next, we tested the wild-type and Δ*lpqf*^{Sm} strains in the presence of imipenem and amoxicillin-clavulanic acid (Figure 45, D & E). At the tested drug concentrations, imipenem and amoxicillin-clavulanic acid did not affect either strain, both showing a similar growth pattern to the 7H9 condition, reaching an OD_{600nm} of approximately 1.3 (Figure 45, A, D, & E). This indicates that the Δ*lpqf*^{Sm} strain is not affected by these β-lactams under the conditions tested (Figure 30).

To rule out any change in growth due to indirect effects on cell wall properties and pathways being interrupted instead of the direct action of β-lactams, rifamycin (Figure 45, F) and chloramphenicol was used (Figure 45, G). The strains grown in rifamycin appeared to follow a similar trend during the lag phase until the 1000-min mark, where the wildtype took longer

to reach OD_{600nm} of 1.0 at the 3000-min mark compared to Δ*lpqf*^{Sm} (OD_{600nm} of 1.0 at 2450 min). This suggests that at sub-MIC levels of rifamycin, the Δ*lpqf*^{Sm} strain exhibited altered growth kinetics compared to wildtype strain (wildtype: $R^2 = 0.9704$, sum of squares = 25.42; Δ*lpqf*^{Sm} $R^2 = 0.9497$, sum of squares = 0.9497), with a mean difference of -0.47 ± 0.0 (Figure 45, F). This result partly aligns with published chemical genomics data from 90 CRISPRi-induced knockdown libraries used to quantify vulnerability, including *lpqf* in *M. tuberculosis* and *M. smegmatis*. For example, Bosch et al. (2021) demonstrated that the fitness of $LpqF^{MTB}$ is affected in the presence of rifamycin, whereas $LpqF^{SMEG}$ was unaffected (pebble, 2020; Bosch et al., 2021). Additionally, with *Tn*-mutants in *M. smegmatis* that have been shown to confer hypersensitivity to rifampin due to disruptions in genes such as arr, which encodes rifampin ADP ribosyltransferase (Alexander, Jones and Liu, 2003). The notable discrepancy between the findings in this study and those in the referenced studies may result from differences in methodologies, such as CRISPRi vs. recombinant gene technology.

In the chloramphenicol-treated cultures, there was a slightly slower growth rate for the wildtype strain, entering the exponential phase at 350 min versus 400 min for Δ*lpqf*^{Sm}. The wildtype grew slightly better than Δ*lpqf*^{Sm} during the transition from the exponential to the late phase (Figure 45, G). Overall, chloramphenicol had no effect on either strain, potentially due to the concentration of this drug being too low. Overall, these results demonstrate that LpqF is not important in sub-MIC concentrations of chloramphenicol. This suggests the drug impact is at least partially limited to β-lactams and potentially rifampicin. To note, unfortunately as with the *M. marinum* strain a complementation strain for these data was omitted due to inefficient complementarity between wildtype and complement strains.

In conclusion, Δ*lpqf*^{Sm} showed similar growth in untreated cultures in 7H9 media. In LB media conditions, untreated cultures of Δ*lpqf*^{Sm} also did not display an advantage but grew less efficiently entering the exponential phase later, reaching a lower OD than the wildtype. The Δ*lpqf*^{Sm} displayed a growth advantage over wildtype in meropenem-treated cultures. Overall, Δ*lpqf*^{Sm} demonstrated a strong growth advantage in the antibiotic-treated cultures in 7H9 compared to the wildtype.

7.2 An *lpqf* transposon mutant has altered peptidoglycan incorporation relative to wildtype *M. marinum*

Having successfully identified morphological defects in the absence of *lpqf*, coupled with the growth advantage in meropenem-treated cells (Figures 50 & 51) and evidence that LpqF is a D,D-CPase (Chapter 5, Figure 41), the impact of LpqF loss on peptidoglycan incorporation at the single-cell level was subsequently investigated. To do this, virtual time-lapse microscopy was utilised, which has been used previously in mycobacteria in studies by García-Heredia et al. (2018), Botella et al. (2017), and Baranowski et al. (2018).

Initially, cells were labelled with HADA for 360 minutes, followed by NADA labelling for 960 minutes, allowing for an independent measurement of peptidoglycan insertion and elongation. HADA allows for the visualisation of amino acid incorporation into nascent peptidoglycan via PBPs, reporting on labelling through 3,4 cross-links while enabling glycosyltransferases to continue glycan polymerisation. Therefore, the dye localises to the poles and cell division sites, indicating new peptidoglycan incorporation (García-Heredia et al., 2018). In contrast, NADA reports on peptidoglycan amino acid exchange via 3,3 cross-linkages, enabling visualisation of peptidoglycan incorporation at older sites and differential synthesis steps (Botella et al., 2017; Montón Silva et al., 2018; García-Heredia et al., 2018; Kuru et al., 2019) (Figure 46, A, B & C).

In this experiment, Δ*lpqf*^{Mm} showed a greater accumulation of NADA along the lateral wall than the wildtype (Figure 46, D). NADA accumulation was measured after an equal amount of incorporation time for both the wildtype and Δ*lpqf*^{Mm} strains. This was found to be significantly different when the length of the zone of incorporation was measured, as well as the width of the cell between NADA incorporation sites ($p < 0.0001$) (Figure 46, E). In contrast, HADA incorporation showed no difference in length between the two strains, but a significant difference in width was observed for Δ*lpqf*^{Mm} ($p < 0.0109$) (Figure 46, D, E). This agrees with the phase contrast results, which showed a wider diameter in Δ*lpqf*^{Mm} at mid-exponential phase (Figure 42). Overall, the examination of NADA demonstrated an accumulation along the lateral cell wall that extended from the pole in the Δ*lpqf*^{Mm} strain compared to the wildtype. This contrasts with the localised HADA labelling observed at and around the poles in the wild type. In the Δ*lpqf*^{Mm} strain, however, the incorporation of HADA exhibited more variability across

the population, as shown in Figure 46, D and E. These data suggest that *lpqf* has a role in the incorporation of peptidoglycan at the poles.

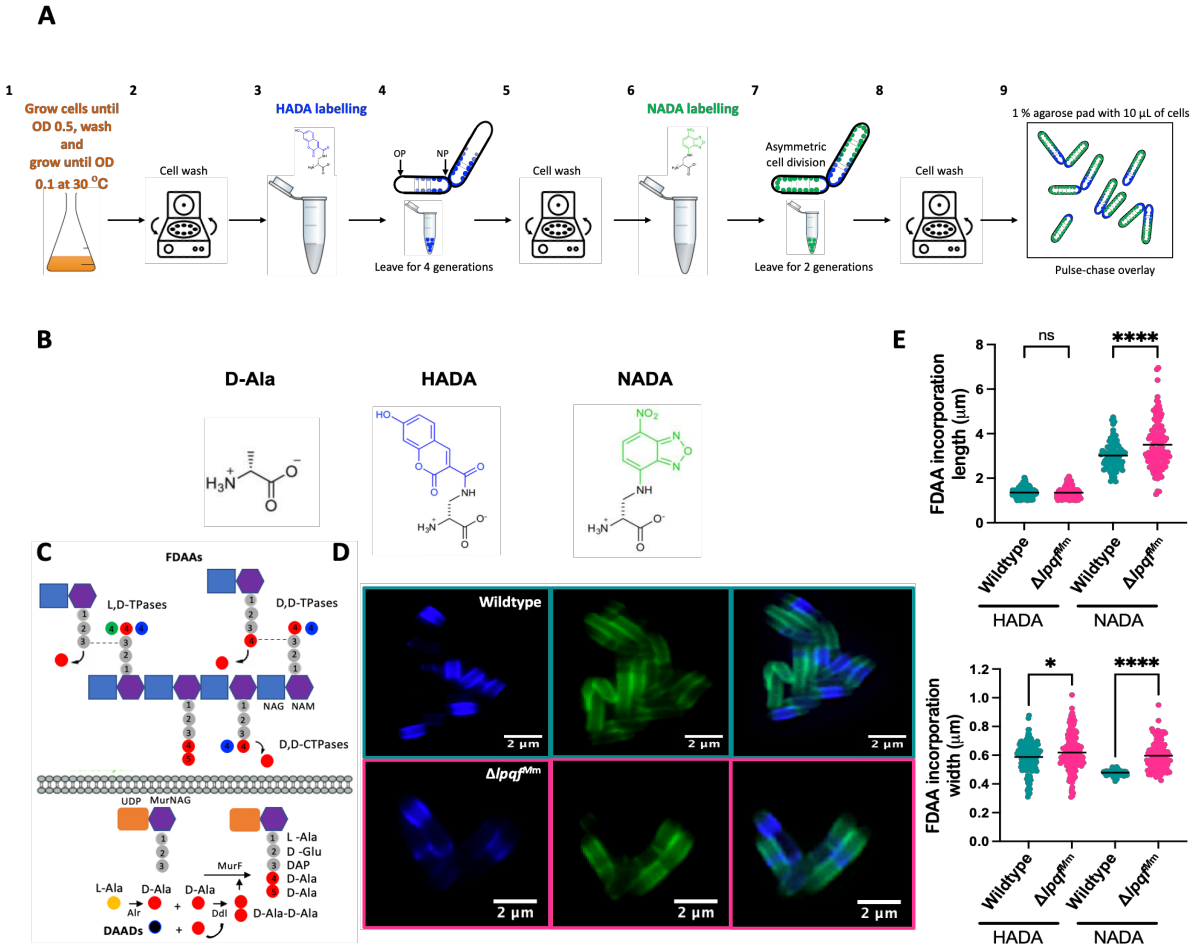


Figure 46: Cell wall labelling of wildtype and Δ*lpqf M. marinum* strains with FDAA dyes HADA and NADA. A diagrammatic representation of the methodology for pulse-chase labelling of *M. marinum* cells with HADA and NADA is shown in (**A**) (for detailed procedures see section 2.9). The steps are briefly summarised as follows: *M. marinum* cell cultures were grown to mid exponential phase (**A**, 1), centrifuged, and washed (**A**, 2). The cells were then resuspended in 7H9 medium and grown late lag phase, after which 500 µM HADA was added. Cultures were incubated for 4-6 generations (~ 6 h) to ensure robust FDAA incorporation (**A**, 3-4). Cells were washed twice with PBS to remove residual HADA (**A**, 5) and resuspended in 7H9 medium. Subsequently, 25 µM NADA was added, and cells were incubated for 2 generations (~ 16 h) for further FDAA incorporation (**A**, 6-7). Cells were gently washed twice in 7H9 (**A**, 8), resuspended in PBS, and applied to agarose pads on slides for visualisation by epifluorescence microscopy (HADA: Em 450 nm, Ex 405 nm; NADA: Em 555 nm, Ex 450 nm) (**A**, 9). NP; new pole, OP; old pole. (**B**) Structures of D-alanine, the FDAAs HADA (blue) and NADA (green) are shown above the corresponding image. (**C**) A basic schematic representation of the cell wall incorporation of D-amino acids for *M. tuberculosis* is provided. (**D**) Epifluorescence images of HADA (blue, left panel), NADA (green, middle panel), and overlay (right panel) are color-coded for wildtype (turquoise) and Δ*lpqf*^{Mm} (pink). Measurements of FDAA incorporation were quantified using MicrobeJ with the maxima setting. FDAA accumulation was measured for NADA and HADA dimensions along the length (**E**) and width (**F**) of each cell for 426 cells, 10 cells per frame. Images are representative of n = 2, and quantitation of each FDAA was analysed via MicrobeJ and GraphPad Prism 10. Error bars represent standard error of the mean. ns: non-significant ($p > 0.05$), * $p < 0.0109$, ****$p < 0.0001$, Welch's T-test (Dunnett's T3 multiple comparison test) ANOVA.

7.3 Discussion

Morphological assessment using phase-contrast microscopy of Δ*lpqf* in *M. marinum* 1218R Δ*lpqf*^{Mm} at lag, mid-exponential, and late-exponential phases revealed no differences at the lag and late-exponential phases. However, a significant difference in cell length was observed at the mid-exponential phase. Specifically, the cell diameter increased during the lag phase and was significantly larger at the mid-exponential phase in the Δ*lpqf*^{Mm} strain compared to the wildtype. Having confirmed a morphological defect for Δ*lpqf* in *M. marinum*, the same criteria were applied using *M. smegmatis* to determine if the defect could be recapitulated across mycobacteria. Despite the significant changes observed in Δ*lpqf*^{Mm} in *M. marinum,* a similar phenotype was not observed in *M. smegmatis,* suggesting that the impact of losing *lpqf* differs between species, potentially due to differences in growth kinetics and environmental niches for each organism.

The next study aimed to determine whether loss of *lpqf* leads to changes in growth kinetics, as might be expected given the observed changes in cell shape. Previous research has demonstrated that mutations causing modest alterations in cell shape changes can result in overall fitness defects in *Caulobacter crescentus* and *E. coli* (Ausmees, Kuhn and Jacobs-Wagner, 2003; Persat, Stone and Gitai, 2014; Cho et al., 2016). The assessment in this study revealed a difference in growth for the Δ*lpqf*^{Mm} strain compared to wildtype under these conditions (Figure 44). Furthermore, a potential complementation strain using *lpqf*::pTIC-Δ*lpqf*^{Mm} was evaluated to determine whether *lpqf* is directly responsible for the defects observed in Δ*lpqf*^{Mm} at both the single-cell and population levels. Unfortunately, the complemented strain did not rescue the phenotype, potentially due to the use of the pTIC plasmid, which requires anhydrotetracycline for induction. This dependency may have interfered with the bacterium's ability to regulate *lpqf* expression. As a result, the addition of anhydrotetracycline likely induced partial expression of LpqF, leading to an incomplete phenotype that did not fully recapitulate the wildtype strain. Despite this, as demonstrated in 7H9 media, Δ*lpqf*^{Mm} morphological defects could indeed be recapitulated, albeit modestly. This complements the data obtained in phase contrast for Δ*lpqf*^{Mm}, which showed longer cell lengths that were more prominent at mid-exponential phase. Taken together this suggests that in the absence of *lpqf,* cell elongation is prolonged due to a lack, but not total loss, of control of new peptidoglycan synthesis at the poles (Figure 45).

Since mycobacteria require access to fatty acids, iron, glycerol, and other carbon sources such as cholesterol for intra- and extracellular growth (Griffin et al., 2012; Knobloch et al., 2020). The Δ*lpqf*^{Sm} strain was investigated to determine whether its growth would be impaired in two rich mediums: 7H9 and LB media. Although LB contains yeast extract, it lacks fatty acids necessary for cell wall biosynthesis, which could potentially impact the growth of Δ*lpqf*^{Sm} compared to its growth in the more optimal 7H9 media.

In untreated cultures in LB media, Δ*lpqf*^{Sm} exhibited a slower growth rate compared to the wildtype strain. In contrast, no difference in growth was observed between Δ*lpqf*^{Sm} and wildtype in 7H9 media. This result differs from the *M. marinum* data described in Figure 44, suggesting species specific effects. These discrepancies may reflect differences in the ecological niches of each *M. smegmatis* and *M. marinum* and the spatiotemporal localisation of peptidoglycan-targeting enzymes. For example, Botella et al. (2017) demonstrated distinct differences in peptidoglycan incorporation between *M. smegmatis* and *M. tuberculosis*. In *M. smegmatis*, peptidoglycan incorporation occurs predominantly at the old pole, whereas in *M. tuberculosis*, it occurs at both poles and is tightly coupled with cell division. Cell elongation in *M. tuberculosis* is dependent on cell length, potentially reflecting differences in the localisation of hydrolases in each species.

Furthermore, other studies have highlighted the importance of preferential growth differences in various environments when deleting genes that encode peptidoglycan-targeting enzymes and serine-threonine kinases involved in regulating cell division and peptidoglycan synthesis, such as *dacB* and *pkn1*. For example, Kandasamy et al. (2020) demonstrated that a double knockout strain Δ*pkn1* and Δ*dacB2* exhibited differential phenotypes, with Δ*pkn1* growing better in liquid media and both Δ*pkn1* and Δ*dacB2* showing improved growth under acidic conditions in THP-1 macrophages.

Following the studies in untreated rich media, the vulnerability of the Δ*lpqf*^{Sm} strain was tested in the presence of the carbapenems doripenem and meropenem in 7H9 media at pH 7.0 in *M. smegmatis*. Using sub-MIC levels of these drugs were used to investigate altered phenotypes without killing the cells. The results for meropenem were clear: with the wildtype strain was unable to grow, while the Δ*lpqf*^{Sm} strain showed growth. In contrast, imipenem did not affect either strain. Notably, these findings differ from the imipenem data obtained in the protein inhibition assay for LpqF against a panel of β-lactams (Chapter 3, Figure 36). However, this

comparison has limitations, as the former involved cellular growth assays, whereas the latter used purified LpqF. This underscores the inherent differences between *in vivo* growth studies and *in vitro* enzyme assays. Finally, the result for imipenem in this *in vivo* study is aligns with a recent study by Kumar et al. (2022), which showed that D,D-CPases (DacB, DacB1, and DacB2), along with PBPs (PBPA and PBPB) in *M. tuberculosis* are insensitive to imipenem.

A caveat in the growth kinetic studies could be that the drug concentrations used might have been too low to exhibit an effect on cell growth. For example, chloramphenicol was shown in this study to have no impact. In contrast, the effects of rifampicin observed in this study could be due to alternative mechanisms, which could be further investigated by using a range of concentrations. For example, Zhu et al (2018) used varying concentrations (0-200 ug/ mL) of rifampicin to induce a sub-population of rifampicin-tolerant bacilli. The authors reported that RpoB is induced from a second promoter leading to reinitiation of growth in the resistant sub-populations. Other studies, such as Piddock, Williams and Ricci, (2000), have explored rifampicin resistance mechanisms, demonstrating the accumulation of rifampicin in *M. tuberculosis* and *M. smegmatis* at sub-MIC concentrations of 0.25 mg/L and 8 mg/L, respectively. Although the concentrations used in our study were optimised in accordance with published data, the growth kinetic studies will need to be repeated at higher sub-MIC concentrations for chloramphenicol and meropenem, as determined using a broth dilution and checkerboard titration assay.

Overall, these data suggest that the loss of *lpqf* provides an advantage in the presence of carbapenems when grown in 7H9 media conditions. The use of rifampicin and chloramphenicol in this study serves as a proof of principle to confirm the direct effects of carbapenems. However, we discovered that rifampicin as well as meropenem has an impact on growth in the absence of *lpqf*. Therefore, we cannot entirely rule out these results are solely a direct effect of the carbapenems. To conclude, the loss of *lpqf* in *M. marinum* and *M. smegmatis* provides an advantage to the Δ*lpqf* strain, supporting our single-cell and preliminary data on its role in the cell wall of these organisms.

Having identified that Δ*lpqf* impacts cell morphology, coupled with the data for D,D-CPase activity of LpqF, a pulse-chase experiment using *M. marinum* strains was undertaken. Here we applied the FDAA probes HADA and NADA (Figure 46). As indicated above, HADA typically reports on peptidoglycan synthesis at the poles and cell division sites, while NADA reports on

lateral cell wall peptidoglycan. This is especially useful for organisms like mycobacteria, which use a smaller portion of the cell and elongate from the poles rather than from the lateral wall, as seen in other rod-shaped bacilli such as *B. subtilis* and *E. coli* (Baranowski, Rego, & Rubin, 2019).

This experiment exploited this unique distinction in mycobacteria to show that, in the absence of *lpqf*, HADA accumulation in and around the polar region became more dispersed but still localised to this area. In contrast, NADA accumulation showed a significantly dispersed gradient that extended around the diameter and along the length of the cell in the absence of *lpqf*. The results obtained in this study for wild-type *M. marinum* appear to corroborate published data, following a similar pattern to peptidoglycan synthesis reported for *M. tuberculosis*. The García-Heredia et al. (2018) study reports that for their wild-type strain, HADA was more concentrated at the polar regions, with accumulation localised at the new pole and dimmer HADA at the old pole, further validating our experimental procedure. In contrast, Baranowski et al. (2018) show a more dispersed labelling of HADA for ΔL,D-TPases in *M. smegmatis*. Overall, the data from this study suggest that *lpqf* mediates peptidoglycan incorporation in and around the polar site in *M. marinum*, and the loss of *lpqf* influences uncontrolled elongation. This could be explained by the loss or reduction of D,D-CPase activity, which cleaves off the last D-alanine and therefore the HADA label from peptidoglycan precursors. This change would not be evident without the use of NADA, which differentiates between new (near the pole) and older (lateral cell wall) peptidoglycan. This implies that in the wild type, *lpqf* reduces the overall labelling efficiency by cleaving off the appended FDAA.

7.4 Conclusion

The results described in this chapter demonstrate that in the absence of *lpqf*, there is a growth advantage in the presence of sub-MIC concentrations of meropenem. Our data support a direct effect of meropenem and not an off-target effect of non-peptidoglycan targeting antibiotics. Additionally, it has been possible to establish a role for *lpqf* in peptidoglycan homeostasis using FDAA incorporation experiments. Although other possibilities exist, as noted in the discussion, the data obtained for HADA and NADA accumulation in the absence of *lpqf* complement the data gathered so far, supporting the hypothesis that LpqF functions as a D,D-CPase.

Chapter 8. Overall discussion

M. tuberculosis remains a serious global threat, partly due to its unusually thick cell wall, which contains mAGP. The foundation of this complex is peptidoglycan, a sugar-amino acid layer built and maintained by enzymes coordinating their functions to enable cell elongation and division, a process intimately linked to arabinogalactan (Al-Jourani et al., 2023; Franklin et al., 2024). Studying these enzymes including how they are induced, regulated, and what they interact with is crucial to understanding how peptidoglycan is maintained. Although, there are many on-going studies in this area, research on D,D-CPases is still behind in comparison to studies in Gram negative and Gram positive bacteria such as *E. coli* and *B. subtilis* respectively. This thesis addressed five fundamental objectives regarding a newly discovered peptidoglycan-targeting enzyme. It answered the five questions embedded within these objectives which were as follows.

Firstly, a potential hit, *Rv3593* or *lpqf,* from an old *Tn*-library which was successfully validated. This thesis addressed the question regarding it catalytic domain and narrowing down on its function in peptidoglycan biogenesis. *In silico* analysis revealed a highly conserved C-terminal, where the active site is located, and a unique N-terminal that consists of an NTF2-like domain. Building on these data, this thesis was able to distinguish between a PBP and β-lactamase, ruling out the latter. This distinction guided the investigation into its binding site using β-lactams associated with PBP inhibition. These data lay the foundation for further investigation into the binding kinetics of β-lactams associated and PBP inhibition which will provide an insight into the high efficacy of meropenem in LpqF.

Secondly, asked the question whether the active site of purified LpqF was open and indeed it was confirmed to be open, accepting β-lactams and being inhibited by the carbapenem class of inhibitors. Furthermore, this thesis demonstrated that LpqF is highly susceptible to the carbapenem meropenem but not to penicillins or cephalosporins. Meropenem is a known inhibitor of L,D-TPases and has also been shown to inhibit D,D-TPases. This is work builds on that knowledge and lays the foundation for further research into reverse engineering the binding mechanisms for LpqF, with potential for developing future, less toxic combination therapies.

Thirdly, after identifying that the catalytic active binding pocket is accessible, the next question was to determine the function the NTF2-domain in the N-terminal. The main question that was asked was whether the $NTF2^{LpqF}$ anchor itself to peptidoglycan, similar to other NTF2-domains like Bd1075 from the Banks et al. (2022) study. However, due to the low conservation $NTF2^{LpqF}$ compared to other published or otherwise NTF2-domain folds, it was challenging to identify residues involved in peptidoglycan attachment. Despite this, a proxy was used, which confirmed that $NTF2^{LpqF}$ is indeed capable of attaching peptidoglycan. Furthermore, this study identified two candidate residues, D58 and R98, whose absence led to partial binding to peptidoglycan, with D85 potentially playing a more critical role than R98. This finding suggests that, despite low conservation reflecting its species-specific niche, $NTF2^{LpqF}$ also facilitates attachment to peptidoglycan, albeit through different residues. Once anchored, it may support a function like acting like a scaffold to allow the C-terminal active site domain location near pentapeptide substrate. However, further investigation will need to be undertaken to investigate these residues and probe for other yet unidentified residues that were missed in the initial crystal contact analysis (see 8.1 conclusion).

Fourthly, this thesis poised the question can LpqF cleave peptidoglycan fragments and indeed. confirmed that LpqF can cleave the final D-alanine from the pentapeptide. Based on these data, it is likely that LpqF plays a key role in maintaining the rod shape of the cell, as observed with other D,D-CPases (Nelson et al., 2001; Pandey et al., 2018). Further work should be undertaken building on these data using pentapeptides specifically found in Gram negative bacteria and mycobacteria, such as. *meso*-DAP type peptidoglycan. As discussed in chapter 5, this would enhance the understanding of the affinity of LpqF to this substrate. Figure 47 outlines the proposed mechanism for LpqF.

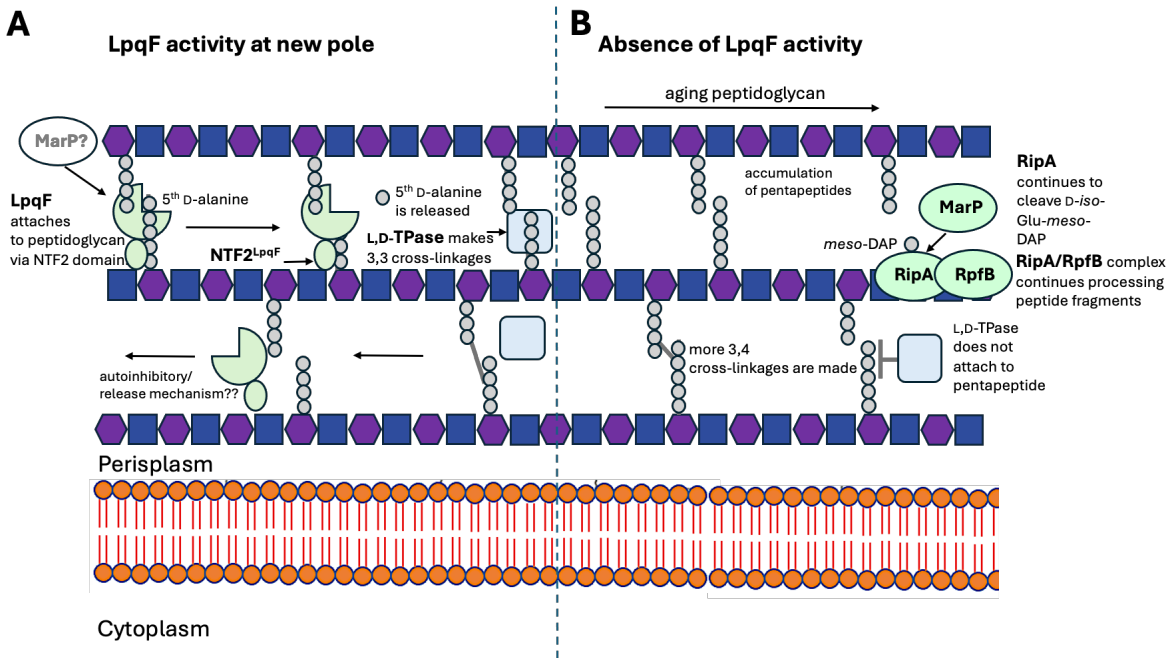


Figure 47: A description of the function for LpqF a new mycobacterial D,D-CPase. (**A**) In the presence of LpqF the fifth D-alanine is clipped off allowing the L,D-TPases access to the newly formed tetrapeptide and thus 3,3 cross-linking can continue. In the absence of LpqF the cell decreases its ability to make newer 3,3 cross links, so the cell elongates but the level of 3,3 cross links is decreased with aging peptidoglycan and higher abundance of 3,4 cross links, leading to less stable peptidoglycan. This suggests LpqF is not a vital enzyme but has a major advantage in low nutrient conditions/late exponential phase. Potentially LpqF is more active during the infection in hypoxic/acidic environments possibly supporting transition from active to dormant when the new cross links are not needed and therefore LpqF is more a regulation enzyme using an autoinhibition mechanism that is yet to be studied (the second NTF2). (**B**) In conclusion, LpqF plays an important role for the cell in peptidoglycan switching from 3,4-3,3 cross-linking. For clarity the other peptidoglycan targeting enzymes have been omitted.

Furthermore, as LpqF is a hydrolase, it is possible that the cell regulates its activity in acidic environments via an activator, such as the acidic serine protease MarP (Rv2671c), similar to RipA (Botella et al., 2017). However, unlike RipA, the data in this study have shown that the active site of LpqF is active at pH 7.0. This suggests that LpqF may be either cleaved to enhance activity or inhibited in more acidic conditions. If the latter is true, it could indicate the presence of a yet unidentified autoinhibition mechanism. This hypothesis should be investigated through pull-down experiments with purified MarP under acidic and low nutrient conditions.

Lastly, growth kinetics demonstrated that the *lpqf* mutant exhibited an altered morphology, displaying a notable growth advantage over the wildtype in the presence of meropenem. While untreated cells showed only a minor difference between mutant and wildtype under normal media conditions. The microscopy data revealed that the mutant had a slight morphological abnormality, with cells being longer and wider at mid-exponential phase. Using FDAA technology and toolkit (Kuru et al., 2012; Kuru et al., 2015), it was possible to associate the mutant with accumulation of FDAA probe NADA and potentially the deposition of older

peptidoglycan along the lateral cell wall of *M. marinum*. This is an important finding because, in mycobacteria, new nascent peptidoglycan is typically inserted into the cell wall at the poles, not laterally. This implies that in the absence of LpqF, there are less 3,3 cross-linking and more 3,4 cross-linking, leading to an increase in cell length (Figure 47). However, although this thesis provides a solid foundation, more data is needed before a definitive conclusion can be made about the extent the impact that *lpqf* has on peptidoglycan cross-linking and regulation (see section 8.1).

8.1 Future work

The main caveat of these data is the lack of complementation work. Recapitulating the substitutions in NTF2^{LpqF} would help to determine whether there is synergism or an additive effect between the peptidoglycan binding residues. This could be achieved by combining two or more of the existing mutants, such as *ntf2*::W56A;W28A, and *ntf2*::D85A;R98A. This approach could also be applied at the population level. For example, recapitulating the Δ*lpqf* mutant in the growth kinetics studies would be useful for analysing growth profiles or even conducting evolution studies to investigate rifampicin and meropenem susceptibilities. Another proven method in mycobacterial genetics could be used to complement Δ*lpqf*. The pMV306 plasmid, commonly used in mycobacterial genetic manipulation (Franklin et al., 2024), can integrate into the chromosome, potentially allowing for better transduction. For example, the *lpqf* gene could be inserted into pMV306 using allelic exchange or Oligonucleotide-Mediated Recombineering followed by Bxb1 Integrase Targeting (ORBIT) as described by Murphy et al. (2018) and Borgers et al. (2019). This could be done in conjunction with CRISPRi, to induce a knock down for Δ*lpqf* mutant. The cells containing the wildtype, Δ*lpqf* and *lpqf*L5::pMV306-Δ*lpqf* could then be passaged *in vitro* (culture plates) at different concentrations of meropenem, doripenem, and/or rifampicin under various media conditions, selecting for resistant cells. Whole genome sequencing could then be performed to determine the mechanisms of resistance or tolerance and how the selected cells acted upon mechanisms. A similar study by Buddle et al. (2024) and vancomycin resistance in DacJ, a D,D-CPase in *Clostridioides difficile* showed reduced fitness of the resistant cells, with two mechanisms of resistance *dacS* and *vanT* demonstrating that resistance in this context is multifactorial. This has implications for the LpqF study, helping us to parse the potential influence of *lpqf* on the surrounding genes.

To determine if LpqF indeed has a second function, as proposed in the FITC-PG associated degradation, it would be relevant to use FITC-pentapeptide along with polymerised peptidoglycan and perform the same experiment with these substrates. This approach would provide the necessary data needed to identify the anomaly seen in FITC-TLC.

Another direction for the $NTF2^{LpqF}$ study could be to ascertain whether the presence of $LpqF^{NTF2}$ enhances PBP activity. The C-terminal region of LpqF, which contains the catalytic domain, could be purified to increase throughput. However, previous attempts to purify the C-terminal alone were hindered by degradation due to its instability. Therefore, the N-terminal region containing the NTF2 domain and the appended second NTF2 domain (Figure 32, A) could be inactivated through genetic modification methods to stabilise, clone and express only the C-terminal. This LpqF variant could then be tested for activity in the same high throughput assays used for degradation analyses, alongside the full length protein and NTF2 only. These experiments would provide insights into whether the active site pocket is occluded by an autoinhibitory mechanism under acidic or low nutrient conditions, or if the activity observed at pH 7.0 is increased.

A further experiment to deepen the investigation into the hydrolysis activity for LpqF to undertake mechanistic studies. This would involve probing the catalytic mechanism of LpqF which would require making site directed mutants in the catalytic pocket and running enzyme kinetics. These mutants could also be applied along with wildtype to test and repeat muropeptide composition analyses for LpqF activity with pentapeptide substrate and whole peptidoglycan as comparisons.

The use of a D,D-CPase activity assay would enhance the results already obtained for LpqF activity. This could be achieved using a fluorescence-coupled assay with whole peptidoglycan, peptidoglycan rich in pentapeptide, and pentapeptide derivatives as substrates for assessment continuous D-alanine release analysis. A spectrophotometer could then detect substrate changes in D-amino acid oxidase-peroxidase at A_{555}, either as an endpoint (Rioseras et al., 2016) or through continuous release, as described in the study by Catherwood et al. (2020). If D-alanine is liberated, a colour change would occur in the presence of phenol due the oxidation of 4-aminoantipyrine to chinoenmine or the conversion of the chromogen amplex red to the dye resorufin, depending on the assay and substrate used (Rioseras et al., 2016; Catherwood et al., 2020). The rate of D-alanine release can be calculated by comparing the rate of change in

presence and absence of the donor substrate. The method from the Catherwood et al. (2020) also allows for monitoring of transpeptidation reactions. For example, adding TPase and an acceptor substrate UDP-Mur*N*Ac-pentapeptide can initiate a transpeptidation reaction, allowing for observation of D-alanine release.

Nuclear magnetic resonance (NMR) could be used as an alternative method to map binding sites, confirm interactions and identify the specific residues that facilitate localisation to particular areas of peptidoglycan. NMR operates by re-orientating atomic nuclei and detecting the absorption of electromagnetic radiation (Slichter, 1996). To detect interactions between $NTF2^{LpqF}$, LpqF and peptidoglycan, the proteins could be labelled with isotopes. For example, NTF2 could be labelled with ^{15}N isotopes, and ligand-protein titrations (e.g., ^{15}N LpqF/$NTF2^{LpqF}$ with muropeptides and pentapeptides) could be performed, as demonstrated by Lin et al. (2021) for Pgp2 and by Mesnage et al. (2014) for the LysM domain of AtlA in *E. coli*. Alternatively, isothermal titration calorimetry (ITC) could be employed, offering the advantage of not requiring labelled enzyme or ligands. For example, full length LpqF and $NTF2^{LpqF}$ could be tested by introducing *meso*-DAP type peptidoglycan ligands and measuring binding affinities through heat displacement (enthalpy changes), which indicates ligand-protein interactions, as described in similar studies on peptidoglycan analysis.

The use of real time analyses for FDAA utilisation *in vitro* could be enhanced by employing high resolution microscopy within an incubator-chamber, using either cell culture plates or a fluid chamber, to visualise real time peptidoglycan synthesis and cell division. The conditions used for the growth in 7H9 at pH 7.0, Sautons medium at pH 5.0, and meropenem treatment could be applied to visualise of the effects on wildtype$^{lpqf\text{Mm}}$ and Δ$lpqf^{\text{Mm}}$ for utilisation and/or accumulation of FDAAs under these conditions. Coupling these analyses with $NTF2^{LpqF}$ morphological studies would contribute to existing data for $NTF2^{LpqF}$ and clarify its role in cell shape maintenance.

To further these investigations and compliment the pulse chase experiment, it would be valuable to determine where LpqF and its mutants, as described above, are localised within the cell and how long they remain active. This could be achieved by using an mCherry plasmid, as described by Botella et al. (2017) and Meiresonne et al. (2017). For example, an LpqF-mCherry strain could be used to identify the approximate location of LpqF within the cell. LpqF-mCherry would likely appear as pinpoints or perhaps more dispersed points, reflecting function

the spaciotemporal dynamics of its D,D-Cpase activity. This could be conducted alongside a wildtype mCherry as a control.

8.2 General conclusion

Overall, this thesis provides compelling evidence that LpqF is a new D,D-CPase in mycobacteria. These data presented, along with the proposed future biochemical and functional experiments, will provide an excellent guide and foundation for the next steps in studying LpqF and other yet unknown D,D-CPases and hydrolases.

Reference:

Abarca, K., Rey-Jurado, E., Muñoz-Durango, N., Yaneisi Vázquez, Soto, J.A., Nicolás M.S. Gálvez, Valdés-Ferrada, J., Iturriaga, C., Urzúa, M., Borzutzky, A., Cerda, J., Villarroel, L., Madrid, V., González, P.A., González-Aramundiz, J.V., Bueno, S.M. and Kalergis, A.M. (2020). Safety and immunogenicity evaluation of recombinant BCG vaccine against respiratory syncytial virus in a randomized, double-blind, placebo-controlled phase I clinical trial. *EClinicalMedicine*, 27, pp.100517–100517. doi:https://doi.org/10.1016/j.eclinm.2020.100517.

Abate, G., Hamzabegovic, F., Eickhoff, C.S. and Hoft, D.F. (2019). BCG Vaccination Induces M. avium and M. abscessus Cross-Protective Immunity. *Frontiers in Immunology*, 10. doi:https://doi.org/10.3389/fimmu.2019.00234.

Abrahams, K.A. and Besra, G.S. (2018). Mycobacterial cell wall biosynthesis: a multifaceted antibiotic target. *Parasitology*, [online] 145(2), pp.116–133. doi:10.1017/S0031182016002377.

Abrahams, K.A., Batt, S.M., Gurcha, S.S., Veerapen, N., Ghader Bashiri and Besra, G.S. (2023). DprE2 is a molecular target of the anti-tubercular nitroimidazole compounds pretomanid and delamanid. *Nature Communications*, 14(1). doi:https://doi.org/10.1038/s41467-023-39300-z.

Acharya, S., Deshpande, P., Asirvatham, E.S., Palkar, A., Sarman, C.J., Laxmeshwar, C., Setia, M.S., Rathod, D., Koli, S., Dale, J., Yeldandi, V., Allam, R., Agarwal, R., Verma, S., Upadhyaya, S. and Nyendak, M. (2022). Utility of the lateral flow urine lipoarabinomannan tuberculosis assay in patients with advanced HIV disease at antiretroviral therapy centres in Mumbai, India. *PLOS ONE*, 17(9), p.e0273970. doi:https://doi.org/10.1371/journal.pone.0273970.

Adediran, S.A., Zhang, Z., Nukaga, M., Palzkill, T. and Pratt, R.F. (2005). The d-Methyl Group in β-Lactamase Evolution: Evidence from the Y221G and GC1 Mutants of the Class C β-Lactamase of *Enterobacter cloacae* P99. *Biochemistry*, 44(20), pp.7543–7552. doi:https://doi.org/10.1021/bi050136f.

Adediran, S.A., Kumar, I., Nagarajan, R., Sauvage, E. and Pratt, R.F. (2010). Kinetics of Reactions of the *Actinomadura* R39 DD-Peptidase with Specific Substrates. *Biochemistry*, 50(3), pp.376–387. doi:https://doi.org/10.1021/bi101760p.

Advani, J., Verma, R., Chatterjee, O., Pachouri, P.K., Upadhyay, P., Singh, R., Yadav, J., Naaz, F., Ravikumar, R., Buggi, S., Suar, M., Gupta, U.D., Pandey, A., Chauhan, D.S., Tripathy, S.P., Gowda, H. and Prasad, T.S.K. (2019). Whole Genome Sequencing of *Mycobacterium tuberculosis* Clinical Isolates From India Reveals Genetic Heterogeneity and Region-Specific Variations That Might Affect Drug Susceptibility. *Frontiers in Microbiology*, [online] 10. doi:https://doi.org/10.3389/fmicb.2019.00309.

Ai, J.-W., Ruan, Q.-L., Liu, Q.-H. and Zhang, W.-H. (2016). Updates on the risk factors for latent tuberculosis reactivation and their managements. *Emerging Microbes & Infections*, 5(1), pp.1–8. doi:https://doi.org/10.1038/emi.2016.10.

Akkermans, R. (2014). Robert Heinrich Herman Koch. *The Lancet Respiratory Medicine*, 2(4), pp.264–265. doi:https://doi.org/10.1016/s2213-2600(14)70018-9.

Akusobi, C., Benghomari, B.S., Zhu, J., Wolf, I.D., Singhvi, S., Dulberger, C.L., Ioerger, T.R. and Rubin, E.J. (2022). Transposon mutagenesis in *Mycobacterium abscessus* identifies an essential penicillin-binding protein involved in septal peptidoglycan synthesis and antibiotic sensitivity. *eLife*, [online] 11, p.e71947. doi:https://doi.org/10.7554/eLife.71947.

Alexander, D.C., Jones, J.R.W. and Liu, J. (2003). A Rifampin-Hypersensitive Mutant Reveals Differences between Strains of *Mycobacterium smegmatis* and Presence of a Novel Transposon, IS *1623*. *Antimicrobial Agents and Chemotherapy*, 47(10), pp.3208–3213. doi:https://doi.org/10.1128/aac.47.10.3208-3213.2003.

Al-Jourani, O., Benedict, S.T., Ross, J., Layton, A.J., van der Peet, P., Marando, V.M., Bailey, N.P., Heunis, T., Manion, J., Mensitieri, F., Franklin, A., Abellon-Ruiz, J., Oram, S.L., Parsons, L., Cartmell, A., Wright, G.S.A.,

Baslé, A., Trost, M., Henrissat, B. and Munoz-Munoz, J. (2023). Identification of D-arabinan-degrading enzymes in mycobacteria. *Nature Communications*, [online] 14(1), p.2233. doi:https://doi.org/10.1038/s41467-023-37839-5.

Al-Orainey, I. (2009). Diagnosis of latent tuberculosis: Can we do better? *Annals of Thoracic Medicine*, 4(1), p.5. doi:https://doi.org/10.4103/1817-1737.44778.

Alaman-Zarate, M.G., Rady, B.J., Evans, C.A., Pian, B., Greetham, D., Marecos-Ortiz, S., Dickman, M.J., Ian DEA. Lidbury, Lovering, A.L., Barstow, B.M. and Stéphane Mesnage (2024). Unusual 1-3 peptidoglycan cross-links in *Acetobacteraceae* are made by L,D-transpeptidases with a catalytic domain distantly related to YkuD domains. *Journal of Biological Chemistry*, 300(1), pp.105494–105494. doi:https://doi.org/10.1016/j.jbc.2023.105494.

Alderwick, L., Harrison, J., Lloyd, G. and Birch, H., 2015. The *Mycobacterial* Cell Wall—Peptidoglycan and Arabinogalactan. *Cold Spring Harbor Perspectives in Medicine*, 5(8), p.a021113.

Alderwick, L.J., Dover, L.G., Veerapen, N., Gurcha, S.S., Kremer, L., Roper, D.L., Pathak, A.K., Reynolds, R.C. and Besra, G.S. (2008). Expression, purification and characterisation of soluble GlfT and the identification of a novel galactofuranosyltransferase Rv3782 involved in priming GlfT-mediated galactan polymerisation in *Mycobacterium tuberculosis*. *Protein Expression and Purification*, [online] 58(2), pp.332–341. doi:https://doi.org/10.1016/j.pep.2007.11.012.

Alderwick, L.J., Lloyd, G.S., Ghadbane, H., May, J.W., Bhatt, A., Eggeling, L., Fütterer, K. and Besra, G.S. (2011). The C-Terminal Domain of the Arabinosyltransferase *Mycobacterium tuberculosis* EmbC Is a Lectin-Like Carbohydrate Binding Module. *PLoS Pathogens*, 7(2), p.e1001299. doi:https://doi.org/10.1371/journal.ppat.1001299.

Alderwick, L.J., Radmacher, E., Seidel, M., Gande, R., Hitchen, P.G., Morris, H.R., Dell, A., Sahm, H., Eggeling, L. and Besra, G.S. (2005). Deletion of Cg-emb in Corynebacterianeae Leads to a Novel Truncated Cell Wall Arabinogalactan, whereas Inactivation of Cg-ubiA Results in an Arabinan-deficient Mutant with a Cell Wall Galactan Core. *Journal of Biological Chemistry*, 280(37), pp.32362–32371. doi:https://doi.org/10.1074/jbc.m506339200.

Alderwick, L.J., Seidel, M., Sahm, H., Besra, G.S. and Eggeling, L. (2006). Identification of a Novel Arabinofuranosyltransferase (AftA) Involved in Cell Wall Arabinan Biosynthesis in *Mycobacterium tuberculosis*. *Journal of Biological Chemistry*, 281(23), pp.15653–15661. doi:https://doi.org/10.1074/jbc.m600045200.

Aldridge, B.B., Fernandez-Suarez, M., Heller, D., Ambravaneswaran, V., Irimia, D., Toner, M. and Fortune, S. (2012). Asymmetry and aging of mycobacterial cells leads to variable growth and antibiotic susceptibility. *Science (New York, N.y.)*, [online] 335(6064), pp.100–104. doi:https://doi.org/10.1126/science.1216166.

Alexander, J.A.N., Chatterjee, S.S., Hamilton, S.M., Eltis, L.D., Chambers, H.F. and Strynadka, N.C.J. (2018). Structural and kinetic analyses of penicillin-binding protein 4 (PBP4)-mediated antibiotic resistance in *Staphylococcus aureus*. *Journal of Biological Chemistry*, 293(51), pp.19854–19865. doi:https://doi.org/10.1074/jbc.ra118.004952.

Aliashkevich, A. and Cava, F. (2021). LD-transpeptidases: the great unknown among the peptidoglycan cross-linkers. *The FEBS Journal*. doi:https://doi.org/10.1111/febs.16066.

Alicja Wysocka, Łukasz Łężniak, Elżbieta Jagielska and Izabela Sabała (2022). Electrostatic Interaction with the Bacterial Cell Envelope Tunes the Lytic Activity of Two Novel Peptidoglycan Hydrolases. *Microbiology spectrum*, 10(3). doi:https://doi.org/10.1128/spectrum.00455-22.

Allen, M., Bailey, C., Cahatol, I., Dodge, L., Yim, J., Kassissa, C., Luong, J., Kasko, S., Pandya, S. and Venketaraman, V. (2015). Mechanisms of Control of *Mycobacterium tuberculosis* by NK Cells: Role of Glutathione. *Frontiers in Immunology*, [online] 6, p.508. doi:https://doi.org/10.3389/fimmu.2015.00508.

Alsenani, T.A., Viviani, S.L., Papp-Wallace, K.M., Bonomo, R.A. and van (2023). Exploring avibactam and relebactam inhibition of *Klebsiella pneumoniae* carbapenemase D179N variant: role of the Ω loop-held deacylation water. *Antimicrobial Agents and Chemotherapy*, 67(10). doi:https://doi.org/10.1128/aac.00350-23.

Ambler, R.P (1980). The structure of β-lactamases (1980) *Philosophical Transactions of the Royal Society of London. B, Biological Sciences*, 289(1036), pp. 321–331. doi:10.1098/rstb.1980.0049.

Ambler, R.P., Coulson, A.F.W., Frère, J.M., Ghuysen, J.M., Joris, B., Forsman, M., Levesque, R.C., Tiraby, G. and Waley, S.G. (1991). A standard numbering scheme for the class A β-lactamases. *Biochemical Journal*, 276(1), pp.269–270. doi:https://doi.org/10.1042/bj2760269.

American Thoracic Society (2000). Diagnostic Standards and Classification of Tuberculosis in Adults and Children. *American Journal of Respiratory and Critical Care Medicine*, [online] 161(4), pp.1376–1395. doi:https://doi.org/10.1164/ajrccm.161.4.16141.

Anderson, J., Adediran, S., Charlier, P., Nguyen-Distèche, M., Frère, J., Nicholas, R., & Pratt, R. (2003). On the substrate specificity of bacterial DD-peptidases: evidence from two series of peptidoglycan-mimetic peptides. *The Biochemical journal*, 373 Pt 3, 949-55. https://doi.org/10.1042/BJ20030217.

André Zapun, Macheboeuf, P. and Vernet, T. (2017). Penicillin-Binding Proteins and β-Lactam Resistance. *Springer eBooks*, pp.177–211. doi:https://doi.org/10.1007/978-3-319-46718-4_13.

Aniefiok John Udoakang, Lindsey, A., Kesego Tapela, Nora Nghochuzie Nganyewo, Frances Ngozi Olisaka, Claudia Adzo Anyigba, Tawiah-Eshun, S., Irene Amoakoh Owusu, Paemka, L., Awandare, G.A. and Quashie, P.K. (2023). The COVID-19, tuberculosis and HIV/AIDS: Ménage à Trois. *Frontiers in Immunology*, 14. doi:https://doi.org/10.3389/fimmu.2023.1104828.

Ankrah, A. O., Glaudemans, A. W. J. M., Maes, A., Van de Wiele, C., Dierckx, R. A. J. O., Vorster, M., & Sathekge, M. M. (2018). Tuberculosis. *Seminars in Nuclear Medicine*, *48*(2), 108–130.

Antonets, K.S. and Nizhnikov, A.A. (2013). SARP: A Novel Algorithm to Assess Compositional Biases in Protein Sequences. *Evolutionary Bioinformatics*, 9, p.EBO.S12299. doi:https://doi.org/10.4137/ebo.s12299.

Antunes, N.T., Lamoureaux, T.L., Toth, M., Stewart, N.K., Frase, H. and Vakulenko, S.B. (2014). Class D β-Lactamases: Are They All Carbapenemases? *Antimicrobial Agents and Chemotherapy*, 58(4), pp.2119–2125. doi:https://doi.org/10.1128/aac.02522-13.

Arai, R., Fukui, S., Kobayashi, N. and Sekiguchi, J. (2012). Solution Structure of IseA, an Inhibitor Protein of DL-Endopeptidases from Bacillus subtilis, Reveals a Novel Fold with a Characteristic Inhibitory Loop. *Journal of biological chemistry/ The Journal of biological chemistry*, 287(53), pp.44736–44748. doi:https://doi.org/10.1074/jbc.m112.414763.

Arango Duque, G. and Descoteaux, A. (2014). Macrophage Cytokines: Involvement in Immunity and Infectious Diseases. *Frontiers in Immunology*, 5(491). doi:https://doi.org/10.3389/fimmu.2014.00491.
Armstrong, T., Fenn, S., & Hardie, K. (2021). Jmm profile: carbapenems: a broad-spectrum antibiotic. Journal of Medical Microbiology, 70(12). https://doi.org/10.1099/jmm.0.001462.

Armstrong, T., Fenn, S.J. and Hardie, K.R. (2021). JMM Profile: Carbapenems: a broad-spectrum antibiotic. *Journal of Medical Microbiology*, [online] 70(12). doi:https://doi.org/10.1099/jmm.0.001462.

Arora, D., Chawla, Y., Basanti Malakar, Singh, A. and Vinay Kumar Nandicoori (2018). The transpeptidase PbpA and noncanonical transglycosylase RodA of Mycobacterium tuberculosis play important roles in regulating bacterial cell lengths. *Journal of Biological Chemistry*, 293(17), pp.6497–6516. doi:https://doi.org/10.1074/jbc.m117.811190.

Arun Kumar Mishra, Alderwick, L.J., Rittmann, D., Raju, Jérôme Nigou, Gilleron, M., Eggeling, L. and Besra, G.S. (2007). Identification of an α(1→6) mannopyranosyltransferase (MptA), involved in *Corynebacterium glutamicum* lipomanann biosynthesis, and identification of its orthologue in *Mycobacterium*

tuberculosis. *Molecular Microbiology*, 65(6), pp.1503–1517. doi:https://doi.org/10.1111/j.1365-2958.2007.05884.x.

Arun Kumar Mishra, Alderwick, L.J., Rittmann, D., Wang, C., Bhatt, A., Jacobs, W.R., Takayama, K., Eggeling, L. and Besra, G.S. (2008). Identification of a novel α(1→6) mannopyranosyltransferase MptB from *Corynebacterium glutamicum* by deletion of a conserved gene, *NCgl1505*, affords a lipomannan- and lipoarabinomannan-deficient mutant. 68(6), pp.1595–1613. doi:https://doi.org/10.1111/j.1365-2958.2008.06265.x.

Asai, M., Konomi Haibara, Masayuki Muroi, Kazuhiko Kintaka and Kishi, T. (1981). Sulfazecin,a novel. BETA.-lactam antibiotic of bacterial origin. Isolation and chemical characterization. *The Journal of Antibiotics*, 34(6), pp.621–627. doi:https://doi.org/10.7164/antibiotics.34.621.

Ates, L.S., Houben, E.N.G. and Bitter, W. (2016). Type VII Secretion: A Highly Versatile Secretion System. *Microbiology Spectrum*, 4(1). doi:https://doi.org/10.1128/microbiolspec.vmbf-0011-2015.
Ausmees, N., Kuhn, J.R. and Jacobs-Wagner, C. (2003). The Bacterial Cytoskeleton. *Cell*, 115(6), pp.705–713. doi:https://doi.org/10.1016/s0092-8674(03)00935-8.

Babajan, B., Chaitanya, M., Rajsekhar, C., Gowsia, D., Madhusudhana, P., Naveen, M., Chitta, S.K. and Anuradha, C.M. (2011). Comprehensive structural and functional characterization of *Mycobacterium tuberculosis* UDP-NAG enolpyruvyl transferase (Mtb-MurA) and prediction of its accurate binding affinities with inhibitors. *Interdisciplinary Sciences: Computational Life Sciences*, 3(3), pp.204–216. doi:10.1007/s12539-011-0100-y.

Backus, K.M., Dolan, M.A., Barry, C.S., Joe, M., McPhie, P., Helena I.M. Boshoff, Lowary, T.L., Davis, B.G. and Barry, C.E. (2014). The Three *Mycobacterium tuberculosis* Antigen 85 Isoforms Have Unique Substrates and Activities Determined by Non-active Site Regions. 289(36), pp.25041–25053. doi:https://doi.org/10.1074/jbc.m114.581579.

Bahadur, R., Chodisetti, P.K. and Reddy, M. (2021). Cleavage of Braun's lipoprotein Lpp from the bacterial peptidoglycan by a paralog of l , D-transpeptidases, LdtF. *Proceedings of the National Academy of Sciences*, 118(19). doi:https://doi.org/10.1073/pnas.2101989118.

Ballister, E.R., Samanovic, M.I. and Darwin, K.H. (2019). *Mycobacterium tuberculosis* Rv2700 Contributes to Cell Envelope Integrity and Virulence. *Journal of Bacteriology*, 201(19). doi:https://doi.org/10.1128/jb.00228-19.

Banaei, N., Gaur, R.L. and Pai, M. (2016). Interferon Gamma Release Assays for Latent Tuberculosis: What Are the Sources of Variability? *Journal of Clinical Microbiology*, 54(4), pp.845–850. doi:https://doi.org/10.1128/jcm.02803-15.

Banks, E.J., Valdivia-Delgado, M., Biboy, J., Wilson, A., Cadby, I.T., Vollmer, W., Lambert, C., Lovering, A.L. and Sockett, R.E. (2022). Asymmetric peptidoglycan editing generates cell curvature in Bdellovibrio predatory bacteria. *Nature Communications*, 13(1). doi:https://doi.org/10.1038/s41467-022-29007-y.

Bansal-Mutalik, R. and Nikaido, H. (2014). Mycobacterial outer membrane is a lipid bilayer and the inner membrane is unusually rich in diacyl phosphatidylinositol dimannosides. *Proceedings of the National Academy of Sciences*, 111(13), pp.4958–4963. doi:https://doi.org/10.1073/pnas.1403078111.

Bansal, A., Kar, D., Murugan, R.A., Mallick, S., Dutta, M., Pandey, S.D., Chowdhury, C. and Ghosh, A.S. (2015). A putative low-molecular-mass penicillin-binding protein (PBP) of *Mycobacterium smegmatis* exhibits prominent physiological characteristics of DD-carboxypeptidase and beta-lactamase. *Microbiology*, 161(5), pp.1081–1091. doi:https://doi.org/10.1099/mic.0.000074.

Banzhaf, M., Yau, H.C., Verheul, J., Lodge, A., Kritikos, G., Mateus, A., Cordier, B., Hov, A.K., Stein, F., Wartel, M., Pazos, M., Solovyova, A.S., Breukink, E., van Teeffelen, S., Savitski, M.M., den Blaauwen, T., Typas, A. and Vollmer, W. (2020). Outer membrane lipoprotein NlpI scaffolds peptidoglycan hydrolases within multi-enzyme complexes in*Escherichia coli*. *The EMBO Journal*, 39(5). doi:https://doi.org/10.15252/embj.2019102246.

Baquero, M.R., Bouzon, M., Quintela, J.C., Ayala, J.A. and Moreno, F. (1996). dacD, an *Escherichia coli* gene encoding a novel penicillin-binding protein (PBP6b) with DD-carboxypeptidase activity. *Journal of Bacteriology*, [online] 178(24), pp.7106–7111. doi:https://doi.org/10.1128/jb.178.24.7106-7111.1996.

Baranowski, C., Rego, E.H. and Rubin, E.J. (2019). The Dream of a *Mycobacterium*. *Microbiology Spectrum*, 7(2). doi:https://doi.org/10.1128/microbiolspec.gpp3-0008-2018.

Baranowski, C., Welsh, M.A., Sham, L.-T., Eskandarian, H.A., Lim, H.C., Kieser, K.J., Wagner, J.C., McKinney, J.D., Fantner, G.E., Ioerger, T.R., Walker, S., Bernhardt, T.G., Rubin, E.J. and Rego, E.H. (2018). Maturing Mycobacterium smegmatis peptidoglycan requires non-canonical crosslinks to maintain shape. *eLife*, 7. doi:https://doi.org/10.7554/elife.37516.

Barbero, N., Barolo, C. and Viscardi, G. (2016). Bovine Serum Albumin Bioconjugation with FITC. *World journal of chemical education*, 4(4), pp.80–85. doi:https://doi.org/10.12691/wjce-4-4-3.

Bardarov, S., Kriakov, J., Carriere, C., Yu, S., Vaamonde, C., McAdam, R.A., Bloom, B.R., Hatfull, G.F. and Jacobs, W.R. (1997). Conditionally replicating mycobacteriophages: A system for transposon delivery to Mycobacterium tuberculosis. *Proceedings of the National Academy of Sciences*, 94(20), pp.10961–10966. doi:https://doi.org/10.1073/pnas.94.20.10961.

Barie, P.S., Narayan, M., Aquino, V.M. and Shapiro, M.J. (2024). Antibiotic use in the intensive care unit: The old and the new. *Elsevier eBooks*, pp.803-814.e1. doi:https://doi.org/10.1016/b978-0-323-69787-3.00130-1.

Barkan, D., Rao, V., Sukenick, G.D. and Glickman, M.S. (2010). Redundant Function of *cmaA2* and *mmaA2* in *Mycobacterium tuberculosis cis* Cyclopropanation of Oxygenated Mycolates. *Journal of Bacteriology*, 192(14), pp.3661–3668. doi:https://doi.org/10.1128/jb.00312-10.

Barna, J.C.J. and Williams, D.H. (1984). The Structure and Mode of Action of Glycopeptide Antibiotics of the Vancomycin Group. *Annual Review of Microbiology*, 38(1), pp.339–357. doi:10.1146/annurev.mi.38.100184.002011.

Barry, C. E., Crick, D. C., and McNeil, M. R. (2007). Targeting the Formation of the Cell Wall Core of M. tuberculosis. *Infectious Disorders - Drug Targets*, 7(2), pp.182–202. doi:https://doi.org/10.2174/187152607781001808.

Bassetti, M., Daniele Roberto Giacobbe, Castaldo, N., Russo, A. and Vena, A. (2021). Role of new antibiotics in extended-spectrum β-lactamase-, AmpC- infections. *Current Opinion in Infectious Diseases*, 34(6), pp.748–755. doi:https://doi.org/10.1097/qco.0000000000000789.

Bastian, I., L Rigouts, A Van Deun and F Portaels (2000). Directly observed treatment, short-course strategy and multidrug-resistant tuberculosis: are any modifications required? *PubMed*, 78(2), pp.238–51.

Batchelder, H.R., Story-Roller, E., Lloyd, E.P., Kaushik, A., Bigelow, K.M., Maggioncalda, E.C., Nuermberger, E.L., Gyanu Lamichhane and Townsend, C.A. (2020). Development of a penem antibiotic against *Mycobacteroides abscessus*. *Communications biology*, 3(1). doi:https://doi.org/10.1038/s42003-020-01475-2.

Batchelder, H.R., Zandi, T.A., Kaushik, A., Naik, A., Story-Roller, E., Maggioncalda, E.C., Gyanu Lamichhane, Nuermberger, E.L. and Townsend, C.A. (2022). Structure–Activity Relationship of Penem Antibiotic Side Chains Used against *Mycobacteria* Reveals Highly Active Compounds. *ACS Infectious Diseases*, 8(8), pp.1627–1636. doi:https://doi.org/10.1021/acsinfecdis.2c00229.

Batt, S., Burke, C., Moorey, A. and Besra, G., 2020. Antibiotics and resistance: the two-sided coin of the mycobacterial cell wall. *The Cell Surface*, 6, p.100044.

Bayot, M.L. and Sharma, S. (2018). *Acid Fast Bacteria*. [online] Nih.gov. Available at: https://www.ncbi.nlm.nih.gov/books/NBK537121/.

Beatriz, C., Juán Manuel Belardinelli, Hugo Adrián Carignano, Buchieri, M.V., Cristian Alejandro Suárez and Héctor Ricardo Morbidoni (2022). Unveiling the Biosynthetic Pathway for Short Mycolic Acids in Nontuberculous Mycobacteria: *Mycobacterium smegmatis* MSMEG_4301 and Its Ortholog *Mycobacterium abscessus* MAB_1915 Are Essential for the Synthesis of α′-Mycolic Acids. *Microbiology spectrum*, 10(4). doi:https://doi.org/10.1128/spectrum.01288-22.

Beauregard, A., Curcio, M.J. and Belfort, M. (2008). The take and give between retrotransposable elements and their hosts. *Annual review of genetics*, [online] 42, pp.587–617. doi:https://doi.org/10.1146/annurev.genet.42.110807.091549.

Becker, K. and Sander, P. (2016). *Mycobacterium tuberculosis* lipoproteins in virulence and immunity - fighting with a double-edged sword. *FEBS Letters*, 590(21), pp.3800–3819. doi:https://doi.org/10.1002/1873-3468.12273.

Behr, M.A., Edelstein, P.H. and Ramakrishnan, L. (2018). Revisiting the timetable of tuberculosis. *BMJ*, [online] 362, p.k2738. doi:https://doi.org/10.1136/bmj.k2738.

Behr, M.A., K Stevenson and V Kapur (2020). *Paratuberculosis: organism, disease, control.* Wallingford, UK Cabi.

Beláňová, M., Petronela Dianišková, Brennan, P.J., Completo, G.C., Rose, N.L., Lowary, T.L. and Katarína Mikušová (2008). Galactosyl Transferases in Mycobacterial Cell Wall Synthesis. *Journal of Bacteriology*, 190(3), pp.1141–1145. doi:https://doi.org/10.1128/jb.01326-07.

Belete, T.M. (2022). Recent Progress in the Development of Novel Mycobacterium Cell Wall Inhibitor to Combat Drug-Resistant Tuberculosis. *Microbiology Insights*, 15, p.117863612210998. doi:https://doi.org/10.1177/11786361221099878.

Bellamy, W.D. and Klimek, J.W. (1948). Some Properties of Penicillin-resistant Staphylococci. *Journal of Bacteriology*, 55(2), pp.153–160. doi:10.1128/jb.55.2.153-160.1948.

Bernadsky, G., Beveridge, T.J. and Clarke, A.J. (1994). Analysis of the sodium dodecyl sulfate-stable peptidoglycan autolysins of select gram-negative pathogens by using renaturing polyacrylamide gel electrophoresis. *Journal of Bacteriology*, 176(17), pp.5225–5232. doi:https://doi.org/10.1128/jb.176.17.5225-5232.1994.

Bespiatykh, D., Bespyatykh, J., Mokrousov, I. and Shitikov, E. (2021). A Comprehensive Map of *Mycobacterium tuberculosis* Complex Regions of Difference. *mSphere*, 6(4). doi:10.1128/msphere.00535-21.

Besra, G. S., Khoo, K. H., McNeil, M. R., Dell, A., Morris, H.R., & Brennan, P. J. (1995). A new interpretation of the structure of the mycolyl-arabinogalactan complex of *Mycobacterium tuberculosis* as revealed through characterization of oligoglycosylalditol fragments by fast-atom bombardment mass spectrometry and 1H nuclear magnetic resonance spectroscopy. *Biochemistry*, 34: 4257–4266.

Betts, J.C., Lukey, P.T., Robb, L.C., McAdam, R.A. and Duncan, K. (2002). Evaluation of a nutrient starvation model of *Mycobacterium tuberculosis* persistence by gene and protein expression profiling. *Molecular Microbiology*, 43(3), pp.717–731. doi:https://doi.org/10.1046/j.1365-2958.2002.02779.x.

Bhamidi, S., Scherman, M. S., Rithner, C. D., Prenni, J. E., Chatterjee, D., Khoo, K. H., and McNeil, M. R. (2008). The identification and location of succinyl residues and the characterization of the interior arabinan region allow for a model of the complete primary structure of *Mycobacterium tuberculosis* mycolyl arabinogalactan. Journal of Biological Chemistry, 283, 12992–13000.

Bhamidi, S., Scherman, M.S., Rithner, C.D., Prenni, J.E., Chatterjee, D., Khoo, K.-H. and McNeil, M.R. (2008). The Identification and Location of Succinyl Residues and the Characterization of the Interior Arabinan Region Allow for a Model of the Complete Primary Structure of *Mycobacterium tuberculosis* Mycolyl Arabinogalactan. *Journal of Biological Chemistry*, 283(19), pp.12992–13000. doi:https://doi.org/10.1074/jbc.m800222200.

Bhat, Z.S., Rather, M.A., Maqbool, M. and Ahmad, Z. (2018). Drug targets exploited in Mycobacterium tuberculosis: Pitfalls and promises on the horizon. *Biomedicine & Pharmacotherapy*, [online] 103, pp.1733–1747. doi:10.1016/j.biopha.2018.04.176.

Bhatnagar, A., Ransom, E.M., Machado, M.-J., Boyd, S., Reese, N., Anderson, K., Lonsway, D., Elkins, C.A., Rasheed, J.K., Patel, J.B., Karlsson, M., Brown, A.C. and Lutgring, J.D. (2020). Assessing the *in vitro* impact of ceftazidime on aztreonam/avibactam susceptibility testing for highly resistant MBL-producing Enterobacterales. *Journal of Antimicrobial Chemotherapy*, [online] 76(4), pp.979–983. doi:https://doi.org/10.1093/jac/dkaa531.

Bhatt, A., Brown, A.K., Singh, A., Minnikin, D.E. and Besra, G.S. (2008). Loss of a mycobacterial gene encoding a reductase leads to an altered cell wall containing beta-oxo-mycolic acid analogs and accumulation of ketones. *Chemistry & Biology*, [online] 15(9), pp.930–939. doi:https://doi.org/10.1016/j.chembiol.2008.07.007.

Bhatt, A., Molle, V., Besra, G.S., Jacobs, W.R. and Kremer, L. (2007). The *Mycobacterium tuberculosis* FAS-II condensing enzymes: their role in mycolic acid biosynthesis, acid-fastness, pathogenesis and in future drug development. *Molecular Microbiology*, 64(6), pp.1442–1454. doi:https://doi.org/10.1111/j.1365-2958.2007.05761.x.

Bhattacharje, G., Ghosh, A. and Das, A.K. (2022). Understanding the Mannose Transfer Mechanism of Mycobacterial Phosphatidyl-myo-inositol Mannosyltransferase A from Molecular Dynamics Simulations. *ACS Omega*, 7(23), pp.19288–19304. doi:https://doi.org/10.1021/acsomega.2c00832.

Bianchet, M.A., Pan, Y.H., Basta, L.A.B., Saavedra, H., Lloyd, E.P., Kumar, P., Mattoo, R., Townsend, C.A. and Lamichhane, G. (2017). Structural insight into the inactivation of *Mycobacterium tuberculosis* non-classical transpeptidase LdtMt2 by biapenem and tebipenem. *BMC Biochemistry*, 18(1). doi:10.1186/s12858-017-0082-4.

Biarrotte-Sorin, S., Hugonnet, J.-E., Delfosse, V., Mainardi, J.-L., Gutmann, L., Arthur, M. and Mayer, C. (2006). Crystal Structure of a Novel β-Lactam-insensitive Peptidoglycan Transpeptidase. *Journal of Molecular Biology*, 359(3), pp.533–538. doi:10.1016/j.jmb.2006.03.014.

BioRender. 2022. *BioRender*. [online] Available at: <https://biorender.com> [Accessed 11 May 2022].

Birch, H.L., Alderwick, L.J., Bhatt, A., Rittmann, D., Krumbach, K., Singh, A., Bai, Y., Lowary, T.L., Eggeling, L. and Besra, G.S. (2008). Biosynthesis of mycobacterial arabinogalactan: identification of a novel α(1→3) arabinofuranosyltransferase. *Molecular Microbiology*. doi:https://doi.org/10.1111/j.1365-2958.2008.06354.x.

Birhanu, A.G., Yimer, S.A., Kalayou, S., Riaz, T., Zegeye, E.D., Holm-Hansen, C., Norheim, G., Aseffa, A., Abebe, M. and Tønjum, T. (2019). Ample glycosylation in membrane and cell envelope proteins may explain the phenotypic diversity and virulence in the Mycobacterium tuberculosis complex. *Scientific Reports*, 9(1). doi:10.1038/s41598-019-39654-9.

Bjerrum, S., Schiller, I., Dendukuri, N., Kohli, M., Nathavitharana, R.R., Zwerling, A.A., Denkinger, C.M., Steingart, K.R. and Shah, M. (2019). Lateral flow urine lipoarabinomannan assay for detecting active tuberculosis in people living with HIV. *Cochrane Database of Systematic Reviews*, 2019(10). doi:https://doi.org/10.1002/14651858.cd011420.pub3.

Black, Gillian F., Dockrell, Hazel M., Crampin, Amelia C., Floyd, S., Weir, Rosemary E., Bliss, L., Sichali, L., Mwaungulu, L., Kanyongoloka, H., Ngwira, B., Warndorff, David K. and Fine, Paul E. M. (2001). Patterns and Implications of Naturally Acquired Immune Responses to Environmental and Tuberculous Mycobacterial Antigens in Northern Malawi. *The Journal of Infectious Diseases*, 184(3), pp.322–329. doi:https://doi.org/10.1086/322042.

Blackswan, O., Medcalf, A., Altink, H., Saavedra, M., Bhattacharya, S., Breve, U. and Tuberculose, H. (2013). *Tuberculosis Tuberculosis A Short History A Short History*. [online] Available at: https://www.york.ac.uk/media/c2d2/media/TB-A%20Short%20History.pdf [Accessed 10 Oct. 2023].

Blackwell, G., Iqbal, Z. and Thomson, N. (2019). Evolution and spread of bacterial transposons. *Access Microbiology*, 1(1A). doi:https://doi.org/10.1099/acmi.ac2019.po0568.

Blanco, N. and Bigi, F. (2023). Deciphering the polycistronic nature of *Mycobacterium tuberculosis* lipoproteins of unknown functions. *bioRxiv (Cold Spring Harbor Laboratory)*. doi:https://doi.org/10.1101/2023.07.16.549196.

Blumberg, P.M. and Strominger, J.L. (1974). Interaction of penicillin with the bacterial cell: penicillin-binding proteins and penicillin-sensitive enzymes. *Bacteriological Reviews*, 38(3), pp.291–335. doi:https://doi.org/10.1128/br.38.3.291-335.1974.

Boelter, G., Bryant, J.A., Doherty, H., Wotherspoon, P., Alodaini, D., Ma, X., Alao, M.B., Moynihan, P.J., Moradigaravand, D., Glinkowska, M., Knowles, T.J., Henderson, I.R. and Banzhaf, M. (2022). The lipoprotein DolP affects cell separation in Escherichia coli, but not as an upstream regulator of NlpD. *Microbiology*, 168(5). doi:https://doi.org/10.1099/mic.0.001197.

Boldrin, F., Ventura, M., Degiacomi, G., Ravishankar, S., Sala, C., Svetlikova, Z., Ambady, A., Dhar, N., Kordulakova, J., Zhang, M., Serafini, A., Vishwas, K.G., Kolly, G.S., Kumar, N., Palù, G., Guerin, M.E., Mikusova, K., Cole, S.T. and Manganelli, R. (2014). The phosphatidyl-myo-inositol mannosyltransferase PimA is essential for Mycobacterium tuberculosis growth in vitro and in vivo. *Journal of bacteriology*, [online] 196(19), pp.3441–51. doi:https://doi.org/10.1128/JB.01346-13.

Bolla, J.R., Sauer, J.B., Wu, D., Mehmood, S., Allison, T.M. and Robinson, C.V. (2018). Direct observation of the influence of cardiolipin and antibiotics on lipid II binding to MurJ. *Nature Chemistry*, 10(3), pp.363–371. doi:10.1038/nchem.2919.

Boneca, I.G., Dussurget, O., Cabanes, D., Nahori, M.-A., Sousa, S., Lecuit, M., Psylinakis, E., Bouriotis, V., Hugot, J.-P., Giovannini, M., Coyle, A., Bertin, J., Namane, A., Rousselle, J.-C., Cayet, N., Prévost, M.-C., Balloy, V., Chignard, M., Philpott, D.J. and Cossart, P. (2007). A critical role for peptidoglycan N-deacetylation inListeriaevasion from the host innate immune system. *Proceedings of the National Academy of Sciences*, 104(3), pp.997–1002. doi:https://doi.org/10.1073/pnas.0609672104.

Borah, K., Mendum, T.A., Hawkins, N.D., Ward, J.L., Beale, M.H., Larrouy-Maumus, G., Bhatt, A., Moulin, M., Haertlein, M., Strohmeier, G., Pichler, H., Forsyth, V.T., Noack, S., Goulding, C.W., McFadden, J. and Beste, D.J.V. (2021). Metabolic fluxes for nutritional flexibility of *Mycobacterium tuberculosis*. *Molecular Systems Biology*, 17(5). doi:https://doi.org/10.15252/msb.202110280.

Borgers, K., Vandewalle, K., Festjens, N. and Callewaert, N. (2019). A guide to *Mycobacterium* mutagenesis. *The FEBS Journal*, 286(19), pp.3757–3774. doi:https://doi.org/10.1111/febs.15041.

Borgers, K., Vandewalle, K., Van Hecke, A., Michielsen, G., Plets, E., van Schie, L., Vanmarcke, S., Schindfessel, L., Festjens, N. and Callewaert, N. (2020). Development of a Counter selectable Transposon To Create Markerless Knockouts from an 18,432-Clone Ordered *Mycobacterium bovis* Bacillus Calmette-Guérin Mutant Resource. *mSystems*, 5(4). doi:https://doi.org/10.1128/msystems.00180-20.

Bosch, B., DeJesus, M.A., Poulton, N.C., Zhang, W., Engelhart, C.A., Zaveri, A., Lavalette, S., Ruecker, N., Trujillo, C., Wallach, J.B., Li, S., Ehrt, S., Chait, B.T., Schnappinger, D. and Rock, J.M. (2021). Genome-wide gene expression tuning reveals diverse vulnerabilities of *M. tuberculosis*. *Cell*, 184(17), pp.4579-4592.e24. doi:https://doi.org/10.1016/j.cell.2021.06.033.

Botella, H., Vaubourgeix, J., Lee, M.H., Song, N., Xu, W., Makinoshima, H., Glickman, M.S. and Ehrt, S. (2017). *Mycobacterium tuberculosis* protease MarP activates a peptidoglycan hydrolase during acid stress. *The EMBO Journal*, 36(4), pp.536–548. doi:https://doi.org/10.15252/embj.201695028.

Botella, H., Yang, G., Ouerfelli, O., Ehrt, S., Nathan, C.F. and Vaubourgeix, J. (2017). Distinct Spatiotemporal Dynamics of Peptidoglycan Synthesis between *Mycobacterium smegmatis* and *Mycobacterium tuberculosis*. *mBio*, 8(5). doi:https://doi.org/10.1128/mbio.01183-17.

Böth, D., Schneider, G. and Schnell, R. (2011). Peptidoglycan Remodeling in *Mycobacterium tuberculosis*: Comparison of Structures and Catalytic Activities of RipA and RipB. *Journal of Molecular Biology*, 413(1), pp.247–260. doi:https://doi.org/10.1016/j.jmb.2011.08.014.

Bouhss, A., Trunkfield, A.E., Bugg, T.D.H. and Mengin-Lecreulx, D. (2008). The biosynthesis of peptidoglycan lipid-linked intermediates. *FEMS Microbiology Reviews*, 32(2), pp.208–233. doi:10.1111/j.1574-6976.2007.00089.x.

Boutte, C.C., Baer, C.E., Papavinasasundaram, K., Liu, W., Chase, M.R., Meniche, X., Fortune, S.M., Sassetti, C.M., Ioerger, T.R. and Rubin, E.J. (2016). A cytoplasmic peptidoglycan amidase homologue controls mycobacterial cell wall synthesis. *eLife*, 5. doi:10.7554/elife.14590.

Boyd, S.E., Holmes, A., Peck, R., Livermore, D.M. and Hope, W.W. (2022). OXA-48-Like β-Lactamases: Global Epidemiology, Treatment Options, and Development Pipeline. 66(8). doi:https://doi.org/10.1128/aac.00216-22.

Brennan, P.J. (2003). Structure, function, and biogenesis of the cell wall of Mycobacterium tuberculosis. *Tuberculosis*, 83(1-3), pp.91–97. doi:https://doi.org/10.1016/s1472-9792(02)00089-6.
Brennan, P.J. and Nikaido, H. (1995). The Envelope of *Mycobacteria*. *Annual Review of Biochemistry*, 64(1), pp.29–63. doi:10.1146/annurev.bi.64.070195.000333.

Brites, D., Loiseau, C., Menardo, F., Borrell, S., Boniotti, M.B., Warren, R., Dippenaar, A., Parsons, S.D.C., Beisel, C., Behr, M.A., Fyfe, J.A., Coscolla, M. and Gagneux, S. (2018). A New Phylogenetic Framework for the Animal-Adapted *Mycobacterium tuberculosis* Complex. *Frontiers in Microbiology*, 9. doi:https://doi.org/10.3389/fmicb.2018.02820.

Brodin, P., Poquet, Y., Levillain, F., Peguillet, I., Larrouy-Maumus, G., Gilleron, M., Ewann, F., Christophe, T., Fenistein, D., Jang, J., Jang, M.-S., Park, S.-J., Rauzier, J., Carralot, J.-P., Shrimpton, R., Genovesio, A., Gonzalo-Asensio, J.A., Puzo, G., Martin, C. and Brosch, R. (2010). High content phenotypic cell-based visual screen identifies *Mycobacterium tuberculosis* acyltrehalose-containing glycolipids involved in phagosome remodeling. *PLoS pathogens*, [online] 6(9), p.e1001100. doi:https://doi.org/10.1371/journal.ppat.1001100.

Bruning, J.B., Murillo, A.C., Chacon, O., Barletta, R.G. and Sacchettini, J.C. (2011). Structure of the *Mycobacterium tuberculosis* d -Alanine: d -Alanine Ligase, a Target of the Antituberculosis Drug d -Cycloserine. *Antimicrobial Agents and Chemotherapy*, 55(1), pp.291–301. doi:10.1128/aac.00558-10.

Buddle, J.E., Thompson, L.M., Williams, A.S., Wright, R.C.T., Durham, W.M., Turner, C.E., Chaudhuri, R.R., Brockhurst, M.A. and Fagan, R.P. (2024). Identification of pathways to high-level vancomycin resistance in *Clostridioides difficile* that incur high fitness costs in key pathogenicity traits. *PLoS Biology*, 22(8), pp.e3002741–e3002741. doi:https://doi.org/10.1371/journal.pbio.3002741.

Bui, T. and Preuss, C.V. (2023). *Cephalosporins*. [online] PubMed. Available at: https://www.ncbi.nlm.nih.gov/books/NBK551517/.

Bullock, T.L., Clarkson, D.W., Kent, H.M. and Stewart, M. (1996). The 1.6 Å Resolution Crystal Structure of Nuclear Transport Factor 2 (NTF2). *Journal of Molecular Biology*, 260(3), pp.422–431. doi:https://doi.org/10.1006/jmbi.1996.0411.

Bush, K. (2017). Game Changers: New β-Lactamase Inhibitor Combinations Targeting Antibiotic Resistance in Gram-Negative Bacteria. *ACS Infectious Diseases*, 4(2), pp.84–87. doi:https://doi.org/10.1021/acsinfecdis.7b00243.

Bush, K. (2018). Past and Present Perspectives on β-Lactamases. *Antimicrobial Agents and Chemotherapy*, 62(10). doi:https://doi.org/10.1128/aac.01076-18.

Bush, K. & Jacoby, G.A. (2010) Updated functional classification of β-lactamases. *Antimicrobial Agents and Chemotherapy*, 54 (3): 969–976. doi:10.1128/aac.01009-09.

Bush, K. and Bradford, P.A. (2016). β-Lactams and β-Lactamase Inhibitors: An Overview. *Cold Spring Harbor Perspectives in Medicine*, [online] 6(8), p.a025247. doi:https://doi.org/10.1101/cshperspect.a025247.

Butler, E.K., Davis, R.M., Bari, V., Nicholson, P.A. and Ruiz, N. (2013). Structure-Function Analysis of MurJ Reveals a Solvent-Exposed Cavity Containing Residues Essential for Peptidoglycan Biogenesis in *Escherichia coli*. *Journal of Bacteriology*, 195(20), pp.4639–4649. doi:10.1128/jb.00731-13.

Cagliero, J., Frédérique Vernel-Pauillac, Murray, G.L., Adler, B., Matsui, M. and Werts, C. (2022). Pathogenic Leptospires Limit Dendritic Cell Activation Through Avoidance of TLR4 and TRIF Signaling. *Frontiers in Immunology*, 13. doi:https://doi.org/10.3389/fimmu.2022.911778.

Callewaert, L. and Michiels, C.W. (2010). Lysozymes in the animal kingdom. *Journal of Biosciences*, [online] 35(1), pp.127–160. doi:https://doi.org/10.1007/s12038-010-0015-5.

Calvet-Seral, J., Estefanía Crespo-Yuste, Mathys, V., Rodriguez-Villalobos, H., Pieter-Jan Ceyssens, Martin, A. and Jesús Gonzalo-Asensio (2023). Targeted Chromosomal Barcoding Establishes Direct Genotype-Phenotype Associations for Antibiotic Resistance in *Mycobacterium abscessus*. doi:https://doi.org/10.1128/spectrum.05344-22.

Camiade, E., Peltier, J., Bourgeois, I., Couture-Tosi, E., Courtin, P., Antunes, A., Chapot-Chartier, M.P., Dupuy, B. and Pons, J.L. (2010). Characterization of Acp, a Peptidoglycan Hydrolase of *Clostridium perfringens* with N-Acetylglucosaminidase Activity That Is Implicated in Cell Separation and Stress-Induced Autolysis. *Journal of Bacteriology*, 192(9), pp.2373–2384. doi:https://doi.org/10.1128/jb.01546-09.

Campelo, T.A., Cardoso de Sousa, P.R., Nogueira, L. de L., Frota, C.C. and Zuquim Antas, P.R. (2021). Revisiting the methods for detecting Mycobacterium tuberculosis: what has the new millennium brought thus far? *Access Microbiology*, [online] 3(7), p.000245. doi:https://doi.org/10.1099/acmi.0.000245.

Cantaloube, S., Veyron-Churlet, R., Haddache, N., Daffé, M. and Zerbib, D. (2011). The *Mycobacterium Tuberculosis* FAS-II Dehydratases and Methyltransferases Define the Specificity of the Mycolic Acid Elongation Complexes. *PLoS ONE*, 6(12), p.e29564. doi:https://doi.org/10.1371/journal.pone.0029564.

Carranza, C. and Chavez-Galan, L. (2019). Several Routes to the Same Destination: Inhibition of Phagosome-Lysosome Fusion by *Mycobacterium tuberculosis*. *The American Journal of the Medical Sciences*, 357(3), pp.184–194. doi:https://doi.org/10.1016/j.amjms.2018.12.003.

Carranza, C., Pedraza-Sanchez, S., de Oyarzabal-Mendez, E. and Torres, M. (2020). Diagnosis for Latent Tuberculosis Infection: New Alternatives. *Frontiers in Immunology*, [online] 11. doi:https://doi.org/10.3389/fimmu.2020.02006.

Casas-Finet, J.R., Jean-Jacques Toulmé, Santus, R. and Maki, A.H. (1988). A maximum of two tryptophan residues in gene-32 protein from phage T4 undergo stacking interactions with single-stranded polynucleotides. *European journal of biochemistry*, 172(3), pp.641–646. doi:https://doi.org/10.1111/j.1432-1033.1988.tb13937.x.

Castanheira, S. and Francisco García-del Portillo (2023). Evidence of two differentially regulated elongasomes in Salmonella. *PubMed*, 6(1). doi:https://doi.org/10.1038/s42003-023-05308-w.

Catalão, M.J., Filipe, S.R., Filipe, S.R. and Pimentel, M. (2019). Revisiting Anti-tuberculosis Therapeutic Strategies That Target the Peptidoglycan Structure and Synthesis. *Frontiers in Microbiology*, [online] 10. doi:10.3389/fmicb.2019.00190.

Catherwood, A.C., Lloyd, A.J., Tod, J.A., Chauhan, S., Slade, S.E., Walkowiak, G.P., Galley, N.F., Punekar, A.S., Smart, K., Rea, D., Evans, N.D., Chappell, M.J., Roper, D.I. and Dowson, C.G. (2020). Substrate and Stereochemical Control of Peptidoglycan Cross-Linking by Transpeptidation by *Escherichia coli* PBP1B. *Journal of the American Chemical Society*, 142(11), pp.5034–5048. doi:https://doi.org/10.1021/jacs.9b08822.

Caulfield, A.J. and Wengenack, N.L. (2016). Diagnosis of active tuberculosis disease: From microscopy to molecular techniques. *Journal of Clinical Tuberculosis and Other Mycobacterial Diseases*, 4, pp.33–43. doi:https://doi.org/10.1016/j.jctube.2016.05.005.

Caveney, N.A., Caballero, G., Voedts, H., Niciforovic, A., Worrall, L.J., Vuckovic, M., Fonvielle, M., Hugonnet, J.-E., Arthur, M. and Strynadka, N.C.J. (2019). Structural insight into YcbB-mediated beta-lactam resistance in Escherichia coli. *Nature Communications*, [online] 10(1). doi:https://doi.org/10.1038/s41467-019-09507-0.

CDC (2019). *History | World TB Day | TB | CDC*. [online] www.cdc.gov. Available at:https://www.cdc.gov/tb/worldtbday/history.htm#:~:text=TB%20in%20humans%20can%20be.

CDC MPEP MTBC DST Report for August 2018 Survey *Mycobacterium tuberculosis* Complex Drug Susceptibility Testing Program Model Performance Evaluation Program Report of Results. (2018). Available at: https://www.cdc.gov/tb/topic/laboratory/mpep/pdf/MPEP_August_2018.pdf [Accessed 11 Feb. 2024].

Champion ™ pET SUMO Protein Expression System For high-level expression and enhanced solubility of recombinant proteins in *E. coli* and cleavage of native protein. (2010). Available at: https://tools.thermofisher.com/content/sfs/manuals/petsumo_man.pdf [Accessed 2 May 2024].

Chatterjee, D. and Khoo, K.-H. (1998). Mycobacterial lipoarabinomannan: An extraordinary lipoheteroglycan with profound physiological effects. *Glycobiology*, 8(2), pp.113–120. doi:10.1093/glycob/8.2.113.

Chemdraw., Professional., 2021., Version 20.1.0.112., Perkin Elmer.

Chen, F., Liu, W., Li, H., Deng, T., Xing, B. and Liu, F. (2022). Rhodamine Fluorophores for STED Super-Resolution Biological Imaging. 2(3). doi:https://doi.org/10.1002/anse.202100066.

Chen, J. (2010). *Identifying Biosynthetic Pathways for Mycobacterial Cell Wall Components Using Transposon Mutagenesis*. Thesis. pp.1–186.

Chen, J. (2010). *Identifying Biosynthetic Pathways for Mycobacterial Cell Wall Components Using Transposon Mutagenesis*. Thesis. pp.1–186.

Chen, J., Kriakov, J., Singh, A., Jacobs, W.R., Besra, G.S. and Bhatt, A. (2009). Defects in glycopeptidolipid biosynthesis confer phage I3 resistance in *Mycobacterium smegmatis*. *Microbiology*, 155(12), pp.4050–4057. doi:https://doi.org/10.1099/mic.0.033209-0.

Chen, J., Zhang, S., Cui, P., Shi, W., Zhang, W. and Zhang, Y. (2017). Identification of novel mutations associated with cycloserine resistance in *Mycobacterium tuberculosis*. *Journal of Antimicrobial Chemotherapy*, 72(12), pp.3272–3276. doi:10.1093/jac/dkx316.

Chen, J., Zhang, S., Cui, P., Shi, W., Zhang, W. and Zhang, Y. (2017). Identification of novel mutations associated with cycloserine resistance in *Mycobacterium tuberculosis*. *Journal of Antimicrobial Chemotherapy*, 72(12), pp.3272–3276. doi:https://doi.org/10.1093/jac/dkx316.

Chen, K.-T., Chen, P.-T., Lin, C.-K., Huang, L.-Y., Hu, C.-M., Chang, Y.-F., Hsu, H.-T., Cheng, T.-J.R., Wu, Y.-T. and Cheng, W.-C. (2016). Structural Investigation of Park's Nucleotide on Bacterial Translocase MraY: Discovery of Unexpected MraY Inhibitors. *Scientific Reports*, 6(1). doi:10.1038/srep31579.

Chen, Y. & Bonnet, R. & Shoichet, B.K. (2007) The acylation mechanism of CTX-m β-lactamase at 0.88 Å Resolution. *Journal of the American Chemical Society*, 129 (17): 5378–5380. doi:10.1021/ja0712064.

Chiaradia, L., Lefebvre, C., Parra, J., Marcoux, J., Burlet-Schiltz, O., Etienne, G., Tropis, M. and Daffé, M. (2017). Dissecting the mycobacterial cell envelope and defining the composition of the native mycomembrane. *Scientific Reports*, [online] 7(1), pp.1–12. doi:https://doi.org/10.1038/s41598-017-12718-4.

Chim, N., Iniguez, A., Nguyen, T.Q. and Goulding, C.W. (2010). Unusual Diheme Conformation of the Heme-Degrading Protein from *Mycobacterium tuberculosis*. *Journal of Molecular Biology*, 395(3), pp.595–608. doi:https://doi.org/10.1016/j.jmb.2009.11.025.

Cho, H., Uehara, T. and Bernhardt, Thomas G. (2014). Beta-Lactam Antibiotics Induce a Lethal Malfunctioning of the Bacterial Cell Wall Synthesis Machinery. *Cell*, [online] 159(6), pp.1300–1311. doi:https://doi.org/10.1016/j.cell.2014.11.017.

Cho, H., Wivagg, C.N., Kapoor, M., Barry, Z., Rohs, P.D.A., Suh, H., Marto, J.A., Garner, E.C. and Bernhardt, T.G. (2016). Bacterial cell wall biogenesis is mediated by SEDS and PBP polymerase families functioning semi-autonomously. *Nature Microbiology*, 1(10). doi:https://doi.org/10.1038/nmicrobiol.2016.172.

Chodisetti, P.K. and Reddy, M. (2019). Peptidoglycan hydrolase of an unusual cross-link cleavage specificity contributes to bacterial cell wall synthesis. *Proceedings of the National Academy of Sciences*, 116(16), pp.7825–7830. doi:https://doi.org/10.1073/pnas.1816893116.

Choudhery, S., Brown, A.J., Akusobi, C., Rubin, E.J., Sassetti, C.M. and Ioerger, T.R. (2021). Modeling Site-Specific Nucleotide Biases Affecting Himar1 Transposon Insertion Frequencies in TnSeq Data Sets. *mSystems*, 6(5). doi:https://doi.org/10.1128/msystems.00876-21.

Chowdhury, C., Kar, D., Dutta, M., Kumar, A. and Ghosh, A.S. (2012). Moderate deacylation efficiency of DacD explains its ability to partially restore beta-lactam resistance in *Escherichia coli* PBP5 mutant. *FEMS Microbiology Letters*, 337(1), pp.73–80. doi:https://doi.org/10.1111/1574-6968.12009.

Chudyk, E.I., Beer, M., Limb, M.A.L., Jones, C.A., Spencer, J., van der Kamp, M.W. and Mulholland, A.J. (2022). QM/MM Simulations Reveal the Determinants of Carbapenemase Activity in Class A β-Lactamases. *ACS Infectious Diseases*, 8(8), pp.1521–1532. doi:https://doi.org/10.1021/acsinfecdis.2c00152.

Cirillo, J.D., Barletta, R.G., Bloom, B.R. and Jacobs, W.R. (1991). A novel transposon trap for mycobacteria: isolation and characterization of IS1096. *Journal of Bacteriology*, 173(24), pp.7772–7780. doi:https://doi.org/10.1128/jb.173.24.7772-7780.1991.

Cole ST, Brosch R, Parkhill J, Garnier T, Churcher C, Harris D, Gordon SV, Eiglmeier K, Gas S, Barry CE, Tekaia F, Badcock K, Basham D, Brown D, Chillingworth T, Connor R, Davies R, Devlin K, Feltwell T, Gentles S, Hamlin N, Holroyd S, Hornsby T, Jagels K, Krogh A, McLean J, Moule S, Murphy L, Oliver K, Osborne J, Quail MA, Rajandream MA, Rogers J, Rutter S, Seeger K, Skelton J, Squares R, Squares S, Sulston JE, Taylor K, Whitehead S, Barrell BG. 1998. Deciphering the biology of *Mycobacterium tuberculosis* from the complete genome sequence. *Nature* 393:537–544. doi: 10.1038/31159.

Cole, S. T., Brosch, R., Parkhill, J., Garnier, T., Churcher, C., Harris, D., et al. (1998). Deciphering the biology of *Mycobacterium tuberculosis* from the complete genome sequence. *Nature* 393, 537–544. doi: 10.1038/31159.

Cole, S.T., Eiglmeier, K., Parkhill, J., James, K.D., Thomson, N.R., Wheeler, P.R., Honoré, N., Garnier, T., Churcher, C., Harris, D., Mungall, K., Basham, D., Brown, D., Chillingworth, T., Connor, R., Davies, R.M., Devlin, K., Duthoy, S., Feltwell, T. and Fraser, A. (2001). Massive gene decay in the leprosy bacillus. *Nature*, 409(6823), pp.1007–1011. doi:https://doi.org/10.1038/35059006.

Comas, I., Coscolla, M., Luo, T., Borrell, S., Holt, K.E., Kato-Maeda, M., Parkhill, J., Malla, B., Berg, S., Thwaites, G., Yeboah-Manu, D., Bothamley, G., Mei, J., Wei, L., Bentley, S., Harris, S.R., Niemann, S., Diel, R., Aseffa, A. and Gao, Q. (2013). Out-of-Africa migration and Neolithic coexpansion of *Mycobacterium tuberculosis* with modern humans. *Nature Genetics*, 45(10), pp.1176–1182. doi:https://doi.org/10.1038/ng.2744.

Comín, J., Otal, I. and Samper, S. (2022). In-depth Analysis of IS6110 Genomic Variability in the *Mycobacterium tuberculosis* Complex. *Frontiers in Microbiology*, 13. doi:https://doi.org/10.3389/fmicb.2022.767912.

Conradie, F., Diacon, A.H., Ngubane, N., Howell, P., Everitt, D., Crook, A.M., Mendel, C.M., Egizi, E., Moreira, J., Timm, J., McHugh, T.D., Wills, G.H., Bateson, A., Hunt, R., Van Niekerk, C., Li, M., Olugbosi, M.

and Spigelman, M. (2020). Treatment of Highly Drug-Resistant Pulmonary Tuberculosis. *New England Journal of Medicine*, 382(10), pp.893–902. doi:https://doi.org/10.1056/nejmoa1901814.

Cookson, B.T., Tyler, A.N. and Goldman, W.E. (1989). Primary structure of the peptidoglycan-derived tracheal cytotoxin of *Bordetella pertussis*. *Biochemistry*, 28(4), pp.1744–1749. doi:https://doi.org/10.1021/bi00430a048.

Correale, S., Ruggiero, A., Capparelli, R., Pedone, E. and Berisio, R. (2013). Structures of free and inhibited forms of the L,D-transpeptidase Ldt_{Mt1} from *Mycobacterium tuberculosis*. *Acta Crystallographica Section D Biological Crystallography*, 69(9), pp.1697–1706. doi:10.1107/s0907444913013085.

Craggs, P.D., Mouilleron, S., Rejzek, M., de Chiara, C., Young, R.J., Field, R.A., Argyrou, A. and de Carvalho, L.P.S. (2018). The Mechanism of Acetyl Transfer Catalyzed by *Mycobacterium tuberculosis* GlmU. *Biochemistry*, 57(24), pp.3387–3401. doi:10.1021/acs.biochem.8b00121.

Crainz, F. (1982). The editions and translations of Dr. Matthew Baillie's Morbid Anatomy. *Medical History*, 26(4), pp.443–452. doi:https://doi.org/10.1017/s0025727300041867.

Crawford, L. and Putnam, D. (2014). Synthesis and Characterization of Macromolecular Rhodamine Tethers and Their Interactions with P-Glycoprotein. *Bioconjugate Chemistry*, 25(8), pp.1462–1469. doi:https://doi.org/10.1021/bc5002196.

Crick DC, Brennan PJ. Biosynthesis of the arabinogalactan-peptidoglycan complex of *Mycobacterium tuberculosis*. In: Daffé M, Reyrat J-M, editors. *The mycobacterial cell envelope.* ASM Press; Washington, DC: 2008. pp. 25–40.

Crick, D.C., Mahapatra, S. and Brennan, P.J. (2001). Biosynthesis of the arabinogalactan-peptidoglycan complex of *Mycobacterium tuberculosis*. *Glycobiology*, 11(9), pp.107R118R. doi:10.1093/glycob/11.9.107r.

Cronin, R.M., Ferrell, M.J., Cahir, C.W., Champion, M.M. and Champion, P.A. (2022). Proteo-genetic analysis reveals clear hierarchy of ESX-1 secretion in *Mycobacterium marinum*. *Proceedings of the National Academy of Sciences of the United States of America*, [online] 119(24). doi:https://doi.org/10.1073/pnas.2123100119.

Crooks, G.E. (2004). WebLogo: A Sequence Logo Generator. *Genome Research*, 14(6), pp.1188–1190. doi:https://doi.org/10.1101/gr.849004.

Crowfoot., D. Bunn., C. Rogers-Low., B. Turner-Jones. (1949). A X-ray crystallographic investigation of the structure of penicillin. In: Clarke HT, Johnson JR, Robinson SR, editors. The chemistry of penicillin. Princeton, New Jersey: *Princeton University Press*; pp. 310 – 367.

Cuff, M.E., Tan, K., C. Hatzos-Skintges, R. Jedrzejczak, J.C. Sacchettini and A. Joachimiak (2015). The crystal structure of D-ALANYL-D-ALANINE CARBOXYPEPTIDASE from *Mycobacterium tuberculosis* H37Rv. doi:https://doi.org/10.2210/pdb4rye/pdb.

Cui, Z., Liu, J., Chang, Y., Lin, D., Luo, D., Ou, J. and Huang, L. (2021). Interaction analysis of *Mycobacterium tuberculosis* between the host environment and highly mutated genes from population genetic structure comparison. *Medicine*, 100(35), p.e27125. doi:https://doi.org/10.1097/md.0000000000027125.

Cunningham, B. and Wells, J. (1989). High-resolution epitope mapping of hGH-receptor interactions by alanine-scanning mutagenesis. *Science*, 244(4908), pp.1081–1085. doi:https://doi.org/10.1126/science.2471267.

CURIOSity Digital Collections. (2022). *Contagion*. [online] Available at: https://curiosity.lib.harvard.edu/contagion/catalog?f%5Bcreators-contributors_ssim%5D%5B%5D=Klebs%2C+E.+%28Edwin%29%2C+1834-1913&f%5Bsubjects_ssim%5D%5B%5D=Tuberculosis--Treatment [Accessed 11 Oct. 2023].

Daffe, M., Brennan, P.J. and McNeil, M. (1990). Predominant structural features of the cell wall arabinogalactan of *Mycobacterium tuberculosis* as revealed through characterization of oligoglycosyl alditol

fragments by gas chromatography/mass spectrometry and by 1H and 13C NMR analyses. *Journal of Biological Chemistry*, 265(12), pp.6734–6743. doi:https://doi.org/10.1016/s0021-9258(19)39211-7.

Daffé, M., Crick, D.C. and Jackson, M. (2014). Genetics of Capsular Polysaccharides and Cell Envelope (Glyco)lipids. *Microbiology Spectrum*, 2(4). doi:https://doi.org/10.1128/microbiolspec.mgm2-0021-2013.

Dajkovic, A., Tesson, B., Chauhan, S., Courtin, P., Keary, R., Flores, P., Marlière, C., Filipe, S.R., Chapot-Chartier, M.-P. and Carballido-Lopez, R. (2017). Hydrolysis of peptidoglycan is modulated by amidation of meso -diaminopimelic acid and Mg2+ in B acillus subtilis. *Molecular Microbiology*, 104(6), pp.972–988. doi:https://doi.org/10.1111/mmi.13673.

Dalhoff, A. (2020). Selective toxicity of antibacterial agents—still a valid concept or do we miss chances and ignore risks? *Infection*, 49(1), pp.29–56. doi:10.1007/s15010-020-01536-y.

Daniel, T.M. (2001). Pioneers of medicine and their impact on tuberculosis. (2001). *Choice Reviews Online*, 38(11), pp.38–622338–6223. doi:https://doi.org/10.5860/choice.38-6223.
Daniel, T.M. (2006). The history of tuberculosis. *Respiratory Medicine*, [online] 100(11), pp.1862–1870. doi:https://doi.org/10.1016/j.rmed.2006.08.006.

Daniel, T.M. and Iversen, P.A. (2015). Hippocrates and tuberculosis. *The International Journal of Tuberculosis and Lung Disease*, [online] 19(4), pp.373–374. doi:https://doi.org/10.5588/ijtld.14.0736.

Darrah, P.A., Zeppa, J.J., Maiello, P., Hackney, J.A., Wadsworth, M.H., Hughes, T.K., Pokkali, S., Swanson, P.A., Grant, N.L., Rodgers, M.A., Kamath, M., Causgrove, C.M., Laddy, D.J., Bonavia, A., Casimiro, D., Lin, P.L., Klein, E., White, A.G., Scanga, C.A. and Shalek, A.K. (2020). Prevention of tuberculosis in macaques after intravenous BCG immunization. *Nature*, [online] 577(7788), pp.95–102. doi:https://doi.org/10.1038/s41586-019-1817-8.

Dartois, V.A. and Rubin, E.J. (2022). Anti-tuberculosis treatment strategies and drug development: Challenges and priorities. *Nature Reviews Microbiology*, 20, pp.685–701. doi:https://doi.org/10.1038/s41579-022-00731-y.

Das, M., David, D., Horo, I., Anouk van Hooij, Tió-Coma, M., Annemieke Geluk and Sundeep Chaitanya Vedithi (2023). Mycobacterium leprae and host immune transcriptomic signatures for reactional states in leprosy. *Frontiers in Microbiology*, 14. doi:https://doi.org/10.3389/fmicb.2023.1113318.

Davenne, T. and McShane, H. (2016). Why don't we have an effective tuberculosis vaccine yet? *Expert Review of Vaccines*, [online] 15(8), pp.1009–1013. doi:https://doi.org/10.1586/14760584.2016.1170599.

Davies, T.A., Shang, W., Bush, K. and Flamm, R.K. (2008). Affinity of Doripenem and Comparators to Penicillin-Binding Proteins in *Escherichia coli* and *Pseudomonas aeruginosa*. *Antimicrobial Agents and Chemotherapy*, [online] 52(4), pp.1510–1512. doi:https://doi.org/10.1128/aac.01529-07.

Davis, J.L. (2018). Pharmacologic Principles. *Equine Internal Medicine*, 4, pp.79–137. doi:https://doi.org/10.1016/b978-0-323-44329-6.00002-4.

de Chiara, C., Homšak, M., Prosser, G.A., Douglas, H.L., Garza-Garcia, A., Kelly, G., Purkiss, A.G., Tate, E.W. and de Carvalho, L.P.S. (2020). D-Cycloserine destruction by alanine racemase and the limit of irreversible inhibition. *Nature Chemical Biology*, 16(6), pp.686–694. doi:https://doi.org/10.1038/s41589-020-0498-9.

De Cock Km and Re, C. (1999). Will DOTS do it? A reappraisal of tuberculosis control in countries with high rates of HIV infection. *PubMed*, 3(6), pp.457–65.

De Maio, F. *et al.* (2020) 'PE_PGRS proteins of *mycobacterium tuberculosis*: A specialized molecular task force at the forefront of host–pathogen interaction', *Virulence*, 11(1), pp. 898–915. doi:10.1080/21505594.2020.1785815.

De Smet, K.A.L., Young, D.B., Duncan, K., Gallagher, A. and Kempsell, K.E. (1999). Alteration of a single amino acid residue reverses fosfomycin resistance of recombinant MurA from *Mycobacterium tuberculosis*. *Microbiology*, 145(11), pp.3177–3184. doi:10.1099/00221287-145-11-3177.

Decuyper, L., Marko Jukič, Stanislav Gobec, Aleš Žula and Matthias D'hooghe (2018). Antibacterial and β-Lactamase Inhibitory Activity of Monocyclic β-Lactams. 38(2), pp.426–503. doi:https://doi.org/10.1002/med.21443.

DeJesus, M. and Ioerger, T. (2017). *TB Genome Annotation Portal*, *Rv3593 (lpqF) - TB Genome Annotation Portal*. Available at: https://orca2.tamu.edu/U19/pages/Rv3593.html (Accessed: 22 May 2023).

DeJesus, M.A., Gerrick, E.R., Xu, W., Park, S.W., Long, J.E., Boutte, C.C., Rubin, E.J., Schnappinger, D., Ehrt, S., Fortune, S.M., Sassetti, C.M. and Ioerger, T.R. (2017). Comprehensive Essentiality Analysis of the *Mycobacterium tuberculosis* Genome via Saturating Transposon Mutagenesis. *mBio*, 8(1). doi:10.1128/mbio.02133-16.

DeJesus, M.A., Gerrick, E.R., Xu, W., Park, S.W., Long, J.E., Boutte, C.C., Rubin, E.J., Schnappinger, D., Ehrt, S., Fortune, S.M., Sassetti, C.M. and Ioerger, T.R. (2017). Comprehensive Essentiality Analysis of the *Mycobacterium tuberculosis* Genome via Saturating Transposon Mutagenesis. *mBio*, 8(1). doi:https://doi.org/10.1128/mbio.02133-16.

Dempwolff, F., Sanchez, S. and Kearns, D.B. (2020). Tn FLX : a Third-Generation mariner -Based Transposon System for *Bacillus subtilis*. *Applied and Environmental Microbiology*, 86(10). doi:https://doi.org/10.1128/aem.02893-19.

Den Blaauwen, T., de Pedro, M.A., Nguyen-Distèche, M. and Ayala, J.A. (2008). Morphogenesis of rod-shaped sacculi. *FEMS Microbiology Reviews*, 32(2), pp.321–344. doi:https://doi.org/10.1111/j.1574-6976.2007.00090.x.

Denome, S.A., Elf, P.K., Henderson, T.A., Nelson, D.E. and Young, K.D. (1999). *Escherichia coli* Mutants Lacking All Possible Combinations of Eight Penicillin Binding Proteins: Viability, Characteristics, and Implications for Peptidoglycan Synthesis. *Journal of Bacteriology*, 181(13), pp.3981–3993. doi:https://doi.org/10.1128/jb.181.13.3981-3993.1999.

Diacon, A.H., van, Barnard, M., Florian von Groote-Bidlingmaier, Lange, C., García-Basteiro, A.L., Esperança Sevene, Lluis Ballell and Barros, D. (2016). β-Lactams against Tuberculosis — New Trick for an Old Dog? 375(4), pp.393–394. doi:https://doi.org/10.1056/nejmc1513236.

Dianišková, P., Korduláková, J., Škovierová, H., Kaur, D., Jackson, M., Brennan, P. and Mikušová, K. (2011). nvestigation of ABC transporter from mycobacterial arabinogalactan biosynthetic cluster. *General Physiology and Biophysics*, 30(3), pp.239–250. doi:https://doi.org/10.4149/gpb_2011_03_239.

Diezel, W., Kopperschläger, G. and Hofmann, E. (1972). An improved procedure for protein staining in polyacrylamide gels with a new type of Coomassie Brilliant Blue. *Analytical Biochemistry*, 48(2), pp.617–620. doi:https://doi.org/10.1016/0003-2697(72)90117-0.

Dinadayala, P., Kaur, D., Berg, S., Amin, A.G., Vissa, V.D., Chatterjee, D., Brennan, P.J. and Crick, D.C. (2006). Genetic Basis for the Synthesis of the Immunomodulatory Mannose Caps of Lipoarabinomannan in Mycobacterium tuberculosis. *Journal of Biological Chemistry*, 281(29), pp.20027–20035. doi:https://doi.org/10.1074/jbc.m603395200.

Dmitriev, B.A., Ehlers, S., Rietschel, E.T. and Brennan, P.J. (2000). Molecular mechanics of the mycobacterial cell wall: From horizontal layers to vertical scaffolds. *International Journal of Medical Microbiology*, 290(3), pp.251–258. doi:10.1016/s1438-4221(00)80122-8.

Doi, Y. (2019). Treatment Options for Carbapenem-resistant Gram-negative Bacterial Infections. *Clinical Infectious Diseases*, 69 (Supplement_7), pp.S565–S575. doi:https://doi.org/10.1093/cid/ciz830. doi:10.1146/annurev.bi.52.070183.004141.

Domingues, S., da Silva, G.J. and Nielsen, K.M. (2012). Integrons. *Mobile Genetic Elements*, 2(5), pp.211–223. doi:https://doi.org/10.4161/mge.22967.

Domínguez, J., Boettger, E.C., Cirillo, D., Cobelens, F., Eisenach, K.D., Gagneux, S., Hillemann, D., Horsburgh, R., Molina-Moya, B., Niemann, S., Tortoli, E., Whitelaw, A. and Lange, C. (2016). Clinical implications of molecular drug resistance testing for *Mycobacterium tuberculosis*: a TBNET/RESIST-TB consensus statement. *The International Journal of Tuberculosis and Lung Disease*, 20(1), pp.24–42. doi:https://doi.org/10.5588/ijtld.15.0221.

Donowitz, G.R. (1989). Third Generation Cephalosporins. *Infectious Disease Clinics of North America*, 3(3), pp.595–612. doi:https://doi.org/10.1016/s0891-5520(20)30291-9.

Dooley, K.E., Kaplan, R., Mwelase, N., Grinsztejn, B., Ticona, E., Lacerda, M., Sued, O., Belonosova, E., Ait-Khaled, M., Angelis, K., Brown, D., Singh, R., Talarico, C.L., Tenorio, A.R., Keegan, M.R., Aboud, M., Dooley, K.E., Richard, K., Noluthando, M. and Beatriz, G. (2019). Dolutegravir-based Antiretroviral Therapy for Patients Coinfected With Tuberculosis and Human Immunodeficiency Virus: A Multicenter, Noncomparative, Open-label, Randomized Trial. *Clinical Infectious Diseases*. doi:https://doi.org/10.1093/cid/ciz256.

Dousa, K.M., Kurz, S.G., Taracila, M.A., Bonfield, T., Bethel, C.R., Barnes, M.D., Suresh Selvaraju, Abdelhamed, A.M., Kreiswirth, B.N., W. Henry Boom, Kasperbauer, S.H., Daley, C.L. and Bonomo, R.A. (2020). Insights into the L,D-Transpeptidases and D,D-Carboxypeptidase of *Mycobacterium abscessus*: Ceftaroline, Imipenem, and Novel Diazabicyclooctane Inhibitors. *Antimicrobial agents and chemotherapy*, 64(8). doi:https://doi.org/10.1128/aac.00098-20.

Downing, K.J., Mischenko, V.V., Shleeva, M.O., Young, D.I., Young, M., Kaprelyants, A.S., Apt, A.S. and Mizrahi, V. (2005). Mutants of *Mycobacterium tuberculosis* Lacking Three of the Five *rpf* -Like Genes Are Defective for Growth In Vivo and for Resuscitation In Vitro. *Infection and Immunity*, 73(5), pp.3038–3043. doi:10.1128/iai.73.5.3038-3043.2005.

Draper P., Khoo K. H., Chatterjee D., Dell A. and Morris H. R. (1997). Galactosamine in walls of slow-growing mycobacteria. Biochemical Journal, 327 (Pt 2), 519–525.

Duan, T., Du, Y., Xing, C., Wang, H.Y. and Wang, R.-F. (2022). Toll-Like Receptor Signaling and Its Role in Cell-Mediated Immunity. *Frontiers in Immunology*, 13. doi:https://doi.org/10.3389/fimmu.2022.812774.

Duarte, R., Lönnroth, K., Carvalho, C., Lima, F., Carvalho, A.C.C., Muñoz-Torrico, M. and Centis, R. (2018). Tuberculosis, social determinants, and co-morbidities (including HIV). *Pulmonology*, [online] 24(2), pp.115–119. doi:https://doi.org/10.1016/j.rppnen.2017.11.003.

Dubé, J.-Y., McIntosh, F. and Behr, M.A. (2022). Mice Dually Disrupted for Nod2 and Mincle Manifest Early Bacteriological Control but Late Susceptibility During *Mycobacterium tuberculosis* Infection. *Frontiers in Immunology*, 13. doi:https://doi.org/10.3389/fimmu.2022.862992.

Dubée, V., Triboulet, S., Mainardi, J.-L., Ethève-Quelquejeu, M., Gutmann, L., Marie, A., Dubost, L., Hugonnet, J.-E. and Arthur, M. (2012). Inactivation of *Mycobacterium tuberculosis* L,D-Transpeptidase Ldt $_{Mt1}$ by Carbapenems and Cephalosporins. *Antimicrobial Agents and Chemotherapy*, 56(8), pp.4189–4195. doi:https://doi.org/10.1128/aac.00665-12.

Dubnau, E., Chan, J., Raynaud, C., Mohan, V.P., Lanéelle, M.-A., Yu, K., Quémard, A., Smith, I. and Daffé, M. (2002). Oxygenated mycolic acids are necessary for virulence of *Mycobacterium tuberculosis* in mice. *Molecular Microbiology*, 36(3), pp.630–637. doi:https://doi.org/10.1046/j.1365-2958.2000.01882.x.

Ducret, A., Quardokus, E.M. and Brun, Y.V. (2016). MicrobeJ, a tool for high throughput bacterial cell detection and quantitative analysis. *Nature Microbiology*, 1(7). doi:https://doi.org/10.1038/nmicrobiol.2016.77.
Dulberger, C., Rubin, E. and Boutte, C., 2019. The mycobacterial cell envelope — a moving target. *Nature Reviews Microbiology*, 18(1), pp.47-59.

Dzhekieva, L., Rocaboy, M., Kerff, F., Charlier, P., Sauvage, E., & Pratt, R. (2010). Crystal structure of a complex between the Actinomadura R39 DD-peptidase and a peptidoglycan-mimetic boronate inhibitor: interpretation of a transition state analogue in terms of catalytic mechanism. Biochemistry, 49(30), 6411-9.

E. Ellen. Nell and Hill, J.H. (1947). Comparison of the in vitro antigonococcal actions of penicillins G, F, K, and X. *American journal of syphilis, gonorrhea, and venereal diseases*, 31(1), pp.14–19.

Eagle, H. (1946). The Relative Activity of Penicillins F, G, K, and X Against Spirochetes and Streptococci *in Vitro*. *Journal of Bacteriology*, 52(1), pp.81–88. doi:https://doi.org/10.1128/jb.52.1.81-88.1946.

Eagle, H. (1947). THE THERAPEUTIC ACTIVITY OF PENICILLINS F, G, K, AND X IN EXPERIMENTAL INFECTIONS WITH PNEUMOCOCCUS TYPE I AND STREPTOCOCCUS PYOGENES. *Journal of Experimental Medicine*, 85(2), pp.175–186. doi:https://doi.org/10.1084/jem.85.2.175.

Ealand, C.S., Asmal, R., Mashigo, L., Campbell, L. and Kana, B.D. (2019). Characterization of putative DD-carboxypeptidase-encoding genes in *Mycobacterium smegmatis*. *Scientific Reports*, 9(1). doi:https://doi.org/10.1038/s41598-019-41001-x.

Ealand, C., Rimal, B., Chang, J., Lethabo Mashigo, Chengalroyen, M., Lusanda Mapela, Germar Beukes, Machowski, E., Kim, S.J. and Kana, B. (2018). Resuscitation-Promoting Factors Are Required for *Mycobacterium smegmatis* Biofilm Formation. *Applied and Environmental Microbiology*, 84(17). doi:https://doi.org/10.1128/aem.00687-18.

Eberhardt, R.Y., Chang, Y., Bateman, A., Murzin, A.G., Axelrod, H.L., Hwang, W.C. and Aravind, L. (2013). Filling out the structural map of the NTF2-like superfamily. *BMC Bioinformatics*, 14(1). doi:https://doi.org/10.1186/1471-2105-14-327.

EBI Web Team (2023). [online] Ebi.ac.uk. Available at: https://www.ebi.ac.uk/thornton-srv/databases/cgi-bin/pdbsum/GetPage.pl?pdbcode=3h3h&template=main.html [Accessed 24 Dec. 2023]. fast.genomics.lbl.gov. (2023). *fast.genomics*. [online] Available at: https://fast.genomics.lbl.gov/cgi/search.cgi [Accessed 3 Dec. 2023].

Eckert, C., Lecerf, M., Dubost, L., Arthur, M. and Mesnage, S. (2006). Functional Analysis of AtlA, the Major N-Acetylglucosaminidase of *Enterococcus faecalis*. *Journal of Bacteriology*, 188(24), pp.8513–8519. doi:https://doi.org/10.1128/jb.01145-06.

Edoo, Z., Arthur, M. and Hugonnet, J.-E. (2017). Reversible inactivation of a peptidoglycan transpeptidase by a β-lactam antibiotic mediated by β-lactam-ring recyclization in the enzyme active site. *Scientific Reports*, [online] 7(1), pp.1–8. doi:https://doi.org/10.1038/s41598-017-09341-8.

Egan, A.J.F., Biboy, J., van't Veer, I., Breukink, E. and Vollmer, W. (2015). Activities and regulation of peptidoglycan synthases. *Philosophical Transactions of the Royal Society B: Biological Sciences*, 370(1679), p.20150031. doi:https://doi.org/10.1098/rstb.2015.0031.

Egan, A.J.F., Errington, J. and Vollmer, W. (2020). Regulation of peptidoglycan synthesis and remodelling. *Nature Reviews. Microbiology*, [online] 18(8), pp.446–460. doi:https://doi.org/10.1038/s41579-020-0366-3.

Egesborg, P., Carlettini, H., Volpato, J.P. and Doucet, N. (2014). Combinatorial active-site variants confer sustained clavulanate resistance in BlaC β-lactamase from *Mycobacterium tuberculosis*. *Protein Science*, 24(4), pp.534–544. doi:https://doi.org/10.1002/pro.2617.

Egorov, A., Rubtsova, M., Grigorenko, V., Uporov, I. and Veselovsky, A. (2019). The Role of the Ω-Loop in Regulation of the Catalytic Activity of TEM-Type β-Lactamases. *Biomolecules*, 9(12), p.854. doi:https://doi.org/10.3390/biom9120854.

Emami, K., Guyet, A., Kawai, Y., Devi, J., Wu, L.J., Allenby, N., Daniel, R.A. and Errington, J. (2017). RodA as the missing glycosyltransferase in *Bacillus subtilis* and antibiotic discovery for the peptidoglycan polymerase pathway. *Nature Microbiology*, 2(3). doi:10.1038/nmicrobiol.2016.253.

Enea Sancho-Vaello, Albesa-Jové, D., Ane Rodrigo-Unzueta and Guerin, M.E. (2017). Structural basis of phosphatidyl-myo-inositol mannosides biosynthesis in mycobacteria. *Biochimica et Biophysica Acta (BBA) - Molecular and Cell Biology of Lipids*, 1862(11), pp.1355–1367. doi:https://doi.org/10.1016/j.bbalip.2016.11.002.

England, K., Boshoff, H.I.M., Arora, K., Weiner, D., Dayao, E., Schimel, D., Via, L.E. and Barry, C.E. (2012). Meropenem-Clavulanic Acid Shows Activity against *Mycobacterium tuberculosis* In Vivo. *Antimicrobial Agents and Chemotherapy*, [online] 56(6), pp.3384–3387. doi:https://doi.org/10.1128/aac.05690-11.

Eniyan, K., Dharavath, S., Vijayan, R., Bajpai, U. and Gourinath, S. (2018). Crystal structure of UDP- N - acetylglucosamine-enolpyruvate reductase (MurB) from *Mycobacterium tuberculosis*. *Biochimica et Biophysica Acta (BBA) - Proteins and Proteomics*, 1866(3), pp.397–406. doi:10.1016/j.bbapap.2017.11.013.

Errington, J. (2015). Bacterial morphogenesis and the enigmatic MreB helix. *Nature Reviews Microbiology*, 13(4), pp.241–248. doi:https://doi.org/10.1038/nrmicro3398.

Espaillat, A., Alvarez, L., Torrens, G., ter Beek, J., Miguel-Ruano, V., Irazoki, O., Gago, F., Hermoso, J.A., Berntsson, R.P.-A. . and Cava, F. (2024). A distinctive family of L,D-transpeptidases catalyzing L-Ala-mDAP crosslinks in Alpha- and Betaproteobacteria. *Nature Communications*, [online] 15(1), p.1343. doi:https://doi.org/10.1038/s41467-024-45620-5.

Espaillat, A., Alvarez, L., Torrens, G., ter Beek, J., Miguel-Ruano, V., Irazoki, O., Gago, F., Hermoso, J.A., Berntsson, R.P.-A. . and Cava, F. (2024). A distinctive family of L,D-transpeptidases catalyzing L-Ala-mDAP crosslinks in Alpha- and Betaproteobacteria. *Nature Communications*, [online] 15(1), p.1343. doi:https://doi.org/10.1038/s41467-024-45620-5.

Espaillat, A., Carrasco-López, C., Bernardo-García, N., Alzoray Rojas-Altuve, Klett, J., Morreale, A., Hermoso, J.A. and Cava, F. (2021). Binding of non-canonical peptidoglycan controls *Vibrio cholerae* broad spectrum racemase activity. *Computational and Structural Biotechnology Journal*, 19, pp.1119–1126. doi:https://doi.org/10.1016/j.csbj.2021.01.031.

Eun Seon Chung, Kar, P., Maliwan Kamkaew, Amir, A. and Aldridge, B.B. (2023). *Mycobacterium tuberculosis* grows linearly at the single-cell level with larger variability than model organisms. *bioRxiv (Cold Spring Harbor Laboratory)*. doi:https://doi.org/10.1101/2023.05.17.541183.

Eun, H.-M., Yapo, A. and Petit, J.-F. (1978). DD-Carboxypeptidase Activity of Membrane Fragments of Mycobacterium smegmatis. Enzymatic Properties and Sensitivity to beta-Lactan Antibiotics. *European Journal of Biochemistry*, 86(1), pp.97–103. doi:https://doi.org/10.1111/j.1432-1033.1978.tb12288.x.

Evans, B. and Amyes, S. (2014). Oxa β-lactamases. Clinical Microbiology Reviews, 27(2), 241-263. https://doi.org/10.1128/cmr.00117-13

Farra, A., Koula, K., Jolly, B.L., Gando, H.G., Ouarandji, L.M., Mossoro-Kpinde, C.D., Manirakiza, A., Simelo, J.P. and de Dieu Iragena, J. (2023). Effectiveness of Xpert MTB/RIF and the Line Probe Assay tests for the rapid detection of drug-resistant tuberculosis in the Central African Republic. *PLOS global public health*, [online] 3(5), p.e0001847. doi:https://doi.org/10.1371/journal.pgph.0001847.

Fedrizzi, T., Meehan, C.J., Grottola, A., Giacobazzi, E., Fregni Serpini, G., Tagliazucchi, S., Fabio, A., Bettua, C., Bertorelli, R., De Sanctis, V., Rumpianesi, F., Pecorari, M., Jousson, O., Tortoli, E. and Segata, N. (2017). Genomic characterization of Nontuberculous Mycobacteria. *Scientific Reports*, 7(1). doi:https://doi.org/10.1038/srep45258.

Fei, Y., Yung Shin Sun, Li, Y., Lau, K., Yu, H., Chokhawala, H.A., Huang, S., Landry, J.P., Chen, X. and Zhu, X. (2011). Fluorescent labeling agents change binding profiles of glycan-binding proteins. *Molecular BioSystems*, 7(12), pp.3343–3343. doi:https://doi.org/10.1039/c1mb05332a.

Feiler, C., Fisher, A.C., Boock, J.T., Marrichi, M.J., Wright, L., Schmidpeter, P.A.M., Blankenfeldt, W., Pavelka, M. and DeLisa, M.P. (2013). Directed Evolution of *Mycobacterium tuberculosis* β-Lactamase Reveals

Gatekeeper Residue That Regulates Antibiotic Resistance and Catalytic Efficiency. *PLoS ONE*, 8(9), p.e73123. doi:https://doi.org/10.1371/journal.pone.0073123.

Feng, S., Liang, L., Shen, C., Lin, D., Li, J., Lyu, L., Liang, W., Zhong, L., Cook, G.M., Doi, Y., Chen, C. and Tian, G. (2022). A CRISPR-guided mutagenic DNA polymerase strategy for the detection of antibiotic-resistant mutations in M. tuberculosis. *Molecular Therapy - Nucleic Acids*, [online] 29, pp.354–367. doi:https://doi.org/10.1016/j.omtn.2022.07.004.

Fennelly, K.P. and Jones-López, E.C. (2015). Quantity and Quality of Inhaled Dose Predicts Immunopathology in Tuberculosis. *Frontiers in Immunology*, [online] 6. doi:https://doi.org/10.3389/fimmu.2015.00313.

Fenton, A.K. and Gerdes, K. (2013). Direct interaction of FtsZ and MreB is required for septum synthesis and cell division in *Escherichia coli*. *The EMBO Journal*, 32(13), pp.1953–1965. doi:https://doi.org/10.1038/emboj.2013.129.

Fercher, C., Probst, I., Kohler, V., Goessweiner-Mohr, N., Arends, K., Grohmann, E., Zangger, K., Meyer, N.H. and Keller, W. (2016). VirB8-like protein TraH is crucial for DNA transfer in *Enterococcus faecalis*. *Scientific Reports*, 6(1). doi:https://doi.org/10.1038/srep24643.

Fernández, M., Conde, S., de la Torre, J., Molina-Santiago, C., Ramos, J.-L. and Duque, E. (2011). Mechanisms of Resistance to Chloramphenicol in *Pseudomonas putida* KT2440. *Antimicrobial Agents and Chemotherapy*, [online] 56(2), pp.1001–1009. doi:https://doi.org/10.1128/aac.05398-11.

Fisher, J. F., & Mobashery, S. (2016). beta-Lactam Resistance Mechanisms: Gram-Positive Bacteria and Mycobacterium tuberculosis. *Cold Spring Harbor Perspect Med, 6*(5). doi: 10.1101/cshperspect.a025221.

Fisher, J.F. and Mobashery, S. (2014). The sentinel role of peptidoglycan recycling in the β-lactam resistance of the Gram-negative *Enterobacteriaceae* and *Pseudomonas aeruginosa*. *Bioorganic Chemistry*, 56, pp.41–48. doi:https://doi.org/10.1016/j.bioorg.2014.05.011.

FLEMING, A. (1945). Penicillin, *Nobel Lecture, December 11.*

Fleming, A. (2001). On the antibacterial action of cultures of a penicillium, with special reference to their use in the isolation of B. influenzae. 1929. 79(8), pp.780–90.

Flores, A.R. (2005). Genetic analysis of the -lactamases of *Mycobacterium tuberculosis* and *Mycobacterium smegmatis* and susceptibility to β-lactam antibiotics. *Microbiology*, 151(2), pp.521–532. doi:https://doi.org/10.1099/mic.0.27629-0.

Forbes, B.A. (2017). Mycobacterial Taxonomy. *Journal of Clinical Microbiology*, [online] 55(2), pp.380–383. doi:https://doi.org/10.1128/JCM.01287-16.

Forrellad, M.A., Klepp, L.I., Gioffré, A., Sabio y García, J., Morbidoni, H.R., Santangelo, M. de la P., Cataldi, A.A. and Bigi, F. (2013). Virulence factors of the *Mycobacterium tuberculosis* complex. *Virulence*, [online] 4(1), pp.3–66. doi:https://doi.org/10.4161/viru.22329.

Franklin, A., Salgueiro, V.C., Layton, A.J., Sullivan, R., Mize, T., Lucía Vázquez-Iniesta, Benedict, S.T., Gurcha, S.S., Itxaso Anso, Besra, G.S., Banzhaf, M., Lovering, A.L., Williams, S.J., Guerin, M.E., Scott, N.E., Prados-Rosales, R., Lowe, E.C. and Moynihan, P.J. (2024). The mycobacterial glycoside hydrolase LamH enables capsular arabinomannan release and stimulates growth. *Nature Communications*, 15(1). doi:https://doi.org/10.1038/s41467-024-50051-3.

Freed, N.E. (2017). Creation of a Dense Transposon Insertion Library Using Bacterial Conjugation in Enterobacterial Strains Such As *Escherichia Coli* or *Shigella flexneri*. *Journal of Visualized Experiments*, (127). doi:https://doi.org/10.3791/56216.

Gagneux, S. (2012). Host–pathogen coevolution in human tuberculosis. *Philosophical Transactions of the Royal Society B: Biological Sciences*, 367(1590), pp.850–859. doi:https://doi.org/10.1098/rstb.2011.0316.

Gallagher, J.T., Morris, A. and Dexter, T.M. (1985). Identification of two binding sites for wheat-germ agglutinin on polylactosamine-type oligosaccharides. *Biochemical Journal*, 231(1), pp.115–122. doi:https://doi.org/10.1042/bj2310115.
Gan, L., Chen, S. and Jensen, G.J. (2008). Molecular organization of Gram-negative peptidoglycan. *Proceedings of the National Academy of Sciences of the United States of America*, [online] 105(48), pp.18953–18957. doi:https://doi.org/10.1073/pnas.0808035105.

Gande, R., Gibson, K.J.C., Brown, A.K., Krumbach, K., Dover, L.G., Sahm, H., Shioyama, S., Oikawa, T., Besra, G.S. and Eggeling, L. (2004). Acyl-CoA Carboxylases (accD2 and accD3), Together with a Unique Polyketide Synthase (Cg-pks), Are Key to Mycolic Acid Biosynthesis in Corynebacterianeae Such as *Corynebacterium glutamicum* and *Mycobacterium tuberculosis*. *Journal of Biological Chemistry*, 279(43), pp.44847–44857. doi:https://doi.org/10.1074/jbc.m408648200.

Gandra, S., Takahashi, S., Mitrani-Gold, F.S., Mulgirigama, A. and Ferrinho, D.A. (2022). A systematic scoping review of faropenem and other oral penems: treatment of *Enterobacterales* infections, development of resistance and cross-resistance to carbapenems. *JAC-Antimicrobial Resistance*, 4(6). doi:https://doi.org/10.1093/jacamr/dlac125.

Gao, J., Wang, L., Jiang, J., Xu, Q., Zeng, N., Lu, B., Yuan, P., Sun, K., Zhou, H. and He, X. (2023). A probiotic bi-functional peptidoglycan hydrolase sheds NOD2 ligands to regulate gut homeostasis in female mice. *Nature communications*, 14(1). doi:https://doi.org/10.1038/s41467-023-38950-3.

Gao, L.-Y., Groger, R.K., Cox, J.S., Beverley, S.M., Lawson, E.H. and Brown, E.J. (2003). Transposon Mutagenesis of *Mycobacterium marinum* Identifies a Locus Linking Pigmentation and Intracellular Survival. *Infection and Immunity*, 71(2), pp.922–929. doi:https://doi.org/10.1128/iai.71.2.922-929.2003.

García-Heredia, A., Pohane, A.A., Melzer, E.S., Carr, C.R., Fiolek, T.J., Rundell, S.R., Lim, H.C., Wagner, J.C., Morita, Y.S., Swarts, B.M. and Siegrist, M.S. (2018). Peptidoglycan precursor synthesis along the sidewall of pole-growing mycobacteria. *eLife*, [online] 7, p.e37243. doi:https://doi.org/10.7554/eLife.37243.

Garde, S., Chodisetti, P.K. and Reddy, M. (2021). Peptidoglycan: Structure, Synthesis, and Regulation. *EcoSal Plus*, [online] 9(2). doi:https://doi.org/10.1128/ecosalplus.esp-0010-2020.

Gazi, I., Johansen, L.B. and Huppertz, T. (2022). Heterogeneity, Fractionation, and Isolation. *Encyclopedia of Dairy Sciences*, pp.881–893. doi:https://doi.org/10.1016/b978-0-12-818766-1.00278-6.

Geiger, T., Pazos, M., Lara-Tejero, M., Vollmer, W. and Galán, J.E. (2018). Peptidoglycan editing by a specific ld-transpeptidase controls the muramidase-dependent secretion of typhoid toxin. *Nature Microbiology*, 3(11), pp.1243–1254. doi:https://doi.org/10.1038/s41564-018-0248-x.

Gérald Larrouy-Maumus, Henrieta Škovierová, Rabeb Dhouib, Shiva Kumar Angala, Zuberogoïtia, S., Hà Phạm, Anne Drumond Villela, Katarína Mikušová, Noguera, A., Gilleron, M., Valentínová, L., Korduláková, J., Brennan, P.J., Puzo, G., Jérôme Nigou and Jackson, M. (2012). A Small Multidrug Resistance-like Transporter Involved in the Arabinosylation of Arabinogalactan and Lipoarabinomannan in *Mycobacteria*. *Journal of Biological Chemistry*, [online] 287(47), pp.39933–39941. doi:https://doi.org/10.1074/jbc.m112.400986.

Gey van Pittius, N.C., Sampson, S.L., Lee, H., Kim, Y., van Helden, P.D. and Warren, R.M. (2006). *BMC Evolutionary Biology*, 6(1), p.95. doi:https://doi.org/10.1186/1471-2148-6-95.

Ghazaei, C. (2018). *Mycobacterium tuberculosis* and lipids: Insights into molecular mechanisms from persistence to virulence. *Journal of Research in Medical Sciences*, [online] 23(1), p.63. doi:https://doi.org/10.4103/jrms.jrms_904_17.

Gholoobi, A., Masoudi-Kazemabad, A., Meshkat, M. and Meshkat, Z. (2014). Comparison of Culture and PCR Methods for Diagnosis of Mycobacterium tuberculosis in Different Clinical Specimens. *Jundishapur Journal of Microbiology*, 7(2). doi:https://doi.org/10.5812/jjm.8939.

Ghosh, A.S., Chowdhury, C. and Nelson, D.E. (2008). Physiological functions of D-alanine carboxypeptidases in Escherichia coli. *Trends in Microbiology*, [online] 16(7), pp.309–317. doi:https://doi.org/10.1016/j.tim.2008.04.006.

Ghosh, A.S., Chowdhury, C. and Nelson, D.E. (2008). Physiological functions of D-alanine carboxypeptidases in Escherichia coli. Trends in Microbiology, [online] 16(7), pp.309–317. doi:https://doi.org/10.1016/j.tim.2008.04.006.

Ghuysen, J.M. (1968). Use of bacteriolytic enzymes in determination of wall structure and their role in cell metabolism. *Bacteriological Reviews*, 32(4_Pt_2), pp.425–464. doi:10.1128/br.32.4_pt_2.425-464.1968.

Ghuysen, J.M. and R Hakenbeck (1994). *Bacterial cell wall*. Amsterdam; New York: Elsevier.

Ghuysen, J.M., Nakel, M. and Kandler, O. (1971). Wall peptidoglycan in *Aerococcus viridans* strains 201 Evans and ATCC 11563 and in *Gaffkya homari* strain ATCC 10400. *Biochemistry*, 10(11), pp.2170–2175. doi:https://doi.org/10.1021/bi00787a033.

Gibbs, C.S. and Zoller, M.J. (1991). Identification of functional residues in proteins by charged-to-alanine scanning mutagenesis. *Methods*, 3(3), pp.165–173. doi:https://doi.org/10.1016/s1046-2023(05)80169-0.

Gibson, K.J.C., Eggeling, L., Maughan, W.N., Krumbach, K., Gurcha, S.S., Nigou, J., Puzo, G., Sahm, H. and Besra, G.S. (2003). Disruption of Cg-Ppm1, a Polyprenyl Monophosphomannose Synthase, and the Generation of Lipoglycan-less Mutants in *Corynebacterium glutamicum*. *Journal of Biological Chemistry*, 278(42), pp.40842–40850. doi:https://doi.org/10.1074/jbc.m307988200.

Gill, C.M., Dolan, L., Piggott, L.M. and McLaughlin, A.M. (2022). New developments in tuberculosis diagnosis and treatment. *Breathe*, [online] 18(1), p.210149. doi:https://doi.org/10.1183/20734735.0149-2021.

Giovanna Valle Germano, André Flores Braga, Mendes, R., Priscila Betoni Ballalai, Cavalcanti, O., Saloum, F., de, A., Cléverson Teixeira Soares, Das, P.K., Milton Ozório Moraes, Carla, A. and Brito, N. (2022). Association of CD209 (DC-SIGN) rs735240 SNV with paucibacillary leprosy in the Brazilian population and its functional effects. *Memorias Do Instituto Oswaldo Cruz*, 117. doi:https://doi.org/10.1590/0074-02760220014.

Glauner, B., Höltje, J.V. and Schwarz, U. (1988). The composition of the murein of Escherichia coli. *Journal of Biological Chemistry*, 263(21), pp.10088–10095. doi:https://doi.org/10.1016/s0021-9258(19)81481-3.

Glickman, M.S. (2003). The mmaA2 Gene of *Mycobacterium tuberculosis* Encodes the Distal Cyclopropane Synthase of the α-Mycolic Acid. *Journal of Biological Chemistry*, 278(10), pp.7844–7849. doi:https://doi.org/10.1074/jbc.m212458200.

Glickman, M.S., Cox, J.S. and Jacobs, W.R. (2000). A Novel Mycolic Acid Cyclopropane Synthetase Is Required for Cording, Persistence, and Virulence of *Mycobacterium tuberculosis*. *Molecular Cell*, 5(4), pp.717–727. doi:https://doi.org/10.1016/s1097-2765(00)80250-6.

Global tuberculosis report 2023. Geneva: World Health Organisation; 2023. Licence: CC BY-NC-SA 3.0 IGO.

Goessweiner-Mohr, N., Grumet, L., Arends, K., Pavkov-Keller, T., Gruber, C.C., Gruber, K., Birner-Gruenberger, R., Kropec-Huebner, A., Huebner, J., Grohmann, E. and Keller, W. (2013). The 2.5 Å Structure of the *Enterococcus* Conjugation Protein TraM resembles VirB8 Type IV Secretion Proteins. *Journal of Biological Chemistry*, 288(3), pp.2018–2028. doi:https://doi.org/10.1074/jbc.m112.428847.

Goffin, C. and Ghuysen, J.-M. (1998). Multimodular Penicillin-Binding Proteins: An Enigmatic Family of Orthologs and Paralogs. *Microbiology and Molecular Biology Reviews*, 62(4), pp.1079–1093. doi:https://doi.org/10.1128/mmbr.62.4.1079-1093.1998.

Goffin, C. and Ghuysen, J.-M. (2002) 'Biochemistry and comparative genomics of SxxK superfamily acyltransferases offer a clue to the mycobacterial paradox: Presence of penicillin-susceptible target proteins

versus lack of efficiency of penicillin as therapeutic agent', *Microbiology and Molecular Biology Reviews*, 66(4), pp. 702–738. doi:10.1128/mmbr.66.4.702-738.2002.

Gold, M.C., Cerri, S., Smyk-Pearson, S., Cansler, M.E., Vogt, T.M., Delepine, J., Ervina Winata, Swarbrick, G., Chua, W.-J., Yu, Lantz, O., Cook, M.C., Null, M.D., Jacoby, D.B., Harriff, M.J., Lewinsohn, D.A., Hansen, T.H. and Lewinsohn, D.M. (2010). Human Mucosal Associated Invariant T Cells Detect Bacterially Infected Cells. *PLOS Biology*, 8(6), pp.e1000407–e1000407. doi:https://doi.org/10.1371/journal.pbio.1000407.

Goldberg, J.A., Kumar, V., Spencer, E.J., Hoyer, D., Marshall, S.H., Hujer, A.M., Hujer, K.M., Bethel, C.R., Papp-Wallace, K.M., Perez, F., Jacobs, M.R., David van Duin, Kreiswirth, B.N., van, Plummer, M.S. and Bonomo, R.A. (2021). A γ-lactam siderophore antibiotic effective against multidrug-resistant *Pseudomonas aeruginosa*, *Klebsiella pneumoniae*, and *Acinetobacter spp*. *European Journal of Medicinal Chemistry*, 220, pp.113436–113436. doi:https://doi.org/10.1016/j.ejmech.2021.113436.

Gong, Y., Wei, C., Wang, J., Mu, N., Lu, Q., Wu, C., Yan, N., Yang, H., Zhao, Y., Yang, X., Gurcha, S.S., Veerapen, N., Batt, S.M., Hao, Z., Da, L., Besra, G.S., Rao, Z. and Zhang, L. (2023). Structure of the priming arabinosyltransferase AftA required for AG biosynthesis of *Mycobacterium tuberculosis*. *Proceedings of the National Academy of Sciences of the United States of America*, 120(23). doi:https://doi.org/10.1073/pnas.2302858120.

González-Leiza, S.M., Miguel and Ayala, J.A. (2011). AmpH, a Bifunctional DD -Endopeptidase and DD -Carboxypeptidase of Escherichia coli. *Journal of Bacteriology*, 193(24), pp.6887–6894. doi:https://doi.org/10.1128/jb.05764-11.

Gonzalo-Asensio, J., Pérez, I., Aguiló, N., Uranga, S., Picó, A., Lampreave, C., Cebollada, A., Otal, I., Samper, S. and Martín, C. (2018). New insights into the transposition mechanisms of IS6110 and its dynamic distribution between *Mycobacterium tuberculosis* Complex lineages. *PLOS Genetics*, 14(4), p.e1007282. doi:https://doi.org/10.1371/journal.pgen.1007282.

Gordon, S.V. and Behr, M.A. (2015). Comparative mycobacteriology of the *Mycobacterium tuberculosis* complex. pp.17–29. doi:https://doi.org/10.1079/9781780643960.0017.

Gouzy, A., Healy, C., Black, K.A., Rhee, K.Y. and Ehrt, S. (2021). Growth of Mycobacterium tuberculosis at acidic pH depends on lipid assimilation and is accompanied by reduced GAPDH activity. *Proceedings of the National Academy of Sciences*, 118(32), p.e2024571118. doi:https://doi.org/10.1073/pnas.2024571118.

GOV.UK. (2022). *National quarterly report of tuberculosis in England: Quarter 3, 2022 provisional data*. [online] Available at: https://www.gov.uk/government/statistics/tuberculosis-in-england-national-quarterly-reports/national-quarterly-report-of-tuberculosis-in-england-quarter-3-2022-provisional-data.

Graham, C., Stansfeld, P., and Rodigues, C. (2023). Conservation-Colab: Consrvation to 3D structure. Github, 10.5281/zenodo.10062701

Grāve, K., Bennett, M.D. and Högbom, M. (2019). Structure of *Mycobacterium tuberculosis* phosphatidylinositol phosphate synthase reveals mechanism of substrate binding and metal catalysis. *Communications Biology*, 2(1). doi:https://doi.org/10.1038/s42003-019-0427-1.

Griffin, J. E., Pandey, A. K., Gilmore, S. A., Mizrahi, V., Mckinney, J. D., Bertozzi, C. R., and Sassetti, C. M. (2012). Cholesterol Catabolism by *Mycobacterium tuberculosis* Requires Transcriptional and Metabolic Adaptations. *Chemistry & Biology*, 19(2), pp.218–227. doi:https://doi.org/10.1016/j.chembiol.2011.12.016.

Griffin, J.E., Gawronski, J.D., DeJesus, M.A., Ioerger, T.R., Akerley, B.J. and Sassetti, C.M. (2011). High-Resolution Phenotypic Profiling Defines Genes Essential for *Mycobacterial* Growth and Cholesterol Catabolism. *PLoS Pathogens*, 7(9), p.e1002251. doi:10.1371/journal.ppat.1002251.

Grzegorzewicz, A.E., Ma, Y., Jones, V., Crick, D., Liav, A. and McNeil, M.R. (2008). Development of a microtitre plate-based assay for lipid-linked glycosyltransferase products using the mycobacterial cell wall

rhamnosyltransferase WbbL. *Microbiology*, 154(12), pp.3724–3730. doi:https://doi.org/10.1099/mic.0.2008/023366-0.

Guerin, M.E., Kaur, D., Somashekar, B.S., Gibbs, S., Gest, P., Chatterjee, D., Brennan, P.J. and Jackson, M. (2009). New Insights into the Early Steps of Phosphatidylinositol Mannoside Biosynthesis in *Mycobacteria*. 284(38), pp.25687–25696. doi:https://doi.org/10.1074/jbc.m109.030593.

Guerin, M.E., Kordulakova, J., Schaeffer, F., Svetlikova, Z., Buschiazzo, A., Giganti, D., Gicquel, B., Mikusova, K., Jackson, M. and Alzari, P.M. (2007). Molecular Recognition and Interfacial Catalysis by the Essential Phosphatidylinositol Mannosyltransferase PimA from Mycobacteria. *Journal of Biological Chemistry*, 282(28), pp.20705–20714. doi:https://doi.org/10.1074/jbc.m702087200.

Guo, R., Passi, K. and Jain, C.K. (2020). Tuberculosis Diagnostics and Localization in Chest X-Rays via Deep Learning Models. *Frontiers in Artificial Intelligence*, 3. doi:https://doi.org/10.3389/frai.2020.583427.

Gupta, A., Wood, R., Kaplan, R., Bekker, L.-G. and Lawn, S.D. (2012). Tuberculosis Incidence Rates during 8 Years of Follow-Up of an Antiretroviral Treatment Cohort in South Africa: Comparison with Rates in the Community. *PLoS ONE*, 7(3), p.e34156. doi:https://doi.org/10.1371/journal.pone.0034156.

Gupta, K, R., Gwin, C.M., Rahlwes, K.C., Biegas, K.J., Wang, C., Jin Ho Park, Liu, J., Swarts, B.M., Morita, Y. and E. Hesper Rego (2022). An essential periplasmic protein coordinates lipid trafficking and is required for asymmetric polar growth in mycobacteria. *eLife*, 11. doi:https://doi.org/10.7554/elife.80395.

Gupta, R.Kr. and Srivastava, R. (2011). Resuscitation Promoting Factors: a Family of Microbial Proteins in Survival and Resuscitation of Dormant *Mycobacteria*. *Indian Journal of Microbiology*, 52(2), pp.114–121. doi:10.1007/s12088-011-0202-6.

Gupta, S.K. and Kumari, S. (2022). Chronic recalcitrant erythema nodosum leprosum: therapeutic dilemma and role of mycobacterium indicus pranii vaccine. *Anais Brasileiros de Dermatologia*, 97(1), pp.49–53. doi:https://doi.org/10.1016/j.abd.2020.08.032.

Gurnani, C.K., Winkle, M., Martorana, A.M., Biboy, J., More, N.K., Moynihan, P.J., Banzhaf, M., Vollmer, W. and Polissi, A. (2021). ActS activates peptidoglycan amidases during outer membrane stress in *Escherichia coli*. *Molecular Microbiology*, 116(1), pp.329–342. doi:https://doi.org/10.1111/mmi.14712.

Gurnani, C.K., Winkle, M., Martorana, A.M., Biboy, J., More, N.K., Moynihan, P.J., Banzhaf, M., Vollmer, W. and Polissi, A. (2021). ActS activates peptidoglycan amidases during outer membrane stress in *Escherichia coli*. *Molecular Microbiology*, 116(1), pp.329–342. doi:https://doi.org/10.1111/mmi.14712.

Gutierrez, M.C., Brisse, S., Brosch, R., Fabre, M., Omaïs, B., Marmiesse, M., Supply, P. and Vincent, V. (2005). Ancient Origin and Gene Mosaicism of the Progenitor of *Mycobacterium tuberculosis*. *PLoS Pathogens*, [online] 1(1), p.e5. doi:https://doi.org/10.1371/journal.ppat.0010005.

Haites, R. E., Morita, Y. S., McConville, M. J., & Billman-Jacobe, H. (2005). Function of phosphatidylinositol in mycobacteria. *Journal of Biological Chemistry,* 280: 10981–10987.

Han, S., Zaniewski, R.P., Marr, E.S., Lacey, B.M., Tomaras, A.P., Evdokimov, A., Miller, J.R. and Shanmugasundaram, V. (2010). Structural basis for effectiveness of siderophore-conjugated monocarbams against clinically relevant strains of *Pseudomonas aeruginosa*. *Proceedings of the National Academy of Sciences*, 107(51), pp.22002–22007. doi:https://doi.org/10.1073/pnas.1013092107.

Hansen, J.M., Golchin, S.A., Veyrier, F.J., Domenech, P., Boneca, I.G., Azad, A.K., Murugesan, Schlesinger, L.S., Maziar Divangahi, Reed, M.B. and Behr, M.A. (2013). N-Glycolylated Peptidoglycan Contributes to the Immunogenicity but Not Pathogenicity of *Mycobacterium tuberculosis*. *The Journal of Infectious Diseases*, 209(7), pp.1045–1054. doi:https://doi.org/10.1093/infdis/jit622.

Hardy, A. (1999). Captain of death: the story of tuberculosis. *Medical History*, 43(1), pp.149–149.

Hargreaves, J.R., Boccia, D., Evans, C.A., Adato, M., Petticrew, M. and Porter, J.D.H. (2011). The Social Determinants of Tuberculosis: From Evidence to Action. *American Journal of Public Health*, [online] 101(4), pp.654–662. doi:https://doi.org/10.2105/ajph.2010.199505.

Harriff, M.J., Cansler, M.E., Toren, K.G., Canfield, E.T., Kwak, S., Gold, M.C. and Lewinsohn, D.M. (2014). Human Lung Epithelial Cells Contain *Mycobacterium tuberculosis* in a Late Endosomal Vacuole and Are Efficiently Recognized by CD8+ T Cells. *PLoS ONE*, 9(5), p.e97515. doi:https://doi.org/10.1371/journal.pone.0097515.

Harrison, J., Lloyd, G., Joe, M., Lowary, T.L., Reynolds, E., Walters-Morgan, H., Bhatt, A., Lovering, A., Besra, G.S. and Alderwick, L.J. (2016). Lcp1 Is a Phosphotransferase Responsible for Ligating Arabinogalactan to Peptidoglycan in *Mycobacterium tuberculosis*. *mBio*, 7(4). doi:10.1128/mbio.00972-16.

Hashish, E., Merwad, A., Elgaml, S., Amer, A., Kamal, H., Elsadek, A., Marei, A. and Sitohy, M. (2018). Mycobacterium marinum infection in fish and man: epidemiology, pathophysiology and management; a review. *The Veterinary Quarterly*, [online] 38(1), pp.35–46. doi:https://doi.org/10.1080/01652176.2018.1447171.

Hatfull, G.F. and Sarkis, G.J. (1993). DNA sequence, structure and gene expression of mycobacteriophage L5: a phage system for mycobacterial genetics. *Molecular Microbiology*, 7(3), pp.395–405. doi:https://doi.org/10.1111/j.1365-2958.1993.tb01131.x.

Hawe, A., Sutter, M. and Jiskoot, W. (2008). Extrinsic Fluorescent Dyes as Tools for Protein Characterization. *Pharmaceutical Research*, 25(7), pp.1487–1499. doi:https://doi.org/10.1007/s11095-007-9516-9.

Hayashi, J.M., Richardson, K., Melzer, E.S., Sandler, S.J., Aldridge, B.B., M. Sloan Siegrist and Morita, Y.S. (2018). Stress-Induced Reorganization of the Mycobacterial Membrane Domain. *MBio*, 9(1). doi:https://doi.org/10.1128/mbio.01823-17.

Healy, C., Gouzy, A. and Ehrt, S. (2020). Peptidoglycan Hydrolases RipA and Ami1 Are Critical for Replication and Persistence of *Mycobacterium tuberculosis* in the Host. *mBio*, 11(2). doi:10.1128/mbio.03315-19.

Healy, C., Gouzy, A. and Ehrt, S. (2020). Peptidoglycan Hydrolases RipA and Ami1 Are Critical for Replication and Persistence of *Mycobacterium tuberculosis* in the Host. *mBio*, 11(2). doi:https://doi.org/10.1128/mbio.03315-19.

Heidrich, C., Templin, M.F., Ursinus, A., Merdanovic, M., Berger, J., Schwarz, H., De Pedro, M.A. and Höltje, J.-V. (2001). Involvement of N-acetylmuramyl-l-alanine amidases in cell separation and antibiotic-induced autolysis of Escherichia coli. *Molecular Microbiology*, 41(1), pp.167–178. doi:https://doi.org/10.1046/j.1365-2958.2001.02499.x.

Henrieta Škovierová, Gérald Larrouy-Maumus, Zhang, J., Kaur, D., Barilone, N., Korduláková, J., Gilleron, M., Stéphanie Guadagnini, Beláňová, M., Marie-Christine Prévost, Gicquel, B., Puzo, G., Chatterjee, D., Brennan, P.J., Jérôme Nigou and Jackson, M. (2009). AftD, a novel essential arabinofuranosyltransferase from mycobacteria. *Glycobiology*, 19(11), pp.1235–1247. doi:https://doi.org/10.1093/glycob/cwp116.

Henrieta Škovierová, Larrouy-Maumus, G., Pham, H., Belanova, M., Barilone, N., Dasgupta, A., Katarína Mikušová, Gicquel, B., Gilleron, M., Brennan, P.J., Puzo, G., Jérôme Nigou and Jackson, M. (2010). Biosynthetic Origin of the Galactosamine Substituent of Arabinogalactan in *Mycobacterium tuberculosis*. 285(53), pp.41348–41355. doi:https://doi.org/10.1074/jbc.m110.188110.

Hernández, S.B., Dörr, T., Waldor, M.K. and Cava, F. (2020). Modulation of Peptidoglycan Synthesis by Recycled Cell Wall Tetrapeptides. *Cell Reports*, 31(4), p.107578. doi:https://doi.org/10.1016/j.celrep.2020.107578.

Hershkovitz, I., Donoghue, H.D., Minnikin, D.E., Besra, G.S., Lee, O.Y-C., Gernaey, A.M., Galili, E., Eshed, V., Greenblatt, C.L., Lemma, E., Bar-Gal, G.K. and Spigelman, M. (2008). Detection and Molecular

Characterization of 9000-Year-Old *Mycobacterium tuberculosis* from a Neolithic Settlement in the Eastern Mediterranean. *PLoS ONE*, [online] 3(10). doi:https://doi.org/10.1371/journal.pone.0003426.

Hett, E.C. and Rubin, E.J. (2008). Bacterial Growth and Cell Division: a Mycobacterial Perspective. *Microbiology and Molecular Biology Reviews*, [online] 72(1), pp.126–156. doi:10.1128/MMBR.00028-07.

Hett, E.C., Chao, M.C. and Rubin, E.J. (2010). Interaction and Modulation of Two Antagonistic Cell Wall Enzymes of Mycobacteria. *PLoS Pathogens*, 6(7), p.e1001020. doi:10.1371/journal.ppat.1001020.

Hodgkin, D.C. (1965). The X-ray Analysis of Complicated Molecules. *Science*, 150(3699), pp.979–988. doi:10.1126/science.150.3699.979.

Holden, E.R., Yasir, M., Turner, A.K., Wain, J., Charles, I.G. and Webber, M.A. (2021). Massively parallel transposon mutagenesis identifies temporally essential genes for biofilm formation in *Escherichia coli*. *Microbial Genomics*, [online] 7(11). doi:https://doi.org/10.1099/mgen.0.000673.

Höltje, J.-V. (1998). Growth of the Stress-Bearing and Shape-Maintaining Murein Sacculus of *Escherichia coli*. *Microbiology and Molecular Biology Reviews*, 62(1), pp.181–203. doi:https://doi.org/10.1128/mmbr.62.1.181-203.1998.

Höltje, J.V., Mirelman, D., Sharon, N. and Schwarz, U. (1975). Novel type of murein transglycosylase in Escherichia coli. *Journal of Bacteriology*, 124(3), pp.1067–1076. doi:10.1128/jb.124.3.1067-1076.1975.

Horvat, R.T. (2015). Gamma Interferon Assays Used in the Diagnosis of Tuberculosis. *Clinical and Vaccine Immunology : CVI*, [online] 22(8), pp.845–849. doi:https://doi.org/10.1128/CVI.00199-15.

Hoyland, Christopher N., Aldridge, C., Cleverley, Robert M., Duchêne, M.-C., Minasov, G., Onopriyenko, O., Sidiq, K., Stogios, Peter J., Anderson, Wayne F., Daniel, Richard A., Savchenko, A., Vollmer, W. and Lewis, Richard J. (2014). Structure of the LdcB LD-Carboxypeptidase Reveals the Molecular Basis of Peptidoglycan Recognition. *Structure*, 22(7), pp.949–960. doi:https://doi.org/10.1016/j.str.2014.04.015.

Hsu, Y.-P., Rittichier, J., Kuru, E., Yablonowski, J., Pasciak, E., Tekkam, S., Hall, E., Murphy, B., Lee, T.K., Garner, E.C., Huang, K.C., Brun, Yves V. and VanNieuwenhze, M.S. (2017). Full color palette of fluorescentd-amino acids for in situ labeling of bacterial cell walls. *Chemical Science*, 8(9), pp.6313–6321. doi:https://doi.org/10.1039/c7sc01800b.

Hughes, D.L. (2017). Patent Review of Manufacturing Routes to Fifth-Generation Cephalosporin Drugs. Part 2, Ceftaroline Fosamil and Ceftobiprole Medocaril. *Organic Process Research & Development*, 21(6), pp.800–815. doi:https://doi.org/10.1021/acs.oprd.7b00143.

Hughes, D.L. (2017). Patent Review of Manufacturing Routes to Fifth-Generation Cephalosporin Drugs. Part 1, Ceftolozane. *Organic Process Research & Development*, 21(3), pp.430–443. doi:https://doi.org/10.1021/acs.oprd.7b00033.

Hugonnet, J.-E. ., Tremblay, L.W., Boshoff, H.I., Barry, C.E. and Blanchard, J.S. (2009). Meropenem-Clavulanate Is Effective Against Extensively Drug-Resistant *Mycobacterium tuberculosis*. *Science*, 323(5918), pp.1215–1218. doi:https://doi.org/10.1126/science.1167498.

Hugonnet, J.-E. and Blanchard, J.S. (2007). Irreversible Inhibition of the *Mycobacterium tuberculosis* β-Lactamase by Clavulanate†. *Biochemistry*, 46(43), pp.11998–12004. doi:10.1021/bi701506h.

Huovinen, P. & Huovinen, S. & Jacoby, G.A. (1988) Sequence of PSE-2 beta-lactamase. *Antimicrobial Agents and Chemotherapy*, 32 (1): 134–136. doi:10.1128/aac.32.1.134.

Huszár, S., Singh, V., Polčicová, A., Baráth, P., Barrio, M.B., Lagrange, S., Leblanc, V., Nacy, C.A., Mizrahi, V. and Mikušová, K. (2017). *N* -Acetylglucosamine-1-Phosphate Transferase, WecA, as a Validated Drug

Target in *Mycobacterium tuberculosis*. *Antimicrobial Agents and Chemotherapy*, 61(11). doi:https://doi.org/10.1128/aac.01310-17.

Hutchison, C.A., Merryman, C., Sun, L., Assad-Garcia, N., Richter, R.A., Smith, H.O. and Glass, J.I. (2019). Polar Effects of Transposon Insertion into a Minimal Bacterial Genome. *Journal of Bacteriology*, 201(19). doi:https://doi.org/10.1128/jb.00185-19.

Hyoun Woo Kim, Ha Na Im, Doo Ri An, Ji Won Yoon, Jun Ho Jang, Shahriar Mobashery, Dusan Hesek, Lee, M., Yoo, J., Cui, M., Choi, S., Kim, C.-H., Nam Yong Lee, Kim, S.-J., Kim, J.-S., Bang, G., Noh, M., Byung Seok Lee, Hye Eun Yoon and Se Won Suh (2015). The Cell Shape-determining Csd6 Protein from *Helicobacter pylori* Constitutes a New Family of L,D-Carboxypeptidase. 290(41), pp.25103–25117. doi:https://doi.org/10.1074/jbc.m115.658781.

Ilona van Alen, Aleksandra Chikunova, Danny, Amber, Timmer, M., Steffen Brünle and Ubbink, M. (2023). Asp179 in the class A β-lactamase from *Mycobacterium tuberculosis* is a conserved yet not essential residue due to epistasis. □*The* □*FEBS journal*, 290(20), pp.4933–4949. doi:https://doi.org/10.1111/febs.16892.

Imada, A., Kitano, K., Kintaka, K., Muroi, M. and Asai, M. (1981). Sulfazecin and isosulfazecin, novel β-lactam antibiotics of bacterial origin. *Nature*, 289(5798), pp.590–591. doi:https://doi.org/10.1038/289590a0.

immunizationdata.who.int. (2022). *WHO Immunization Data portal*. [online] Available at: https://immunizationdata.who.int.

Iobst, S.T., Wormald, M.R., Weis, W.I., Dwek, R.A. and Drickamer, K. (1994). Binding of sugar ligands to Ca(2+)-dependent animal lectins. I. Analysis of mannose binding by site-directed mutagenesis and NMR. *Journal of Biological Chemistry*, 269(22), pp.15505–15511. doi:https://doi.org/10.1016/s0021-9258(17)40708-3.

Jacobs, C., Frère, J.-M. and Normark, S. (1997). Cytosolic Intermediates for Cell Wall Biosynthesis and Degradation Control Inducible β-Lactam Resistance in Gram-Negative Bacteria. *Cell*, 88(6), pp.823–832. doi:https://doi.org/10.1016/s0092-8674(00)81928-5.

Jacoby, G.A. (2009). AmpC -Lactamases. *Clinical Microbiology Reviews*, [online] 22(1), pp.161–182. doi:https://doi.org/10.1128/cmr.00036-08.

Jamet, S., Quentin, Y., Coudray, C., Texier, P., Laval, F., Mamadou Daffé, Gwennaele Fichant and Cam, K. (2015). Evolution of Mycolic Acid Biosynthesis Genes and Their Regulation during Starvation in *Mycobacterium tuberculosis*. *Journal of Bacteriology*, 197(24), pp.3797–3811. doi:https://doi.org/10.1128/jb.00433-15.

Jana, M., Ghosh, A., Santra, A., Kar, R.K., Misra, A.K. and Bhunia, A. (2017). Synthesis of novel muramic acid derivatives and their interaction with lysozyme: Action of lysozyme revisited. *Journal of Colloid and Interface Science*, [online] 498, pp.395–404. doi:https://doi.org/10.1016/j.jcis.2017.03.060.

Jankute, M., Cox, J.A.G., Harrison, J. and Besra, G.S. (2015). Assembly of the *Mycobacterial* Cell Wall. *Annual Review of Microbiology*, 69(1), pp.405–423. doi:https://doi.org/10.1146/annurev-micro-091014-104121.

Jaurin, B. & Grundström, T. (1981) AMPC cephalosporinase of escherichia coli K-12 has a different evolutionary origin from that of beta-lactamases of the penicillinase type. *Proceedings of the National Academy of Sciences*, 78 (8): 4897–4901. doi:10.1073/pnas.78.8.4897.

Javid, A., Cooper, C., Singh, A., Schindler, S., Hänisch, M., Marshall, R.L., Kalscheuer, R., Bavro, V.N. and Bhatt, A. (2019). The mycolic acid reductase Rv2509 has distinct structural motifs and is essential for growth in slow-growing mycobacteria. *Molecular Microbiology*, 113(2), pp.521–533. doi:https://doi.org/10.1111/mmi.14437.

Jensen, S.E. and Campbell, J.N. (1976). Peptidoglycan biosynthesis in *Micrococcus luteus* (*sodonensis*): transglycosidase and phosphodiesterase activities in membrane preparations. *Journal of Bacteriology*, 127(1), pp.309–318. doi:https://doi.org/10.1128/jb.127.1.309-318.1976.

Jin, Y., Xin, Y., Zhang, W. and Ma, Y. (2010). *Mycobacterium tuberculosis* Rv1302 and *Mycobacterium smegmatis* MSMEG-4947 have WecA function and MSMEG-4947 is required for the growth of M. smegmatis. *FEMS Microbiology Letters*, 310(1), pp.54–61. doi:https://doi.org/10.1111/j.1574-6968.2010.02045.x.

Johansen, M.D., Kasparian, J.A., Hortle, E., Britton, W.J., Purdie, A.C. and Oehlers, S.H. (2018). *Mycobacterium marinum* infection drives foam cell differentiation in zebrafish infection models. *Developmental & Comparative Immunology*, [online] 88, pp.169–172. doi:https://doi.org/10.1016/j.dci.2018.07.022.

Johnson, J.W., Fisher, J.F. and Mobashery, S. (2012). Bacterial cell-wall recycling. *Annals of the New York Academy of Sciences*, 1277(1), pp.54–75. doi:https://doi.org/10.1111/j.1749-6632.2012.06813.x.

Joint center for structural genomics (jcsg). (2009). Crystal structure of snoal-Like protein of unknown function (yp_438428.1) from *Burkholderia thailandensis* e264 at 1.60 a resolution. To be published.

Juan, C., Torrens, G., González-Nicolau, M. and Oliver, A. (2017b). Diversity and regulation of intrinsic β-lactamases from non-fermenting and other Gram-negative opportunistic pathogens. *FEMS Microbiology Reviews*, 41(6), pp.781–815. doi:https://doi.org/10.1093/femsre/fux043.

Jullian, M., Hernandez, A., Maurras, A., Puget, K., Amblard, M., Martínez, J., & Subra, G. (2009). N-terminus FITC labeling of peptides on solid support: the truth behind the spacer. Tetrahedron Letters, 50, 260-263.

K.M. Nampoothiri, R. Rubex, Patel, A.K., Narayanan, S.S., Krishna, S., Das, S.M. and Pandey, A. (2008). Molecular cloning, overexpression and biochemical characterization of hypothetical β-lactamases of *Mycobacterium tuberculosis* H37Rv. *Journal of applied microbiology*, 105(1), pp.59–67. doi:https://doi.org/10.1111/j.1365-2672.2007.03721.x.

Kaderabkova, N., Bharathwaj, M., Furniss, R.C.D., Gonzalez, D., Palmer, T. and Mavridou, D.A.I. (2022). The biogenesis of β-lactamase enzymes. *Microbiology*, 168(8). doi:https://doi.org/10.1099/mic.0.001217.

Källenius, G., Correia-Neves, M., Buteme, H., Hamasur, B. and Svenson, S.B. (2016). Lipoarabinomannan, and its related glycolipids, induce divergent and opposing immune responses to *Mycobacterium tuberculosis* depending on structural diversity and experimental variations. *Tuberculosis*, 96, pp.120–130. doi:https://doi.org/10.1016/j.tube.2015.09.005.

Kana, B.D., Gordhan, B.G., Downing, K.J., Sung, N., Vostroktunova, G., Machowski, E.E., Tsenova, L., Young, M., Kaprelyants, A., Kaplan, G. and Mizrahi, V. (2008). The resuscitation-promoting factors of *Mycobacterium tuberculosis* are required for virulence and resuscitation from dormancy but are collectively dispensable for growth in vitro. *Molecular Microbiology*, 67(3), pp.672–684. doi:10.1111/j.1365-2958.2007.06078.x.

Kanabalan, R.D., Lee, L.J., Lee, T.Y., Chong, P.P., Hassan, L., Ismail, R. and Chin, V.K. (2021). Human tuberculosis and *Mycobacterium tuberculosis* complex: A review on genetic diversity, pathogenesis and omics approaches in host biomarkers discovery. *Microbiological Research*, 246, p.126674. doi:https://doi.org/10.1016/j.micres.2020.126674.

Kandasamy, S., Palaniyandi, K., Gupta, U.D. and Narayanan, S. (2020). Double deletion of PknI/DacB2 leads to attenuation of *Mycobacterium tuberculosis* for growth and virulence. *Tuberculosis*, 123, p.101957. doi:https://doi.org/10.1016/j.tube.2020.101957.

Kang, C.-M., Nyayapathy, S., Lee, J.-Y., Suh, J.-W. and Husson, R.N. (2008). Wag31, a homologue of the cell division protein DivIVA, regulates growth, morphology and polar cell wall synthesis in mycobacteria. *Microbiology*, 154(3), pp.725–735. doi:https://doi.org/10.1099/mic.0.2007/014076-0.

Kang, S.-M. and Kim, D.-H. (2024). Structural Insights into the Penicillin-Binding Protein 4 (DacB) from *Mycobacterium tuberculosis*. *International Journal of Molecular Sciences*, 25(2), pp.983–983. doi:https://doi.org/10.3390/ijms25020983.

Kanno, A.I., Goulart, C., Leite, L.C.C., Pagliarone, A.C. and Nascimento, I.P. (2019). A Bivalent Recombinant *Mycobacterium bovis* BCG Expressing the S1 Subunit of the Pertussis Toxin Induces a Polyfunctional $CD4^{+}$T Cell Immune Response. *BioMed Research International*, 2019, pp.1–7. doi:https://doi.org/10.1155/2019/9630793.

Karl Bernhard Lehmann and Rudolf Otto Neumann (1896). *Atlas und Grundriss der Bakteriologie und Lehrbuch der speziellen bakteriologischen Diagnostik*.

Kartmann, B., Stengler, S. and Niederweis, M. (1999). Porins in the Cell Wall of *Mycobacterium tuberculosis*. *Journal of Bacteriology*, 181(20), pp.6543–6546. doi:https://doi.org/10.1128/jb.181.20.6543-6546.1999.

Katoch, K., Muniyandi, M., Singh, M., Singh, M. and Rajshekhar, K. (2021). Cost-effectiveness of incorporating *Mycobacterium indicus pranii* vaccine to multidrug therapy in newly diagnosed leprosy cases for better treatment outcomes & immunoprophylaxis in contacts as leprosy control measures for National Leprosy Eradication Programme in India. *Indian Journal of Medical Research*, 154(1), p.121. doi:https://doi.org/10.4103/ijmr.ijmr_661_20.

Kaur, D., Guerin, M.E., Škovierová, H., et al. (2009). Chapter 2 Biogenesis of the Cell Wall and Other Glycoconjugates of *Mycobacterium tuberculosis*. *Advances in Applied Microbiology*. doi:10.1016/S0065-2164(09)69002-X.

Kaur, D., Obregón-Henao, A., Pham, H., Chatterjee, D., Brennan, P.J. and Jackson, M. (2008). Lipoarabinomannan of *Mycobacterium*: Mannose capping by a multifunctional terminal mannosyltransferase. *Proceedings of the National Academy of Sciences*, 105(46), pp.17973–17977. doi:https://doi.org/10.1073/pnas.0807761105.

Kaur, P., Rausch, M., Basanti Malakar, Watson, U., Damle, N.P., Chawla, Y., Srinivasan, S., Sharma, K., Schneider, T., Gagan Deep Jhingan, Saini, D., Mohanty, D., Grein, F. and Vinay Kumar Nandicoori (2019). LipidII interaction with specific residues of *Mycobacterium tuberculosis* PknB extracytoplasmic domain governs its optimal activation. *Nature communications*, 10 (1). doi:https://doi.org/10.1038/s41467-019-09223-9.

Kaushik, A., Ammerman, N.C., Liu, J., Martins, O., Kreiswirth, B.N., Gyanu Lamichhane, Parrish, N. and Nuermberger, E.L. (2019). *In Vitro* Activity of the New β-Lactamase Inhibitors Relebactam and Vaborbactam in Combination with β-Lactams against *Mycobacterium abscessus* Complex Clinical Isolates. *Antimicrobial Agents and Chemotherapy*, 63(3). doi:https://doi.org/10.1128/aac.02623-18.

Kaushik, A., Makkar, N., Pandey, P., Parrish, N., Singh, U. and Lamichhane, G. (2015). Carbapenems and Rifampin Exhibit Synergy against *Mycobacterium tuberculosis* and *Mycobacterium abscessus*. *Antimicrobial Agents and Chemotherapy*, [online] 59(10), pp.6561–6567. doi:https://doi.org/10.1128/AAC.01158-15.

Kawai, F., Clarke, T., Roper, D.I., Gab Jo Han, Kwang Yeon Hwang, Satoru Unzai, Obayashi, E., Sam Yong Park and Tame, J.R.H. (2010). Crystal Structures of Penicillin-Binding Proteins 4 and 5 from Haemophilus influenzae. *Journal of Molecular Biology*, 396(3), pp.634–645. doi:https://doi.org/10.1016/j.jmb.2009.11.055.

Kieser, K.J. and Rubin, E.J. (2014). How sisters grow apart: mycobacterial growth and division. *Nature Reviews Microbiology*, 12(8), pp.550–562. doi:https://doi.org/10.1038/nrmicro3299.

Kieser, K.J., Baranowski, C., Chao, M.C., Long, J.E., Sassetti, C.M., Waldor, M.K., Sacchettini, J.C., Ioerger, T.R. and Rubin, E.J. (2015). Peptidoglycan synthesis in *Mycobacterium tuberculosis* is organized into networks with varying drug susceptibility. *Proceedings of the National Academy of Sciences*, 112(42), pp.13087–13092. doi:10.1073/pnas.1514135112.

Kieser, K.J., Boutte, C.C., Kester, J.C., Baer, C.E., Barczak, A.K., Meniche, X., Chao, M.C., E. Hesper Rego, Sassetti, C.M., Fortune, S.M. and Rubin, E.J. (2015b). Phosphorylation of the Peptidoglycan Synthase PonA1 Governs the Rate of Polar Elongation in *Mycobacteria*. *PLOS pathogens*, 11(6), pp.e1005010–e1005010. doi:https://doi.org/10.1371/journal.ppat.1005010.

Kieswetter, N.S., Ozturk, M., Jones, S.-S., Senzani, S., Chengalroyen, M.D., Brombacher, F., Kana, B. and Guler, R. (2021b). Deletion of N-acetylmuramyl-L-alanine amidases alters the host immune response to *Mycobacterium tuberculosis* infection. *Virulence*, 12(1), pp.1227–1238. doi:https://doi.org/10.1080/21505594.2021.1914448.

Killick, K.E., Ní Cheallaigh, C., O'Farrelly, C., Hokamp, K., MacHugh, D.E. and Harris, J. (2013). Receptor-mediated recognition of mycobacterial pathogens. *Cellular Microbiology*, [online] 15(9), pp.1484–1495. doi:https://doi.org/10.1111/cmi.12161.

Kim, D., Kim, S., Kwon, Y., Kim, Y., Park, H., Kwak, K., Lee, H., Lee, J.H., Jang, K.-M., Kim, D., Lee, S.H. and Kang, L.-W. (2023). Structural Insights for β-Lactam Antibiotics. *Biomolecules & Therapeutics*, [online] 31(2), pp.141–147. doi:https://doi.org/10.4062/biomolther.2023.008.

Kim, S.K., Dickinson, M.S., Finer-Moore, J., Guan, Z., Kaake, R.M., Echeverria, I., Chen, J., Pulido, E.H., Sali, A., Krogan, N.J., Rosenberg, O.S. and Stroud, R.M. (2023). Structure and dynamics of the essential endogenous mycobacterial polyketide synthase Pks13. *Nature Structural & Molecular Biology*. doi:https://doi.org/10.1038/s41594-022-00918-0.

Kishida, H., Satoru Unzai, Roper, D.I., Lloyd, A.J., Park, S.-Y. and Jeremy (2006). Crystal Structure of Penicillin Binding Protein 4 (dacB) from *Escherichia coli*, both in the Native Form and Covalently Linked to Various Antibiotics. 45(3), pp.783–792. doi:https://doi.org/10.1021/bi051533t.

Kitzis, M.D., Acar, J.F. and Gutmann, L. (1989). Antibacterial activity of meropenem against Gram-negative bacteria with a permeability defect and against staphylococci. *Journal of Antimicrobial Chemotherapy*, 24(suppl A), pp.125–132. doi:https://doi.org/10.1093/jac/24.suppl_a.125.

Kitzmiller, C.E., Cheng, T.-Y., Prandi, J., Sparks, I.L., D. Branch Moody and Morita, Y.S. (2024). Detergent-induced quantitatively limited formation of diacyl phosphatidylinositol dimannoside in Mycobacterium smegmatis. *Journal of lipid research*, pp.100533–100533. doi:https://doi.org/10.1016/j.jlr.2024.100533.

Kleinnijenhuis, J., Oosting, M., Joosten, L. A. B., et al. (2011) Innate Immune Recognition of *Mycobacterium tuberculosis*. *Clinical and Developmental Immunology*, 405310.

Klink, M., Brzezinska, M., Szulc, I., Brzostek, A., Kielbik, M., Sulowska, Z. and Dziadek, J. (2013). Cholesterol Oxidase Is Indispensable in the Pathogenesis of *Mycobacterium tuberculosis*. *PLoS ONE*, 8(9), p.e73333. doi:https://doi.org/10.1371/journal.pone.0073333.

Knobloch, P., Hendrik Koliwer-Brandl, Arnold, F.M., Hanna, N., Gonda, I., Adenau, S., Personnic, N., Barisch, C., Seeger, M.A., Soldati, T. and Hilbi, H. (2020). *Mycobacterium marinum* produces distinct mycobactin and carboxymycobactin siderophores to promote growth in broth and phagocytes. *Cellular microbiology*, 22(5). doi:https://doi.org/10.1111/cmi.13163.

Knott-Hunziker V, Waley SG, Orlek BS, Sammes PG. (1979). Penicillinase active sites: labelling of serine-44 in beta-lactamase I by 6beta-bromopenicillanic acid. *FEBS Lett* 99:59–61.

Kohli, M., Schiller, I., Dendukuri, N., Yao, M., Dheda, K., Denkinger, C.M., Schumacher, S.G. and Steingart, K.R. (2021). Xpert MTB/RIF Ultra and Xpert MTB/RIF assays for extrapulmonary tuberculosis and rifampicin resistance in adults. *Cochrane Database of Systematic Reviews*. doi:https://doi.org/10.1002/14651858.cd012768.pub3.

Korduláková, J., Gilleron, M., Katarína Mikušová, Puzo, G., Brennan, P.J., Gicquel, B. and Jackson, M. (2002). Definition of the First Mannosylation Step in Phosphatidylinositol Mannoside Synthesis. 277(35), pp.31335–31344. doi:https://doi.org/10.1074/jbc.m204060200.

Korza, H.J. and Matthias Bochtler (2005). *Pseudomonas aeruginosa* LD-Carboxypeptidase, a Serine Peptidase with a Ser-His-Glu Triad and a Nucleophilic Elbow*. 280(49), pp.40802–40812. doi:https://doi.org/10.1074/jbc.m506328200.

Kotani S, Yanagida I, Kato K and Matsuda T (1970). Studies on peptides, glycopeptides and antigenic polysaccharide-glycopeptide complexes isolated from an L-11 enzyme lysate of the cell walls of *Mycobacterium tuberculosis* strain H37Rv. *PubMed*, 13(4), pp.249–75.

Kovacevic, S., Anderson, D., Morita, Y. S., Patterson, J., Haites, R., McMillan, B.N., Coppel, R., McConville, M.J., & Billman-Jacobe, H. (2006). Identification of a novel protein with a role in lipoarabinomannan biosynthesis in mycobacteria. *Journal of Biological Chemistry*, 281: 9011–9017.

KREMER, L., DOVER, L.G., CARRÈRE, S., NAMPOOTHIRI, K.M., LESJEAN, S., BROWN, A.K., BRENNAN, P.J., MINNIKIN, D.E., LOCHT, C. and BESRA, G.S. (2002). Mycolic acid biosynthesis and enzymic characterization of the β-ketoacyl-ACP synthase A-condensing enzyme from *Mycobacterium tuberculosis*. *Biochemical Journal*, 364(2), pp.423–430. doi:https://doi.org/10.1042/bj20011628.
Kremer, L., Dover, L.G., Morehouse, C.B., Hitchin, P., Everett, M.G., Morris, H.R., Dell, A., Brennan, P.J., McNeil, M.R., Flaherty, C., Duncan, K. and Besra, G.S. (2001). Galactan Biosynthesis in Mycobacterium tuberculosis. 276(28), pp.26430–26440. doi:https://doi.org/10.1074/jbc.m102022200.

Kremer, L., K. Madhavan Nampoothiri, Lesjean, S., Dover, L.G., Graham, S., Betts, J., Brennan, P.J., De, M., Locht, C. and Besra, G.S. (2001). Biochemical Characterization of Acyl Carrier Protein (AcpM) and Malonyl-CoA:AcpM Transacylase (mtFabD), Two Major Components of *Mycobacterium tuberculosis* Fatty Acid Synthase II. 276(30), pp.27967–27974. doi:https://doi.org/10.1074/jbc.m103687200.

Kriakov, J., Lee, S. hee and Jacobs, W.R. (2003). Identification of a Regulated Alkaline Phosphatase, a Cell Surface-Associated Lipoprotein, in *Mycobacterium smegmatis*. *Journal of Bacteriology*, 185(16), pp.4983–4991. doi:https://doi.org/10.1128/jb.185.16.4983-4991.2003.

Kuan, R., Muskat, K., Peters, B. and Lindestam Arlehamn, C.S. (2020). Is mapping the BCG vaccine-induced immune responses the key to improving the efficacy against tuberculosis? *Journal of Internal Medicine*, 288(6), pp.651–660. doi:https://doi.org/10.1111/joim.13191.

Kuhn, M.L., Alexander, E., G. Minasov, Page, H.J., Z. Warwrzak, L. Shuvalova, Flores, K., Wilson, D.J., Shi, C., Aldrich, C.C. and Anderson, W.F. (2016). Structure of the Essential *Mtb* FadD32 Enzyme: A Promising Drug Target for Treating Tuberculosis. *ACS Infectious Diseases*, 2(8), pp.579–591. doi:https://doi.org/10.1021/acsinfecdis.6b00082.

Kühner, D., Stahl, M., Demircioglu, D.D. and Bertsche, U. (2014). From cells to muropeptide structures in 24 h: Peptidoglycan mapping by UPLC-MS. *Scientific Reports*, 4(1). doi:https://doi.org/10.1038/srep07494.

Kuk, A.C.Y., Mashalidis, E.H. and Lee, S.-Y. (2016). Crystal structure of the MOP flippase MurJ in an inward-facing conformation. *Nature Structural & Molecular Biology*, 24(2), pp.171–176. doi:10.1038/nsmb.3346.

Kulasekara, H.D. (2014). Transposon Mutagenesis. *Methods in Molecular Biology*, pp.501–519. doi:https://doi.org/10.1007/978-1-4939-0473-0_39.

Kumaragurubaran Karthik, Subramanian, S., Michael Vinoli Priyadharshini, Ayyaru Jawahar, Subbaiyan Anbazhagan, Ramaiyan Selvaraju Kathiravan, Thomas, P., R. Narendra Babu, K.G. Tirumurugaan and Gopal Dhinakar Raj (2023). Whole genome sequencing and comparative genomics of *Mycobacterium orygis* isolated from different animal hosts to identify specific diagnostic markers. *Frontiers in Cellular and Infection Microbiology*, [online] 13. doi:https://doi.org/10.3389/fcimb.2023.1302393.

Kumar, P., Arora, K., Lloyd, J.R., Lee, I.Y., Nair, V., Fischer, E., Boshoff, H.I.M. and Barry, C.E. (2012). Meropenem inhibits D, D-carboxypeptidase activity in *Mycobacterium tuberculosis*. *Molecular Microbiology*, 86(2), pp.367–381. doi:10.1111/j.1365-2958.2012.08199.x.

Kumar, P., Arora, K., Lloyd, J.R., Lee, I.Y., Nair, V., Fischer, E., Boshoff, H.I.M. and Barry, C.E. (2012). Meropenem inhibits D,D-carboxypeptidase activity in *Mycobacterium tuberculosis*. *Molecular Microbiology*, 86(2), pp.367–381. doi:https://doi.org/10.1111/j.1365-2958.2012.08199.x.

Kumar, P., Das, G. and Bhaskar, S. (2019). Mycobacterium indicus pranii therapy induces tumor regression in MyD88- and TLR2-dependent manner. *BMC Research Notes*, 12(1). doi:https://doi.org/10.1186/s13104-019-4679-0.

Kumar, P., Kaushik, A., Bell, D.T., Chauhan, V., Xia, F., Stevens, R.L. and Gyanu Lamichhane (2017). Mutation in an Unannotated Protein Confers Carbapenem Resistance in Mycobacterium tuberculosis. *Antimicrobial agents and chemotherapy*, 61(3). doi:https://doi.org/10.1128/aac.02234-16.

Kumarasiri, M., Zhang, W., Shi, Q., Fisher, J.F. and Mobashery, S. (2014). Protonation states of active-site lysines of penicillin-binding protein 6 from Escherichia coli and the mechanistic implications. *Proteins: Structure, Function, and Bioinformatics*, 82(7), pp.1348–1358. doi:10.1002/prot.24501.

Kurosu, M., Mahapatra, S., Narayanasamy, P. and Crick, D.C. (2007). Chemoenzymatic synthesis of Park's nucleotide: toward the development of high-throughput screening for MraY inhibitors. *Tetrahedron Letters*, 48(5), pp.799–803. doi:10.1016/j.tetlet.2006.11.160.

Kuru, E., Hughes, H.V., Brown, P.J., Hall, E., Tekkam, S., Cava, F., de Pedro, M.A., Brun, Y.V. and VanNieuwenhze, M.S. (2012). In Situ Probing of Newly Synthesized Peptidoglycan in Live Bacteria with Fluorescent D-Amino Acids. *Angewandte Chemie International Edition*, 51(50), pp.12519–12523. doi:https://doi.org/10.1002/anie.201206749.

Kuru, E., Radkov, A., Meng, X., Egan, A., Alvarez, L., Dowson, A., Booher, G., Breukink, E., Roper, D.I., Cava, F., Vollmer, W., Brun, Y. and VanNieuwenhze, M.S. (2019). Mechanisms of Incorporation for D-Amino Acid Probes That Target Peptidoglycan Biosynthesis. *ACS Chemical Biology*, 14(12), pp.2745–2756. doi:https://doi.org/10.1021/acschembio.9b00664.

Kuru, E., Tekkam, S., Hall, E., Brun, Y.V. and Van Nieuwenhze, M.S. (2014). Synthesis of fluorescent D-amino acids and their use for probing peptidoglycan synthesis and bacterial growth in situ. *Nature Protocols*, 10(1), pp.33–52. doi:https://doi.org/10.1038/nprot.2014.197.

Kwan, C. and Qiao, Y. (2023). Mechanistic Insights into the Activities of Major Families of Enzymes in Bacterial Peptidoglycan Assembly and Breakdown. *ChemBioChem*, 24(7). doi:https://doi.org/10.1002/cbic.202200693.

Labischinski, H., Goodell, E.W., Goodell, A. and Hochberg, M.L. (1991). Direct proof of a 'more-than-single-layered' peptidoglycan architecture of Escherichia coli W7: a neutron small-angle scattering study. *Journal of Bacteriology*, 173(2), pp.751–756. doi:https://doi.org/10.1128/jb.173.2.751-756.1991.

Lai, G.C., Cho, H. and Bernhardt, T.G. (2017). The mecillinam resistome reveals a role for peptidoglycan endopeptidases in stimulating cell wall synthesis in Escherichia coli. *PLOS Genetics*, 13(7), p.e1006934. doi:https://doi.org/10.1371/journal.pgen.1006934.

Lang, P.A., Raj, R., Tumber, A., Lohans, C.T., Rabe, P., Robinson, C.V., Brem, J. and Schofield, C.J. (2022). Studies on enmetazobactam clarify mechanisms of widely used β-lactamase inhibitors. *Proceedings of the National Academy of Sciences*, 119(18). doi:https://doi.org/10.1073/pnas.2117310119.

Larkins-Ford, J., Degefu, Y.N., Van, N., Sokolov, A. and Aldridge, B.B. (2022). Design principles to assemble drug combinations for effective tuberculosis therapy using interpretable pairwise drug response measurements. *Cell Reports. Medicine*, [online] 3(9), p.100737. doi:https://doi.org/10.1016/j.xcrm.2022.100737.

Lavollay, M., Arthur, M., Fourgeaud, M., Dubost, L., Marie, A., Veziris, N., et al. (2008). The peptidoglycan of stationary-phase *Mycobacterium tuberculosis* predominantly contains cross-links generated by L, D-transpeptidation. *J. Bacteriol.* 190, 4360–4366. doi: 10.1128/JB.00239-08.

Lebacle, C., Loriot, Y. and Irani, J. (2021). BCG-unresponsive high-grade non-muscle invasive bladder cancer: what does the practicing urologist need to know? *World Journal of Urology*. doi:https://doi.org/10.1007/s00345-021-03666-w.

LECHEVALIER, M.P. and LECHEVALIER, H. (1970). Chemical composition as a criterion in the classification of aerobic actinomycetes. *International Journal of Systematic Bacteriology*, 20(4), pp.435–443. doi:https://doi.org/10.1099/00207713-20-4-435.

Lecoq, L., Dubée, V., Sébastien Triboulet, Bougault, C.M., Jean-Emmanuel Hugonnet, Arthur, M. and Jean-Pierre Simorre (2013). Structure of *Enterococcus faecium* L,D-Transpeptidase Acylated by Ertapenem Provides Insight into the Inactivation Mechanism. 8(6), pp.1140–1146. doi:https://doi.org/10.1021/cb4001603.

Leduc, M., Frehel, C., Siegel, E. and Van Heijenoort, J. (1989). Multilayered Distribution of Peptidoglycan in the Periplasmic Space of Escherichia coli. *Microbiology*, 135(5), pp.1243–1254. doi:https://doi.org/10.1099/00221287-135-5-1243.

Lee, A., Wu, S.-W., Scherman, M.S., Torrelles, J.B., Chatterjee, D., McNeil, M.R. and Khoo, K.-H. (2006). Sequencing of Oligoarabinosyl Units Released from *Mycobacterial* Arabinogalactan by Endogenous Arabinanase: Identification of Distinctive and Novel Structural Motifs. *Biochemistry*, 45(51), pp.15817–15828. doi:https://doi.org/10.1021/bi060688d.
Lee, D., Das, S., Dawson, N.L., Dobrijevic, D., Ward, J. and Orengo, C. (2016). Novel Computational Protocols for Functionally Classifying and Characterising Serine Beta-Lactamases. *PLoS computational biology*, [online] 12(6), p.e1004926. doi:https://doi.org/10.1371/journal.pcbi.1004926.

Lee, R., Hsu, T., Huang, S., Hsieh, S., Wong, C., & Lee, Y. (2011). Survey of immune-related, mannose/fucose-binding C-type lectin receptors reveals widely divergent sugar-binding specificities. *Glycobiology*, 21 4, 512-20. https://doi.org/10.1093/glycob/cwq193.

Lee, T.K. and Huang, K.C. (2013). The role of hydrolases in bacterial cell-wall growth. *Current Opinion in Microbiology*, 16(6), pp.760–766. doi:https://doi.org/10.1016/j.mib.2013.08.005.

Lefebvre, C., Wafa Frigui, Slama, N., Françoise Lauzeral-Vizcaino, Constant, P., Lemassu, A., Parish, T., Eynard, N., Mamadou Daffé, Brosch, R. and Annaïk Quémard (2020). Discovery of a novel dehydratase of the fatty acid synthase type II critical for ketomycolic acid biosynthesis and virulence of *Mycobacterium tuberculosis*. *Scientific Reports*, 10(1). doi:https://doi.org/10.1038/s41598-020-58967-8.

Lekshmi Narendrakumar, Chakraborty, M., Kumari, S., Paul, D. and Das, B. (2023). β-Lactam potentiators to re-sensitize resistant pathogens: Discovery, development, clinical use and the way forward. 13. doi:https://doi.org/10.3389/fmicb.2022.1092556.

Lemoine, F., Domelevo Entfellner, J.-B. ., Wilkinson, E., Correia, D., Dávila Felipe, M., De Oliveira, T. and Gascuel, O. (2018). Renewing Felsenstein's Phylogenetic Bootstrap in the Era of Big Data. *Nature*, [online] 556(7702), pp.452–456. doi:https://doi.org/10.1038/s41586-018-0043-0.

Leonard, D.A., Bonomo, R.A. and Powers, R.A. (2013). CLASS D β-LACTAMASES: A RE-APPRAISAL AFTER FIVE DECADES. *Accounts of chemical research*, [online] 46(11), pp.2407–2415. doi:https://doi.org/10.1021/ar300327a.

Letunic, I. and Bork, P. (2021). Interactive Tree Of Life (iTOL) v5: an online tool for phylogenetic tree display and annotation. *Nucleic Acids Research*, 49(W1), pp.W293–W296. doi:https://doi.org/10.1093/nar/gkab301.

Levefaudes, M., Patin, D., Célia de Sousa-d'Auria, Chami, M., Didier Blanot, Hervé, M., Arthur, M., Houssin, C. and Mengin-Lecreulx, D. (2015). Diaminopimelic Acid Amidation in *Corynebacteriales*. 290(21), pp.13079–13094. doi:https://doi.org/10.1074/jbc.m115.642843.

Levitte, S., Adams, Kristin N., Berg, Russell D., Cosma, Christine L., Urdahl, Kevin B. and Ramakrishnan, L. (2016). Mycobacterial Acid Tolerance Enables Phagolysosomal Survival and Establishment of Tuberculous Infection In Vivo. *Cell Host & Microbe*, 20(2), pp.250–258. doi:https://doi.org/10.1016/j.chom.2016.07.007.

Leyh-Bouille, M. *et al.* (1970) 'LL-diaminopimelic acid containing peptidoglycans in walls of streptomyces sp. and of clostridium perfringens (type A)', *Biochemistry*, 9(15), pp. 2944–2952. doi:10.1021/bi00817a002.

Li, D. and Wu, M. (2021). Pattern recognition receptors in health and diseases. *Signal Transduction and Targeted Therapy*, 6(1), pp.1–24. doi:https://doi.org/10.1038/s41392-021-00687-0.

Li, S.-Y., Höltje, J.-V. and Young, K.D. (2004). Comparison of high-performance liquid chromatography and fluorophore-assisted carbohydrate electrophoresis methods for analyzing peptidoglycan composition of Escherichia coli. *Analytical Biochemistry*, [online] 326(1), pp.1–12. doi:https://doi.org/10.1016/j.ab.2003.11.007.

Li, W.-J., Li, D.-F., Hu, Y.-L., Zhang, X.-E., Bi, L.-J. and Wang, D.-C. (2013). Crystal structure of L,D-transpeptidase LdtMt2 in complex with meropenem reveals the mechanism of carbapenem against Mycobacterium tuberculosis. *Cell Research*, 23(5), pp.728–731. doi:https://doi.org/10.1038/cr.2013.53.

Li, Y., Wang, J., Wang, R. and Cai, Y. (2020). Double-carbapenem therapy in the treatment of multidrug resistant Gram-negative bacterial infections: a systematic review and meta-analysis. *BMC Infectious Diseases*, 20(1). doi:https://doi.org/10.1186/s12879-020-05133-0.

Li, Y., Wang, Y. and Liu, X. (2012). The Role of Airway Epithelial Cells in Response to Mycobacteria Infection. *Clinical and Developmental Immunology*, [online] 2012. doi:https://doi.org/10.1155/2012/791392.

Li, Y., Wei, Y., Guo, X., Li, X., Lu, L., Hu, L. and He, Z. (2024). Insertion sequence transposition activates anti mycobacteriophage immunity through an *lsr2*-silenced lipid metabolism gene island. *mLife*, 3(1), pp.87–100. doi:https://doi.org/10.1002/mlf2.12106.

Libby, R.L. and Holmberg, N.L. (1945). The Activity of Penicillins G and X *in Vitro*. *Science*, 102(2647), pp.303–304. doi:https://doi.org/10.1126/science.102.2647.303.

Liebenberg, D., Gordhan, B.G. and Kana, B.D. (2022). Drug resistant tuberculosis: Implications for transmission, diagnosis, and disease management. *Frontiers in Cellular and Infection Microbiology*, 12. doi:https://doi.org/10.3389/fcimb.2022.943545.

Lim, D. and Strynadka, N.C.J. (2002). Structural basis for the β lactam resistance of PBP2a from methicillin-resistant Staphylococcus aureus. *Nature Structural Biology*. doi:https://doi.org/10.1038/nsb858.

Lin, C., Chan, Vermeulen, J., Brockerman, J.A., Soni, A., Tanner, M.A., Gaynor, E.C., McIntosh, L.P., Jean-Pierre Simorre and Murphy, M.P. (2021). Peptidoglycan binding by a pocket on the accessory NTF2-domain of Pgp2 directs helical cell shape of Campylobacter jejuni. 296, pp.100528–100528. doi:https://doi.org/10.1016/j.jbc.2021.100528.

Lin, P.L. and Flynn, J.L. (2010). Understanding Latent Tuberculosis: A Moving Target. *Journal of Immunology (Baltimore, Md. : 1950)*, [online] 185(1), pp.15–22. doi:https://doi.org/10.4049/jimmunol.0903856.

Lin, X. and Kück, U. (2022). Cephalosporins as key lead generation beta-lactam antibiotics. *Applied Microbiology and Biotechnology*, [online] 106(24), pp.8007–8020. doi:https://doi.org/10.1007/s00253-022-12272-8.

Lisa, M.-N., Palacios, A.R., Aitha, M., González, M.M., Moreno, D.M., Crowder, M.W., Bonomo, R.A., Spencer, J., Tierney, D.L., Llarrull, L.I. and Vila, A.J. (2017). A general reaction mechanism for carbapenem hydrolysis by mononuclear and binuclear metallo-β-lactamases. *Nature Communications*, [online] 8(1), p.538. doi:https://doi.org/10.1038/s41467-017-00601-9.

Liu, R., Miller, P.A. and Miller, M.J. (2021). Conjugation of Aztreonam, a Synthetic Monocyclic β-Lactam Antibiotic, to a Siderophore Mimetic Significantly Expands Activity Against Gram-Negative Bacteria. *ACS Infectious Diseases*, 7(11), pp.2979–2986. doi:https://doi.org/10.1021/acsinfecdis.1c00458.

Liu, Y., Nadhira Kaffah, Sufyan Pandor, Sartain, M.J. and Larrouy-Maumus, G. (2023). Ion mobility mass spectrometry for the study of mycobacterial mycolic acids. *Scientific Reports*, 13(1). doi:https://doi.org/10.1038/s41598-023-37641-9.

Lohans, C.T. & Brem, J. & Schofield, C.J. (2017) New Delhi metallo-β-lactamase 1 catalyzes avibactam and Aztreonam hydrolysis. *Antimicrobial Agents and Chemotherapy*, 61 (12). doi:10.1128/aac.01224-17.

López-Zabalza, M. J., Sanz, S., Iriarte, A., López-Moratalla, N., & Santiago, E. (1990). Modification of skeletal S-1 with fluorescein isothiocyanate. Comparative biochemistry and physiology. B, Comparative biochemistry, 96(1), 101-5.

Loraine, J., Pu, F., Turapov, O. and Mukamolova, G.V. (2016). Development of an *In Vitro* Assay for Detection of Drug-Induced Resuscitation-Promoting-Factor-Dependent *Mycobacteria*. *Antimicrobial Agents and Chemotherapy*, 60(10), pp.6227–6233. doi:https://doi.org/10.1128/aac.00518-16.

Loudon, R.G. and Rena Marie Roberts (1967). Droplet expulsion from the respiratory tract. *PubMed*, 95(3), pp.435–42. doi:https://doi.org/10.1164/arrd.1967.95.3.435.

Lovering, A.L., de Castro, L.H., Lim, D. and Strynadka, N.C.J. (2007). Structural Insight into the Transglycosylation Step of Bacterial Cell-Wall Biosynthesis. *Science*, 315(5817), pp.1402–1405. doi:https://doi.org/10.1126/science.1136611.

Lovering, A.L., Safadi, S.S. and Strynadka, N.C.J. (2012). Structural Perspective of Peptidoglycan Biosynthesis and Assembly. *Annual Review of Biochemistry*, 81(1), pp.451–478. doi:https://doi.org/10.1146/annurev-biochem-061809-112742.

Lowary, T.L. (2016). Twenty Years of Mycobacterial Glycans: Furanosides and Beyond. 49(7), pp.1379–1388. doi:https://doi.org/10.1021/acs.accounts.6b00164.

Lu, J., Wu, T., Zhang, B., Liu, S., Song, W., Qiao, J. and Ruan, H. (2021). Types of nuclear localization signals and mechanisms of protein import into the nucleus. *Cell Communication and Signaling*, [online] 19(1). doi:https://doi.org/10.1186/s12964-021-00741-y.

Lu, Q., Zhang, W., Fang, J., Zheng, J., Dong, C. and Xiong, S. (2020). *Mycobacterium tuberculosis* Rv1096, facilitates mycobacterial survival by modulating the NF-κB/MAPK pathway as peptidoglycan N-deacetylase. *Molecular Immunology*, 127, pp.47–55. doi:https://doi.org/10.1016/j.molimm.2020.08.005.

Lu, Z., Wang, H., Zhang, A., Liu, X., Zhou, W., Yang, C., Guddat, L., Yang, H., Schofield, C.J. and Rao, Z. (2020). Structures of *Mycobacterium tuberculosis* Penicillin-Binding Protein 3 in Complex with Five β-Lactam Antibiotics Reveal Mechanism of Inactivation. *Molecular Pharmacology*, [online] 97(4), pp.287–294. doi:https://doi.org/10.1124/mol.119.118042.

Ludwiczak, P., Bordat, Y., Martin, C., Puzo, G., Gilleron, M. and Gicquel, B. (2002). *Mycobacterium tuberculosis* phoP mutant: lipoarabinomannan molecular structure. *Microbiology*, 148(10), pp.3029–3037. doi:https://doi.org/10.1099/00221287-148-10-3029.

Lunge, A. Gupta, R., Choudhary, E. and Agarwal, N. (2020). The unfoldase ClpC1 of *Mycobacterium tuberculosis* regulates the expression of a distinct subset of proteins having intrinsically disordered termini. *Journal of Biological Chemistry*, 295(28), pp.9455–9473. doi:https://doi.org/10.1074/jbc.ra120.013456.

Lupoli, T.J., Tsukamoto, H., Doud, E.H., Wang, T.-S.A., Walker, S. and Kahne, D. (2011). Transpeptidase-Mediated Incorporation of D-Amino Acids into Bacterial Peptidoglycan. *Journal of the American Chemical Society*, [online] 133(28), pp.10748–10751. doi:10.1021/ja2040656.

Ma, Y., Pan, F. and McNeil, M. (2002). Formation of dTDP-Rhamnose Is Essential for Growth of *Mycobacteria*. *Journal of Bacteriology*, 184(12), pp.3392–3395. doi:https://doi.org/10.1128/jb.184.12.3392-3395.2002.

MacGurn, J.A. and Cox, J.S. (2007). A Genetic Screen for *Mycobacterium tuberculosis* Mutants Defective for Phagosome Maturation Arrest Identifies Components of the ESX-1 Secretion System. *Infection and Immunity*, 75(6), pp.2668–2678. doi:https://doi.org/10.1128/iai.01872-06.

Macheboeuf, P. & Contreras-Martel, C. & Job, V. & et al. (2006) Penicillin binding proteins: Key players in bacterial cell cycle and drug resistance processes. *FEMS Microbiology Reviews*, 30 (5): 673–691. doi:10.1111/j.1574-6976.2006.00024.x.

Macheboeuf, P., Lemaire, D., Martins, A.D.S., Dideberg, O., Jamin, M. and Dessen, A. (2008). Trapping of an Acyl–Enzyme Intermediate in a Penicillin-binding Protein (PBP)-catalyzed Reaction. *Journal of Molecular Biology*, 376(2), pp.405–413. doi:10.1016/j.jmb.2007.10.066.

Machowski, E., Senzani, S., Ealand, C. and Kana, B. (2014). Comparative genomics for mycobacterial peptidoglycan remodelling enzymes reveals extensive genetic multiplicity. *BMC Microbiology*, 14(1), p.75. doi:10.1186/1471-2180-14-75.

Madhab Sapkota, Ravi K.R. Marreddy, Wu, X., Kumar, M. and Hurdle, J.G. (2020). The early stage peptidoglycan biosynthesis Mur enzymes are antibacterial and antisporulation drug targets for recurrent *Clostridioides difficile* infection. *Anaerobe*, 61, pp.102129–102129. doi:https://doi.org/10.1016/j.anaerobe.2019.102129.

MAEDA, H. (1980). A New Lysozyme Assay Based on Fluorescence Polarization or Fluorescence Intensity Utilizing a Fluorescent Peptidoglycan Substrate 1. *The Journal of Biochemistry*, 88(4), pp.1185–1191. doi:https://doi.org/10.1093/oxfordjournals.jbchem.a133073.

Maeda, N., Nigou, J., Herrmann, J.-L., Jackson, M., Amara, A., Lagrange, P.H., Puzo, G., Gicquel, B. and Neyrolles, O. (2002). The Cell Surface Receptor DC-SIGN Discriminates between *Mycobacterium* Species through Selective Recognition of the Mannose Caps on Lipoarabinomannan. *Journal of Biological Chemistry*, 278(8), pp.5513–5516. doi:10.1074/jbc.c200586200.

Magnet, S., Bellais, S., Dubost, L., Fourgeaud, M., Mainardi, J.-L. ., Petit-Frere, S., Marie, A., Mengin-Lecreulx, D., Arthur, M. and Gutmann, L. (2007). Identification of the L,D-Transpeptidases Responsible for Attachment of the Braun Lipoprotein to *Escherichia coli* Peptidoglycan. *Journal of Bacteriology*, 189(10), pp.3927–3931. doi:https://doi.org/10.1128/jb.00084-07.

Magnet, S., Dubost, L., Marie, A., Arthur, M. and Gutmann, L. (2008). Identification of the L,D-Transpeptidases for Peptidoglycan Cross-Linking in *Escherichia coli*. *Journal of Bacteriology*, 190(13), pp.4782–4785. doi:https://doi.org/10.1128/jb.00025-08.

Mahamaya Biswal, Lu, J. and Song, J. (2022). SARS-CoV-2 Nucleocapsid Protein Targets a Conserved Surface Groove of the NTF2-like Domain of G3BP1. *Journal of Molecular Biology/Journal of molecular biology*, 434(9), pp.167516–167516. doi:https://doi.org/10.1016/j.jmb.2022.167516.

Mahapatra, S., Crick, D.C., McNeil, M.R. and Brennan, P.J. (2007). Unique Structural Features of the Peptidoglycan of Mycobacterium leprae. *Journal of Bacteriology*, 190(2), pp.655–661. doi:10.1128/jb.00982-07.

Mahapatra, S., Piechota, C., Gil, F., Ma, Y., Huang, H., Scherman, M.S., Jones, V., Pavelka, M.S., Moniz-Pereira, J., Pimentel, M., McNeil, M.R. and Crick, D.C. (2013). Mycobacteriophage Ms6 LysA: a Peptidoglycan Amidase and a Useful Analytical Tool. *Applied and Environmental Microbiology*, 79(3), pp.768–773. doi:https://doi.org/10.1128/aem.02263-12.

Mahapatra, S., Scherman, H., Brennan, P.J. and Crick, D.C. (2005). N Glycolylation of the Nucleotide Precursors of Peptidoglycan Biosynthesis of *Mycobacterium*s pp. Is Altered by Drug Treatment. *Journal of Bacteriology*, 187(7), pp.2341–2347. doi:10.1128/jb.187.7.2341-2347.2005.

Mahapatra, S., Yagi, T., Belisle, J.T., Espinosa, B.J., Hill, P.J., McNeil, M.R., Brennan, P.J. and Crick, D.C. (2005). Mycobacterial Lipid II Is Composed of a Complex Mixture of Modified Muramyl and Peptide Moieties

Linked to Decaprenyl Phosphate. *Journal of Bacteriology*, 187(8), pp.2747–2757. doi:https://doi.org/10.1128/jb.187.8.2747-2757.2005.

Mainardi, J.-L., Fourgeaud, M., Hugonnet, J.-E., Dubost, L., Brouard, J.-P., Ouazzani, J., Rice, L.B., Gutmann, L. and Arthur, M. (2005). A Novel Peptidoglycan Cross-linking Enzyme for a β-Lactam-resistant Transpeptidation Pathway. *Journal of Biological Chemistry*, 280(46), pp.38146–38152. doi:10.1074/jbc.m507384200.

Mairi, A., Pantel, A., Sotto, A., Lavigne, J.-P. and Touati, A. (2017). OXA-48-like carbapenemases producing *Enterobacteriaceae* in different niches. *European Journal of Clinical Microbiology & Infectious Diseases*, [online] 37(4), pp.587–604. doi:https://doi.org/10.1007/s10096-017-3112-7.

Maitra, A., Munshi, T., Healy, J., Martin, L.T., Vollmer, W., Keep, N.H. and Bhakta, S. (2019). Cell wall peptidoglycan in *Mycobacterium tuberculosis*: An Achilles' heel for the TB-causing pathogen. *FEMS Microbiology Reviews*, [online] 43(5), pp.548–575. doi:10.1093/femsre/fuz016.

Malakhov, M.P., Mattern, M.R., Malakhova, O.A., Drinker, M., Weeks, S.D. and Butt, T.R. (2004). SUMO fusions and SUMO-specific protease for efficient expression and purification of proteins. *Journal of Structural and Functional Genomics*, 5(1/2), pp.75–86. doi:https://doi.org/10.1023/b:jsfg.0000029237.70316.52.
Malcolm GP Page (2007). Emerging cephalosporins. *Expert Opinion on Emerging Drugs*, 12(4), pp.511–524. doi:https://doi.org/10.1517/14728214.12.4.511.

Malhotra, K.T. and Nicholas, R.A. (1992). Substitution of lysine 213 with arginine in penicillin-binding protein 5 of *Escherichia coli* abolishes D-alanine carboxypeptidase activity without affecting penicillin binding. *Journal of Biological Chemistry*, 267(16), pp.11386–11391. doi:https://doi.org/10.1016/s0021-9258(19)49922-5.

Marblestone, J.G. (2006). Comparison of SUMO fusion technology with traditional gene fusion systems: Enhanced expression and solubility with SUMO. *Protein Science*, 15(1), pp.182–189. doi:https://doi.org/10.1110/ps.051812706.

Marrakchi, H., Ducasse, S., Labesse, G., Montrozier, H., Margeat, E., Emorine, L., Charpentier, X., Daffé, M. and QuémardA. (2002). MabA (FabG1), a *Mycobacterium tuberculosis* protein involved in the long-chain fatty acid elongation system FAS-II. *Microbiology*, 148(4), pp.951–960. doi:https://doi.org/10.1099/00221287-148-4-951.

Marrakchi, H., Lanéelle, M.-A. and Daffé, M. (2014). Mycolic Acids: Structures, Biosynthesis, and Beyond. *Chemistry & Biology*, [online] 21(1), pp.67–85. doi:https://doi.org/10.1016/j.chembiol.2013.11.011.

Martinelli, D. and Pavelka, M.S. (2016). The RipA and RipB Peptidoglycan Endopeptidases Are Individually Nonessential to *Mycobacterium smegmatis*. *Journal of Bacteriology*, 198(9), pp.1464–1475. doi:https://doi.org/10.1128/jb.00059-16.

Massova, I. and Mobashery, S. (1998). Kinship and Diversification of Bacterial Penicillin-Binding Proteins and β-Lactamases. *Antimicrobial Agents and Chemotherapy*, [online] 42(1), pp.1–17. doi:https://doi.org/10.1128/aac.42.1.1.

Matias, V.R.F., Al-Amoudi, A., Dubochet, J. and Beveridge, T.J. (2003). Cryo-Transmission Electron Microscopy of Frozen-Hydrated Sections of *Escherichia coli* and *Pseudomonas aeruginosa*. *Journal of Bacteriology*, 185(20), pp.6112–6118. doi:https://doi.org/10.1128/jb.185.20.6112-6118.2003.

Matsuhashi, M. (1966). Biosynthesis in the bacterial cell wall. *Tanpakushitsu Kakusan Koso* 11: 875–886.
Mavrici, D., Marakalala, M.J., Holton, J.M., Prigozhin, D.M., Gee, C.L., Zhang, Y.J., Rubin, E.J. and Alber, T. (2014). *Mycobacterium tuberculosis* FtsX extracellular domain activates the peptidoglycan hydrolase, RipC. *Proceedings of the National Academy of Sciences*, 111(22), pp.8037–8042. doi:https://doi.org/10.1073/pnas.1321812111.

Maya-Martinez, R., Alexander, J.A.N., Otten, C.F., Ayala, I., Vollmer, D., Gray, J., Bougault, C.M., Burt, A., Laguri, C., Fonvielle, M., Arthur, M., Strynadka, N.C.J., Vollmer, W. and Simorre, J.-P. (2019). Recognition of

Peptidoglycan Fragments by the Transpeptidase PBP4 From *Staphylococcus aureus*. *Frontiers in Microbiology*, 9. doi:10.3389/fmicb.2018.03223.

McClintock, B. (1950). The origin and behavior of mutable loci in maize. *Proceedings of the National Academy of Sciences*, 36(6), pp.344–355. doi:https://doi.org/10.1073/pnas.36.6.344.

McClintock, B. (1953). INDUCTION OF INSTABILITY AT SELECTED LOCI IN MAIZE. *Genetics*, 38(6), pp.579–599. doi:https://doi.org/10.1093/genetics/38.6.579.

McKinney, R.M., Churchill, F.C., Spillane, J.T. and Pearce, G.W. (1969). Characterization of fluorescein isothiocyanate dyes by infrared and thin-layer chromatography methods. *Analytical Biochemistry*, 29(3), pp.526–532. doi:https://doi.org/10.1016/0003-2697(69)90337-6.

McNeil, M., Daffe, M. and Brennan, P.J. (1991). Location of the mycolyl ester substituents in the cell walls of mycobacteria. *Journal of Biological Chemistry*, [online] 266(20), pp.13217–13223. doi:https://doi.org/10.1016/S0021-9258(18)98826-5.

McNeil, M., Wallner, S.J., Hunter, S.W. and Brennan, P.J. (1987). Demonstration that the galactosyl and arabinosyl residues in the cell-wall arabinogalactan of *Mycobacterium leprae* and *Mycobacterium tuberculosis* are furanoid. *Carbohydrate Research*, 166(2), pp.299–308. doi:https://doi.org/10.1016/0008-6215(87)80065-4.

Meberg, B.M., Sailer, F.C., Nelson, D.E. and Young, K.D. (2001). Reconstruction of *Escherichia coli* mrcA (PBP 1a) Mutants Lacking Multiple Combinations of Penicillin Binding Proteins. *Journal of Bacteriology*, 183(20), pp.6148–6149. doi:https://doi.org/10.1128/jb.183.20.6148-6149.2001.

Meeske, A.J., Riley, E.P., Robins, W.P., Uehara, T., Mekalanos, J.J., Kahne, D., Walker, S., Kruse, A.C., Bernhardt, T.G. and Rudner, D.Z. (2016). SEDS proteins are a widespread family of bacterial cell wall polymerases. *Nature*, 537(7622), pp.634–638. doi:10.1038/nature19331.

Mehta, S.C., Furey, I.M., Pemberton, O.A., Boragine, D.M., Chen, Y. and Palzkill, T. (2021). KPC-2 β-lactamase enables carbapenem antibiotic resistance through fast deacylation of the covalent intermediate. *Journal of Biological Chemistry*, 296, p.100155. doi:https://doi.org/10.1074/jbc.ra120.015050.

Meiresonne, N.Y., van der Ploeg, R., Hink, M.A. and den Blaauwen, T. (2017). Activity-Related Conformational Changes in D,D-Carboxypeptidases Revealed by In Vivo Periplasmic Förster Resonance Energy Transfer Assay in Escherichia coli. *mBio*, [online] 8(5). doi:https://doi.org/10.1128/mBio.01089-17.

Mekonen, H., Negesse, A., Dessie, G., Desta, M., Mihiret, G.T., Tarik, Y.D., Kitaw, T.M. and Getaneh, T. (2024). Impact of HIV coinfection on tuberculosis treatment outcomes in Ethiopia: a systematic review and meta-analysis. *BMJ Open*, [online] 14(7), p.e087218. doi:https://doi.org/10.1136/bmjopen-2024-087218.

Melanny Ika Sulistyowaty, Galih Satrio Putra, Juni Ekowati, Tri Widiandani and Matsunami, K. (2023). In silico study of phytochemicals contained in *brucea javanica* in inhibiting the InhA enzyme as antituberculosis. *Journal of Public Health in Africa*. doi:https://doi.org/10.4081/jphia.2023.2518.

Melek Özkan, Hilal Yılmaz, Pınar Ergenekon, Esra Meşe Erdoğan and Mustafa Erbakan (2024). Microbial membrane transport proteins and their biotechnological applications. *PubMed*, 40(2). doi:https://doi.org/10.1007/s11274-024-03891-6.

Melly, G., Stokas, H., Dunaj, J.L., Hsu, F., Malligarjunan Rajavel, Su, C., Yu, E. and Purdy, G.E. (2019). Structural and functional evidence that lipoprotein LpqN supports cell envelope biogenesis in *Mycobacterium tuberculosis*. *Journal of Biological Chemistry*, [online] 294(43), pp.15711–15723. doi:https://doi.org/10.1074/jbc.ra119.008781.

Melzer, E.S., Kado, T., Alam García-Heredia, Gupta, K.R., Meniche, X., Morita, Y.S., Sassetti, C.M., Rego, E.H. and Siegrist, M.S. (2022). Cell Wall Damage Reveals Spatial Flexibility in Peptidoglycan Synthesis and a Nonredundant Role for RodA in *Mycobacteria*. *Journal of Bacteriology*, 204(6). doi:https://doi.org/10.1128/jb.00540-21.

Mencarini, J., Spinicci, M., Zammarchi, L. and Bartoloni, A. (2023). Tuberculosis in the European Region. [online] doi:https://doi.org/10.1007/s40475-023-00287-8.

Meng, E.C., Goddard, T.D., Pettersen, E.F., Couch, G.S., Pearson, Z.J., Morris, J.H. and Ferrin, T.E. (2023). UCSF ChimeraX: Tools for Structure Building and Analysis. *Protein Science: A Publication of the Protein Society*, [online] 32(11), p.e4792. doi:https://doi.org/10.1002/pro.4792.

Meng, E.C., Pettersen, E.F., Couch, G.S., Huang, C.C. and Ferrin, T.E. (2006). Tools for integrated sequence-structure analysis with UCSF Chimera. *BMC Bioinformatics*, 7(1), p.339. doi:https://doi.org/10.1186/1471-2105-7-339.

Mengin-Lecreulx, D., Texier, L., Rousseau, M. and van Heijenoort, J. (1991). The murG gene of *Escherichia coli* codes for the UDP-N-acetylglucosamine: N-acetylmuramyl-(pentapeptide) pyrophosphoryl-undecaprenol N-acetylglucosamine transferase involved in the membrane steps of peptidoglycan synthesis. *Journal of Bacteriology*, 173(15), pp.4625–4636. doi:10.1128/jb.173.15.4625-4636.1991.

Menon, D., Singh, K., Pinto, S.M., Nandy, A., Jaisinghani, N., Kutum, R., Dash, D., Prasad, T.S.K. and Gandotra, S. (2019). Quantitative Lipid Droplet Proteomics Reveals *Mycobacterium tuberculosis* Induced Alterations in Macrophage Response to Infection. *ACS Infectious Diseases*, 5(4), pp.559–569. doi:https://doi.org/10.1021/acsinfecdis.8b00301.

Merck.com. (2024). *Facing global shortage, Merck commits to meeting patient demand*. [online] Available at: https://www.merck.com/stories/facing-a-global-shortage-merck-commits-to-meeting-patient-demand/ [Accessed 20 Feb. 2024].

Mesnage, S., Dellarole, M., Baxter, N.J., Rouget, J.-B., Dimitrov, J.D., Wang, N., Fujimoto, Y., Hounslow, A.M., Lacroix-Desmazes, S., Fukase, K., Foster, S.J. and Williamson, M.P. (2014). Molecular basis for bacterial peptidoglycan recognition by LysM domains. *Nature Communications*, 5(1). doi:https://doi.org/10.1038/ncomms5269.

Michel van Kempen, Kim, S., Tumescheit, C., Milot Mirdita, Lee, J., Cameron, Johannes Söding and Steinegger, M. (2023). Fast and accurate protein structure search with Foldseek. doi:https://doi.org/10.1038/s41587-023-01773-0.

Migliori GB, Centis R, D'Ambrosio L, Spanevello A, Borroni E, Cirillo DM, Sotgiu G. 2012. Totally drug-resistant and extremely drug-resistant tuberculosis: the same disease? Clinical Infectious Disease. 54:1379–1380. doi: 10.1093/cid/cis128.

Mikoulinskaia, G.V., Prokhorov, D.A., Chernyshov, S.V., Sitnikova, D.S., Arakelian, A.G. and Uversky, V.N. (2023). Conservative Tryptophan Residue in the Vicinity of an Active Site of the M15 Family L,D-Peptidases: A Key Element in the Catalysis. *International journal of molecular sciences*, [online] 24(17), pp.13249–13249. doi:https://doi.org/10.3390/ijms241713249.

Mikušová, K., Beláňová, M., Korduláková, J., Honda, K., McNeil, M.R., Mahapatra, S., Crick, D.C. and Brennan, P.J. (2006). Identification of a Novel Galactosyl Transferase Involved in Biosynthesis of the *Mycobacterial* Cell Wall. *Journal of Bacteriology*, 188(18), pp.6592–6598. doi:https://doi.org/10.1128/jb.00489-06.

Mikusová, K., Huang, H., Yagi, T., Holsters, M., Vereecke, D., D'Haeze, W., Scherman, M.S., Brennan, P.J., McNeil, M.R. and Crick, D.C. (2005). Decaprenylphosphoryl arabinofuranose, the donor of the D-arabinofuranosyl residues of mycobacterial arabinan, is formed via a two-step epimerization of decaprenylphosphoryl ribose. *Journal of bacteriology*, [online] 187(23), pp.8020–5. doi:https://doi.org/10.1128/JB.187.23.8020-8025.2005.

Mills, J.N., Motichka, K., Jucker, M., Henry H.L. Wu, Uhlik, B.C., Stern, R.M., Scherman, M.S., Vissa, V.D., Pan, F., Kundu, M., Fang, Y. and McNeil, M.R. (2004). Inactivation of the *Mycobacterial* Rhamnosyltransferase, Which Is Needed for the Formation of the Arabinogalactan-Peptidoglycan Linker, Leads to Irreversible Loss of Viability. 279(42), pp.43540–43546. doi:https://doi.org/10.1074/jbc.m407782200.

Minnikin, D.E., Lee, O.Y. and Wu, H.H.T. (2015). Pathophysiological Implications of Cell Envelope Structure in Mycobacterium tuberculosis and Related Taxa. In *Tuberculosis - Expanding Knowledge*. doi:dx.doi.org/10.5772/59585.

Mirdita, M., Schütze, K., Moriwaki, Y., Heo, L., Ovchinnikov, S. and Steinegger, M. (2022). ColabFold: making protein folding accessible to all. *Nature Methods*, [online] 19, pp.1–4. doi:https://doi.org/10.1038/s41592-022-01488-1.

Mirzayev, F., Viney, K., Linh, N.N., Gonzalez-Angulo, L., Gegia, M., Jaramillo, E., Zignol, M. and Kasaeva, T. (2020). World Health Organization recommendations on the treatment of drug-resistant tuberculosis, 2020 update. *European Respiratory Journal*, [online] 57(6). doi: https://doi.org/10.1183/13993003.03300-2020.

Mishra, A.K., Driessen, N.N., Appelmelk, B.J. and Besra, G.S. (2011). Lipoarabinomannan and related glycoconjugates: structure, biogenesis and role in *Mycobacterium tuberculosis* physiology and host–pathogen interaction. *FEMS Microbiology Reviews*, 35(6), pp.1126–1157. doi:10.1111/j.1574-6976.2011.00276.x.

Mishra, A.K., Krumbach, K., Rittmann, D., Appelmelk, B.J., Pathak, V., Pathak, A.K., Jérome Nigou, Jeroen Geurtsen, Eggeling, L. and Besra, G.S. (2011). Lipoarabinomannan biosynthesis in *Corynebacterineae*: the interplay of two α(1→2)-mannopyranosyltransferases MptC and MptD in mannan branching. *Molecular Microbiology*, 80(5), pp.1241–1259. doi:https://doi.org/10.1111/j.1365-2958.2011.07640.x.

Mohammadi, T., van Dam, V., Sijbrandi, R., Vernet, T., Zapun, A., Bouhss, A., Diepeveen-de Bruin, M., Nguyen-Distèche, M., de Kruijff, B. and Breukink, E. (2011). Identification of FtsW as a transporter of lipid-linked cell wall precursors across the membrane. *The EMBO Journal*, 30(8), pp.1425–1432. doi:10.1038/emboj.2011.61.

Montón Silva, A., Otten, C., Biboy, J., Breukink, E., VanNieuwenhze, M., Vollmer, W. and den Blaauwen, T. (2018). The Fluorescent D-Amino Acid NADA as a Tool to Study the Conditional Activity of Transpeptidases in *Escherichia coli*. *Frontiers in Microbiology*, 9. doi:https://doi.org/10.3389/fmicb.2018.02101.

Moon, T.M., D'Andréa, É.D., Lee, C.W., Soares, A., Jakoncic, J., Desbonnet, C., Garcia-Solache, M., Rice, L.B., Page, R. and Peti, W. (2018). The structures of penicillin-binding protein 4 (PBP4) and PBP5 from *Enterococci* provide structural insights into β-lactam resistance. *Journal of Biological Chemistry*, 293(48), pp.18574–18584. doi:https://doi.org/10.1074/jbc.ra118.006052.

Mora-Ochomogo, M. and Lohans, C.T. (2021). β-Lactam antibiotic targets and resistance mechanisms: from covalent inhibitors to substrates. *RSC Medicinal Chemistry*, 12(10), pp.1623–1639. doi:https://doi.org/10.1039/d1md00200g.

Morino, Y., & Tanase, S. (1978). Chemical structure of the active site of pig heart mitochondrial aspartate aminotransferase labeled with beta-chloro-l-alanine. The Journal of biological chemistry, 253(1), 252-6.

Morita, Y.S., Castro, B., Waller, R.F., Kurokawa, K., M.F. Sernee, Nakatani, F., Haites, R.E., Billman-Jacobe, H., McConville, M.J., Maeda, Y. and Kinoshita, T. (2006). PimE Is a Polyprenol-phosphate-mannose-dependent Mannosyltransferase That Transfers the Fifth Mannose of Phosphatidylinositol Mannoside in *Mycobacteria*. 281(35), pp.25143–25155. doi:https://doi.org/10.1074/jbc.m604214200.

Morlot, C., Uehara, T., Marquis, K.A., Bernhardt, T.G. and Rudner, D.Z. (2010). A highly coordinated cell wall degradation machine governs spore morphogenesis in *Bacillus subtilis*. *Genes & Development*, 24(4), pp.411–422. doi:https://doi.org/10.1101/gad.1878110.

Morris, R.P., Nguyen, L., Gatfield, J., Visconti, K., Nguyen, K., Schnappinger, D., Ehrt, S., Liu, Y., Heifets, L., Pieters, J., Schoolnik, G. and Thompson, C.J. (2005). Ancestral antibiotic resistance in Mycobacterium tuberculosis. *Proceedings of the National Academy of Sciences*, [online] 102(34), pp.12200–12205. doi:https://doi.org/10.1073/pnas.0505446102.

Moynihan, P.J. and Clarke, A.J. (2011). O-Acetylated peptidoglycan: Controlling the activity of bacterial autolysins and lytic enzymes of innate immune systems. *The International Journal of Biochemistry & Cell Biology*, 43(12), pp.1655–1659. doi:https://doi.org/10.1016/j.biocel.2011.08.007.

Moynihan, P.J., Cadby, I.T., Veerapen, N., Jankute, M., Crosatti, M., Mukamolova, G.V., Lovering, A.L. and Besra, G.S. (2019). The hydrolase LpqI primes mycobacterial peptidoglycan recycling. *Nature Communications*, 10(1). doi:https://doi.org/10.1038/s41467-019-10586-2.

Mukamolova, G.V., Obolbek Turapov, Malkin, J., Woltmann, G. and Barer, M.R. (2010). Resuscitation-promoting Factors Reveal an Occult Population of Tubercle Bacilli in Sputum. 181(2), pp.174–180. doi:https://doi.org/10.1164/rccm.200905-0661oc.

Mukonzo, J., Aklillu, E., Marconi, V. and Schinazi, R.F. (2019). Potential drug–drug interactions between antiretroviral therapy and treatment regimens for multi-drug resistant tuberculosis: Implications for HIV care of MDR-TB co-infected individuals. *International Journal of Infectious Diseases*, 83, pp.98–101. doi:https://doi.org/10.1016/j.ijid.2019.04.009.

Mullin, N.P., Hall, K.T. and Taylor, M.E. (1994). Characterization of ligand binding to a carbohydrate-recognition domain of the macrophage mannose receptor. *Journal of Biological Chemistry*, 269(45), pp.28405–28413. doi:https://doi.org/10.1016/s0021-9258(18)46942-6.

Munshi, T., Gupta, A., Evangelopoulos, D., Guzman, J.D., Gibbons, S., Keep, N.H. and Bhakta, S. (2013). Characterisation of ATP-Dependent Mur Ligases Involved in the Biogenesis of Cell Wall Peptidoglycan in Mycobacterium tuberculosis. *PLoS ONE*, 8(3), p.e60143. doi:10.1371/journal.pone.0060143.

Murphy, K.C., Nelson, S.J., Nambi, S., Papavinasasundaram, K., Baer, C.E. and Sassetti, C.M. (2018). ORBIT: a New Paradigm for Genetic Engineering of *Mycobacterial* Chromosomes. *mBio*, 9(6). doi:https://doi.org/10.1128/mbio.01467-18.

Murzyn, K., Róg, T. and Pasenkiewicz-Gierula, M. (2005). Phosphatidylethanolamine-Phosphatidylglycerol Bilayer as a Model of the Inner Bacterial Membrane. *Biophysical Journal*, 88(2), pp.1091–1103. doi:https://doi.org/10.1529/biophysj.104.048835.

Myers, J.B., Zaegel, V., Coultrap, S.J., Miller, A.P., Bayer, K.U. and Reichow, S.L. (2017). The CaMKII holoenzyme structure in activation-competent conformations. *Nature Communications*, 8(1). doi:https://doi.org/10.1038/ncomms15742.

Naas, T. & Oueslati, S. & Bonnin, R.A. & et al. (2017) Beta-lactamase database (BLDB) – structure and function. *Journal of Enzyme Inhibition and Medicinal Chemistry*, 32 (1): 917–919. doi:10.1080/14756366.2017.1344235.

Nagata, Y., Mori, K., Takagi, M., Murzin, A.G. and Damborský, J. (2001). Identification of protein fold and catalytic residues of γ-hexachlorocyclohexane dehydrochlorinase LinA. *Proteins: Structure, Function, and Bioinformatics*, 45(4), pp.471–477. doi:https://doi.org/10.1002/prot.10007.

Nakiyingi, L., Bwanika, J.M., Ssengooba, W., Mubiru, F., Nakanjako, D., Joloba, M.L., Mayanja-Kizza, H. and Manabe, Y.C. (2021). Chest X-ray interpretation does not complement Xpert MTB/RIF in diagnosis of smear-negative pulmonary tuberculosis among TB-HIV co-infected adults in a resource-limited setting. *BMC Infectious Diseases*, 21(1). doi:https://doi.org/10.1186/s12879-020-05752-7.

Nantongo, M., Nguyen, D.C., Bethel, C.R., Taracila, M.A., Li, Q., Dousa, K.M., Shin, E., Kurz, S.G., Nguyen, L., Kreiswirth, B.N., W. Henry Boom, Plummer, M.S. and Bonomo, R.A. (2024). Durlobactam, a Diazabicyclooctane β-Lactamase Inhibitor, Inhibits BlaC and Peptidoglycan Transpeptidases of *Mycobacterium tuberculosis*. *ACS infectious diseases*. doi:https://doi.org/10.1021/acsinfecdis.4c00119.

Nataraj, V., Varela, C., Javid, A., Singh, A., Besra, G.S. and Bhatt, A. (2015). Mycolic acids: deciphering and targeting the Achilles' heel of the tubercle bacillus. *Molecular Microbiology*, [online] 98(1), pp.7–16. doi:10.1111/mmi.13101.

Nath Jha, A., Vishveshwara, S. and Banavar, J.R. (2010). Amino acid interaction preferences in proteins. *Protein Science*, 19(3), pp.603–616. doi:https://doi.org/10.1002/pro.339.

NCBI (2023). *BLAST: Basic Local Alignment Search Tool*. [online] Nih.gov. Available at: https://blast.ncbi.nlm.nih.gov/Blast.cgi.

nebasechanger.neb.com. (2023). *NEBaseChanger*. [online] Available at: https://nebasechanger.neb.com.

Nel, H.J., du Plessis, N., Kleynhans, L., Loxton, A.G., van Helden, P.D. and Walzl, G. (2014). *Mycobacterium bovis* BCG infection severely delays Trichuris muris expulsion and co-infection suppresses immune responsiveness to both pathogens. *BMC Microbiology*, [online] 14(1), p.9. doi:https://doi.org/10.1186/1471-2180-14-9.

Nelson, D.E. and Young, K.D. (2001). Contributions of PBP 5 and dd -Carboxypeptidase Penicillin Binding Proteins to Maintenance of Cell Shape in *Escherichia coli*. *Journal of Bacteriology*, 183(10), pp.3055–3064. doi:https://doi.org/10.1128/jb.183.10.3055-3064.2001.

Nelson, D.E. and Young, K.D. (2001). Contributions of PBP 5 and DD-Carboxypeptidase Penicillin Binding Proteins to Maintenance of Cell Shape in *Escherichia coli*. *Journal of Bacteriology*, 183(10), pp.3055–3064. doi:https://doi.org/10.1128/jb.183.10.3055-3064.2001.

Nemmara, V.V., Dzhekieva, L., Subarno Sarkar, K., Adediran, S.A., Duez, C., Nicholas, R.A. and Pratt, R.F. (2011). Substrate Specificity of Low-Molecular Mass Bacterial DD-Peptidases. *Biochemistry*, 50(46), pp.10091–10101. doi:https://doi.org/10.1021/bi201326a.

Neu, H.C. (1974). Cefoxitin, a Semisynthetic Cephamycin Antibiotic: Antibacterial Spectrum and Resistance to Hydrolysis by Gram-Negative Beta-Lactamases. *Antimicrobial Agents and Chemotherapy*, 6(2), pp.170–176. doi:https://doi.org/10.1128/aac.6.2.170.

Neuhoff, V., Stamm, R. and Eibl, H. (1985). Clear background and highly sensitive protein staining with Coomassie Blue dyes in polyacrylamide gels: A systematic analysis. *Electrophoresis*, 6(9), pp.427–448. doi:https://doi.org/10.1002/elps.1150060905.

Ngadjeua, F., Braud, E., Saidbakhrom Saidjalolov, Iannazzo, L., Schnappinger, D., Ehrt, S., Jean-Emmanuel Hugonnet, Mengin-Lecreulx, D., Patin, D., Mélanie Ethève-Quelquejeu, Fonvielle, M. and Arthur, M. (2018). Critical Impact of Peptidoglycan Precursor Amidation on the Activity of L,D-Transpeptidases from *Enterococcus faecium* and *Mycobacterium tuberculosis*. *Chemistry - A European Journal*, 24(22), pp.5743–5747. doi:https://doi.org/10.1002/chem.201706082.

Ngadjeua, F., Braud, E., Saidbakhrom Saidjalolov, Iannazzo, L., Schnappinger, D., Ehrt, S., Jean-Emmanuel Hugonnet, Mengin-Lecreulx, D., Patin, D., Mélanie Ethève-Quelquejeu, Fonvielle, M. and Arthur, M. (2018). Critical Impact of Peptidoglycan Precursor Amidation on the Activity of l,d-Transpeptidases from *Enterococcus faecium* and *Mycobacterium tuberculosis*. *Chemistry - A European Journal*, 24(22), pp.5743–5747. doi:https://doi.org/10.1002/chem.201706082.

Nguyen, L. and Thompson, C., 2006. Foundations of antibiotic resistance in bacterial physiology: the mycobacterial paradigm. *Trends in Microbiology*, 14(7), pp.304-312.

Nguyen, P.P., Kado, T., Prithviraj, M., Siegrist, M.S. and Morita, Y.S. (2022). Inositol acylation of phosphatidylinositol mannosides: a rapid mass response to membrane fluidization in mycobacteria. *Journal of Lipid Research*, 63(9), p.100262. doi:https://doi.org/10.1016/j.jlr.2022.100262.

NICE (2024). *Overview | Tuberculosis | Guidance | NICE*. [online] Nice.org.uk. Available at: https://www.nice.org.uk/guidance/NG33.

NICE. (2024). *BNF is only available in the UK*. [online] Available at: https://bnf.nice.org.uk/treatment-summaries/cephalosporins/#:~:text=Cefotaxime%2C%20ceftazidime%20and%20ceftriaxone%20are [Accessed 9 Mar. 2024].

Nickels, J.D., Chatterjee, S., Barmak Mostofian, Stanley, C.B., Ohl, M., Piotr Zolnierczuk, Schulz, R., Dean, Standaert, R.F., Elkins, J.G., Cheng, X. and Katsaras, J. (2017). *Bacillus subtilis* Lipid Extract, A Branched-Chain Fatty Acid Model Membrane. □*The* □*journal of physical chemistry letters*, 8(17), pp.4214–4217. doi:https://doi.org/10.1021/acs.jpclett.7b01877.

Nicola, G., Fedarovich, A., Nicholas, R.A. and Davies, C.J. (2005). A large displacement of the SXN motif of Cys115-modified penicillin-binding protein 5 from *Escherichia coli*. 392(1), pp.55–63. doi:https://doi.org/10.1042/bj20050449.

Nicola, G., Tomberg, J., Pratt, R.F., Nicholas, R.A. and Davies, C. (2010). Crystal Structures of Covalent Complexes of β-Lactam Antibiotics with *Escherichia coli* Penicillin-Binding Protein 5: Toward an Understanding of Antibiotic Specificity. *Biochemistry*, 49(37), pp.8094–8104. doi:https://doi.org/10.1021/bi100879m.

Niederweis, M., Danilchanka, O., Huff, J., Hoffmann, C. and Engelhardt, H. (2010b). Mycobacterial outer membranes: in search of proteins. *Trends in Microbiology*, 18(3), pp.109–116. doi:https://doi.org/10.1016/j.tim.2009.12.005.

Nigou, J., Gilleron, M., Rojas, M., García, L.F., Thurnher, M. and Puzo, G. (2002). *Mycobacterial* lipoarabinomannans: modulators of dendritic cell function and the apoptotic response. *Microbes and Infection*, 4(9), pp.945–953. doi:10.1016/s1286-4579(02)01621-0.

Nikitushkin, V.D., Demina, G.R., Shleeva, M.O., Guryanova, S.V., Ruggiero, A., Berisio, R. and Kaprelyants, A.S. (2015). A product of RpfB and RipA joint enzymatic action promotes the resuscitation of dormant mycobacteria. *FEBS Journal*, 282(13), pp.2500–2511. doi:10.1111/febs.13292.

Nordmann, P., Bouvier, M. and Laurent Poirel (2023). Efficacy of ceftazidime-avibactam, meropenem-vaborbactam, and imipenem-relebactam combinations against carbapenemase-producing *Enterobacterales* in Switzerland. *European Journal of Clinical Microbiology & Infectious Diseases*, 42(9), pp.1145–1152. doi:https://doi.org/10.1007/s10096-023-04647-0.

Nowiński, A., S Wesołowski and Korzeniewska-Koseła, M. (2023). The impact of comorbidities on tuberculosis treatment outcomes in Poland: a national cohort study. *Frontiers in Public Health*, 11. doi:https://doi.org/10.3389/fpubh.2023.1253615.

Odone, A., Amadasi, S., White, R.G., Cohen, T., Grant, A.D. and Houben, R.M.G.J. (2014). The Impact of Antiretroviral Therapy on Mortality in HIV Positive People during Tuberculosis Treatment: A Systematic Review and Meta-Analysis. *PLoS ONE*, 9(11), p.e112017. doi:https://doi.org/10.1371/journal.pone.0112017.

Ohnishi, R., Ishikawa, S. and Sekiguchi, J. (1999). Peptidoglycan Hydrolase LytF Plays a Role in Cell Separation with CwlF during Vegetative Growth of *Bacillus subtilis*. *Journal of Bacteriology*, 181(10), pp.3178–3184. doi:https://doi.org/10.1128/jb.181.10.3178-3184.1999.

Okafor, C.N., Rewane, A. and Momodu, I.I. (2020). *Bacillus Calmette Guerin (BCG)*. [online] PubMed. Available at: https://www.ncbi.nlm.nih.gov/books/NBK538185/.

Okamoto, M.P., Nakahiro, R.K., Chin, A., Bedikian, A. and Gill, M.A. (1994). Cefepime: A new fourth-generation cephalosporin. *American Journal of Health-System Pharmacy*, 51(4), pp.463–477. doi:https://doi.org/10.1093/ajhp/51.4.463.

Olivença, F., Ferreira, C., Nunes, A., Silveiro, C., Pimentel, M., Gomes, J.P. and Catalão, M.J. (2022). Identification of drivers of mycobacterial resistance to peptidoglycan synthesis inhibitors. *Frontiers in Microbiology*, 13. doi:https://doi.org/10.3389/fmicb.2022.985871.

Osborn, M., Stachulski, N., Sun, H., Blais, J., Venishetty, V., Raccuglia, M., Kankam, M., Colvin, R. and Segal, F. (2019). A First-in-Human Study To Assess the Safety and Pharmacokinetics of LYS228, a Novel Intravenous

Monobactam Antibiotic in Healthy Volunteers. *Antimicrobial Agents and Chemotherapy*, [online] 63(7). doi:https://doi.org/10.1128/AAC.02592-18.

Ouellette, M., Bissonnette, L. and Roy, P.H. (1987). Precise insertion of antibiotic resistance determinants into Tn21-like transposons: nucleotide sequence of the OXA-1 beta-lactamase gene. *Proceedings of the National Academy of Sciences*, 84(21), pp.7378–7382. doi:https://doi.org/10.1073/pnas.84.21.7378.

Pan, W., Lyness Matizirofa, Workman, L., Hawkridge, T., Hanekom, W.A., Mahomed, H., Hussey, G. and Hatherill, M. (2009). Comparison of Mantoux and Tine Tuberculin Skin Tests in BCG-Vaccinated Children Investigated for Tuberculosis. *PLOS ONE*, 4(11), pp.e8085–e8085. doi:https://doi.org/10.1371/journal.pone.0008085.

Panas, M.D., Ahola, T. and McInerney, G.M. (2014). The C-Terminal Repeat Domains of nsP3 from the Old World Alphaviruses Bind Directly to G3BP. *Journal of Virology*, [online] 88(10), pp.5888–5893. doi:https://doi.org/10.1128/jvi.00439-14.

Panas, M.D., Schulte, T., Thaa, B., Sandalova, T., Kedersha, N., Achour, A. and McInerney, G.M. (2015). Viral and Cellular Proteins Containing FGDF Motifs Bind G3BP to Block Stress Granule Formation. *PLOS Pathogens*, 11(2), p.e1004659. doi:https://doi.org/10.1371/journal.ppat.1004659.

Panas, M.D., Varjak, M., Lulla, A., Er Eng, K., Merits, A., Karlsson Hedestam, G.B. and McInerney, G.M. (2012). Sequestration of G3BP coupled with efficient translation inhibits stress granules in Semliki Forest virus infection. *Molecular Biology of the Cell*, 23(24), pp.4701–4712. doi:https://doi.org/10.1091/mbc.e12-08-0619.

Pandey, N. and Cascella, M. (2019). *Beta Lactam Antibiotics*. [online] Nih.gov. Available at: https://www.ncbi.nlm.nih.gov/books/NBK545311/.

Pandey, S.D., Pal, S., Kumar N, G., Bansal, A., Mallick, S. and Ghosh, A.S. (2018). Two DD-Carboxypeptidases from Mycobacterium smegmatis Affect Cell Surface Properties through Regulation of Peptidoglycan Cross-Linking and Glycopeptidolipids. *Journal of Bacteriology*, 200 (14). doi:10.1128/jb.00760-17.

Pandey, S.D., Pal, S., Kumar N, G., Bansal, A., Mallick, S. and Ghosh, A.S. (2018). Two DD - Carboxypeptidases from *Mycobacterium smegmatis* Affect Cell Surface Properties through Regulation of Peptidoglycan Cross-Linking and Glycopeptidolipids. *Journal of Bacteriology*, 200(14). doi:https://doi.org/10.1128/jb.00760-17.

Papp-Wallace, K.M., Endimiani, A., Taracila, M.A. and Bonomo, R.A. (2011). Carbapenems: Past, Present, and Future. *Antimicrobial Agents and Chemotherapy*, 55(11), pp.4943–4960. doi:https://doi.org/10.1128/aac.00296-11.

Park, S. and Cho, H. (2022). The Tol-Pal System Plays an Important Role in Maintaining Cell Integrity During Elongation in *Escherichia coli*. *Frontiers in Microbiology*, 13. doi:https://doi.org/10.3389/fmicb.2022.891926.

Park, Y., Taguchi, A., Vadim Baidin, Kahne, D. and Walker, S. (2023). A Time-Resolved FRET Assay Identifies a Small Molecule that Inhibits the Essential Bacterial Cell Wall Polymerase FtsW. 62(25). doi:https://doi.org/10.1002/anie.202301522.

Pasipanodya, J.G. and Gumbo, T. (2013). A Meta-Analysis of Self-Administered vs Directly Observed Therapy Effect on Microbiologic Failure, Relapse, and Acquired Drug Resistance in Tuberculosis Patients. *Clinical Infectious Diseases*, 57(1), pp.21–31. doi:https://doi.org/10.1093/cid/cit167.

Patel, P.M., Camps, N., Rivera, C.I., Tuda, C. and VanOstran, G. (2022). *Mycobacterium marinum* Infection and Interferon-Gamma Release Assays Cross-Reactivity: A Case Report. *Cureus*. doi:https://doi.org/10.7759/cureus.21420.

PaweŁczyk, J. and Kremer, L. (2014). The Molecular Genetics of Mycolic Acid Biosynthesis. *Microbiology Spectrum*, 2(4). doi:https://doi.org/10.1128/microbiolspec.mgm2-0003-2013.

Payen, M.C., De Wit, S., Martin, C., Sergysels, R., Muylle, I., Van Laethem, Y. and Clumeck, N. (2012). Clinical use of the meropenem-clavulanate combination for extensively drug-resistant tuberculosis [Case study]. *The International Journal of Tuberculosis and Lung Disease*, 16(4), pp.558–560. doi:https://doi.org/10.5588/ijtld.11.0414.

pebble (2020). *Rv3593 (lpqF*. [online] Rockefeller.edu. Available at: https://pebble.rockefeller.edu/genes/H37Rv/RVBD3593/# [Accessed 18 Aug. 2024].

Peddireddy, V., Doddam, S.N. and Ahmed, N. (2017). Mycobacterial Dormancy Systems and Host Responses in Tuberculosis. *Frontiers in Immunology*, [online] 8. doi:10.3389/fimmu.2017.00084.

Peitsaro, N., Polianskyte, Z., Tuimala, J., Pörn-Ares, I., Liobikas, J., Speer, O., Lindholm, D., Thompson, J. and Eriksson, O. (2008). Evolution of a family of metazoan active-site-serine enzymes from penicillin-binding proteins: a novel facet of the bacterial legacy. *BMC Evolutionary Biology*, 8(1), p.26. doi:https://doi.org/10.1186/1471-2148-8-26.

Peng, W., Zou, L., Suresh Bhamidi, McNeil, M.R. and Lowary, T.L. (2012). The Galactosamine Residue in *Mycobacterial* Arabinogalactan Is α-Linked. *The Journal of Organic Chemistry*, 77(21), pp.9826–9832. doi:https://doi.org/10.1021/jo301393s.

Perkowski, E.F., Zulauf, K.E., D. Weerakoon, Hayden, J.D., Ioerger, T.R., Oreper, D., Gomez, S.M., Sacchettini, J.C. and Braunstein, M. (2017). The EXIT Strategy: an Approach for Identifying Bacterial Proteins Exported during Host Infection. 8(2). doi:https://doi.org/10.1128/mbio.00333-17.

Persat, A., Stone, H.A. and Gitai, Z. (2014). The curved shape of *Caulobacter crescentus* enhances surface colonization in flow. *Nature Communications*, 5(1). doi:https://doi.org/10.1038/ncomms4824.

Peters, K., Kannan, S., Rao, V.A., Biboy, J., Vollmer, D., Erickson, S.W., Lewis, R.J., Young, K.D. and Vollmer, W. (2016). The Redundancy of Peptidoglycan Carboxypeptidases Ensures Robust Cell Shape Maintenance in *Escherichia coli*. *mBio*, [online] 7(3). doi:https://doi.org/10.1128/mbio.00819-16.

Phil Hogarth & Jasson Sawyer. (2023). aphascience.blog.gov.uk. *New APHA tools for the fight against bovine TB - APHA Science Blog*. [online] Available at: https://aphascience.blog.gov.uk/2023/03/24/tb-day-2023/.

Philippon, A., Arlet, G., Labia, R. and Iorga, B.I. (2022). Class C β-Lactamases: Molecular Characteristics. *Clinical Microbiology Reviews*, 35(3). doi:https://doi.org/10.1128/cmr.00150-21.

Piddock, L.J.V., Williams, K.J. and Ricci, V. (2000). Accumulation of rifampicin by *Mycobacterium aurum*, Mycobacterium *smegmatis* and *Mycobacterium tuberculosis. Journal of Antimicrobial Chemotherapy, 45(2),* pp.159–165. doi:https://doi.org/10.1093/jac/45.2.159.

Pidgeon, S.E., Apostolos, A.J., Nelson, J.M., Shaku, M., Rimal, B., Islam, M.N., Crick, D.C., Kim, S.J., Pavelka, M.S., Kana, B.D. and Pires, M.M. (2019). L,D-Transpeptidase Specific Probe Reveals Spatial Activity of Peptidoglycan Cross-Linking. *ACS Chemical Biology*. doi:10.1021/acschembio.9b00427.

Pisabarro, A.G., de Pedro, M.A. and Vázquez, D. (1985). Structural modifications in the peptidoglycan of *Escherichia coli* associated with changes in the state of growth of the culture. *Journal of Bacteriology*, 161(1), pp.238–242. doi:https://doi.org/10.1128/jb.161.1.238-242.1985.

Pizarro, R.A., Fernanáez, R.O. and Orce, L.V. (1988). Peptidoglycan hydrolases in an autolytic mutant of *Salmonella typhimurium*. *Archives Internationales de Physiologie et de Biochimie*, 96(3), pp.171–177. doi:https://doi.org/10.3109/13813458809075941.

Poirel, L., Potron, A. and Nordmann, P. (2012). OXA-48-like carbapenemases: the phantom menace. *Journal of Antimicrobial Chemotherapy*, 67(7), pp.1597–1606. doi:https://doi.org/10.1093/jac/dks121.

Popham, D.L., Gilmore, M.E. and Setlow, P. (1999). Roles of Low-Molecular-Weight Penicillin-Binding Proteins in *Bacillus subtilis* Spore Peptidoglycan Synthesis and Spore Properties. *Journal of Bacteriology*, 181(1), pp.126–132. doi:https://doi.org/10.1128/jb.181.1.126-132.1999.

Porfírio, S., Carlson, R. and Azadi, P., 2019. Elucidating Peptidoglycan Structure: An Analytical Toolset. *Trends in Microbiology*, 27(7), pp.653-654.

Porter, C.J., Bantwal, R., Bannam, T.L., Rosado, C.J., Pearce, M.C., Adams, V., Lyras, D., Whisstock, J.C. and Rood, J.I. (2011). The conjugation protein TcpC from Clostridium perfringens is structurally related to the type IV secretion system protein VirB8 from Gram-negative bacteria. *Molecular Microbiology*, 83(2), pp.275–288. doi:https://doi.org/10.1111/j.1365-2958.2011.07930.x.

Portevin, D., de Sousa-D'Auria, C., Houssin, C., Grimaldi, C., Chami, M., Daffe, M. and Guilhot, C. (2003). A polyketide synthase catalyzes the last condensation step of mycolic acid biosynthesis in mycobacteria and related organisms. *Proceedings of the National Academy of Sciences*, 101(1), pp.314–319. doi:https://doi.org/10.1073/pnas.0305439101.

Potron, A., Poirel, L. and Nordmann, P. (2015). Emerging broad-spectrum resistance in *Pseudomonas aeruginosa* and *Acinetobacter baumannii* : Mechanisms and epidemiology. *International Journal of Antimicrobial Agents*, 45(6), pp.568–585. doi:https://doi.org/10.1016/j.ijantimicag.2015.03.001.

Pradhan, G., Pattnaik, M., Sethy, H., Patnaik, J., Mohanty, T. and Giri, P. (2019). Diagnosis and treatment of pulmonary tuberculosis in one day : Way forward for END TB Strategy 2015. *Journal of Family Medicine and Primary Care*, 8(1), p.184. doi:https://doi.org/10.4103/jfmpc.jfmpc_358_16.

Pratt, R.F. and McLeish, M.J. (2010). Structural relationship between the active sites of β-lactam-recognizing and amidase signature enzymes: convergent evolution? *Biochemistry*, [online] 49(45), pp.9688–9697. doi:https://doi.org/10.1021/bi1012222.

Pray, L. (2013). *Transposons | Learn Science at Scitable*. [online] Nature.com. Available at: https://www.nature.com/scitable/topicpage/transposons-the-jumping-genes-518/.

Prigozhin, D.M., Krieger, I.V., Huizar, J.P., Mavrici, D., Waldo, G.S., Hung, L.-W., Sacchettini, J.C., Terwilliger, T.C. and Alber, T. (2014). Subfamily-Specific Adaptations in the Structures of Two Penicillin-Binding Proteins from *Mycobacterium tuberculosis*. *PLoS ONE*, 9(12), p.e116249. doi:https://doi.org/10.1371/journal.pone.0116249.

Prosser, G.A. and Carvalho, L.P.S. (2013). Kinetic mechanism and inhibition of *Mycobacterium tuberculosis* D-alanine: D-alanine ligase by the antibiotic D-cycloserine. *The FEBS Journal*, 280(4), pp.1150–1166. doi:10.1111/febs.12108.

Pryka, R.D. and Haig, G.M. (1994). Meropenem: a new carbapenem antimicrobial. *The Annals of Pharmacotherapy*, [online] 28(9), pp.1045–1054. doi:https://doi.org/10.1177/106002809402800910.
Qiao, Y., Lebar, M.D., Schirner, K., Schaefer, K., Tsukamoto, H., Kahne, D. and Walker, S. (2014). Detection of Lipid-Linked Peptidoglycan Precursors by Exploiting an Unexpected Transpeptidase Reaction. *Journal of the American Chemical Society*, 136(42), pp.14678–14681. doi:https://doi.org/10.1021/ja508147s.

Qin, L., Gao, S., Wang, J., Zheng, R., Lu, J. and Hu, Z. (2013). The Conservation and Application of Three Hypothetical Protein Coding Gene for Direct Detection of *Mycobacterium tuberculosis* in Sputum Specimens. *PLoS ONE*, 8(9), p.e73955. doi:https://doi.org/10.1371/journal.pone.0073955.

Qin, Z.Z., Ahmed, S., Sarker, M.S., Paul, K., Adel, A.S.S., Naheyan, T., Barrett, R., Banu, S. and Creswell, J. (2021). Tuberculosis detection from chest x-rays for triaging in a high tuberculosis-burden setting: an evaluation of five artificial intelligence algorithms. *The Lancet Digital Health*, [online] 3(9), pp.e543–e554. doi:https://doi.org/10.1016/S2589-7500(21)00116-3.

Rahman, K., Jamal, M., Chen, X., Zhou, W., Yang, B., Zou, Y., Xu, W., Lei, Y., Wu, C., Cao, X., Tyagi, R., Naeem, M.A., Lin, D., Habib, Z., Peng, N., Fu, Z.F. and Cao, G. (2021). Reprogramming *Mycobacterium*

tuberculosis CRISPR System for Gene Editing and Genome-wide RNA Interference Screening. *Genomics, Proteomics & Bioinformatics*. [online] doi:https://doi.org/10.1016/j.gpb.2021.01.008.

Rajaram, M.V.S., Brooks, M.N., Morris, J.D., Torrelles, J.B., Azad, A.K. and Schlesinger, L.S. (2010). *Mycobacterium tuberculosis* Activates Human Macrophage Peroxisome Proliferator-Activated Receptor Linking Mannose Receptor Recognition to Regulation of Immune Responses. *The Journal of Immunology*, 185(2), pp.929–942. doi:https://doi.org/10.4049/jimmunol.1000866.

Ramakrishnan, L., Tran, H.T., Federspiel, N.A. and Falkow, S. (1997). A crtB homolog essential for photochromogenicity in *Mycobacterium marinum*: isolation, characterization, and gene disruption via homologous recombination. *Journal of bacteriology*, 179(18), pp.5862–5868. doi:https://doi.org/10.1128/jb.179.18.5862-5868.1997.

Rana, A.K., Singh, A., Gurcha, S.S., Cox, L.R., Bhatt, A. and Besra, G.S. (2012). Ppm1-Encoded Polyprenyl Monophosphomannose Synthase Activity Is Essential for Lipoglycan Synthesis and Survival in Mycobacteria. *PLoS ONE*, 7(10), p.e48211. doi:https://doi.org/10.1371/journal.pone.0048211.

Rastoder, E., Shaker, S.B., Naqibullah, M., Wille, M.M.W., Lund, M., Wilcke, J.T., Seersholm, N. and Jensen, S.G. (2019). Chest x-ray findings in tuberculosis patients identified by passive and active case finding: A retrospective study. *Journal of Clinical Tuberculosis and Other Mycobacterial Diseases*, 14, pp.26–30. doi:https://doi.org/10.1016/j.jctube.2019.01.003.

Raymond, J.B., Mahapatra, S., Crick, D.C. and Pavelka, M.S. (2004). Identification of thenamHGene, Encoding the Hydroxylase Responsible for the N-Glycolylation of the *Mycobacterial* Peptidoglycan. *Journal of Biological Chemistry*, 280(1), pp.326–333. doi:https://doi.org/10.1074/jbc.m411006200.

Raz, A., Talay, S.R. and Fischetti, V.A. (2012). Cellular aspects of the distinct M protein and SfbI anchoring pathways in Streptococcus pyogenes. *Molecular Microbiology*, 84(4), pp.631–647. doi:https://doi.org/10.1111/j.1365-2958.2012.08047.x.

Reddi, P.P., Amin, A.G., Khandekar, P.S. and Talwar, G.P. (1994). Molecular definition of unique species status of *Mycobacterium* w; a candidate leprosy vaccine strain. *PubMed*, 62(2), pp.229–36.

Ren, H., Dover, L.G., Islam, S.T., Alexander, D.C., Chen, J.M., Besra, G.S. and Liu, J. (2007). Identification of the lipooligosaccharide biosynthetic gene cluster from *Mycobacterium marinum*. *Molecular Microbiology*, 63(5), pp.1345–1359. doi:https://doi.org/10.1111/j.1365-2958.2007.05603.x.

Reuper, H., Amari, K. and Krenz, B. (2021). Analyzing the G3BP-like gene family of *Arabidopsis thaliana* in early turnip mosaic virus infection. *Scientific Reports*, 11(1). doi:https://doi.org/10.1038/s41598-021-81276-7.

Reva, O., Korotetskiy, I., and Ilin, A. (2015) Role of the horizontal gene exchange in evolution of pathogenic *Mycobacteria*. BMC Evol Biol 15 Suppl 1: S2.

Ribbeck, K. (1998). NTF2 mediates nuclear import of Ran. *The EMBO Journal*, 17(22), pp.6587–6598. doi:https://doi.org/10.1093/emboj/17.22.6587.

Rich, M., Khan, U., Zeng, C., LaHood, A., Franke, M.F., Atwood, S., Mathieu Bastard, Erlina Burhan, Danielyan, N., Dzhazibekova, P.M., Demekech Gadissa, Ghafoor, A., Hewison, C., Mahmud İslam, Kazmi, E., Khan, P., Lecca, L., Llang Bridget Maama, Melikyan, N. and Ye Yint Naing (2023). Outcomes of WHO-conforming, longer, all-oral multidrug-resistant TB regimens and analysis implications. *International Journal of Tuberculosis and Lung Disease*, 27(6), pp.451–457. doi:https://doi.org/10.5588/ijtld.22.0613.

Richards, A.S., Sossen, B., Emery, J.C., Horton, K.C., Heinsohn, T., Frascella, B., Balzarini, F., Oradini-Alacreu, A., Brit Häcker, Odone, A., McCreesh, N., Grant, A.D., Kranzer, K., Cobelens, F., Esmail, H. and Rein (2023). Quantifying progression and regression across the spectrum of pulmonary tuberculosis: a data synthesis study. *The Lancet Global Health*. doi:https://doi.org/10.1016/s2214-109x(23)00082-7.

Riggs-Shute, S.D., Falkinham, J.O. and Yang, Z. (2020). Construction and Use of Transposon MycoTetOP2 for Isolation of Conditional *Mycobacteria* Mutants. *Frontiers in microbiology*, 10. doi:https://doi.org/10.3389/fmicb.2019.03091.

Rimal, B., Senzani, S., Ealand, C., Lamichhane, G., Kana, B. and Kim, S.J. (2022). Peptidoglycan compositional analysis of *Mycobacterium smegmatis* using high-resolution LC–MS. *Scientific Reports*, 12(1). doi:https://doi.org/10.1038/s41598-022-15324-1.

Rioseras, B., Yagüe, P., López-García, M.T., Gonzalez-Quiñonez, N., Binda, E., Marinelli, F. and Manteca, A. (2016). Characterization of SCO4439, a D-alanyl-D-alanine carboxypeptidase involved in spore cell wall maturation, resistance and germination in *Streptomyces coelicolor*. *Scientific Reports*, 6(1). doi:https://doi.org/10.1038/srep21659.

Risso, V.A., Gavira, J.A., Gaucher, E.A. and Sanchez-Ruiz, J.M. (2014). Phenotypic comparisons of consensus variants versus laboratory resurrections of Precambrian proteins. *Proteins: Structure, Function, and Bioinformatics*, 82(6), pp.887–896. doi:https://doi.org/10.1002/prot.24575.

Rocaboy, M., Herman, R., Sauvage, E., Remaut, H., Moonens, K., Terrak, M., Charlier, P. and Kerff, F. (2013). The crystal structure of the cell division amidase AmiC reveals the fold of the AMIN domain, a new peptidoglycan binding domain. *Molecular Microbiology*, p.n/a-n/a. doi:https://doi.org/10.1111/mmi.12361.

Roguin, A. (2006). Rene Theophile Hyacinthe Laennec (1781-1826): The Man Behind the Stethoscope. *Clinical Medicine & Research*, 4(3), pp.230–235. doi:https://doi.org/10.3121/cmr.4.3.230.

Romano, M., Aryan, E., Korf, H., Bruffaerts, N., Franken, C.L.M.C., Ottenhoff, T.H.M. and Huygen, K. (2012). Potential of *Mycobacterium tuberculosis* resuscitation-promoting factors as antigens in novel tuberculosis sub-unit vaccines. *Microbes and Infection*, 14(1), pp.86–95. doi:10.1016/j.micinf.2011.08.011.

Rose, N.L., Completo, G.C., Lin, S.-J., McNeil, M., Palcic, M.M. and Lowary, T.L. (2006). Expression, Purification, and Characterization of a Galactofuranosyltransferase Involved in *Mycobacterium tuberculosis* Arabinogalactan Biosynthesis. *Journal of the American Chemical Society*, 128(20), pp.6721–6729. doi:https://doi.org/10.1021/ja058254d.

Roumestand, C., Leiba, J., Galophe, N., Margeat, E., Padilla, A., Bessin, Y., Barthe, P., Molle, V. and Cohen-Gonsaud, M. (2011). Structural Insight into the *Mycobacterium tuberculosis* Rv0020c Protein and Its Interaction with the PknB Kinase. *Structure*, 19(10), pp.1525–1534. doi:https://doi.org/10.1016/j.str.2011.07.011.

ROWE, M.T. and DONAGHY, J. (2008). Mycobacterium bovis: the importance of milk and dairy products as a cause of human tuberculosis in the UK. A review of taxonomy and culture methods, with particular reference to artisanal cheeses. *International Journal of Dairy Technology*, 61(4), pp.317–326. doi:https://doi.org/10.1111/j.1471-0307.2008.00433.x.

Rowland, C.E., Newman, H., Martin, T.T., Dods, R., Nikolaos Bournakas, Wagstaff, J.M., Lewis, N., Stanway, S.J., Balmforth, M., Kessler, C., Katerine van Rietschoten, Bellini, D., Roper, D.I., Lloyd, A.J., Dowson, C.G., Skynner, M.J., Beswick, P. and Dawson, M.J. (2024). Discovery and chemical optimisation of a Potent, Bi-cyclic (Bicycle®) Antimicrobial Inhibitor of *Escherichia coli* PBP3. *bioRxiv (Cold Spring Harbor Laboratory)*. doi:https://doi.org/10.1101/2024.03.20.581580.

Roy, A., Yang, J. and Zhang, Y. (2012). COFACTOR: an accurate comparative algorithm for structure-based protein function annotation. *Nucleic Acids Research*, 40(W1), pp.W471–W477. doi:https://doi.org/10.1093/nar/gks372.

Rubin, E.J., Akerley, B.J., Novik, V.N., Lampe, D.J., Husson, R.N. and Mekalanos, J.J. (1999). In vivo transposition of mariner-based elements in enteric bacteria and mycobacteria. *Proceedings of the National Academy of Sciences*, [online] 96(4), pp.1645–1650. doi:https://doi.org/10.1073/pnas.96.4.1645.

Ruggiero, A., Marasco, D., Squeglia, F., Soldini, S., Pedone, E., Pedone, C. and Berisio, R. (2010). Structure and Functional Regulation of RipA, a *Mycobacterial* Enzyme Essential for Daughter Cell Separation. *Structure*, 18(9), pp.1184–1190. doi:https://doi.org/10.1016/j.str.2010.06.007.

Ruggiero, A., Squeglia, F., Romano, M., Vitagliano, L., De Simone, A. and Berisio, R. (2016). Structure and dynamics of the multi-domain resuscitation promoting factor RpfB from *Mycobacterium tuberculosis*. *Journal of Biomolecular Structure and Dynamics*, 35(6), pp.1322–1330. doi:10.1080/07391102.2016.1182947.

Ruiz, N. (2015). Lipid Flippases for Bacterial Peptidoglycan Biosynthesis. *Lipid Insights*, 8s1, p.LPI.S31783. doi:10.4137/lpi.s31783.

Russell-Goldman, E., Xu, J., Wang, X., Chan, J. and Tufariello, J.M. (2008). A Mycobacterium tuberculosis Rpf Double-Knockout Strain Exhibits Profound Defects in Reactivation from Chronic Tuberculosis and Innate Immunity Phenotypes. *Infection and Immunity*, 76(9), pp.4269–4281. doi:10.1128/iai.01735-07.

Ryu, B.H., Ngo, T.D., Yoo, W., Lee, S., Kim, B.-Y., Lee, E., Kim, K.K. and Kim, T.D. (2016). Biochemical and Structural Analysis of a Novel Esterase from *Caulobacter crescentus* related to Penicillin-Binding Protein (PBP). *Scientific Reports*, 6(1). doi:https://doi.org/10.1038/srep37978.

Saavedra, J.T., Schwartzman, J.A. and Gilmore, M.S. (2017). Mapping Transposon Insertions in Bacterial Genomes by Arbitrarily Primed PCR. *Current Protocols in Molecular Biology*, 118(1). doi:https://doi.org/10.1002/cpmb.38.

Sacco, E., Covarrubias, A.S., O'Hare, H.M., Carroll, P., Eynard, N., Jones, T.A., Parish, T., Daffe, M., Backbro, K. and Quemard, A. (2007). The missing piece of the type II fatty acid synthase system from *Mycobacterium tuberculosis*. *Proceedings of the National Academy of Sciences*, 104(37), pp.14628–14633. doi:https://doi.org/10.1073/pnas.0704132104.

Saha, C.K., Sanches Pires, R., Brolin, H., Delannoy, M. and Atkinson, G.C. (2020). FlaGs and webFlaGs: discovering novel biology through the analysis of gene neighbourhood conservation. *Bioinformatics*, 37(9), pp.1312–1314. doi:https://doi.org/10.1093/bioinformatics/btaa788.

Salomon, A., Law, S., Johnson, C., Baddeley, A., Rangaraj, A., Singh, S. and Daftary, A. (2022). Interventions to improve linkage along the HIV-tuberculosis care cascades in low- and middle-income countries: A systematic review and meta-analysis. *PLOS ONE*, 17(5), p.e0267511. doi:https://doi.org/10.1371/journal.pone.0267511.

Sanders, A.N. and Pavelka, M.S. (2013). Phenotypic analysis of *Eschericia coli* mutants lacking l,d-transpeptidases. *Microbiology*, 159(Pt_9), pp.1842–1852. doi:https://doi.org/10.1099/mic.0.069211-0.

Saqib, M., Khatri, R., Singh, B., Gupta, A., Kumar, A. and Bhaskar, S. (2016). *Mycobacterium indicus pranii* as a booster vaccine enhances BCG induced immunity and confers higher protection in animal models of tuberculosis. *Tuberculosis*, 101, pp.164–173. doi:https://doi.org/10.1016/j.tube.2016.10.002.

Saran, K., Iyengar, S.S., Sinha, N., Kumar Abhishek, Kumar, A. and Prakash, J. (2023). Role of *Mycobacterium indicus pranii* in clinical outcomes in patients with sepsis: A systematic review and meta-analysis of randomised controlled trials. *Indian Journal of Anaesthesia*, 67(12), pp.1029–1035. doi:https://doi.org/10.4103/ija.ija_726_23.

Sarkar, P., Yarlagadda, V., Ghosh, C. and Haldar, J. (2017). A Review on Cell Wall Synthesis Inhibitors with an Emphasis on Glycopeptide Antibiotics. *MedChemComm*, [online] 8(3), pp.516–533. doi:10.1039/c6md00585c.
Sarkar, S., Chatterjee, A. and Biswas, K. (2023). A Recent Update on Rhodamine Dye Based Sensor Molecules: A Review. *Critical Reviews in Analytical Chemistry*, pp.1–27. doi:https://doi.org/10.1080/10408347.2023.2169598.

Sasidharan, K., Martinez-Vernon, A.S., Chen, J., Fu, T. and Soyer, O.S. (2018). A low-cost DIY device for high resolution, continuous measurement of microbial growth dynamics. [online] doi:https://doi.org/10.1101/407742.

Sassetti, C.M., Boyd, D.H. and Rubin, E.J. (2003). Genes required for mycobacterial growth defined by high density mutagenesis. *Molecular microbiology*, [online] 48(1), pp.77–84. doi:https://doi.org/10.1046/j.1365-2958.2003.03425.x.

Sassine, J., Xu, M., Sidiq, K.R., Emmins, R., Errington, J. and Daniel, R.A. (2017). Functional redundancy of division specific penicillin-binding proteins in *Bacillus subtilis*. *Molecular Microbiology*, 106(2), pp.304–318. doi:10.1111/mmi.13765.

Sauvage, E. and Terrak, M. (2016). Glycosyltransferases and Transpeptidases/Penicillin-Binding Proteins: Valuable Targets for New Antibacterials. *Antibiotics*, 5(1), p.12. doi:10.3390/antibiotics5010012.

Sauvage, E., Duez, C., Herman, R., Kerff, F., Petrella, S., Anderson, J.W., Adediran, S.A., Pratt, R.F., Frère, J.-M. and Charlier, P. (2007). Crystal Structure of the *Bacillus subtilis* Penicillin-binding Protein 4a, and its Complex with a Peptidoglycan Mimetic Peptide. *Journal of Molecular Biology*, 371(2), pp.528–539. doi:https://doi.org/10.1016/j.jmb.2007.05.071.

Sauvage, E., Herman, R., Petrella, S., Duez, C., Fabrice Bouillenne, Jean-Marie Frère and Charlier, P. (2005). Crystal Structure of the Actinomadura R39 DD-peptidase Reveals New Domains in Penicillin-binding Proteins. 280(35), pp.31249–31256. doi:https://doi.org/10.1074/jbc.m503271200.

Sauvage, E., Kerff, F., Terrak, M., Ayala, J.A. and Charlier, P. (2008). The penicillin-binding proteins: structure and role in peptidoglycan biosynthesis. *FEMS Microbiology Reviews*, 32(3), pp.556–556. doi:10.1111/j.1574-6976.2008.00115.x.

Sauvage, E., Powell, A.J., Heilemann, J., Josephine, H.R., Charlier, P., Davies, C. and Pratt, R.F. (2008). Crystal Structures of Complexes of Bacterial DD-Peptidases with Peptidoglycan-Mimetic Ligands: The Substrate Specificity Puzzle. *Journal of Molecular Biology/Journal of molecular biology*, 381(2), pp.383–393. doi:https://doi.org/10.1016/j.jmb.2008.06.012.

Savková, K., Stanislav Huszár, Baráth, P., Zuzana Pakanová, Stanislav Kozmon, Vancová, M., Tesařová, M., Jaroslav Blaško, Kaliňák, M., Singh, V., Korduláková, J. and Katarína Mikušová (2021). An ABC transporter Wzm–Wzt catalyzes translocation of lipid-linked galactan across the plasma membrane in mycobacteria. *Proceedings of the National Academy of Sciences of the United States of America*, 118(17). doi:https://doi.org/10.1073/pnas.2023663118.

Schaefer, K., Owens, T.W., Page, J.E., Santiago, M., Kahne, D. and Walker, S. (2020). Structure and reconstitution of a hydrolase complex that may release peptidoglycan from the membrane after polymerization. *Nature Microbiology*, 6(1), pp.34–43. doi:https://doi.org/10.1038/s41564-020-00808-5.

Schaeffer, M.L., Agnihotri, G., Craig Alan Volker, Kallender, H., Brennan, P.J. and Lonsdale, J. (2001). Purification and Biochemical Characterization of the *Mycobacterium tuberculosis* β-Ketoacyl-acyl Carrier Protein Synthases KasA and KasB. *Journal of Biological Chemistry*, 276(50), pp.47029–47037. doi:https://doi.org/10.1074/jbc.m108903200.

Scherman, H., Kaur, D., Pham, H., Henrieta Škovierová, Jackson, M. and Brennan, P.J. (2009). Identification of a Polyprenylphosphomannosyl Synthase Involved in the Synthesis of *Mycobacterial* Mannosides. *Journal of Bacteriology*, 191(21), pp.6769–6772. doi:https://doi.org/10.1128/jb.00431-09.

Schiebel, J., Kapilashrami, K., Fekete, A., Bommineni, G.R., Schaefer, C.M., Mueller, M.J., Tonge, P.J. and Kisker, C. (2013). Structural Basis for the Recognition of Mycolic Acid Precursors by KasA, a Condensing Enzyme and Drug Target from *Mycobacterium Tuberculosis*. *Journal of Biological Chemistry*, 288(47), pp.34190–34204. doi:https://doi.org/10.1074/jbc.m113.511436.
Schleifer, K, H and Kandler, O. 1973. Peptidoglycan Types of Bacterial Cell Walls and Their Taxonomic Implications. *Bacteriological Reviews* 37(2), pp.258-258.

Schlesinger, L. S. (1993). Macrophage phagocytosis of virulent but not attenuated strains of *Mycobacterium tuberculosis* is mediated by mannose receptors in addition to complement receptors. *Journal of Immunology,* 1;150 (7): 2920-30.

Schulz, G.E. (2011). Protein Modifications Giving Rise to Homo-oligomers. *Progress in Molecular Biology and Translational Science*, pp.187–229. doi:https://doi.org/10.1016/b978-0-12-415906-8.00006-6.

Schwefel, D., Maierhofer, C., Beck, J., Seeberger, S., Diederichs, K., Möller, H.M., Welte, W. and Wittmann, V. (2010). Structural Basis of Multivalent Binding to Wheat Germ Agglutinin. 132(25), pp.8704–8719. doi:https://doi.org/10.1021/ja101646k.

Seeliger, J.C., Holsclaw, C.M., Schelle, M.W., Zsofia Botyanszki, Gilmore, S., Tully, S., Niederweis, M., Cravatt, B.F., Leary, J.A. and Bertozzi, C.R. (2012). Elucidation and Chemical Modulation of Sulfolipid-1 Biosynthesis in *Mycobacterium tuberculosis*. *Journal of Biological Chemistry*, 287(11), pp.7990–8000. doi:https://doi.org/10.1074/jbc.m111.315473.

Sehnal, D. (2023). *MotiveValidator | WebChemistry*. [online] webchem.ncbr.muni.cz. Available at: http://webchem.ncbr.muni.cz/Platform/MotiveValidator.

Seidel, M., Alderwick, L.J., Birch, H.L., Sahm, H., Eggeling, L. and Besra, G.S. (2007). Identification of a Novel Arabinofuranosyltransferase AftB Involved in a Terminal Step of Cell Wall Arabinan Biosynthesis in *Corynebacterianeae*, such as *Corynebacterium glutamicum* and *Mycobacterium tuberculosis*. *Journal of Biological Chemistry*, 282(20), pp.14729–14740. doi:https://doi.org/10.1074/jbc.m700271200.

Sester, M., Giehl, C., McNerney, R., Kampmann, B., Walzl, G., Cuchí, P., Wingfield, C., Lange, C., Migliori, G.B., Kritski, A.L. and Meyerhans, A. (2010). Challenges and perspectives for improved management of HIV/*Mycobacterium tuberculosis* co-infection. *European Respiratory Journal*, [online] 36(6), pp.1242–1247. doi:https://doi.org/10.1183/09031936.00040910.

Shah, M., Hanrahan, C., Wang, Z.Y., Dendukuri, N., Lawn, S.D., Denkinger, C.M. and Steingart, K.R. (2016). Lateral flow urine lipoarabinomannan assay for detecting active tuberculosis in HIV-positive adults. *Cochrane Database of Systematic Reviews*. doi:https://doi.org/10.1002/14651858.cd011420.pub2.

Shaku, M.T., Ocius, K.L., Apostolos, A.J., Pires, M.M., VanNieuwenhze, M.S., Dhar, N. and Kana, B.D. (2023). Amidation of glutamate residues in mycobacterial peptidoglycan is essential for cell wall cross-linking. *Frontiers in Cellular and Infection Microbiology*, 13. doi:https://doi.org/10.3389/fcimb.2023.1205829.

Shaler, C.R., Horvath, C., Lai, R. and Xing, Z. (2012). Understanding Delayed T-Cell Priming, Lung Recruitment, and Airway Luminal T-Cell Responses in Host Defense against Pulmonary Tuberculosis. *Clinical and Developmental Immunology*, [online] 2012, p.e628293. doi:https://doi.org/10.1155/2012/628293.

Sham, L.-T. ., Butler, E.K., Lebar, M.D., Kahne, D., Bernhardt, T.G. and Ruiz, N. (2014). MurJ is the flippase of lipid-linked precursors for peptidoglycan biogenesis. *Science*, 345(6193), pp.220–222. doi:10.1126/science.1254522.

Shangguan, Y., Guo, W., Feng, X., Shi, Y., Li, X., Pan, Z., Hu, M., Shi, J., Ding, C., Xia, J., Hu, W., Ji, Z., Zhao, C., Li, Y., He, Z., Jin, L., Tao, X., Zhu, X., Zhang, X. and Song, Q. (2023). Randomized control study of the use of faropenem for treating patients with pulmonary tuberculosis. *International Journal of Infectious Diseases*, [online] 132, pp.99–107. doi:https://doi.org/10.1016/j.ijid.2023.04.388.

Shapiro, A.B., Moussa, S.H., McLeod, S.M., Durand-Réville, T. and Miller, A.A. (2021). Durlobactam, a New Diazabicyclooctane β-Lactamase Inhibitor for the Treatment of *Acinetobacter* Infections in Combination With Sulbactam. *Frontiers in Microbiology*, 12. doi:https://doi.org/10.3389/fmicb.2021.709974.

Sharma, A., Equbal, Md.J., Pandey, S., Sheikh, J.A., Ehtesham, N.Z., Hasnain, S.E. and Chaudhuri, T.K. (2017). Immunodominant proteinMIP_05962 from *Mycobacterium indicus pranii* displays chaperone activity. *The FEBS Journal*, 284(9), pp.1338–1354. doi:https://doi.org/10.1111/febs.14057.

Sharma, M., Zhang, S., Niu, L., Lewinsohn, D., Zhang, X. and Huang, S. (2020). Mucosal-Associated Invariant T Cells Develop an Innate-Like Transcriptomic Program in Anti-mycobacterial Responses. *Frontiers in Immunology*, 11. doi:https://doi.org/10.3389/fimmu.2020.01136.

Sharma, P., Misra, R.S., Kar, H.K., Mukherjee, A., Poricha, D., Kaur, H., Mukherjee, R. and Rani, R. (2000). Mycobacterium w vaccine, a useful adjuvant to multidrug therapy in multibacillary leprosy: a report on hospital based immunotherapeutic clinical trials with a follow-up of 1-7 years after treatment. *Leprosy Review*, [online] 71(2), pp.179–192. doi:https://doi.org/10.5935/0305-7518.20000020.

Sharma, S.K., Katoch, K., Sarin, R., Balambal, R., Kumar Jain, N., Patel, N., Murthy, K.J.R., Singla, N., Saha, P.K., Khanna, A., Singh, U., Kumar, S., Sengupta, A., Banavaliker, J.N., Chauhan, D.S., Sachan, S., Wasim, M., Tripathi, S., Dutt, N. and Jain, N. (2017). Efficacy and Safety of *Mycobacterium indicus pranii* as an adjunct therapy in Category II pulmonary tuberculosis in a randomized trial. *Scientific Reports*, 7(1). doi:https://doi.org/10.1038/s41598-017-03514-1.

Shchelik, I.S. and Gademann, K. (2021). Synthesis and antimicrobial evaluation of new cephalosporin derivatives containing cyclic disulfide moieties. *bioRxiv (Cold Spring Harbor Laboratory)*. doi:https://doi.org/10.1101/2021.11.03.467114.

Shen, Y. (2002). Adaptive Immune Response of Vgamma 2Vdelta 2+ T Cells During Mycobacterial Infections. *Science*, 295(5563), pp.2255–2258. doi:https://doi.org/10.1126/science.1068819.

Shenderov, K., Barber, D.L., Mayer-Barber, K.D., Gurcha, S.S., Jankovic, D., Feng, C.G., Oland, S., Hieny, S., Caspar, P., Yamasaki, S., Lin, X., Jenny P.-Y. Ting, Giorgio Trinchieri, Besra, G.S., Cerundolo, V. and Sher, A. (2013). Cord Factor and Peptidoglycan Recapitulate the Th17-Promoting Adjuvant Activity of *Mycobacteria* through Mincle/CARD9 Signaling and the Inflammasome. *Journal of Immunology*, 190(11), pp.5722–5730. doi:https://doi.org/10.4049/jimmunol.1203343.

Shi, L.-B., Berg, S., Lee, A., Spencer, J.R., Zhang, J., Vissa, V.D., McNeil, M.R., Khoo, K.-H. and Chatterjee, D. (2006). The Carboxy Terminus of EmbC from *Mycobacterium smegmatis* Mediates Chain Length Extension of the Arabinan in Lipoarabinomannan. *Journal of Biological Chemistry*, 281(28), pp.19512–19526. doi:https://doi.org/10.1074/jbc.m513846200.

Shi, Q., Meroueh, S.O., Fisher, J.F. and Mobashery, S. (2008). Investigation of the Mechanism of the Cell Wall dd-Carboxypeptidase Reaction of Penicillin-Binding Protein 5 of *Escherichia coli* by Quantum Mechanics/Molecular Mechanics Calculations. *Journal of the American Chemical Society*, 130(29), pp.9293–9303. doi:https://doi.org/10.1021/ja801727k.

Shimokawa, M., Akihiro Ishiwata, Kashima, T., Nakashima, C., Li, J., Fukushima, R., Sawai, N., Miku Nakamori, Tanaka, Y., Kudo, A., Sae Morikami, Iwanaga, N., Akai, G., Shimizu, N., Arakawa, T., Yamada, C., Kitahara, K., Tanaka, K., Ito, Y. and Shinya Fushinobu (2023). Identification and characterization of endo-α-, exo-α-, and exo-β-d-arabinofuranosidases degrading lipoarabinomannan and arabinogalactan of mycobacteria. *Nature communications*, [online] 14(1). doi:https://doi.org/10.1038/s41467-023-41431-2.

Shockman, G.D. and Höltje, J. (1994). Microbial peptidoglycan (murein) hydrolases. *New comprehensive biochemistry*, 27, pp.131–166.

Shrive, A.K., Martin, C., Burns, I., Paterson, J.M., Martin, J.D., Townsend, J.P., Waters, P., Clark, H.W., Kishore, U., Reid, K.B.M. and Greenhough, T.J. (2009). Structural Characterisation of Ligand-Binding Determinants in Human Lung Surfactant Protein D: Influence of Asp325. *Journal of Molecular Biology*, 394(4), pp.776–788. doi:https://doi.org/10.1016/j.jmb.2009.09.057.

Siegel, S.D., Amer, B.R., Wu, C., Sawaya, M.R., Gosschalk, J.E., Clubb, R.T. and Ton-That, H. (2019). Structure and Mechanism of LcpA, a Phosphotransferase That Mediates Glycosylation of a Gram-Positive Bacterial Cell Wall-Anchored Protein. *MBio*, 10(1). doi:https://doi.org/10.1128/mbio.01580-18.

Siegrist, C.-A. . (2007). Mechanisms Underlying Adverse Reactions to Vaccines. *Journal of Comparative Pathology*, 137, pp.S46–S50. doi:https://doi.org/10.1016/j.jcpa.2007.04.012.

Siegrist, M. Sloan and Bertozzi, Carolyn R. (2014). *Mycobacterial* Lipid Logic. *Cell Host & Microbe*, 15(1), pp.1–2. doi:https://doi.org/10.1016/j.chom.2013.12.005.

Silva, Govender, T., Glenn, Kruger, H.G., Jerônimo Lameira, Roitberg, A.E. and Cláudio Nahum Alves (2015). Simulating the inhibition reaction of *Mycobacterium tuberculosis* L,D-transpeptidase 2 by carbapenems. *Chemical communications*, 51(63), pp.12560–12562. doi:https://doi.org/10.1039/c5cc03202d.

Silva, J.R.A., Roitberg, A.E. and Alves, C.N. (2014). Catalytic Mechanism of L, D-Transpeptidase 2 from *Mycobacterium tuberculosis* Described by a Computational Approach: Insights for the Design of New Antibiotics Drugs. *Journal of Chemical Information and Modeling*, 54(9), pp.2402–2410. doi:10.1021/ci5003069.

Singh, P., Rameshwaram, N.R., Ghosh, S. and Mukhopadhyay, S. (2018). Cell envelope lipids in the pathophysiology of Mycobacterium tuberculosis. *Future Microbiology*, 13(6), pp.689–710. doi:https://doi.org/10.2217/fmb-2017-0135.

Singh, S., Gumbo, T., Alffenaar, J.-W., Boorgula, G.D., Thomas, T.A., Dheda, K., Malinga, L., Raj, P., Aryal, S. and Srivastava, S. (2023). Meropenem-vaborbactam restoration of first-line drugs' efficacy and comparison of meropenem-vaborbactam-moxifloxacin versus BPaL MDR-TB regimen. *International Journal of Antimicrobial Agents*, [online] p.106968. doi:https://doi.org/10.1016/j.ijantimicag.2023.106968.

Singh, S.K., Parveen, S., SaiSree, L. and Reddy, M. (2015). Regulated proteolysis of a cross-link–specific peptidoglycan hydrolase contributes to bacterial morphogenesis. *Proceedings of the National Academy of Sciences*, 112(35), pp.10956–10961. doi:https://doi.org/10.1073/pnas.1507760112.

Singh, S.K., SaiSree, L., Amrutha, R.N. and Reddy, M. (2012). Three redundant murein endopeptidases catalyse an essential cleavage step in peptidoglycan synthesis of *Escherichia coli* K12. *Molecular Microbiology*, 86(5), pp.1036–1051. doi:https://doi.org/10.1111/mmi.12058.

Singh, V., Grzegorzewicz, A.E., Fienberg, S., Müller, R., Lutete Peguy Khonde, Sanz, O., Alfonso, S., Urones, B., Drewes, G., Bantscheff, M., Ghidelli-Disse, S., Ioerger, T.R., Bhanupriya Angala, Liu, J., Lee, R.E., Sacchettini, J.C., Krieger, I.V., Jackson, M., Chibale, K. and Ghorpade, S.R. (2022). 1,3-Diarylpyrazolyl-acylsulfonamides Target HadAB/BC Complex in *Mycobacterium tuberculosis*. *ACS Infectious Diseases*, 8(11), pp.2315–2326. doi:https://doi.org/10.1021/acsinfecdis.2c00392.

Singhania, A., Dubelko, P., Kuan, R., Chronister, W.D., Muskat, K., Das, J., Phillips, E.J., Mallal, S.A., Seumois, G., Vijayanand, P., Sette, A., Lerm, M., Peters, B. and Lindestam Arlehamn, C. (2021). CD4+CCR6+ T cells dominate the BCG-induced transcriptional signature. *eBioMedicine*, [online] 74, p.103746. doi:https://doi.org/10.1016/j.ebiom.2021.103746.

Sinha, P., Srivastava, G.N., Tripathi, R., Mishra, M.N. and Anupurba, S. (2020). Detection of mutations in the rpoB gene of rifampicin-resistant *Mycobacterium tuberculosis* strains inhibiting wild type probe hybridization in the MTBDR plus assay by DNA sequencing directly from clinical specimens. *BMC Microbiology*, 20(1). doi:https://doi.org/10.1186/s12866-020-01967-5.

Sinha, R.K. and Rosenthal, R.S. (1980). Release of soluble peptidoglycan from growing conococci: demonstration of anhydro-muramyl-containing fragments. *Infection and Immunity*, 29(3), pp.914–925. doi:https://doi.org/10.1128/iai.29.3.914-925.1980.

Skoog, K., Bruzell, F.S., Ducroux, A., Hellberg, M., Johansson, H., Lehtiö, J., Högbom, M. and Daley, D.O. (2011). Penicillin-binding protein 5 can form a homo-oligomeric complex in the inner membrane of Escherichia coli. *Protein Science*, 20(9), pp.1520–1529. doi:https://doi.org/10.1002/pro.677.
Slichter, C.P. (1996). *Principles of magnetic resonance*. Berlin ; New York: Springer.

Small, J.L., O'Donoghue, A.J., Boritsch, E.C., Tsodikov, O.V., Knudsen, G.M., Vandal, O., Craik, C.S. and Ehrt, S. (2013). Substrate Specificity of MarP, a Periplasmic Protease Required for Resistance to Acid and Oxidative Stress in *Mycobacterium tuberculosis*. *Journal of Biological Chemistry*, 288(18), pp.12489–12499. doi:https://doi.org/10.1074/jbc.m113.456541.

Smith C (2023) Discovery of Diagnostic Methods and Therapeutic Drugs against Tuberculosis Infection. Mycobacterial Diseases. 13.338.

Smith, A., Brownawell, A. and Macara, I.G. (1998). Nuclear import of Ran is mediated by the transport factor NTF2. *Current Biology*, 8(25), pp.1403-S1. doi:https://doi.org/10.1016/s0960-9822(98)00023-2.

Snapper, S.B., Melton, R.E., Mustafa, S., Kieser, T. and Jacobs, W.R. (1990). Isolation and characterization of efficient plasmid transformation mutants of *Mycobacterium smegmatis*. *Molecular Microbiology*, [online] 4(11), pp.1911–1919. doi:https://doi.org/10.1111/j.1365-2958.1990.tb02040.x.

Soetaert, K., Rens, C., Wang, X.-M., De Bruyn, J., Lanéelle, M.-A., Laval, F., Lemassu, A., Daffé, M., Bifani, P., Fontaine, V. and Lefèvre, P. (2015). Increased Vancomycin Susceptibility in *Mycobacteria*: a New Approach To Identify Synergistic Activity against Multidrug-Resistant *Mycobacteria*. *Antimicrobial Agents and Chemotherapy*, 59(8), pp.5057–5060. doi:10.1128/aac.04856-14.

Soleimanpour, S., Yaghoubi, A., Sadat Seddighinia, F. and Rezaee, S.A.R. (2022). A century of attempts to develop an effective tuberculosis vaccine: Why they failed? *International Immunopharmacology*, 109, p.108791. doi:https://doi.org/10.1016/j.intimp.2022.108791.

Soroka, D., Ourghanlian, C., Compain, F., Fichini, M., Dubée, V., Mainardi, J.-L., Hugonnet, J.-E. and Arthur, M. (2016). Inhibition of β-lactamases of mycobacteria by avibactam and clavulanate. *Journal of Antimicrobial Chemotherapy*, p.dkw546. doi:https://doi.org/10.1093/jac/dkw546.

Sparks, I.L., Derbyshire, K.M., Jacobs, W.R. and Morita, Y. (2023). *Mycobacterium smegmatis*: The Vanguard of *Mycobacterial* Research. *Journal of Bacteriology*, 205(1). doi:https://doi.org/10.1128/jb.00337-22.

Sparks, I.L., Kado, T., Malavika Prithviraj, Japinder Nijjer, Yan, J. and Morita, Y.S. (2024). Lipoarabinomannan mediates localized cell wall integrity during division in mycobacteria. *Nature communications*, 15(1). doi:https://doi.org/10.1038/s41467-024-46565-5.

Spratt BG, & Pardee AB (1975). Penicillin-binding proteins and cell shape in *E. coli*. Nature, 254(5500), 516–517.

Spratt, B.G. (1975) Distinct penicillin binding proteins involved in the division, elongation, and shape of escherichia coli K12. *Proceedings of the National Academy of Sciences*, 72 (8): 2999–3003. doi:10.1073/pnas.72.8.2999.

Squeglia, F., Ruggiero, A. and Berisio, R. (2017). Chemistry of Peptidoglycan in *Mycobacterium tuberculosis* Life Cycle: An off-the-wall Balance of Synthesis and Degradation. *Chemistry - A European Journal*, 24(11), pp.2533–2546. doi:https://doi.org/10.1002/chem.201702973.

Sridharan, S., Wang, L., Brown, A.K., Dover, L.G., Kremer, L., Besra, G.S. and Sacchettini, J.C. (2007). X-Ray Crystal Structure of *Mycobacterium tuberculosis* β-Ketoacyl Acyl Carrier Protein Synthase II (mtKasB). *Journal of Molecular Biology*, 366(2), pp.469–480. doi:https://doi.org/10.1016/j.jmb.2006.11.006.

Steggerda, S.M., Black, B.E. and Paschal, B.M. (2000). Monoclonal Antibodies to NTF2 Inhibit Nuclear Protein Import by Preventing Nuclear Translocation of the GTPase Ran. *Molecular Biology of the Cell*, 11(2), pp.703–719. doi:https://doi.org/10.1091/mbc.11.2.703.

Stinear, T.P., Seemann, T., Harrison, P.F., Jenkin, G.A., Davies, J.K., Johnson, P.D.R., Abdellah, Z., Arrowsmith, C., Chillingworth, T., Churcher, C., Clarke, K., Cronin, A., Davis, P., Goodhead, I., Holroyd, N., Jagels, K., Lord, A., Moule, S., Mungall, K. and Norbertczak, H. (2008). Insights from the complete genome sequence of *Mycobacterium marinum* on the evolution of *Mycobacterium tuberculosis*. *Genome Research*, [online] 18(5), pp.729–741. doi:https://doi.org/10.1101/gr.075069.107.

Stogios, P.J. and Savchenko, A. (2020). Molecular mechanisms of vancomycin resistance. *Protein Science*, 29(3), pp.654–669. doi:https://doi.org/10.1002/pro.3819.

Su, H., Sheng, X. and Liu, Y. (2016). Insights into the catalytic mechanism of *N*-acetylglucosaminidase glycoside hydrolase from Bacillus subtilis: a QM/MM study. *Organic & Biomolecular Chemistry*, 14(13), pp.3432–3442. doi:https://doi.org/10.1039/c6ob00320f.

Suen, T.K., Simone, Li, W., Charlotte, Valerie, Mourits, V.P., Dijkstra, H., Lemmers, H., Bhat, J., Xu, C.-J., Joosten, L.A.B., Schultze, J.L., Li, Y., Placek, K. and Netea, M.G. (2023). BCG vaccination induces innate immune memory in γδ T cells in humans. *Journal of Leukocyte Biology*, 115(1), pp.149–163. doi:https://doi.org/10.1093/jleuko/qiad103.

Susie Coutinho Liedke, Daniel Zamith Miranda, Kamilla Xavier Gomes, Luis, J., Frases, S., Nosanchuk, J.D., Rodrigues, M.L., Nimrichter, L., José Mauro Peralta and Guimarães, A.J. (2017). Characterization of the antifungal functions of a WGA-Fc (IgG2a) fusion protein binding to cell wall chitin oligomers. *Scientific Reports*, 7(1). doi:https://doi.org/10.1038/s41598-017-12540-y.

Susser, M. and Stein, Z. (2009). *Eras in Epidemiology*. doi:https://doi.org/10.1093/acprof:oso/9780195300666.001.0001.

Suthar, A.B., Lawn, S.D., del Amo, J., Getahun, H., Dye, C., Sculier, D., Sterling, T.R., Chaisson, R.E., Williams, B.G., Harries, A.D. and Granich, R.M. (2012). Antiretroviral Therapy for Prevention of Tuberculosis in Adults with HIV: A Systematic Review and Meta-Analysis. *PLoS Medicine*, 9(7), p.e1001270. doi:https://doi.org/10.1371/journal.pmed.1001270.

Suyama, M., Doerks, T., Braun, I.C., Sattler, M., Izaurralde, E. and Bork, P. (2000). Prediction of structural domains of TAP reveals details of its interaction with p15 and nucleoporins. *EMBO Reports*, 1(1), pp.53–58. doi:https://doi.org/10.1093/embo-reports/kvd009.

Suzuki, H. & Nishimura, Y. & Hirota, Y. (1978) On the process of cellular division in escherichia coli: A series of mutants of E. coli altered in the penicillin-binding proteins. *Proceedings of the National Academy of Sciences*, 75 (2): 664–668. doi:10.1073/pnas.75.2.664.

Svetitsky, S., Leibovici, L. and Paul, M. (2009). Comparative Efficacy and Safety of Vancomycin versus Teicoplanin: Systematic Review and Meta-Analysis. *Antimicrobial Agents and Chemotherapy*, 53(10), pp.4069–4079. doi:10.1128/aac.00341-09.

Sykes, R.B., Cimarusti, C.M., Bonner, D.P., Bush, K., Floyd, D.M., Georgopapadakou, N.H., Koster, W.M., Liu, W.C., Parker, W.L., Principe, P.A., Rathnum, M.L., Slusarchyk, W.A., Trejo, W.H. and Wells, J.S. (1981). Monocyclic beta-lactam antibiotics produced by bacteria. *Nature*, [online] 291(5815), pp.489–491. doi:https://doi.org/10.1038/291489a0.

T. E. W. Feltkamp (1970). Conjugation of fluorescein isothiocyanate to antibodies. I. Experiments on the conditions of conjugation. *PubMed*, 18(6), pp.865–73.

Tabrah F. L. (2011). Koch's postulates, carnivorous cows, and tuberculosis today. *Hawaii medical journal*, *70*(7), 144–148.

Taguchi, A., Welsh, M.A., Marmont, L.S., Lee, W., Sjodt, M., Kruse, A.C., Kahne, D., Bernhardt, T.G. and Walker, S. (2019). FtsW is a peptidoglycan polymerase that is functional only in complex with its cognate penicillin-binding protein. *Nature Microbiology*, [online] 4(4), pp.587–594. doi:10.1038/s41564-018-0345-x.

Taiana Tainá Silva-Pereira, Naila Cristina Soler-Camargo and Marcia, A. (2024). Diversification of gene content in the *Mycobacterium tuberculosis* complex is determined by phylogenetic and ecological signatures. *Microbiology spectrum*. doi:https://doi.org/10.1128/spectrum.02289-23.

Tao, W., Ivanovska, V., Schweickert, B. and Muller, A. (2019). Proxy indicators for antibiotic consumption; surveillance needed to control antimicrobial resistance. *Bulletin of the World Health Organization*, 97(1), pp.3–3A. doi:https://doi.org/10.2471/blt.18.227348.

Tellier, R., Li, Y., Cowling, B.J. and Tang, J.W. (2019). Recognition of aerosol transmission of infectious agents: a commentary. *BMC Infectious Diseases*, 19(1). doi:https://doi.org/10.1186/s12879-019-3707-y.

Templin, M.F. (1999) 'A defect in cell wall recycling triggers autolysis during the stationary growth phase of escherichia coli', *The EMBO Journal*, 18(15), pp. 4108–4117. doi:10.1093/emboj/18.15.4108.

Terradot, L., Bayliss, R., Oomen, C., Leonard, G.A., Baron, C. and Waksman, G. (2005). Structures of two core subunits of the bacterial type IV secretion system, VirB8 from Brucella suis and ComB10 from Helicobacter pylori. *Proceedings of the National Academy of Sciences*, 102(12), pp.4596–4601. doi:https://doi.org/10.1073/pnas.0408927102.

The Telegraph. (2010). *London 'the TB capital of Europe'*. [online] Available at: https://www.telegraph.co.uk/news/health/news/8206887/London-the-TB-capital-of-Europe.html.

Thomsen Vf and So, L. (1962). [In vitro activity of penicillin. Comparative studies on benzylpenicillin, phenoxymethylpenicillin, phenoxyethylpenicillin and dimethoxyphenylpenicillin]. *PubMed*, 67, pp.111–9.

Tipper, D.J. & Strominger, J.L. (1965) Mechanism of action of Penicillins: A proposal based on their structural similarity to acyl-D-alanyl-D-alanine. *Proceedings of the National Academy of Sciences*, 54 (4): 1133–1141. doi:10.1073/pnas.54.4.1133.

Tomanicek, S.J. & Wang, K.K. & Weiss, K.L. & et al. (2010) The active site protonation states of perdeuterated toho-1 β-lactamase determined by neutron diffraction support a role for GLU166 as the general base in acylation. *FEBS Letters*, 585 (2): 364–368. doi:10.1016/j.febslet.2010.12.017

Tortoli, E., Fedrizzi, T., Meehan, C.J., Trovato, A., Grottola, A., Giacobazzi, E., Serpini, G.F., Tagliazucchi, S., Fabio, A., Bettua, C., Bertorelli, R., Frascaro, F., De Sanctis, V., Pecorari, M., Jousson, O., Segata, N. and Cirillo, D.M. (2017). The new phylogeny of the genus *Mycobacterium* : The old and the news. *Infection, Genetics and Evolution*, 56, pp.19–25. doi:https://doi.org/10.1016/j.meegid.2017.10.013.

Tortoli, E., Meehan, C.J., Grottola, A., Fregni Serpini, G., Fabio, A., Trovato, A., Pecorari, M. and Cirillo, D.M. (2019). Genome-based taxonomic revision detects a number of synonymous taxa in the genus *Mycobacterium*. *Infection, Genetics and Evolution*, 75, p.103983. doi:https://doi.org/10.1016/j.meegid.2019.103983.

Toth, M., Antunes, N.T., Stewart, N.K., Frase, H., Bhattacharya, M., Smith, C.A. and Vakulenko, S.B. (2016). Class D β-lactamases do exist in Gram-positive bacteria. *Nature Chemical Biology*, [online] 12(1), pp.9–14. doi:https://doi.org/10.1038/nchembio.1950.

Tran, T., Bonham, A.J., Chan, E.D. and Honda, J.R. (2019). A paucity of knowledge regarding nontuberculous mycobacterial lipids compared to the tubercle bacillus. *Tuberculosis*, [online] 115, pp.96–107. doi:https://doi.org/10.1016/j.tube.2019.02.008.

Trivedi, O.A., Arora, P., Sridharan, V., Tickoo, R., Mohanty, D. and Gokhale, R.S. (2004). Enzymic activation and transfer of fatty acids as acyl-adenylates in mycobacteria. *Nature*, 428(6981), pp.441–445. doi:https://doi.org/10.1038/nature02384.

Trivedi, R.R., Crooks, J.A., Auer, G.K., Pendry, J., Foik, I.P., Siryaporn, A., Abbott, N.L., Gitai, Z. and Weibel, D.B. (2018). Mechanical Genomic Studies Reveal the Role of d -Alanine Metabolism in *Pseudomonas aeruginosa* Cell Stiffness. *mBio*, [online] 9(5). doi:https://doi.org/10.1128/mbio.01340-18.

Tufariello, J.M., Mi, K., Xu, J., Manabe, Y.C., Kesavan, A.K., Drumm, J., Tanaka, K., Jacobs, W.R. and Chan, J. (2006). Deletion of the *Mycobacterium tuberculosis* Resuscitation-Promoting Factor Rv1009 Gene Results in Delayed Reactivation from Chronic Tuberculosis. *Infection and Immunity*, 74(5), pp.2985–2995. doi:10.1128/iai.74.5.2985-2995.2006.

Tufariello, J.M., Jacobs, W.R. and Chan, J. (2004). Individual *Mycobacterium tuberculosis* Resuscitation-Promoting Factor Homologues Are Dispensable for Growth *In Vitro* and *In Vivo*. *Infection and Immunity*, 72(1), pp.515–526. doi:https://doi.org/10.1128/iai.72.1.515-526.2004.

Turapov, O., Forti, F., Kadhim, B., Ghisotti, D., Sassine, J., Straatman-Iwanowska, A., Bottrill, A.R., Moynihan, P.J., Wallis, R., Barthe, P., Cohen-Gonsaud, M., Ajuh, P., Vollmer, W. and Mukamolova, G.V. (2018). Two Faces of CwlM, an Essential PknB Substrate, in *Mycobacterium tuberculosis*. *Cell Reports*, 25(1), pp.57-67.e5. doi:10.1016/j.celrep.2018.09.004.

Turnbull, W.B., Shimizu, K.H., Chatterjee, D., Homans, S.W. and Treumann, A. (2004). Identification of the 5-Methylthiopentosyl Substituent in *Mycobacterium tuberculosis* Lipoarabinomannan. *Angewandte Chemie International Edition*, 43(30), pp.3918–3922. doi:https://doi.org/10.1002/anie.200454119.

Turner, J. and Torrelles, J.B. (2018). Mannose-capped lipoarabinomannan in *Mycobacterium tuberculosis* pathogenesis. *Pathogens and Disease*, 76(4). doi:https://doi.org/10.1093/femspd/fty026.

Turner, J., Muraoka, A., Bedenbaugh, M., Childress, B., Pernot, L., Wiencek, M. and Peterson, Y.K. (2022). The Chemical Relationship Among Beta-Lactam Antibiotics and Potential Impacts on Reactivity and Decomposition. *Frontiers in Microbiology*, 13. doi:https://doi.org/10.3389/fmicb.2022.807955.

Turner, R.D., Vollmer, W. and Foster, S.J. (2014). Different walls for rods and balls: the diversity of peptidoglycan. *Molecular Microbiology*, 91(5), pp.862–874. doi:https://doi.org/10.1111/mmi.12513.

Twining, S.S. (1984). Fluorescein isothiocyanate-labeled casein assay for proteolytic enzymes. 143(1), pp.30–34. doi:https://doi.org/10.1016/0003-2697(84)90553-0.

Typas, A. & Banzhaf, M. & Gross, C.A. & et al. (2011) From the regulation of peptidoglycan synthesis to bacterial growth and morphology. *Nature Reviews Microbiology*, 10 (2): 123–136. doi:10.1038/nrmicro2677.

UCL (2010). *London - the tuberculosis capital of Europe*. [online] UCL News. Available at: https://www.ucl.ac.uk/news/2010/dec/london-tuberculosis-capital-europe#:~:text=The%20UK%20is%20the%20only [Accessed 12 Oct. 2023].

Uehara, T., Dinh, T. and Bernhardt, T.G. (2009). LytM-Domain Factors Are Required for Daughter Cell Separation and Rapid Ampicillin-Induced Lysis in Escherichia coli. *Journal of Bacteriology*, 191(16), pp.5094–5107. doi:https://doi.org/10.1128/jb.00505-09.

Unicef (2023). *Vaccination and Immunization Statistics - UNICEF DATA*. [online] UNICEF DATA. Available at: https://data.unicef.org/topic/child-health/immunization/.

United Nations (2023). *The Sustainable Development Goals Report 2023: Special Edition*. [online] unstats.un.org. Available at: https://unstats.un.org/sdgs/report/2023/.

Urbach, C., Evrard, C., Vaidas Pudzaitis, Fastrez, J., Soumillion, P. and Declercq, J. (2009). Structure of PBP-A from *Thermosynechococcus elongatus*, a Penicillin-Binding Protein Closely Related to Class A β-Lactamases. *Journal of Molecular Biology*, 386(1), pp.109–120. doi:https://doi.org/10.1016/j.jmb.2008.12.001.

Vaekova, R.S., Jaiswal, D., Sehnal, D., Ionescu, C.-M. ., Geidl, S., Pravda, L., Horsky, V., Wimmerova, M. and Ko a, J. (2014). MotiveValidator: interactive web-based validation of ligand and residue structure in biomolecular complexes. *Nucleic Acids Research*, 42(W1), pp.W227–W233. doi:https://doi.org/10.1093/nar/gku426.

Valegård, K., Iqbal, A., Kershaw, N.J., Ivison, D., Généreux, C., Dubus, A., Blikstad, C., Demetriades, M., Hopkinson, R.J., Lloyd, A.J., Roper, D.I., Schofield, C.J., Andersson, I. and McDonough, M.A. (2013).

Structural and mechanistic studies of theorf12gene product from the clavulanic acid biosynthesis pathway. *Acta Crystallographica Section D Biological Crystallography*, 69(8), pp.1567–1579. doi:https://doi.org/10.1107/s0907444913011013.

Valegård, K., Iqbal, A., Kershaw, N.J., Ivison, D., Généreux, C., Dubus, A., Blikstad, C., Demetriades, M., Hopkinson, R.J., Lloyd, A.J., Roper, D.I., Schofield, C.J., Andersson, I. and McDonough, M.A. (2013). Structural and mechanistic studies of theorf12gene product from the clavulanic acid biosynthesis pathway. *Acta Crystallographica Section D Biological Crystallography*, 69(8), pp.1567–1579. doi:https://doi.org/10.1107/s0907444913011013.

van Alen, I., Chikunova, A., Safeer, A.A., Ahmad, M.U.D., Perrakis, A. and Ubbink, M. (2021). The G132S Mutation Enhances the Resistance of *Mycobacterium tuberculosis* β-Lactamase against Sulbactam. *Biochemistry*, 60(28), pp.2236–2245. doi:10.1021/acs.biochem.1c00168.

van den Ent, F. and Löwe, J. (2006). RF cloning: A restriction-free method for inserting target genes into plasmids. *Journal of Biochemical and Biophysical Methods*, [online] 67(1), pp.67–74. doi:https://doi.org/10.1016/j.jbbm.2005.12.008.

van der Linden, M.P.G., de Haan, L., Dideberg, O. and Keck, W. (1994). Site-directed mutagenesis of proposed active-site residues of penicillin-binding protein 5 from *Escherichia coli*. *Biochemical Journal*, 303(2), pp.357–362. doi:https://doi.org/10.1042/bj3030357.

van Teeseling, M.C.F., de Pedro, M.A. and Cava, F. (2017). Determinants of Bacterial Morphology: From Fundamentals to Possibilities for Antimicrobial Targeting. *Frontiers in Microbiology*, [online] 8. doi:https://doi.org/10.3389/fmicb.2017.01264.

Vandal, O.H., Pierini, L.M., Schnappinger, D., Nathan, C.F. and Ehrt, S. (2008). A membrane protein preserves intrabacterial pH in intraphagosomal *Mycobacterium tuberculosis*. *Nature Medicine*, 14(8), pp.849–854. doi:https://doi.org/10.1038/nm.1795.

Vasstrand, E.N., Miron, T. and Jensen, H.B. (1987). Partial characterization of a peptidoglycan-protein complex from *Fusobacterium nucleatum* Fev1. *Acta Odontologica Scandinavica*, 45(3), pp.213–226. doi:https://doi.org/10.3109/00016358709098861.

Vector Labs, (2023). *Lectins: Wheat Germ Agglutinin (WGA), Biotinylated*. [online] Available at: https://vectorlabs.com/products/biotinylated-wheat-germ-agglutinin-wga [Accessed 2 Feb. 2024].

Velayati, A.A. and Farnia, P. (2017). The Species Concept. *Atlas of Mycobacterium Tuberculosis*, [online] pp.1–16. Available at: https://www.sciencedirect.com/science/article/pii/B9780128038086000013 [Accessed 19 April. 2022].

Vermassen, A., Leroy, S., Talon, R., Provot, C., Popowska, M. and Desvaux, M. (2019). Cell Wall Hydrolases in Bacteria: Insight on the Diversity of Cell Wall Amidases, Glycosidases and Peptidases Toward Peptidoglycan. *Frontiers in Microbiology*, 10. doi:10.3389/fmicb.2019.00331.

Veronique De Jager, Gupte, N., Nunes, S., Barnes, G.L., Christiaan, R., Mostert, J., Dorman, S.E., Abulfathi, A.A., Upton, C.M., Faraj, A., Nuermberger, E.L., Gyanu Lamichhane, Svensson, E.M., Ulrika Simonsson, Diacon, A.H. and Dooley, K.E. (2022). Early Bactericidal Activity of Meropenem plus Clavulanate (with or without Rifampin) for Tuberculosis: The COMRADE Randomized, Phase 2A Clinical Trial. *American Journal of Respiratory and Critical Care Medicine*, 205(10), pp.1228–1235. doi:https://doi.org/10.1164/rccm.202108-1976oc.

Via, L.E., Deretic, D., Ulmer, R.J., Hibler, N.S., Huber, L.A. and Deretic, V. (1997). Arrest of mycobacterial phagosome maturation is caused by a block in vesicle fusion between stages controlled by rab5 and rab7. *The Journal of biological chemistry*, [online] 272(20), pp.13326–31. doi:https://doi.org/10.1074/jbc.272.20.13326.

Vitale, A., Pessi, G., Urfer, M., Locher, H.H., Zerbe, K., Obrecht, D., Robinson, J.A. and Eberl, L. (2020). Identification of Genes Required for Resistance to Peptidomimetic Antibiotics by Transposon Sequencing. *Frontiers in Microbiology*, [online] 11. doi:https://doi.org/10.3389/fmicb.2020.01681.

Voladri, R.K., Lakey, D.L., Hennigan, S.H., Menzies, B.E., Edwards, K.M. and Kernodle, D.S. (1998). Recombinant expression and characterization of the major beta-lactamase of *Mycobacterium tuberculosis*. *Antimicrobial Agents and Chemotherapy*, [online] 42(6), pp.1375–1381. doi:https://doi.org/10.1128/AAC.42.6.1375.

Vollmer, W. and Bertsche, U. (2008). Murein (peptidoglycan) structure, architecture and biosynthesis in Escherichia coli. Biochimica et Biophysica Acta (BBA) - Biomembranes, 1778(9), pp.1714–1734. doi:10.1016/j.bbamem.2007.06.007.

Vollmer, W. and Höltje, J.-V. (2004). The Architecture of the Murein (Peptidoglycan) in Gram-Negative Bacteria: Vertical Scaffold or Horizontal Layer(s)? *Journal of Bacteriology*, 186(18), pp.5978–5987. doi:https://doi.org/10.1128/jb.186.18.5978-5987.2004.

Vollmer, W. and Tomasz, A. (2000). The pgdA Gene Encodes for a Peptidoglycan N-Acetylglucosamine Deacetylase in *Streptococcus pneumoniae*. *Journal of Biological Chemistry*, 275(27), pp.20496–20501. doi:https://doi.org/10.1074/jbc.m910189199.

Vollmer, W.; Joris, B.; Charlier, P.; Foster, S. Bacterial peptidoglycan (murein) hydrolases. (2008). FEMS Microbiology. Rev. 32, 259–286.

Waddington, K. (2004). To Stamp Out 'So Terrible a Malady': Bovine Tuberculosis and Tuberculin Testing in Britain, 1890–1939. *Medical History*, 48(1), pp.29–48. doi:https://doi.org/10.1017/s0025727300007043.

Wang, F., Cassidy, C. and Sacchettini, J.C. (2006). Crystal Structure and Activity Studies of the *Mycobacterium tuberculosis* β-Lactamase Reveal Its Critical Role in Resistance to β-Lactam Antibiotics. *Antimicrobial Agents and Chemotherapy*, 50(8), pp.2762–2771. doi:https://doi.org/10.1128/aac.00320-06.

Watt, S.R. and Clarke, A.J. (1994). Role of autolysins in the EDTA-induced lysis of *Pseudomonas aeruginosa*. *FEMS Microbiology Letters*, [online] 124(1), pp.113–119. doi:https://doi.org/10.1111/j.1574-6968.1994.tb07270.x.

Waxman, D.J. and Strominger, J.L. (1983). Penicillin-Binding Proteins and the Mechanism of Action of Beta-Lactam Antibiotics. *Annual Review of Biochemistry*, 52(1), pp.825–869. doi:10.1146/annurev.bi.52.070183.004141.

Waxman, D.J., Arima, H. and Strominger, J.L. (1982). Amino acid sequence homologies between *Escherichia coli* penicillin-binding protein 5 and class a β-lactamases. *FEBS Letters*, 139(2), pp.159–163. doi:https://doi.org/10.1016/0014-5793(82)80840-5.

Weerdenburg, E.M., Abdallah, A., Farania Rangkuti, El, A., Otto, T.D., Adroub, S.A., Molenaar, D., Ummels, R., Kars ter Veen, Gunny van Stempvoort, Astrid, Ali, S., Langridge, G.C., Thomson, N.R., Pain, A. and Bitter, W. (2015). Genome-Wide Transposon Mutagenesis Indicates that *Mycobacterium marinum* Customizes Its Virulence Mechanisms for Survival and Replication in Different Hosts. *Infection and Immunity*, 83(5), pp.1778–1788. doi:https://doi.org/10.1128/iai.03050-14.

White, A.D., Sarfas, C., West, K., Sibley, L.S., Wareham, A.S., Clark, S., Dennis, M.J., Williams, A., Marsh, P.D. and Sharpe, S.A. (2015). Evaluation of the Immunogenicity of *Mycobacterium bovis* BCG Delivered by Aerosol to the Lungs of Macaques. *Clinical and Vaccine Immunology*, 22(9), pp.992–1003. doi:https://doi.org/10.1128/cvi.00289-15.

Whitley, K.D., Jukes, C., Tregidgo, N., Karinou, E., Almada, P., Cesbron, Y., Henriques, R., Dekker, C. and Holden, S. (2021). FtsZ treadmilling is essential for Z-ring condensation and septal constriction initiation in Bacillus subtilis cell division. *Nature Communications*, [online] 12(1), p.2448. doi:https://doi.org/10.1038/s41467-021-22526-0.

WHO (2007) *The Use of Liquid Medium for Culture and DST.* Geneva: World Health Organization.

WHO (2011). Use of tuberculosis release assays (IGRAs) in low and middle-income countries. World Health Organization Policy.

WHO (2015). Implementing tuberculosis diagnostics. http://www.who.int/tb/publications/implementing_TB_diagnostics/en/ doi:WHO/HTM/TB/2015.11.

WHO (2019). Lateral flow urine lipoarabinomannan assay (LF-LAM) for the diagnosis of active tuberculosis in people living with HIV, 2019 Update. WHO/CDS/TB/2019.16

WHO (2023). *Tuberculosis*. [online] World Health Organization. Available at: https://www.who.int/news-room/fact-sheets/detail/tuberculosis.

WHO consolidated guidelines on tuberculosis: Module 4: treatment - drug-resistant tuberculosis treatment, 2022 update. (2022). [online] *PubMed*. Geneva: World Health Organization. Available at: https://www.ncbi.nlm.nih.gov/books/NBK588564/ [Accessed 11 Feb. 2024].

WHO policy statement (2022). Geneva: World Health Organization. Licence: CC BY-NC-SA 3.0 IGO.

Wietzerbin-Falszpan, J., Das, B.C., Azuma, I., Adam, A., Petit, J.F. and Lederer, E. (1970). Isolation and mass spectrometric identification of the peptide subunits of mycobacterial cell walls. *Biochemical and Biophysical Research Communications*, 40(1), pp.57–63. doi:10.1016/0006-291x(70)91045-4.

Wietzerbin, J., Das, B.C., Petit, J.F., Lederer, E., Leyh-Bouille, M. and Ghuysen, J.M. (1974). Occurrence of D-alanyl-(D)-meso-diaminopimelic acid and meso-diaminopimelyl-meso-diaminopimelic acid interpeptide linkages in the peptidoglycan of *Mycobacteria*. *Biochemistry*, 13(17), pp.3471–3476. doi:https://doi.org/10.1021/bi00714a008.

Wilson, V.G. and Heaton, P.R. (2008). Ubiquitin proteolytic system: focus on SUMO. *Expert Review of Proteomics*, 5(1), pp.121–135. doi:https://doi.org/10.1586/14789450.5.1.121.

Wivagg, C.N. and Hung, D.T. (2012). Resuscitation-Promoting Factors Are Required for β-Lactam Tolerance and the Permeability Barrier in *Mycobacterium tuberculosis*. *Antimicrobial Agents and Chemotherapy*, 56(3), pp.1591–1594. doi:10.1128/aac.06027-11.

Wivagg, C.N., Bhattacharyya, R.P. and Hung, D.T. (2014). Mechanisms of β-lactam killing and resistance in the context of Mycobacterium tuberculosis. *The Journal of Antibiotics*, 67(9), pp.645–654. doi:10.1038/ja.2014.94.

Woo Cheol Lee, Jang, A., Lee, J.-Y. and Kim, Y. (2021). Structural implication of substrate binding by peptidoglycan remodeling enzyme MepS. *Biochemical and Biophysical Research Communications*, 583, pp.178–183. doi:https://doi.org/10.1016/j.bbrc.2021.10.050.

Wood, R., Middelkoop, K., Myer, L., Grant, A.D., Whitelaw, A., Lawn, S.D., Kaplan, G., Huebner, R., McIntyre, J. and Bekker, L.-G. (2007). Undiagnosed Tuberculosis in a Community with High HIV Prevalence. *American Journal of Respiratory and Critical Care Medicine*, 175(1), pp.87–93. doi:https://doi.org/10.1164/rccm.200606-759oc.

World Health Organisation (2022). *Global Tuberculosis Report 2022*. [online] www.who.int. Available at: https://www.who.int/teams/global-tuberculosis-programme/tb-reports/global-tuberculosis-report-2022.

World Health Organisation (2023). *Guidelines on the management of latent tuberculosis infection*. [online] www.who.int. Available at: https://www.who.int/publications/i/item/9789241548908.

World Health Organization (2021). *Global tuberculosis report 2021*. [online] www.who.int. Available at: https://www.who.int/publications/i/item/9789240037021.

World Health Organization (2023). Roadmap towards ending TB in children and adolescents, third edition. Geneva: Licence: CC BY-NC-SA 3.0 IGO.

World Health Organization (2023). *SDG Target 3.3 Communicable diseases*. [online] www.who.int. Available at: https://www.who.int/data/gho/data/themes/topics/sdg-target-3_3-communicable-diseases.

World Health Organization (2023). *Strategic and Technical Advisory Group for Tuberculosis (STAG-TB)*. World Health Organization.

World Health Organization (2023). universal access to rapid tuberculosis diagnostics. Geneva: World Health Organization; 2023. Licence: CC BY-NC-SA 3.0 IGO.

Wu, R., Clancy, S. and A. Joachimiak (2012). The crystal structure of beta-lactamase from *Sphaerobacter thermophilus* DSM 20745. doi:https://doi.org/10.2210/pdb4ewf/pdb.

Wu, X., Yang, Y., Han, Y., Zhang, J., Liang, Y., Li, H., Li, B. and Wang, L. (2008). Effect of recombinant Rv1009 protein on promoting the growth of *Mycobacterium tuberculosis*. *Journal of Applied Microbiology*, 105(4), pp.1121–1127. doi:https://doi.org/10.1111/j.1365-2672.2008.03850.x.

www.ebi.ac.uk. (2023). *InterPro*. [online] Available at: https://www.ebi.ac.uk/interpro/result/InterProScan/iprscan5-R20231220-203920-0181-83465985-p1m/ [Accessed 20 Dec. 2023].

www.gavi.org. (2022). *5 ancient diseases and what the ancients said about them | Gavi, the Vaccine Alliance*. [online] Available at: https://www.gavi.org/vaccineswork/5-ancient-diseases-and-what-ancients-said-about-them.

www.gavi.org. (2023). *Vaccine profiles: Tuberculosis | Gavi, the Vaccine Alliance*. [online] Available at: https://www.gavi.org/vaccineswork/routine-vaccines-tuberculosis.

www.genome.jp. (2021). *KEGG Genome Browser - mtu*. [online] Available at: https://www.genome.jp/genome/mtu+Rv3593 [Accessed 5 Nov. 2023].

www.stoptb.org. (2019). *IGRA test for latent TB infection now available through the Stop TB Partnership's Global Drug Facility | Stop TB Partnership*. [online] Available at: https://www.stoptb.org/news/igra-test-latent-tb-infection-now-available-through-stop-tb-partnerships-global-drug-facility.

www.uniprot.org. (n.d.). *UniProt*. [online] Available at: https://www.uniprot.org/uniprotkb/O06155/entry [Accessed 30 Apr. 2024].

www.who.int. (2023). *What's new in the TB section of the 2023 WHO Model Lists of Essential Medicines*. [online] Available at: https://www.who.int/news/item/09-08-2023-what-s-new-in-the-tb-section-of-the-2023-who-model-lists-of-essential-medicines.

Xie, M., Li, Y., Xu, L., Zhang, S., Ye, H., Sun, F., Mei, R. and Su, X. (2021). Optimization of bacterial cytokine protein production by response surface methodology for environmental bioremediation. *RSC advances*, [online] 11(57), pp.36105–36115. doi:https://doi.org/10.1039/d1ra03565g.

Xu, X., Dong, B., Peng, L., Gao, C., He, Z., Wang, C. and Zeng, J. (2022). Anti-tuberculosis drug development via targeting the cell envelope of *Mycobacterium tuberculosis*. *Frontiers in Microbiology*, 13. doi:https://doi.org/10.3389/fmicb.2022.1056608.

Xu, Z., Meshcheryakov, V.A., Poce, G. and Chng, S.-S. (2017). MmpL3 is the flippase for mycolic acids in mycobacteria. *Proceedings of the National Academy of Sciences*, 114(30), pp.7993–7998. doi:https://doi.org/10.1073/pnas.1700062114.

Yamada, M., Tachibana, T., Imamoto, N. and Yoneda, Y. (1998). Nuclear transport factor p10/NTF2 functions as a Ran–GDP dissociation inhibitor (Ran-GDI). *Current Biology*, 8(24), pp.1339-S2. doi:https://doi.org/10.1016/s0960-9822(07)00566-0.

Yang, H., Kruh-Garcia, N.A. and Dobos, K.M. (2012). Purified protein derivatives of tuberculin — past, present, and future. *FEMS Immunology & Medical Microbiology*, 66(3), pp.273–280. doi:https://doi.org/10.1111/j.1574-695x.2012.01002.x.

Yao, Y., Barghava, N., Kim, J., Niederweis, M. and Marassi, F.M. (2012). Molecular Structure and Peptidoglycan Recognition of *Mycobacterium tuberculosis* ArfA (Rv0899). *Journal of Molecular Biology*, 416(2), pp.208–220. doi:https://doi.org/10.1016/j.jmb.2011.12.030.

Young, D.B., Gideon, H.P. and Wilkinson, R.J. (2009). Eliminating latent tuberculosis. *Trends in Microbiology*, [online] 17(5), pp.183–188. doi:https://doi.org/10.1016/j.tim.2009.02.005.

Yu, H., Rao, X. and Zhang, K. (2017). Nucleoside diphosphate kinase (Ndk): A pleiotropic effector manipulating bacterial virulence and adaptive responses. *Microbiological Research*, [online] 205, pp.125–134. doi:https://doi.org/10.1016/j.micres.2017.09.001.

Zandi, T.A. and Townsend, C.A. (2021). Competing off-loading mechanisms of meropenem from an L,D-transpeptidase reduce antibiotic effectiveness. *Proceedings of the National Academy of Sciences*, 118(27). doi:https://doi.org/10.1073/pnas.2008610118.

Zapun, A., Philippe, J., Abrahams, K.A., Signor, L., Roper, D.I., Breukink, E. and Vernet, T. (2013). *In vitro* Reconstitution of Peptidoglycan Assembly from the Gram-Positive Pathogen *Streptococcus pneumoniae*. *ACS Chemical Biology*, 8(12), pp.2688–2696. doi:https://doi.org/10.1021/cb400575t.

Zeng, D., Debabov, D., Hartsell, T.L., Cano, R.J., Adams, S., Schuyler, J.A., McMillan, R. and Pace, J.L. (2016). Approved Glycopeptide Antibacterial Drugs: Mechanism of Action and Resistance. *Cold Spring Harbor Perspectives in Medicine*, 6(12), p.a026989. doi:10.1101/cshperspect.a026989.

Zeng, J., Platig, J., Cheng, T.-Y., Ahmed, S., Skaf, Y., Potluri, L.-P., Schwartz, D., Steen, H., D. Branch Moody and Husson, R.N. (2020). Protein kinases PknA and PknB independently and coordinately regulate essential *Mycobacterium tuberculosis* physiologies and antimicrobial susceptibility. *PLOS pathogens*, 16(4), pp.e1008452–e1008452. doi:https://doi.org/10.1371/journal.ppat.1008452.

Zeng, X. and Lin, J. (2013). Beta-lactamase induction and cell wall metabolism in Gram-negative bacteria. *Frontiers in Microbiology*, [online] 4(128). doi:https://doi.org/10.3389/fmicb.2013.00128.

Zhanel, G.G., Pozdirca, M., Golden, A.R., Lawrence, C.K., Zelenitsky, S., Berry, L., Schweizer, F., Bay, D., Adam, H., Zhanel, M.A., Lagacé-Wiens, P., Walkty, A., Irfan, N., Naber, K., Lynch, J.P. and Karlowsky, J.A. (2022). Sulopenem: An Intravenous and Oral Penem for the Treatment of Urinary Tract Infections Due to Multidrug-Resistant Bacteria. *Drugs*, 82(5), pp.533–557. doi:https://doi.org/10.1007/s40265-022-01688-1.

Zhang HM, Hao Q. (2011). Crystal structure of NDM-1 reveals a common β-lactam hydrolysis mechanism. *FASEB J* 25:2574–2582.

Zhang Z, Pang Y, Wang Y, Liu C, Zhao Y. (2014). Beijing genotype of *Mycobacterium tuberculosis* is significantly associated with linezolid resistance in multidrug-resistant and extensively drug-resistant tuberculosis in China. International Journal Antimicrobial Agents **43**:231–235. doi: 10.1016/j.ijantimicag.2013.12.007.

Zhang, C., Freddolino, P.L. and Zhang, Y. (2017). COFACTOR: improved protein function prediction by combining structure, sequence and protein–protein interaction information. *Nucleic Acids Research*, 45(W1), pp.W291–W299. doi:https://doi.org/10.1093/nar/gkx366.

Zhang, D., de Souza, R.F., Anantharaman, V., Iyer, L.M. and Aravind, L. (2012). Polymorphic toxin systems: Comprehensive characterization of trafficking modes, processing, mechanisms of action, immunity and ecology using comparative genomics. *Biology Direct*, 7(1). doi:https://doi.org/10.1186/1745-6150-7-18.

Zhang, Q., Wook Bin Lee, Ji Seon Kang, Lark Kyun Kim and Kim, Y.-J. (2018). Integrin CD11b negatively regulates Mincle-induced signaling via the Lyn–SIRPα–SHP1 complex. *Experimental & Molecular Medicine*, 50(2), pp.e439–e439. doi:https://doi.org/10.1038/emm.2017.256.

Zhang, W., Li, S., Ma, L., Ding, W. and Xu, Y. (2019). Identification of a novel carboxypeptidase encoded by Rv3627c that plays a potential role in mycobacteria morphology and cell division. *Enzyme and Microbial Technology*, 126, pp.32–40. doi:https://doi.org/10.1016/j.enzmictec.2019.03.003.

Zhang, W., Shi, Q., Meroueh, S.O., Vakulenko, S.B. and Mobashery, S. (2007). Catalytic Mechanism of Penicillin-Binding Protein 5 of *Escherichia coli*. *Biochemistry*, 46(35), pp.10113–10121. doi:https://doi.org/10.1021/bi700777x.
Zhang, Z., Bulloch, E.M.M., Bunker, R.D., Baker, E.N., Squire, C.J. (2009). Structure and function of GlmU from *Mycobacterium tuberculosis*. *Acta Crystallographica, Section D, Biological Crystallography.* 2009;65:275–283. doi: 10.1107/S0907444909001036.

Zhao Y, Xu S, Wang L, Chin DP, Wang S, Jiang G, Xia H, Zhou Y, Li Q, Ou X, Pang Y, Song Y, Zhao B, Zhang H, He G, Guo J, Wang Y. 2012. National survey of drug-resistant tuberculosis in China. New England Journal Medicine. 366:2161–2170. doi: 10.1056/NEJMoa1108789.

Zhao, Q., Leung, S., Corbett, A.H. and Meier, I. (2006). Identification and Characterization of the *Arabidopsis* Orthologs of Nuclear Transport Factor 2, the Nuclear Import Factor of Ran. *Plant Physiology*, 140(3), pp.869–878. doi:https://doi.org/10.1104/pp.105.075499.

Zheng, S., Sham, L.-T., Rubino, F.A., Brock, K.P., Robins, W.P., Mekalanos, J.J., Marks, D.S., Bernhardt, T.G. and Kruse, A.C. (2018). Structure and mutagenic analysis of the lipid II flippase MurJ from *Escherichia coli*. *Proceedings of the National Academy of Sciences*, 115(26), pp.6709–6714. doi:https://doi.org/10.1073/pnas.1802192115.

Zhou, S., Wang, W., Zhou, X., Zhang, Y., Lai, Y., Tang, Y., Xu, J., Li, D., Lin, J., Yang, X., Ran, T., Chen, H., Guddat, L.W., Wang, Q., Gao, Y., Rao, Z. and Gong, H. (2021). Structure of *Mycobacterium tuberculosis* cytochrome bcc in complex with Q203 and TB47, two anti-TB drug candidates. *eLife*, [online] 10, p.e69418. doi:https://doi.org/10.7554/eLife.69418.

Zhu, J.-H., Wang, B.-W., Pan, M., Zeng, Y.-N., Rego, H. and Javid, B. (2018). Rifampicin can induce antibiotic tolerance in mycobacteria via paradoxical changes in rpoB transcription. *Nature Communications*, [online] 9(1), p.4218. doi:https://doi.org/10.1038/s41467-018-06667-3.

Zhu, L., Prasanti Yerramilli, Pruitt, L., Mishra, A., Olsen, R.J., Beres, S.B., Waller, A.S. and Musser, J.M. (2021). Functional Insights into the High-Molecular-Mass Penicillin-Binding Proteins of *Streptococcus agalactiae* Revealed by Gene Deletion and Transposon Mutagenesis Analysis. *Journal of bacteriology*, 203(17). doi:https://doi.org/10.1128/jb.00234-21.

Zink, A.R., Sola, C., Reischl, U., Grabner, W., Rastogi, N., Wolf, H. and Nerlich, A.G. (2003). Characterization of *Mycobacterium tuberculosis* Complex DNAs from Egyptian Mummies by Spoligotyping. *Journal of Clinical Microbiology*, [online] 41(1), pp.359–367. doi:https://doi.org/10.1128/jcm.41.1.359-367.2003.

Zuber, B., Chami, M., Houssin, C., Dubochet, J., Griffiths, G. and Daffé, M. (2008). Direct Visualization of the Outer Membrane of *Mycobacteria* and *Corynebacteria* in Their Native State. *Journal of Bacteriology*, 190(16), pp.5672–5680. doi:10.1128/jb.01919-07.